frontiers | Research Topics

Molecular and immune influences in the progression of gliomas

Edited by
Haotian Zhao and Maria Caffo

Published in
Frontiers in Oncology
Frontiers in Neurology

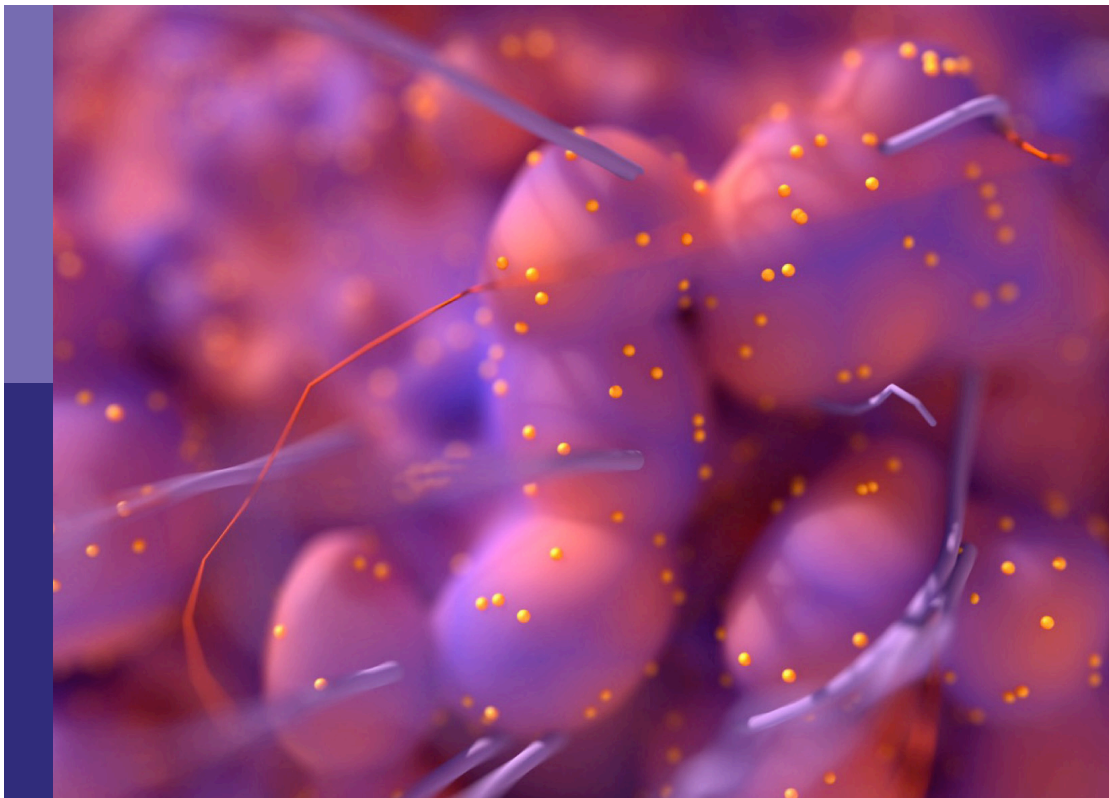

ISSN 1664-8714
ISBN 978-2-83251-683-6
DOI 10.3389/978-2-83251-683-6

About Frontiers

Frontiers is more than just an open access publisher of scholarly articles: it is a pioneering approach to the world of academia, radically improving the way scholarly research is managed. The grand vision of Frontiers is a world where all people have an equal opportunity to seek, share and generate knowledge. Frontiers provides immediate and permanent online open access to all its publications, but this alone is not enough to realize our grand goals.

Frontiers journal series

The Frontiers journal series is a multi-tier and interdisciplinary set of open-access, online journals, promising a paradigm shift from the current review, selection and dissemination processes in academic publishing. All Frontiers journals are driven by researchers for researchers; therefore, they constitute a service to the scholarly community. At the same time, the *Frontiers journal series* operates on a revolutionary invention, the tiered publishing system, initially addressing specific communities of scholars, and gradually climbing up to broader public understanding, thus serving the interests of the lay society, too.

Dedication to quality

Each Frontiers article is a landmark of the highest quality, thanks to genuinely collaborative interactions between authors and review editors, who include some of the world's best academicians. Research must be certified by peers before entering a stream of knowledge that may eventually reach the public - and shape society; therefore, Frontiers only applies the most rigorous and unbiased reviews. Frontiers revolutionizes research publishing by freely delivering the most outstanding research, evaluated with no bias from both the academic and social point of view. By applying the most advanced information technologies, Frontiers is catapulting scholarly publishing into a new generation.

What are Frontiers Research Topics?

Frontiers Research Topics are very popular trademarks of the *Frontiers journals series*: they are collections of at least ten articles, all centered on a particular subject. With their unique mix of varied contributions from Original Research to Review Articles, Frontiers Research Topics unify the most influential researchers, the latest key findings and historical advances in a hot research area.

Find out more on how to host your own Frontiers Research Topic or contribute to one as an author by contacting the Frontiers editorial office: frontiersin.org/about/contact

Molecular and immune influences in the progression of gliomas

Topic editors

Haotian Zhao — New York Institute of Technology, United States

Maria Caffo — University of Messina, Italy

Citation

Zhao, H., Caffo, M., eds. (2023). *Molecular and immune influences in the progression of gliomas*. Lausanne: Frontiers Media SA.

doi: 10.3389/978-2-83251-683-6

Table of contents

frontiers | Frontiers in Oncology

TYPE Editorial
PUBLISHED 01 February 2023
DOI 10.3389/fonc.2023.1102445

OPEN ACCESS

EDITED AND REVIEWED BY
David D. Eisenstat,
Royal Children's Hospital, Australia

*CORRESPONDENCE
Haotian Zhao
hzhao10@nyit.edu

SPECIALTY SECTION
This article was submitted to Neuro-Oncology and Neurosurgical Oncology, a section of the journal Frontiers in Oncology

RECEIVED 18 November 2022
ACCEPTED 09 January 2023
PUBLISHED 01 February 2023

CITATION
Malik K, Mian N, Caffo M and Zhao H (2023) Editorial: Molecular and immune influences in the progression of gliomas. *Front. Oncol.* 13:1102445. doi: 10.3389/fonc.2023.1102445

Editorial: Molecular and immune influences in the progression of gliomas

Karan Malik[1], Noreen Mian[1], Maria Caffo[2] and Haotian Zhao[1]*

[1]Department of Biomedical Sciences, College of Osteopathic Medicine, New York Institute of Technology, Old Westbury, NY, United States, [2]Department of Biomedical and Dental Sciences and Morpho-Functional Imaging, Unit of Neurosurgery, Messina, Italy

KEYWORDS

glioma, tumor microenvironment, biomarker, immune suppression, epithelial to mesenchymal transition, autophagy, long non-coding RNA, microRNA

Editorial on the Research Topic
Molecular and immune influences in the progression of gliomas

Diffuse gliomas are a heterogeneous group of tumors that represent the most prevalent and lethal primary tumors of the brain (1). High-grade gliomas are among the most difficult cancers to treat, for which first-line therapy – a combination of maximal surgical resection, radiotherapy, and chemotherapy with temozolomide (TMZ) – remains unchanged over a decade with few effective targeted therapies (2). Histologically, gliomas are categorized into four grades by WHO. Grade I gliomas usually grow slowly and behave in a more benign manner. Grade II and III gliomas can grow more rapidly and frequently require more aggressive treatment. Grade IV gliomas, also known as glioblastoma (GBM), is the most common and clinically aggressive gliomas, with median overall survival for patients with GBM at ~ 15 months (2). At the genomics level, gliomas in adults comprise two major groups based on the mutational status of isocitrate dehydrogenase genes *IDH1* and *IDH2*. Although IDH-mutant gliomas usually start as lower histologic grade tumors with improved prognosis, they often progress to higher grades. In contrast, IDH-wild-type gliomas typically present as GBM (2).

Multi-omics and recent technological advances such as single-cell techniques have provided a detailed and expanding appreciation of glioma intertumoral and intratumoral heterogeneity at genetic and epigenetic levels (3). The interactions with these heterogeneous components result in profoundly diverse phenotypic outcomes that contribute to adaptative responses and therapeutic resistance in this group of highly resilient disease. Importantly, heterogeneous cell populations within the tumor microenvironment (TME) represent an important aspect of glioma pathogenesis. Besides neuroglial cell types, gliomas are enriched for tumor-associated macrophages (TAM), while the maturation of natural killer (NK) cells is also affected in different glioma subtypes. The abundance of TAMs and low levels of infiltrating T cells constitute an immunosuppressive TME for adult gliomas (Figure 1A) (3, 4). With recent success of immunomodulatory therapy in diverse cancer types, there is significant interest in the study of immune regulation in the TME of glioma, and its implication in immunotherapy.

This topic introduces current developments in molecular and immune-mediated mechanisms in gliomas. One important goal was to investigate potential biomarkers in gliomas which may be useful tools in predicting behaviors of subpopulations of immune

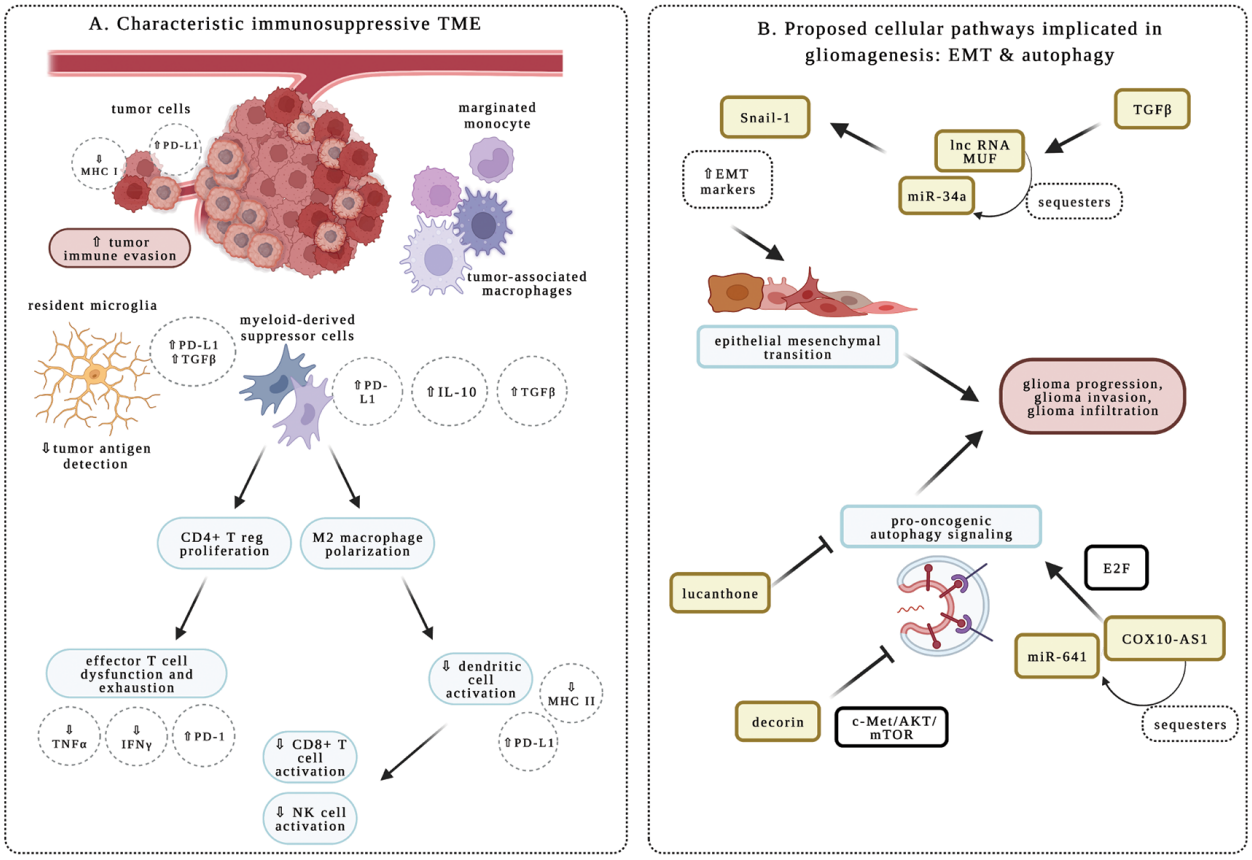

FIGURE 1
Schematic representation of immune and molecular regulation in glioma microenvironment. **(A)** Immunosuppression in glioma tumor microenvironment (TME). Immune responses are impacted by diverse cell types in the TME. Studies in the research topic highlight the importance of characterizing the immune phenotype in glioma. Tumor-associated macrophages (TAMs) include resident microglia, monocytes that will differentiate into M2- versus M1-predominant macrophages, and myeloid-derived suppressor cells (MDSCs), which are peripherally derived immunocytes that marginate through the blood-brain barrier. These cells are characteristic of an immunosuppressive TME and secrete key growth factors including interleukin 10 (IL-10) and transforming growth factor-beta (TGFß) to support an oncogenic niche. Cells of lymphoid origin, including T cells and natural killer (NK) cells; as well as other peripheral infiltrating cells, such as dendritic cells (DCs), are reported to be sparse within TME. MDSCs have been shown to prime CD4+ regulatory T cells (Treg) for an immunosuppressive and anergic role within gliomas. MDSC-primed Treg suppresses CD8+ effector T cell response, and contributes to effector T cell exhaustion through the downregulation of major histocompatibility complex class I molecules (MHC-I), suppression of signaling by interferon (IFN)-γ and tumor necrosis factor (TNF)-α, and upregulation of programmed cell death ligand 1 (PD-L1). The M2-polarized macrophages typically downregulate the expression of MHC-II and PD-L1 to suppress the activation of CD8+ T cells, NK cells, and DCs in the TME, thereby contributing to the immunosuppressive properties of TME. **(B)** Epithelial to mesenchymal transition (EMT) and autophagy in glioma. Studies in this research topic illustrate how cellular and molecular aspects of autophagy and EMT facilitate glioma infiltration, recurrence, and progression. COX10-AS1 is a lnc-RNA that is shown to upregulate pro-oncogenic autophagy signaling mechanisms *via* the E2F family of proteins. Decorin is an extracellular matrix component that inhibits autophagy *via* c-Met/Akt/mTOR signaling, and may function as a novel therapeutic target. Lucanthone is effective in inhibiting autophagy, glioma cell proliferation and survival. And TGFß within the TME is shown to promote EMT, as evident by upregulation of EMT markers like Snail-1 *via* miR-34a sequestration by the lnc-RNA MUF. Created with BioRender.com.

infiltrates and in determining which glioma subtypes may be amenable to genotoxic and immunomodulatory therapies. A systematic review was performed investigating proteins, nucleic acids, circulating cells, and metabolites, as potential blood-based biomarkers for glioma (Ali et al.). Around 200 targets are categorized according to their clinical utility in predicting recurrence, identifying highly infiltrative glioma subtypes, and optimizing therapeutic management. The study found that panels of microRNAs and proteins are the most promising biomarkers, while a selection of single biomarkers may also be useful. Consistently, several manuscripts drew on multiple modalities including the study of institution-specific patient cohorts, bioinformatics, and multi-omics data from The Cancer Genome Atlas (TCGA) and Chinese Glioma Genome Atlas (CGGA). TAMs in glioma can arise from resident microglia or monocytes of peripheral circulation (4). They are engaged in immunosuppression and have unique gene signatures for macrophage activation and increased chemokine/cytokine signaling, which is associated with poor prognosis in glioma patients (Figure 1A) (3, 4). CHI3L2 (Chitinase-3-Like Protein 2) is a member of chitinase-like proteins in the glycoside hydrolase 18 family (5), and SIGLEC9 (sialic acid-binding Ig-like lectin-9) is a new member of the Siglec subgroup of the immunoglobulin superfamily expressed in monocytes, neutrophils, T cells and NK cells (6). Two research teams found respectively that elevated levels of CHI3L2 (Liu et al.), or SIGLEC9 (Xu et al.), are associated with poor

prognosis and increased immune infiltrates in glioma. CHI3L2 expression is closely related to different activation states of TAMs and induces the apoptosis of CD8+ T cells (Liu et al.). Similarly, SIGLEC9 expression is positively correlated with myeloid-derived suppressor cell infiltration, immune suppression, TAM proliferation and functions (Xu et al.). Therefore, high levels of CHI3L2 or SIGLEC9 could act as unfavorable prognostic factors in glioma patients.

The interactions of malignant cells with immune cells represent critical events in tumor progression (3, 4). However, the molecular details underlying these interactions remain unclear. Three groups discovered that the expression of Tumor necrosis factor receptor superfamily member 12A (TNFRSF12A) (Zhang et al.), methyltransferase like 7B (METTL7B) (Xiong et al.), or Caspase 6 (CASP6) (Guo et al.) in tumor cells is associated with reduced survival in glioma patients, respectively. Further analysis revealed a significant correlation of their expression with immune cell infiltration and immune checkpoints. Knockdown of METTL7B (Xiong et al.) or CASP6 (Guo et al.) inhibits glioma proliferation, suggesting that they contribute to the progression of glioma. These genes could be viable prognostic biomarkers and potential immunotherapeutic targets in glioma.

Predicting the infiltrative behavior of glioma is difficult from a clinical-translational perspective. A prognostic and diagnostic MRI protocol to screen for aggressive and invasive gliomas has been proposed (Li et al.). In a single-center case series, it was shown that T2/FLAIR abnormality could be an indicator of GBM progression, especially for new lesions disseminating from primary sites. It should be noted that these studies report preliminary analysis of candidate indicators of tumor progression and prognosis.

One of the major obstacles to successful treatment of glioma arises from its invasive behavior that enables escape from complete surgical resection and chemo- and radiation therapy (2). Recent work indicates that epithelial to mesenchymal transition (EMT) represents a critical state that promotes glioma infiltration and progression (Figure 1B) (7, 8). One group showed that long non-coding RNA (lncRNA) MUF is specifically upregulated by TGFβ (Shree et al.). LncRNA-MUF functions as a sponge for microRNA 34a (miR-34a), promoting the expression of EMT markers. Knockdown of lncRNA-MUF reduces proliferation, migration, and invasion of glioma cells, and sensitizes them to TMZ-induced apoptosis.

Autophagy has two counterbalancing arms in cancer: one that impairs proliferation and invasion, while the other may contribute to tumor progression, invasion, and EMT (Figure 1B) (9, 10). Decorin, a proteoglycan in the extracellular matrix, downregulates the expression of EMT markers, suppresses glioma cell migration and invasion (Jia et al.). These effects are achieved through inhibiting autophagy by activating the c-Met/AKT/mTOR axis. In agreement, it has been demonstrated that COX10-AS1, a lncRNA associated with autophagy, promotes glioma progression by sequestering miR-641 to regulate E2F6 (Liu et al.). To complement this work, another study showed that lucanthone, an orally bioavailable and anti-schistosomal agent, acts as an autophagy inhibitor in glioma cells to enhance TMZ efficacy, and suppresses the growth of glioma cells (Radin et al.). Therefore, the unique biology of glioma invasion and progression revealed by these studies will provide potential therapeutic targets.

In summary, the Research Topic of "Molecular and Immune Influences in the Progression of Gliomas" presents novel preclinical and clinical work in glioma progression and resistance. The diverse work will contribute to developmental therapeutics and the search for clinically adaptable biomarkers to evaluate the anti-glioma therapy, to assess disease response, and to monitor for resistance and recurrence. These studies highlight the importance of multimodal and multidisciplinary approaches in the study of glioma.

Author contributions

All authors listed have made a substantial, direct, and intellectual contribution to the work, and approved it for publication.

Funding

HZ is supported by the New York Institute of Technology and National Cancer Institute (R01CA220551) of National Institutes of Health. KM is supported by the New York Institute of Technology College of Osteopathic Medicine Academic Scholarship.

Conflict of interest

The authors declare that the research was conducted in the absence of any commercial or financial relationships that could be construed as a potential conflict of interest.

Publisher's note

References

1. Ostrom QT, Gittleman H,, Fulop J, Liu M, Blanda R, Kromer C, et al. CBTRUS statistical report: primary brain and central nervous system tumors diagnosed in the United States in 2008–2012. *Neuro Oncol* (2015) 17:iv1–iv62.

2. Horbinski C, Berger T, Packer RJ, Wen PY. Clinical implications of the 2021 edition of the WHO classification of central nervous system tumours. *Nat Rev Neurol* (2022) 18:515–29. doi: 10.1038/s41582-022-00679-w

3. Nicholson JG, Fine HA. Diffuse glioma heterogeneity and its therapeutic implications. *Cancer Discovery* (2021) 11:575–90. doi: 10.1158/2159-8290.CD-20-1474

4. Andersen BM, Faust Akl C, Wheeler MA, Chiocca EA, Reardon DA, Quintana FJ. Glial and myeloid heterogeneity in the brain tumour microenvironment. *Nat Rev Cancer* (2021) 21:786–802. doi: 10.1038/s41568-021-00397-3

5. Du H, Masuko-Hongo K, Nakamura H, Xiang Y, Bao CD, Wang XD, et al. The prevalence of autoantibodies against cartilage intermediate layer protein, YKL-39, osteopontin, and cyclic citrullinated peptide in patients with early-stage knee osteoarthritis: evidence of a variety of autoimmune processes. *Rheumatol Int* (2005) 26:35–41. doi: 10.1007/s00296-004-0497-2

6. Ibarlucea-Benitez I, Weitzenfeld P, Smith P, Ravetch JV. Siglecs-7/9 function as inhibitory immune checkpoints *in vivo* and can be targeted to enhance therapeutic antitumor immunity. *Proc Natl Acad Sci U.S.A.* (2021) 118. doi: 10.1073/pnas.2107424118

7. Colella B, Faienza F, Di Bartolomeo S. EMT regulation by autophagy: A new perspective in glioblastoma biology. *Cancers (Basel)* (2019) Mar 6; 11(3):312. doi: 10.3390/cancers11030312

8. Li H, Li J, Chen L, Qi S, Yu S, Weng Z, et al. HERC3-mediated SMAD7 ubiquitination degradation promotes autophagy-induced EMT and chemoresistance in glioblastoma. *Clin Cancer Res* (2019) 25:3602–16. doi: 10.1158/1078-0432.CCR-18-3791

9. Niclou SP, Golebiewska A. Turning strength into weakness: protein degradation and autophagy as therapeutic targets in glioblastoma? *Neuro Oncol* (2021) 23:1041–3. doi: 10.1093/neuonc/noab099

10. Manea AJ, Ray SK. Regulation of autophagy as a therapeutic option in glioblastoma. *Apoptosis* (2021) 26:574–99. doi: 10.1007/s10495-021-01691-z

frontiers in Oncology

ORIGINAL RESEARCH
published: 15 April 2021
doi: 10.3389/fonc.2021.611038

CHI3L2 Is a Novel Prognostic Biomarker and Correlated With Immune Infiltrates in Gliomas

Liling Liu[1,2†], Yuanzhong Yang[1,2†], Hao Duan[2,3†], Jiahua He[1,2], Lu Sun[1,2], Wanming Hu[1,2] and Jing Zeng[1,2*]*

[1] Department of Pathology, Sun Yat-Sen University Cancer Center, Guangzhou, China, [2] State Key Laboratory of Oncology in Southern China, Sun Yat-Sen University Cancer Center, Guangzhou, China, [3] Department of Neurosurgery, Sun Yat-Sen University Cancer Center, Guangzhou, China

CHI3L2 (Chitinase-3-Like Protein 2) is a member of chitinase-like proteins (CLPs), which belong to the glycoside hydrolase 18 family. Its homologous gene, CHI3L1, has been extensively studied in various tumors and has been shown to be related to immune infiltration in breast cancer and glioblastoma. High CHI3L2 expression was reported to be associated with poor prognosis in breast cancer and renal cell carcinoma. However, the prognostic significance of CHI3L2 in glioma and its correlation between immune infiltration remains unclear. In this study, we examined 288 glioma samples by immunohistochemistry to find that CHI3L2 is expressed in tumor cells and macrophages in glioma tissues and highly expressed in glioblastoma and IDH wild-type gliomas. Relationships between CHI3L2 expression and clinical features (grade, age, Ki67 index, P53, PHH3 (mitotic figures), ATRX, TERTp, MGMTp, IDH, and 1p/19q co-deleted status) were evaluated. Kaplan-Meier survival was conducted to show high CHI3L2 expression in tumor cells (TC) and macrophage cells (MC) indicated poor prognosis in diffusely infiltrating glioma (DIG), lower-grade glioma (LGG), and IDH wild-type gliomas (IDH-wt). The overall survival time was higher in patients with dual-low CHI3L2 expression in TC and MC compared to those in patients with non-dual CHI3L2 expression and dual high expression in DIG and IDH wild-type gliomas. By univariate and multivariate analysis, we found that high CHI3L2 expression in tumor cells was an independent unfavorable prognostic factor in glioma patients. Moreover, we used two datasets (TCGA and CGGA) to verify the results of our study and explore the potential functional role of CHI3L2 by GO and KEGG analyses in gliomas. TIMER platform analysis indicated CHI3L2 expression was closely related to diverse marker genes of tumor immune infiltrating cells, including monocytes, TAMs, M1 macrophages, M2 macrophages, TGFβ1+ Treg and T cell exhaustion in GBM and LGG. Western Blot validated CHI3L2 is expressed in glioma cells and microglia cells. The results of flow cytometry showed that CHI3L2 induces the apoptosis of CD8+ T cells. In conclusion, these results demonstrate CHI3L2 is related to poor prognosis and immune infiltrates in gliomas, suggesting it may serve as a promising prognostic biomarker and represent a new target for glioma patients.

Keywords: CHI3L2, gliomas, CGGA, TCGA, prognosis, immune infiltrates

OPEN ACCESS

Edited by:
Manabu Kinoshita, Asahikawa Medical University, Japan

Reviewed by:
Koji Takano, Osaka International Cancer Institute, Japan
Rui-Chao Chai, Capital Medical University, China

****Correspondence:***
Jing Zeng
zengjing@sysucc.org.cn
Wanming Hu
huwm@sysucc.org.cn

[†]These authors have contributed equally to this work

Specialty section:
This article was submitted to Neuro-Oncology and Neurosurgical Oncology, a section of the journal Frontiers in Oncology

Received: *28 September 2020*
Accepted: *23 March 2021*
Published: *15 April 2021*

Citation:
Liu L, Yang Y, Duan H, He J, Sun L, Hu W and Zeng J (2021) CHI3L2 Is a Novel Prognostic Biomarker and Correlated With Immune Infiltrates in Gliomas. Front. Oncol. 11:611038. doi: 10.3389/fonc.2021.611038

INTRODUCTION

Gliomas comprise the bulk of primary brain tumors in adults (1). Diffuse glioma is histopathologically classified into grade II-IV according to morphological criteria, including mitotic count, nuclear atypia, microvascular proliferation, and necrosis. Glioblastoma multiform (GBM) is categorized as one of the most malignant subtypes (2, 3). The 2016 World Health Organization (WHO) classification of adult diffuse glioma combines tumor histological morphology and molecular features, including the isocitrate dehydrogenase (IDH) mutation and the chromosomal arms 1p and 19q complete deletion (1p/19q co-deletion) (4). Even combining maximal surgical resection and radiotherapy with adjuvant temozolomide, tumor recurrence is inevitable and the prognosis of gliomas remains very poor (5). Consequently, it is an urgent demand to discover the potential molecular characteristics of gliomas and look for more effective treatment strategies.

CHI3L2 (Chitinase-3-Like Protein 2), also known as YKL39, is a kind of secretory protein. It is a member of chitinase-like proteins (CLPs) which include CHI3L1, CHI3L2, SI-CLP, YM1 and YM2. CHI3L2 was originally isolated from the culture medium of primary human articular cartilage cells (6). It has two physiological activities, one is to induce autoimmune response (7), the other is to participate in tissue remodeling, both of which may lead to disease progression. Previous studies showed CHI3L2 mRNA is significantly up-regulated in osteoarthritis, Alzheimer's disease, multiple sclerosis, and amyotrophic lateral sclerosis patients (8–11). CHI3L2 was secreted by microglia/astrocytes and could increase monocyte/macrophage infiltration, angiogenesis, and neuronal death in amyotrophic lateral sclerosis (11). It is not yet clear what type of cells CHI3L2 is expressed in gliomas. However, previous studies on CHI3L2 have shown that macrophages are a possible source of CHI3L2 in tumors (12–15). CHI3L2 has a high degree of sequence identity with CHI3L1, but no cross-reactivity has been observed (16–18). There have been many studies on the correlations between CHI3L1 and the progression of a number of cancers (19–22). In recent years, the relationship between tumor immune microenvironment and immunotherapy has received more and more attention. It was also reported CHI3L1 was related to immune infiltration in breast cancer and glioblastoma (23, 24). However, the data about the role of CHI3L2 in cancers and its association with immune infiltrates are fragmentary. Previous studies reported that CHI3L2 was overexpressed in tumor-associated macrophages and related to poor outcomes in breast cancer and renal cell carcinoma (13–15). Studies have been shown that CHI3L2 mRNA expression was increased in gliomas (18, 25, 26). However, the prognostic significance of CHI3L2 and its correlation with immune infiltrates in glioma remain unclear.

To systematically explore the CHI3L2 protein expression in diffusely infiltrating glioma, we first evaluated the CHI3L2 expression levels of 288 glioma tissues by immunohistochemistry (IHC) and analyzed the association between CHI3L2 levels and clinicopathological parameters. Moreover, we took advantage of CHI3L2 transcriptional data of gliomas in The Cancer Genome Atlas (TCGA) and the Chinese Glioma Genome Atlas (CGGA) datasets to validate our findings. Gene Ontology (GO) and Kyoto Encyclopedia of Genes and Genomes (KEGG) pathway analyses were used to explore the potential biological process and pathways of CHI3L2 in glioma. The Tumor IMmune Estimation Resource (TIMER) platform was used to explore the correlations between CHI3L2 and diverse marker genes of tumor immune infiltrates. Finally, we further verified the results through Western Blot and flow cytometry. In gliomas, this is the first comprehensive study to elaborate on the clinical significance of CHI3L2, its influence on prognosis and its correlation with immune infiltrates.

Abbreviations: CHI3L2, Chitinase-3-Like Protein 2; CGGA, Chinese Glioma Genome Atlas; CLPs, chitinase-like proteins; Cor, R-value of Spearman's correlation; CAMs, cell adhesion molecules; DEGs, differentially expressed genes; DIG, diffusely infiltrating glioma; FISH, fluorescent in situ hybridization; GBM, glioblastoma multiforme; GO, Gene Ontology; IHC, immunohistochemistry; IDH, isocitrate dehydrogenase; KEGG, Kyoto Encyclopedia of Gene and Genomes; LGG, lower-grade glioma; TAM, tumor-associated macrophage; TCGA, The Cancer Genome Atlas; TIMER, Tumor IMmune Estimation Resource; Treg, regulatory T cell; WHO, World Health Organization.

MATERIALS AND METHODS

Samples

We enrolled 288 glioma patients (WHO grade II-IV) operated at the Sun Yat-sen University Cancer Center (Guangzhou, China) from January 2009 to January 2016. The median follow-up time was 54 months. Follow-up was last done in June 2019. The detailed clinical data are listed in **Table S1**. There were 167 males and 121 females. The median age of all patients at initial diagnosis was 43 years (range 7-78years). According to MRI imaging, 278 cases of glioma were located on the supratentorial and 10 cases of glioma were located infratentorial. 264 out of 288 patients received postoperative adjuvant treatment (radiotherapy or chemotherapy). The median overall survival time of all patients was 27 months (range 0-110 months). This cohort included 112 cases of astrocytoma, 45 cases of oligodendroglial gliomas and 131 cases of glioblastoma (WHO IV). All samples were ethically approved for use based on informed consent.

Cell Culture

The human glioma cell lines and a human microglia cell line were purchased from the American Type Culture Collection resource center. The human glioma cells were maintained in Dulbecco's modified Eagle's medium (DMEM) supplemented with 10% heat-inactivated fetal bovine serum (FBS) and the human microglia cells were cultured in Minimum Essential Medium (MEM) with 10% FBS at 37 °C in a humidified incubator containing 5% CO2. Peripheral blood mononuclear cells (PBMC) were isolated by Ficoll-Hypaque density gradient centrifugation (Solarbio, Beijing, China). CD8+ T cell were separated by positive selection from PBMCs with CD8 magnetic beads and cultured in RPMI-1640 medium supplemented with 10% human serum, 5% L-glutamine-

penicillin-streptomycin solution (Sigma-Aldrich, USA), CD3/CD28 antibody (Biolegend, USA) (25ul/ml) and IL-2 (100IU/ml) in 24-well plates. After culturing for 24 hours, add the corresponding concentration of human CHI3L2 protein (Sino Biological, Beijing, China) to T cells and culture for 72 hours at 37 °C in a humidified incubator containing 5% CO2.

Immunohistochemistry (IHC), Molecular Genetics and Assessment Standard

Immunohistochemistry was essentially performed as previously reported (27). These tissue specimens were incubated with CHI3L2 rabbit polyclonal antibody (#22164, SAB, Maryland, USA). Immunohistochemical evaluation was independently conducted by two pathologists blinded for patient characteristics and outcome, and CHI3L2 expression by tumor cells and macrophage cells was scored separately. The discrepancies were resolved by consensus under a microscope for multi-viewing. A semi-quantitative IHC scoring criterion was used to determine the CHI3L2 protein expression levels in tumor cells. The percentage of positive cells and staining intensity were assessed to improve accuracy. The percent positivity of staining cells range from 0 to 4: 0, none; 1, 1%-25%; 2, 26%-50%; 3, 51%-75%; 4, 76%-100%. The intensity of staining was graded from 0 to 3 (0, no staining; 1, weak; 2, moderate and 3, strong). Then, we obtained the final IHC score by multiplying the proportion score by the intensity score of staining. We chose 4.5, which was determined by the Youden index as an optimal cutoff point to separate low CHI3L2 expression (score of 0-4.5) from high CHI3L2 expression (score>4.5) in tumor cells. For the macrophage cells, we only count the number of CHI3L2 positive staining macrophages, regardless of the staining intensity. We designed 7.5 determined by Youden index as an optimal cutoff point to differentiate low expression (number≤7.5) from high expression (number>7.5) in macrophages.

The other antibody markers including PHH3, P53, Ki67, ATRX, CD163, CD4, CD8, and CD20 were also used by immunohistochemistry tests. We detected MGMT promoter methylated status, TERT promoters and IDH mutation status by Sanger sequencing. 1p and 19q deletion status was detected using fluorescent in situ hybridization (FISH). The detailed protocol and assessment standard were described as a previous study (28).

Bioinformatic Analysis in Cancer Datasets

The CHI3L2 RNA-seq data were downloaded from http://www.cgga.org.cn/. We totally analyzed 601 TCGA RNA-seq cohort and 608 CGGA RNA-seq cohort of gliomas, ranging from WHO grade II to grade IV.

To identify the CHI3L2-related genes, the limma package of R software was used to screen out the differentially expressed genes (DEGs). The top 26 hub genes of the overlapping DEGs were built via the plug-in molecular complex detection and cytoHubba of Cytoscape. To explore the functions and pathways of CHI3L2-related genes, we performed GO and KEGG analyses on ClueGo and Metascape websites. The TIMER platform (https://cistrome.shinyapps.io/timer/) (29, 30) was performed to explore the association between CHI3L2 and marker sets of tumor immune infiltrates in GBM and LGG (31).

Western Blot

Total protein was extracted from seven human glioma cell lines and one human microglia cell line (HMC3). 30 ug of protein was loaded onto 10% SDSPAGE and electrophoretically transferred to PVDF membranes. After blocking, the membranes were incubated with primary antibody against CHI3L2 (1:1000 dilutions, rabbit polyclonal anti-CHI3L2, #22164, SAB, Maryland, USA). The membranes were then incubated with horseradish peroxidase-linked anti-rabbit antibody (at a 1:3000 dilution, Santa Cruz Biotechnology, Inc., Santa Cruz, Calif., USA). B-Actin was served as a loading control.

Flow Cytometry Analysis

Apoptosis was examined by flow cytometric analysis. Cells were collected, washed with PBS, and incubated with annexin V-FITC and PI (BD Biosciences, San Jose, CA, USA) for 15 minutes. Then cell apoptosis was analyzed by flow cytometry (FACS Calibur, Becton Dickinson, Sparks, MD) according to the manufacturer's instruction. FlowJo (Treestar, USA) software was used for the analysis of flow cytometry data. The results are expressed as mean ± SD of three independent experiments.

Statistical Analysis

GraphPad Prism 8 and SPSS 22 software were performed for statistical analyses. The measurement data are represented as mean ± SD. The Chi-square test was conducted to explore the correlations between CHI3L2 levels and clinicopathological features. Kaplan-Meier analysis was conducted for the overall survival of glioma patients with the log-rank test. The Cox proportional hazards regression model was used for univariate and multivariate analyses to evaluate the independence of CHI3L2 in predicting prognosis. The association between CHI3L2 and marker genes of immune infiltrating cells was assessed by Spearman's correlation coefficients. $P < 0.05$ was regarded as statistically significant.

RESULTS

The Expression Levels of CHI3L2 in Glioma Samples and Its Correlation With Clinicopathological Parameters

We detected CHI3L2 protein expression levels in histological sections from patients with different glioma grades by immunohistochemistry (IHC). Among the 288 glioma specimens inspected, we found CHI3L2 was mainly stained in tumor cells, as well as macrophage cells. **Figures 1A–D** showed different IHC staining intensity of CHI3L2 in glioma tissues. **Figures 1E, F** mainly showed CHI3L2+ macrophages in glioma tissues. The IHC score of CHI3L2 in tumor cells and density of CHI3L2+ macrophages in different glioma subgroups are shown in **Figure 2**. We found the expression levels of CHI3L2 in tumor

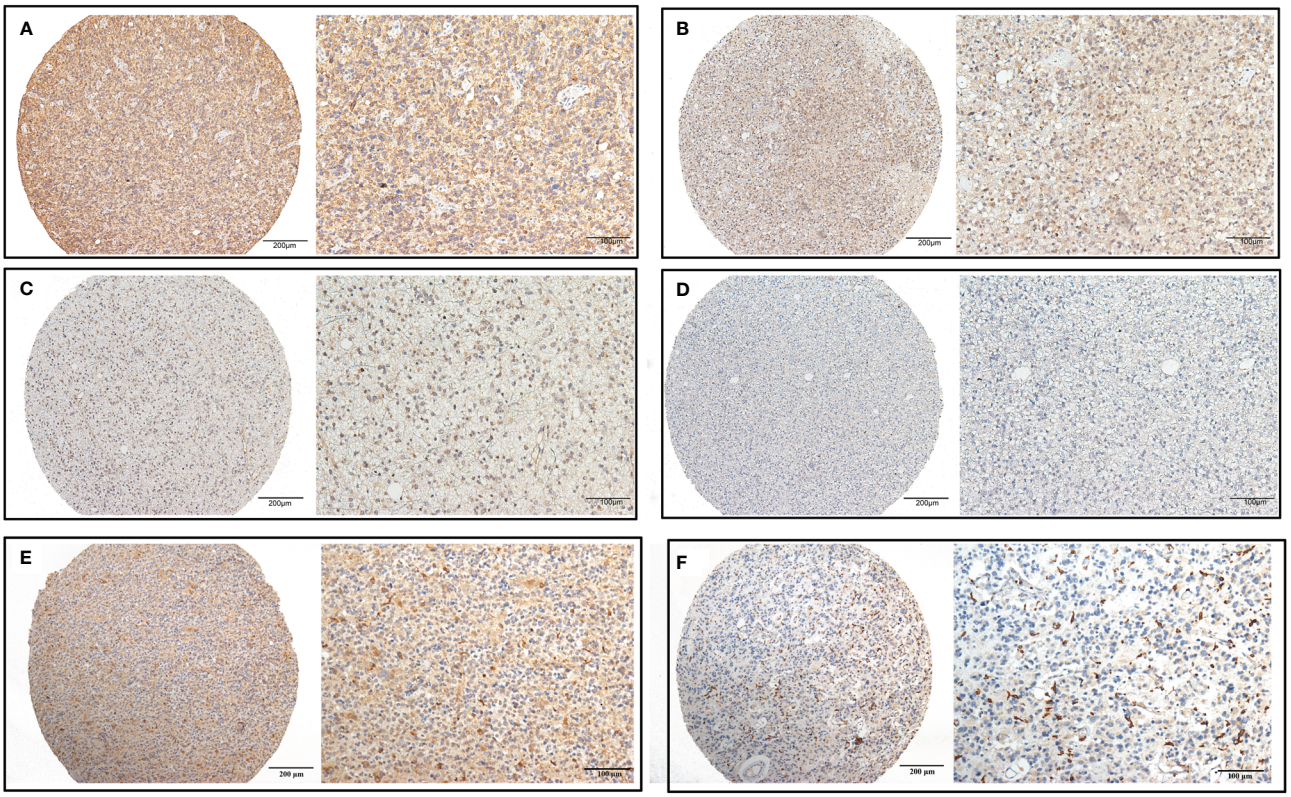

FIGURE 1 | CHI3L2 protein expression was detected by IHC. Representative images of strong **(A)**, moderate **(B)**, weak **(C)**, and negative **(D)** staining of CHI3L2 are shown. Representative images of the high density of CHI3L2+ macrophages in strong **(E)** and weak **(F)** staining glioma tissues are shown.

cells were upregulated with increasing WHO grade of gliomas (**Figure 2A**), but there was no significant difference in CHI3L2+ macrophage density between WHO II and WHO III gliomas (**Figure 2D**). The CHI3L2 expression levels of GBM were significantly increased compared with LGG (WHO II-III) (P<0.001) in tumor cells (**Figure 2B**) and macrophages (**Figure 2E**). A significant increase of CHI3L2 expression levels was found in IDH-wildtype gliomas compared with IDH-mutant gliomas (P<0.001) in tumor cells (**Figure 2C**) and macrophages (**Figure 2F**). We further analyze the CHI3L2 IHC score and density of CHI3L2+ macrophages in diffusely infiltrating glioma of new molecular classification, including IDH mutant without 1p/19q codeleted gliomas, IDH mutant with 1p/19q codeleted gliomas, and IDH wild-type gliomas (**Figures S1A, B**). We found the expression of CHI3L2 is not related to the status of 1p/19q codeleted in IDH mutant gliomas.

Based on the expression levels of CHI3L2 in tumor cells and macrophage cells, we evaluated the association between CHI3L2 staining and clinicopathological factors, as listed in **Table 1**. In tumor cells, we found significant correlations between CHI3L2 expression and WHO grade (P<0.001), age (P=0.001), Ki67 (P<0.001), P53 (P=0.034), PHH3 (mitotic figures) (P<0.001), ATRX protein expression (P=0.026), IDH (P<0.001) and 1p/19q codeleted (P=0.002). In macrophage cells, CHI3L2 is strongly correlated with WHO grade (P<0.001), gender (P=0.008), age (P=0.006), Ki67 (P<0.001), PHH3 (mitotic figures) (P<0.001), and IDH status (P<0.001). However, CHI3L2 expression levels of glioma cells were not significantly related to gender, location, TERT promoter mutation status, and MGMT promoter methylated status. In macrophage cells, CHI3L2 expression has no correlation with location, P53, ATRX protein expression, MGMT promoter methylated status, TERT promoter mutation, and 1p/19q codeleted status.

Impact of CHI3L2 Expression on the Prognosis of Gliomas

To explore the prognostic significance of CHI3L2 in gliomas, we performed the Kaplan-Meier method and log-rank test. We found high CHI3L2 expression levels of tumor cells and macrophages significantly predicted worse overall survival in diffusely infiltrating glioma (DIG) (**Figures 3A, D**) and lower-grade glioma (LGG) patients (**Figures 3B, E**). However, there was no statistical significance difference in GBM in our cohort (**Figures 3C, F**). When considering the CHI3L2 expression of tumor cells and macrophages together, we found the overall survival time was higher in patients with dual-low CHI3L2 expression in TC and MC compared to those in patients with non-dual CHI3L2 expression and dual high expression in DIG (**Figure 3G**), but this difference is not statistically significant in LGG and GBM (**Figures 3H, I**). Similarly, we also analyze the

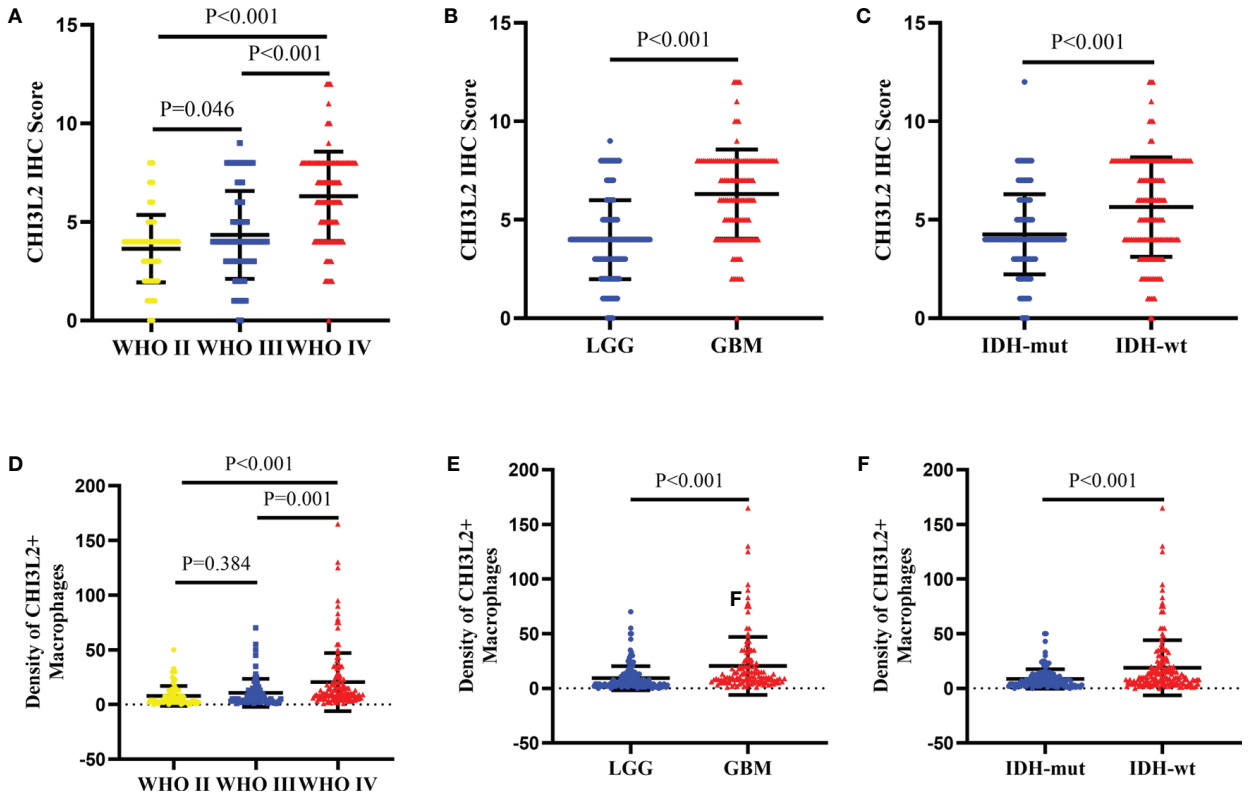

FIGURE 2 | The protein expression levels of CHI3L2 in different subgroups of gliomas. **(A)** The IHC score in diffusely infiltrating glioma (WHO II-IV). **(B)** The IHC score in LGG and GBM. **(C)** The IHC score in diffusely infiltrating glioma with different IDH status. **(D)** The density of CHI3L2+ macrophages in diffusely infiltrating glioma (WHO II-IV). **(E)** The density of CHI3L2+ macrophages in LGG and GBM. **(F)** The density of CHI3L2+ macrophages in diffusely infiltrating glioma with different IDH status.

effect of CHI3L2 on the prognosis in the new molecular classification of glioma. We found CHI3L2 expression in tumor cells is closely related to the prognosis of all new molecular classification of glioma, and high CHI3L2 expression in tumor cells, macrophages and TC + MC predicted poor outcome for IDH wild-type gliomas (**Figure S2**). Furthermore, we found regardless of whether patients with glioma have methylation of the MGMT promoter or have received adjuvant therapy, high CHI3L2 indicates a poor prognosis for glioma (**Figure S3**).

Additionally, to evaluate the independent risk factors for prognosis of glioma, we conducted the univariate analysis (**Table 2**) and multivariate analysis (**Table 3**). In univariate analysis, CHI3L2 expression in tumor cells, CHI3L2+ macrophage cells density, CHI3L2 expression in both tumor cells and macrophage cells (TC + MC), grade, age, location, adjuvant therapy, Ki67 index, PHH3 (mitotic figures), IDH, and 1p/19q codeleted status were shown to be prognostic variables for the prognosis of overall survival in glioma patients (**Table 2**). Then we included the prognostic variables in the univariate analysis (P<0.05) into the multivariate analysis. We found CHI3L2 expression in tumor cells, location, Ki67, IDH, 1p/19q codeleted were independent prognostic factors in gliomas (**Table 3**).

Validation of CHI3L2 mRNA Expression Levels and Prognostic Effect in TCGA and CGGA Datasets

To further verify the results of our study, we collected a total of 601 glioma samples from the TCGA dataset and 608 glioma samples from the CGGA dataset to analyze the CHI3L2 mRNA expression. In the TCGA dataset, CHI3L2 mRNA levels were significantly increased in GBM (WHO IV) compared with WHO II, WHO III, and LGG patients (**Figures 4A, B**). CHI3L2 mRNA expression levels were significantly higher in IDH wild-type gliomas compared with IDH mutant gliomas (**Figure 4C**). Similar results were also obtained in the CGGA dataset (**Figures 4D–F**). We further analyze the CHI3L2 mRNA expression levels in new molecular classification of diffusely infiltrating glioma, including IDH mutant without 1p/19q codeleted gliomas, IDH mutant with 1p/19q codeleted gliomas, and IDH wild-type gliomas, in TCGA and CGGA database (**Figure S4A** and **Figure S4B**). We found CHI3L2 mRNA expression levels in IDH wild-type gliomas are higher than IDH mutant gliomas. Gliomas with IDH mutant and 1p/19q codeleted have higher CHI3L2 mRNA levels than gliomas with IDH mutant and non-1p/19q codeleted. Moreover, we performed Kaplan-Meier analysis to confirm whether CHI3L2 mRNA levels could predict poor prognosis of gliomas in datasets.

TABLE 1 | Correlation between CHI3L2 expression and clinicopathologic parameters in gliomas.

Parameters	CHI3L2 inTumor cells		P value	CHI3L2 inMacrophage cells		P value
	Low	High		Low	High	
Grade						
LGG	117	40	<0.001	96	61	<0.001
GBM	34	97		37	94	
Gender						
Male	81	86	0.117	66	101	0.008
Female	70	51		67	54	
Age						
<55	127	92	0.001	111	108	0.006
≥55	24	45		22	47	
Location						
Supratentorial	144	134	0.257	127	151	0.372
Infratentorial	7	3		6	4	
Ki67						
<10%	51	11	<0.001	42	20	<0.001
≥10%	100	126		91	135	
P53						
<10%	61	39	0.034	49	51	0.484
≥10%	90	98		84	104	
PHH3						
<5/10HPF	87	23	<0.001	67	43	<0.001
≥5/10HPF	64	114		66	112	
ATRX						
Negative	74	85	0.026	76	83	0.541
Positive	77	52		57	72	
TERTp						
Wild type	81	66	0.354	74	73	0.148
Mutant	70	71		59	82	
IDH						
Wild type	64	98	<0.001	59	103	<0.001
Mutant	87	39		74	52	
1p/19q Codeleted						
Yes	35	13	0.002	26	22	0.224
No	116	124		107	133	
MGMTp						
Methylated	73	69	0.732	66	76	0.920
Unmethylated	78	68		67	79	

P-value: Chi-square test.

As shown in **Figure 5**, patients with high CHI3L2 mRNA levels correspond to shorter survival time in all glioma subgroups both in the TCGA (**Figures 5A–C**) and CGGA (**Figures 5D–F**) datasets. Similarly, we also verified the effect of CHI3L2 on the prognosis in the new molecular classification of glioma in database (**Figure S5**). Except for gliomas with IDH mutant and non-1p/19q codeleted in the TCGA dataset, high levels of CHI3L2 mRNA in any other subgroup indicate a poor prognosis, whether in the TCGA or CGGA dataset.

Predicted Functions and Pathways of CHI3L2 in Gliomas

The GBM and LGG RNA-seq data were from TCGA and CGGA datasets. Limma package in R software was conducted to screen out the differentially expressed genes (DEGs) with the cut-off criterion of adjusted P< 0.05 and |log2FC| > 1. We identified 1356 overlapping DEGs which were aberrantly expressed in TCGA and CGGA datasets (**Figure 6A**). The top 26 hub genes were screened via the plug-in molecular complex detection and cytoHubba of Cytoscape (**Figure 6B**). GO analysis was performed to show the overlapping DEGs were involved in several biological processes, including angiogenesis, immune, and inflammatory response (**Figure 6C**). The KEGG pathways enriched in several classic signaling pathways, such as cell adhesion molecules (CAMs) and PI3K-Akt signaling pathways (**Figure 6D**).

The Correlation Between CHI3L2 and Markers of Immune Infiltrates in Gliomas

Infiltrating immune cells are important components of the tumor microenvironment and are frequently associated with tumor behavior and patient outcomes. Since GO analysis revealed that CHI3L2 was related to the immune response, we further explored the infiltration of immune cells in gliomas. To estimate the relevance of CHI3L2 and diverse immune cell markers, we used the TIMER platform to investigate correlations between CHI3L2 levels and markers of diverse immune cells, included monocytes, TAMs (tumor-associated macrophages), M1 and M2 macrophages, Tregs (regulatory T cells), exhausted T cells, CD8+ T cells, T cells (general), B cells and neutrophils in GBM and LGG (**Table 4**). We found CHI3L2 was significantly associated with marker sets of monocytes, TAMs, and M2 macrophages in GBM and LGG. Particularly, we showed the scatter plots of association between CHI3L2 and the marker sets of monocytes, TAMs, M1 phenotype, and M2 phenotype in GBM and LGG (**Figures 7A–H**). We also found significant correlations between CHI3L2 and some markers of Treg and T cell exhaustion, such as TGFβ1, CTLA4, TIM-3, and GZMB. Since Treg and T cell exhaustion play an important role in tumor immune escape. We believe CHI3L2 may also play an immunomodulation role in gliomas. In addition, we used several clinical commonly immune cell markers, including CD163, CD4, CD8, CD20, to perform immunohistochemical test on glioma samples, and found that CHI3L2+ macrophages have a certain correlation with CD163+ M2 macrophages (r=0.547, p<0.001), CD4+ T cells (r=0.330, p<0.001), CD8+ T cells (r=0.389, p<0.001), and CD20+ B cells (r=0.237, p<0.001) in gliomas (**Figure S6**).

The Expression of CHI3L2 in Glioma Cell Lines and Its Effect on CD8+ T Cells

The expression of CHI3L2 in glioblastoma cells (U251, U87, T98G, DBTRG, A172, LN229) and microglia cell (HMC3) has been verified by Western Blot (**Figure 8A**). **Figure 8A** shows that CHI3L2 is expressed in glioblastoma cell lines and a microglia cell line. It is strongly expressed in the glioblastoma cell lines U87, U251, LN229, A172 and the microglia cell line HMC3, while the expression in the glioblastoma cell lines T98G and DBTRG is weak. **Figure 8B** is the result of flow cytometry analysis. The left image is a representative sorting that lists the percentage of cells in each quadrant: bottom left-live cells; top left-mechanically damaged cells; bottom right-early apoptosis; top right- late apoptosis. The cellular apoptotic rate was a sum of early and late apoptotic rates. The proportion of apoptotic cells in the control group was 28.1%, the proportion of apoptotic cells in the 0.5ug/ml CHI3L2 group was 33.6%, and the proportion of apoptotic cells in the 2.5ug/ml CHI3L2

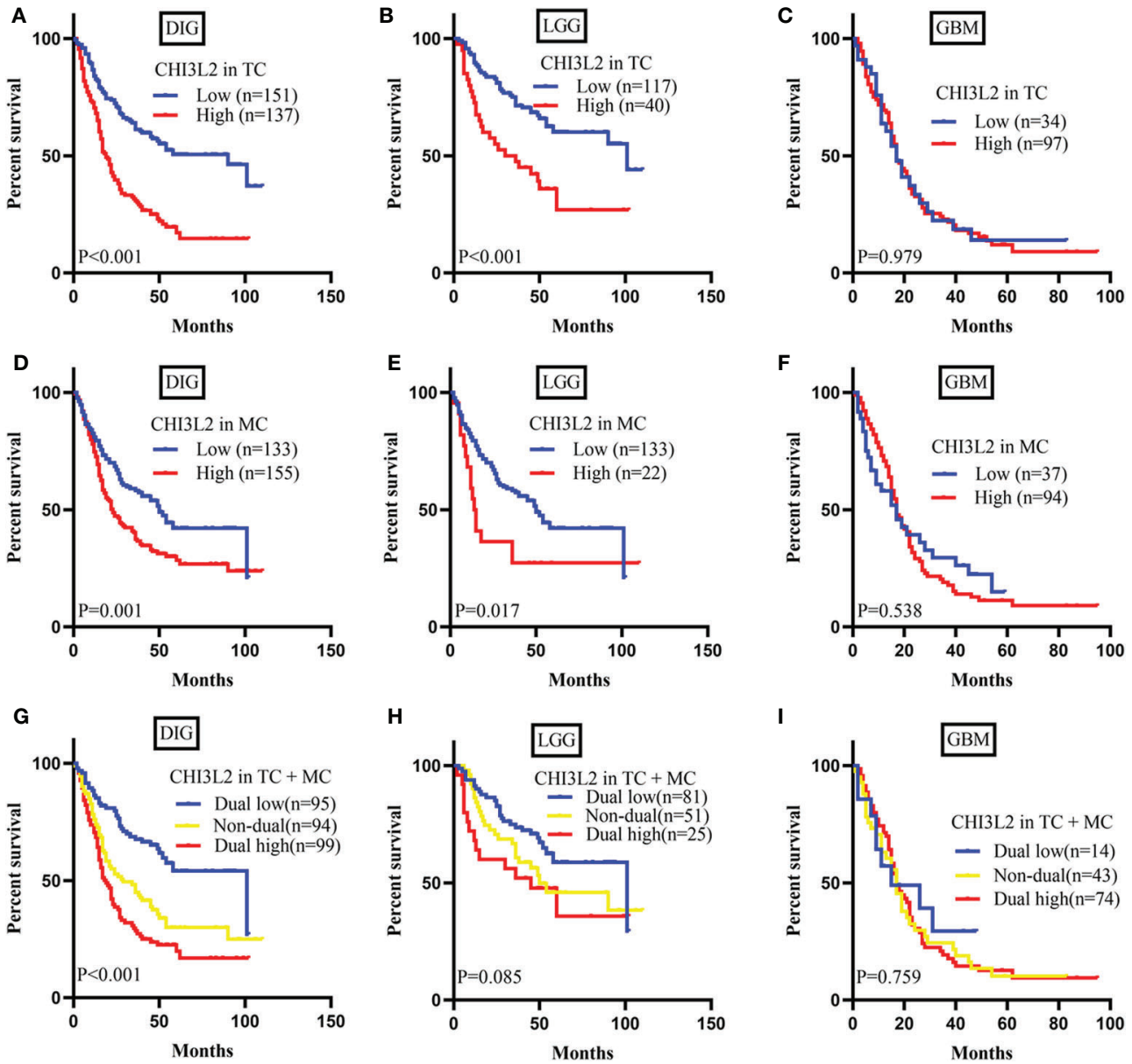

FIGURE 3 | CHI3L2 protein expression affects overall survival (OS) in glioma patients. Kaplan-Meier curves showing a correction of CHI3L2 expression with OS in tumor cells **(A–C)**, macrophage cells **(D–F)**, and tumor cells + macrophages cells **(G–I)** of diffusely infiltrating glioma (DIG), LGG, and GBM.

group was 35.9%. The right chart shows the percentage of apoptotic cells of three independent experiments. The result of flow cytometric analysis demonstrated that the apoptotic proportion of CD8+ T cells increases with increasing CHI3L2 concentration, indicating CHI3L2 may be related to immunosuppression.

DISCUSSION

At present, the outcome of most glioma is very poor, even with the use of comprehensive treatment strategies. It has been widely reported that the therapeutic resistance of glioma is closely related to its unique metabolic mechanism and the surrounding complex immunosuppressive microenvironment (32–34). Therefore, exploring reliable prognostic biomarkers and personalized treatment strategies for this disease are urgently needed. In the present study, CHI3L2 has been identified as a novel prognostic biomarker and associated with tumor immune infiltration markers in gliomas, which indicate CHI3L2 may serve as a target for glioma treatment in the future.

CHI3L2, as a member of the glycoside hydrolases 18 family, can act as a cytokine and growth factor but lacks chitinase activity (17). It was found produced by tumor-associated macrophages in breast cancer (13, 14). In renal cell carcinoma,

TABLE 2 | Univariate analysis of prognostic variables of overall survival.

Variables	Univariate analysis		
	HR	95%CI	P
CHI3L2 expression in tumor cells (low vs. high)	2.564	1.890-3.479	**<0.001**
CHI3L2+ macrophage cells density (low vs. high)	1.650	1.217-2.238	**0.001**
CHI3L2 in TC + MC (dual low vs. dual high)	3.017	2.035-4.472	**<0.001**
CHI3L2 in TC + MC (dual low vs. non-dual)	2.094	1.396-3.140	**<0.001**
Grade (LGG vs. GBM)	3.642	2.663-4.983	**<0.001**
Gender (Male vs. Female)	0.747	0.551-1.014	0.061
Age (<55 vs. ≥55 years)	2.135	1.545-2.951	**<0.001**
Location (Supratentorial vs. Infratentorial)	2.374	1.165-4.837	**0.017**
Adjuvant therapy (no vs. yes)	3.036	1.421-6.485	**0.004**
Ki67 (<10% vs. ≥10%)	3.501	2.190-5.596	**<0.001**
P53 (<10% vs. ≥10%)	1.220	0.887-1.676	0.221
PHH3 (<5/10HPF vs. ≥5/10HPF)	2.756	1.963-3.868	**<0.001**
ATRX (negative vs. positive)	1.225	0.907-1.654	0.185
TERTp (wild-type vs. mutant)	1.136	0.845-1.527	0.399
MGMTp (methylated vs. unmethylated)	0.876	0.651-1.178	0.381
IDH (wild-type vs. mutant)	0.202	0.142-0.286	**<0.001**
1p/19q Codeleted (no vs. yes)	0.165	0.084-0.322	**<0.001**

TABLE 3 | Multivariate analysis of prognostic variables of overall survival.

Variables	Multivariate analysis		
	HR	95%CI	P
CHI3L2 expression in tumor cells (low vs. high)	1.466	1.011-2.125	0.044
CHI3L2+ macrophage cells density (low vs. high)	1.002	0.719-1.398	0.990
Grade (LGG vs. GBM)	1.017	0.604-1.715	0.949
Age (<55 vs. ≥55 years)	1.350	0.956-1.907	0.088
Location (Supratentorial vs. Infratentorial)	2.393	1.120-5.112	0.024
Adjuvant therapy (no vs. yes)	1.783	0.794-4.001	0.161
Ki67 (<10% vs. ≥10%)	2.683	1.552-4.639	<0.001
PHH3 (<5/10HPF vs. ≥5/10HPF)	0.949	0.556-1.621	0.848
IDH (wild-type vs. mutant)	0.368	0.244-0.556	<0.001
1p/19q Codeleted (no vs. yes)	0.275	0.131-0.575	0.001

CHI3L2 was mainly expressed in tumor cells and tumor-associated macrophages (15). Previous studies revealed CHI3L2 significantly increased in glioblastoma by northern blot hybridization and western blotting analysis and activated signal-regulated kinases ERK1/ERK2 leading to the initiation of

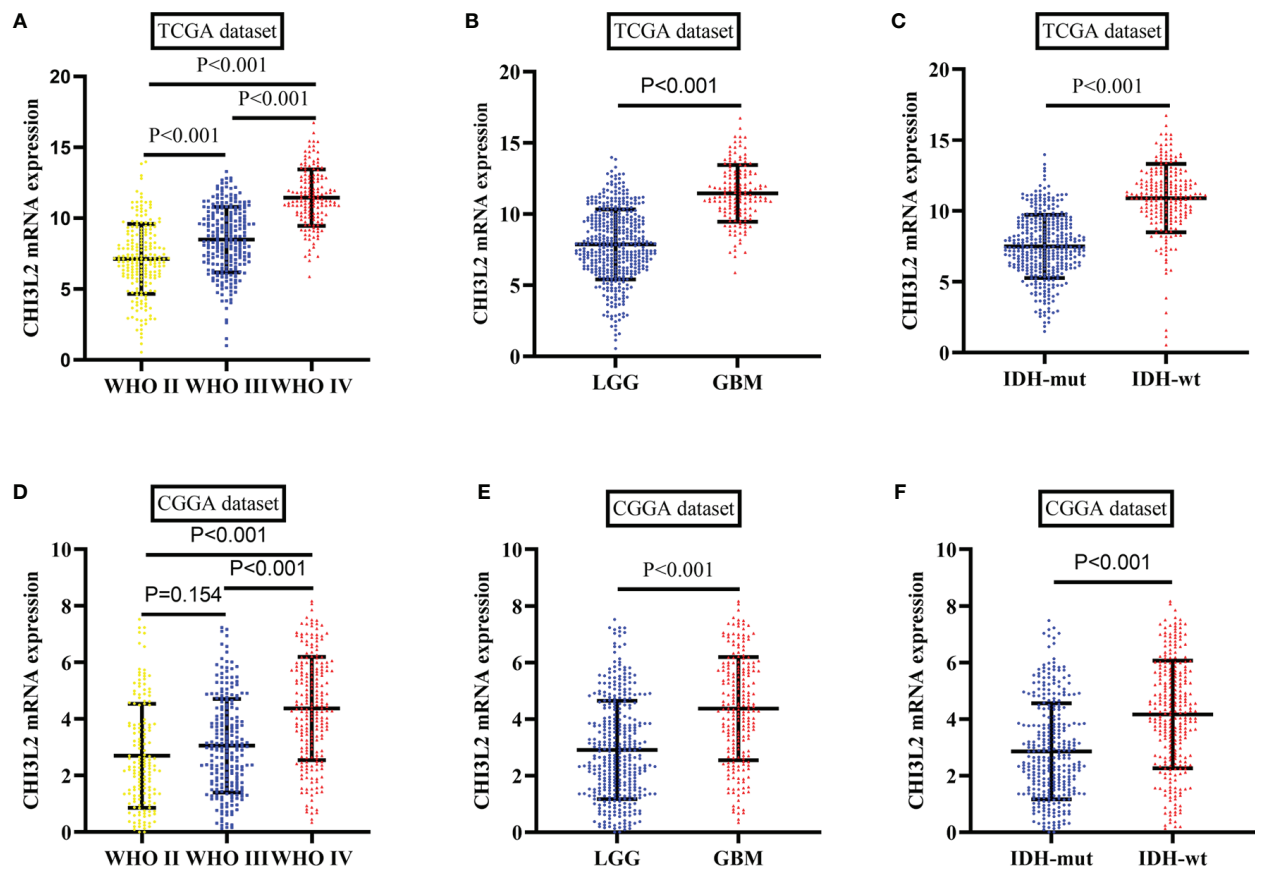

FIGURE 4 | The mRNA expression levels of CHI3L2 in gliomas in TCGA and CGGA datasets. **(A)** CHI3L2 mRNA levels in diffusely infiltrating glioma (WHO II-IV) in the TCGA dataset. **(B)** CHI3L2 mRNA levels in LGG and GBM in TCGA dataset. **(C)** CHI3L2 mRNA levels in diffusely infiltrating glioma with different IDH status in TCGA dataset. **(D)** CHI3L2 mRNA levels in diffusely infiltrating glioma (WHO II-IV) in the CGGA dataset. **(E)** CHI3L2 mRNA levels in LGG and GBM in CGGA dataset. **(F)** CHI3L2 mRNA levels in diffusely infiltrating glioma with different IDH status in CGGA dataset.

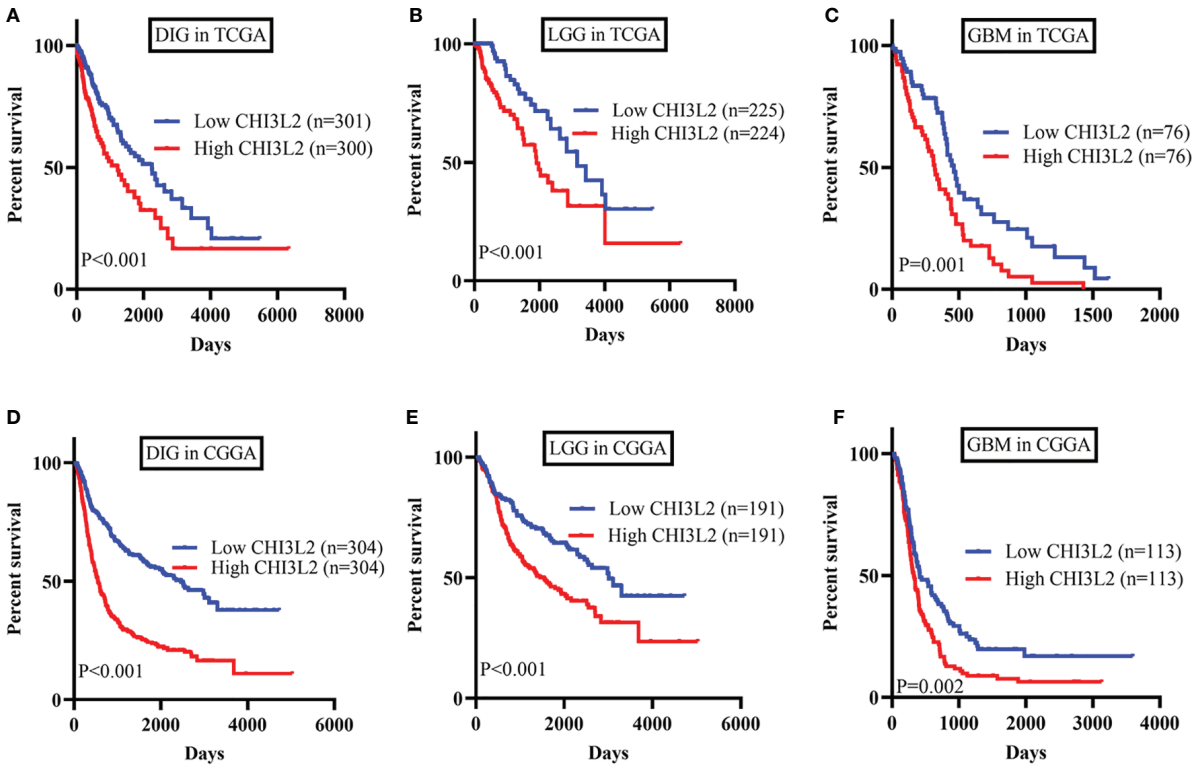

FIGURE 5 | The prognostic impact of CHI3L2 mRNA levels in gliomas in TCGA and CGGA datasets. Kaplan-Meier curves reveal high CHI3L2 mRNA levels predict short overall survival time in diffusely infiltrating glioma (DIG), LGG, and GBM in the TCGA dataset **(A–C)** and CGGA dataset **(D–F)**.

MAP kinase signaling cascade in 293 and U87 MG cells (18, 26). However, the correlations between CHI3L2 expression and clinicopathological features, the association with tumor-infiltrating immune cells, the prognostic value of CHI3L2, and its other functions in gliomas are still unknown.

Our study showed CHI3L2 expressed in tumor cells and macrophage cells in glioma tissues and particularly up-regulated in GBM and IDH wild-type gliomas. The Kaplan-Meier curves reveal higher CHI3L2 expression levels correlated with short overall survival in diffusely infiltrating glioma, lower-grade glioma, and IDH wild-type gliomas. High CHI3L2 expression indicates a poor prognosis for glioma patients, regardless of whether the MGMT promoter is methylated or has received adjuvant therapy. Cox proportional hazards regression model indicates CHI3L2 expression in tumor cells is an independent prognostic indicator of glioma. TCGA and CGGA datasets further confirm our findings. However, it should be pointed out that no significant differences between high CHI3L2 and poor prognosis in GBM were achieved in our cohort, which is different from the results (The relationship between high CHI3L2 mRNA expression and short overall survival time were statistically significant in all subgroups) in TCGA and CGGA datasets. We believe there are two reasons for the inconsistent results. One probable reason is the difference in detection levels. The relative expression levels of CHI3L2 mRNA were detected using high-throughput sequencing in TCGA and CGGA datasets, but CHI3L2 expression levels in our samples were assessed at protein levels by immunohistochemistry. Another possible reason is the difference in sample size. Accordingly, we intend to enlarge our sample size in the following study.

Based on these results, we further performed GO and KEGG pathway analyses to conclude the CHI3L2-related genes were involved in several biological processes, including angiogenesis, immune, and inflammatory response, and enriched in several classic signaling pathways, including cell adhesion molecules and PI3K-Akt signaling pathway. It has been reported that CHI3L2 acts as a powerful monocyte chemotactic factor and angiogenesis stimulating factor in breast cancer (14). A recent review also reported CHI3L2 acts as a new target for anti-angiogenic therapy in breast cancer patients (35). The angiogenesis function of CHI3L2 may be responsible for the poor prognosis of glioma, which needs further confirmation by follow-up studies. A recent review reported the role of cell adhesion molecules (CAM) in immune responses and tumor microenvironment——Cell adhesion molecules affect the antigen-presenting function, and inhibit the development of regulated cells and the leaching of regulatory cells into tumors, thus promoting tumor immune escape (36). Our study showed CHI3L2 expressed in tumor cells and macrophages in glioma tissues. A previous study suggests human glioma- infiltrating macrophages have similar functions to CAM in mediated immune responses (37). It was also

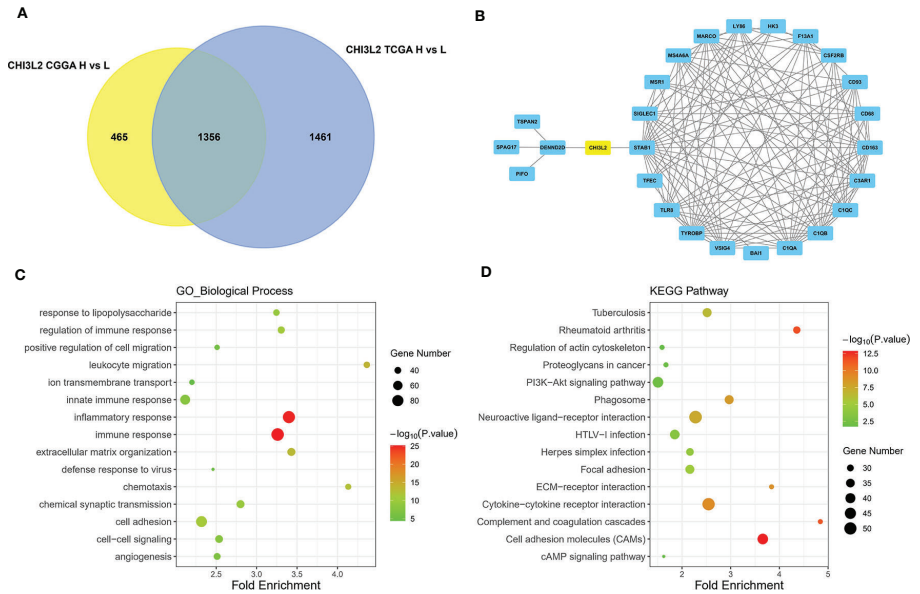

FIGURE 6 | Identification of DEGs, hub genes, functions, and pathways of CHI3L2 in gliomas. **(A)** The Venn diagrams show a total of 1356 overlapping DEGs identified from TCGA and CGGA datasets. **(B)** The 26 hub genes are screened out by the cytoHubba plugin of Cytoscape software. **(C)** GO analysis shows multiple biological processes of the overlapping DEGs. **(D)** Several pathways of the overlapping DEGs are identified by KEGG analysis.

TABLE 4 | Correlation analysis between CHI3L2 and markers of immune cells in GBM and LGG.

Description	Gene markers	GBM		LGG	
		Cor	P	Cor	P
Monocyte	CD86	0.456	***	0.601	***
	CD115 (CSF1R)	0.462	***	0.442	***
TAM	CCL2	0.669	***	0.592	***
	CD68	0.455	***	0.668	***
	IL10	0.482	***	0.538	***
M1 Macrophage	INOS (NOS2)	-0.029	0.722	-0.155	***
	IRF5	0.383	***	0.579	***
	COX2 (PTGS2)	0.467	***	0.165	***
M2 Macrophage	CD163	0.499	***	0.523	***
	VSIG4	0.466	***	0.493	***
	MS4A4A	0.473	***	0.560	***
Treg	FOXP3	0.098	0.228	-0.084	0.056
	CCR8	0.151	0.062	0.183	***
	STAT5B	-0.030	0.714	-0.110	*
	TGFβ1	0.315	***	0.526	***
T cell exhaustion	PD-1 (PDCD1)	0.039	0.629	0.539	***
	CTLA4	0.323	**	0.381	***
	LAG3	-0.144	0.076	0.201	***
	TIM-3 (HAVCR2)	0.456	***	0.630	***
	GZMB	0.318	**	0.352	***
T cell (general)	CD3D	0.303	***	0.572	***
	CD3E	0.281	***	0.615	***
	CD2	0.319	***	0.626	***
CD8+ T cell	CD8A	-0.002	0.984	0.316	***
	CD8B	0.149	0.067	0.289	***
B cell	CD19	0.174	*	0.375	***
	CD79A	0.015	0.859	0.257	***
Neutrophils	CD66b (CEACAM8)	-0.101	0.214	0.014	0.756
	CD11b (ITGAM)	0.451	***	0.514	***
	CCR7	0.203	*	0.412	***

*Cor, R-value of Spearman's correlation. (*P < 0.05; **P < 0.01; ***P < 0.001).*

reported that CAMs are potential prognostic biomarkers and attractive therapeutic targets for glioblastoma (38). A previous study suggested PI3K-Akt signaling pathway activation, to some extent, affects the activity of most immune cell types. PI3K-AKT-mTOR pathway plays a certain role in regulating immunosuppression in tumor microenvironment (39). We speculate CHI3L2 may be able to act as immunomodulation through this pathway. Additionally, we have learned in previous studies that CHI3L1 (the homologous gene of CHI3L2) may be used as an immunomodulatory factor to affect the therapeutic efficacy of PI3K/AKT-based pathway inhibitors in glioblastoma (40). CHI3L1 also plays a key role in inducing immunosuppression and metastasis in breast cancer. CHI3L1 up-regulates pro-inflammatory mediators, CCL2, CXCL2 and MMP-9, all of which contribute to tumor growth and metastasis, and treatment with chitin can significantly reduce these effects (23). These studies provide a reference for us to further explore the internal mechanism of CHI3L2 in immune infiltration.

Based on the analysis of the TIMER platform, the correlations between CHI3L2 and markers of immune cells imply CHI3L2 may play a part in immunomodulation in GBM and LGG. Our results suggest CHI3L2 expression has strong correlations with marker sets, include CD86 and CSF1R of monocytes, CCL2, CD68, and IL 10 of TAMs and CD163, VSIG4, and MS4A4A of M2 macrophages in GBM and LGG. A study has shown that purified CHI3L2 strongly induces the migration of freshly isolated human CD14+ monocytes (14). It was reported that CD163 could act as a regulator of immune response and the potential to be a target to suppress immune escape and recover the function of T-cell populations in gliomas (41). In our experiments, we also found a strong correlation between CHI3L2 and CD163 (**Figure S6**). Additionally, there was a

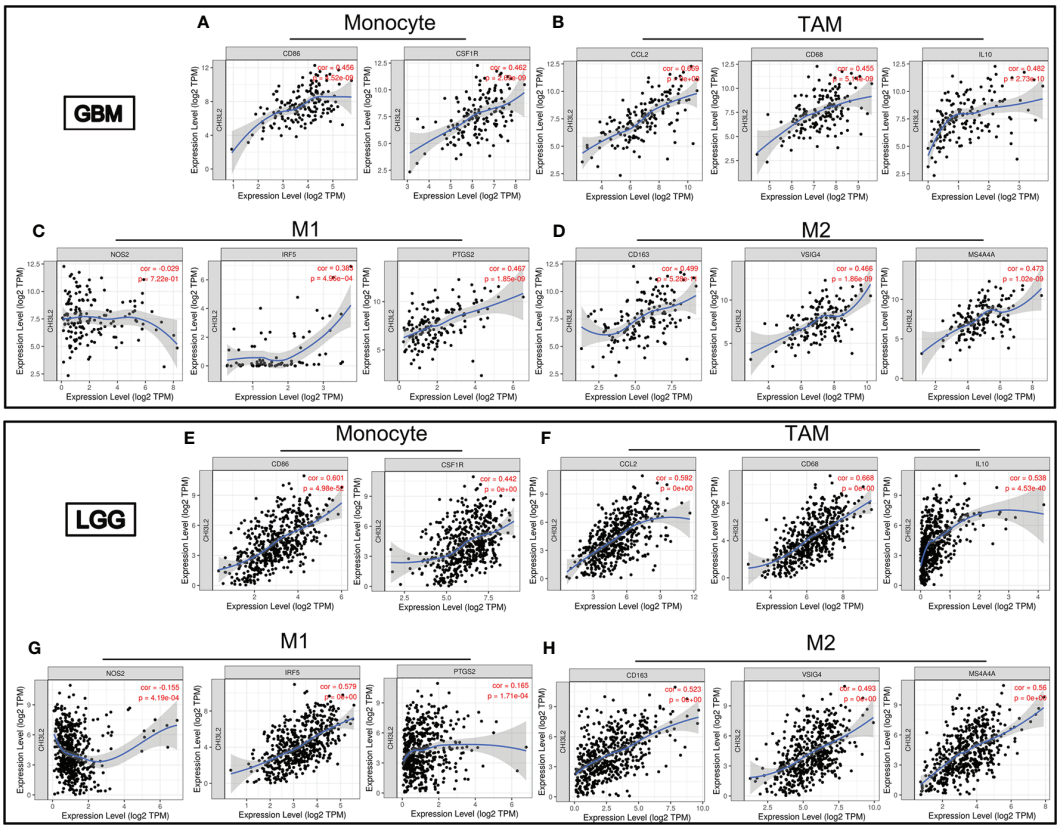

FIGURE 7 | CHI3L2 expression correlates with marker sets of immune cells in GBM and LGG. Scatter plots illustrate correlations between CHI3L2 and markers of monocytes (CD 86 and CSF1R), TAMs (CCL2, CD68 and IL10), M1 (NOS2, IRF5, and PTGS2), and M2 macrophages (CD163, VSIG4, and MS4A4A) in GBM **(A–D)** and LGG **(E–H)**.

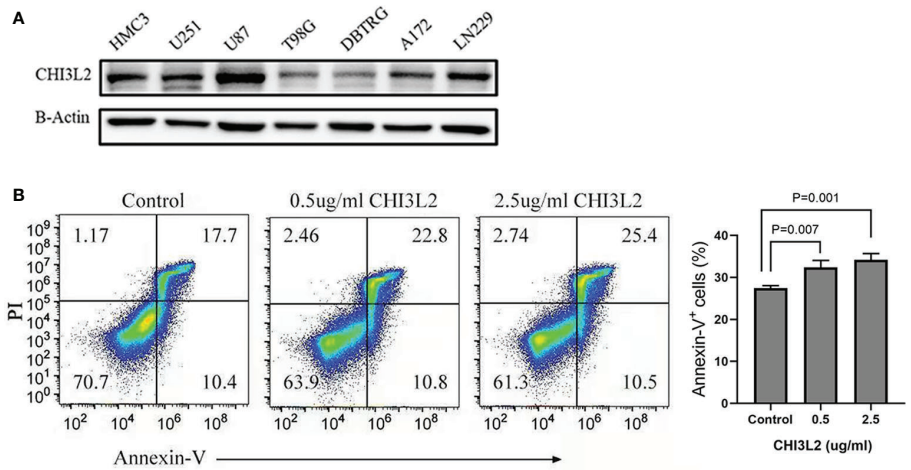

FIGURE 8 | The expression of CHI3L2 was verified by Western Blot and the proportion of CD8+ T cell apoptosis was analyzed by flow cytometry. **(A)** Western blot of seven human glioma cell lines and one human microglia cell line (HMC3) reveals robust CHI3L2 protein expression. **(B)** CD8+ T cells were cultured with 10% serum media and treated with or without CHI3L2 for 72 hours. Cell apoptosis was analyzed by using FITC-annexin V-based flow cytometry, the cellular apoptotic rate was a sum of early and late apoptotic rates. Left, the representative sorting. Right, quantified result of three independent experiments.

significant relationship between CHI3L2 and marker genes of Treg and T cell exhaustion, including TGFβ1, CTLA4, TIM-3, and GZMB. In the tumor microenvironment, TGFβ can serve as an anti-tumor immunosuppressive factor and play an essential part in Treg cells (42). It was reported that only TGFβ, the key regulatory factor of tumor progression, was able to stimulate CHI3L2 mRNA levels in human macrophages in vitro (43). TGF-β, which can be secreted by both microglial cells and glioma cells, participates in the functional transformation of macrophages into immunosuppressive and pro-invasive phenotypes, which supports tumor growth (44, 45). Macrophages are believed to be activated microglia within the central nervous system. Our data show that CHI3L2 is expressed in tumor cells and macrophages in glioma tissues, and has a certain correlation with TGF-β, further suggesting that CHI3L2 may also have the function of inhibiting tumor immune regulation and promoting tumor growth. Similarly, CTLA4 and TIM-3 can induce T cell exhaustion via direct mechanisms through the interactions with their ligands, leading to impaired T cell activation, inhibition of T cell proliferation, and impaired cytokine release (46). The correlation between CHI3L2 and T cell exhaustion markers indicates CHI3L2 may play a part in mediating T cell depletion. Our flow cytometry results further confirmed that CHI3L2 can induce CD8+ T cell apoptosis, indicating that CHI3L2 has the potential to promote tumor immune escape. However, how CHI3L2 protein promotes the apoptosis of CD8+ T cells needs to be further explored in future research.

The limitations of this study are as follows: First, the sample size of gliomas for IHC is limited. Second, we did not accurately define the type of CHI3L2 + macrophages. In addition, further experimental investigation and analysis are needed to gain insights into the underlying mechanisms.

In conclusion, our study suggests CHI3L2 may be a promising prognostic biomarker that contributes to poor prognosis for gliomas. CHI3L2 may also play an important role in immunomodulation, suggesting CHI3L2 may serve as a novel therapeutic target for glioma patients.

DATA AVAILABILITY STATEMENT

The raw data supporting the conclusions of this article will be made available by the authors, without undue reservation.

ETHICS STATEMENT

The studies involving human participants were reviewed and approved by Sun Yat-Sen University Cancer Center. Written informed consent to participate in this study was provided by the participants' legal guardian/next of kin.

AUTHOR CONTRIBUTIONS

LL and WH designed the study and wrote the manuscript. LL, WH, JH, HD, and LS acquired the data. YY and HD provided help for the IHC test and Flow cytometry analysis. LL, YY, and WH performed the data analysis. WH and JZ reviewed the manuscript. All authors contributed to the article and approved the submitted version.

SUPPLEMENTARY MATERIAL

The Supplementary Material for this article can be found online at: https://www.frontiersin.org/articles/10.3389/fonc.2021.611038/full#supplementary-material

REFERENCES

1. Ostrom QT, Gittleman H, Truitt G, Boscia A, Kruchko C, Barnholtz-Sloan JS. CBTRUS Statistical Report: Primary Brain and Other Central Nervous System Tumors Diagnosed in the United States in 2011-2015. *Neuro-Oncology* (2018) 20:1–86. doi: 10.1093/neuonc/noy131
2. Louis DN, Ohgaki H, Wiestler OD, Cavenee WK, Burger PC, Jouvet A, et al. The 2007 WHO Classification of Tumours of the Central Nervous System. *Acta Neuropathol* (2007) 114(2):97–109. doi: 10.1007/s00401-007-0243-4
3. Molinaro AM, Taylor JW, Wiencke JK, Wrensch MR. Genetic and Molecular Epidemiology of Adult Diffuse Glioma. *Nat Rev Neurol* (2019) 15(7):405–17. doi: 10.1038/s41582-019-0220-2
4. Louis DN, Perry A, Reifenberger G, von Deimling A, Figarella-Branger D, Cavenee WK, et al. The 2016 World Health Organization Classification of Tumors of the Central Nervous System: A Summary. *Acta Neuropathol* (2016) 131(6):803–20. doi: 10.1007/s00401-016-1545-1
5. Van Meir EG, Hadjipanayis CG, Norden AD, Shu HK, Wen PY, Olson JJ. Exciting New Advances in Neuro-Oncology The Avenue to a Cure for Malignant Glioma. *Ca-Cancer J Clin* (2010) 60(3):166–93. doi: 10.3322/caac.20069
6. Steck E, Breit S, Breusch SJ, Axt M, Richter W. Enhanced Expression of the Human Chitinase 3-like 2 Gene (YKL-39) but not Chitinase 3-like 1 Gene (YKL-40) in Osteoarthritic Cartilage. *Biochem Biophys Res Commun* (2002) 299(1):109–15. doi: 10.1016/s0006-291x(02)02585-8
7. Du H, Masuko-Hongo K, Nakamura H, Xiang Y, Bao CD, Wang XD, et al. The Prevalence of Autoantibodies Against Cartilage Intermediate Layer Protein, YKL-39, Osteopontin, and Cyclic Citrullinated Peptide in Patients with Early-Stage Knee Osteoarthritis: Evidence of a Variety of Autoimmune Processes. *Rheumatol Int* (2005) 26(1):35–41. doi: 10.1007/s00296-004-0497-2
8. Miyatake K, Tsuji K, Yamaga M, Yamada J, Matsukura Y, Abula K, et al. Human YKL39 (Chitinase 3-like Protein 2), an Osteoarthritis-Associated Gene, Enhances Proliferation and Type II Collagen Expression in ATDC5 Cells. *Biochem Biophys Res Commun* (2013) 431(1):52–7. doi: 10.1016/j.bbrc.2012.12.094
9. Sanfilippo C, Malaguarnera L, Di Rosa M. Chitinase Expression in Alzheimer's Disease and Non-Demented Brains Regions. *J Neurol Sci* (2016) 369:242–9. doi: 10.1016/j.jns.2016.08.029
10. Hinsinger G, Galeotti N, Nabholz N, Urbach S, Rigau V, Demattei C, et al. Chitinase 3-like Proteins as Diagnostic and Prognostic Biomarkers of Multiple Sclerosis. *Mult Scler J* (2015) 21(10):1251–61. doi: 10.1177/1352458514561906
11. Sanfilippo C, Longo A, Lazzara F, Cambria D, Distefano G, Palumbo M, et al. CHI3L1 and CHI3L2 Overexpression in Motor Cortex and Spinal Cord of sALS Patients. *Mol Cell Neurosci* (2017) 85:162–9. doi: 10.1016/j.mcn.2017.10.001
12. Colton CA, Mott RT, Sharpe H, Xu Q, Van Nostrand WE, Vitek MP. Expression Profiles for Macrophage Alternative Activation Genes in AD and in Mouse Models of AD. *J Neuroinflamm* (2006) 3:27. doi: 10.1186/1742-2094-3-27
13. Litviakov N, Tsyganov M, Larionova I, Ibragimova M, Deryusheva I, Kazantseva P, et al. Expression of M2 Macrophage Markers YKL-39 and

CCL18 in Breast Cancer is Associated With the Effect of Neoadjuvant Chemotherapy. *Cancer Chemother Pharmacol* (2018) 82(1):99–109. doi: 10.1007/s00280-018-3594-8
14. Liu T, Larionova I, Litviakov N, Riabov V, Zavyalova M, Tsyganov M, et al. Tumor-Associated Macrophages in Human Breast Cancer Produce New Monocyte Attracting and Pro-Angiogenic Factor YKL-39 Indicative for Increased Metastasis After Neoadjuvant Chemotherapy. *Oncoimmunology* (2018) 7(6):e1436922. doi: 10.1080/2162402x.2018.1436922
15. Pusztai C, Yusenko MV, Banyai D, Szanto A, Kovacs G. M2 Macrophage Marker Chitinase 3-Like 2 (CHI3L2) Associates With Progression of Conventional Renal Cell Carcinoma. *Anticancer Res* (2019) 39(12):6939–43. doi: 10.21873/anticanres.13915
16. Hu B, Trinh K, Figueira WF, Price PA. Isolation and Sequence of a Novel Human Chondrocyte Protein Related to Mammalian Members of the Chitinase Protein Family. *J Biol Chem* (1996) 271(32):19415–20. doi: 10.1074/jbc.271.32.19415
17. Kzhyshkowska J, Yin S, Liu T, Riabov V, Mitrofanova I. Role of Chitinase-Like Proteins in Cancer. *Biol Chem* (2016) 397(3):231–47. doi: 10.1515/hsz-2015-0269
18. Kavsan V, Dmitrenko V, Boyko O, Filonenko V, Avdeev S, Areshkov P, et al. Overexpression of YKL-39 Gene in Glial Brain Tumors. *Scholarly Res Exchange* (2008) 2008:1–8. doi: 10.3814/2008/814849
19. Johansen JS, Drivsholm L, Price PA, Christensen IJ. High Serum YKL-40 Level in Patients With Small Cell Lung Cancer is Related to Early Death. *Lung Cancer (Amsterdam Netherlands)* (2004) 46(3):333–40. doi: 10.1016/j.lungcan.2004.05.010
20. Hormigo A, Gu B, Karimi S, Riedel E, Panageas KS, Edgar MA, et al. YKL-40 and Matrix Metalloproteinase-9 as Potential Serum Biomarkers for Patients with High-Grade Gliomas. *Clin Cancer Res* (2006) 12(19):5698–704. doi: 10.1158/1078-0432.Ccr-06-0181
21. Johansen JS. Serum YKL-40, A New Prognostic Biomarker in Cancer Patients? *Cancer Epidemiol Biomarkers Prev* (2006) 15(2):194–202. doi: 10.1158/1055-9965.Epi-05-0011
22. Bi J, Lau SH, Lv ZL, Xie D, Li W, Lai YR, et al. Overexpression of YKL-40 is an Independent Prognostic Marker in Gastric Cancer. *Hum Pathol* (2009) 40 (12):1790–7. doi: 10.1016/j.humpath.2009.07.005
23. Libreros S, Garcia-Areas R, Shibata Y, Carrio R, Torroella-Kouri M, Iragavarapu-Charyulu V. Induction of Proinflammatory Mediators by CHI3L1 is Reduced by Chitin Treatment: Decreased Tumor Metastasis in a Breast Cancer Model. *Int J Cancer* (2012) 131(2):377–86. doi: 10.1002/ijc.26379
24. Xiao K, Tan J, Yuan J, Peng G, Long W, Su J, et al. Prognostic Value and Immune Cell Infiltration of Hypoxic Phenotype-Related Gene Signatures in Glioblastoma Microenvironment. *J Cell Mol Med* (2020) 24:13235–47. doi: 10.1111/jcmm.15939
25. Saidi A, Javerzat S, Bellahcène A, De Vos J, Bello L, Castronovo V, et al. Experimental Anti-Angiogenesis Causes Upregulation of Genes Associated With Poor Survival in Glioblastoma. *Int J Cancer* (2008) 122(10):2187–98. doi: 10.1002/ijc.23313
26. Areshkov PA, Kavsan VM. Chitinase 3-like Protein 2 (CHI3L2, YKL-39) Activates Phosphorylation of Extracellular Signal-Regulated Kinases ERK1/ERK2 in Human Embryonic Kidney (HEK293) and Human Glioblastoma (U87 MG) Cells. *TSitologiia i Genetika* (2010) 44(1):3–9. doi: 10.3103/s0095452710010019
27. Hu W, Yang Y, Xi S, Sai K, Su D, Zhang X, et al. Expression of CPEB4 in Human Glioma and Its Correlations With Prognosis. *Medicine* (2015) 94(27): e979. doi: 10.1097/md.0000000000000979
28. Hu WM, Wang F, Xi SY, Zhang X, Lai JP, Wu HY, et al. Practice of the New Integrated Molecular Diagnostics in Gliomas: Experiences and New Findings in a Single Chinese Center. *J Cancer* (2020) 11(6):1371–82. doi: 10.7150/jca.38603
29. Li T, Fan J, Wang B, Traugh N, Chen Q, Liu JS, et al. TIMER: A Web Server for Comprehensive Analysis of Tumor-Infiltrating Immune Cells. *Cancer Res* (2017) 77(21):e108–e10. doi: 10.1158/0008-5472.Can-17-0307
30. Li T, Fu J, Zeng Z, Cohen D, Li J, Chen Q, et al. TIMER2.0 for Analysis of Tumor-Infiltrating Immune Cells. *Nucleic Acids Res* (2020) 48(W1):W509–w14. doi: 10.1093/nar/gkaa407
31. Pan JH, Zhou H, Cooper L, Huang JL, Zhu SB, Zhao XX, et al. LAYN Is a Prognostic Biomarker and Correlated With Immune Infiltrates in Gastric and Colon Cancers. *Front Immunol* (2019) 10:6. doi: 10.3389/fimmu.2019.00006
32. Reardon DA, Freeman G, Wu C, Chiocca EA, Wucherpfennig KW, Wen PY, et al. Immunotherapy Advances for Glioblastoma. *Neuro Oncol* (2014) 16 (11):1441–58. doi: 10.1093/neuonc/nou212
33. Yan D, Kowal J, Akkari L, Schuhmacher AJ, Huse JT, West BL, et al. Inhibition of Colony Stimulating Factor-1 Receptor Abrogates Microenvironment-Mediated Therapeutic Resistance in Gliomas. *Oncogene* (2017) 36(43):6049–58. doi: 10.1038/onc.2017.261
34. Ma Q, Long W, Xing C, Chu J, Luo M, Wang HY, et al. Cancer Stem Cells and Immunosuppressive Microenvironment in Glioma. *Front Immunol* (2018) 9:2924. doi: 10.3389/fimmu.2018.02924
35. Kzhyshkowska J, Larionova I, Liu T. YKL-39 as a Potential New Target for Anti-Angiogenic Therapy in Cancer. *Front Immunol* (2019) 10:2930. doi: 10.3389/fimmu.2019.02930
36. Harjunpää H, Llort Asens M, Guenther C, Fagerholm SC. Cell Adhesion Molecules and Their Roles and Regulation in the Immune and Tumor Microenvironment. *Front Immunol* (2019) 10:1078. doi: 10.3389/fimmu.2019.01078
37. Hussain SF, Yang D, Suki D, Aldape K, Grimm E, Heimberger AB. The Role of Human Glioma-Infiltrating Microglia/Macrophages in Mediating Antitumor Immune Responses. *Neuro Oncol* (2006) 8(3):261–79. doi: 10.1215/15228517-2006-008
38. Turaga SM, Lathia JD. Adhering Towards Tumorigenicity: Altered Adhesion Mechanisms in Glioblastoma Cancer Stem Cells. *CNS Oncol* (2016) 5(4):251–9. doi: 10.2217/cns-2016-0015
39. O'Donnell JS, Massi D, Teng MWL, Mandala M. PI3K-AKT-mTOR Inhibition in Cancer Immunotherapy, Redux. *Semin Cancer Biol* (2018) 48:91–103. doi: 10.1016/j.semcancer.2017.04.015
40. Wang Y, Wong CW, Yan M, Li L, Liu T, Or PM, et al. Differential Regulation of the Pro-Inflammatory Biomarker, YKL-40/CHI3L1, by PTEN/Phosphoinositide 3-kinase and JAK2/STAT3 Pathways in Glioblastoma. *Cancer Lett* (2018) 429:54–65. doi: 10.1016/j.canlet.2018.04.040
41. Liu S, Zhang C, Maimela NR, Yang L, Zhang Z, Ping Y, et al. Molecular and Clinical Characterization of CD163 Expression via Large-Scale Analysis in Glioma. *Oncoimmunology* (2019) 8(7):1601478. doi: 10.1080/2162402x.2019.1601478
42. Tu E, Chia PZ, Chen W. TGFβ in T Cell Biology and Tumor Immunity: Angel or Devil? *Cytokine Growth Factor Rev* (2014) 25(4):423–35. doi: 10.1016/j.cytogfr.2014.07.014
43. Gratchev A, Schmuttermaier C, Mamidi S, Gooi L, Goerdt S, Kzhyshkowska J. Expression of Osteoarthritis Marker YKL-39 is Stimulated by Transforming Growth Factor Beta (TGF-beta) and IL-4 in Differentiating Macrophages. *Biomarker Insights* (2008) 3:39–44. doi: 10.1177/117727190800300003
44. Wesolowska A, Kwiatkowska A, Slomnicki L, Dembinski M, Master A, Sliwa M, et al. Microglia-derived TGF-beta as an Important Regulator of Glioblastoma Invasion–an Inhibition of TGF-Beta-Dependent Effects by shRNA Against Human TGF-Beta Type II Receptor. *Oncogene* (2008) 27 (7):918–30. doi: 10.1038/sj.onc.1210683
45. Gieryng A, Pszczolkowska D, Walentynowicz KA, Rajan WD, Kaminska B. Immune microenvironment of gliomas. *Lab Invest* (2017) 97(5):498–518. doi: 10.1038/labinvest.2017.19
46. Saleh R, Taha RZ, Toor SM, Sasidharan Nair V, Murshed K, Khawar M, et al. Expression of Immune Checkpoints and T Cell Exhaustion Markers in Early and Advanced Stages of Colorectal Cancer. *Cancer Immunol Immunother CII* (2020) 69(10):1989–99. doi: 10.1007/s00262-020-02593-w

Conflict of Interest: The authors declare that the research was conducted in the absence of any commercial or financial relationships that could be construed as a potential conflict of interest.

frontiers in Oncology

ORIGINAL RESEARCH
published: 16 April 2021
doi: 10.3389/fonc.2021.643159

A Novel Immune-Related Prognostic Biomarker and Target Associated With Malignant Progression of Glioma

Yu Zhang[1†], Xin Yang[1†], Xiao-Lin Zhu[1†], Zhuang-Zhuang Wang[1], Hao Bai[1], Jun-Jie Zhang[1], Chun-Yan Hao[2] and Hu-Bin Duan[1,3*]*

[1] Department of Neurosurgery, First Hospital of Shanxi Medical University, Taiyuan, China, [2] Department of Geriatrics, First Hospital of Shanxi Medical University, Taiyuan, China, [3] Department of Neurosurgery, Lvliang People's Hospital, Lvliang, China

OPEN ACCESS

Edited by:
Mahua Dey,
University of Wisconsin-Madison,
United States

Reviewed by:
Maria Caffo,
University of Messina, Italy
Shweta Tiwary,
National Institutes of Health (NIH),
United States

***Correspondence:**
Hu-Bin Duan
hubinduan68@163.com
Chun-Yan Hao
haochunyan68@126.com

[†]These authors have contributed equally to this work

Specialty section:
This article was submitted to Neuro-Oncology and Neurosurgical Oncology, a section of the journal Frontiers in Oncology

Received: 17 December 2020
Accepted: 23 March 2021
Published: 16 April 2021

Citation:
Zhang Y, Yang X, Zhu X-L, Wang Z-Z, Bai H, Zhang J-J, Hao C-Y and Duan H-B (2021) A Novel Immune-Related Prognostic Biomarker and Target Associated With Malignant Progression of Glioma. Front. Oncol. 11:643159. doi: 10.3389/fonc.2021.643159

Background: Glioma is one of the most common malignancies in the central nervous system and has limited effective therapeutic options. Therefore, we sought to identify a suitable target for immunotherapy.

Materials and Methods: We screened prognostic genes for glioma in the CGGA database and GSE43378 dataset using survival analysis, receiver operating characteristic (ROC) curves, independent prognostic analysis, and clinical correlation analysis. The results were intersected with immune genes from the ImmPort database through Venn diagrams to obtain likely target genes. The target genes were validated as prognostically relevant immune genes for glioma using survival, ROC curve, independent prognostic, and clinical correlation analyses in samples from the CGGA database and GSE43378 dataset, respectively. We also constructed a nomogram using statistically significant glioma prognostic factors in the CGGA samples and verified their sensitivity and specificity with ROC curves. The functions, pathways, and co-expression-related genes for the glioma target genes were assessed using PPI networks, enrichment analysis, and correlation analysis. The correlation between target gene expression and immune cell infiltration in glioma and the relationship with the survival of glioma patients were investigated using the TIMER database. Finally, target gene expression in normal brain, low-grade glioma, and high-grade glioma tissues was detected using immunohistochemical staining.

Results: We identified TNFRSF12A as the target gene. Satisfactory results from survival, ROC curve, independent prognosis, and clinical correlation analyses in the CGGA and GSE43378 samples verified that TNFRSF12A was significantly associated with the prognosis of glioma patients. A nomogram was constructed using glioma prognostic correlates, including TNFRSF12A expression, primary-recurrent-secondary (PRS) type, grade, age, chemotherapy, IDH mutation, and 1p19q co-deletion in CGGA samples with an AUC value of 0.860, which illustrated the accuracy of the prognosis prediction. The results of the TIMER analysis validated the significant correlation of TNFRSF12A with

immune cell infiltration and glioma survival. The immunohistochemical staining results verified the progressive up-regulation of TNFRSF12A expression in normal brain, low-grade glioma, and high-grade glioma tissues.

Conclusion: We concluded that TNFRSF12A was a viable prognostic biomarker and a potential immunotherapeutic target for glioma.

Keywords: glioma, prognosis, immune, malignant progression, TNFRSF12A

INTRODUCTION

Gliomas are the most common primary intracranial tumors, accounting for 81% of intracranial malignancies (1). In the past, the categories of astrocytoma, oligodendroglioma, oligoastrocytoma, and ependymoma, were commonly used for the pathological classification of gliomas in clinical practice (2). The World Health Organization (WHO) recently proposed a novel glioma classification method based on the presence or absence of IDH mutations and 1p/19q co-deletion (3). These new classifications have effectively promoted the progress of molecular diagnosis and treatment of glioma, resulting in molecular detection becoming an increasingly important component of glioma diagnosis and treatment. With rapid developments in biomedical research, the procedures for tumor exploration, localization, and surgical treatment of brain tumors are gradually improving. However, conventional surgical resection cannot completely remove all brain tumors, and often, residual tumor cells remain. Although postoperative chemoradiotherapy can prolong the survival of some patients, the overall prognosis is poor (1, 4–7). Suppression or eradication of glioma cells through specific immune targets is a potential therapeutic strategy to improve glioma treatment. For example, it has been reported that the accumulation of regulatory T (T reg) cells in glioblastoma (GBM) contributes to the suppression of anti-tumor immunity, and the combined blockade of IL-12 and CTLA-4 acts on CD4 (+) cells, resulting in the reduction of FoxP3 (+) T reg cells and increases in effector T cells, thereby inhibiting tumor growth (8). Also, evidence suggests that elevated expression of PD-L1 protein can suppress immune processes (9). PD-L1 inhibition therapy resulted in a significant inhibitory effect on GBM (10). Thus, to identify similar novel immune-related prognostic markers and targets, we used CGGA, GEO, and ImmPort databases to screen for glioma prognostication-related immune genes. We analyzed and validated the possibility that the identified genes could serve as glioma prognostic markers and therapeutic targets using various methods.

MATERIALS AND METHODS

Data Preparation

The mRNAseq 693 and mRNAseq 325 glioma sample data were downloaded from the Chinese Cerebral Glioma Genome Atlas (CGGA) database (http://www.cgga.org.cn/download.jsp), which contains mRNA expression and clinical profiles, for which samples with incomplete information had been previously identified and separated out. The GSE43378 chip-containing gene expression profiles and clinical profiles for the glioma samples were extracted from the Gene Expression Omnibus (GEO) database (https://www.ncbi.nlm.nih.gov/geo/). The GSE43378 profile was based on the GPL570 [HG-U133 Plus2] Affymetrix Human Genome U133 Plus 2.0 Array platform. We performed gene annotation for the mRNA expression data from the glioma samples in the CGGA database and GSE43378 data set, respectively. The expression was processed by taking log2 [data = log2(data+1)] and correcting for the batch effect, then combined with the clinical data.

Target Gene Screening

We obtained a list of immune-related genes from the ImmPort database (https://www.immport.org/shared/home). The ImmPort project is a platform for collecting, organizing, and sharing immunology-related research. The platform contained experimental data and metadata that described the study objectives and data generation methods. We conducted survival, ROC curve, independent prognostic, and clinical correlation analyses to batch screen the genes from the CGGA and GSE43378 glioma samples. We selected the gene clusters that were significantly associated with the survival, prognosis, and clinical features of glioma patients. The filtration criteria are shown in **Figure 1**. A p-value <0.05 was set as the threshold for statistically significant differences. The intersection was determined between glioma-related genes and ImmPort immune-related genes using the Venn online web program (http://bioinformatics.psb.ugent.be/webtools/Venn/). The less studied single genes that were identified were selected for additional analysis. Single gene expression data were extracted and combined with clinical data. The differential expression of target genes in low-grade glioma (LGG), GBM, and normal samples was verified using the GEPIA database (http://gepia.cancer-pku.cn/), which integrated gene expression profiles from the TCGA and GTEx projects and contained RNA sequencing expression profiles from 9,736 tumors and 8,587 normal samples.

Survival Analysis

We used R statistical software (Version 4.0.2) to conduct all survival analyses. The samples from the CGGA and GSE43378 data were initially grouped based on median single gene

Abbreviations: LGG, low-grade glioma; GO, Gene Ontology; KEGG, Kyoto Encyclopedia of Genes and Genomes; PPI, Protein-Protein Interaction; IHC, immunohistochemistry.

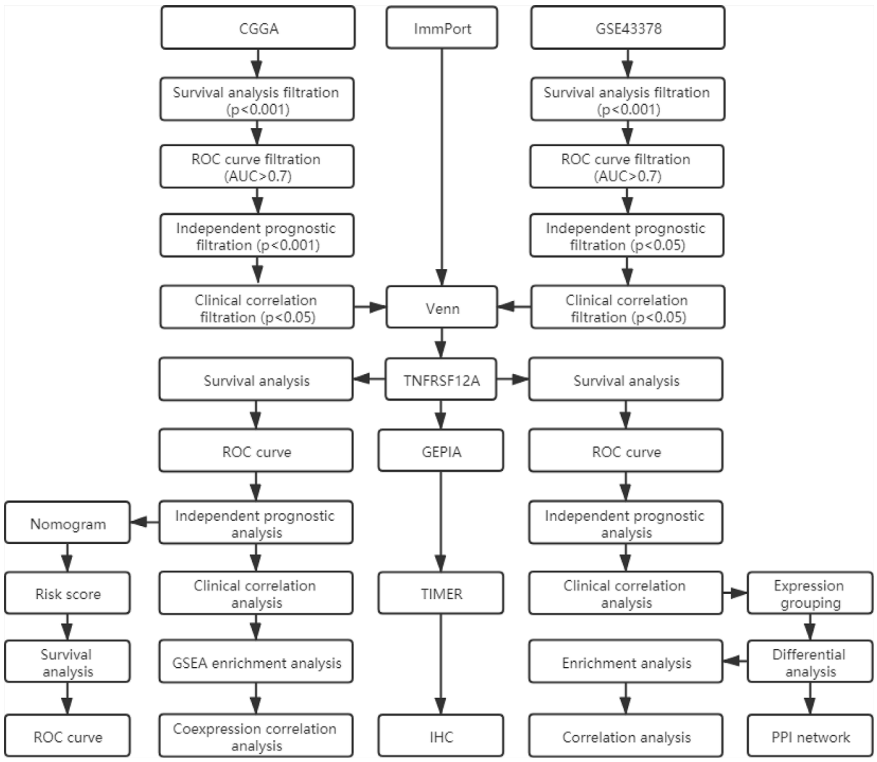

FIGURE 1 | The work flow diagram of this study.

expression. Survival analysis was conducted in the different groups to detect the correlation between gene expression levels and glioma prognosis in the patients. Differences of $p < 0.05$ were considered to be statistically significant.

Receiver Operating Characteristic (ROC) Curves

To validate the accuracy of single genes for predicting survival in patients with glioma, 1-year, 3-year, and 5-year survival ROC curves were plotted using R statistical software (Version 4.0.2). Area under curve (AUC) values were calculated to assess the validity of the model. AUC values of 0.5–0.7 were considered moderate, 0.7–0.9 were considered better, and >0.9 was superior.

Independent Prognostic Analysis

To determine the prognostic factors associated with glioma patients, we performed univariate and multivariate independent prognostic analyses on the samples from the CGGA and GSE43378 data using R statistical software (Version 4.0.2). The variables used for screening the CGGA data included single gene expression, primary-recurrent-secondary (PRS) type, histology, grade, gender, age, radiation therapy, chemotherapy, IDH mutations, and 1p19q co-deletion. The variables used to screen the GSE43378 data included single gene expression, histology, grade, gender, and age. Age was stratified at 41 years. Differences of $p < 0.05$ were considered statistically significant. Non-statistically significant variables were excluded.

Prognostic Nomogram Construction

A nomogram was constructed based on statistically significant prognostic factors collected from the CGGA data using R statistical software (Version 4.0.2), and risk scores were calculated. Based on the median risk score value, samples were classified into high- and low-risk groups. Survival analysis was performed for the different groups. A p-value <0.05 was considered to be statistically significant. We used ROC curves to assess the sensitivity and specificity of the nomogram model.

Clinical Correlation Analysis

To evaluate the correlation between single genes and clinical features of glioma patients, we performed correlation analysis for single gene expression and clinical features for the CGGA and GSE43378 data, respectively. A p-value <0.05 indicated that single genes were significantly correlated with the corresponding clinical features.

Differential Analysis, PPI Network, and Enrichment Analysis

The glioma samples from the GSE43378 dataset were grouped based on median single gene expression. Differentially expressed genes (DEGs) were obtained through analysis ($|\log FC| > 0.5$,

adjP < 0.05), and volcano plots were constructed. Twenty of the highest significantly up-regulated and 20 of the lowest significantly down-regulated DEGs were extracted to plot correlation heat maps. Potential protein interactions between the DEGs were assessed using the STRING database (https://string-db.org/). Based on a score of >0.4 as the PPI extraction criterion, a PPI network was visualized using Cytoscape software (www.cytoscape.org/). Gene Ontology (GO) function annotation and KEGG pathway enrichment analysis were conducted to explore the functions and pathways enriched with the DEGs (Count ≥ 10, adjP < 0.05). We also grouped the samples in the CGGA database using median single gene expression values. GSEA enrichment analysis was performed for the different groups. Finally, we obtained the top five GO function and KEGG pathway enriched by sample genes in high-expression group and low-expression group ($p < 0.05$).

Correlation Analysis

We analyzed the correlation between the target genes and the sample genes from the CGGA and GSE43378 data and selected the genes that were significantly correlated with the target (cor > 0.5, $p < 0.001$). The correlation analysis was conducted using the limma package from R statistical software (Version 4.0.2). The top 20 genes in the CGGA and GSE43378 data that were positively correlated or negatively correlated with the target gene were selected and used to construct a correlation heat map. Finally, the top five genes in the CGGA and GSE43378 data that were positively and negatively correlated with the target genes were selected and plotted as correlation circles.

Immune Cell Infiltration

The TIMER database (https://cistrome.shinyapps.io/timer/) was used to detect the infiltration of immune cells in tumor tissues based on RNA-Seq expression. Six types of immune cells were assessed, including B cells, CD4+ T cells, CD8+ T cells, neutrophils, macrophages, and dendritic cells. The gene module for TIMER was used to assess the correlation between single gene expression levels and infiltration of the six immune cell types in LGG and GBM patients. The survival module was used to assess the correlation between single genes, the six types of immune cell infiltration, and survival of LGG and GBM patients using the Cox proportional risk model. TIMER also was used to draw Kaplan-Meier plots for immune infiltration and genes to visualize differences in survival. The split percentage of patients (% = 50%) with a p-value <0.05 was considered to be statistically significant.

Immunohistochemistry

Immunohistochemical staining was used to detect the expression of target immune-related genes in normal brain, low-grade glioma, and high-grade glioma tissues. The experiments that utilized human tissue were approved by the ethics committee of the First Hospital of Shanxi Medical University. Two samples of normal brain tissue in patients with epilepsy, two samples of low-grade glioma, and four high-grade glioma samples were collected from the First Hospital of Shanxi Medical University. All postoperative tissues were examined pathologically in the Department of Pathology, First Hospital of Shanxi Medical University. After routine paraffin-embedding, tissue sections were obtained, placed on glass microscope slides, de-paraffinized, and rehydrated. Antigen retrieval and blocking of endogenous peroxidases were performed, followed by exposure to monogenic polyclonal antibodies (Sangon, Shanghai, China) and enzyme-labeled IgG polymers. Antibody presence was visualized using a diaminobenzidine (DAB) chromogenic solution and hematoxylin as a counterstain.

RESULTS

Target Gene Identification

In this study, 131 glioma prognosis-associated genes were collected from CGGA samples through survival, ROC curve, independent prognostic, and clinical correlation analyses. In addition, 162 glioma prognosis-associated genes were collected from GSE43378 samples, and 1,793 immune-related genes were identified in the ImmPort immune gene list (**Table 1**). The intersection of the glioma prognosis-related genes from the CGGA, GES43378, and immune-related genes from the ImmPort platform was identified using the Venn online web program (**Figure 1**). Three immune genes related to glioma prognosis were identified as TGFB2, VIM, and TNFRSF12A (**Figure 2A**). We chose TNFRSF12A as the target of our study. The results of the GEPIA analysis revealed that the expression of TNFRSF12A was significantly up-regulated in LGG and GBM patient tissues compared to normal tissues (**Figures 2B, C**).

Survival Analysis and ROC Curves

The survival data from glioma patients in the CGGA and GSE43378 datasets were significantly different between the high and low TNFRSF12A expression groups ($p < 0.001$). The survival time for the glioma patients in the high expression group was significantly shorter, suggesting that TNFRSF12A hyperexpression might be a risk factor for a poor prognosis of glioma patients (**Figures 2D, E**). The AUC values for the 1-year, 3-year, and 5-year survival ROC curves for the CGGA samples were 0.813, 0.798, and 0.750, respectively (**Figure 3A**), and for the GSE43378 samples were 0.847, 0.863, and 0.750, respectively (**Figure 3B**). The AUC values for both groups were high, which validated the accuracy of TNFRSF12A as a prognostic gene in predicting survival time in glioma patients.

Univariate and Multivariate Independent Prognostic Analyses

Three variables unrelated to glioma prognosis were excluded by univariate and multivariate independent prognostic analysis in

TABLE 1 | The number of samples and genes screened in CGGA and GSE43378.

Database ID	Sample	Gene
CGGA	749	131
GSE43378	50	162
ImmPort	–	1,793
Total number	799	2,086

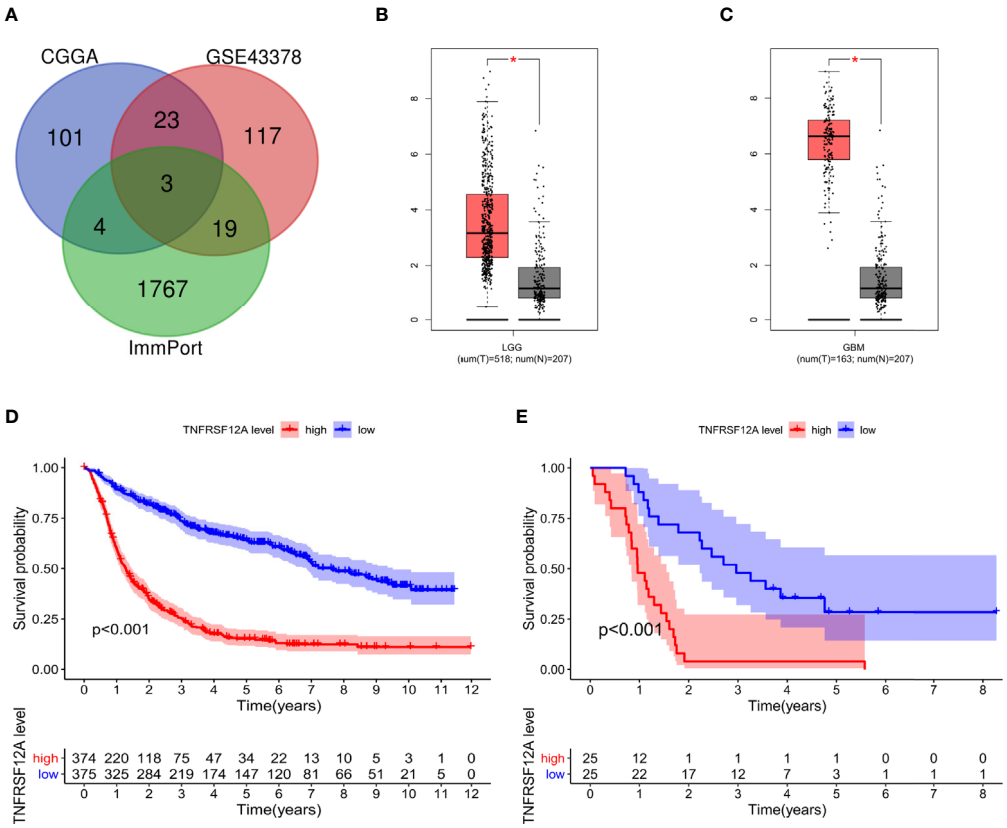

FIGURE 2 | **(A)** Venn diagram identifying the intersection of glioma prognostic genes from CGGA and GSE43378 data and immune genes from ImmPort. **(B)** Expression of TNFRSF12A in LGG and normal samples. **(C)** Expression of TNFRSF12A in GBM and normal samples. **(D)** Survival analysis of glioma patients in the high and low expression groups of TNFRSF12A in CGGA. **(E)** Survival analysis of glioma patients in the high and low expression groups of TNFRSF12A in GSE43378. *$p < 0.05$

the CGGA data, which were histology, gender, and radiation therapy ($p > 0.05$, **Figures 4A, B**). Three variables were excluded in the GSE43378 data, which were histology, grade, and gender ($p > 0.05$, **Figures 4C, D**). Independent prognostic analysis of both groups illustrated that the expression level of TNFRSF12A was an independent prognostic factor for glioma (**Table 2**).

Prognostic Nomogram Construction

We constructed a nomogram based on seven meaningful prognosis-related variables in the CGGA data, including TNFRSF12A expression, PRS type, grade, age, chemotherapy, IDH mutations, and 1p19q co-deletion. One-year, 3-year, and 5-year survival rates for glioma patients were predicted based on the nomogram score (**Figure 5**). The results of the risk curve and survival analyses revealed that low-risk patients survived longer than high-risk patients (**Figures 6A–C**). The AUC value of the ROC curve was 0.860, which validated the accuracy of the nomogram (**Figure 6D**).

Clinical Correlation Verification

Clinical correlation analysis of the CGGA data demonstrated that the expression level for TNFRSF12A was significantly correlated with PRS type, histology, grade, age, chemotherapy, IDH mutations, and 1p19q co-deletion in glioma samples. TNFRSF12A expression was higher in patients >41 years of age compared to patients ≤41 years of age (**Figure 7A**) and higher in recurrent and secondary gliomas than in primary gliomas (**Figure 7B**). TNFRSF12A exhibited higher expression in wildtype and 1p19q non-coding glioma compared to IDH mutants or 1p19q co-deletions (**Figures 7C, D**). The expression of TNFRSF12A was up-regulated as the glioma grade increased (**Figure 7E**). GBM patients exhibited the highest expression levels among all subtypes (**Figure 7F**). TNFRSF12A expression decreased in patients who underwent chemotherapy (**Figure G**). Expression of TNFRSF12A was significantly correlated with histology and grade in glioma patients and independent of age and gender, as seen in the GSE43378 samples (**Figures 7H, I**). Moreover, TNFRSF12A expression was up-regulated as the glioma grade increased (**Figure 7J**). The expression of TNFRSF12A in GBM patients was highest among all glioma subtypes (**Figure 7K**).

Differential Analysis, PPI Network, and Enrichment Analysis

Glioma samples from GSE43378 samples were grouped based on the median expression level of TNFRSF12A for differential analysis,

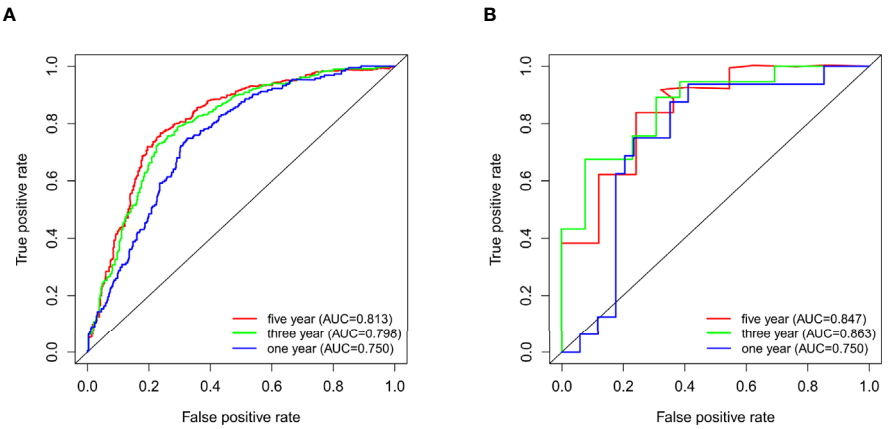

FIGURE 3 | **(A)** ROC curves for 1-, 3-, and 5-year survival of patients in CGGA. **(B)** ROC curves for 1-, 3-, and 5-year survival of patients in GSE43378.

and 645 DEGs were identified (**Figure 8A**). Twenty of the highest significantly up-regulated and 20 of the lowest significantly down-regulated DEGs were plotted using a heat map (**Figure 8B**). Potential protein interactions between the DEGs were assessed using the STRING online database. Two hundred three nodes and 642 edges of the PPI network were visualized using Cytoscape software (**Figure 8C**). The enrichment analysis for the DEGs revealed that the main enriched GO functions of the DEGs

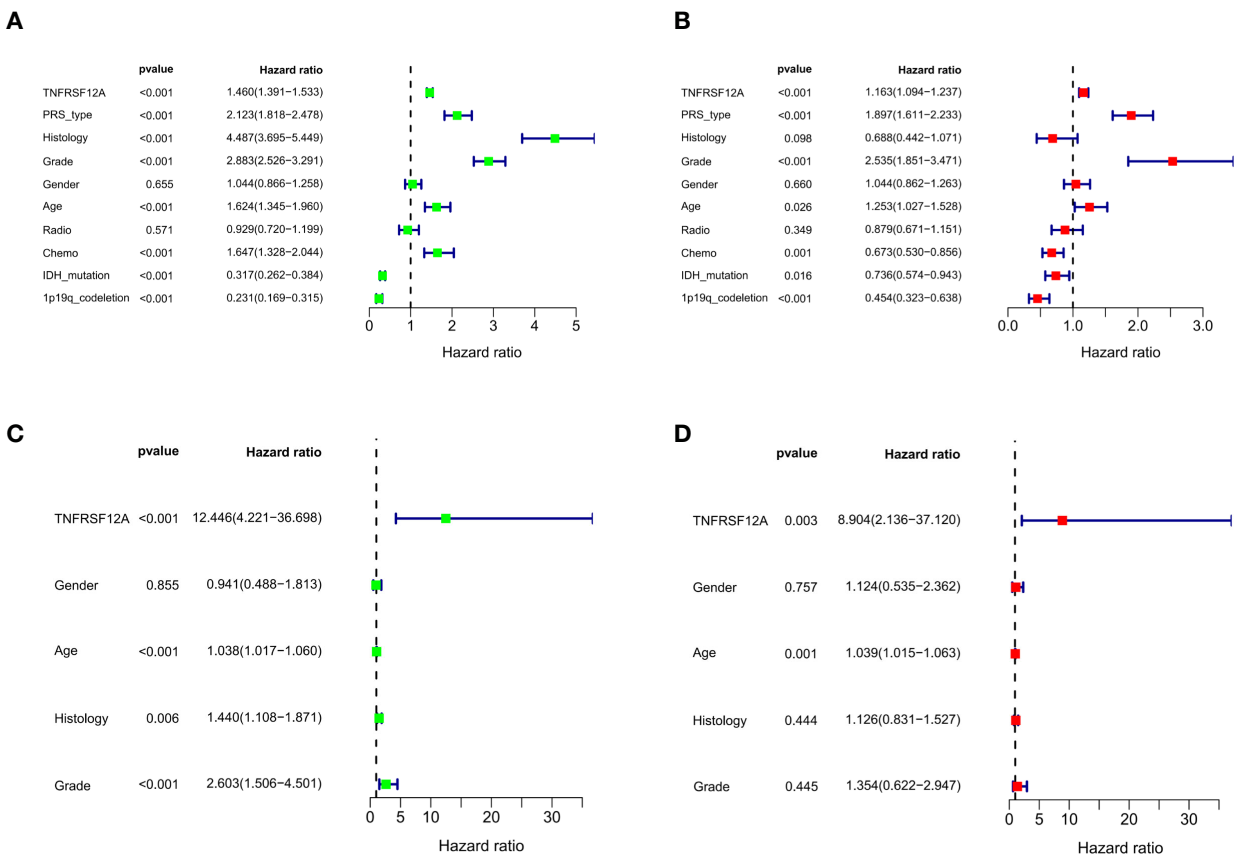

FIGURE 4 | **(A)** Univariate independent prognostic analysis of samples in CGGA. **(B)** Multivariate independent prognostic analysis of samples in CGGA. **(C)** Univariate independent prognostic analysis of samples in GSE43378. **(D)** Multivariate independent prognostic analysis of samples in GSE43378.

TABLE 2 | Univariate and multivariate independent prognostic analysis of glioma patients in CGGA and GSE43378.

	Parameters	Univariate analysis				Multivariate analysis				
		HR	HR.95L	HR.95H	p value	HR	HR.95L	HR.95H	p value	
CGGA	TNFRSF12A	1.46	1.39	1.53	5.41E-53	1.16	1.09	1.23	1.37E-06	<0.05
	PRS_type	2.12	1.81	2.47	1.79E-21	1.89	1.61	2.23	1.47E-14	<0.05
	Histology	4.48	3.69	5.44	7.38E-52	0.68	0.44	1.07	0.097813569	
	Grade	2.88	2.52	3.29	1.44E-55	2.53	1.85	3.47	6.67E-09	<0.05
	Gender	1.04	0.86	1.25	0.655307114	1.04	0.86	1.26	0.659748289	
	Age	1.62	1.34	1.96	4.49E-07	1.25	1.02	1.52	0.026094249	<0.05
	Radio	0.92	0.71	1.19	0.570623486	0.87	0.67	1.15	0.349417608	
	Chemo	1.64	1.32	2.04	5.71E-06	0.67	0.52	0.85	0.001260157	<0.05
	IDH_mutation	0.31	0.26	0.38	3.84E-32	0.73	0.57	0.94	0.015520671	<0.05
	1p19q_codeletion	0.23	0.16	0.31	2.08E-20	0.45	0.32	0.63	5.19E-06	<0.05
GSE43378	TNFRSF12A	12.44	4.22	36.69	4.87E-06	8.90	2.13	37.11	0.00268473	<0.05
	Gender	0.94	0.48	1.81	0.855389498	1.12	0.53	2.36	0.757094847	
	Age	1.03	1.01	1.06	0.000468367	1.03	1.01	1.06	0.001305705	<0.05
	Histology	1.43	1.10	1.87	0.006370135	1.12	0.83	1.52	0.44409736	
	Grade	2.60	1.50	4.50	0.000616173	1.35	0.62	2.94	0.444637821	

were extracellular matrix organization, extracellular structure organization, regulation of peptidase activity, negative regulation of hydrolase activity, regulation of endopeptidase activity, negative regulation of proteolysis, negative regulation of endopeptidase activity, and negative regulation of peptidase activity (**Figure 9A**). The DEGs were predominantly enriched for the cytokine-cytokine receptor interaction and neuroactive ligand-receptor interaction pathways (**Figure 9B**). The main enrichment GO functions for the sample genes from the TNFRSF12A high expression group in the CGGA data were actin filament-based transport, basement membrane, collagen binding, collagen-containing extracellular matrix, and negative regulation of cell cycle G1-S phase transition. The primary enriched GO functions for the low expression group were axolemma, glutamate receptor activity, inhibitory postsynaptic potential, and synaptic vesicle exocytosis regulation (**Figure 9C**). The main enrichment pathways for the sample genes from the TNFRSF12A high expression group were bladder cancer, cell adhesion molecule cams, cytokine-cytokine receptor interaction, ECM receptor interaction, focal adhesion, hematopoietic cell lineage, the JAK/STAT signaling pathway, leukocyte

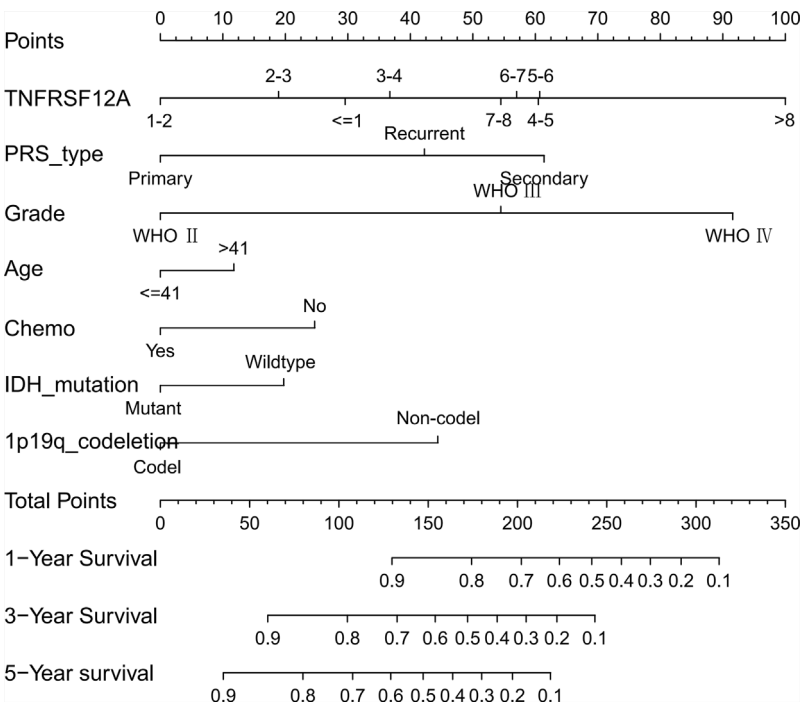

FIGURE 5 | Nomogram of 1-year, 3-year, and 5-year survival in glioma patients with CGGA.

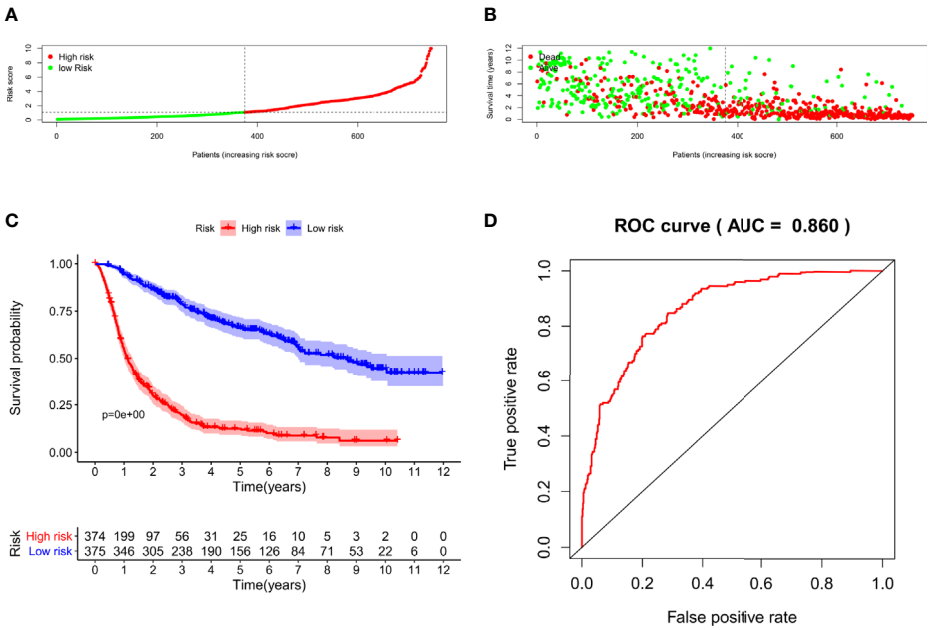

FIGURE 6 | **(A)** Risk score grouping of samples in CGGA. **(B)** Survival time corresponding to the patient risk score in CGGA. **(C)** Survival analysis of patients in high-risk and low-risk groups. **(D)** ROC curve for the nomogram.

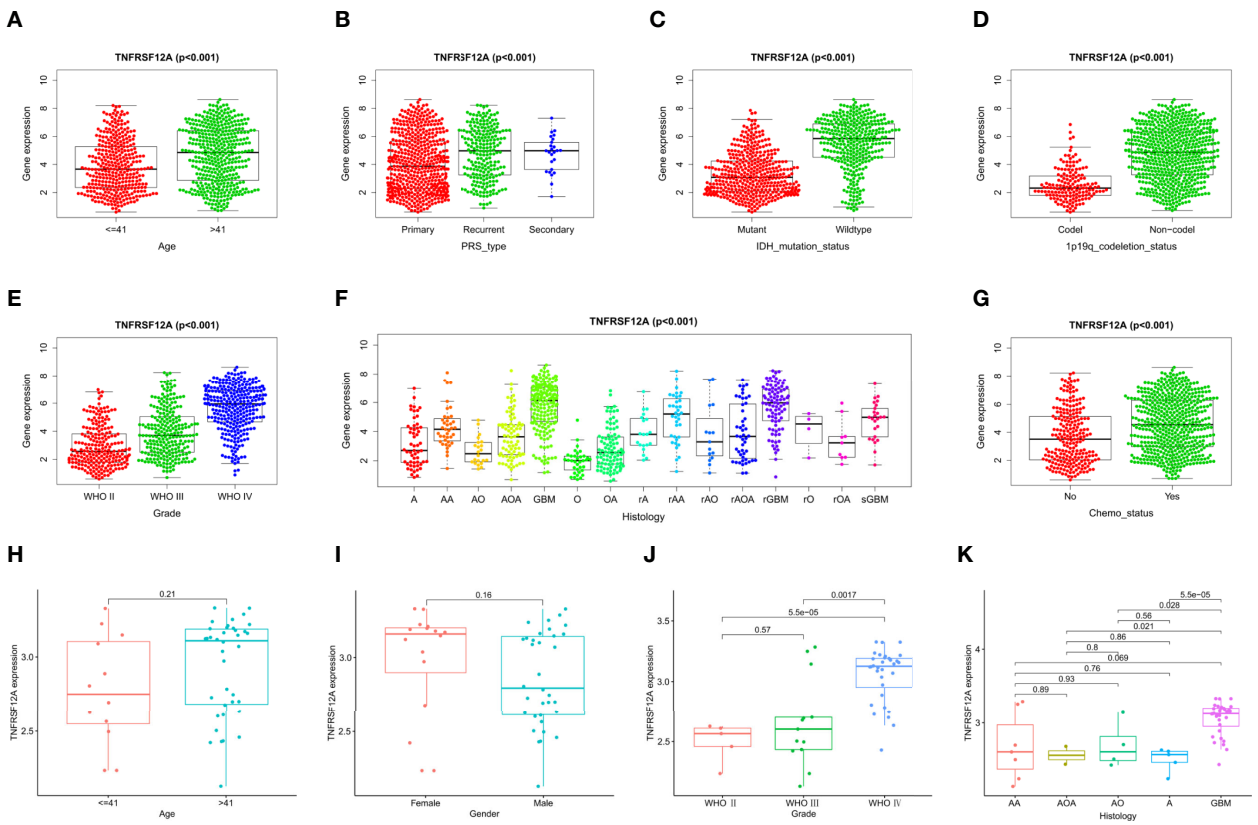

FIGURE 7 | Correlation analysis of TNFRSF12A expression levels and clinical features in glioma patients. CGGA: **(A)** Age. **(B)** PRS type. **(C)** IDH mutation. **(D)** 1p19q co-deletion. **(E)** Grade. **(F)** Histology. **(G)** Chemotherapy. GSE43378: **(H)** Age, **(I)** Gender, **(J)** Grade. **(K)** Histology.

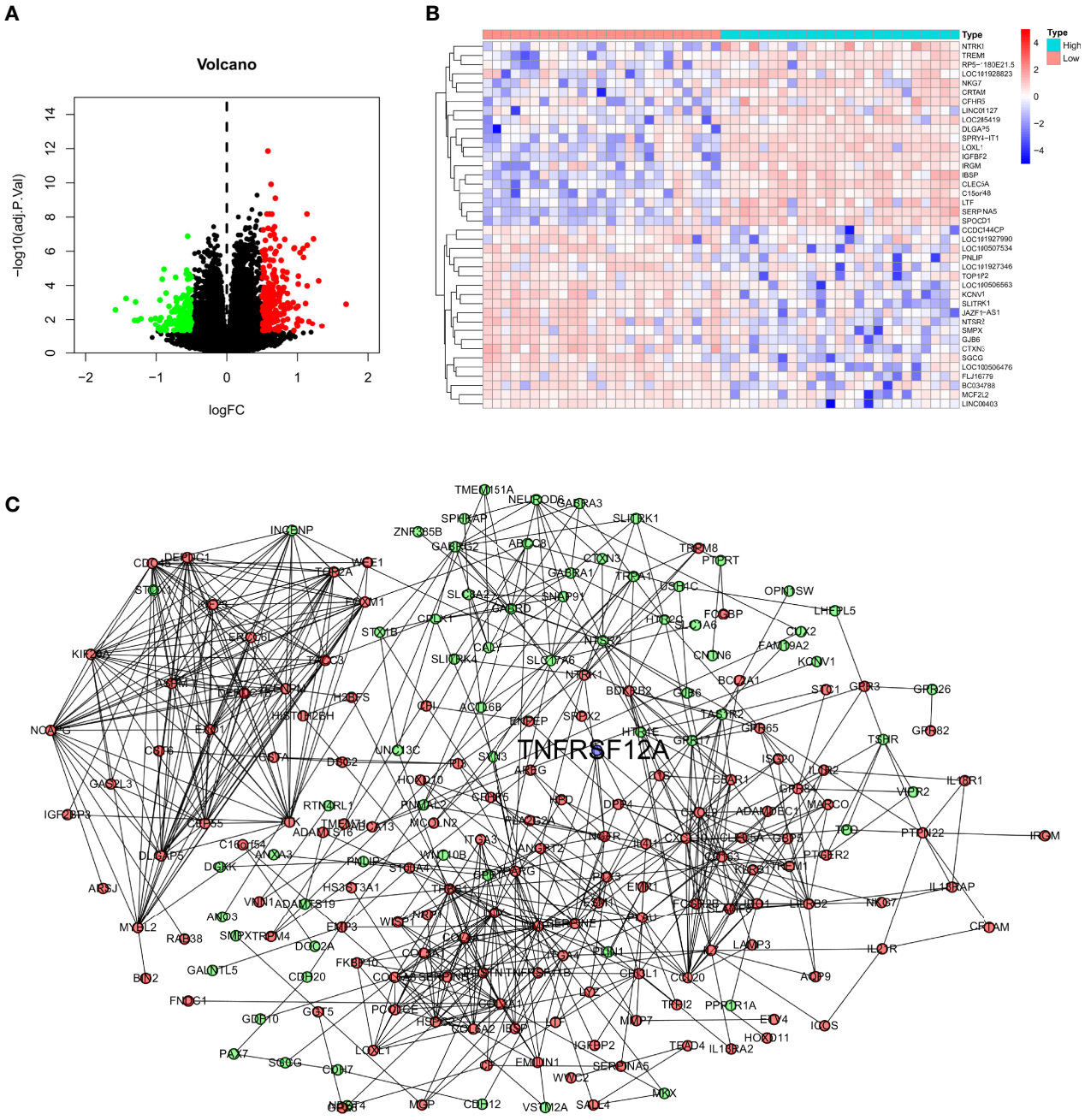

FIGURE 8 | **(A)** Volcano map of DEGs in GSE43378. **(B)** Correlation heat map of the 20 up- and down-regulated most significant DEGs in GSE43378. **(C)** PPI network for DEGs of GSE43378 in String database, red dots indicate up-regulated genes, green dots indicate down-regulated genes, and blue dots indicate target gene.

transendothelial migration, natural killer cell-mediated cytotoxicity, and the Toll-like-receptor signaling pathway. No significantly enriched pathways were found in the low-expression group (**Figure 9D**).

Correlation Analysis

The correlation heat map indicated that the 20 genes with the highest significant positive correlations with TNFRSF12A in the CGGA samples were ANXA2, VIM, SERPINH1, ANXA1, TAGLN2, PLAU, SPOCD1, PYGL, SRPX2, SERPINE1, ITGA5, CHI3L1, VASP, CCDC109B, IGFBP2, CLCF1, MMP14, SOCS3, MIR4435-1HG, and METTL7B. The 20 genes with the highest significant negative correlations were AMER3, REPS2, RP5-1119A7.17, SVOP, JPH3, ELFN2, NSG2, CPLX2, KCNIP3, SCN3B, ARPP21, PTPRT, ST6GAL2, GABRB3, CRY2, KCNJ11, TUB, TNR, DGCR5, and KCNIP2. The correlation diagram is seen

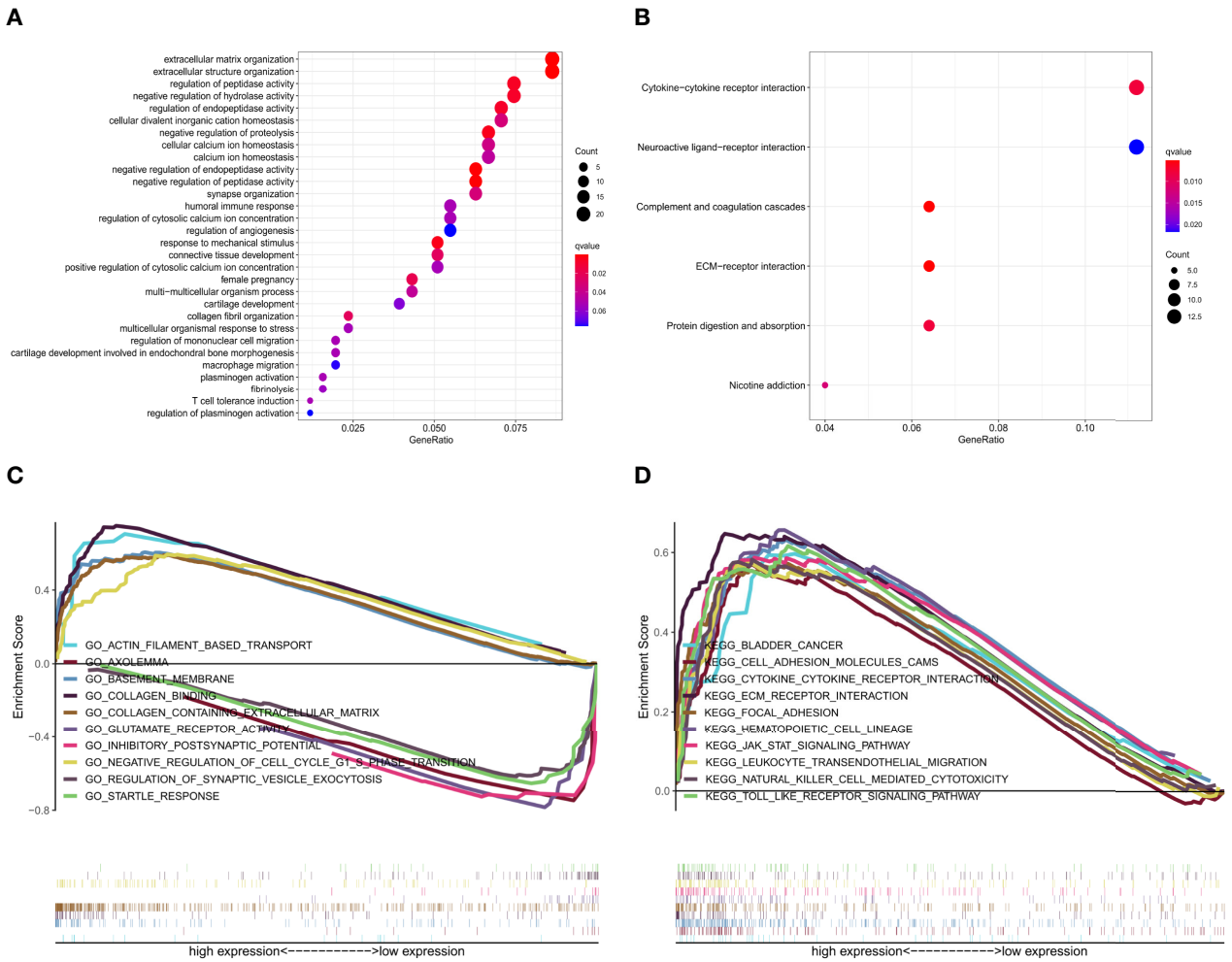

FIGURE 9 | **(A)** GO enrichment analysis of DEGs in GSE43378. **(B)** KEGG pathway enrichment analysis of DEGs in GSE43378. **(C)** GSEA GO enrichment analysis of genes in CGGA. **(D)** GSEA KEGG pathway enrichment analysis of genes in CGGA.

in **Figure 10A**. The correlation circle shows the top five genes with positive and negative correlations (**Figure 10B**). The correlation heat map showed that the 20 genes with the highest significant positive correlations with TNFRSF12A in the GSE43378 samples were CLIC1, C1R, TIMP1, VIM, SPOCD1, CASP4, FAM129A, TAGLN2, TNFRSF1A, IBSP, ISG20, BCAT1, VMP1, OST4, SERPING1, TUBB6, PRSS23, SSR3, LAMC1, and UGCG. The 20 genes with the highest significant negative correlations were SCAPER, SLC6A1, NR1D2, CRTAC1, ZRANB1, TET1, EPB41L4A-AS1, ANKRD46, LOC283588, OAT, PDZD8, C5orf30, NIFK-AS1, CNRIP1, AKT3, LOC102725017, MAPT, RP1-193H18.2, KIF3A, and BC022047 (**Figure 10C**). The correlation circle shows the top five genes with positive and negative correlations (**Figure 10D**).

Immune Cell Infiltration

Gene module analysis using TIMER demonstrated that TNFRSF12A expression in LGG patients was directly correlated with the infiltration of B cells, CD4+ T cells, CD8+ T cells, neutrophils, macrophages, and dendritic cells (all $p < 0.05$, **Figure 11A**). The expression of TNFRSF12A in GBM patients was inversely correlated with the infiltration of B cells (cor = −0.134, p = 6.01e-03), and directly correlated with the infiltration of dendritic cells (cor = 0.456, p = 7.62e-23) (**Figure 11B**). TNFRSF12A expression in LGG patients showed a significant positive correlation with several classical immune checkpoints (PDCD1, CD274, PDCD1LG2, CTLA4, LAG3, and HAVCR2) (all $p < 0.05$, **Figure 11C**). TNFRSF12A expression in GBM patients showed a positive correlation with two classical immune checkpoints CD274 (cor = 0.452, p = 6.44e-09) and PDCD1LG2 (cor = 0.234, p = 3.73e-03), while LAG3 (cor = −0.206, p = 1.07e-02) exhibited a negative correlation (**Figure 11D**). Analysis of Cox proportional risk models using the survival module showed that the infiltration of CD8+ T cells, macrophages, neutrophils, and the expression of TNFRSF12A were highly associated with the survival of LGG patients. Dendritic cell infiltration and TNFRSF12A

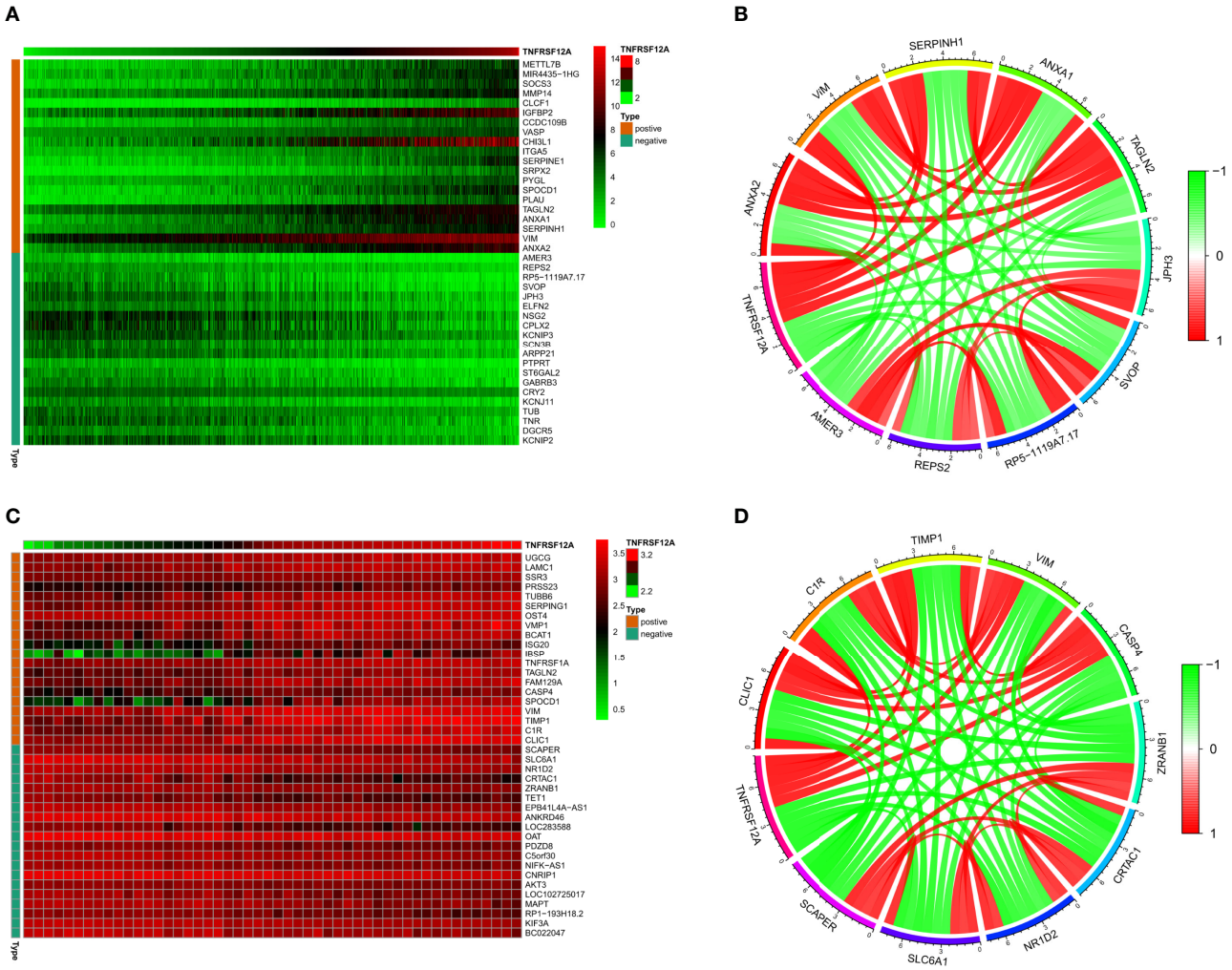

FIGURE 10 | **(A)** Correlation heat map of the top 20 positively and negatively correlated genes with TNFRSF12A in CGGA. **(B)** Correlation circles for the top 5 positively and negatively correlated genes with TNFRSF12A in CGGA. **(C)** Correlation heat map of the top 20 positively and negatively correlated genes with TNFRSF12A in GSE43378. **(D)** Correlation circles for the top 5 positively and negatively correlated genes with TNFRSF12A in GSE43378.

expression were significantly associated with the survival of GBM patients (**Table 3**). The Kaplan-Meier diagram showed that survival of LGG patients was significantly associated with the expression of TNFRSF12A and the infiltration of six types of immune cells, including B cells, CD4+ T cells, CD8+ T cells, neutrophils, macrophages, and dendritic cells (all $p < 0.05$, **Figure 11E**). The survival of GBM patients was correlated with the infiltration of dendritic cells ($p = 0.002$, **Figure 11F**).

Immunohistochemistry

The differences in TNFRSF12A expression in normal brain, low-grade glioma, and high-grade glioma tissues were detected using immunohistochemical staining. The results revealed that TNFRSF12A was primarily expressed in the cytoplasm of cells, and TNFRSF12A expression was significantly higher in gliomas compared with normal brain tissue (**Figure 12**). In addition, the expression of TNFRSF12A was significantly higher in high-grade gliomas than low-grade gliomas (**Figure 12**). The immunohistochemical staining results validated the previous dataset analyses indicating that TNFRSF12A expression was progressively up-regulated in normal tissues, low-grade gliomas, and high-grade gliomas.

DISCUSSION

Currently, 19 tumor necrosis factors (TNF) and 29 tumor necrosis factor receptors (TNFR) have been identified in humans. After binding, these receptors and ligands maintain the body's homeostasis by regulating cytokine production and controlling cell survival. Numerous studies have shown that these proteins function in human immune responses (11–13).

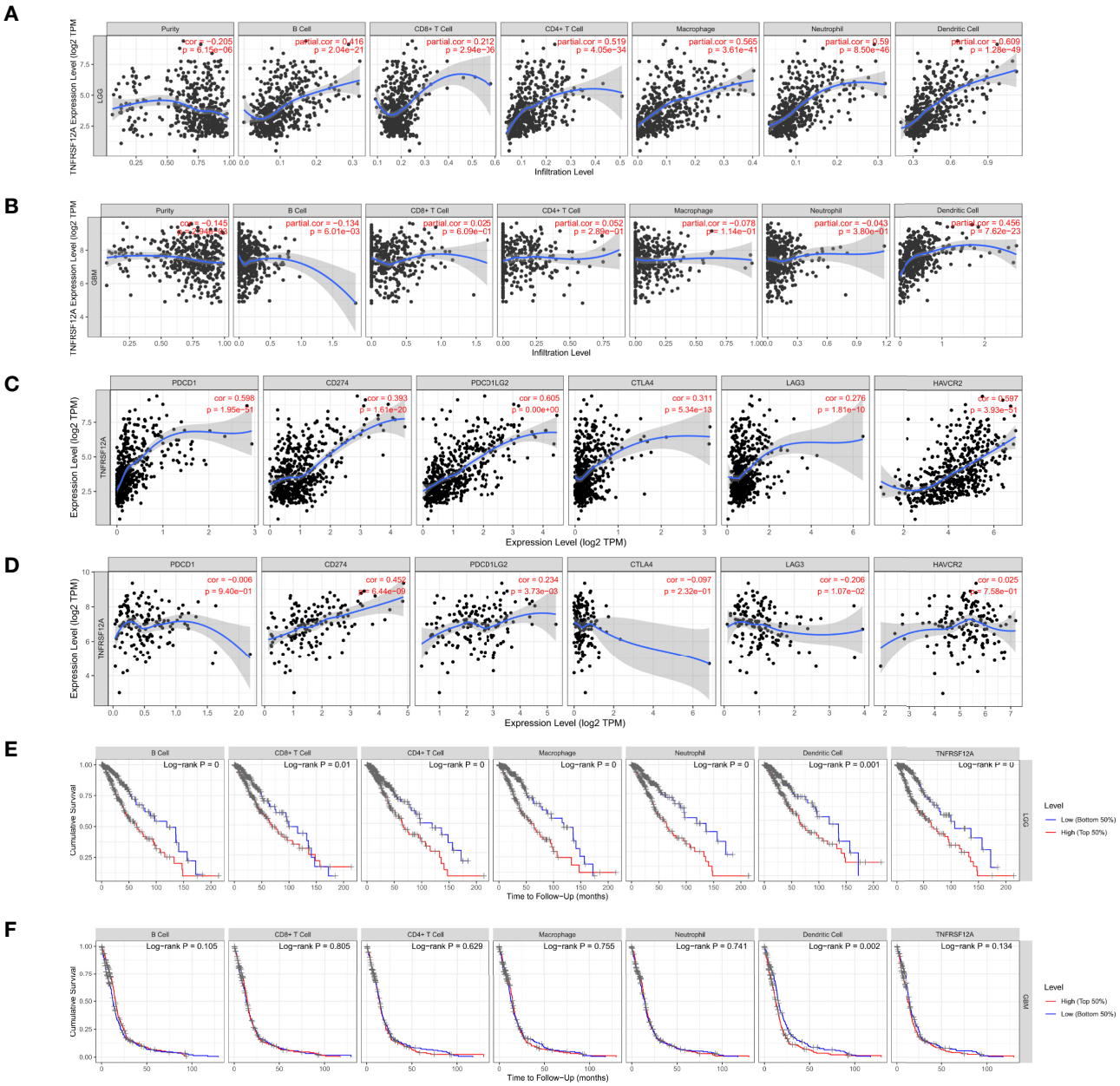

FIGURE 11 | **(A)** Correlation between TNFRSF12A expression in LGG and infiltration of six immune cells. **(B)** Correlation between TNFRSF12A expression in GBM and infiltration of six immune cells. **(C)** Correlation between TNFRSF12A and six classical immune checkpoints in LGG. **(D)** Correlation between TNFRSF12A and six classical immune checkpoints in GBM. **(E)** KM curve of LGG patient survival with TNFRSF12A expression and infiltration of six immune cells. **(F)** KM curve of GBM patient survival with TNFRSF12A expression and infiltration of six immune cells.

Numerous TNF family proteins are highly expressed in tumors and exert modulatory effects (14). For example, tumor necrosis factor receptor 12 (TNFR12) regulates the immune tolerance of B cells and myeloid-derived suppressor cells (15) while tumor necrosis factor receptor 14 (TNFR14) regulates the immune activation of T cells (16).

Using a comprehensive analysis based on multiple databases, we focused on TNFRSF12A, which is significantly overexpressed in gliomas (17). TNFRSF12A, member 12A of the tumor necrosis factor receptor superfamily, also known as fibroblast growth factor-inducible 14 (FN14), is widely expressed in most healthy tissues but exhibits low expression in the brain (18, 19). Tumor necrosis factor-like weak inducer of apoptosis (TWEAK), the ligand of TNFRSF12A, is a type II transmembrane protein (20). Together, they constitute the TWEAK/TNFRSF12A signaling pathway that is involved in multiple biological processes,

TABLE 3 | Cox proportional risk model of TNFRSF12A expression and infiltration of six immune cells in LGG and GBM.

		coef	HR	95%CI_l	95%CI_u	p.value	sig
LGG	B_cell	2.741	15.499	0.052	4580.118	0.345	
	CD8_Tcell	7.710	2231.271	2.152	2312937.870	0.030	*
	CD4_Tcell	1.471	4.354	0.001	17479.969	0.728	
	Macrophage	4.311	74.512	1.262	4398.821	0.038	*
	Neutrophil	−8.154	0.000	0.000	0.598	0.036	*
	Dendritic	−1.202	0.301	0.005	17.319	0.561	
	TNFRSF12A	0.479	1.614	1.397	1.864	0.000	***
GBM	B_cell	−0.519	0.595	0.341	1.039	0.068	·
	CD8_Tcell	0.241	1.272	0.861	1.879	0.227	
	CD4_Tcell	0.135	1.144	0.600	2.182	0.683	
	Macrophage	0.069	1.071	0.573	2.003	0.830	
	Neutrophil	0.396	1.486	0.670	3.299	0.330	
	Dendritic	0.284	1.329	1.004	1.758	0.047	*
	TNFRSF12A	0.123	1.131	1.017	1.259	0.023	*

*$P < 0.05$, ***$P < 0.001$.

including proliferation, differentiation, migration, cell death (apoptosis and necrosis), angiogenesis, and inflammation (21, 22). The expression of TNFRSF12A markedly increases in damaged tissue, autoimmune diseases, and inflammatory diseases such as SLE and autoimmune myocarditis (23, 24). Numerous studies have shown that TNFRSF12A participates in the regulation of essential signaling pathways in many tumors. In gastric cancer, TNFRSF12A is involved in the activation of the PI3K/Akt and NF-kB signaling pathways, which ultimately leads to the development of gastric cancer (25, 26). TNFRSF12A also participates in activating the JAK/STAT signaling pathway in non-small cell lung cancers (27) and the NF-kB signaling pathway in prostate cancer (28, 29). The signaling pathways activated by TNFRSF12A ultimately lead to tumor cell invasion

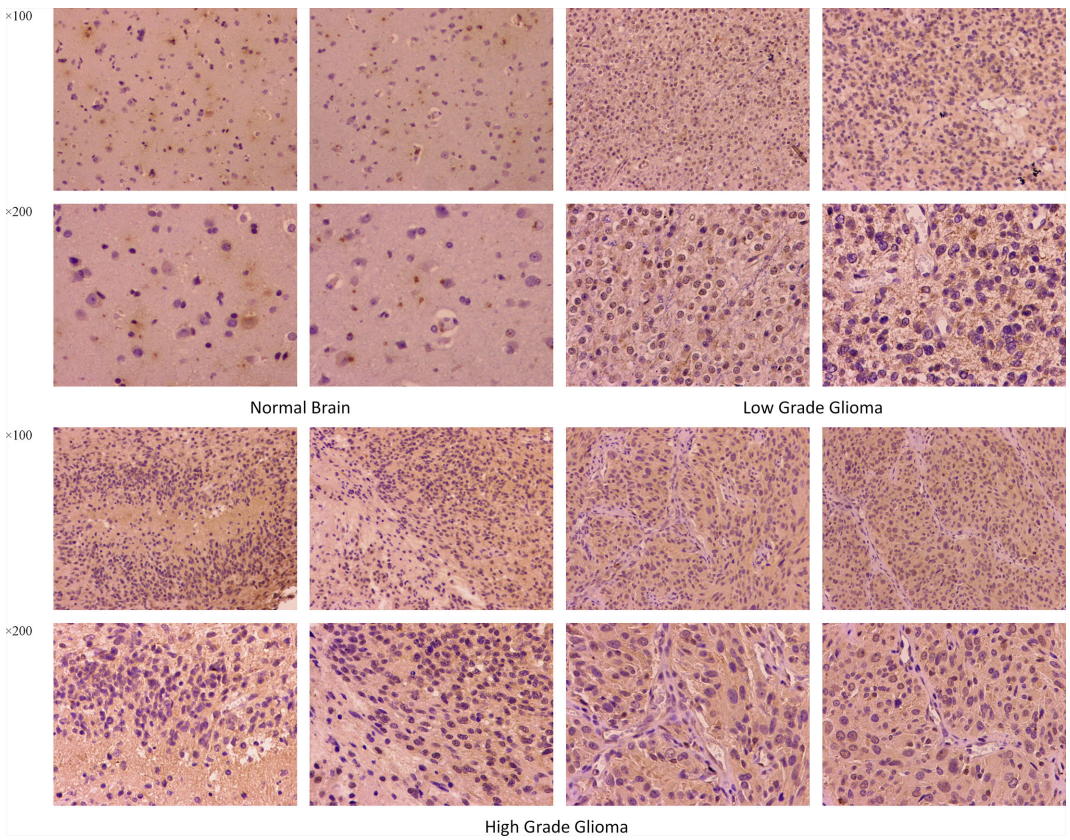

FIGURE 12 | Immumohistochemical staining for TNFRSF12A expression in normal brain, low-grade glioma and high-grade glioma tissues. Magnification, ×100, ×200.

and migration. TNFRSF12A was found to be significantly overexpressed in gliomas. The overexpression of TNFRSF12A in glioma cell lines significantly increased cell migration and invasion, which demonstrated the tumor-promoting effects of TNFRSF12A (17, 30). It has been reported that the expression of TNFRSF12A was significantly higher in recurring gliomas than in newly diagnosed primary tumors (31). In our study, we found that the TNFRSF12A expression levels increased with the grade of the glioma. This observation is supported by several previous studies (17, 32). Thus, we suggest that TNFRSF12A contributes to the progression of glioma. According to survival analysis, TNFRSF12A expression was associated with a shortened survival in glioma patients. Previous studies have demonstrated that overexpression of TNFRSF12A in tumors results in malignancy (17, 33). However, these experimental interventions might present stronger specific effects than the actual physiological processes in the tumor because the experimental process might result in TNFRSF12A expression levels that far exceed those in actual tumors (34).

Anti-TNFRSF12A antibodies can inhibit tumor growth moderately and significantly prolong life expectancy by alleviating tumor-induced weight loss (35). This suggests that anti-TNFRSF12A antibodies prevent tumors from auto-damage and deterioration, which could preserve body mass. Interestingly, TNFRSF12A presented high integrity and independence with respect to its signaling processes and regulated downstream pathways without modification (36). Therefore, our results supported the conclusion that TNFRSF12A expression could serve as an independent high-risk predictor for glioma patients.

Currently, the administration of temozolomide (TMZ) can prolong the survival of a subset of glioma patients to some extent. However, most patients develop therapeutic resistance during treatment (37). With the accumulation of oncogenetic mutations, low-grade gliomas eventually are likely to develop into high-grade gliomas (38). Specifically, TMZ treatment results in genetic alterations and biological changes in GBM cells. For example, mutations occurring at high frequencies can result in DNA mismatch repair (39). Moreover, the accumulation of mutations also causes over-activation of the PI3K/Akt/mTOR signaling pathway (40, 41). TNFRSF12A is expressed at low levels in TMZ-sensitive gliomas and highly expressed in TMZ-resistant gliomas. Moreover, in TMZ-sensitive and TMZ-resistant glioma cell lines, lower and higher TNFRSF12A levels were expressed, respectively. Cells with drug-resistant properties exhibited an enhanced migratory capacity compared to cells without drug-resistant properties. This suggests that TNFRSF12A might be responsible for the increased migration of drug-resistant tumor cells (42). Glioma cells that are less sensitive to TMZ presented higher expression of TWEAK, TNFRSF12A, and NF-kb. Thus, the TWEAK/TNFRSF12A/NF-kb axis might participate in the drug resistance exhibited by some gliomas (43).

IDH was chosen as a classification criterion by WHO in 2016. Patients with IDH mutations presented significantly longer survival periods than those without mutations (44, 45). Furthermore, IDH mutations increased sensitivity to TMZ by disrupting the repair process of parp1-mediated DNA (46). In our analysis, TNFRSF12A was more highly expressed in IDH wild-type gliomas than gliomas with IDH mutations. One study reported that TNFRSF12A promoted the invasive phenotype of IDH1 wild-type gliomas, while IDH1-mutant gliomas exhibited low TNFRSF12A mRNA and protein levels compared with IDH1 wild-type gliomas (47).

Modern oncology has begun to experiment with gene target therapy, which is characterized by the fact that target drugs can focus on individual genes or proteins and affect specific cell types of tumors without many of the side effects associated with traditional chemotherapeutic drugs (48). There are numerous potential approaches to tumor therapy using TNFRSF12A as a target. With the goal of inhibiting the TWEAK/TNFRSF12A signaling pathway, Yin et al. studied a preparation called RG7212, which inhibits TWEAK binding to TNFRSF12A. RG7212 effectively inhibited tumor growth in athymic (nude) mice tumor xenograft models of renal cell carcinoma (ACHN, Caki-1), breast cancer (MDA-MB-231), and non-small cell lung cancer (Calu-3) (49). Roos et al. identified aurintricarboxylic acid (ATA) as an inhibitor of TWEAK/TNFRSF12A/NF-κB signaling. Through inhibition of Rac1 activation, ATA inhibited the TWEAK-induced glioma cell invasion process but did not affect cell viability or TNFRSF12A expression (50). It has been well-established that excessive activation of the TWEAK/TNFRSF12A signaling pathway promotes glioma growth (17, 33). However, it has also been reported that the function of this pathway can be achieved by the expression of TNRSF12A alone (36). Therefore, it is not certain whether inhibition of this signaling pathway could provide possible clinical therapeutic effects in glioma treatment.

Preparations made by combining a targeted polypeptide with a toxin is termed a targeted toxin, which is a class of drugs that can be internalized by and kill tumor cells (51, 52). Currently, the anti-TNFRSF12A monoclonal antibody, ITEM4, has been used for this purpose (53–55). Researchers have conjugated ITEM4 with recombinant gelonin (rGel), and this preparation exhibits significant anticancer properties in bladder cancer cell xenografts (53). In another study that used TNFRSF12A as the target, researchers synthesized an immunoconjugate using recombinant gelonin toxin and ITEM4, which produced significant tumor-inhibiting results in a breast cancer xenograft model (54). Zhou et al. used ITEM4 as an antibody to study two immunotoxins. One immunotoxin was a chemical conjugate composed of the rGel toxin and the anti-TNFRSF12A antibody, ITEM-4, and the other was a humanized, dimeric single-chain antibody of ITEM-4 fused to rGel. Both immunotoxins produced significant inhibitory effects on melanoma (MDA-MB-435) in xenograft mice (55). Importantly, these studies involved *in vivo* experiments, demonstrating that TNFRSF12A is a viable potential immune target.

To achieve more effective drug delivery, researchers have developed novel nanomaterial methodologies. They have processed synthetic nanomaterials with a 100 nm carboxylate-modified polystyrene modification combined with ITEM4. This new mode of administration has many advantages. First, it selectively binds TNFRSF12A, but not the brain extracellular matrix, which reduces the non-specific binding of targeted

nanoparticles in the brain. Second, it can associate with and be internalized by TNFRSF12A-positive GBM cells. Finally, it has good tissue penetration. A previous study demonstrated that nanoparticles targeting TNFRSF12A more accurately localized to gliomas compared to untargeted TNFRSF12A nanoparticles (56). Recently, Wadajkar et al. synthesized degradable nanoparticles by processing poly(lactic-co-glycolic acid) (PLGA) and PLGA-polyethylene glycol (PLGA-PEG) polymers. Nanoparticles bound to ITEM-4 exhibited minimal binding to extracellular brain components, extremely strong binding to TNFRSF12A, and increased uptake into brain tumor cells. Compared with unbound ITEM-4 nanoparticles, ITEM-4-bound nanoparticles were retained longer in the tumor (57). In summary, multiple research results have proven that TNFRSF12A is a potential glioma therapeutic target.

CONCLUSION

Overall, TNFRSF12A is significantly overexpressed in gliomas and closely associated with inflammatory processes. Studies have revealed that specific drug modifications can improve the precision therapy of TNFRSF12A for gliomas. Our analysis provides a more comprehensive demonstration of the roles of TNFRSF12A in glioma progression. In conclusion, TNFRSF12A can serve as an independent risk factor to predict prognosis and has tremendous value in glioma immunotherapy.

DATA AVAILABILITY STATEMENT

The original contributions presented in the study are included in the article/supplementary material. Further inquiries can be directed to the corresponding authors.

ETHICS STATEMENT

The studies involving human participants were reviewed and approved by the Ethics Committee of the First Hospital of Shanxi Medical University. The patients/participants provided their written informed consent to participate in this study.

AUTHOR CONTRIBUTIONS

YZ, XY, and X-LZ contributed to the entire project, from the design proposal, to the collection and collation of data, to the writing of the paper. Z-ZW helped retrieve and organize the data, while HB and J-JZ were responsible for statistical analysis. C-YH and H-BD are responsible for supervising and providing financial support. All authors contributed to the article and approved the submitted version.

FUNDING

This work was supported by the National Natural Science Foundation of China Youth Fund (30600637); China Postdoctoral Science Foundation Special Grant (2019T120195); Key Grants for Returning Students from Shanxi Province (2016-4).

ACKNOWLEDGMENTS

Thanks to the CGGA, GEO (GSE43378), ImmPort, GEPIA, and TIMER databases for open data.

REFERENCES

1. Ostrom QT, Bauchet L, Davis FG, Deltour I, Fisher JL, Langer CE, et al. The epidemiology of glioma in adults: a "state of the science" review. *Neuro Oncol* (2014) 16:896–913. doi: 10.1093/neuonc/nou087
2. Camelo-Piragua S, Kesari S. Further understanding of the pathology of glioma: implications for the clinic. *Expert Rev Neurother* (2016) 16:1055–65. doi: 10.1080/14737175.2016.1194755
3. Wesseling P, Capper D. WHO 2016 Classification of gliomas. *Neuropathol Appl Neurobiol* (2018) 44:139–50. doi: 10.1111/nan.12432
4. Gittleman H, Sloan AE, Barnholtz-Sloan JS. An independently validated survival nomogram for lower-grade glioma. *Neuro Oncol* (2020) 22:665–74. doi: 10.1093/neuonc/noz191
5. Lan Q, Zhu Q, Xu L, Xu T. Application of 3D-Printed Craniocerebral Model in Simulated Surgery for Complex Intracranial Lesions. *World Neurosurg* (2020) 134:e761–70. doi: 10.1016/j.wneu.2019.10.191
6. Lakomkin N, Hadjipanayis CG. Fluorescence-guided surgery for high-grade gliomas. *J Surg Oncol* (2018) 118:356–61. doi: 10.1002/jso.25154
7. Ramayya AG, Chen HI, Marcotte PJ, Brem S, Zager EL, Osiemo B, et al. Assessing variability in surgical decision making among attending neurosurgeons at an academic center. *J Neurosurg* (2019) 132:1970–6. doi: 10.3171/2019.2.jns182658
8. Vom Berg J, Vrohlings M, Haller S, Haimovici A, Kulig P, Sledzinska A, et al. Intratumoral IL-12 combined with CTLA-4 blockade elicits T cell-mediated glioma rejection. *J Exp Med* (2013) 210:2803–11. doi: 10.1084/jem.20130678
9. Wang X, Guo G, Guan H, Yu Y, Lu J, Yu J. Challenges and potential of PD-1/PD-L1 checkpoint blockade immunotherapy for glioblastoma. *J Exp Clin Cancer Res* (2019) 38:87. doi: 10.1186/s13046-019-1085-3
10. Bloch O, Lim M, Sughrue ME, Komotar RJ, Abrahams JM, O'Rourke DM, et al. Autologous Heat Shock Protein Peptide Vaccination for Newly Diagnosed Glioblastoma: Impact of Peripheral PD-L1 Expression on Response to Therapy. *Clin Cancer Res* (2017) 23:3575–84. doi: 10.1158/1078-0432.ccr-16-1369
11. Dostert C, Grusdat M, Letellier E, Brenner D. The TNF Family of Ligands and Receptors: Communication Modules in the Immune System and Beyond. *Physiol Rev* (2019) 99:115–60. doi: 10.1152/physrev.00045.2017
12. Yepes M. TWEAK and Fn14 in the Neurovascular Unit. *Front Immunol* (2013) 4:367:367. doi: 10.3389/fimmu.2013.00367
13. Prinz-Hadad H, Mizrachi T, Irony-Tur-Sinai M, Prigozhina TB, Aronin A, Brenner T, et al. Amelioration of autoimmune neuroinflammation by the fusion molecule Fn14·TRAIL. *J Neuroinflamm* (2013) 10:36. doi: 10.1186/1742-2094-10-36
14. Annibaldi A, Meier P. Checkpoints in TNF-Induced Cell Death: Implications in Inflammation and Cancer. *Trends Mol Med* (2018) 24:49–65. doi: 10.1016/j.molmed.2017.11.002
15. Mancusi A, Alvarez M, Piccinelli S, Velardi A, Pierini A. TNFR2 signaling modulates immunity after allogeneic hematopoietic cell

transplantation. *Cytokine Growth Factor Rev* (2019) 47:54–61. doi: 10.1016/j.cytogfr.2019.05.001
16. Šedý JR, Ramezani-Rad P. HVEM network signaling in cancer. *Adv Cancer Res* (2019) 142:145–86. doi: 10.1016/bs.acr.2019.01.004
17. Tran NL, McDonough WS, Savitch BA, Fortin SP, Winkles JA, Symons M, et al. Increased fibroblast growth factor-inducible 14 expression levels promote glioma cell invasion via Rac1 and nuclear factor-kappaB and correlate with poor patient outcome. *Cancer Res* (2006) 66:9535–42. doi: 10.1158/0008-5472.can-06-0418
18. Winkles JA. The TWEAK-Fn14 cytokine-receptor axis: discovery, biology and therapeutic targeting. *Nat Rev Drug Discovery* (2008) 7:411–25. doi: 10.1038/nrd2488
19. Burkly LC. TWEAK/Fn14 axis: the current paradigm of tissue injury-inducible function in the midst of complexities. *Semin Immunol* (2014) 26:229–36. doi: 10.1016/j.smim.2014.02.006
20. Wiley SR, Cassiano L, Lofton T, Davis-Smith T, Winkles JA, Lindner V, et al. A novel TNF receptor family member binds TWEAK and is implicated in angiogenesis. *Immunity* (2001) 15:837–46. doi: 10.1016/s1074-7613(01)00232-1
21. Burkly LC, Michaelson JS, Zheng TS. TWEAK/Fn14 pathway: an immunological switch for shaping tissue responses. *Immunol Rev* (2011) 244:99–114. doi: 10.1111/j.1600-065X.2011.01054.x
22. Boulamery A, Desplat-Jégo S. Regulation of Neuroinflammation: What Role for the Tumor Necrosis Factor-Like Weak Inducer of Apoptosis/Fn14 Pathway? *Front Immunol* (2017) 8:1534. doi: 10.3389/fimmu.2017.01534
23. Stock AD, Wen J, Putterman C. Neuropsychiatric Lupus, the Blood Brain Barrier, and the TWEAK/Fn14 Pathway. *Front Immunol* (2013) 4:484. doi: 10.3389/fimmu.2013.00484
24. Nikolopoulos D, Fanouriakis A, Boumpas DT. Update on the pathogenesis of central nervous system lupus. *Curr Opin Rheumatol* (2019) 31:669–77. doi: 10.1097/bor.0000000000000065
25. Kwon OH, Kim JH, Kim SY, Kim YS. TWEAK/Fn14 signaling mediates gastric cancer cell resistance to 5-fluorouracil via NF-κB activation. *Int J Oncol* (2014) 44:583–90. doi: 10.3892/ijo.2013.2211
26. Liu JY, Jiang L, He T, Liu JJ, Fan JY, Xu XH, et al. NETO2 promotes invasion and metastasis of gastric cancer cells via activation of PI3K/Akt/NF-κB/Snail axis and predicts outcome of the patients. *Cell Death Dis* (2019) 10:162. doi: 10.1038/s41419-019-1388-5
27. Sun Y, Han Y, Wang X, Wang W, Wang X, Wen M, et al. Correlation of EGFR Del 19 with Fn14/JAK/STAT signaling molecules in non-small cell lung cancer. *Oncol Rep* (2016) 36:1030–40. doi: 10.3892/or.2016.4905
28. Ruiz-Plazas X, Rodríguez-Gallego E, Alves M, Altuna-Coy A, Lozano-Bartolomé J, Portero-Otin M, et al. Biofluid quantification of TWEAK/Fn14 axis in combination with a selected biomarker panel improves assessment of prostate cancer aggressiveness. *J Transl Med* (2019) 17:307. doi: 10.1186/s12967-019-2053-6
29. Li L, Ameri AH, Wang S, Jansson KH, Casey OM, Yang Q, et al. EGR1 regulates angiogenic and osteoclastogenic factors in prostate cancer and promotes metastasis. *Oncogene* (2019) 38:6241–55. doi: 10.1038/s41388-019-0873-8
30. Tran NL, McDonough WS, Donohue PJ, Winkles JA, Berens TJ, Ross KR, et al. The human Fn14 receptor gene is up-regulated in migrating glioma cells in vitro and overexpressed in advanced glial tumors. *Am J Pathol* (2003) 162:1313–21. doi: 10.1016/s0002-9440(10)63927-2
31. Hersh DS, Harder BG, Roos A, Peng S, Heath JE, Legesse T, et al. The TNF receptor family member Fn14 is highly expressed in recurrent glioblastoma and in GBM patient-derived xenografts with acquired temozolomide resistance. *Neuro Oncol* (2018) 20:1321–30. doi: 10.1093/neuonc/noy063
32. Li A, Walling J, Ahn S, Kotliarov Y, Su Q, Quezado M, et al. Unsupervised analysis of transcriptomic profiles reveals six glioma subtypes. *Cancer Res* (2009) 69:2091–9. doi: 10.1158/0008-5472.can-08-2100
33. Fortin SP, Ennis MJ, Schumacher CA, Zylstra-Diegel CR, Williams BO, Ross JT, et al. Cdc42 and the guanine nucleotide exchange factors Ect2 and trio mediate Fn14-induced migration and invasion of glioblastoma cells. *Mol Cancer Res* (2012) 10:958–68. doi: 10.1158/1541-7786.mcr-11-0616
34. Perez JG, Tran NL, Rosenblum MG, Schneider CS, Connolly NP, Kim AJ, et al. The TWEAK receptor Fn14 is a potential cell surface portal for targeted delivery of glioblastoma therapeutics. *Oncogene* (2016) 35:2145–55. doi: 10.1038/onc.2015.310
35. Johnston AJ, Murphy KT, Jenkinson L, Laine D, Emmrich K, Faou P, et al. Targeting of Fn14 Prevents Cancer-Induced Cachexia and Prolongs Survival. *Cell* (2015) 162:1365–78. doi: 10.1016/j.cell.2015.08.031
36. Brown SA, Cheng E, Williams MS, Winkles JA. TWEAK-independent Fn14 self-association and NF-κB activation is mediated by the C-terminal region of the Fn14 cytoplasmic domain. *PloS One* (2013) 8:e65248. doi: 10.1371/journal.pone.0065248
37. Hombach-Klonisch S, Mehrpour M, Shojaei S, Harlos C, Pitz M, Hamai A, et al. Glioblastoma and chemoresistance to alkylating agents: Involvement of apoptosis, autophagy, and unfolded protein response. *Pharmacol Ther* (2018) 184:13–41. doi: 10.1016/j.pharmthera.2017.10.017
38. Wang J, Cazzato E, Ladewig E, Frattini V, Rosenbloom DI, Clonal evolution of glioblastoma under therapy. *Nat Genet* (2016) 48:768–76. doi: 10.1038/ng.3590
39. Kim H, Zheng S, Amini SS, Virk SM, Mikkelsen T, Brat DJ, et al. Whole-genome and multisector exome sequencing of primary and post-treatment glioblastoma reveals patterns of tumor evolution. *Genome Res* (2015) 25:316–27. doi: 10.1101/gr.180612.114
40. Byron SA, Tran NL, Halperin RF, Phillips JJ, Kuhn JG, de Groot JF, et al. Prospective Feasibility Trial for Genomics-Informed Treatment in Recurrent and Progressive Glioblastoma. *Clin Cancer Res* (2018) 24:295–305. doi: 10.1158/1078-0432.ccr-17-0963
41. Johnson BE, Mazor T, Hong C, Barnes M, Aihara K, McLean CY, et al. Mutational analysis reveals the origin and therapy-driven evolution of recurrent glioma. *Science* (2014) 343:189–93. doi: 10.1126/science.1239947
42. Cherry EM, Lee DW, Jung JU, Sitcheran R. Tumor necrosis factor-like weak inducer of apoptosis (TWEAK) promotes glioma cell invasion through induction of NF-κB-inducing kinase (NIK) and noncanonical NF-κB signaling. *Mol Cancer* (2015) 14:9. doi: 10.1186/s12943-014-0273-1
43. Ensign SP, Roos A, Mathews IT, Dhruv HD, Tuncali S, Sarkaria JN, et al. SGEF Is Regulated via TWEAK/Fn14/NF-κB Signaling and Promotes Survival by Modulation of the DNA Repair Response to Temozolomide. *Mol Cancer Res* (2016) 14:302–12. doi: 10.1158/1541-7786.mcr-15-0183
44. Su YT, Phan FP, Wu J. Perspectives on IDH Mutation in Diffuse Gliomas. *Trends Cancer* (2018) 4:605–7. doi: 10.1016/j.trecan.2018.06.006
45. Eckel-Passow JE, Lachance DH, Molinaro AM, Walsh KM, Decker PA, Sicotte H, et al. Glioma Groups Based on 1p/19q, IDH, and TERT Promoter Mutations in Tumors. *N Engl J Med* (2015) 372:2499–508. doi: 10.1056/NEJMoa1407279
46. Lu Y, Kwintkiewicz J, Liu Y, Tech K, Frady LN, Su YT, et al. Chemosensitivity of IDH1-Mutated Gliomas Due to an Impairment in PARP1-Mediated DNA Repair. *Cancer Res* (2017) 77:1709–18. doi: 10.1158/0008-5472.can-16-2773
47. Hersh DS, Peng S, Dancy JG, Galisteo R, Eschbacher JM, Castellani RJ, et al. Differential expression of the TWEAK receptor Fn14 in IDH1 wild-type and mutant gliomas. *J Neuro-Oncol* (2018) 138:241–50. doi: 10.1007/s11060-018-2799-3
48. Krishnamurthy N, Kurzrock R. Targeting the Wnt/beta-catenin pathway in cancer: Update on effectors and inhibitors. *Cancer Treat Rev* (2018) 62:50–60. doi: 10.1016/j.ctrv.2017.11.002
49. Yin X, Luistro L, Zhong H, Smith M, Nevins T, Schostack K, et al. RG7212 anti-TWEAK mAb inhibits tumor growth through inhibition of tumor cell proliferation and survival signaling and by enhancing the host antitumor immune response. *Clin Cancer Res* (2013) 19:5686–98. doi: 10.1158/1078-0432.ccr-13-0405
50. Roos A, Dhruv HD, Mathews IT, Inge LJ, Tuncali S, Hartman LK, et al. Identification of aurintricarboxylic acid as a selective inhibitor of the TWEAK-Fn14 signaling pathway in glioblastoma cells. *Oncotarget* (2017) 8:12234–46. doi: 10.18632/oncotarget.14685
51. Bolognesi A, Polito L. Immunotoxins and other conjugates: pre-clinical studies. *Mini Rev Med Chem* (2004) 4:563–83. doi: 10.2174/1389557043403864
52. Pastan I, Hassan R, FitzGerald DJ, Kreitman RJ. Immunotoxin treatment of cancer. *Annu Rev Med* (2007) 58:221–37. doi: 10.1146/annurev.med.58.070605.115320
53. Zhou H, Marks JW, Hittelman WN, Yagita H, Cheung LH, Rosenblum MG, et al. Development and characterization of a potent immunoconjugate

targeting the Fn14 receptor on solid tumor cells. *Mol Cancer Ther* (2011) 10:1276–88. doi: 10.1158/1535-7163.mct-11-0161
54. Zhou H, Hittelman WN, Yagita H, Cheung LH, Martin SS, Winkles JA, et al. Antitumor activity of a humanized, bivalent immunotoxin targeting fn14-positive solid tumors. *Cancer Res* (2013) 73:4439–50. doi: 10.1158/0008-5472.can-13-0187
55. Zhou H, Ekmekcioglu S, Marks JW, Mohamedali KA, Asrani K, Phillips KK, et al. The TWEAK receptor Fn14 is a therapeutic target in melanoma: immunotoxins targeting Fn14 receptor for malignant melanoma treatment. *J Invest Dermatol* (2013) 133:1052–62. doi: 10.1038/jid.2012.402
56. Schneider CS, Perez JG, Cheng E, Zhang C, Mastorakos P, Hanes J, et al. Minimizing the non-specific binding of nanoparticles to the brain enables active targeting of Fn14-positive glioblastoma cells. *Biomaterials* (2015) 42:42–51. doi: 10.1016/j.biomaterials.2014.11.054
57. Wadajkar AS, Dancy JG, Roberts NB, Connolly NP, Strickland DK, Winkles JA, et al. Decreased non-specific adhesivity, receptor targeted (DART) nanoparticles exhibit improved dispersion, cellular uptake, and tumor retention in invasive gliomas. *J Contr Rel* (2017) 267:144–53. doi: 10.1016/j.jconrel.2017.09.006

Conflict of Interest: The authors declare that the research was conducted in the absence of any commercial or financial relationships that could be construed as a potential conflict of interest.

frontiers in Oncology

ORIGINAL RESEARCH
published: 29 April 2021
doi: 10.3389/fonc.2021.650534

High Level of METTL7B Indicates Poor Prognosis of Patients and Is Related to Immunity in Glioma

Yujia Xiong[1], *Mingxuan Li*[1], *Jiwei Bai*[2], *Yutao Sheng*[1] *and Yazhuo Zhang*[1,2,3,4*]

[1] *Beijing Neurosurgical Institute, Capital Medical University, Beijing, China,* [2] *Department of Neurosurgery, Beijing Tiantan Hospital, Capital Medical University, Beijing, China,* [3] *Beijing Institute for Brain Disorders Brain Tumor Center, Beijing, China,* [4] *China National Clinical Research Center for Neurological Diseases, Beijing, China*

Glioma is the most common primary intracranial malignant tumor in adults. Although there have been many efforts on potential targeted therapy of glioma, the patient's prognosis remains dismal. Methyltransferase Like 7B (METTL7B) has been found to affect the development of a variety of tumors. In this study, we collected RNA-seq data of glioma in CGGA and TCGA, analyzed them separately. Then, Kaplan-Meier survival analysis, univariate and multivariate Cox analysis, and receiver operating characteristic curve (ROC curve) analysis were used to evaluate the effect of METTL7B on prognosis. Gene Ontology (GO), Kyoto Encyclopedia of Genes and Genomes (KEGG), Gene Set Enrichment Analysis (GSEA) enrichment analyses were used to identify the function or pathway associated with METTL7B. Moreover, the ESTIMATE algorithm, Cibersort algorithm, Spearman correlation analysis, and TIMER database were used to explore the relationship between METTL7B and immunity. Finally, the role of METTL7B was explored in glioma cells. We found that METTL7B is highly expressed in glioma, and high expression of METTL7B in glioma is associated with poor prognosis. In addition, there were significant differences in immune scores and immune cell infiltration between the two groups with different expression levels of METTL7B. Moreover, METTL7B was also correlated with immune checkpoints. Knockdown of METTL7B revealed that METTL7B promoted the progression of glioma cells. The above results indicate that METTL7B affects the prognosis of patients and is related to tumor immunity, speculating that METTL7B may be a new immune-related target for the treatment of glioma.

Keywords: glioma, METTL7B, immune, prognosis, CGGA TCGA

OPEN ACCESS

Edited by:
Matthias Preusser,
Medical University of Vienna, Austria

Reviewed by:
Simon Hanft,
Westchester Medical Center,
United States
Yu Ping,
First Affiliated Hospital of Zhengzhou University, China

****Correspondence:***
Yazhuo Zhang
zyz2004520@yeah.net

Specialty section:
This article was submitted to Neuro-Oncology and Neurosurgical Oncology, a section of the journal Frontiers in Oncology

Received: *07 January 2021*
Accepted: *06 April 2021*
Published: *29 April 2021*

Citation:
Xiong Y, Li M, Bai J, Sheng Y and Zhang Y (2021) High Level of METTL7B Indicates Poor Prognosis of Patients and Is Related to Immunity in Glioma. Front. Oncol. 11:650534. doi: 10.3389/fonc.2021.650534

INTRODUCTION

Glioma is the most common primary malignant brain tumor in adults (1, 2). Glioma can be divided into low grade glioma (WHO grade II/III, LGG) and glioblastoma (WHO grade IV, GBM) (3). WHO 2016 classified glioma according to molecular pathological type (IDH mutation and 1p/19q Codeletion), which will be helpful for clinical treatment (4, 5). Currently, surgery,

radiotherapy, and alkylating agent are the main treatment options for glioma (6–8). However, the prognosis of glioma as a whole is poor (9, 10). Recent studies find that tumor immune response plays an essential role in glioma (11–13), suggesting the promising prospect of immune therapy for glioma therapy.

METTL7B, located at chromosome 12q13.2, is correlated with methyltransferase activity and s-adenosine methionine-dependent methyltransferase activity. It has been found that METTL7B contributes to the occurrence and development of breast cancer, thyroid cancer, and lung cancer (14–16). Moreover, recent research revealed that METTL7B may regulate immunity by regulating the methylation of the FOX3P promoter (17), a novel immune-associated gene.

The current study analyzed the glioma transcriptome data in the TCGA and CGGA database and found that METTL7B is highly expressed in glioma and is correlated with multiple clinical features of glioma. Moreover, patients with high METTL7B levels have a poor prognosis. At the same time, we analyzed the differential genes between the two groups with high and low expression of METTL7B and performed enrichment analysis based on the differential genes, and the results indicated enrichment of several immune-related functions and pathways. The results showed that METTL7B is positively correlated with the ESTIMATE score. Also, we found that METTL7B is associated with multiple immune checkpoints, and the immune cell subpopulations may be associated with METTL7B. Moreover, knockdown of METTL7B decreased the proliferation, migration, and invasion ability of glioma cells. In summary, our findings revealed that METTL7B affects the prognosis of patients and is involved in tumor immunity in glioma.

MATERIALS AND METHODS

Data Download and Collation

We downloaded the glioma RNA-seq data (total 698 cases, glioblastoma (GBM) 169 cases, low-grade glioma (LGG) 529 cases), and clinical data (1114 cases, GBM+LGG) from the TCGA website (http://www.tcga.org/). After deleting the missing samples of clinical data, gene expression and the corresponding clinical documents of 640 cases were obtained. RNA-seq and clinical data for glioma (325 + 693 cases) were downloaded from the CGGA website (http://www.cgga.org.cn). For batch correction and integration, the LIMMA (18) package and SVA (19) package were used.

GEPIA Analysis and HPA Analysis

The GEPIA website was used to analyze the differences between the METTL7B gene expression levels in glioma (LGG and GBM) and normal samples. Moreover, we used the GEPIA website to draw Kaplan–Meier (20) curves for survival analysis in the TCGA database. We further verified the METTL7B protein levels of normal samples and glioma samples using the Human Protein Atlas (HPA website, http://www.proteinatlas.org).

Prognostic Analysis

Kaplan-Meier curve was used for survival analysis. We used R software to load the survival package (https://CRAN.R-project.org/package=survival) and the survminer package (https://CRAN.R-project.org/package=survivalminer) to draw the Kaplan-Meier curve on glioma samples of the CGGA database. We also performed univariate and multivariate Cox analysis, and receiver operating characteristic curve (ROC) survival analysis was performed using the survivalROC package (https://CRAN.R-project.org/package=survivalROC).

Differential Gene Enrichment Analysis

Differential analysis was performed using the LIMMA package. The clusterProfiler (21) package and enrichplot package (https://github.com/GuangchuangYu/enrichplot) was applied to perform the GO and KEGG enrichment analysis of differential genes. In addition, GSEA software was used to analyze the GO and KEGG pathways between the high and low levels of METTL7B.

Immune Evaluation

The immune score of samples was assessed in the R software using the ESTIMATE package (https://R-Forge.R-project.org/projects/estimate/). Cibersort (22) algorithm was applied to analyze the correlations between METTL7B and 22 immune cell subsets. Tumor Immune Estimation Resource (TIMER, https://cistrome.shinyapps.io/timer/) was further used to analyze the relationship between different immune cells and prognosis in GBM and LGG and the correlations between METTL7B and immune cells.

Cell Line and Transfection

U87 Glioma cell line, purchased from the American Type Culture Collection, was cultured in DMEM (Thermo Fisher Scientific) supplemented with 10% fetal bovine serum in an incubator at 37°C and 5% CO2. The METTL7B small interfering RNA (siRNA) and negative control (NC) were obtained from the Guangzhou RiboBio Co., Ltd. Cells were seeded in the 6-well plate (5×10^5 cells per well)were transfected with siRNAs and NC with the help of lipofectamine 3000.

Quantitative Reverse Transcription Polymerase Chain Reaction (qRT-PCR) and Western Blot

Two days after transfection, cells were collected for RNA using Trizol reagent (Invitrogen). The cDNA was further synthesized using the SuperScript III First Strand Synthesis System (Invitrogen). QuantStudio 5 (Applied Biosystems) was used to perform the qRT-PCR. The expression of METTL7B was normalized to GAPDH. The primers of MTEEL7B were as following: CCTGCCTAGACCCAAATCCC (forward) and AAACCGCTCATATTGGAGGTG (reverse). For western blot, mouse METTL7B antibody (Santa Cruz Biotechnology, sc-398626, 1:500) was used as primary antibody, and the β-actin was applied as the control.

CCK8, Migration, and Invasion Assay

Glioma cells were cultured in the 96-well plate ($5x10^3$ cells per well) for 24 hours before transfection. Cells were then treated with METTL7B siRNAs or NC, and the optical density (OD) values at 450nm at several time points were assessed after the 3h-

incubation of 10ul CCK8 assay at 37°C. $1x10^5$ glioma cells transfected with METTL7B siRNAs and NC were seeded in the transwell chamber (Corning) with (For invasion) or without (For migration) Matrigel. After 4 hours (migration) and 8 hours (invasion), the cells at the bottom surface of the filters were fixed and stained with 0.1% crystal violet.

Statistical Analysis

The R software (version 3.6.3) was used for the statistical analysis. The median value of METTL7B expression was considered as the cutoff value to separate patients into the high and low groups. The Circlize (23) and Corrplot packages (https://github.com/taiyun/corrplot) were used to map the correlation circles. Other R packages, "ggplot2", "ggpubr", "vioplot" were applied to visualize the results of data analysis. Wilcoxon Signed Rank test and Student's t test were used for statistical analysis between two groups, while the Kruskal-Wallis test was applied for statistical tests of more than two groups. When p less than 0.05, we considered the difference to be statistically significant.

RESULTS

METTL7B Is Highly Expressed in Glioma and Is Related to Patient Prognosis

The expression of METTL7B in tumor samples of glioma and normal samples was evaluated using the GEPIA website and we found that METTL7B is highly expressed in both LGG and GBM samples (**Figure 1A**). Similarly, the protein level of METTL7B in glioma samples was also higher compared to that in normal samples in the HPA database (**Figure 1B**). Next, we analyzed the relationships between METTL7B expression level and the clinicopathological characteristics of glioma patients, showing that the expression of METTL7B was significantly correlated with age, tumor stage, pathology, and IDH1mutation ($p < 0.001$), but not with gender or radiotherapy in glioma ($p > 0.05$) (**Figure 2**, **Table 1**, **Supplementary Figure 1**).

Kaplan-Meier survival analysis indicated that the high expression of METTL7B was significantly correlated with poor prognosis (p <0.001, **Figures 3A, B**). Furthermore, univariate Cox analysis identified METTL7B as a risk factor, and subsequent multivariate Cox analysis revealed that METTL7B is independently associated with the prognosis in glioma (**Figures 3C–F**). Moreover, we confirmed that PRS type, histology, grade, chemotherapy, IDH mutation, and 1p19q codeletion could also affect the prognosis of the patients (**Figures 3C–F**).

In addition, the ROC curve analysis suggested that METTL7B shows satisfactory performance in predicting the 1-year, 3-year, and 5-year survival rates of patients (all AUC>0.7) (**Figures 3G, H**).

TABLE 1 | Differences in clinical characteristics between the high and low METTL7B expression groups.

Database	Clinical features	P-value
TCGA	Histology	<0.001*
TCGA	Grade	<0.001*
TCGA	Gender	0.48
TCGA	Age	<0.001*
TCGA	IDH mutation	<0.001*
CGGA	PRS type	<0.001*
CGGA	Histology	<0.001*
CGGA	Grade	<0.001*
CGGA	Gender	0.64
CGGA	Age	<0.001*
CGGA	Radio status	0.63
CGGA	Chemo status	<0.001*
CGGA	IDH mutation status	<0.001*
CGGA	1p19q codeletion status	<0.001*

indicated $p < 0.05$; PRS, primary and recurrent status.

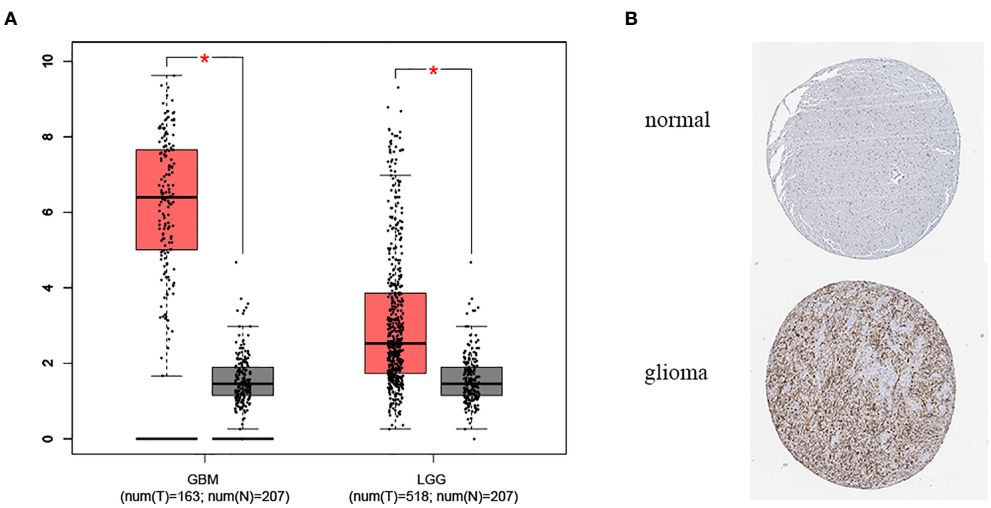

FIGURE 1 | The expression level of METTL7B in glioma. **(A)** Expression of METTL7B in glioma and normal tissues in GEPIA database. **(B)** The protein level of METTL7B in glioma and normal tissues based on the Human Protein Atlas. *p < 0.05.

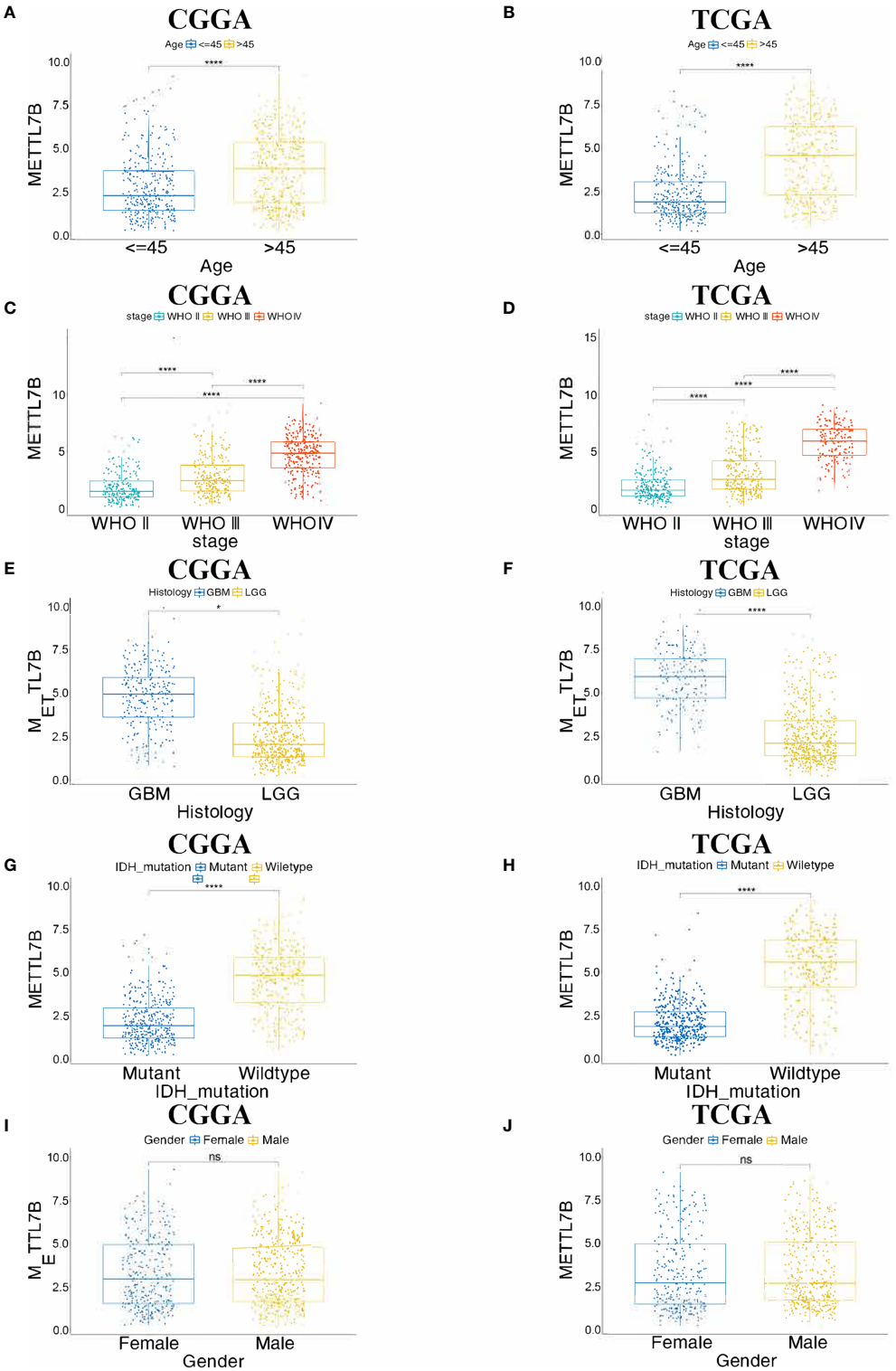

FIGURE 2 | Correlation between the expression of METTL7B and clinical features using CGGA and TCGA database. **(A, B)** Differential expression of METTL7B was significantly related to the age of the patients, **(C, D)** WHO stage of glioma, **(E, F)** histology, **(G, H)** IDH_mutation. **(I, J)** The expression level of METTL7B was not correlated with the Gender of patients. *p < 0.05; ****p < 0.0001; ns, not significant.

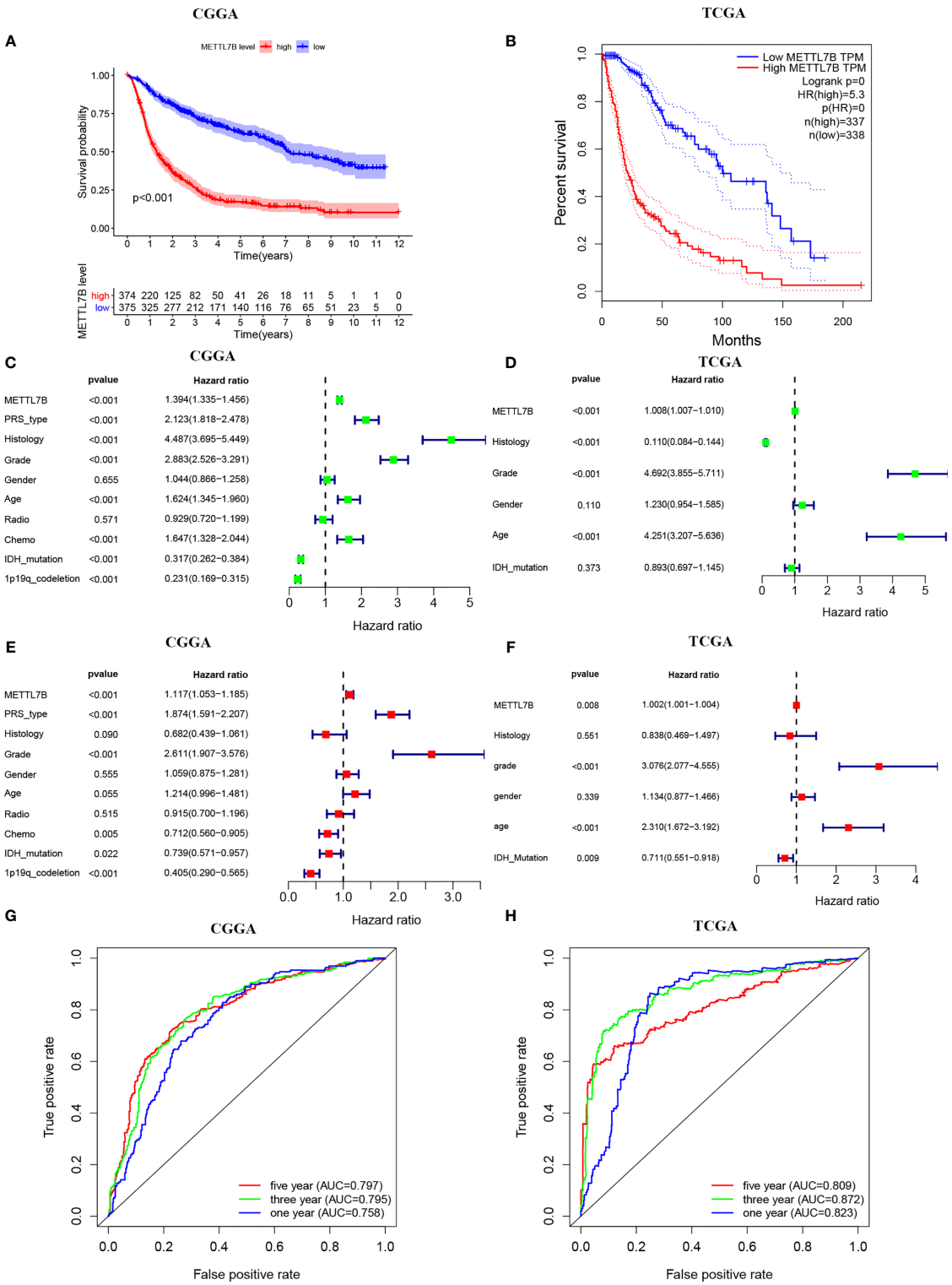

FIGURE 3 | Survival analysis of METTL7B in CGGA and TCGA patients. **(A, B)** Kaplan-Meier survival curves in the high and low expressions of METTL7B groups. **(C, D)** Univariate Cox analysis of METTL7B. **(E, F)** Multivariate Cox analysis of METTL7B. **(G, H)** ROC analysis of METTL7B for 1, 3, and 5-year survival.

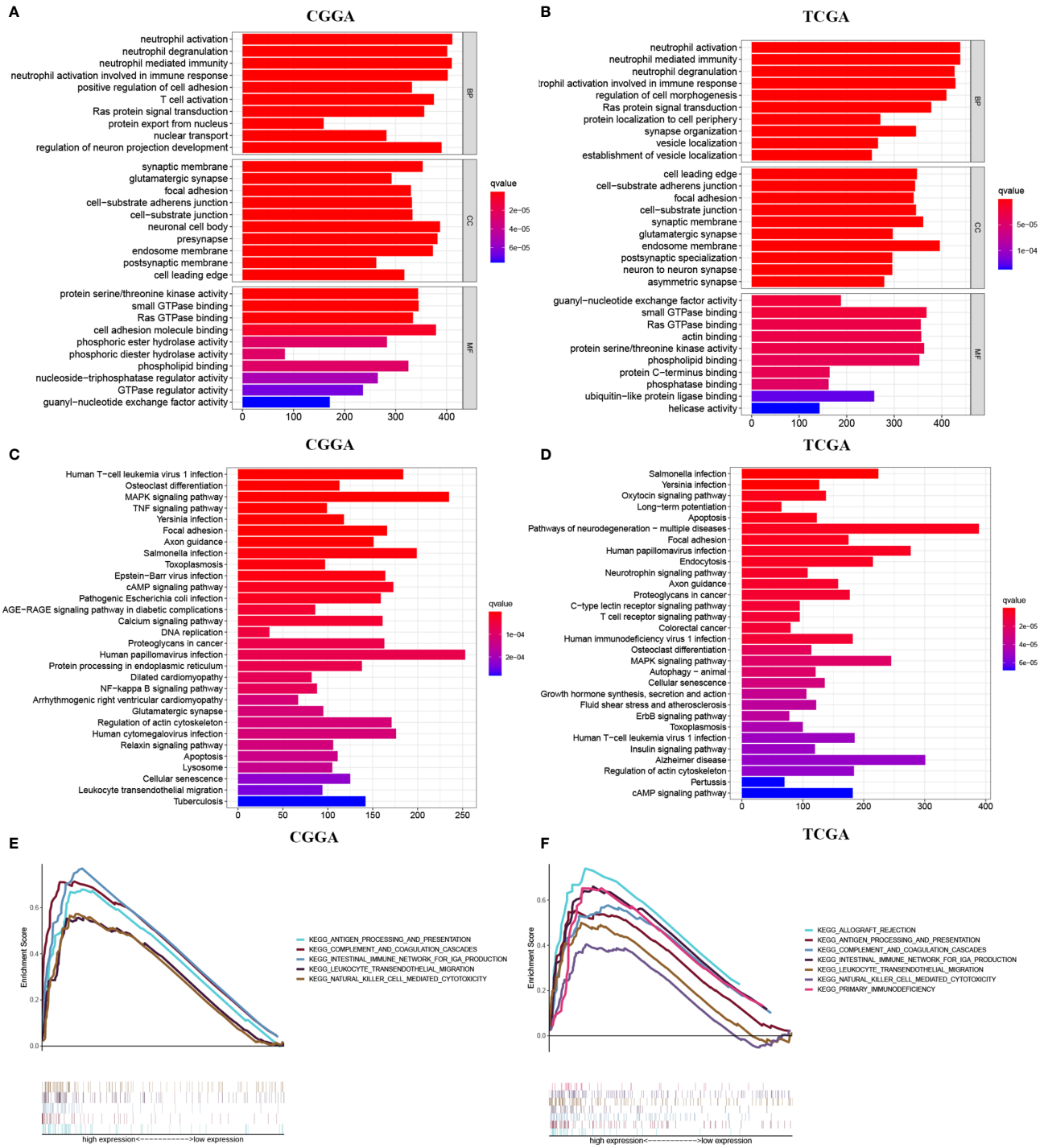

FIGURE 4 | Differential gene enrichment analysis between different METTL7B groups. **(A, B)** Top 10 GO terms, involving BP, CC, and MF. **(C, D)** Top 30 KEGG pathways. **(E, F)** GSEA enrichment analysis revealed potential associations between METTL7B and several immune-associated pathways.

Differential Gene Enrichment Analysis Between METTL7B Groups

We then analyzed the different genes, and the heatmap was developed to show the top 100 up-regulated and the top 100 down-regulated differential genes between the two groups (**Supplementary Figure 2, Supplementary Table 1**). Further GO enrichment analysis of differential genes revealed that METTL7B may be associated with neutrophil-mediated

immunity, neutrophil activation, neutrophil activation involved in immune response, neutrophil degranulation, T cell activation, and other immune-related functions (**Figures 4A, B**). Interestingly, KEGG analysis further suggested that METTL7B may be involved in some immune-related and previously recognized oncogenic pathways such as TNF signaling pathway, T cell receptor signaling pathway, NF-kappaB signaling pathway, MAPK signaling pathway, human T-cell leukemia virus type 1 infection, salmonella infection, and Yersinia infection, (**Figures 4C, D**). In addition, GSEA enrichment analysis in TCGA and CGGA databases also indicated significant enrichment of multiple immune-related functions and pathways (**Figures 4E, F**, **Supplementary Figure 3**). The above results indicated that METTL7B may function *via* the involvement of the tumor immune microenvironment. Thus, we further analyzed the relationship between METTL7B and tumor immunity.

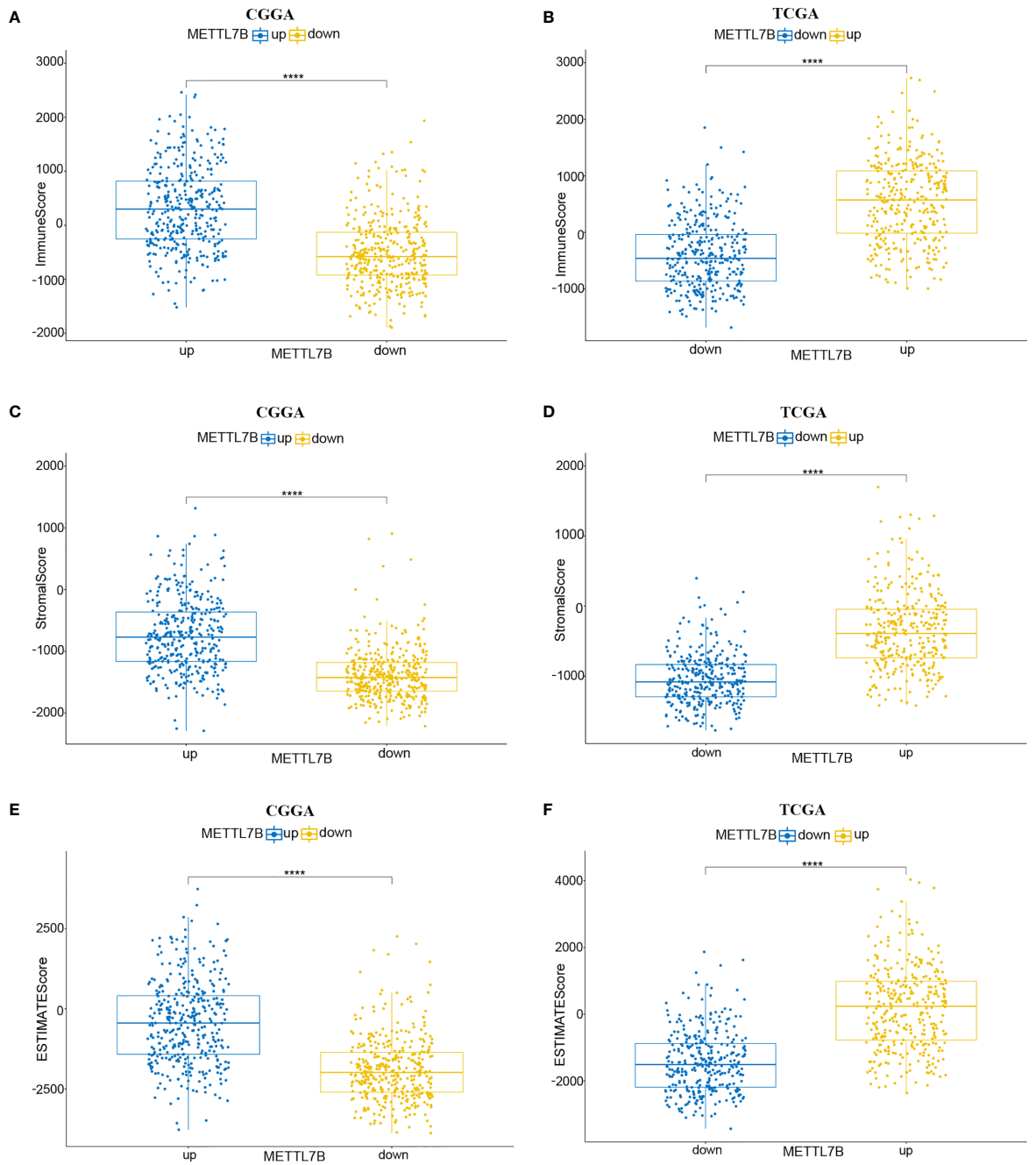

FIGURE 5 | Relationship between ESTIMATE score and METTL7B expression level in CGGA and TCGA patients. **(A, B)** Immunescore, **(C, D)** stromalscore, and **(E, F)** ESTIMATEscore were higher in the group with higher METTL7B expression. ****p < 0.0001.

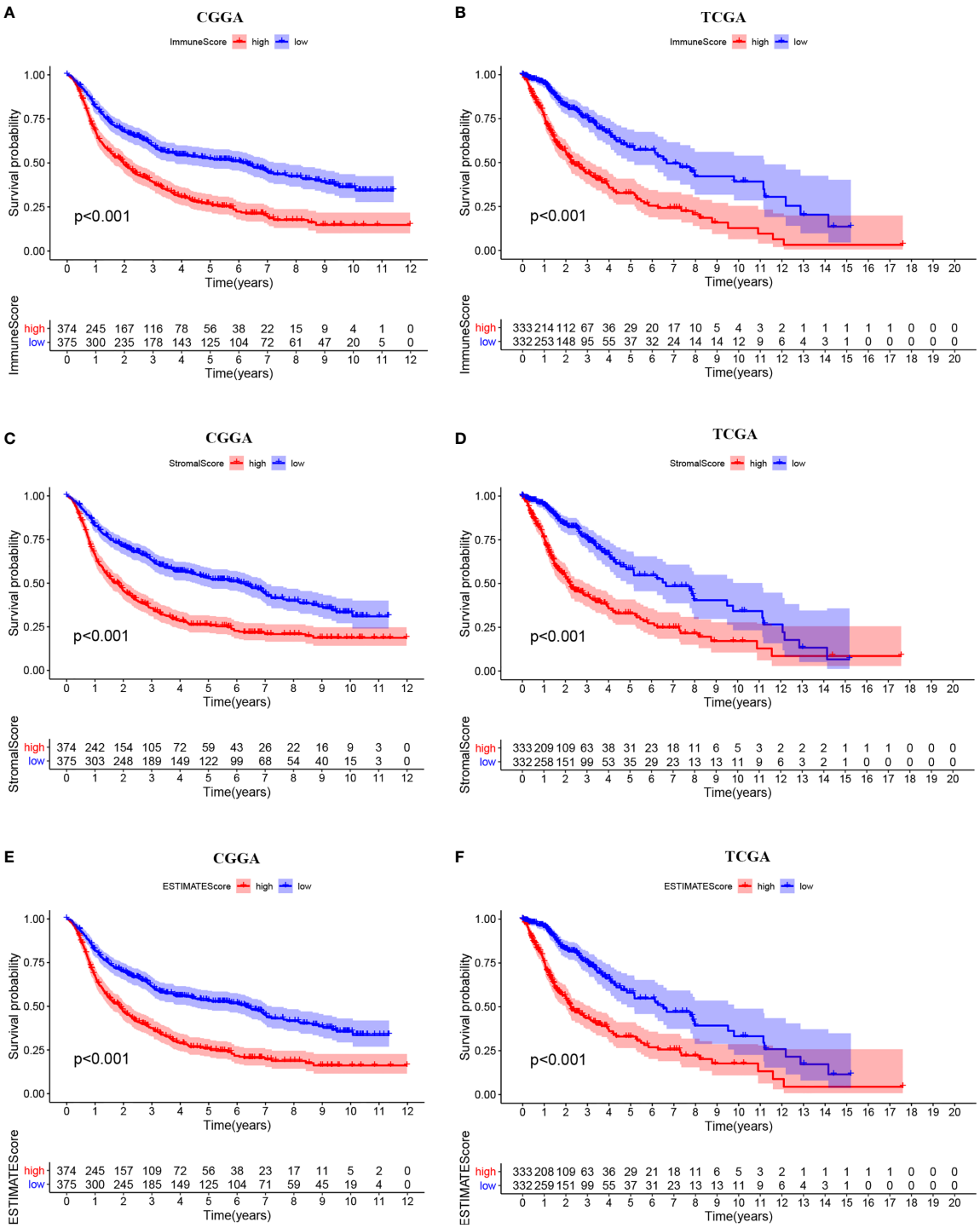

FIGURE 6 | Kaplan-Meier survival curves of ESTIMATE score. High levels of **(A, B)** immunescore, **(C, D)** stromalscore, and **(E, F)** ESTIMATEscore correlated with poor prognosis.

METTL7B Is Involved in Tumor Immunity in Glioma

The ESTIMATE algorithm was performed to assess the immune levels of glioma patients, showing the significant differences (p<0.001) in the immune score, stromal score, and ESTIMATE score between the patients with high and low METTL7B expression. Specifically, the immune score, stromal score, and ESTIMATE score of the high expression METTL7B patients

were all higher (**Figure 5**). Moreover, high immune score, high stromal score, and high ESTIMATE score were all associated with poor prognosis in glioma (**Figure 6**). Univariate cox analysis also confirmed the survival performance of the immune score, stromal score, and ESTIMATE score (**Supplementary Figure 4**). We further explored the correlations between METTL7B and immune checkpoints and identified that METTL7B is positively correlated with several immune checkpoints PD1, PDL1, CTLA4, LAG3, and TIM3 (**Figure 7**). Moreover, we analyzed the proportion of 22 immune cells in the two groups by the Cibersort algorithm, revealing that there were significant differences in T cells CD8, NK cells activated, Monocyte, Macrophages M1, Macrophages M2, and Neutrophils between the two groups with high and low METTL7B expression level (**Figures 8A, B**, **Supplementary Table 2**). The correlations between METTL7B and 22 kinds of immune cells were further analyzed by Spearman correlation analysis, and we found that METTL7B may correlate with multiple immune cells, including Neutrophils, MacrophagesM1, MacrophagesM2, T cells, and other immune cells (**Figures 8C–J**, **Supplementary Table 3**). Further analysis showed that compared with M1 chemokine, METTL7B was mainly related to M2 chemokine (**Supplementary Figure 5**). Finally, we used the TIMER database to explore these correlations in LGG or GBM patients alone. And the results suggested that in LGG patients, B cell, CD8+ T cell, CD4+ T cell, Macrophage, and Neutrophil significantly affect the prognosis ($p<0.05$), and were still correlated with METTL7B expression, while no correlations were found in GBM patients (**Figure 9**). In summary, the above findings showed that METTL7B is associated with the immune score, immune checkpoints, and immune cell infiltration in glioma patients.

Inhibition of METTL7B Decreased the Proliferation, Migration, and Invasion Ability of Glioma Cells

To further validate the potential oncogenic role of METTL7B in glioma, we explored its function in the glioma cell line. Cells were treated with three siRNAs targeting METTL7B (si-METTL7B-1, si-METTL7B-2, and si-METTL7B-3), and the qRT-PCR (**Figure 10A**) and western blot (**Figure 10B**) revealed that si-METTL7B-1 and si-METTL7B-3 effectively inhibited the expression of METTL7B. Therefore, the two siRNAs were selected for further experiments. Cell proliferation ability was significantly reduced after METTL7B knockdown (**Figure 10C**). Moreover, inhibition of METTL7B significantly decreased the cell migration and invasion ability (**Figures 10D–F**).

DISCUSSION

Glioma is the most common primary tumor of the central nervous system, accounting for 15% of all brain tumors (24). At present, the effect of targeted drug therapy is not satisfactory (13). Among glioma, glioblastomas are highly resistant to many chemotherapeutic drugs (25). Recent studies have shown that radiotherapy combined with chemotherapy can improve patient survival (26), however, the prognosis of patients is dismal (27). Exploring new therapeutic targets and targeted therapeutic drugs for glioma patients are of no delay.

In this study, Kaplan-Meier analysis, univariate and multivariate Cox analysis, and ROC curve were employed to analyze the relationships between METTL7B and the clinical characteristics and prognosis of patients. Moreover, GO, KEGG, and GSEA enrichment analysis was conducted to identify the

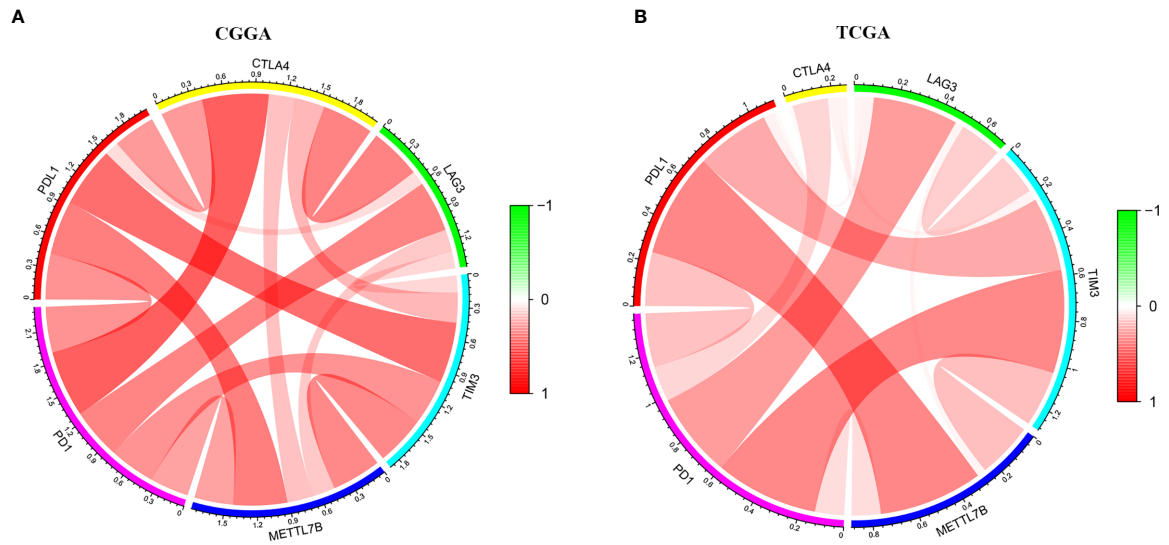

FIGURE 7 | The circle diagram showed that METTL7B was positively correlated with multiple immune checkpoints, PD1, PDL1, CTLA4, LAG3, and TIM3 in glioma patients. **(A)** CGGA. **(B)** TCGA.

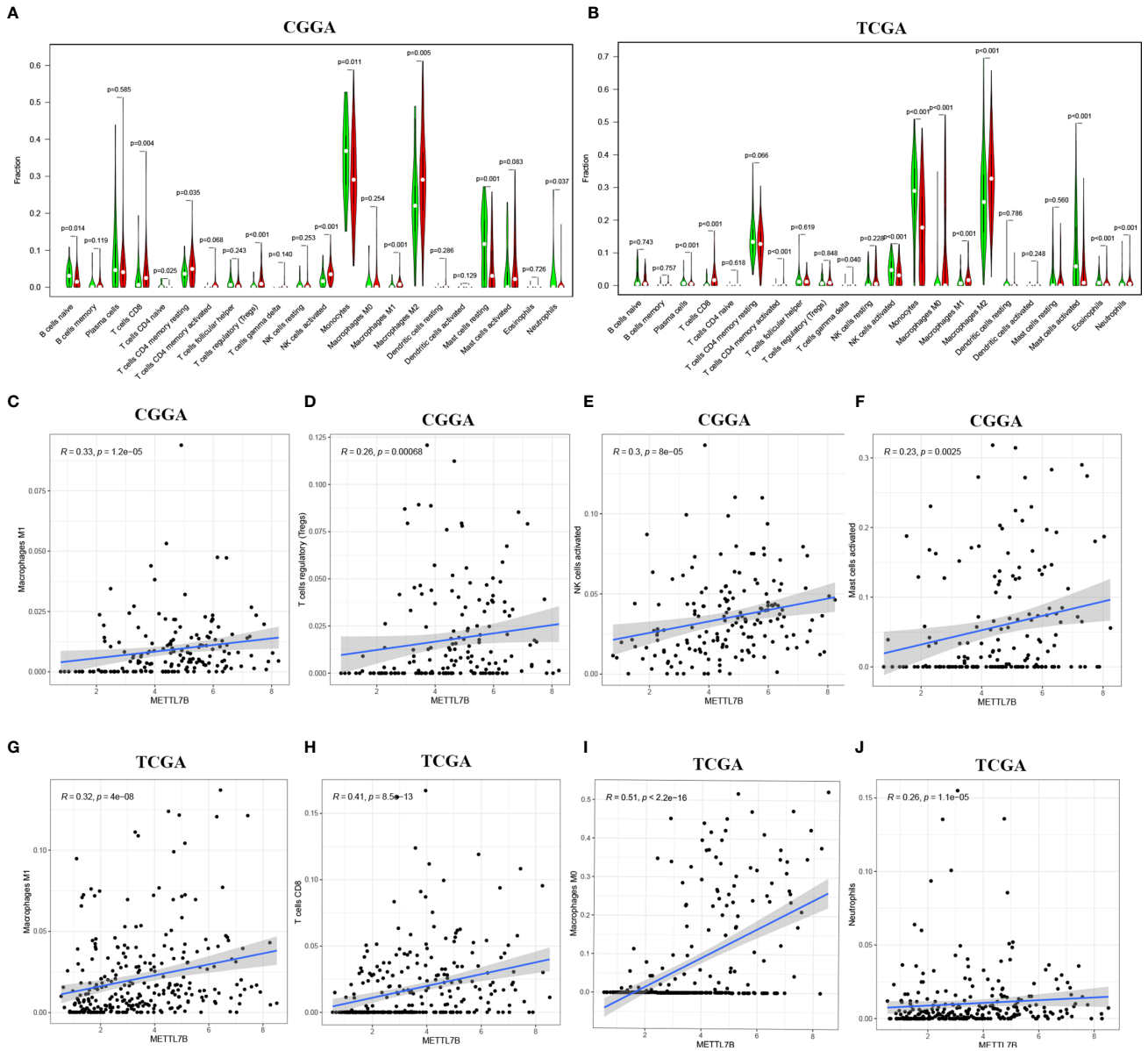

FIGURE 8 | Proportions of the 22 types of tumor-infiltrate immune cells in different METTL7B groups in **(A)** CGGA and **(B)** TCGA. Correlation analysis between METTL7B and 22 kinds of immune cells in glioma. METTL7B was positively associated with **(C)** Macrophages M1, **(D)** T cells regulatory, **(E)** NK cells activated, **(F)** Mast cells activated in CGGA. **(G)** Macrophages M1, **(H)** T cells CD8, **(I)** Macrophages M0, **(J)** Neutrophils infiltration were positively correlated with METTL7B expression in TCGA.

potential mechanisms of METTL7B in glioma. Further analysis of immune infiltration was carried out to explore the relationship between the patient's prognosis and immune cells. Importantly, the relationships between METTL7B and immune checkpoints were analyzed, and the differences of 22 kinds of immune cells in patients with high and low METTL7B levels were further analyzed. Finally, the role of METTL7B in glioma cells was explored.

METTL7B is associated with the development of a variety of tumors, while its role in glioma has not been previously studied. Through GEPIA analysis, we found that METTL7B was highly expressed in glioma (LGG and GBM), and the expression of METTL7B in GBM was increased compared to that of LGG. Similarly, HPA results also support the high expression of METTL7B in glioma. These results suggest that METTL7B may contribute to glioma progression. Further analysis identified that the expression of METTL7B was higher in glioma with a higher WHO grade and the METTL7B level in IDH1 wild-type was higher than that of mutant type. Accumulating studies have shown that IDH1 mutations are

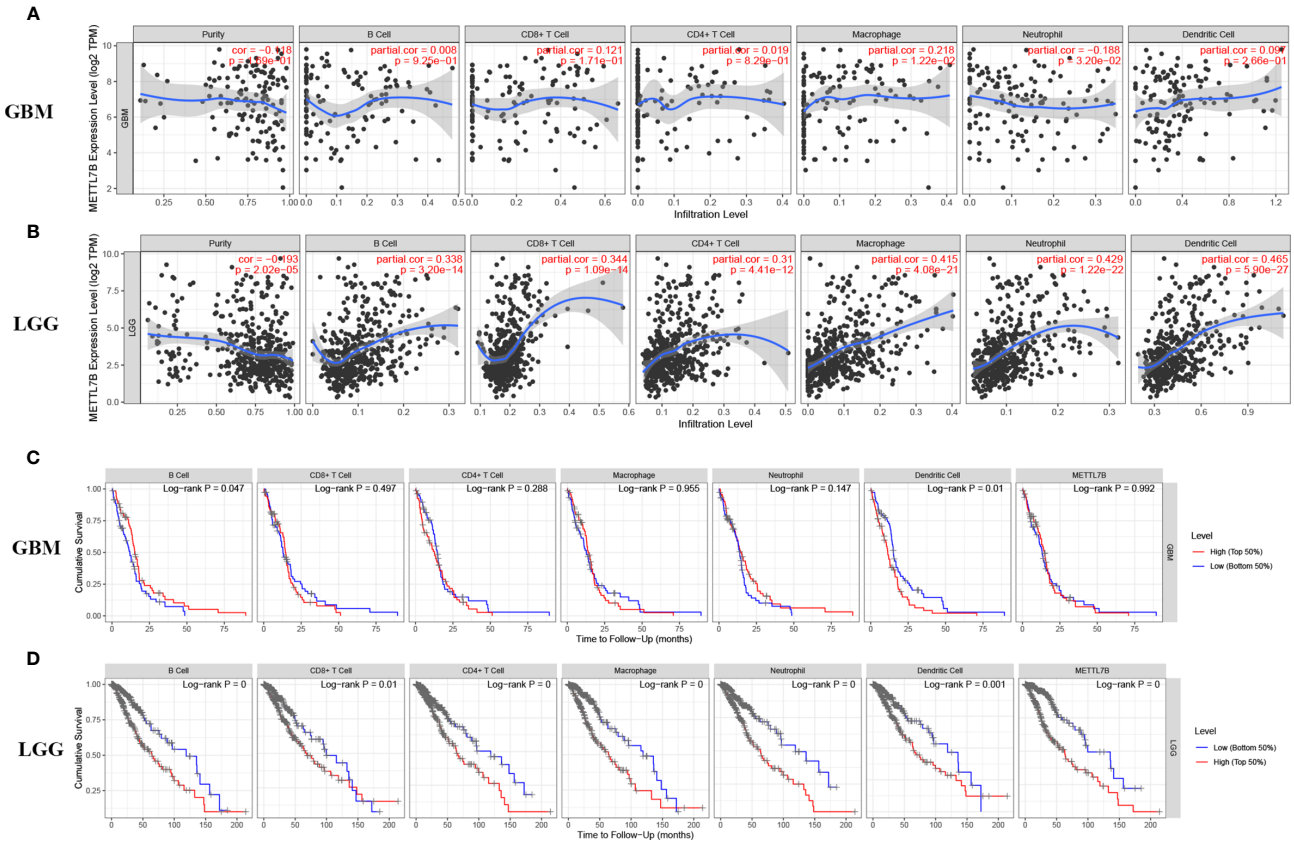

FIGURE 9 | The relationship between METTL7B expression level, tumor purity, and immune cell infiltration was explored using the TIMER database. METTL7B was significantly correlated with immune cell infiltration in **(A)** GBM and **(B)** LGG patients. Kaplan-Meier survival analysis of several immune cells in **(C)** GBM and **(D)** LGG patients.

related to the occurrence and development of glioma (28), and IDH1 mutations are more common in LGG(WHO II, WHO III) than in GBM(WHO IV) (29). Therefore, we speculated that the higher expression of METTL7B in GBM patients might due to more GBM patients are IDH wild-type tumors, which expressed higher METTL7B levels.

The Kaplan-Meier curves of METTL7B indicated that METTL7B significantly affected the prognosis of glioma patients. To verify the role of METTL7B in the prognosis of glioma patients, univariate and multivariate Cox analyses were conducted, which suggested that METTL7B might independently predict the prognosis of glioma patients. ROC curve further verified our results, the analysis of CGGA and TCGA databases showed that the performance of METTL7B for 1-year, 3-year, and 5-year OS prediction was satisfactory.

To explore the possible mechanism of METTL7B affecting the survival of patients, GO and KEGG enrichment analyses were performed based on the differentially expressed genes between METTL7B groups, and the results suggested various immune-related pathways. In addition, GSEA enrichment analysis further revealed enrichment of multiple immune-related functions and pathways. Therefore, we assumed that METTL7B may function *via* regulation of tumor immunity, such as regulation of neutrophils, T cell activation, and B cell-mediated immunity, which was not revealed in previous studies.

Patients with higher expression of METTL7B had a higher ESTIMATE score, stromal score, and immune score, which were adverse prognosis factors, further confirming that METTL7B may participate in the tumor immune microenvironment. Moreover, METTL7B was positively correlated with multiple immune checkpoints. Studies have shown that the upregulation of immune checkpoints such as PD-L1, CTLA-4, TIM-3, and LAG3 in glioma helps tumor immune evasion, leading to T cell dysfunction (30–32), suggesting that METTL7B may promote tumor immune evasion by upregulating the expression of immune checkpoints. We also used the Cibersort to evaluate the ratio of different immune cells which found significant differences between the different METTL7B expression groups. Wherein, Neutrophils, Macrophages M1, Macrophages M2, and T cells correlated with the expression of METTL7B, which validated the immune-related findings of the enrichment of differentially expressed genes. Macrophages are the main immune cells in glioma and can be polarized into M1 and M2 macrophages under the influence of chemokines (33). M2

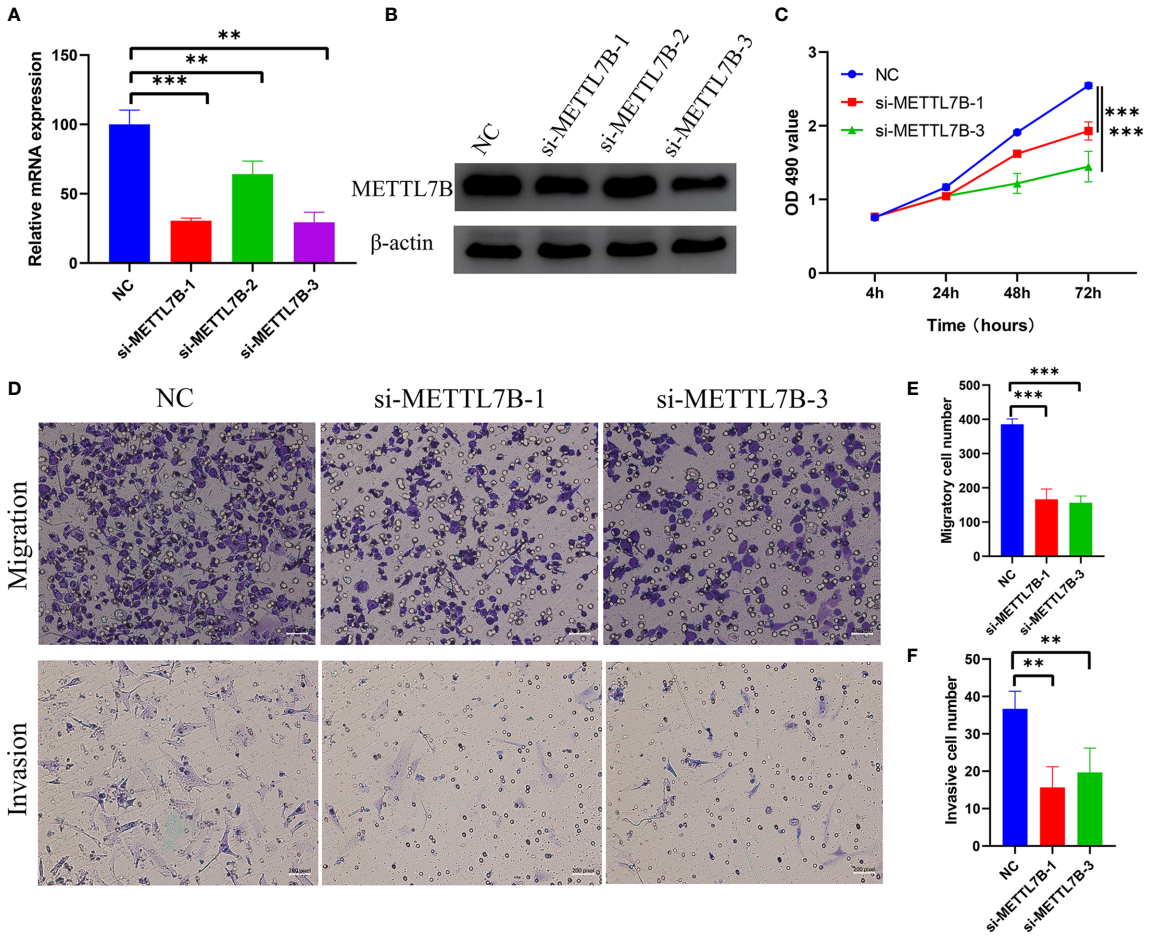

FIGURE 10 | **(A)** qRT-PCR revealed that the METTL7B mRNA level was significantly suppressed using METTL7B siRNAs. **(B)** Western blotting indicated that the expression of METTL7B was decreased after treated with METTL7B siRNAs. **(C)** CCK8 assay showed that the proliferation ability of glioma cells was significantly decreased after knockdown of METTL7B. **(D–F)** Transwell assay revealed that knockdown of METTL7B inhibited the migration and invasion ability of glioma cells. Magnification, 200X. **p < 0.01; ***p < 0.001.

macrophages are an immunosuppressive phenotype in gliomas and are associated with the poor prognosis of patients (34). Our analysis found that METTL7B was mainly related to M2 chemokine, and thus we speculated that METTL7B might contribute to a tumor microenvironment favorable for tumor growth by promoting the differentiation of macrophages into M2 type. Collectively, our study found that the high expression of METTL7B was associated with poor prognosis in glioma patients, which may be mediated *via* inhibiting tumor immunity. Finally, the results of the TIMER database suggested that in LGG patients, several immune cells influenced patients prognosis and were associated with METTL7B expression, while these results were not consistent in GBM, suggesting the complex mechanisms of METTL7B in glioma and the latent function difference of METTL7B between LGG and GBM. Further mechanism exploration is highly warranted.

In the current study, glioma patients from TCGA and CGGA databases were simultaneously analyzed, and the consistent results of the two databases made our results more reliable. After analysis, we found a new glioma prognostic gene, METTL7B, which is also closely related to immunity. The result has not been reported in previous studies, so our study may influence the future diagnosis and treatment of glioma. However, our study also has several limitations. The function and potential mechanisms of METTL7B in glioma cells were not assessed in the current study. Moreover, the association between METTL7B and tumor immune microenvironment remains further validation. Finally, the role of METL7B in some special glioma types, such as diffuse midline glioma, remains further discussed.

CONCLUSION

Our study revealed a novel prognostic gene, METTL7B, in glioma. Patients with high METTL7B expression have a poor prognosis and show a distinct immune landscape compared to

those with low expression, identifying METTL7B as a promising target for drug and immune therapy in glioma.

DATA AVAILABILITY STATEMENT

Publicly available datasets were analyzed in this study. This data can be found here: http://www.tcga.org, http://www.cgga.org.cn.

ETHICS STATEMENT

Ethical review and approval was not required for the study on human participants in accordance with the local legislation and institutional requirements. The patients/participants provided their written informed consent to participate in this study.

AUTHOR CONTRIBUTIONS

YX and YZ designed the study. YX wrote the manuscript and performed bioinformatics analysis. ML, JB, and YS contributed to manuscript discussion, figures and tables. All authors contributed to the article and approved the submitted version.

FUNDING

This study was supported by the National Natural Science Foundation of China (81771489); supported by Beijing Municipal Science & Technology Commission (Z171100000117002).

ACKNOWLEDGMENTS

We are grateful to the work of TCGA and CGGA members.

SUPPLEMENTARY MATERIAL

The Supplementary Material for this article can be found online at: https://www.frontiersin.org/articles/10.3389/fonc.2021.650534/full#supplementary-material

REFERENCES

1. Ostrom QT, Cote DJ, Ascha M, Kruchko C, Barnholtz-Sloan JS. Adult Glioma Incidence and Survival by Race or Ethnicity in the United States From 2000 to 2014. *JAMA Oncol* (2018) 4:1254–62. doi: 10.1001/jamaoncol.2018.1789
2. Lapointe S, Perry A, Butowski NA. Primary Brain Tumours in Adults. *Lancet (London England)* (2018) 392:432–46. doi: 10.1016/s0140-6736(18)30990-5
3. Berghoff AS, Kiesel B, Widhalm G, Wilhelm D, Rajky O, Kurscheid S, et al. Correlation of Immune Phenotype With IDH Mutation in Diffuse Glioma. *Neuro-oncology* (2017) 19:1460–8. doi: 10.1093/neuonc/nox054
4. Wesseling P, Capper D. Who 2016 Classification of Gliomas. *Neuropathol Appl Neurobiol* (2018) 44:139–50. doi: 10.1111/nan.12432
5. Pekmezci M, Rice T, Molinaro AM, Walsh KM, Decker PA, Hansen H, et al. Adult Infiltrating Gliomas With WHO 2016 Integrated Diagnosis: Additional Prognostic Roles of ATRX and TERT. *Acta Neuropathol* (2017) 133:1001–16. doi: 10.1007/s00401-017-1690-1
6. Weller M, Wick W, Aldape K, Brada M, Berger M, Pfister SM, et al. Glioma. *Nat Rev Dis Primers* (2015) 1:15017. doi: 10.1038/nrdp.2015.17
7. Buckner JC, Shaw EG, Pugh SL, Chakravarti A, Gilbert MR, Barger GR, et al. Radiation Plus Procarbazine, CCNU, and Vincristine in Low-Grade Glioma. *New Engl J Med* (2016) 374:1344–55. doi: 10.1056/NEJMoa1500925
8. Tan MSY, Sandanaraj E, Chong YK, Lim SW, Koh LWH, Ng WH, et al. A STAT3-based Gene Signature Stratifies Glioma Patients for Targeted Therapy. *Nat Commun* (2019) 10:3601. doi: 10.1038/s41467-019-11614-x
9. Day BW, Lathia JD, Bruce ZC, D'Souza RCJ, Baumgartner U, Ensbey KS, et al. The Dystroglycan Receptor Maintains Glioma Stem Cells in the Vascular Niche. *Acta Neuropathol* (2019) 138:1033–52. doi: 10.1007/s00401-019-02069-x
10. Sturm D, Pfister SM, Jones DTW. Pediatric Gliomas: Current Concepts on Diagnosis, Biology, and Clinical Management. *J Clin Oncol: Off J Am Soc Clin Oncol* (2017) 35:2370–7. doi: 10.1200/jco.2017.73.0242
11. Galstyan A, Markman JL, Shatalova ES, Chiechi A, Korman AJ, Patil R, et al. Blood-Brain Barrier Permeable Nano Immunoconjugates Induce Local Immune Responses for Glioma Therapy. *Nat Commun* (2019) 10:3850. doi: 10.1038/s41467-019-11719-3
12. Garofalo S, D'Alessandro G, Chece G, Brau F, Maggi L, Rosa A, et al. Enriched Environment Reduces Glioma Growth Through Immune and non-Immune Mechanisms in Mice. *Nat Commun* (2015) 6:6623. doi: 10.1038/ncomms7623
13. Ruan S, Xie R, Qin L, Yu M, Xiao W, Hu C, et al. Aggregable Nanoparticles-Enabled Chemotherapy and Autophagy Inhibition Combined With Anti-PD-L1 Antibody for Improved Glioma Treatment. *Nano Lett* (2019) 19:8318–32. doi: 10.1021/acs.nanolett.9b03968
14. Ye D, Jiang Y, Sun Y, Li Y, Cai Y, Wang Q, et al. METTL7B Promotes Migration and Invasion in Thyroid Cancer Through Epithelial-Mesenchymal Transition. *J Mol Endocrinol* (2019) 63:51–61. doi: 10.1530/JME-18-0261
15. McKinnon CM, Mellor H. The Tumor Suppressor RhoBTB1 Controls Golgi Integrity and Breast Cancer Cell Invasion Through METTL7B. *BMC Cancer* (2017) 17:145. doi: 10.1186/s12885-017-3138-3
16. Liu D, Li W, Zhong F, Yin J, Zhou W, Li S, et al. Mettl7b Is Required for Cancer Cell Proliferation and Tumorigenesis in Non-Small Cell Lung Cancer. *Front Pharmacol* (2020) 11:178. doi: 10.3389/fphar.2020.00178
17. Abdel-Hameed EA, Ji H, Sherman KE, Shata MT. Epigenetic Modification of FOXP3 in Patients With Chronic HIV Infection. *J Acquired Immune Deficiency Syndromes (1999)* (2014) 65:19–26. doi: 10.1097/QAI.0b013e3182a1bca4
18. Ritchie ME, Phipson B, Wu D, Hu Y, Law CW, Shi W, et al. Limma Powers Differential Expression Analyses for RNA-sequencing and Microarray Studies. *Nucleic Acids Res* (2015) 43:e47. doi: 10.1093/nar/gkv007
19. Leek JT, Johnson WE, Parker HS, Jaffe AE, Storey JD. The Sva Package for Removing Batch Effects and Other Unwanted Variation in High-Throughput Experiments. *Bioinf (Oxford England)* (2012) 28:882–3. doi: 10.1093/bioinformatics/bts034
20. Dudley WN, Wickham R, Coombs N. An Introduction to Survival Statistics: Kaplan-Meier Analysis. *J Advanced Practitioner Oncol* (2016) 7:91–100. doi: 10.6004/jadpro.2016.7.1.8
21. Yu G, Wang LG, Han Y, He QY. clusterProfiler: An R Package for Comparing Biological Themes Among Gene Clusters. *Omics: J Integr Biol* (2012) 16:284–7. doi: 10.1089/omi.2011.0118
22. Newman AM, Liu CL, Green MR, Gentles AJ, Feng W, Xu Y, et al. Robust Enumeration of Cell Subsets From Tissue Expression Profiles. *Nat Methods* (2015) 12:453–7. doi: 10.1038/nmeth.3337
23. Gu Z, Gu L, Eils R, Schlesner M, Brors B. Circlize Implements and Enhances Circular Visualization in R. *Bioinf (Oxford England)* (2014) 30:2811–2. doi: 10.1093/bioinformatics/btu393
24. Ostrom QT, Gittleman H, Truitt G, Boscia A, Kruchko C, Barnholtz-Sloan JS. Cbtrus Statistical Report: Primary Brain and Other Central Nervous System

Tumors Diagnosed in the United States in 2011-2015. *Neuro-oncology* (2018) 20:iv1–86. doi: 10.1093/neuonc/noy131
25. Gusyatiner O, Hegi ME. Glioma Epigenetics: From Subclassification to Novel Treatment Options. *Semin Cancer Biol* (2018) 51:50–8. doi: 10.1016/j.semcancer.2017.11.010
26. Perry JR, Laperriere N, O'Callaghan CJ, Brandes AA, Menten J, Phillips C, et al. Short-Course Radiation Plus Temozolomide in Elderly Patients With Glioblastoma. *New Engl J Med* (2017) 376:1027–37. doi: 10.1056/NEJMoa1611977
27. Gilbert MR, Dignam JJ, Armstrong TS, Wefel JS, Blumenthal DT, Vogelbaum MA, et al. A Randomized Trial of Bevacizumab for Newly Diagnosed Glioblastoma. *New Engl J Med* (2014) 370:699–708. doi: 10.1056/NEJMoa1308573
28. Miroshnikova YA, Mouw JK, Barnes JM, Pickup MW, Lakins JN, Kim Y, et al. Tissue Mechanics Promote IDH1-dependent Hif1α-Tenascin C Feedback to Regulate Glioblastoma Aggression. *Nat Cell Biol* (2016) 18:1336–45. doi: 10.1038/ncb3429
29. Bai H, Harmancı AS, Erson-Omay EZ, Li J, Coşkun S, Simon M, et al. Integrated Genomic Characterization of IDH1-mutant Glioma Malignant Progression. *Nat Genet* (2016) 48:59–66. doi: 10.1038/ng.3457
30. Du L, Lee JH, Jiang H, Wang C, Wang S, Zheng Z, et al. beta-Catenin Induces Transcriptional Expression of PD-L1 to Promote Glioblastoma Immune Evasion. *J Exp Med* (2020) 217(11):e20191115. doi: 10.1084/jem.20191115
31. Xue S, Hu M, Iyer V, Yu J. Blocking the PD-1/PD-L1 Pathway in Glioma: A Potential New Treatment Strategy. *J Hematol Oncol* (2017) 10:81. doi: 10.1186/s13045-017-0455-6
32. Woroniecka K, Chongsathidkiet P, Rhodin K, Kemeny H, Dechant C, Farber SH, et al. T-Cell Exhaustion Signatures Vary With Tumor Type and Are Severe in Glioblastoma. *Clin Cancer Res* (2018) 24:4175–86. doi: 10.1158/1078-0432.Ccr-17-1846
33. Wei J, Chen P, Gupta P, Ott M, Zamler D, Kassab C, et al. Immune Biology of Glioma-Associated Macrophages and Microglia: Functional and Therapeutic Implications. *Neuro-oncology* (2020) 22:180–94. doi: 10.1093/neuonc/noz212
34. Chen Y, Song Y, Du W, Gong L, Chang H, Zou Z. Tumor-Associated Macrophages: An Accomplice in Solid Tumor Progression. *J Biomed Sci* (2019) 26:78. doi: 10.1186/s12929-019-0568-z

Conflict of Interest: The authors declare that the research was conducted in the absence of any commercial or financial relationships that could be construed as a potential conflict of interest.

frontiers in Oncology

SYSTEMATIC REVIEW
published: 04 June 2021
doi: 10.3389/fonc.2021.665235

Blood-Based Biomarkers for Glioma in the Context of Gliomagenesis: A Systematic Review

*Hamza Ali[1], Romée Harting[1], Ralph de Vries[2], Meedie Ali[1], Thomas Wurdinger[1] and Myron G. Best[1]**

[1] Department of Neurosurgery, Brain Tumor Center Amsterdam, Cancer Center Amsterdam, Amsterdam UMC, VU University Medical Center and Academic Medical Center, Amsterdam, Netherlands, [2] Medical Library, Vrije Universiteit, Amsterdam, Netherlands

OPEN ACCESS

Edited by:
Jose R. Pineda, University of the Basque Country, Spain

Reviewed by:
Lisa Shaw, University of Central Lancashire, United Kingdom
Juan Manuel Sepulveda Sanchez, University Hospital October 12, Spain

***Correspondence:**
Myron G. Best
m.g.best@amsterdamumc.nl

Specialty section:
This article was submitted to Neuro-Oncology and Neurosurgical Oncology, a section of the journal Frontiers in Oncology

Received: *07 February 2021*
Accepted: *18 May 2021*
Published: *04 June 2021*

Citation:
Ali H, Harting R, de Vries R, Ali M, Wurdinger T and Best MG (2021) Blood-Based Biomarkers for Glioma in the Context of Gliomagenesis: A Systematic Review. Front. Oncol. 11:665235. doi: 10.3389/fonc.2021.665235

Background: Gliomas are the most common and aggressive tumors of the central nervous system. A robust and widely used blood-based biomarker for glioma has not yet been identified. In recent years, a plethora of new research on blood-based biomarkers for glial tumors has been published. In this review, we question which molecules, including proteins, nucleic acids, circulating cells, and metabolomics, are most promising blood-based biomarkers for glioma diagnosis, prognosis, monitoring and other purposes, and align them to the seminal processes of cancer.

Methods: The Pubmed and Embase databases were systematically searched. Biomarkers were categorized in the identified biomolecules and biosources. Biomarker characteristics were assessed using the area under the curve (AUC), accuracy, sensitivity and/or specificity values and the degree of statistical significance among the assessed clinical groups was reported.

Results: 7,919 references were identified: 3,596 in PubMed and 4,323 in Embase. Following screening of titles, abstracts and availability of full-text, 262 articles were included in the final systematic review. Panels of multiple biomarkers together consistently reached AUCs >0.8 and accuracies >80% for various purposes but especially for diagnostics. The accuracy of single biomarkers, consisting of only one measurement, was far more variable, but single microRNAs and proteins are generally more promising as compared to other biomarker types.

Conclusion: Panels of microRNAs and proteins are most promising biomarkers, while single biomarkers such as GFAP, IL-10 and individual miRNAs also hold promise. It is possible that panels are more accurate once these are involved in different, complementary cancer-related molecular pathways, because not all pathways may be dysregulated in cancer patients. As biomarkers seem to be increasingly dysregulated in patients with short survival, higher tumor grades and more pathological tumor types, it can be hypothesized that more pathways are dysregulated as the degree of malignancy of the

glial tumor increases. Despite, none of the biomarkers found in the literature search seem to be currently ready for clinical implementation, and most of the studies report only preliminary application of the identified biomarkers. Hence, large-scale validation of currently identified and potential novel biomarkers to show clinical utility is warranted.

Keywords: diagnostics, liquid biopsy, blood, glioblastoma, glioma

INTRODUCTION

Gliomas, and especially glioblastomas, are one of the most devastating primary tumors of the central nervous system with a dismal prognosis. Definite diagnosis of the disease is particularly dependent on tumor tissue assessment, though repetitive collection of tumor tissue to track tumor molecular evolution and/or tumor progression and regression is not desired. Part of such follow-up monitoring can be done *via* (advanced) imaging techniques. Also, the past years a plethora of research has been published in which blood-based biomarkers for glioma were utilized with various purposes. This is in line with the upcoming field of so-called 'liquid biopsies' in other (solid) tumor types. Blood-based biomarkers were found to be helpful as (early) diagnostic markers, including tumor grade and brain disease differentiating markers, prognostic, predictive, and monitoring markers (1–3) in glioma patients. Early diagnostic blood markers are biomarkers that can be utilized to predict development of glioma in individuals years before clinical or radiological signs can be noticed. These markers may be useful to screen patients with familial disorders such as neurofibromatosis type I, Li–Fraumeni syndrome and others that are at risk of development of a glioma (4). The term 'diagnostic marker' in this systematic review implies markers that were used to differentiate between healthy individuals and glioma patients. The terms 'tumor grade and brain disease/tumor type-differentiating markers' are employed to further classify glial tumors in glioma patients. Predictive markers can be employed to predict response to therapy and thus aid in correct therapy selection by examining the expression of histopathological features present in the glial tumor. Lastly, monitoring markers can be used to monitor tumor volume or monitor tumor progression as opposed to pseudoprogression after treatment. Tumor volume monitoring biomarkers that are stated in this review, were mainly used to predict tumor volume pre-treatment, but may also have use as volume monitoring markers after treatment. An example of how the different biomarker types may be employed during the clinical course of a typical glioma patient is detailed in **Figure 1**. Here, the timing of different biomarker types during and before treatment of future glioma patients is illustrated, along a timeline of clinical events in high- and low-grade glioma patients. Currently, it remains unclear which biomarkers or which combination of biomarkers will have most clinical utility. The aim of this systematic review is to identify and highlight the most promising and well-researched blood-based biomarkers for patients with glioma. Identification of a novel biomarker should start with the desired clinical groups to separate in mind. Distinguishing these groups should have clinical relevance, e.g. monitoring progression of lower-grade glioma patients to a secondary glioblastoma thereby tailoring treatment and providing prognostic information, or identification of patients with glioblastoma on treatment that develop tumor pseudo-progression as opposed to true-progression, thereby optimizing treatment schedules. With this, we believe that a promising biomarker should meet several criteria. First, the accuracy of the biomarker should be sufficiently high, measure exactly the difference between the clinically relevant groups without contribution from confounding variables, and adjusted towards its clinical context. For example, a diagnostic biomarker should be very precise, whereas predictive biomarkers should be very specific In order to not withhold patients potential therapeutic options. Second, a biomarker should be resistant to inter- and intra-individual factors, such as diurnal variation, body temperature, comorbidities, medication, radiation therapy, exercise, fasting, sex, and race. Following, the analytical devices that are used to measure the biomarker should be relatively cheap, easy to operate, sensitive in determining low concentrations of biomarker and specific for the biomarker, avoiding false-positive test results. Lastly, the biomarker should have been tested in several (preferably independent) studies with large patient populations, which include independent validation cohorts. Here, we provide a useful and easily accessible overview of the studies performed so far, after which we discuss the most promising markers that may deserve further validation. The review has been subdivided into several biosources and biomolecules as illustrated in **Figure 2**, and will close with a discussion of this dynamic field.

METHODS

Search Strategy and Study Selection

We conducted systematic searches in the bibliographic databases PubMed and Embase from inception up to August 7, 2020. The following terms, including synonyms and closely related words, as index terms or free-text words were used: "Glioma", "Blood", "Biomarkers". These were combined with possible purposes of biomarkers such as prognosis, diagnosis, monitoring and other related terms. Duplicate articles were excluded. The references of the identified articles were searched for relevant publications. The full search strategies for PubMed and Embase can be found in **Supplemental Tables 1** and **2**. Three authors independently screened all potentially relevant titles and abstracts for eligibility. If necessary, the full-text article was reassessed for the eligibility criteria. Differences in judgement were resolved through a

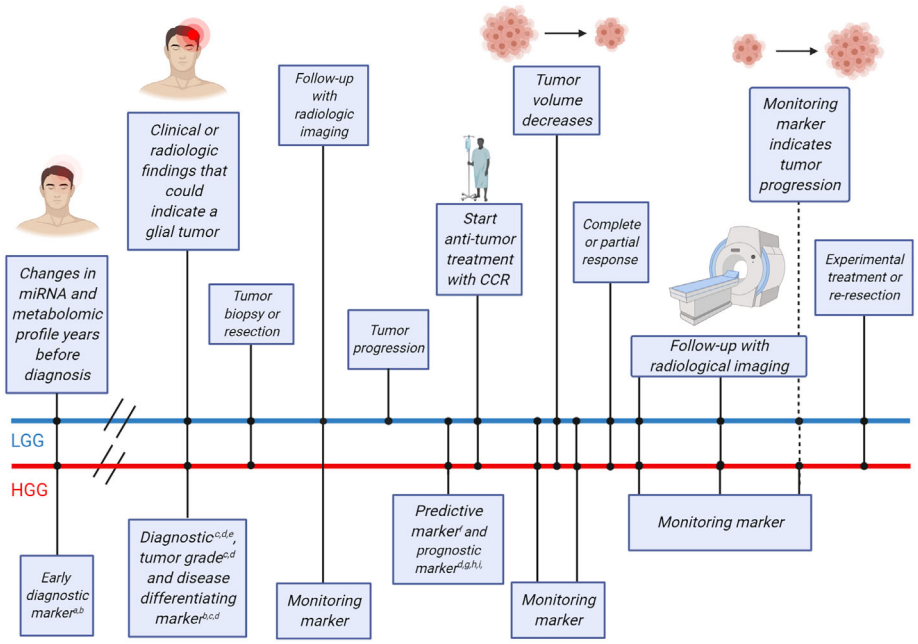

FIGURE 1 | Timeline of clinical events for glioma patients and possible blood-based biomarkers that could be employed at different points in time. The straight lines indicate timelines for two example glioma patients [upper blue line for a lower-grade glioma (LGG) patient, lower red line for a high-grade glioma (HGG) patient]. Clinical events that occur on either timeline are indicated using dots and the clinical events are described in boxes connected to the dots. Early diagnostic markers have been found more than two decades before glioma diagnosis and could be used as a screening tool in the healthy population for patients older than 50 years. At the time of clinical or radiological findings that may indicate the growth of a glial tumor, diagnostic, tumor grade and disease differentiating biomarkers may be used to supplement the diagnostic procedure. Following, surgery (tumor tissue biopsy and/or tumor resection) may be performed, including either tumor resection or only a tumor tissue biopsy for definite histopathological diagnosis. At this point, the brain tumor is identified as a HGG or LGG. Following discussion of the case in a multidisciplinary tumor board, treatment may be initiated in patients with more malignant tumor types, while patients with less malignant tumor types may be subjected to frequent follow-up using monitoring markers and radiological imaging to monitor potential tumor progression. At the moment of tumor progression in patients with less malignant tumors or directly after surgical resection in patients with malignant tumors, predictive markers may provide additional information on the potential benefit of adjuvant treatment. Anti-tumor treatment with conventional chemo- and/or radiotherapy (CCR) is currently usually initiated at this point. Monitoring blood markers can detect tumor volume decrease over time. Patients with complete or partial response can be followed using radiological imaging and monitoring markers to distinguish between tumor progression or pseudoprogression. Patients with stable disease, progressive disease or tumor progression after complete or partial response may be admitted for experimental treatments. For each biomarker purpose, several potential blood-based biomarkers are listed [a]*Tocopherols;* [b]*miR-21;* [c]*GFAP;* [d]*Panels of miRNAs, proteins and metabolites;* [e]*IL-10;* [f]*NLR;* [g]*YKL-40;* [h]*F-NLR;* [i]*F-NLR-AGR.* Figure was adapted from "Cell Transfer Protocol", by BioRender.com (2021). Retrieved from: https://app.biorender.com/biorender-templates.

consensus procedure. Studies were included if they met all of the following criteria: i) Histologically proven glial tumors; ii) Measured biomarker concentrations in whole blood, serum or plasma; iii) Correlation of the biomarkers with at least one of the following: glial tumor diagnosis, glial tumor grade, (glial) tumor type such as astrocytoma or oligodendroglioma, overall survival of patients, glial tumor manifestation prior to diagnosis, and tumor burden; iv) Included measures, such as Area Under the Curve (AUC), accuracy, hazard ratio (HR), sensitivity, specificity values and/or the degree of significance using a p-value. We excluded studies if they i) Reported on biomarkers found in CSF, tumor tissue or other non-hematogenous fluids such as cyst fluid; ii) Were of the following publication types: editorials, letters, interviews, case reports, animal studies, in vitro studies, pediatric studies, or (systematic) reviews; iii) Did not analyze biomarker value in a glioma-only (sub)group; iv) Reported on prognostic biomarkers when patients with glial tumors were treated with experimental treatments; v) Were published in languages other than English; vi) Described biomarker(s) which lacked substantial evidence relative to the biomarker categories. Substantial evidence is quantified as able to differentiate between clinically relevant groups in at least four independent studies. The process of retrieving all articles relevant to our systematic review is summarized in a Preferred Reporting Items for Systematic Reviews and Meta-Analyses (PRISMA) flowchart (see **Figure 3**).

Data Extraction and Study Quality Assessment

Details per study (e.g. biosource and biomolecule), study population type (e.g. glioma or glioblastoma patients) and marker clinical group separating ability quantified as AUC, sensitivity, specificity, accuracy or hazard ratio can be found in the **Supplementary Materials**. In the **Supplementary Tables**, biomarkers are separated by purpose as diagnostic (**Supplemental Tables 3–5**), prognostic (**Supplemental Table 6**),

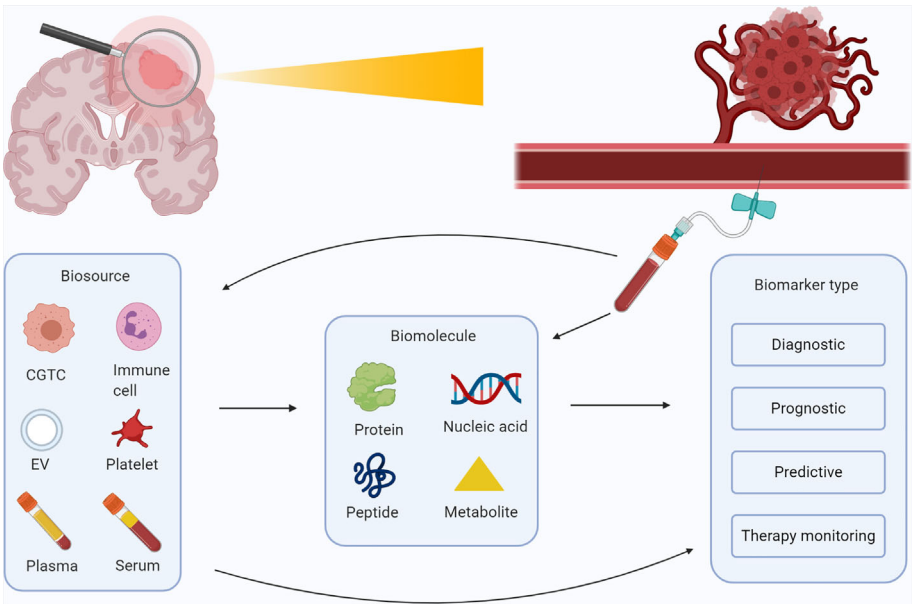

FIGURE 2 | Overview of possible blood-based biomarkers for glioma and their purposes. Schematic overview of the several biosources (plasma, serum, extracellular vesicles, blood platelets, circulating immune cells, and circulating glioma tumor cells) and biomolecules (proteins, nucleic acids, metabolomics and peptides) that are identified for patients with glioma. These biomolecules can be collected in a vial of blood, and employed as a diagnostic, prognostic, predictive, or therapy monitoring marker. Figure was created with BioRender.com.

predictive (**Supplemental Table 7**), and therapy monitoring (**Supplemental Tables 8** and **9**) markers. A separate table with panels of biomarkers and their potential function has been added as well (**Supplemental Table 10**). The summarized methodologies and results of included studies were used to critically assess the quality of the included studies. The evaluation of study quality is discussed in the results section.

RESULTS

Study Selection and Characteristics of Selected Studies

The literature search generated a total of 7,919 references of which 3,596 were identified in PubMed and 4,323 in Embase, of which 262 studies were eligible for inclusion (**Figure 3**). A plethora of biomarkers were identified that could differentiate between clinically relevant patient groups. However, most markers were only found to be dysregulated in one group as compared to the other in only one or two studies. Therefore, we describe in this systematic review only markers that could differentiate between clinically relevant groups with significant results in at least four independent studies. We regarded these as the most promising biomarkers. Many studies did not include large patient or control populations of >100 patients or any validation cohort at all. Also, studies often did not report biomarker accuracies. The markers were divided into four relevant biomolecule groups: proteins, nucleic acids, circulating cells and metabolomics, and the most promising markers within these categories are discussed below. Due to word restrictions, we decided to report on glioma patients in general, and in most cases not per histopathological subtype separately, though we do understand that such separation is of clinical importance. The histopathological classification of gliomas is continuously developing with implementation of multiple (novel) molecular tissue markers (4). Hence, in retrospect it is not always possible to correlate the patients' diagnoses as provided in the identified studies to the current standards. We decided to report the diagnosis as provided in the referenced studies.

PROTEINS AND PEPTIDES

Interleukins

Interleukins (ILs) are a group of cytokine proteins usually secreted by inflammatory cells by means of inter-inflammatory cell communication. Interleukins can promote or inhibit carcinogenesis. It is possible that glial tumors create a protumor environment by actively secreting (5, 6) and/or recruiting brain-resident cells such as microglia to stimulate the secretion of cytokines with pro-tumorigenic functions (7). Interleukins such as IL-1b (8–12), IL-6 (8–10, 13–17) and IL-10 (8, 10, 13, 18–23) have been found to be increased in glioma patients compared to healthy individuals. Accuracies of AUC = 0.9-1.0 (13) and a sensitivity 95% and specificity of 85% (19), have been found. However, IL-1b (21, 24) and IL-6 (21, 22, 25, 26) concentrations were also found to not be changed compared to controls or even decreased in glioma patients compared to

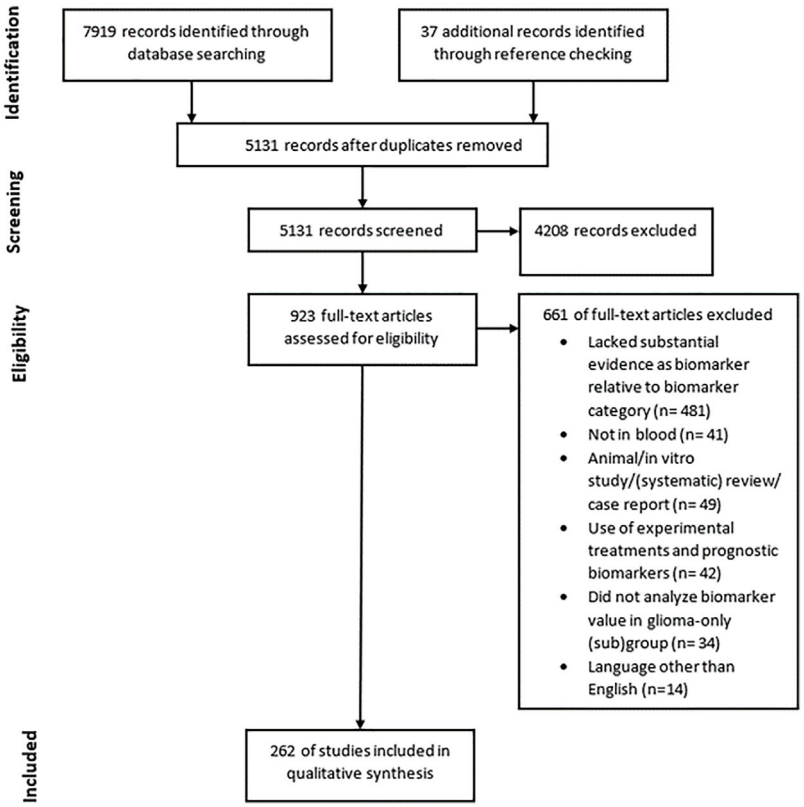

FIGURE 3 | PRISMA diagram showing the amount of records found through database searching and reference checking, the amount of records screened and removed using exclusion criteria and the amount of records included in the final qualitative synthesis.

controls. IL-1b (12) and IL-6 (17) levels may also be increased in patients with higher glioma grades, however other studies could not find a significant difference in IL-6 concentrations between patients with higher and lower glioma grades (25–27). Furthermore, IL-6 (17, 28) and IL-10 (21) have been found to be correlated with worse survival, but other studies could not confirm this for IL-6 (14, 25, 29–31). Thus, interleukins may be potential biomarkers, especially for glioma diagnosis.

S100 Protein Superfamily

Several S100-family members have been reported to contribute *in vivo* to tumor growth, metastasis, angiogenesis and immune invasion (32). Proteins from the S100 protein family including S100A8, S100A9 and S100B have been found to be increased in the blood of glioma patients compared to healthy individuals in multiple studies (33–39). However, it has also been reported that S100B is not changed in glioma patients compared to controls (40). Furthermore, it is unclear whether proteins of the S100-family are correlated with tumor grade (38, 40), tumor volume (39, 40) and survival (34, 41, 42). The accuracy of the inflammatory biomarker S100A8 is promising with a diagnostic AUC of 0.9 in glioblastoma patients (34). Glioblastoma and anaplastic astrocytoma patients could be differentiated with an AUC of 0.7 (34).

TNF Protein Superfamily

Tumor necrosis factor (TNF) was reported to be a major mediator of cancer-related inflammation and is elevated in cancer patients with poor prognosis (43). In vitro studies with glioma cells have shown that TNF can stimulate angiogenesis, downregulate the tumor suppressor gene PTEN and increase glioma cell invasiveness (44). Currently it is unclear whether TNF-alfa and TNF-beta are increased (9, 10, 14, 45), decreased (16, 20) or not changed in the blood of glioma patients (8, 13, 31).

Acute-Phase Reactant Proteins and Other Inflammatory Protein Markers

Acute-phase (reactant) proteins (APRPs) are proteins that become increased (positive APRPs) or decreased (negative APRPs) in serum or plasma by at least 25% in response to an inflammatory stimulus (46). As gliomas and other cancers are characterized by chronic inflammation, it is possible that APRPs are altered in patients with cancer and can be employed as biomarkers. Indeed, in many other cancer types positive APRPs such as α1-antitrypsin and ceruloplasmin have been found to be increased, while negative APRPs such as kininogen and α2-HS glycoprotein are found to be decreased (47). Similarly, in glioma patients many positive APRPs such as haptoglobin (48–51) or CRP (14, 48, 52, 53) were increased compared to healthy

individuals with AUCs around 0.8 (50, 52, 53) (see **Supplemental Table 3**). However, it is not clear whether negative APRPs and markers of reduced inflammation such as albumin, the prognostic nutritional index (PNI) and the albumin-globulin-ratio are decreased or remain unchanged (54, 55). Glioma tumor grade may be correlated with an increase of positive APRPs and a decrease of negative APRPs. The positive APRP fibrinogen was increased in patients with higher tumor grades (56–58) and similar results were also found for the related inflammatory marker F-NLR-AGR (57). The negative APRP marker albumin was decreased (56, 58) in patients with higher tumor grades, as is for the serum markers Albumin-Globulin-Ratio (AGR) and PNI (54–56, 58, 59), but these significant results were refuted in other studies (55, 57). The grade discriminative AUCs of both positive and negative APRPs were between 0.6 and 0.7 (54, 56, 58).

Several positive APRPs have been found to be dysregulated in patients with glioma with longer compared to shorter survival. The inflammatory marker CRP has been found to be decreased in the serum of patients with longer survival (52, 60, 61), but the prognostic value was low [(HR)=1.0] (52). However, significant results could not be confirmed elsewhere despite large patients series and multivariate analyses (14, 28, 62, 63). Furthermore, fibrinogen (56, 57, 64), fibrinogen-NLR score (64), F-NLR-AGR (57) and fibrinogen-albumin score (65) were all increased in glioma patients with worse survival. HRs were between 1.5-3.8 for fibrinogen and its related markers. Negative APRPs and markers of reduced inflammation such as albumin (56, 66–68), AGR (57, 69, 70), PNI (59, 69, 71), and the Sanbo Scoring System (72), were elevated in patients with prolonged survival compared to patients with shorter survival. However, other studies could not find a significant relationship between albumin (70, 71, 73, 74), AGR (75), PNI (74, 76) and survival. Lastly, APRPs may also have use as a marker to differentiate between glioma patients and patients with other intracranial diseases and as markers to detect IDH1-mutation and MGMT-methylation status. However, research on these topics is scarce at this moment. In all, it seems that positive APRPs and markers of increased inflammation are increased while negative APRPs and markers of reduced inflammation are decreased in patients with glial tumors and in particular patients with more malignant glial tumors (see **Supplemental Tables 3**–**8**).

GFAP

Glial fibrillary acidic protein (GFAP) is a protein that is mainly expressed by astrocytes and aids in the maintenance of astrocytic structure and stability. Blood levels of GFAP can be increased after injury of the brain through strokes (77), traumatic brain injuries (78), and after brain surgery, including glioma resection (79–81). The blood levels are typically increased in the context of destruction of glial cells and opening of the blood-brain-barrier. As both usually do not occur in non-acute brain diseases such as multiple sclerosis or brain metastases, GFAP may be a specific marker for gliomas. Indeed, GFAP values (38, 80, 82–85) were found to be elevated in glioblastoma patients, but diagnostic sensitivities were rather variable: between 33% and 86% of glioblastoma had elevated GFAP concentrations (38, 82–86). GFAP diagnostic specificities were more uniform and ranged between 85-100% (80, 82, 84). However, GFAP concentrations were not elevated in the circulation of glioma patients with tumor grades lower than grade IV (80, 82, 85). Furthermore, GFAP was increased in patients with glioblastoma as compared to patients with lower tumor grades (38, 80, 82–85, 87) and in glioblastoma patients compared to patients with other brain pathologies such as brain metastases, meningioma or pituitary adenoma (38, 81, 82, 84–86, 88). Also, GFAP levels were increased in patients with worse survival (80, 84), greater tumor volume (40, 80, 82, 86, 88), higher Ki67 proliferation index and lack of IDH1-mutation (80). However, it was not always confirmed that circulating GFAP is correlated to tumor volume and survival (83). Thus, GFAP is a promising marker and might have value as biomarker for glioblastoma diagnosis, grade and tumor type differentiation.

YKL-40

YKL-40 is a glycoprotein that is secreted by macrophages, chondrocytes and several cancer cell types (89), including glioma cells (90). The exact functions of YKL-40 in cancer are unknown, however, it may stimulate angiogenesis, cell proliferation, prevent cell apoptosis (91), and aid in tissue remodeling during inflammation (89). YKL-40 is found to be increased in cancer and in inflammatory diseases such as Crohn's disease, COPD, ulcerative colitis and others (89). YKL-40 was found to be increased in glioma patients as compared to healthy individuals (86, 92–95). The AUC in one study was 0.9 (93). Furthermore, YKL-40 is increased in patients with high-grade glioma compared to patients with low-grade glioma (93, 94, 96). Also, high baseline YKL-40 and increases in YKL-40 during treatment were correlated with worse survival in glioma patients with hazard ratios between 1-2.2 (25, 95–98). However, it was also found that YKL-40 was not correlated with survival (99) and tumor volume (94, 96, 97). In all, YKL-40 is an interesting marker, especially for predicting patient survival.

VEGF

The vascular endothelial growth factor (VEGF) is one of the growth factors that aids in glioma neovascularization and a well-studied biomarker in glioma patients. VEGF has been researched extensively and has been found to be increased in glioma patients (10, 12, 14, 16, 100–107). However, multiple other studies did not find a significant difference (22, 24, 108–111). The same controversial results were also found in other studies when VEGF was used as a blood biomarker for other purposes such as tumor grade differentiating marker (12, 102, 103, 112, 113), tumor type differentiating marker for patients with glioblastoma and patients with intracranial metastases (103, 104, 114) and prognostic marker in patients that received several types of therapies (14, 19, 29, 31, 112, 115). It remains unclear why such differences have been found. It is possible that patient populations were too small to find a significant effect as both in studies with and without a significant effect of VEGF, most of the studies included small patient populations (<100 patients). Hence, VEGF does not seem to be a promising blood biomarker at this moment.

Coagulation in Glioma

It is well known that cancer causes hypercoagulability that can result in venous thromboembolisms (VTE), disseminated intravascular coagulation and other coagulation disorders. The relation between brain cancer and thrombo-embolic events seems to be especially strong, as brain tumor patients had the second highest rate of thrombo-embolic events from malignancies in 18 organs (116). It is possible that this hypercoagulable state can be retraced in the blood of glioma patients if procoagulant factors are increased while anti-coagulant factors are decreased. It was seen that a multitude of coagulation markers and procoagulant factors were significantly increased in the circulation of glioma patients compared to healthy individuals such as prothrombin factor 1 + 2 (14), tissue factor (117), coagulation factor VII (19) and P-selectin (118). Procoagulant markers correlated with tumor grade and worse prognosis (see **Supplemental Tables 4** and **6**). Especially fibrinogen is well researched and often found to be correlated with grade (56–58) and survival in glioma (56, 57) and glioblastoma (56, 64) patients with moderate grade differentiating abilities (56, 58) and moderate prognostic abilities (HR=1.5) (64). Contrary, anti-clotting factors were also found to be increased (see **Supplemental Tables 3**, **4** and **6**). Here, it may be possible that anti-clotting factors are reactively increased as a response to the prothrombotic state that is created by the tumor. However, it is also possible that the tumor stimulates the increase in anti-thrombotic proteins, as these may facilitate metastasis by degrading the extracellular matrix and allowing tumor cells to invade blood vessels (119).

Panels of Peptides and Proteins

Biomarker panels of two to over 100 markers were used with various purposes in glioma patients. In general, larger panels could differentiate between patients and controls or different patient groups with different grades, tumor types or survival with higher accuracies. Inflammation, immune response and cell proliferation related markers were dysregulated such as interleukins (13), TNF-alfa (13), CRP (52), YKL-40 (86) and FGF-basic (13). Functional analysis revealed enrichment of pathways that are dysregulated in cancer cells such as apoptosis pathways, immune function pathways and others (13, 52). Several protein and peptide panels could differentiate between glioma patients and healthy individuals with high accuracies with sensitivities and specificities >85% (13, 52, 86, 120–123). Only two panels had modest value as diagnostic markers with an AUC of 0.6 (16) and 74% accuracy (124). One protein panel (122) and several proteins or peptides from other panels (120, 123) could also differentiate between glioma patients with different tumor grades. Lastly, panels could differentiate between patients with better and worse prognosis (16, 125), and between patients with different intracranial tumors (123).

NUCLEIC ACIDS

MicroRNAs

miRNAs are short, single-stranded RNAs of approximately 22 nucleotides in length, which bind and regulate translational repression or degradation of messenger and other RNAs (126). MicroRNAs may be ideal blood-based biomarkers as they are easily accessible in body fluids (127), are stable under harsh extrinsic conditions such as significant changes in temperature (128), and are protected from intrinsic conditions such as degradation by RNAses (129). Indeed, microRNAs can be found in biofluids such as serum, plasma, urine and cerebrospinal fluid and have shown to be deregulated in various cancer types such as renal cell carcinoma (130) and melanoma (131). Also, research is accumulating indicating that the blood of glioma patients has a unique miRNA expression pattern. However, it has been noted that miRNAs may not be good biomarkers as the brain has little influence on miRNA concentrations in blood as compared to other organs (132) and because differences in blood cell counts may more prominently influence variation in circulating miRNA profiles (133, 134). Despite that, miR-21 (135–143), miR-182 (144–148) and miR-222 (139, 149, 150) were all found to be increased in the blood of glioma patients as compared to healthy individuals. However, miR-21 (151, 152) and miR-222 (136) were also found to not have significantly different results in patients compared to controls. Diagnostic sensitivities and specificities of the miRNAs in glioma patients ranged from 47% to perfect accuracy (136, 139, 141, 148, 149). miR-21 (136, 139), miR-182 (146, 147) and miR-222 (139) were also correlated with tumor grade and an AUC of 0.8 was reported for miR-21 (139). Furthermore, miR-21 (143) and miR-222 (139) might also have use as a marker to differentiate between glial tumors and other intracranial tumors. Lastly, miR-21 (141), miR-182 (148, 153) and miR-222 (149, 150) may have value as prognostic markers and HRs of 1.3 (148) and 2.8 (149) have been reported. Remarkably, it was also found that miR-21 was upregulated years before glioma manifestation in patients (154).

Panels of microRNAs

In general, combination of microRNAs increased the accuracies of markers as compared to single microRNAs. Small panels of microRNAs which studied marker concentrations in two or three microRNAs could differentiate between glioma patients and controls with an AUC of 0.8 (139) and sensitivities and specificities between 70%-100% (138, 155–157). When larger miRNA panels were used, diagnostic accuracies of tests tended to increase. Using a panel of nine miRNAs as diagnostic markers, 50 and 90 glioma patients could be differentiated from healthy individuals with high accuracy with an AUC of 1.0 (151) and accuracy of 99.8% (137), respectively. However, a 180-miRNA panel in whole blood could distinguish between glioblastoma patients and healthy individuals with 'just' 81% accuracy (158). Patients with glioblastoma could be differentiated from lower grade patients with an AUC of 0.9 (159), also certain miRNA combinations were highly prognostic for glioma patients with HRs of 3.1 (151) and 0.4 (160), or could differentiate between patients with different brain tumors with an AUC of 0.8 (157). Lastly, the development of pulmonary embolisms could be predicted in glioma patients with an AUC of 0.8 (161).

Cell-Free DNA

Cell-free DNA (cfDNA) refers to fragmented DNA freely circulating outside of cells in blood plasma. cfDNA partly consists of DNA derived from tumor cells. cfDNA is often

analyzed by examining circulating DNA from patients and searching whether there are tumor-specific mutations, deletions and/or amplifications present. The majority of cfDNA is released by non-tumor cells including (neighboring) inflammatory, stromal and other (healthy) cells, thereby searching for tumor-derived materials is considered to be a needle in a haystack. While both serum and plasma were used as biosource for cfDNA, it has been reported that serum contains around six times as much amounts of free cfDNA as compared to plasma with low levels of contaminating extraneous DNA released from leukocytes (162). Evidence is accumulating that the amount of cfDNA molecules and individual sequences of cfDNA can be employed as tumor biomarkers. First, it has been shown that total number of cfDNA molecules can be used as diagnostic marker to differentiate between glioma patients and controls (163, 164), tumor type differentiating marker (163), tumor progression marker (165), and prognostic marker (164). However, it remains unclear whether total cfDNA can also be used as a marker to estimate and monitor tumor burden (164–166). Furthermore, mutations and copy number variations in cfDNA can also be utilized to differentiate between glioma patients and controls (164, 166–170). Diagnostic sensitivities ranged from 50% to near perfect accuracies. Especially selection of cfDNA fragments between 90-150 base-pairs drastically improved detection accuracies. Moreover, mutations in therapeutically relevant genes such as TP53 and EGFR could also be found in cfDNA (164, 167) but were not always concordant with mutations in tumor tissue.

An alternative and highly potential biomarker may be methylation patterns in cfDNA of glioma patients. DNA methylation is one of three epigenetic mechanisms used to alter gene expression and can contribute to cancer development through regional hypermethylation and global hypomethylation (171). Methylation of tumor suppressor genes can silence tumor suppressor genes, while global hypomethylation of repetitive genomic elements can lead to elevated expression of oncogenes and chromosomal instability (171). In cfDNA of glioma patients, global hypomethylation of repetitive Alu elements and regional methylation of tumor suppressor genes such as MGMT were studied. Global hypomethylation of Alu elements was correlated with glioma diagnosis, higher tumor grade, shorter survival and lower Karnofsky Performance Score (172, 173). Also, it was recently reported that cfDNA methylation profiles have remarkable diagnostic capabilities in high-grade as well as in low-grade glioma with AUCs near 1.0. cfDNA methylation profiles also displayed high brain tumor differentiating capabilities with AUCs between 0.7-0.8 (174). Concordance of promoter methylation in tumor suppressor genes such as MGMT in cfDNA with their counterparts inside tumors, was observed with varying sensitivities 31%-80% but with high specificities all near 100% (175–182). Lastly, lack of MGMT promoter methylation in cfDNA could be used as a prognostic marker with hazard ratios between 2.0-2.2 (180, 182). While cfDNA methylation methods are of interest as markers with multiple purposes, so far the patient populations in which these methods were studied were often small (50 or less patients).

CIRCULATING CELLS, EXTRACELLULAR VESICLES, AND METABOLOMICS

Circulating Glioma Cells

It has been suggested that circulating tumor cells (CTCs) are the driving cells of tumor metastasis. Extracranial metastases occur very rarely in patients with glioma and with an (estimated) incidence of less than 0.5% (183, 184). Despite this, several research efforts have been investigating the existence of circulating glial tumor cells (CGTCs) using a variety of methods, with highly variable results. Diagnostic sensitivities were reported between 21%-80% (185–192). Apart from diagnosis, CGTCs might also have other purposes. However, the cells were often not correlated with tumor grade (187, 190, 192), survival (188) or tumor burden (189) and they could not be used to differentiate between different glial tumor types (187). Interestingly, CGTCs have also been investigated as a tool to differentiate between tumor recurrence and radiation necrosis (192), and to differentiate between pseudoprogression and actual tumor progression (186, 190, 191), though such applications are definitely not ready for implementation in the current daily clinics.

Blood Platelets

It is well documented that platelets influence cancer cells in multiple ways, for example, platelets are known to promote tumor angiogenesis, tumor cell proliferation, metastasis and aid in immune surveillance escape of tumor cells (193). Because platelets stimulate tumor activities to a large degree, it is possible that platelet counts and content are altered as well in patients with glioma. However, currently platelet counts have variable results as biomarkers in glioma. Platelet counts were found to be increased in glioma patients (93, 100, 194) as well as non-significantly changed (54, 55, 118, 194) compared to healthy individuals. In most studies, platelets were observed to be non-significantly altered in patients with higher grade glioma compared to lower grade glioma (54, 58, 93, 195–197). Furthermore, there is overwhelming evidence that platelet counts are not correlated with patient prognosis in glioma patients (62, 70, 71, 93, 198–205). Moreover, platelet counts are not different in glioma patients as compared to other intracranial pathologies such as epilepsy and non-glial brain tumors (54, 206, 207). Aside platelet counts, researchers, amongst us, have noted that platelets may have altered protein content (208) and RNA content, due to sequestration of tumor-derived RNAs. The RNA content of these so-called 'tumor-educated-platelets' (TEPs) may be employed to distinguish cancer patients from healthy individuals (209). Also other research groups have confirmed that TEPs have good accuracy in distinguishing between healthy individuals and patients with various types of cancer (210–214). There are many obstacles that can interfere with the results of the TEPs such as age-related factors (215, 216), pre-analytical variables, and inflammatory and cardiovascular disease (217). Despite this, our data suggests that platelet RNA profiles may be employed for diagnostics of lower-grade glioma and glioblastoma, and potentially tumor

treatment monitoring (209, 218, 219). Hence, platelets may contain promising information regarding the presence and treatment response of glioma.

White Blood Cells

In glioma patients it was often observed that WBC counts were increased compared to controls (21, 54, 55, 100, 118, 220). However, it was also found that leukocytes are not significantly changed in glioma patients compared to controls (21, 194), potentially due to dexamethasone use (221–224). Furthermore, it remains unclear whether WBCs are correlated with higher tumor grades (54, 55, 195, 201, 225, 226) and worse survival (23, 61, 62, 71, 201, 227) as many studies reported both statistically significant and non-significant results (144). Moreover, it was found that leukocyte counts were increased in glioma patients compared to patients with neuromas (54), non-lesional epilepsy (54) and meningioma (54, 161) and lack of IDH-mutation (201). However, it was also found that WBCs are not different in glioma as compared to meningioma patients (55). At this moment, total white blood cell counts are not considered promising as a blood-based marker for glioma.

Lymphocytes

Lymphocytes mainly consist out of three groups: T-cells (CD-3+), B-cells (CD-20+) and NK-cells (CD-56+). It was found in multiples studies that total lymphocyte numbers are not changed in glioma patients as compared to controls (21, 55, 100, 194, 228, 229). However, significant decreases in total lymphocytes were noted as well in glioma patients (54, 206, 228). This significant decrease might be attributed partly due to the use of dexamethasone (229). Total lymphocyte counts were lower in patients with higher tumor grades (54, 55, 196, 197, 201) and one study reported a tumor grade differentiating AUC of 0.6. Also, many studies reported that total lymphocyte numbers were not correlated with survival in glioma patients (62, 70, 71, 74, 198, 201, 202, 204, 205, 227, 230–233) though two studies reported that increased numbers of total lymphocytes were associated with prolonged survival (234, 235). Furthermore, total lymphocytes were not changed in glioma patients as compared to patients with brain metastases (206, 207), but it remains unclear whether total lymphocytes are changed in glioma patients as compared to meningioma (54, 55, 206) and epilepsy patients (54, 206). However, lymphocytes were also not correlated to tumor grade in two other studies (58, 196) or with IDH-1/2 mutation status (201, 236).

Total T-cells numbers were seen to be significantly decreased in glioma patients in multiple studies with high statistical significance (20, 21, 23, 229, 237, 238). Two other studies did not find a difference in malignant glioma patients (21, 24). Corticosteroids usually did not influence total T-cell counts (21, 23, 223), however, in one study corticosteroids did cause a significant decrease in CD3+-cell counts (229). Thus, more research is needed to determine whether CD3+ cells are altered in glioma patients. It may be possible that T-cells are decreased because of a decrease in CD4+-cells, which has often been reported in glioma patients (20, 21, 23, 229, 238–240). However, other studies did not find a significant difference between glioma patients and controls (21, 241, 242) in terms of CD4+-counts in blood. CD4+-cells have been found to be negatively correlated with glial tumor grade (20, 243) as well as to not be correlated with increasing tumor grades in glioma patients. Decrease in CD4+-cell counts was inversely related to survival in glioma patients (233, 243), but not related to IDH1-status (236).

There is little evidence for NK-cells as blood-based glioma biomarker. In several studies NK-cells (CD3+/CD56+, CD3-/CD56+ or CD16+/CD56+) were not significantly altered as compared to healthy individuals in glioma patients (23, 229, 244, 245). However, certain NK-cell populations were seen to be significantly decreased (23, 245) or increased (238) in glioma patients. Also, CD16+/CD56+-NK-cells had prognostic value (23). CD8+-cell counts were not altered in glioma patients in most studies (21, 238, 239, 242). It remains unclear whether CD8-cell counts are correlated with patient survival (23, 233) and lower tumor grades (20). There is a lot of controversial evidence concerning the value of lymphocytes and subpopulations of lymphocytes as biomarkers in glioma and glioblastoma patients. However, the majority of studies agree that total T-cells and CD4+-cells may be promising as a diagnostic marker.

Neutrophils

Neutrophils were found to be increased in glioma patients compared to controls in the majority of the studies (21, 54, 55, 194, 220). Furthermore, higher-grade glioma patients were often reported to have increased neutrophil counts as compared to patients with lower-grade glioma (54, 55, 58, 196, 197, 201, 226, 246). Grade differentiating AUCs between 0.6-0.7 were reported (55, 58, 201). It remains unclear whether neutrophils are related to IDH mutation status (201, 236). Moreover, glioma patients had higher neutrophils compared to patients with a meningioma (54, 161), neuromas (54) or epilepsy (54, 206). It was also found that there was no difference between glioma or glioblastoma patients and meningioma patients (55, 206), between glioma or glioblastoma and metastases (206, 207) and grade III and grade IV glioma patients (227) in terms of neutrophil counts. Multiple studies reported that neutrophil counts had no prognostic value in glioma patients (62, 70, 71, 198, 204, 205, 230, 234), however, other studies found a negative correlation of neutrophil counts with survival in glioma (201, 227, 231, 247) with HRs around 1.6 (227, 231). Thus, neutrophil count might be valuable as diagnostic and grade differentiating marker.

Monocytes

It remains unclear whether monocyte counts (CD14+-cells and/or CD16+-cells) are changed in glioma patients compared to controls (54, 55, 106, 194, 229, 244, 248) or are related to tumor grade (54, 55, 58, 197, 225, 246). However, monocytes with reduced immune function and with mainly immunosuppressive functions such as M2-macrophages (245, 249, 250) and HLA-DR-low and HLA-DR-negative monocytes were significantly increased in glioma patients as compared to controls (21, 244, 251), but cell counts might be confounded by dexamethasone use (229). Also, less pro-inflammatory M1-macrophages were

observed in glioma patients (249, 250). Total monocyte counts could not be correlated to prognosis (62, 71, 227, 231). Monocytes were found to not be different in glioblastoma patients as compared to patients with brain metastases (207) and increased in glioma patients compared to epilepsy (54), meningioma (54, 55), or acoustic neuroma (54).

Neutrophil-Lymphocyte-Ratio

The Neutrophil-lymphocyte-ratio (NLR) may be a promising marker for multiple types of cancers (252–255) and has the potential to fulfill various biomarker roles. It is unclear how the NLR can be dysregulated. However, a hypothesis is that tumors, including glioblastoma (256), secrete hematopoietic factors such as granulocyte-colony stimulating factor, granulocyte macrophage-colony stimulating factor and IL-1 and IL-6, which stimulate proliferation of neutrophils (257, 258). Also, tumors can secrete neutrophil attractant chemokines (259) and turn neutrophils from foe into friend *via* the secretion of TGF-beta (260). Tumor-associated neutrophils can stimulate vascularization of the tumor and inhibit lymphocyte function, weakening the antitumor response (261). NLR and the derived NLR (dNLR; absolute neutrophil count/(WBC count minus absolute neutrophil count) were increased in glioma patients compared to controls (54, 55, 194, 206, 262). Glioma patients with low NLR or derived NLR had longer survival in multiple studies with large patient populations (57, 63, 64, 69, 75, 93, 201, 203, 204, 225, 226, 230, 234, 262–269) with HRs mostly between 1.7 and 2.4. On the contrary, multiple studies including those with larger patient populations could not find a correlation between NLR and survival in glioma patients (62, 71, 198, 200, 205, 227, 247, 270). Furthermore, there is overwhelming evidence that NLR is significantly increased in patients with higher-grade glioma as compared to patients with lower-grade glioma (54–57, 93, 195, 197, 200, 201, 213, 266, 271, 272). The AUC to differentiate between patients with higher-grade and lower-grade glioma was mostly between 0.6 and 0.7. It remains unclear whether NLR values are increased in glioma patients compared to patients with meningioma (54, 55, 206) or intracerebral metastases (206, 207), although it may be increased as compared to patients with epilepsy (54, 206) or acoustic neuroma (54). Also, NLR values might be correlated with IDH-mutation status (56, 63, 69, 201, 225, 226, 267) and increased tissue Ki-67 expression (267, 271). Finally, high NLR correlated with tumor relapse (264), and decrease in NLR during treatment with radiotherapy and concomitant temozolomide was correlated with pseudoprogression (265). To conclude, NLR might be correlated with clinicopathological markers, survival and tumor grade. However, there is a lot of conflicting evidence for most of these markers. There is overwhelming evidence that NLR is related to tumor grade, but the accuracies reported are too limited to apply NLR as a definite diagnostics biomarker in the clinics.

Platelet-Lymphocyte-Ratio and Monocyte-Lymphocyte Ratio

It remains unclear whether the platelet-lymphocyte-ratio (PLR) and monocyte-lymphocyte-ratio may have use as a blood-based marker in glioma. Controversial results have been found for both PLR (54, 55, 206) and MLR (54, 194) as diagnostic markers to differentiate between glioma patients and controls. Similar controversial results have also been found for PLR (54–56, 197, 201, 263, 266, 271) and MLR (54, 58, 197, 266, 271) as tumor grade differentiating markers. PLR (63, 64, 69, 71, 75, 198, 204, 205, 263, 266, 267, 269) as well as MLR (69, 71, 75, 267, 271) were found to not be prognostic in glioma patients in the majority of studies. However, PLR and MLR might have some value as brain disease differentiating marker for glioma patients as these markers were significantly different in glioma patients as compared to patients with epilepsy (54, 206) and non-glial brain malignancies metastases (54, 55, 206, 207). Both markers were rarely correlated with tumor tissue IDH-mutation (56, 63, 69, 201, 267) or MGMT-methylation status, and Ki-67 proliferation index (267, 271).

Systemic Immune Inflammation Index

The systemic immune inflammation (SII) index can be calculated as follows: platelets * (neutrophils/lymphocytes). A high SII-index was correlated with short survival in patients with different cancer types (273–275). In glioma, an increased SII-index was found in patients with higher tumor grades (58, 70, 195, 196) with AUCs of 0.6-0.8 (58, 196), respectively. The SII-index was correlated with poorer prognosis (70, 267), and patients with tumors with higher tissue Ki-67 proliferation index (196), but was not correlated with tumor size (70).

Dendritic Cells

Dendritic cells are antigen presenting cells that can present antigens for example from tumor cells to T-cells, which subsequently activates these T-cells. Total dendritic cells and its subpopulations (myeloid/conventional dendritic cells and plasmacytoid dendritic cells) were found to be decreased in blood of glioma patients compared to controls (21, 243, 276), and these cell populations were also decreased in glioblastoma patients compared to patients with lower tumor grades (243). Furthermore, it was reported that an immature dendritic cell population with increased immunoinhibitory effects on cells (277) becomes increased in glioma patients, especially in patients with higher tumor grades (243). Therefore, glial tumors might actively weaken a patient's immune system.

Myeloid-Derived Suppressor Cells

Myeloid-derived suppressor cells (MDSCs) are immunoinhibitory cells originating from monocytes. MDSCs might be formed during direct cell-cell contact with tumor cells possibly during infiltration of the glial tumor (106). There are variable results concerning in which glioma patients MDSC counts are changed. Total MDSCs (33, 278–280), monocytic MDSCs (21, 33, 280, 281) and granulocytic MDSCs (33, 278–281) were often significantly increased in glioblastoma patients but non-significantly altered in patients with lower grades. Furthermore, MDSCs were increased in patients with poor prognosis (30) and in glioblastoma patients as compared to other patients with intracranial tumors such as anaplastic glioma or meningioma (251).

Regulatory T-Cells

Tregs are known for their immunosuppressive functions (282) and have been shown to be associated with poor patient prognosis in various cancer types (283). Tregs have been found to be significantly increased in the blood of glioblastoma patients as compared to healthy individuals (23, 229, 240, 284, 285). However, Tregs were also found to be non-significantly altered in glioma (21, 23, 241, 286) or even significantly decreased (237, 240).

Extracellular Vesicles

Extracellular vesicles (EVs) are microparticles that are 30 to 10.000 nanometer in diameter. These vesicles are released by cells and can carry proteins, lipids and nucleic acids from one cell to another, thereby facilitating communication between cells (287). Extracellular vesicles can be released from the plasma membrane itself as microvesicles or can be released after fusion of endosomes inside a cell with the plasma membrane as exosomes (288). In glioma patients numbers of EVs (289, 290), microparticles (291) and exosomes (292) in blood were increased as compared to healthy individuals. EVs could potentially also be used as markers for tumor relapse (289) or tumor progression as opposed to pseudoprogression (293). Furthermore, the cargo of EVs can be employed as biomarkers. The protein cargo level – that is the total amount of protein loaded – from glioma patients might have value as diagnostic marker (294, 295). Also, the protein cargo itself is dysregulated and can be used to differentiate between a group of healthy individuals and patients with less malignant glial tumors, which have similar protein cargo, and patients with highly malignant glial tumors (296). EV protein cargo from glioblastoma patients was enriched in proteins that were associated with inflammation, immune response, members of the complement coagulation cascade and others (289). Other studies found a decrease in immune system related proteins IFN-γ, IL-10, and IL-3 within plasma exosomes from glioma patients (292). Furthermore, RNA inside exosomes may increase tumor cell invasion and repress apoptosis (297). Lastly, the surface protein profile of EVs are dysregulated (298, 299) and can be used as biomarkers to differentiate between glioma patients and healthy individuals with high accuracy.

Single Metabolites and Metabolomic Panels

Metabolomics is the analysis of small molecules in a biofluid, cell, tissue, organ or organism (300) and can be used to study metabolic pathways within the organism. Combinations of metabolites such as creatine, glucose and lactate could differentiate patients with brain tumors, glioblastoma, oligodendroglioma, glial tumor, or astrocytoma from healthy individuals with very high accuracy (AUC: 0.9-1.0) (301). Patients with higher grade and lower grade tumors could be differentiated with AUC of 0.7 (301) or 91% accuracy (302). Tumor type differentiating metabolomic panels had variable accuracies with AUCs between 0.4-0.8 (301, 303). Tumor tissue IDH-mutation status could be predicted with an accuracy of 94% (302). Single metabolites (303, 304) and metabolite combinations (303) could predict survival of glioma patients, even with near perfect accuracies. Remarkably, serum metabolites such as tocopherols were found in two studies that could predict glioblastoma up to 22 years before manifestation (305) and glioma patients up to 9 years before manifestation (306). The metabolic pathways that were dysregulated were often involved energy metabolism including amino acid metabolism (302, 303, 306, 307), lipid metabolism (303, 306, 307), nucleic acid metabolism (302) and carbohydrate metabolism (302, 306, 307). Glucose and lactate in particular are interesting markers and had value as blood biomarkers with several purposes, possibly due to their role in the Warburg effect. Glucose levels were reported to be increased in patients with higher tumor grades (308) or worse survival (308–311). One study reported that this was independent of the degree of disability, tumor grade, diabetes, prolonged dexamethasone use, or subsequent treatment modalities (309). Furthermore, it has been found that glucose was related to tumor progression and it was higher in patients with glial brain tumors such as glioblastoma and oligodendrogliomas, but not in meningioma, as compared to healthy individuals (301). Pre-treatment lactate levels (302, 312, 313) were increased in patients with high-grade glioma compared to low-grade glioma patients with AUCs of 0.7 (312) and 1.0 (313), and could potentially also be used as a diagnostic marker (307).

Assessment of Risk of Bias and Reproducibility of Included Studies

Using summaries of the methodology and results of the studies that we referenced here (see **Supplemental Tables 3–9**), we assessed risk of bias in the biomarker studies, similar to some degree to the QUADAS-2 (314) and REMARK (315) guidelines for quality assessment of diagnostic and prognostic biomarker studies. We noted several limitations in the studies that were reviewed concerning study population size, presentation of results and registration of effect of intrinsic and extrinsic factors that could influence marker levels. Apart from markers that are measured on a routine basis such as some APRPs or inflammatory cell populations in clinical chemistry labs, the study populations of markers are often small (often <100 individuals included). Also, small validation cohorts are used or validation cohorts were not included at all. Primarily glioblastoma patients are included in the studies that we referenced here. Patients with lower-grade gliomas are rarely included or comprise a small portion of the entire patient population. Therefore, it is unclear whether the biomarkers that we selected as being most promising, will be of value in particularly these patients. Furthermore, the majority of studies only reported the p-values of biomarkers and not the value of biomarkers quantified as accuracy, sensitivity, specificity and/or hazard ratio, and these could not be deduced from the available and presented data. Therefore, it is unclear what the clinical value of most biomarkers is. Lastly, it is largely unknown to what extent biomarkers are affected by extrinsic factors such as anti-tumor therapy, use of (co-)medication, choice of analytical methods, and by intra-individual factors such as race,

comorbidities and others. Co-medication use by patients before sampling, such as corticosteroid use, is reported in some studies. Use of other medication, e.g. anti-diabetic and anti-epileptic drugs, is rarely reported. Most studies that reported use of these drugs did not (statistically) analyze the effect of these drugs on the biomarkers that were studied, a potential bias that should be taken into account when interpreting these data.

In order to assess the potential reproducibility, and ultimately clinical validation, of the most promising markers GFAP, IL-10, and miR-21, we precisely evaluated the available studies using dedicated guidelines. The MIQE guideline was employed for the miRNA (316), whereas we had to adjust existing guidelines to assess the studies for GFAP and IL-10 (**Supplementary Table 12**), as to the best of our knowledge no such guidelines are available for ELISA/immunoassays. As can be seen in **Supplementary Figure 1**, for GFAP and IL-10 essential factors of the study design such as the number of included patients, protein detection methods and kits were almost always mentioned. However, other important factors such as the used (analytical) instrumentation, sample storage and sample preparation procedures were rarely reported. Also, it was often not reported whether samples were quality controlled by evaluating intra-assay and inter-assay variability. Furthermore, test accuracy is often not reported which makes it unclear whether the tests will have value in the clinical settings. Lastly, factors such as comedication use, histopathological marker presence and tumor volume are rarely reported, which can have significant impact on biomarker concentrations. For miR-21, several categories of the guidelines were often sufficiently described such as experimental design, sample processing and storage. However, other categories such as 'nucleic acid extraction', 'qPCR target information' and 'qPCR protocol' were rarely sufficiently described or not described at all (**Supplementary Figure 2**). In all, it again highlights that adequate reporting of employed methods is of importance to ensure reproducibility of the identified biomarker.

Thus, it can be concluded that there is room for improvement in biomarker studies in multiple domains of methodology and results presentation, as has been reported by other (systematic) reviews (317–319). The biomarker studies that we referenced here may not be of the highest possible quality and cannot be used to determine immediately which biomarkers will have clinical value. However, they can still be used to determine which biomarkers are promising for further research, as markers that have shown great clinical group differentiating abilities in multiple studies may still hold clinical value despite the bias in results and methodologies present in the studies.

DISCUSSION

Glioma is still one of the most devastating diseases with high burden. Any additional information that can be obtained from the patient regarding tumor development, growth, behavior, and vulnerabilities, in a least minimally invasive way is desired. Many studies have been published, and included in this systematic review, that identified potential circulating biomarkers for patients with glioma, at each point in the glioma patients clinical course (**Figure 1**). Unfortunately, none of the biomarkers is in our opinion ready for direct clinical implementation.

As opposed to tumor tissue biomarkers, such as MGMT methylation, 1p/19q codeletion, IDH1-mutations, and the recently introduced methylation profiling (320) in glioma, blood-based markers often reflect local or systemic responses of the endogenous processes to the presence of a tumor. Direct measurement of glioma-derived circulating cells and genomic aberrations is an exception in this view. Cells, cell ratios and APRPs that are often measured in complete blood counts (CBCs), are attractive biomarkers as CBCs are regularly used in the clinic and extensive research has already been performed on their utility as biomarkers. However, they are possibly insufficiently accurate biomarkers for clinical utility as a single marker or in combination with other cells, cell ratios or APRPs. An explanation for the worse performance of single markers as opposed to panels of markers may be interpreted using the framework of hallmarks and enabling characteristics of cancer, as formulated in the seminal article by Hanahan and Weinberg (321). Hallmarks are traits unique to cancer cells and enabling characteristics are traits that lead to the development of such hallmarks. In this framework, blood biomarkers including VEGF, miR-182 and YKL-40 may be mediating factors that enable cancer cells to contain the hallmarks 'inducing angiogenesis', 'resisting cell death' and 'tissue invasion'. Other biomarkers such as lactate concentrations and CGTC can be seen as an expression of the hallmarks or enabling characteristics 'deregulated cellular energetics' and 'activating invasion and metastasis'. Inflammatory cells may be promoting the enabling characteristic 'tumor promoting inflammation' (see **Supplemental Table 11** and **Figure 4**). As single blood markers have low to modest accuracies and value as biomarkers but panels of biomarkers often have higher accuracies, it can be hypothesized that screening of multiple markers involved in multiple hallmarks or enabling characteristics may improve biomarker accuracy. This hypothesis can be supported by the fact that diagnostic sensitivity of inflammatory cells such as NLR, PLR, neutrophils and others is limited with diagnostic and tumor grade and tumor type differentiating AUCs between 0.6-0.7 (54–56, 58, 201). Similar results also have been found for APRPs with AUCs between 0.5-0.7 (54–56, 58). Combination of inflammatory cell populations (54, 56, 58) or APRPs (56), as well as combination of inflammatory cell populations with APRPs (54, 56), does not increase accuracy in a meaningful way (144). Thus, it is possible that both APRPs as well as inflammatory cell populations already reflect alterations in the inflammation enabling characteristic and combination of these markers does not further improve marker accuracies. Also, panels of biomarkers often have higher accuracies than single biomarkers irrespective of the biomarker function and these panels contain biomarkers involved in multiple pathways related to the hallmarks of cancer and its enabling characteristics (13, 52, 155). Furthermore, our analysis indicates that biomarker levels become increasingly dysregulated as tumors increase in

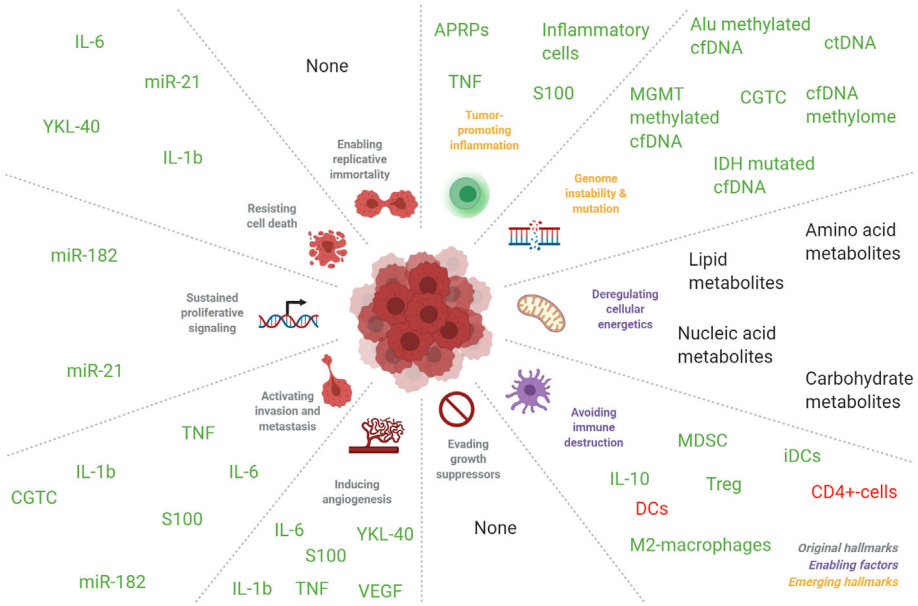

FIGURE 4 | Correlation of blood-based biomarkers in patients with glioma with seminal events in tumorigenesis. Blood biomarkers in glioma patients are implicated in the molecular pathways as detailed by Hanahan and Weinberg (321). Markers colored in green were mostly found to be increased in the circulation of glioma patients compared to healthy individuals, and in glioma patients with more malignant tumors compared to patients with less malignant tumors. Markers that were inversely correlated were colored in red. Markers without color were found to be either significantly increased or decreased in the formerly mentioned groups. The abbreviation "DC" indicates dendritic cells and "iDC" indicates immature dendritic cells. Adapted from "Hallmarks of Cancer: Circle", by BioRender.com (2021). Retrieved from: https://app.biorender.com/biorender-templates.

TABLE 1 | Advantages and disadvantages of the biomarkers.

Nucleic acids (miRNA, cfDNA, RNA, DNA methylation)	
Advantages	**Disadvantages**
If well-designed highly specific	Long turn-around when using next-generation sequencing approaches
For certain methods such as digital droplet PCR highly sensitive, also depending on patient population and tumor stage	Expensive test requirements, esp. with next-generation sequencing
Measurements can be multiplexed and analysis of panels is possible	Requires high-quality RNA isolates
Well-established isolation and detection methods	Clonal hematopoiesis may confound mutation analysis
Provides information on (epi)genomic and transcriptomic levels	May not provide actionable information
Proteins and peptides	
Advantages	**Disadvantages**
Long-term experience with protein-based tests in current clinical practice	Can be less specific
Usually low costs for tests	Limited stability
Easily standardized protocols	
Sensitive test methodologies	
Circulating cells (white blood cells, blood platelets, lymphocytes, etc.)	
Advantages	**Disadvantages**
Measurement routinely available in clinical chemistry labs	Reduced specificity
Rapid test results	No direct measurement of tumor-derived materials; surrogate markers
	Some circulating cells, esp. immune cells, require more specialized isolation and quantification methodologies
Circulating glioma cells and extracellular vesicles	
Advantages	**Disadvantages**
Directly tumor-derived markers, therefore highly specific	May require expensive, technically-challenging, and time-consuming isolation procedures
Enables for testing of panels of (genetic) markers	No gold standard for isolation
Protects markers from degrading enzymes in plasma	Reduced sensitivity, esp. in lower tumor stages
Circulating glioma cells may allow for functional analysis and drug screens	Long turn-around when using next-generation sequencing approaches

malignancy, as biomarker levels are often positively correlated with tumor grade, worse survival and/or more malignant tumor types. Therefore, cellular hallmarks might develop in more cancer cells as tumor malignancy increases and this may be reflected in the dysregulation of circulating biomarkers. With this in mind, we propose to introduce multi-biosource, multi-biomolecule-based blood tests for glioma patients. Keeping the criteria for biomarker test development as discussed above in mind, such tests may likely include (components of) a miRNA, protein, or platelet RNA panel, perhaps including the already promising single markers miR-21, IL-10, and GFAP. These panels likely include multiple components of the tumor progression, are less resistant to confounding variables due to its high dimensions, and far more accurate than a single measured biomarker. Also, complementary implementation of several biomarker types may make synergistically use of each other's advantages, and perhaps at least partially reduce each other's disadvantages (**Table 1**) (144).

Hence, additional validation of the currently most promising markers (**Figure 4**) is also required. Aside analysis of blood, other biofluids such as urine or perhaps cerebrospinal fluid may also be rich sources of biomarkers. Recent analysis has shown that tumor evolution could be tracked *via* repeated CSF samplings (322). Similarly, perhaps also other body fluids such as saliva, sputum, or breathing air may contain molecular information traceable to a primary glioma. We believe that blood-based biomarkers may currently only at maximum complement the current methods to diagnose and/or monitor a glioma, such as clinical symptoms, imaging, and tissue collection *via* tumor resection or (stereotactic) biopsy. It may very well be anticipated that blood-based biomarkers are included in a future setting in clinical decision making, for example in multidisciplinary tumor boards, once such biomarkers are thoroughly validated. For this, systematic biobanking of blood from glioma patients is required. Such biobanking requires research funds that support these efforts, as well as research project that in a dedicated way screen for relevant and valuable biomarkers in well-annotated, large, and homogeneous patient series. It is of importance that any future biomarker discovery or validation research is reported according to the highest standards, facilitating reproducibility of the found results. Alternatively, we believe that any clinical trial, even in a phase 1 stage, should include a blood-biomarker branch in the trial design, in order to at least aim to discover a companion diagnostics biomarker. Also, blood-based biomarkers that may complement current imaging methods for the identification of true tumor progression versus pseudo-tumor progression is required.

In all, the glioma research community should be encouraged towards additional identification and inclusion of blood-based biomarker research in a clinical setting. While currently at the stage of analytical validation and start of clinical validation, further studies should focus on demonstrating its clinical utility.

DATA AVAILABILITY STATEMENT

The original contributions presented in the study are included in the article/**Supplementary Material**. Further inquiries can be directed to the corresponding author.

AUTHOR CONTRIBUTIONS

HA, RH, and MGB developed the search strategy and developed the selection criteria. HA, RH, and MA selected studies for inclusion through title, abstract, and full-text screening. HA, TW, and MGB drafted the manuscript. All authors contributed to the article and approved the submitted version.

FUNDING

Financial support was provided by stichting STOPHersentumoren.nl (TW and MGB).

SUPPLEMENTARY MATERIAL

The Supplementary Material for this article can be found online at: https://www.frontiersin.org/articles/10.3389/fonc.2021.665235/full#supplementary-material

REFERENCES

1. Best MG, Sol N, Zijl S, Reijneveld JC, Wesseling P, Wurdinger T. Liquid Biopsies in Patients With Diffuse Glioma. *Acta Neuropathol* (2015) 129:849–65. doi: 10.1007/s00401-015-1399-y
2. Zachariah MA, Oliveira-Costa JP, Carter BS, Stott SL, Nahed BV. Blood-Based Biomarkers for the Diagnosis and Monitoring of Gliomas. *Neuro Oncol* (2018) 20:1155–61. doi: 10.1093/neuonc/noy074
3. Holdhoff M, Yovino SG, Boadu O, Grossman SA. Blood-Based Biomarkers for Malignant Gliomas. *J Neurooncol* (2013) 113:345–52. doi: 10.1007/s11060-013-1144-0
4. Weller M, van den Bent M, Preusser M, Le Rhun E, Tonn JC, Minniti G, et al. EANO Guidelines on the Diagnosis and Treatment of Diffuse Gliomas of Adulthood. *Nat Rev Clin Oncol* (2020) 17:30. doi: 10.1038/s41571-020-00447-z
5. Tarassishin L, Casper D, Lee SC. Aberrant Expression of Interleukin-1β and Inflammasome Activation in Human Malignant Gliomas. *PloS One* (2014) 9:e103432. doi: 10.1371/journal.pone.0103432
6. Van Meir E, Sawamura Y, Diserens A-CC, Hamou M-FF, de Tribolet N. Human Glioblastoma Cells Release Interleukin 6 in Vivo and In Vitro. *Cancer Res* (1990) 50:6683–8.
7. a Dzaye OD, Hu F, Derkow K, Haage V, Euskirchen P, Harms C, et al. Glioma Stem Cells But Not Bulk Glioma Cells Upregulate IL-6 Secretion in Microglia/Brain Macrophages Via Toll-like Receptor 4 Signaling. *J Neuropathol Exp Neurol* (2016) 75:429–40. doi: 10.1093/jnen/nlw016
8. Nijaguna MB, Patil V, Urbach S, Shwetha SD, Sravani K, Hegde AS, et al. Glioblastoma-Derived Macrophage Colony-Stimulating Factor (MCSF) Induces Microglial Release of Insulin-Like Growth Factor-Binding Protein 1 (IGFBP1) to Promote Angiogenesis. *J Biol Chem* (2015) 290:23401–15. doi: 10.1074/jbc.M115.664037
9. Ren J, Jia P, Feng H, Li X, Zhao J, Sun Y. Involvement of Poly(Adp-Ribose) Polymerase-1 in Chinese Patients With Gliomaa Potential Target for Effective Patient Care. *Int J Biol Markers* (2018) 33:68–72. doi: 10.5301/ijbm.5000267

10. Albulescu R, Codrici E, Popescu ID, Mihai S, Necula LG, Petrescu D, et al. Cytokine Patterns in Brain Tumour Progression. *Mediators Inflamm* (2013) 2013:979748. doi: 10.1155/2013/979748
11. Gao Y, Zhang E, Liu B, Zhou K, He S, Feng L, et al. Integrated Analysis Identified Core Signal Pathways and Hypoxic Characteristics of Human Glioblastoma. *J Cell Mol Med* (2019) 23:6228–37. doi: 10.1111/jcmm.14507
12. Shamsdin SA, Mehrafshan A, Rakei SM, Mehrabanilare D. Evaluation of VEGF, FGF and PDGF and Serum Levels of Inflammatory Cytokines in Patients With Glioma and Meningioma in Southern Iran. *Asian Pac J Cancer Prev* (2019) 20:2883–90. doi: 10.31557/APJCP.2019.20.10.2883
13. Nijaguna MB, Patil V, Hegde AS, Chandramouli BA, Arivazhagan A, Santosh V, et al. An Eighteen Serum Cytokine Signature for Discriminating Glioma From Normal Healthy Individuals. *PloS One* (2015) 10:e0137524. doi: 10.1371/journal.pone.0137524
14. Reynés G, Vila V, Martín M, Parada A, Fleitas T, Reganon E, et al. Circulating Markers of Angiogenesis, Inflammation, and Coagulation in Patients With Glioblastoma. *J Neurooncol* (2011) 102:35–41. doi: 10.1007/s11060-010-0290-x
15. Deniz ÇD, Gürbilek M, Koç M. Prognostic Value of Interferon-Gamma, Interleukin-6, and Tumor Necrosis Factor-Alpha in the Radiation Response of Patients Diagnosed With Locally Advanced Non-Small-Cell Lung Cancer and Glioblastoma Multiforme. *Turk J Med Sci* (2018) 48:117–23. doi: 10.3906/sag-1611-77
16. Carlsson A, Persson O, Ingvarsson J, Widegren B, Salford L, Borrebaeck CAKK, et al. Plasma Proteome Profiling Reveals Biomarker Patterns Associated With Prognosis and Therapy Selection in Glioblastoma Multiforme Patients. *Proteomics Clin Appl* (2010) 4:591–602. doi: 10.1002/prca.200900173
17. Shan Y, He X, Song W, Han D, Niu J, Wang J. Role of IL-6 in the Invasiveness and Prognosis of Glioma. *Int J Clin Exp Med* (2015) 8:9114–20.
18. Hands JR, Abel P, Ashton K, Dawson T, Davis C, Lea RW, et al. Investigating the Rapid Diagnosis of Gliomas From Serum Samples Using Infrared Spectroscopy and Cytokine and Angiogenesis Factors. *Anal Bioanal Chem* (2013) 405:7347–55. doi: 10.1007/s00216-013-7163-z
19. Xu BJ, An QA, Gowda SS, Yan W, Pierce LA, Abel TW, et al. Identification of Blood Protein Biomarkers That Aid in the Clinical Assessment of Patients With Malignant Glioma. *Int J Oncol* (2012) 40:1995–2003. doi: 10.3892/ijo.2012.1355
20. Gousias K, Markou M, Arzoglou V, Voulgaris S, Vartholomatos G, Kostoula A, et al. Frequent Abnormalities of the Immune System in Gliomas and Correlation With the WHO Grading System of Malignancy. *J Neuroimmunol* (2010) 226:136–42. doi: 10.1016/j.jneuroim.2010.05.027
21. Löhr M, Freitag B, Technau A, Krauss J, Monoranu C-MM, Rachor J, et al. High-Grade Glioma Associated Immunosuppression Does Not Prevent Immune Responses Induced by Therapeutic Vaccines in Combination With Treg Depletion. *Cancer Immunol Immunother* (2018) 67:1545–58. doi: 10.1007/s00262-018-2214-0
22. Kmiecik J, Poli A, Brons NHC, Waha A, Eide GE, Enger PØ, et al. Elevated CD3+ and CD8+ Tumor-Infiltrating Immune Cells Correlate With Prolonged Survival in Glioblastoma Patients Despite Integrated Immunosuppressive Mechanisms in the Tumor Microenvironment and at the Systemic Level. *J Neuroimmunol* (2013) 264:71–83. doi: 10.1016/j.jneuroim.2013.08.013
23. Mostafa H, Pala A, Högel J, Hlavac M, Dietrich E, Westhoff MA, et al. Immune Phenotypes Predict Survival in Patients With Glioblastoma Multiforme. *J Hematol Oncol* (2016) 9:77. doi: 10.1186/s13045-016-0272-3
24. Bryant NL, Suarez-Cuervo C, Gillespie GY, Markert JM, Nabors LB, Meleth S, et al. Characterization and Immunotherapeutic Potential of γδ T-cells in Patients With Glioblastoma. *Neuro Oncol* (2009) 11:357–67. doi: 10.1215/15228517-2008-111
25. Holst CB, Christensen IJ, Skjøth-Rasmussen J, Hamerlik P, Poulsen HS, Johansen JS. Systemic Immune Modulation in Gliomas: Prognostic Value of Plasma IL-6, YKL-40, and Genetic Variation in YKL-40. *Front Oncol* (2020) 10:478. doi: 10.3389/fonc.2020.00478
26. Doroudchi M, Pishe ZG, Malekzadeh M, Golmoghaddam H, Taghipour M, Ghaderi A. Elevated Serum IL-17A But Not IL-6 in Glioma Versus Meningioma and Schwannoma. *Asian Pac J Cancer Prev* (2013) 14:5225–30. doi: 10.7314/APJCP.2013.14.9.5225
27. Hu J, Mao Y, Li M, Lu Y. The Profile of Th17 Subset in Glioma. *Int Immunopharmacol* (2011) 11:1173–9. doi: 10.1016/j.intimp.2011.03.015
28. Bunevicius A, Radziunas A, Tamasauskas S, Tamasauskas A, Laws ER, Iervasi G, et al. Prognostic Role of High Sensitivity C-reactive Protein and Interleukin-6 in Glioma and Meningioma Patients. *J Neurooncol* (2018) 138:351–8. doi: 10.1007/s11060-018-2803-y
29. Demirci U, Yaman M, Buyukberber S, Coskun U, Baykara M, Uslu K, et al. Prognostic Importance of Markers for Inflammation, Angiogenesis and Apoptosis in High Grade Glial Tumors During Temozolomide and Radiotherapy. *Int Immunopharmacol* (2012) 14:546–9. doi: 10.1016/j.intimp.2012.08.007
30. Marinari E, Allard M, Gustave R, Widmer V, Philippin G, Merkler D, et al. Inflammation and Lymphocyte Infiltration are Associated With Shorter Survival in Patients With High-Grade Glioma. *Oncoimmunology* (2020) 9:1779990. doi: 10.1080/2162402X.2020.1779990
31. Chiorean R, Berindan-Neagoe I, Braicu C, Florian IS, Leucuta D, Crisan D, et al. Quantitative Expression of Serum Biomarkers Involved in Angiogenesis and Inflammation, in Patients With Glioblastoma Multiforme: Correlations With Clinical Data. *Cancer Biomark* (2014) 14:185–94. doi: 10.3233/CBM-130310
32. Bresnick AR, Weber DJ, Zimmer DB. S100 Proteins in Cancer. *Nat Rev Cancer* (2015) 15:96–109. doi: 10.1038/nrc3893
33. Gielen PR, Schulte BM, Kers-Rebel ED, Verrijp K, Bossman SAJFH, Ter Laan M, et al. Elevated Levels of Polymorphonuclear Myeloid-Derived Suppressor Cells in Patients With Glioblastoma Highly Express S100A8/9 and Arginase and Suppress T Cell Function. *Neuro Oncol* (2016) 18:1253–64. doi: 10.1093/neuonc/now034
34. Arora A, Patil V, Kundu P, Kondaiah P, Hegde AS, Arivazhagan A, et al. Serum Biomarkers Identification by iTRAQ and Verification by MRM: S100A8/S100A9 Levels Predict Tumor-Stroma Involvement and Prognosis in Glioblastoma. *Sci Rep* (2019) 9:1–12. doi: 10.1038/s41598-019-39067-8
35. Popescu ID, Codrici E, Albulescu L, Mihai S, Enciu AM, Albulescu R, et al. Potential Serum Biomarkers for Glioblastoma Diagnostic Assessed by Proteomic Approaches. *Proteome Sci* (2014) 12:47. doi: 10.1186/s12953-014-0047-0
36. Gautam P, Nair SC, Gupta MK, Sharma R, Polisetty RV, Uppin MS, et al. Proteins With Altered Levels in Plasma From Glioblastoma Patients as Revealed by iTRAQ-Based Quantitative Proteomic Analysis. *PloS One* (2012) 7:e46153. doi: 10.1371/journal.pone.0046153
37. Zupancic K, Blejec A, Herman A, Veber M, Verbovsek U, Korsic M, et al. Identification of Plasma Biomarker Candidates in Glioblastoma Using an Antibody-Array-Based Proteomic Approach. *Radiol Oncol* (2014) 48:257–66. doi: 10.2478/raon-2014-0014
38. Lyubimova NV, Toms MG, Popova EE, Bondarenko YV, Krat VB, Kushlinskii NE, et al. Neurospecific Proteins in the Serum of Patients With Brain Tumors. *Eksp Biol Med* (2010) 150:678–81. doi: 10.1007/s10517-011-1236-9
39. Oktay K, Olguner SK, Sarac ME, Mazhar KÖ, Çetinalp NE, GEZERCAN4 Y, et al. Evaluation of Serum S100b Values in High Grade Glioma Patients. *J Neurol Sci* (2015) 32:738–46. doi: 10.1007/s11060-016-2204-z
40. Brommeland T, Rosengren L, Fridlund S, Hennig R, Isaksen V. Serum Levels of Glial Fibrillary Acidic Protein Correlate to Tumour Volume of High-Grade Gliomas. *Acta Neurol Scand* (2007) 116:380–4. doi: 10.1111/j.1600-0404.2007.00889.x
41. Vos MJ, Postma TJ, Martens F, Uitdehaag BMJ, Blankenstein MA, Vandertop WP, et al. Serum Levels of S-100B Protein and Neuron-specific Enolase in Glioma Patients: A Pilot Study. *Anticancer Res* (2004) 24:2511–4.
42. Holla FK, Postma TJ, Blankenstein MA, van Mierlo TJM, Vos MJ, Sizoo EM, et al. Prognostic Value of the S100B Protein in Newly Diagnosed and Recurrent Glioma Patients: A Serial Analysis. *J Neurooncol* (2016) 129:525–32. doi: 10.1007/s11060-016-2204-z
43. Balkwill F. Tumour Necrosis Factor and Cancer. *Nat Rev Cancer* (2009) 9:361–71. doi: 10.1038/nrc2628
44. Villeneuve J, Tremblay P, Vallières L. Tumor Necrosis Factor Reduces Brain Tumor Growth by Enhancing Macrophage Recruitment and Microcyst Formation. *Cancer Res* (2005) 65:3928–36. doi: 10.1158/0008-5472.CAN-04-3612
45. Rahbar A, Cederarv M, Wolmer-Solberg N, Tammik C, Stragliotto G, Peredo I, et al. Enhanced Neutrophil Activity is Associated With Shorter

Time to Tumor Progression in Glioblastoma Patients. *Oncoimmunology* (2016) 5:e1075693. doi: 10.1080/2162402X.2015.1075693
46. Kushner AM I. Acute Phase Proteins as Disease Markers. *Disease Markers J* (1987) 5: (1):1–11. Pubmed.
47. Pang WW, Abdul-Rahman PS, Wan-Ibrahim WI, Hashim OH. Can the Acute-Phase Reactant Proteins be Used as Cancer Biomarkers? *Int J Biol Markers* (2010) 25:1–11. doi: 10.1177/172460081002500101
48. Weiss JF, Morantz RA, Bradley WP, Chretien PB. Serum Acute-Phase Proteins and Immunoglobulins in Patients With Gliomas. *Cancer Res* (1979) 39:542–4.
49. Matsuura H, Nakazawa S. Prognostic Significance of Serum Alpha 1-Acid Glycoprotein in Patients With Glioblastoma Multiforme: A Preliminary Communication. *Neurosurg Psychiatry* (1985) 48:835–7. doi: 10.1136/jnnp.48.8.835
50. Mohan Kumar D, Thota B, Vijay Shinde S, Prasanna KV, Hegde AS, Arivazhagan A, et al. Proteomic Identification of Haptoglobin Alpha2 as a Glioblastoma Serum Biomarker: Implications in Cancer Cell Migration and Tumor Growth. *J Proteome Res* (2010) 9:5557–67. doi: 10.1021/pr1001737
51. Gollapalli K, Ray S, Srivastava R, Renu D, Singh P, Dhali S, et al. Investigation of Serum Proteome Alterations in Human Glioblastoma Multiforme. *Proteomics* (2012) 12:2378–90. doi: 10.1002/pmic.201200002
52. Nijaguna MB, Schröder C, Patil V, Shwetha SD, Hegde AS, Chandramouli BA, et al. Definition of a Serum Marker Panel for Glioblastoma Discrimination and Identification of Interleukin 1β in the Microglial Secretome as a Novel Mediator of Endothelial Cell Survival Induced by C-reactive Protein. *J Proteomics* (2015) 128:251–61. doi: 10.1016/j.jprot.2015.07.026
53. Miyauchi E, Furuta T, Ohtsuki S, Tachikawa M, Uchida Y, Sabit H, et al. Identification of Blood Biomarkers in Glioblastoma by SWATH Mass Spectrometry and Quantitative Targeted Absolute Proteomics. *PloS One* (2018) 13:e0193799. doi: 10.1371/journal.pone.0193799
54. Zheng SH, Huang JL, Chen M, Wang BL, Ou QS, Huang SY. Diagnostic Value of Preoperative Inflammatory Markers in Patients With Glioma: A Multicenter Cohort Study. *J Neurosurg* (2018) 129:583–92. doi: 10.3171/2017.3.JNS161648
55. Liu S, Zhu Y, Zhang C, Meng X, Sun B, Zhang G, et al. The Clinical Significance of Soluble Programmed Cell Death-Ligand 1 (sPD-L1) in Patients With Gliomas. *Front Oncol* (2020) 10:9. doi: 10.3389/fonc.2020.00009
56. Wang PF, Meng Z, Song HW, Yao K, Duan ZJ, Yu CJ, et al. Preoperative Changes in Hematological Markers and Predictors of Glioma Grade and Survival. *Front Pharmacol* (2018) 9:886. doi: 10.3389/fphar.2018.00886
57. Wu Y, Song Z, Sun K, Rong S, Gao P, Wang F, et al. A Novel Scoring System Based on Peripheral Blood Test in Predicting Grade and Prognosis of Patients With Glioma. *Onco Targets Ther* (2019) 12:11413–23. doi: 10.2147/OTT.S236598
58. Huang Z, Wu L, Hou Z, Zhang P, Li G, Xie J. Eosinophils and Other Peripheral Blood Biomarkers in Glioma Grading: A Preliminary Study. *BMC Neurol* (2019) 19:313. doi: 10.1186/s12883-019-1549-2
59. He ZQ, Ke C, Al-Nahari F, Duan H, Guo CC, Wang Y, et al. Low Preoperative Prognostic Nutritional Index Predicts Poor Survival in Patients With Newly Diagnosed High-Grade Gliomas. *J Neurooncol* (2017) 132:239–47. doi: 10.1007/s11060-016-2361-0
60. Tadej Strojnik TŠ and TTL. Prognostic Value of Erythrocyte Sedimentation Rate and C-Reactive Protein in the Blood of Patients With Glioma. *Anticancer Res* (2014) 34:339–47.
61. Pierscianek D, Ahmadipour Y, Michel A, Chihi M, Oppong MD, Kebir S, et al. Prediction of Preoperative Survival in Patients With Glioblastoma by Routine Inflammatory Laboratory Parameters. *Anticancer Res* (2020) 40:1161–6. doi: 10.21873/anticanres.14058
62. Maas SLN, Draaisma K, Snijders TJ, Senders JT, Berendsen S, Seute T, et al. Routine Blood Tests Do Not Predict Survival in Patients With Glioblastoma—Multivariable Analysis of 497 Patients. *World Neurosurg* (2019) 126:e1081–91. doi: 10.1016/j.wneu.2019.03.053
63. Auezova R, Ivanova N, Akshulakov S, Zhetpisbaev B, Kozhakhmetova A, Ryskeldiyev N, et al. Isocitrate Dehydrogenase 1 Mutation is Associated With Reduced Levels of Inflammation in Glioma Patients. *Cancer Manag Res* (2019) 11:3227–36. doi: 10.2147/CMAR.S195754
64. Hao Y, Li X, Chen H, Huo H, Liu Z, Tian F, et al. A Cumulative Score Based on Preoperative Neutrophil-Lymphocyte Ratio and Fibrinogen in Predicting Overall Survival of Patients With Glioblastoma Multiforme. *World Neurosurg* (2019) 128:e427–33. doi: 10.1016/j.wneu.2019.04.169
65. He ZQ, Duan H, Ke C, Zhang XH, Guo CC, Al-Nahari F, et al. Evaluation of Cumulative Prognostic Score Based on Pretreatment Plasma Fibrinogen and Serum Albumin Levels in Patients With Newly Diagnosed High-Grade Gliomas. *Oncotarget* (2017) 8:49605–14. doi: 10.18632/oncotarget.17849
66. Han S, Huang Y, Li Z, Hou H, Wu A. The Prognostic Role of Preoperative Serum Albumin Levels in Glioblastoma Patients. *BMC Cancer* (2015) 15:108. doi: 10.1186/s12885-015-1125-0
67. Schwartzbaum JA, Lal P, Evanoff W, Mamrak S, Yates A, Barnett GH, et al. Presurgical Serum Albumin Levels Predict Survival Time From Glioblastoma Multiforme. *J Neurooncol* (1999) 43:35–41. doi: 10.1023/A:1006269413998
68. Borg N, Guilfoyle MR, Greenberg DC, Watts C, Thomson S. Serum Albumin and Survival in Glioblastoma Multiforme. *J Neurooncol* (2011) 105:77–81. doi: 10.1007/s11060-011-0562-0
69. Wang PF, Song HW, Cai HQ, Kong LW, Yao K, Jiang T, et al. Preoperative Inflammation Markers and IDH Mutation Status Predict Glioblastoma Patient Survival. *Oncotarget* (2017) 8:50117–23. doi: 10.18632/oncotarget.15235
70. Liang R, Li J, Tang X, Liu Y. The Prognostic Role of Preoperative Systemic Immune-Inflammation Index and Albumin/Globulin Ratio in Patients With Newly Diagnosed High-Grade Glioma. *Clin Neurol Neurosurg* (2019) 184:105397. doi: 10.1016/j.clineuro.2019.105397
71. Zhou XW, Dong H, Yang Y, Luo JW, Wang X, Liu YH, et al. Significance of the Prognostic Nutritional Index in Patients With Glioblastoma: A Retrospective Study. *Clin Neurol Neurosurg* (2016) 151:86–91. doi: 10.1016/j.clineuro.2016.10.014
72. Wang PF, Zhang J, Cai HQ, Meng Z, Yu CJ, Li SW, et al. Sanbo Scoring System, Based on Age and Pre-Treatment Hematological Markers, is a Non-Invasive and Independent Prognostic Predictor for Patients With Primary Glioblastomas: A Retrospective Multicenter Study. *J Cancer* (2019) 10:5654–60. doi: 10.7150/jca.33047
73. Xu WZ, Li F, Xu ZK, Chen X, Sun B, Cao JW, et al. Preoperative Albumin-to-Globulin Ratio and Prognostic Nutrition Index Predict Prognosis for Glioblastoma. *Onco Targets Ther* (2017) 10:725–33. doi: 10.2147/OTT.S127441
74. Rigamonti A, Imbesi F, Silvani A, Lamperti E, Agostoni E, Porcu L, et al. Prognostic Nutritional Index as a Prognostic Marker in Glioblastoma: Data From a Cohort of 282 Italian Patients. *J Neurol Sci* (2019) 400:175–9. doi: 10.1016/j.jns.2019.04.002
75. Zhang ZY, Zhan YB, Zhang FJ, Yu B, Ji YC, Zhou JQ, et al. Prognostic Value of Preoperative Hematological Markers Combined With Molecular Pathology in Patients With Diffuse Gliomas. *Aging (Albany NY)* (2019) 11:6252–72. doi: 10.18632/aging.102186
76. Ding JD, Yao K, Wang PF, Yan CX. Clinical Significance of Prognostic Nutritional Index in Patients With Glioblastomas. *Medicine (United States)* (2018) 97:e13218. doi: 10.1097/MD.0000000000013218
77. Vos PE, Jacobs B, Andriessen TMJC, Lamers KJB, Borm GF, Beems T, et al. GFAP and S100B are Biomarkers of Traumatic Brain Injury: An Observational Cohort Study. *Neurology* (2010) 75:1786–93. doi: 10.1212/WNL.0b013e3181fd62d2
78. Herrmann M, Vos P, Wunderlich MT, De Bruijn CHMM, Lamers KJB. Release of Glial Tissue-Specific Proteins After Acute Stroke: A Comparative Analysis of Serum Concentrations of Protein S-100B and Glial Fibrillary Acidic Protein. *Stroke* (2000) 31:2670–7. doi: 10.1161/01.STR.31.11.2670
79. Husain H, Savage W, Grossman SA, Ye X, Burger PC, Everett A, et al. Pre- and Post-Operative Plasma Glial Fibrillary Acidic Protein Levels in Patients With Newly Diagnosed Gliomas. *J Neurooncol* (2012) 109:123–7. doi: 10.1007/s11060-012-0874-8
80. Kiviniemi A, Gardberg M, Frantzén J, Parkkola R, Vuorinen V, Pesola M, et al. Serum Levels of GFAP and EGFR in Primary and Recurrent High-Grade Gliomas: Correlation to Tumor Volume, Molecular Markers, and Progression-Free Survival. *J Neurooncol* (2015) 124:237–45. doi: 10.1007/s11060-015-1829-7
81. Baumgarten P, Quick-Weller J, Gessler F, Wagner M, Tichy J, Forster MT, et al. Pre- and Early Postoperative GFAP Serum Levels in Glioma and Brain Metastases. *J Neurooncol* (2018) 139:541–6. doi: 10.1007/s11060-018-2898-1

82. Jung CS, Foerch C, Schänzer A, Heck A, Plate KH, Seifert V, et al. Serum GFAP is a Diagnostic Marker for Glioblastoma Multiforme | Brain | Oxford Academic. *Brain* (2007) 130:3336–41. doi: 10.1093/brain/awm263
83. Vietheer JM, Rieger J, Wagner M, Senft C, Tichy J, Foerch C. Serum Concentrations of Glial Fibrillary Acidic Protein (GFAP) do Not Indicate Tumor Recurrence in Patients With Glioblastoma. *J Neurooncol* (2017) 135:193–9. doi: 10.1007/s11060-017-2565-y
84. Lyubimova NV, Timofeev YS, Mitrofanov AA, Bekyashev AK, Goncharova ZA, Kushlinskii NE. Glial Fibrillary Acidic Protein in the Diagnosis and Prognosis of Malignant Glial Tumors. *Bull Exp Biol Med* (2020) 168:503–6. doi: 10.1007/s10517-020-04741-9
85. Ilhan-Mutlu A, Wagner L, Widhalm G, Wöhrer A, Bartsch S, Czech T, et al. Exploratory Investigation of Eight Circulating Plasma Markers in Brain Tumor Patients. *Neurosurg Rev* (2013) 36:45–56. doi: 10.1007/s10143-012-0401-6
86. Gállego Pérez-Larraya J, Paris S, Idbaih A, Dehais C, Laigle-Donadey F, Navarro S, et al. Diagnostic and Prognostic Value of Preoperative Combined GFAP, IGFBP-2, and YKL-40 Plasma Levels in Patients With Glioblastoma. *Cancer* (2014) 120:3972–80. doi: 10.1002/cncr.28949
87. Husain H, Savage W, Everett A, Ye X, Blair C, Romans KE, et al. The Role of Plasma GFAP as a Biomarker for Glioblastoma. *J Clin Oncol* (2011) 29:2095–5. doi: 10.1200/jco.2011.29.15_suppl.2095
88. Tichy J, Spechtmeyer S, Mittelbronn M, Hattingen E, Rieger J, Senft C, et al. Prospective Evaluation of Serum Glial Fibrillary Acidic Protein (GFAP) as a Diagnostic Marker for Glioblastoma. *J Neurooncol* (2015) 126:361–9. doi: 10.1007/s11060-015-1978-8
89. Llorens F, Thüne K, Tahir W, Kanata E, Diaz-Lucena D, Xanthopoulos K, et al. YKL-40 in the Brain and Cerebrospinal Fluid of Neurodegenerative Dementias. *Mol Neurodegener* (2017) 12:83. doi: 10.1186/s13024-017-0226-4
90. Horbinski C, Wang G, Wiley CA. YKL-40 is Directly Produced by Tumor Cells and is Inversely Linked to EGFR in Glioblastomas. *Int J Clin Exp Pathol* (2010) 3:226–37.
91. Schultz NA, Johansen JS. YKL-40-a Protein in the Field of Translational Medicine: A Role as a Biomarker in Cancer Patients? *Cancers (Basel)* (2010) 2:1453–91. doi: 10.3390/cancers2031453
92. Kazakova MH, Staneva DN, Koev IG, Staikov DG, Mateva N, Timonov PT, et al. Protein and mRNA levels of YKL-40 in high-grade glioma. *Folia Biol* (2014) 60:261–70.
93. Gandhi P, Khare R, VasudevGulwani H, Kaur S. Circulatory YKL-40 & NLR: Underestimated Prognostic Indicators in Diffuse Glioma. *Int J Mol Cell Med* (2018) 7:111–8. doi: 10.22088/IJMCM.BUMS.7.2.111
94. Tanwar MK, Gilbert MR, Holland EC. Gene Expression Microarray Analysis Reveals YKL-40 to be a Potential Serum Marker for Malignant Character in Human Glioma. *Cancer Res* (2002) 62:4364–8.
95. Bernardi D, Padoan A, Ballin A, Sartori M, Manara R, Scienza R, et al. Serum YKL-40 Following Resection for Cerebral Glioblastoma. *J Neurooncol* (2012) 107:299–305. doi: 10.1007/s11060-011-0762-7
96. Iwamoto FM, Hottinger AF, Karimi S, Riedel E, Dantis J, Jahdi M, et al. Serum YKL-40 is a Marker of Prognosis and Disease Status in High-Grade Gliomas. *Neuro Oncol* (2011) 13:1244–51. doi: 10.1093/neuonc/nor117
97. Hormigo A, Gu B, Karimi S, Riedel E, Panageas KS, Edgar MA, et al. YKL-40 and Matrix Metalloproteinase-9 as Potential Serum Biomarkers for Patients With High-Grade Gliomas. *Clin Cancer Res* (2006) 12:5698–704. doi: 10.1158/1078-0432.CCR-06-0181
98. Chandra A, Jahangiri A, Chen W, Nguyen AT, Yagnik G, Pereira MP, et al. Clonal ZEB1-driven Mesenchymal Transition Promotes Targetable Oncologic Antiangiogenic Therapy Resistance. *Cancer Res* (2020) 80:1498–511. doi: 10.1158/0008-5472.CAN-19-1305
99. van Linde ME, van der Mijn JC, Pham TV, Knol JC, Wedekind LE, Hovinga KE, et al. Evaluation of Potential Circulating Biomarkers for Prediction of Response to Chemoradiation in Patients With Glioblastoma. *J Neurooncol* (2016) 129:221–30. doi: 10.1007/s11060-016-2178-x
100. Corsini E, Ciusani E, Gaviani P, Silvani A, Canazza A, Bernardi G, et al. Decrease in Circulating Endothelial Progenitor Cells in Treated Glioma Patients. *J Neurooncol* (2012) 108:123–9. doi: 10.1007/s11060-012-0805-8
101. Salmaggi A, Eoli M, Frigerio S, Silvani A, Gelati M, Corsini E, et al. Intracavitary VEGF, bFGF, IL-8, IL-12 Levels in Primary and Recurrent Malignant Glioma. *J Neurooncol* (2003) 62:297–303. doi: 10.1023/A:1023367223575
102. Yang J, Zhao Z, Zhong X. Correlation Analysis of the Clinicopathological Features of Glioma and Expression of p53 and VEGF. *Int J Clin Exp Med* (2017) 10:3606–11.
103. Nowacka A, Smuczyński W, Rość D, Woźniak—Dąbrowska K, Śniegocki M. Serum VEGF-A Concentrations in Patients With Central Nervous System (CNS) Tumors. *PloS One* (2018) 13:e0192395. doi: 10.1371/journal.pone.0192395
104. Rafat N, Beck GC, Schulte J, Tuettenbeg J, Vajkoczy P. Circulating Endothelial Progenitor Cells in Malignant Gliomas. Clinical Article. *J Neurosurg* (2010) 112:43–9. doi: 10.3171/2009.5.JNS081074
105. Reynés G, Martínez-Sales V, Vila V, Balañá C, Pérez-Segura P, Vaz MA, et al. Phase II Trial of Irinotecan and Metronomic Temozolomide in Patients With Recurrent Glioblastoma. *Anticancer Drugs* (2016) 27:133–7. doi: 10.1097/CAD.0000000000000314
106. Rodrigues JC, Gonzalez GC, Zhang L, Ibrahim G, Kelly JJ, Gustafson MP, et al. Normal Human Monocytes Exposed to Glioma Cells Acquire Myeloid-Derived Suppressor Cell-Like Properties. *Neuro Oncol* (2010) 12:351–65. doi: 10.1093/neuonc/nop023
107. Labussière M, Cheneau C, Prahst C, Gállego Pérez-Larraya J, Farina P, Lombardi G, et al. Angiopoietin-2 May be Involved in the Resistance to Bevacizumab in Recurrent Glioblastoma. *Cancer Invest* (2016) 34:39–44. doi: 10.3109/07357907.2015.1088948
108. Ribom D, Larsson A, Pietras K, Smits A. Growth Factor Analysis of Low-Grade Glioma CSF: PDGF and VEGF are Not Detectable. *Neurol Sci* (2003) 24:70–3. doi: 10.1007/s100720300075
109. Takano S, Yoshii Y, Kondo S, Suzuki H, Maruno T, Shirai S, et al. Concentration of Vascular Endothelial Growth Factor in the Serum and Tumor Tissue of Brain Tumor Patients. *Cancer Res* (1996) 56:2185–90.
110. Stockhammer G, Obwegeser A, Kostron H, Schumacher P, Muigg A, Felber S, et al. Vascular Endothelial Growth Factor (VEGF) is Elevated in Brain Tumor Cysts and Correlates With Tumor Progression. *Acta Neuropathol* (2000) 100:101–5. doi: 10.1007/s004010051199
111. Crocker M, Ashley S, Giddings I, Petrik V, Hardcastle A, Aherne W, et al. Serum Angiogenic Profile of Patients With Glioblastoma Identifies Distinct Tumor Subtypes and Shows That TIMP-1 is a Prognostic Factor. *Neuro Oncol* (2011) 13:99–108. doi: 10.1093/neuonc/noq170
112. Peles E, Lidar Z, Simon AJ, Grossman R, Nass D, Ram Z. Angiogenic Factors in the Cerebrospinal Fluid of Patients With Astrocytic Brain Tumors. *Neurosurgery* (2004) 55:562–7. doi: 10.1227/01.NEU.0000134383.27713.9A
113. Nazari PMS, Marosi C, Moik F, Riedl J, Özer Ö, Berghoff AS, et al. Low Systemic Levels of Chemokine C-C Motif Ligand 3 (CCL3) are Associated With a High Risk of Venous Thromboembolism in Patients With Glioma. *Cancers (Basel)* (2019) 11:2020. doi: 10.3390/cancers11122020
114. Ilhan A, Gartner W, Neziri D, Czech T, Base W, Hörl WH, et al. Angiogenic Factors in Plasma of Brain Tumour Patients. *Anticancer Res* (2009) 29:731–6. Pubmed.
115. Tabouret E, Boudouresque F, Barrie M, Matta M, Boucard C, Loundou A, et al. Association of Matrix Metalloproteinase 2 Plasma Level With Response and Survival in Patients Treated With Bevacizumab for Recurrent High-Grade Glioma. *Neuro Oncol* (2014) 16:392–9. doi: 10.1093/neuonc/not226
116. Levitan N, Dowlati A, Remick SC, Tahsildar HI, Sivinski LD, Beyth R, et al. Rates of Initial and Recurrent Thromboembolic Disease Among Patients With Malignancy Versus Those Without Malignancy: Risk Analysis Using Medicare Claims Data. *Medicine (Baltimore)* (1999) 78:285–91. doi: 10.1097/00005792-199909000-00001
117. Rość D, Grabarczyk E, Bierwagen M, Wierciński M, Góralczyk K, Haor B, et al. A Preliminary Estimation of Tissue Factor Pathway Inhibitor (TFPI) and Protein C in Patients With Intracranial Tumors. *Adv Clin Exp Med* (2017) 26:1219–24. doi: 10.17219/acem/67760
118. Marx S, Splittstöhser M, Kinnen F, Moritz E, Joseph C, Paul S, et al. Platelet Activation Parameters and Platelet-Leucocyte-Conjugate Formation in Glioblastoma Multiforme Patients. *Oncotarget* (2018) 9:25860–76. doi: 10.18632/oncotarget.25395
119. Kwaan HC, Mazar AP, McMahon BJ. The Apparent uPA/PAI-1 Paradox in Cancer: More Than Meets the Eye. *Semin Thromb Hemost* (2013) 39:382–91. doi: 10.1055/s-0033-1338127
120. Li Z, Lu H, Yang J, Zeng X, Zhao L, Li H, et al. Analysis of the Raw Serum Peptidomic Pattern in Glioma Patients. *Clin Chim Acta* (2013) 425:221–6. doi: 10.1016/j.cca.2013.08.002

121. Villanueva J, Philip J, Entenberg D, Chaparro CA, Tanwar MK, Holland EC, et al. Serum Peptide Profiling by Magnetic Particle-Assisted, Automated Sample Processing and MALDI-TOF Mass Spectrometry. *Anal Chem* (2004) 76:1560–70. doi: 10.1021/ac0352171
122. Liu J, Zheng S, Yu Jk, Zhang Jm, Chen Z. Serum Protein Fingerprinting Coupled With Artificial Neural Network Distinguishes Glioma From Healthy Population or Brain Benign Tumor. *J Zhejiang Univ Sci B* (2005) 6:4–10. doi: 10.1631/jzus.2005.b0004
123. Zhang H, Wu G, Tu H, Huang F. Discovery of Serum Biomarkers in Astrocytoma by SELDI-TOF MS and Proteinchip Technology. *J Neurooncol* (2007) 84:315–23. doi: 10.1007/s11060-007-9376-5
124. Vaitkiene P, Urbanaviciute R, Grigas P, Steponaitis G, Tamasauskas A, Skiriutė D. Identification of Astrocytoma Blood Serum Protein Profile. *Cells* (2019) 9:16. doi: 10.3390/cells9010016
125. Zhenjiang L, Rao M, Luo X, Valentini D, von Landenberg A, Meng Q, et al. Cytokine Networks and Survivin Peptide-Specific Cellular Immune Responses Predict Improved Survival in Patients With Glioblastoma Multiforme. *EBioMedicine* (2018) 33:49–56. doi: 10.1016/j.ebiom.2018.06.014
126. Kim VN, Han J, Siomi MC. Biogenesis of Small RNAs in Animals. *Nat Rev Mol Cell Biol* (2009) 10:126–39. doi: 10.1038/nrm2632
127. Weber JA, Baxter DH, Zhang S, Huang DY, Huang KH, Lee MJ, et al. The microRNA Spectrum in 12 Body Fluids. *Clin Chem* (2010) 56:1733–41. doi: 10.1373/clinchem.2010.147405
128. Wang J, Che F, Zhang J, Zhang M, Xiao S, Liu Y, et al. Diagnostic and Prognostic Potential of Serum Cell-Free microRNA-214 in Glioma. *World Neurosurg* (2019) 125:e1217–25. doi: 10.1016/j.wneu.2019.02.009
129. Vickers KC, Palmisano BT, Shoucri BM, Shamburek RD, Remaley AT. MicroRNAs are Transported in Plasma and Delivered to Recipient Cells by High-Density Lipoproteins. *Nat Cell Biol* (2011) 13:423–35. doi: 10.1038/ncb2210
130. Fedorko M, Stanik M, Iliev R, Redova-Lojova M, Machackova T, Svoboda M, et al. Combination of MiR-378 and MiR-210 Serum Levels Enables Sensitive Detection of Renal Cell Carcinoma. *Int J Mol Sci* (2015) 16:23382–9. doi: 10.3390/ijms161023382
131. Kanemaru H, Fukushima S, Yamashita J, Honda N, Oyama R, Kakimoto A, et al. The Circulating microRNA-221 Level in Patients With Malignant Melanoma as a New Tumor Marker. *J Dermatol Sci* (2011) 61:187–93. doi: 10.1016/j.jdermsci.2010.12.010
132. Chen G, Wang J, Cui Q. Could Circulating miRNAs Contribute to Cancer Therapy? *Trends Mol Med* (2013) 19:71–3. doi: 10.1016/j.molmed.2012.10.006
133. Pritchard CC, Kroh E, Wood B, Arroyo JD, Dougherty KJ, Miyaji MM, et al. Blood Cell Origin of Circulating microRNAs: A Cautionary Note for Cancer Biomarker Studies. *Cancer Prev Res* (2012) 5:492–7. doi: 10.1158/1940-6207.CAPR-11-0370
134. Keller A, Leidinger P, Bauer A, Elsharawy A, Haas J, Backes C, et al. Toward the Blood-Borne miRNome of Human Diseases. *Nat Methods* (2011) 8:841–3. doi: 10.1038/nmeth.1682
135. Siegal T, Charbit H, Paldor I, Zelikovitch B, Canello T, Benis A, et al. Dynamics of Circulating Hypoxia-Mediated miRNAs and Tumor Response in Patients With High-Grade Glioma Treated With Bevacizumab. *J Neurosurg* (2016) 125:1008–15. doi: 10.3171/2015.8.JNS15437
136. Wang Q, Li P, Li A, Jiang W, Wang H, Wang J, et al. Plasma Specific miRNAs as Predictive Biomarkers for Diagnosis and Prognosis of Glioma. *J Exp Clin Cancer Res* (2012) 31:97. doi: 10.1186/1756-9966-31-97
137. Morokoff A, Jones J, Nguyen H, Ma C, Lasocki A, Gaillard F, et al. Serum microRNA is a Biomarker for Post-Operative Monitoring in Glioma. *J Neurooncol* (2020) 149:391–400. doi: 10.1007/s11060-020-03566-w
138. Ivo D'Urso P, Fernando D'Urso O, Damiano Gianfreda C, Mezzolla V, Storelli C, Marsigliante S. miR-15b and miR-21 as Circulating Biomarkers for Diagnosis of Glioma. *Curr Genomics* (2015) 16:304–11. doi: 10.2174/1389202916666150707155610
139. Santangelo A, Imbrucè P, Gardenghi B, Belli L, Agushi R, Tamanini A, et al. A microRNA Signature From Serum Exosomes of Patients With Glioma as Complementary Diagnostic Biomarker. *J Neurooncol* (2018) 136:51–62. doi: 10.1007/s11060-017-2639-x
140. ParvizHamidi M, Haddad G, Ostadrahimi S, Ostadrahimi N, Sadeghi S, Fayaz S, et al. Circulating miR-26a and miR-21 as Biomarkers for Glioblastoma Multiform. *Biotechnol Appl Biochem* (2019) 66:261–5. doi: 10.1002/bab.1707
141. Labib EM, Ezz LR, Arab E, Ghanem HM, Hassan RE, Swellam M. Relevance of Circulating MiRNA-21 and MiRNA-181 in Prediction of Glioblastoma Multiforme Prognosis Relevance of Circulating MiRNA-21 and MiRNA-181 in Prediction of Glioblastoma Multiforme Prognosis. *Arch Physiol Biochem* (2020) 21:1–6. doi: 10.1080/13813455.2020.1739716
142. Ilhan-Mutlu A, Wagner L, Wöhrer A, Furtner J, Widhalm G, Marosi C, et al. Plasma Microrna-21 Concentration may be a Useful Biomarker in Glioblastoma Patients. *Cancer Invest* (2012) 30:615–21. doi: 10.3109/07357907.2012.708071
143. Yang K, Wang S, Cheng Y, Tian Y, Hou J. Role of miRNA-21 in the Diagnosis and Prediction of Treatment Efficacy of Primary Central Nervous System Lymphoma. *Oncol Lett* (2019) 17:3475–81. doi: 10.3892/ol.2019.9941
144. Lu Z, Tang H, Wu D, Xia Y, Wu M, Yi X, et al. Amplified Voltammetric Detection of miRNA From Serum Samples of Glioma Patients Via Combination of Conducting Magnetic Microbeads and Ferrocene-Capped Gold Nanoparticle/Streptavidin Conjugates. *Biosens Bioelectron* (2016) 86:502–7. doi: 10.1016/j.bios.2016.07.010
145. Wang J, Yi X, Tang H, Han H, Wu M, Zhou F. Direct Quantification of MicroRNA At Low Picomolar Level in Sera of Glioma Patients Using a Competitive Hybridization Followed by Amplified Voltammetric Detection. *Anal Chem* (2012) 84:6400–6. doi: 10.1021/ac203368h
146. Wang J, Lu Z, Tang H, Wu L, Wang Z, Wu M, et al. Multiplexed Electrochemical Detection of MiRNAs From Sera of Glioma Patients At Different Stages Via the Novel Conjugates of Conducting Magnetic Microbeads and Diblock Oligonucleotide-Modified Gold Nanoparticles. *Anal Chem* (2017) 89:10834–40. doi: 10.1021/acs.analchem.7b02342
147. Li J, Yuan H, Xu H, Zhao H, Xiong N. Hypoxic Cancer-Secreted Exosomal Mir-182-5p Promotes Glioblastoma Angiogenesis by Targeting Kruppel-Like Factor 2 and 4. *Mol Cancer Res* (2020) 18:1218–31. doi: 10.1158/1541-7786.MCR-19-0725
148. Xiao Y, Zhang L, Song Z, Guo C, Zhu J, Li Z, et al. Potential Diagnostic and Prognostic Value of Plasma Circulating Microrna-182 in Human Glioma. *Med Sci Monit* (2016) 22:855–62. doi: 10.12659/MSM.897164
149. Zhang R, Pang B, Xin T, Guo H, Xing Y, Xu S, et al. Plasma miR-221/222 Family as Novel Descriptive and Prognostic Biomarkers for Glioma. *Mol Neurobiol* (2016) 53:1452–60. doi: 10.1007/s12035-014-9079-9
150. Swellam M, Ezz El Arab L, Al-Posttany AS, B. Said S. Clinical Impact of Circulating Oncogenic MiRNA-221 and MiRNA-222 in Glioblastoma Multiform. *J Neurooncol* (2019) 144:545–51. doi: 10.1007/s11060-019-03256-2
151. Zhi F, Shao N, Wang R, Deng D, Xue L, Wang Q, et al. Identification of 9 Serum microRNAs as Potential Noninvasive Biomarkers of Human Astrocytoma. *Neuro Oncol* (2015) 17:383–91. doi: 10.1093/neuonc/nou169
152. Shi R, Wang PY, Li XY, Chen JX, Li Y, Zhang XZ, et al. Exosomal Levels of miRNA-21 From Cerebrospinal Fluids Associated With Poor Prognosis and Tumor Recurrence of Glioma Patients. *Oncotarget* (2015) 6:26971–81. doi: 10.18632/oncotarget.4699
153. Zhao H, Shen J, Hodges TR, Song R, Fuller GN, Heimberger AB. Serum microRNA Profiling in Patients With Glioblastoma: A Survival Analysis. *Mol Cancer* (2017) 16:59. doi: 10.1186/s12943-017-0628-5
154. Ilhan-Mutlu A, Wagner L, Wöhrer A, Jungwirth S, Marosi C, Fischer P, et al. Blood Alterations Preceding Clinical Manifestation of Glioblastoma. *Cancer Invest* (2012) 30:625–9. doi: 10.3109/07357907.2012.725443
155. Ebrahimkhani S, Vafaee F, Hallal S, Wei H, Lee MYT, Young PE, et al. Deep Sequencing of Circulating Exosomal microRNA Allows non-Invasive Glioblastoma Diagnosis. *NPJ Precis Oncol* (2018) 2:1–9. doi: 10.1038/s41698-018-0071-0
156. Manterola L, Guruceaga E, Pérez-Larraya JG, González-Huarriz M, Jauregui P, Tejada S, et al. A Small Noncoding RNA Signature Found in Exosomes of GBM Patient Serum as a Diagnostic Tool. *Neuro Oncol* (2014) 16:520–7. doi: 10.1093/neuonc/not218
157. Ohno M, Matsuzaki J, Kawauchi J, Aoki Y, Miura J, Takizawa S, et al. Assessment of the Diagnostic Utility of Serum Microrna Classification in Patients With Diffuse Glioma. *JAMA Netw Open* (2019) 2:e1916953. doi: 10.1001/jamanetworkopen.2019.16953
158. Roth P, Wischhusen J, Happold C, Chandran PA, Hofer S, Eisele G, et al. A Specific miRNA Signature in the Peripheral Blood of Glioblastoma Patients. *J Neurochem* (2011) 118:449–57. doi: 10.1111/j.1471-4159.2011.07307.x

159. Regazzo G, Terrenato I, Spagnuolo M, Carosi M, Cognetti G, Cicchillitti L, et al. A Restricted Signature of Serum miRNAs Distinguishes Glioblastoma From Lower Grade Gliomas. *J Exp Clin Cancer Res* (2016) 35:124. doi: 10.1186/s13046-016-0393-0
160. Qian Z, Li Y, Fan X, Zhang C, Wang Y, Jiang T, et al. Prognostic Value of a microRNA Signature as a Novel Biomarker in Patients With Lower-Grade Gliomas. *J Neurooncol* (2018) 137:127–37. doi: 10.1007/s11060-017-2704-5
161. Oto J, Plana E, Solmoirago MJ, Fernández-Pardo Á, Hervás D, Cana F, et al. MicroRNAs and Markers of Neutrophil Activation as Predictors of Early Incidental Post-Surgical Pulmonary Embolism in Patients With Intracranial Tumors. *Cancers (Basel)* (2020) 12:1–19. doi: 10.3390/cancers12061536
162. Umetani N, Hiramatsu S, Hoon DSB. Higher Amount of Free Circulating DNA in Serum Than in Plasma is Not Mainly Caused by Contaminated Extraneous DNA During Separation. *Ann N Y Acad Sci* (2006) 1075:299–307. doi: 10.1196/annals.1368.040
163. Faria G, Silva E, Da Fonseca C, Quirico-Santos T. Circulating Cell-Free DNA as a Prognostic and Molecular Marker for Patients With Brain Tumors Under Perillyl Alcohol-Based Therapy. *Int J Mol Sci* (2018) 19:1610. doi: 10.3390/ijms19061610
164. Bagley SJ, Ali Nabavizadeh S, Mays JJ, Till JE, Ware JB, Levy S, et al. Clinical Utility of Plasma Cell-Free DNA in Adult Patients With Newly Diagnosed Glioblastoma: A Pilot Prospective Study. *Clin Cancer Res* (2020) 26:397–407. doi: 10.1158/1078-0432.CCR-19-2533
165. Nørøxe DS, Østrup O, Yde CW, Ahlborn LB, Nielsen FC, Michaelsen SR, et al. Cell-Free DNA in Newly Diagnosed Patients With Glioblastoma – A Clinical Prospective Feasibility Study. *Oncotarget* (2019) 10:4397–406. doi: 10.18632/oncotarget.27030
166. Nabavizadeh SA, Ware JB, Guiry S, Nasrallah MP, Mays JJ, Till JE, et al. Imaging and Histopathologic Correlates of Plasma Cell-Free DNA Concentration and Circulating Tumor DNA in Adult Patients With Newly Diagnosed Glioblastoma. *Neurooncol Adv* (2020) 2:1–9. doi: 10.1093/noajnl/vdaa016
167. Piccioni DE, Achrol AS, Kiedrowski LA, Banks KC, Boucher N, Barkhoudarian G, et al. Analysis of Cell-Free Circulating Tumor DNA in 419 Patients With Glioblastoma and Other Primary Brain Tumors. *CNS Oncol* (2019) 8:CNS34. doi: 10.2217/cns-2018-0015
168. Ahmed K, Govardhan H, Roy M, Naveen T, Siddanna P, Sridhar P, et al. Cell-Free Circulating Tumor DNA in Patients With High-Grade Glioma as Diagnostic Biomarker - A Guide to Future Directive. *Indian J Cancer* (2019) 56:65–9. doi: 10.4103/ijc.IJC_551_17
169. Mouliere F, Chandrananda D, Piskorz AM, Moore EK, Morris J, Ahlborn LB, et al. Enhanced Detection of Circulating Tumor DNA by Fragment Size Analysis. *Sci Transl Med* (2018) 10:4921. doi: 10.1126/scitranslmed.aat4921
170. Bettegowda C, Sausen M, Leary RJ, Kinde I, Wang Y, Agrawal N, et al. Detection of Circulating Tumor DNA in Early- and Late-Stage Human Malignancies. *Sci Transl Med* (2014) 6:24. doi: 10.1126/scitranslmed.3007094
171. Yoshida T, Yamashita S, Takamura-Enya T, Niwa T, Ando T, Enomoto S, et al. Alu and Satα Hypomethylation in Helicobacter Pylori-Infected Gastric Mucosae. *Int J Cancer* (2011) 128:33–9. doi: 10.1002/ijc.25534
172. Chen J, Gong M, Lu S, Liu F, Xia L, Nie D, et al. Detection of Serum Alu Element Hypomethylation for the Diagnosis and Prognosis of Glioma. *J Mol Neurosci* (2013) 50:368–75. doi: 10.1007/s12031-013-0014-8
173. Chen J, Huan W, Zuo H, Zhao L, Huang C, Liu X, et al. Alu Methylation Serves as a Biomarker for Non-Invasive Diagnosis of Glioma. *Oncotarget* (2016) 7:26099–106. doi: 10.18632/oncotarget.8318
174. Nassiri F, Chakravarthy A, Feng S, Shen SY, Nejad R, Zuccato JA, et al. Detection and Discrimination of Intracranial Tumors Using Plasma Cell-Free DNA Methylomes. *Nat Med* (2020) 26:1044–7. doi: 10.1038/s41591-020-0932-2
175. Lavon I, Refael M, Zelikovitch B, Shalom E, Siegal T. Serum DNA can Define Tumor-Specific Genetic and Epigenetic Markers in Gliomas of Various Grades. *Neuro Oncol* (2010) 12:173–80. doi: 10.1093/neuonc/nop041
176. Wang Z, Jiang W, Wang Y, Guo Y, Cong Z, Du F, et al. MGMT Promoter Methylation in Serum and Cerebrospinal Fluid as a Tumor-Specific Biomarker of Glioma. *BioMed Rep* (2015) 3:543–8. doi: 10.3892/br.2015.462
177. Majchrzak-Celińska A, Paluszczak J, Kleszcz R, Magiera M, Barciszewska AM, Nowak S, et al. Detection of MGMT, RASSF1A, p15INK4B, and p14ARF Promoter Methylation in Circulating Tumor-Derived DNA of Central Nervous System Cancer Patients. *J Appl Genet* (2013) 54:335–44. doi: 10.1007/s13353-013-0149-x
178. Weaver KD, Grossman SA, Herman JG. Methylated Tumor-Specific DNA as a Plasma Biomarker in Patients With Glioma. *Cancer Invest* (2006) 24:35–40. doi: 10.1080/07357900500449546
179. Estival A, Sanz C, Ramirez JL, Velarde JM, Domenech M, Carrato C, et al. Pyrosequencing Versus Methylation-Specific PCR for Assessment of MGMT Methylation in Tumor and Blood Samples of Glioblastoma Patients. *Sci Rep* (2019) 9:11125. doi: 10.1038/s41598-019-47642-2
180. Balañá C, Carrato C, Ramírez JL, Cardona AF, Berdiel M, Sánchez JJ, et al. Tumour and Serum MGMT Promoter Methylation and Protein Expression in Glioblastoma Patients. *Clin Transl Oncol* (2011) 13:677–85. doi: 10.1007/s12094-011-0714-x
181. Balaña C, Ramirez JL, Taron M, Roussos Y, Ariza A, Ballester R, et al. O6-methyl-guanine-DNA Methyltransferase Methylation in Serum and Tumor DNA Predicts Response to 1,3-Bis(2-Chloroethyl)-1-nitrosourea But Not to Temozolamide Plus Cisplatin in Glioblastoma Multiforme. *Clin Cancer Res* (2003) 9:1461–8. Pubmed.
182. Fiano V, Trevisan M, Trevisan E, Senetta R, Castiglione A, Sacerdote C, et al. MGMT Promoter Methylation in Plasma of Glioma Patients Receiving Temozolomide. *J Neurooncol* (2014) 117:347–57. doi: 10.1007/s11060-014-1395-4
183. Schuster H, Jellinger K, Gund A, Reǵele H. Extracranial Metastases of Anaplastic Cerebral Gliomas. *Acta Neurochir (Wien)* (1976) 35:247–59. doi: 10.1007/BF01406121
184. Campbell AN, Chan HSL, Becker LE, Daneman A, Park TS, Hoffman HJ. Extracranial Metastases in Childhood Primary Intracranial Tumors. A Report of 21 Cases and Review of the Literature. *Cancer* (1984) 53:974–81. doi: 10.1002/1097-0142(19840215)53:4<974::AID-CNCR2820530426>3.0.CO;2-C
185. Müller C, Holtschmidt J, Auer M, Heitzer E, Lamszus K, Schulte A, et al. Cancer: Hematogenous Dissemination of Glioblastoma Multiforme. *Sci Transl Med* (2014) 6:247. doi: 10.1126/scitranslmed.3009095
186. Sullivan JP, Nahed BV, Madden MW, Oliveira SM, Springer S, Bhere D, et al. Brain Tumor Cells in Circulation are Enriched for Mesenchymal Gene Expression. *Cancer Discov* (2014) 4:1299–309. doi: 10.1158/2159-8290.CD-14-0471
187. Bang-Christensen SR, Pedersen RS, Pereira MA, Clausen TM, Løppke C, Sand NT, et al. Capture and Detection of Circulating Glioma Cells Using the Recombinant VAR2CSA Malaria Protein. *Cells* (2019) 8:998. doi: 10.3390/cells8090998
188. Lynch D, Powter B, Po JW, Cooper A, Garrett C, Koh E-SS, et al. Isolation of Circulating Tumor Cells From Glioblastoma Patients by Direct Immunomagnetic Targeting. *Appl Sci* (2020) 10:3338. doi: 10.3390/app10093338
189. Krol I, Castro-Giner F, Maurer M, Gkountela S, Szczerba BM, Scherrer R, et al. Detection of Circulating Tumour Cell Clusters in Human Glioblastoma. *Br J Cancer* (2018) 119:487–91. doi: 10.1038/s41416-018-0186-7
190. Zhang W, Bao L, Yang S, Qian Z, Dong M, Yin L, et al. Tumor-Selective Replication Herpes Simplex Virus-Based Technology Significantly Improves Clinical Detection and Prognostication of Viable Circulating Tumor Cells. *Oncotarget* (2016) 7:39768–83. doi: 10.18632/oncotarget.9465
191. MacArthur KM, Kao GD, Chandrasekaran S, Alonso-Basanta M, Chapman C, Lustig RA, et al. Detection of Brain Tumor Cells in the Peripheral Blood by a Telomerase Promoter-Based Assay. *Cancer Res* (2014) 74:2152–9. doi: 10.1158/0008-5472.CAN-13-0813
192. Gao F, Cui Y, Jiang H, Sui D, Wang Y, Jiang Z, et al. Circulating Tumor Cell is a Common Property of Brain Glioma and Promotes the Monitoring System. *Oncotarget* (2016) 7:71330–40. doi: 10.18632/oncotarget.11114
193. Schlesinger M. Role of Platelets and Platelet Receptors in Cancer Metastasis 06 Biological Sciences 0601 Biochemistry and Cell Biology. *J Hematol Oncol* (2018) 11:1–15. doi: 10.1186/s13045-018-0669-2
194. Subeikshanan V, Dutt A, Basu D, Tejus MN, Maurya VP, Madhugiri VS. A Prospective Comparative Clinical Study of Peripheral Blood Counts and Indices in Patients With Primary Brain Tumors. *J Postgrad Med* (2016) 62:86–90. doi: 10.4103/0022-3859.180551
195. Xu W, Wang D, Zheng X, Ou Q, Huang L, Ou Q. Sex-Dependent Association of Preoperative Hematologic Markers With Glioma Grade and Progression. *J Neurooncol* (2018) 137:279–87. doi: 10.1007/s11060-017-2714-3

196. Liang R, Chen N, Li M, Wang X, Mao Q, Liu Y. Significance of Systemic Immune-Inflammation Index in the Differential Diagnosis of High- and Low-Grade Gliomas. *Clin Neurol Neurosurg* (2018) 164:50–2. doi: 10.1016/j.clineuro.2017.11.011
197. Kemerdere R, Akgun MY, Toklu S, Alizada O, Tanriverdi T. Preoperative Systemic Inflammatory Markers in Low- and High-Grade Gliomas: A Retrospective Analysis of 171 Patients. *Heliyon* (2019) 5:e01681. doi: 10.1016/j.heliyon.2019.e01681
198. Lopes M, Carvalho B, Vaz R, Linhares P. Influence of Neutrophil–Lymphocyte Ratio in Prognosis of Glioblastoma Multiforme. *J Neurooncol* (2018) 136:173–80. doi: 10.1007/s11060-017-2641-3
199. Brockmann MA, Giese A, Mueller K, Kaba FJ, Lohr F, Weiss C, et al. Preoperative Thrombocytosis Predicts Poor Survival in Patients With Glioblastoma. *Neuro Oncol* (2007) 9:335–42. doi: 10.1215/15228517-2007-013
200. Auezova R, Ryskeldiev N, Doskaliyev A, Kuanyshev Y, Zhetpisbaev B, Aldiyarova N, et al. Association of Preoperative Levels of Selected Blood Inflammatory Markers With Prognosis in Gliomas. *Onco Targets Ther* (2016) 9:6111–7. doi: 10.2147/OTT.S113606
201. Wang Z, Zhong L, Li G, Huang R, Wang Q, Wang Z, et al. Pre-Treatment Neutrophils Count as a Prognostic Marker to Predict Chemotherapeutic Response and Survival Outcomes in Glioma: A Single-Center Analysis of 288 Cases. *Am J Transl Res* (2020) 12:90–104.
202. Williams M, Zi, Liu W, Woolf D, Hargreaves S, Michalarea V, Menashy R, et al. Change in Platelet Levels During Radiotherapy With Concurrent and Adjuvant Temozolomide for the Treatment of Glioblastoma: A Novel Prognostic Factor for Survival. *J Cancer Res Clin Oncol* (2012) 138:1683–8. doi: 10.1007/s00432-012-1243-x
203. McNamara MG, Lwin Z, Jiang H, Templeton AJ, Zadeh G, Bernstein M, et al. Factors Impacting Survival Following Second Surgery in Patients With Glioblastoma in the Temozolomide Treatment Era, Incorporating Neutrophil/Lymphocyte Ratio and Time to First Progression. *J Neurooncol* (2014) 117:147–52. doi: 10.1007/s11060-014-1366-9
204. Han S, Liu Y, Li Q, Li Z, Hou H, Wu A. Pre-Treatment Neutrophil-to-Lymphocyte Ratio is Associated With Neutrophil and T-Cell Infiltration and Predicts Clinical Outcome in Patients With Glioblastoma. *BMC Cancer* (2015) 15:617. doi: 10.1186/s12885-015-1629-7
205. Yersal Ö, Odabaşi E, Özdemir Ö, Kemal Y. Prognostic Significance of Pre –Treatment Neutrophil–to–Lymphocyte Ratio and Platelet–to–Lymphocyte Ratio in Patients With Glioblastoma. *Mol Clin Oncol* (2018) 9:453. doi: 10.3892/mco.2018.1695
206. Kayhan A, Korkmaz TS, Baran O, Kemerdere R, Yeni SN, Tanriverdi T. Preoperative Systemic Inflammatory Markers in Different Brain Pathologies: An Analysis of 140 Patients. *Turk Neurosurg* (2019) 29:799–803. doi: 10.5137/1019-5149.JTN.24244-18.2
207. Baran O, Kemerdere R, Korkmaz TS, Kayhan A, Tanriverdi T. Can Preoperative Neutrophil to Lymphocyte, Lymphocyte to Monocyte, or Platelet to Lymphocyte Ratios Differentiate Glioblastoma From Brain Metastasis? *Medicine (United States)* (2019) 98:e18306. doi: 10.1097/MD.0000000000018306
208. Campanella R, Guarnaccia L, Cordiglieri C, Trombetta E, Caroli M, Carrabba G, et al. Tumor-Educated Platelets and Angiogenesis in Glioblastoma: Another Brick in the Wall for Novel Prognostic and Targetable Biomarkers, Changing the Vision From a Localized Tumor to a Systemic Pathology. *Cells* (2020) 9:294. doi: 10.3390/cells9020294
209. Best MG, Sol N, Kooi I, Tannous J, Westerman BA, Rustenburg F, et al. RNA-Seq of Tumor-Educated Platelets Enables Blood-Based Pan-Cancer, Multiclass, and Molecular Pathway Cancer Diagnostics. *Cancer Cell* (2015) 28:666–76. doi: 10.1016/j.ccell.2015.09.018
210. Liefaard MC, Lips E, Best M, Sol N, Veld SI'T, Rookus M, et al. RNA Signatures From Tumor-Educated Platelets (TEP) Enable Detection of Early-Stage Breast Cancer. *Ann Oncol* (2019) 30. doi: 10.1093/annonc/mdz095.036
211. Sheng M, Dong Z, Xie Y. Identification of Tumor-Educated Platelet Biomarkers of Non-Small-Cell Lung Cancer. *Onco Targets Ther* (2018) 11:8143–51. doi: 10.2147/OTT.S177384
212. Xue L, Xie L, Song X, Song X. Expression and Significance of ACIN1 mRNA in Platelets of Lung Cancer. *Chin J Lung Cancer* (2018) 21:677–81. doi: 10.3779/j.issn.1009-3419.2018.09.05
213. Xing S, Zeng T, Xue N, He Y, Lai YZ, Li HL, et al. Development and Validation of Tumor-Educated Blood Platelets Integrin Alpha 2b (ITGA2B) RNA for Diagnosis and Prognosis of non-Small-Cell Lung Cancer Through RNA-Seq. *Int J Biol Sci* (2019) 15:1977–92. doi: 10.7150/ijbs.36284
214. Asghar S, Waqar W, Umar M, Manzoor S. Tumor Educated Platelets, a Promising Source for Early Detection of Hepatocellular Carcinoma: Liquid Biopsy an Alternative Approach to Tissue Biopsy. *Clin Res Hepatol Gastroenterol* (2020) 44:836–44. doi: 10.1016/j.clinre.2020.03.023
215. Campbell RA, Franks Z, Bhatnagar A, Rowley JW, Manne BK, Supiano MA, et al. Granzyme A in Human Platelets Regulates the Synthesis of Proinflammatory Cytokines by Monocytes in Aging. *J Immunol* (2018) 200:295–304. doi: 10.4049/jimmunol.1700885
216. Simon LM, Edelstein LC, Nagalla S, Woodley AB, Chen ES, Kong X, et al. Human Platelet microRNA-mRNA Networks Associated With Age and Gender Revealed by Integrated Plateletomics. *Blood* (2014) 123:e37–45. doi: 10.1182/blood-2013-12-544692
217. Best MG, Vancura A, Wurdinger T. Platelet RNA as a Circulating Biomarker Trove for Cancer Diagnostics. *J Thromb Haemost* (2017) 15:1295–306. doi: 10.1111/jth.13720
218. Sol N, In 't Veld GJG, Vancura A, Tjerkstra M, Leurs C, Rustenburg FO, et al. Tumor-Educated Platelet RNA for the Detection and (Pseudo)Progression Monitoring of Glioblastoma. *Cell Rep Med* (2020) 1:100101. doi: 10.1016/j.xcrm.2020.100101
219. Best MG, In 't Veld SGJG, Sol N, Wurdinger T. RNA Sequencing and Swarm Intelligence–Enhanced Classification Algorithm Development for Blood-Based Disease Diagnostics Using Spliced Blood Platelet RNA. *Nat Protoc* (2019) 14:1206–34. doi: 10.1038/s41596-019-0139-5
220. Fossati G, Ricevuti G, Edwards SW, Walker C, Dalton A, Rossi ML. Neutrophil Infiltration Into Human Gliomas. *Acta Neuropathol* (1999) 98:349–54. doi: 10.1007/s004010051093
221. Serra-Bonett N, Al Snih S, Rodriguez MA. Effect of Low-Dose Prednisone on Leukocyte Counts and Subpopulations in Patients With Rheumatoid Arthritis. *J Clin Rheumatol* (2009) 15:148–9. doi: 10.1097/RHU.0b013e3181a3ac2d
222. Shoenfeld Y, Gurewich Y, Gallant LA, Pinkhas J. Prednisone-Induced Leukocytosis. Influence of Dosage, Method and Duration of Administration on the Degree of Leukocytosis. *Am J Med* (1981) 71:773–8. doi: 10.1016/0002-9343(81)90363-6
223. Olnes MJ, Kotliarov Y, Biancotto A, Cheung F, Chen J, Shi R, et al. Effects of Systemically Administered Hydrocortisone on the Human Immunome. *Sci Rep* (2016) 6:1–15. doi: 10.1038/srep23002
224. Frenkel A, Kachko E, Novack V, Klein M, Brotfain E, Koyfman L, et al. The Association of Glucocorticosteroid Treatment With WBC Count in Patients With COPD Exacerbation. *J Clin Med* (2019) 8:1697. doi: 10.3390/jcm8101697
225. Wang ZL, Zhang CB, Liu YQ, Wang Z, Jiang T. Peripheral Blood Test Provides a Practical Method for Glioma Evaluation and Prognosis Prediction. *CNS Neurosci Ther* (2019) 25:876–83. doi: 10.1111/cns.13120
226. Weng W, Chen X, Gong S, Guo L, Zhang X. Preoperative Neutrophil–Lymphocyte Ratio Correlated With Glioma Grading and Glioblastoma Survival. *Neurol Res* (2018) 40:917–22. doi: 10.1080/01616412.2018.1497271
227. Schernberg A, Nivet A, Dhermain F, Ammari S, Escande A, Pallud J, et al. Neutrophilia as a Biomarker for Overall Survival in Newly Diagnosed High-Grade Glioma Patients Undergoing Chemoradiation. *Clin Transl Radiat Oncol* (2018) 10:47–52. doi: 10.1016/j.ctro.2018.04.002
228. Adachi-Hayama M, Adachi A, Shinozaki N, Matsutani T, Hiwasa T, Takiguchi M, et al. Circulating Anti-Filamin C Autoantibody as a Potential Serum Biomarker for Low-Grade Gliomas. *BMC Cancer* (2014) 14:452. doi: 10.1186/1471-2407-14-452
229. Gustafson MP, Lin Y, New KC, Bulur PA, O'Neill BP, Gastineau DA, et al. Systemic Immune Suppression in Glioblastoma: The Interplay Between CD14 +HLA-DR Lo/Neg Monocytes, Tumor Factors, and Dexamethasone. *Neuro Oncol* (2010) 12:631–44. doi: 10.1093/neuonc/noq001
230. Bambury RM, Teo MY, Power DG, Yusuf A, Murray S, Battley JE, et al. The Association of Pre-Treatment Neutrophil to Lymphocyte Ratio With Overall Survival in Patients With Glioblastoma Multiforme. *J Neurooncol* (2013) 114:149–54. doi: 10.1007/s11060-013-1164-9
231. Bertaut A, Truntzer C, Madkouri R, Kaderbhai CG, Derangère V, Vincent J, et al. Blood Baseline Neutrophil Count Predicts Bevacizumab Efficacy in Glioblastoma. *Oncotarget* (2016) 7:70948–58. doi: 10.18632/oncotarget.10898
232. Boonyawan K, Hess KR, Yang J, Long L, Wang Q, Ezhilarasan R, et al. A Relative Increase in Circulating Platelets Following Chemoradiation Predicts

for Poor Survival of Patients With Glioblastoma. *Oncotarget* (2017) 8:90488–95. doi: 10.18632/oncotarget.21799
233. Gousias K, Voulgaris S, Vartholomatos G, Voulgari P, Kyritsis AP, Markou M. Prognostic Value of the Preoperative Immunological Profile in Patients With Glioblastoma. *Surg Neurol Int* (2014) 5:89. doi: 10.4103/2152-7806.134104
234. Gan Y, Zhou X, Niu X, Li J, Wang T, Zhang H, et al. Neutrophil/Lymphocyte Ratio is an Independent Prognostic Factor in Elderly Patients With High-Grade Gliomas. *World Neurosurg* (2019) 127:e261–7. doi: 10.1016/j.wneu.2019.03.085
235. Vaios EJ, Winter SF, Muzikansky A, Nahed BV, Dietrich J. Eosinophil and Lymphocyte Counts Predict Bevacizumab Response and Survival in Recurrent Glioblastoma. *Neurooncol Adv* (2020) 2:1–11. doi: 10.1093/noajnl/vdaa031
236. Capper D, von Deimling A, Brandes AA, Carpentier AF, Kesari S, Sepulveda-Sanchez JM, et al. Biomarker and Histopathology Evaluation of Patients With Recurrent Glioblastoma Treated With Galunisertib, Lomustine, or the Combination of Galunisertib and Lomustine. *Int J Mol Sci* (2017) 18:995. doi: 10.3390/ijms18050995
237. Wiencke JK, Accomando WP, Zheng S, Patoka J, Dou X, Phillips JJ, et al. Epigenetic Biomarkers of T-Cells in Human Glioma. *Epigenetics* (2012) 7:1391–402. doi: 10.4161/epi.22675
238. Bahador M, Gras Navarro A, Rahman MA, Dominguez-Valentin M, Sarowar S, Ulvestad E, et al. Increased Infiltration and Tolerised Antigen-Specific CD8+ TEM Cells in Tumor But Not Peripheral Blood Have No Impact on Survival of HCMV+ Glioblastoma Patients. *Oncoimmunology* (2017) 6: e1336272. doi: 10.1080/2162402X.2017.1336272
239. Bhondeley MK, Mehra RD, Mehra NK, Mohapatra AK, Tandon PN, Roy VB S. Imbalances in T Cell Subpopulations in Human Gliomas in. *J Neurosurg* (1988) 68:589–93. doi: 10.3171/jns.1988.68.4.0589
240. Fecci PE, Mitchell DA, Whitesides JF, Xie W, Friedman AH, Archer GE, et al. Increased Regulatory T-Cell Fraction Amidst a Diminished CD4 Compartment Explains Cellular Immune Defects in Patients With Malignant Glioma. *Cancer Res* (2006) 66:3294–302. doi: 10.1158/0008-5472.CAN-05-3773
241. Vasco C, Canazza A, Rizzo A, Mossa A, Corsini E, Silvani A, et al. Circulating T Regulatory Cells Migration and Phenotype in Glioblastoma Patients: An In Vitro Study. *J Neurooncol* (2013) 115:353–63. doi: 10.1007/s11060-013-1236-x
242. Mohme M, Schliffke S, Maire CL, Runger A, Glau L, Mende KC, et al. Immunophenotyping of Newly Diagnosed and Recurrent Glioblastoma Defines Distinct Immune Exhaustion Profiles in Peripheral and Tumor-Infiltrating Lymphocytes. *Clin Cancer Res* (2018) 24:4187–200. doi: 10.1158/1078-0432.CCR-17-2617
243. Gousias K, von Ruecker A, Voulgari P, Simon M. Phenotypical Analysis, Relation to Malignancy and Prognostic Relevance of ICOS + T Regulatory and Dendritic Cells in Patients With Gliomas. *J Neuroimmunol* (2013) 264:84–90. doi: 10.1016/j.jneuroim.2013.09.001
244. Ogden AT, Horgan D, Waziri A, Anderson D, Louca J, McKhann GM, et al. Defective Receptor Expression and Dendritic Cell Differentiation of Monocytes in Glioblastomas. *Neurosurgery* (2006) 59:902–10. doi: 10.1227/01.NEU.0000233907.03070.7B
245. Li X, Wang B, Gu L, Zhang J, Li X, Gao L, et al. Tim-3 Expression Predicts the Abnormal Innate Immune Status and Poor Prognosis of Glioma Patients. *Clin Chim Acta* (2018) 476:178–84. doi: 10.1016/j.cca.2017.11.022
246. Wilson JRF, Saeed F, Tyagi AK, Goodden JR, Sivakumar G, Crimmins D, et al. Pre-Operative Neutrophil Count and Neutrophil-Lymphocyte Count Ratio (NLCR) in Predicting the Histological Grade of Paediatric Brain Tumours: A Preliminary Study. *Acta Neurochir (Wien)* (2018) 160:793–800. doi: 10.1007/s00701-017-3388-5
247. Evans SM, Putt M, Yang X-Y, Lustig RA, Martinez-Lage M, Williams D, et al. Initial Evidence That Blood-Borne Microvesicles are Biomarkers for Recurrence and Survival in Newly Diagnosed Glioblastoma Patients. *J Neurooncol* (2016) 127:391–400. doi: 10.1007/s11060-015-2051-3
248. Pinton L, Masetto E, Vettore M, Solito S, Magri S, D'Andolfi M, et al. The Immune Suppressive Microenvironment of Human Gliomas Depends on the Accumulation of Bone Marrow-Derived Macrophages in the Center of the Lesion. *J Immunother Cancer* (2019) 7:58. doi: 10.1186/s40425-019-0536-x
249. Guo Y, Hong W, Zhang P, Han D, Fang Y, Tu J, et al. Abnormal Polarization of Macrophage-Like Cells in the Peripheral Blood of Patients With Glioma. *Oncol Lett* (2020) 20:947–54. doi: 10.3892/ol.2020.11602
250. Vidyarthi A, Agnihotri T, Khan N, Singh S, Tewari MK, Radotra BD, et al. Predominance of M2 Macrophages in Gliomas Leads to the Suppression of Local and Systemic Immunity. *Cancer Immunol Immunother* (2019) 68:1995–2004. doi: 10.1007/s00262-019-02423-8
251. Sippel TR, White J, Nag K, Tsvankin V, Klaassen M, Kleinschmidt-DeMasters BK, et al. Neutrophil Degranulation and Immunosuppression in Patients With GBM: Restoration of Cellular Immune Function by Targeting Arginase I. *Clin Cancer Res* (2011) 17:6992–7002. doi: 10.1158/1078-0432.CCR-11-1107
252. Templeton AJ, McNamara MG, Šeruga B, Vera-Badillo FE, Aneja P, Ocaña A, et al. Prognostic Role of Neutrophil-to-Lymphocyte Ratio in Solid Tumors: A Systematic Review and Meta-Analysis. *J Natl Cancer Inst* (2014) 106:dju124. doi: 10.1093/jnci/dju124
253. Chen J, Deng Q, Pan Y, He B, Ying H, Sun H, et al. Prognostic Value of Neutrophil-to-Lymphocyte Ratio in Breast Cancer. *FEBS Open Bio* (2015) 5:502–7. doi: 10.1016/j.fob.2015.05.003
254. Shimada H, Takiguchi N, Kainuma O, Soda H, Ikeda A, Cho A, et al. High Preoperative Neutrophil-Lymphocyte Ratio Predicts Poor Survival in Patients With Gastric Cancer. *Gastric Cancer* (2010) 13:170–6. doi: 10.1007/s10120-010-0554-3
255. Ferrucci PF, Ascierto PA, Pigozzo J, Vecchio MD, Maio M, Cappellini GCA, et al. Baseline Neutrophils and Derived Neutrophil-to-Lymphocyte Ratio: Prognostic Relevance in Metastatic Melanoma Patients Receiving Ipilimumab. *Ann Oncol* (2016) 27:732–8. doi: 10.1093/annonc/mdw016
256. Tweardy DJ, Cannizzaro LA, Palumbo AP, Shane S, Huebner K, Vantuinen P, et al. Molecular Cloning and Characterization of a cDNA for Human Granulocyte Colony-Stimulating Factor (G-CSF) From a Glioblastoma Multiforme Cell Line and Localization of the G-CSF Gene to Chromosome Band 17q21. *Oncogene Res* (1987) 1:209–20.
257. Teramukai S, Kitano T, Kishida Y, Kawahara M, Kubota K, Komuta K, et al. Pretreatment Neutrophil Count as an Independent Prognostic Factor in Advanced Non-Small-Cell Lung Cancer: An Analysis of Japan Multinational Trial Organisation LC00-03. *Eur J Cancer* (2009) 45:1950–8. doi: 10.1016/j.ejca.2009.01.023
258. Lechner MG, Liebertz DJ, Epstein AL. Characterization of Cytokine-Induced Myeloid-Derived Suppressor Cells From Normal Human Peripheral Blood Mononuclear Cells. *J Immunol* (2010) 185:2273–84. doi: 10.4049/jimmunol.1000901
259. Balkwill F, Mantovani A. Inflammation and Cancer: Back to Virchow? *Lancet* (2001) 357:539–45. doi: 10.1016/S0140-6736(00)04046-0
260. Fridlender ZG, Sun J, Kim S, Kapoor V, Cheng G, Ling L, et al. Polarization of Tumor-Associated Neutrophil Phenotype by TGF-β: "N1" Versus "N2" Tan. *Cancer Cell* (2009) 16:183–94. doi: 10.1016/j.ccr.2009.06.017
261. Uribe-Querol E, Rosales C. Neutrophils in Cancer: Two Sides of the Same Coin. *J Immunol Res* (2015) 2015:983698. doi: 10.1155/2015/983698
262. Wiencke JK, Koestler DC, Salas LA, Wiemels JL, Roy RP, Hansen HM, et al. Immunomethylomic Approach to Explore the Blood Neutrophil Lymphocyte Ratio (NLR) in Glioma Survival. *Clin Epigenet* (2017) 9:10. doi: 10.1186/s13148-017-0316-8
263. Wang J, Xiao W, Chen W, Hu Y. Prognostic Significance of Preoperative Neutrophil-to-Lymphocyte Ratio and Platelet-to-Lymphocyte Ratio in Patients With Glioma. *EXCLI J* (2019) 17:505–12. doi: 10.17179/excli2017-978
264. Tan Z, Shen L, Wu H, Deng L, Li Z, Huang X. Preoperative Neutrophil/Lymphocyte Ratio Is an Independent Prognostic Biomarker in Patients With Low-Grade Gliomas. *World Neurosurg* (2019) 132:e585–90. doi: 10.1016/j.wneu.2019.08.068
265. Huang Y, Ding H, Wu Q, Li Z, Li H, Li S, et al. Neutrophil–Lymphocyte Ratio Dynamics are Useful for Distinguishing Between Recurrence and Pseudoprogression in High-Grade Gliomas. *Cancer Manag Res* (2019) 11:6003–9. doi: 10.2147/CMAR.S202546
266. Bao Y, Yang M, Jin C, Hou S, Shi B, Shi J, et al. Preoperative Hematologic Inflammatory Markers as Prognostic Factors in Patients With Glioma. *World Neurosurg* (2018) 119:e710–6. doi: 10.1016/j.wneu.2018.07.252
267. Lv Y, Zhang S, Liu Z, Tian Y, Liang N, Zhang J. Prognostic Value of Preoperative Neutrophil to Lymphocyte Ratio is Superior to Systemic Immune Inflammation Index for Survival in Patients With Glioblastoma. *Clin Neurol Neurosurg* (2019) 181:24–7. doi: 10.1016/j.clineuro.2019.03.017
268. Alexiou G, Vartholomatos E, Voulgaris S, Zagorianakou P. Prognostic Significance of Neutrophil-to-Lymphocyte Ratio in Glioblastoma.

Neuroimmunol Neuroinflamm (2014) 1:131–4. doi: 10.4103/2347-8659.143666

269. Kaya V, Yildirim M, Yazici G, Yalçin AY, Orhan N, Güzel A. Prognostic Significance of Indicators of Systemic Inflammatory Responses in Glioblastoma Patients. *Asian Pac J Cancer Prev* (2017) 18:3287–91. doi: 10.22034/APJCP.2017.18.12.3287
270. Brenner A, Friger M, Geffen DB, Kaisman-Elbaz T, Lavrenkov K. The Prognostic Value of the Pretreatment Neutrophil/Lymphocyte Ratio in Patients With Glioblastoma Multiforme Brain Tumors: A Retrospective Cohort Study of Patients Treated With Combined Modality Surgery, Radiation Therapy, and Temozolomide Chemotherapy. *Oncology* (2019) 97:255–63. doi: 10.1159/000500926
271. Weng Y, Zhang X, Han J, Ouyang L, Liang M, Shi Z, et al. Do Selected Blood Inflammatory Markers Combined With Radiological Features Predict Proliferation Index in Glioma Patients? *World Neurosurg* (2018) 118:e137–46. doi: 10.1016/j.wneu.2018.06.142
272. Zadora P, Dabrowski W, Czarko K, Smolen A, Kotlinska-Hasiec E, Wiorkowski K, et al. Preoperative Neutrophil-Lymphocyte Count Ratio Helps Predict the Grade of Glial Tumor – A Pilot Study. *Neurol Neurochir Pol* (2015) 49:41–4. doi: 10.1016/j.pjnns.2014.12.006
273. Hong X, Cui B, Wang M, Yang Z, Wang L, Xu Q. Systemic Immune-Inflammation Index, Based on Platelet Counts and Neutrophil-Lymphocyte Ratio, is Useful for Predicting Prognosis in Small Cell Lung Cancer. *Tohoku J Exp Med* (2015) 236:297–304. doi: 10.1620/tjem.236.297
274. Hu B, Yang XR, Xu Y, Sun YF, Sun C, Guo W, et al. Systemic Immune-Inflammation Index Predicts Prognosis of Patients After Curative Resection for Hepatocellular Carcinoma. *Clin Cancer Res* (2014) 20:6212–22. doi: 10.1158/1078-0432.CCR-14-0442
275. Chen Z, Shao Y, Wang K, Cao W, Xiong Y, Wu R, et al. Prognostic Role of Pretreatment Serum Albumin in Renal Cell Carcinoma: A Systematic Review and Meta-Analysi. *Onco Targets Ther* (2016) 9:6701–10. doi: 10.2147/OTT.S108469
276. Pinzon-Charry A, Ho CSK, Laherty R, Maxwell T, Walker D, Gardiner RA, et al. A Population of HLA-DR+ Immature Cells Accumulates in the Blood Dendritic Cell Compartment of Patients With Different Types of Cancer. *Neoplasia* (2005) 7:1112–22. doi: 10.1593/neo.05442
277. Male D, Brostoff J, Roth D, Roitt I. *Immunology*, *8th Edition*. (2012) Elsevier. p. 482.
278. Raychaudhuri B, Ireland PRJ, Ko J, Rini B, Borden EC, Garcia J, et al. Myeloid-Derived Suppressor Cell Accumulation and Function in Patients With Newly Diagnosed Glioblastoma. *Neuro Oncol* (2011) 13:591–9. doi: 10.1093/neuonc/nor042
279. Gabrusiewicz K, Rodriguez B, Wei J, Hashimoto Y, Healy LM, Maiti SN, et al. Glioblastoma-Infiltrated Innate Immune Cells Resemble M0 Macrophage Phenotype. *JCI Insight* (2016) 1:e85841. doi: 10.1172/jci.insight.85841
280. Gielen PR, Schulte BM, Kers-Rebel ED, Verrijp K, Petersen-Baltussen HMJM, Ter Laan M, et al. Increase in Both CD14-Positive and CD15-Positive Myeloid-Derived Suppressor Cell Subpopulations in the Blood of Patients With Glioma But Predominance of CD15-Positive Myeloid-Derived Suppressor Cells in Glioma Tissue. *J Neuropathol Exp Neurol* (2015) 74:390–400. doi: 10.1097/NEN.0000000000000183
281. Dubinski D, Wölfer J, Hasselblatt M, Schneider-Hohendorf T, Bogdahn U, Stummer W, et al. CD4+ T Effector Memory Cell Dysfunction is Associated With the Accumulation of Granulocytic Myeloid-Derived Suppressor Cells in Glioblastoma Patients. *Neuro Oncol* (2016) 18:807–18. doi: 10.1093/neuonc/nov280
282. Sakaguchi S. Naturally Arising CD4+ Regulatory T Cells for Immunologic Self-Tolerance and Negative Control of Immune Responses. *Annu Rev Immunol* (2004) 22:531–62. doi: 10.1146/annurev.immunol.21.120601.141122
283. Facciabene A, Motz GT, Coukos G. T-Regulatory Cells: Key Players in Tumor Immune Escape and Angiogenesis. *Cancer Res* (2012) 72:2162–71. doi: 10.1158/0008-5472.CAN-11-3687
284. Andaloussi A, Lesniak MS. An Increase in CD4+CD25+FOXP3+ Regulatory T Cells in Tumor-Infiltrating Lymphocytes of Human Glioblastoma Multiforme. *Neuro Oncol* (2006) 8:234–43. doi: 10.1215/15228517-2006-006
285. Li Z, Liu X, Guo R, Wang P. CD4+Foxp3− Type 1 Regulatory T Cells in Glioblastoma Multiforme Suppress T Cell Responses Through Multiple Pathways and are Regulated by Tumor-Associated Macrophages. *Int J Biochem Cell Biol* (2016) 81:1–9. doi: 10.1016/j.biocel.2016.09.013
286. Jacobs JFM, Idema AJ, Bol KF, Nierkens S, Grauer OM, Wesseling P, et al. Regulatory T Cells and the PD-L1/PD-1 Pathway Mediate Immune Suppression in Malignant Human Brain Tumors. *Neuro Oncol* (2009) 11:394–402. doi: 10.1215/15228517-2008-104
287. Willms E, Cabañas C, Mäger I, Wood MJA, Vader P. Extracellular Vesicle Heterogeneity: Subpopulations, Isolation Techniques, and Diverse Functions in Cancer Progression. *Front Immunol* (2018) 9:1. doi: 10.3389/fimmu.2018.00738
288. Stahl PD, Raposo G. Extracellular Vesicles: Exosomes and Microvesicles, Integrators of Homeostasis. *Physiology (Bethesda)* (2019) 34:169–77. doi: 10.1152/physiol.00045.2018
289. Osti D, Bene MD, Rappa G, Santos M, Matafora V, Richichi C, et al. Clinical Significance of Extracellular Vesicles in Plasma From Glioblastoma Patients. *Clin Cancer Res* (2019) 25:266–76. doi: 10.1158/1078-0432.CCR-18-1941
290. Ricklefs FL, Maire CL, Reimer R, Dührsen L, Kolbe K, Holz M, et al. Imaging Flow Cytometry Facilitates Multiparametric Characterization of Extracellular Vesicles in Malignant Brain Tumours. *J Extracell Vesicles* (2019) 8:1588555. doi: 10.1080/20013078.2019.1588555
291. Reynés G, Vila V, Fleitas T, Reganon E, Font de Mora J, Jordá M, et al. Circulating Endothelial Cells and Procoagulant Microparticles in Patients With Glioblastoma: Prognostic Value. *PloS One* (2013) 8:e69034. doi: 10.1371/journal.pone.0069034
292. Cumba Garcia LM, Peterson TE, Cepeda MA, Johnson AJ, Parney IF. Isolation and Analysis of Plasma-Derived Exosomes in Patients With Glioma. *Front Oncol* (2019) 10:3338. doi: 10.3389/fonc.2019.00651
293. Koch CJ, Lustig RA, Yang XY, Jenkins WT, Wolf RL, Martinez-Lage M, et al. Microvesicles as a Biomarker for Tumor Progression Versus Treatment Effect in Radiation/Temozolomide-Treated Glioblastoma Patients. *Transl Oncol* (2014) 7:752–8. doi: 10.1016/j.tranon.2014.10.004
294. Muller L, Muller-Haegele S, Mitsuhashi M, Gooding W, Okada H, Whiteside TL. Exosomes Isolated From Plasma of Glioma Patients Enrolled in a Vaccination Trial Reflect Antitumor Immune Activity and Might Predict Survival. *Oncoimmunology* (2015) 4:e1008347. doi: 10.1080/2162402X.2015.1008347
295. Lei YY, Li YT, Hu QL, Wang J, Sui AX. Prognostic Impact of Neutrophil-to-Lymphocyte Ratio in Gliomas: A Systematic Review and Meta-Analysis. *World J Surg Oncol* (2019) 17:1–8. doi: 10.1186/s12957-019-1686-5
296. Hallal S, Azimi A, Wei H, Ho N, Lee MYT, Sim H-W, et al. A Comprehensive Proteomic SWATH-MS Workflow for Profiling Blood Extracellular Vesicles: A New Avenue for Glioma Tumour Surveillance. *Int J Mol Sci* (2020) 21:4754. doi: 10.3390/ijms21134754
297. Ding C, Yi X, Wu X, Bu X, Wang D, Wu Z, et al. Exosome-Mediated Transfer of circRNA CircNFIX Enhances Temozolomide Resistance in Glioma. *Cancer Lett* (2020) 479:1–12. doi: 10.1016/j.canlet.2020.03.002
298. Shao H, Chung J, Balaj L, Charest A, Bigner DD, Carter BS, et al. Protein Typing of Circulating Microvesicles Allows Real-Time Monitoring of Glioblastoma Therapy. *Nat Med* (2012) 18:1835–40. doi: 10.1038/nm.2994
299. Wang H, Jiang D, Li W, Xiang X, Zhao J, Yu B, et al. Evaluation of Serum Extracellular Vesicles as Noninvasive Diagnostic Markers of Glioma. *Theranostics* (2019) 9:5347–58. doi: 10.7150/thno.33114
300. Johnson CH, Patterson AD, Idle JR, Gonzalez FJ. Xenobiotic Metabolomics: Major Impact on the Metabolome. *Annu Rev Pharmacol Toxicol* (2012) 52:37–56. doi: 10.1146/annurev-pharmtox-010611-134748
301. Baranovičová E, Galanda T, Galanda M, Jozef H, Kolarovszki B, Richterová R, et al. Metabolomic Profiling of Blood Plasma in Patients With Primary Brain Tumours: Basal Plasma Metabolites Correlated With Tumour Grade and Plasma Biomarker Analysis Predicts Feasibility of the Successful Statistical Discrimination From Healthy Subjects - a P. *IUBMB Life* (2019) 71:1994–2002. doi: 10.1002/iub.2149
302. Zhao H, Heimberger AB, Lu Z, Wu X, Hodges TR, Song R, et al. Metabolomics Profiling in Plasma Samples From Glioma Patients Correlataes With Tumor Phenotypes. *Oncotarget* (2016) 7:20486–95. doi: 10.18632/oncotarget.7974
303. Mörén L, Tommy Bergenheim A, Ghasimi S, Brännström T, Johansson M, Antti H. Metabolomic Screening of Tumor Tissue and Serum in Glioma Patients Reveals Diagnostic and Prognostic Information. *Metabolites* (2015) 5:502–20. doi: 10.3390/metabo5030502

304. Shen J, Song R, Hodges TR, Heimberger AB, Zhao H. Identification of Metabolites in Plasma for Predicting Survival in Glioblastoma. *Mol Carcinog* (2018) 57:1078–84. doi: 10.1002/mc.22815
305. Björkblom B, Wibom C, Jonsson P, Mörén L, Andersson U, Johannesen TB, et al. Metabolomic Screening of Pre-Diagnostic Serum Samples Identifies Association Between α- and γ-Tocopherols and Glioblastoma Risk. *Oncotarget* (2016) 7:37043–53. doi: 10.18632/oncotarget.9242
306. Huang J, Weinstein SJ, Kitahara CM, Karoly ED, Sampson JN, Albanes D. A Prospective Study of Serum Metabolites and Glioma Risk. *Oncotarget* (2017) 8:70366–77. doi: 10.18632/oncotarget.19705
307. Kelimu A, Xie R, Zhang K, Zhuang Z, Mamtimin B, Sheyhidin I. Metabonomic Signature Analysis in Plasma Samples of Glioma Patients Based on 1H-Nuclear Magnetic Resonance Spectroscopy. *Neurol India* (2016) 64:246–51. doi: 10.4103/0028-3886.177606
308. Zhao S, Cai J, Li J, Bao G, Li D, Li Y, et al. Bioinformatic Profiling Identifies a Glucose-Related Risk Signature for the Malignancy of Glioma and the Survival of Patients. *Mol Neurobiol* (2017) 54:8203–10. doi: 10.1007/s12035-016-0314-4
309. McGirt MJ, Chaichana KL, Gathinji M, Attenello F, Than K, Ruiz AJ, et al. Persistent Outpatient Hyperglycemia is Independently Associated With Decreased Survival After Primary Resection of Malignant Brain Astrocytomas. *Neurosurgery* (2008) 63:286–91. doi: 10.1227/01.NEU.0000315282.61035.48
310. Mayer A, Vaupel P, Struss HG, Giese A, Stockinger M, Schmidberger H. Strong Adverse Prognostic Impact of Hyperglycemic Episodes During Adjuvant Chemoradiotherapy of Glioblastoma Multiforme. *Strahlenther Onkol* (2014) 190:933–8. doi: 10.1007/s00066-014-0696-z
311. Derr RL, Ye X, Islas MU, Desideri S, Saudek CD, Grossman SA. Association Between Hyperglycemia and Survival in Patients With Newly Diagnosed Glioblastoma. *J Clin Oncol* (2009) 27:1082–6. doi: 10.1200/JCO.2008.19.1098
312. Shih CC, Lee TS, Tsuang FY, Lin PL, Cheng YJ, Cheng HL, et al. Pretreatment Serum Lactate Level as a Prognostic Biomarker in Patients Undergoing Supratentorial Primary Brain Tumor Resection. *Oncotarget* (2017) 8:63715–23. doi: 10.18632/oncotarget.18891
313. Branco M, Linhares P, Carvalho B, Santos P, Costa BM, Vaz R. Serum Lactate Levels are Associated With Glioma Malignancy Grade. *Clin Neurol Neurosurg* (2019) 186:105546. doi: 10.1016/j.clineuro.2019.105546
314. Whiting PF, Rutjes AWS, Westwood ME, Mallett S, Deeks JJ, Reitsma JB, et al. Quadas-2: A Revised Tool for the Quality Assessment of Diagnostic Accuracy Studies. *Ann Intern Med* (2011) 155:529–36. doi: 10.7326/0003-4819-155-8-201110180-00009
315. McShane LM, Altman DG, Sauerbrei W, Taube SE, Gion M, Clark GM. Reporting Recommendations for Tumour MARKer Prognostic Studies (REMARK). *Br J Cancer* (2005) 93:387–91. doi: 10.1038/sj.bjc.6602678
316. Bustin SA, Benes V, Garson JA, Hellemans J, Huggett J, Kubista M, et al. The MIQE Guidelines: Minimum Information for Publication of Quantitative Real-Time PCR Experiments. *Clin Chem* (2009) 55:611–22. doi: 10.1373/clinchem.2008.112797
317. Iafolla MAJ, Picardo S, Aung K, Hansen AR. Systematic Review and REMARK Scoring of Renal Cell Carcinoma Prognostic Circulating Biomarker Manuscripts. *PloS One* (2019) 14:e0222359. doi: 10.1371/journal.pone.0222359
318. Raza IJ, Tingate CA, Gkolia P, Romero L, Tee JW, Hunn MK. Blood Biomarkers of Glioma in Response Assessment Including Pseudoprogression and Other Treatment Effects: A Systematic Review. *Front Oncol* (2020) 10:1191. doi: 10.3389/fonc.2020.01191
319. Bustin S, Nolan T. Talking the Talk, But Not Walking the Walk: RT-qPCR as a Paradigm for the Lack of Reproducibility in Molecular Research. *Eur J Clin Invest* (2017) 47:756–74. doi: 10.1111/eci.12801
320. Capper D, Jones DTW, Sill M, Hovestadt V, Schrimpf D, Sturm D, et al. DNA Methylation-Based Classification of Central Nervous System Tumours. *Nature* (2018) 555:469–74. doi: 10.1038/nature26000
321. Hanahan D, Weinberg RA. Hallmarks of Cancer: The Next Generation. *Cell* (2011) 144:646–74. doi: 10.1016/j.cell.2011.02.013
322. Miller AM, Shah RH, Pentsova EI, Pourmaleki M, Briggs S, Distefano N, et al. Tracking Tumour Evolution in Glioma Through Liquid Biopsies of Cerebrospinal Fluid. *Nature* (2019) 565:654–8. doi: 10.1038/s41586-019-0882-3

Conflict of Interest: The authors declare that the research was conducted in the absence of any commercial or financial relationships that could be construed as a potential conflict of interest.

frontiers in Oncology

ORIGINAL RESEARCH
published: 26 July 2021
doi: 10.3389/fonc.2021.648152

The COX10-AS1/miR-641/E2F6 Feedback Loop Is Involved in the Progression of Glioma

Liang Liu[†], *Xiaojian Li*[†], *Heming Wu*, *Yong Tang*, *Xiang Li* and *Yan Shi*[*]

Department of Neurosurgery, Nanjing First Hospital, Nanjing Medical University, Nanjing, China

OPEN ACCESS

Edited by:
Haotian Zhao,
New York Institute of Technology, United States

Reviewed by:
Hongwei Zhu,
Third Xiangya Hospital, Central South University, China
Desi Shang,
Harbin Medical University, China

***Correspondence:**
Yan Shi
shiyan9568@foxmail.com

[†]*These authors have contributed equally to this work*

Specialty section:
This article was submitted to Neuro-Oncology and Neurosurgical Oncology, a section of the journal Frontiers in Oncology

Received: *31 December 2020*
Accepted: *16 April 2021*
Published: *26 July 2021*

Citation:
Liu L, Li X, Wu H, Tang Y, Li X and Shi Y (2021) The COX10-AS1/miR-641/E2F6 Feedback Loop Is Involved in the Progression of Glioma. Front. Oncol. 11:648152. doi: 10.3389/fonc.2021.648152

Glioma is the most common primary tumour of the central nervous system and is considered one of the greatest challenges for neurosurgery. Mounting evidence has shown that lncRNAs participate in various biological processes of tumours, including glioma. This study aimed to reveal the role and relevant mechanism of COX10-AS1 in glioma. The expression of COX10-AS1, miR-641 and E2F6 was measured by qRT-PCR and/or western blot. Clone formation assays, EdU assays, Transwell assays and tumour xenograft experiments were performed to evaluate the effects of COX10-AS1, miR-641 and E2F6 on glioma proliferation, migration and invasion. Luciferase reporter assays, RNA pull-down assays and ChIP assays were conducted to analyse the relationship among COX10-AS1, miR-641 and E2F6. We demonstrated that COX10-AS1 was upregulated in glioma tissues and cell lines, which was related to the grade of glioma and patient survival. Next, through functional assays, we found that COX10-AS1 influenced the proliferation, migration and invasion of glioma cell lines. Then, with the help of bioinformatics analysis, we confirmed that COX10-AS1 regulated glioma progress by acting as a sponge of miR-641 to regulate E2F6. Moreover, further study indicated that E2F6 could promote COX10-AS1 expression by binding to its promoter region. Taken together, the data indicated that COX10-AS1 acts as an oncogene in combination with COX10-AS1/miR-641/E2F6 in glioma, which may be beneficial to the diagnosis and treatment of glioma.

Keywords: long non-coding RNA, COX10-AS1, E2F6, glioma, feedback loop

INTRODUCTION

Glioma is the most common primary tumour in the central nervous system, accounting for approximately 60% of all intracranial primary tumours (1, 2). Glioblastoma multiforme (GBM) is the most lethal type of glioma according to the grade of malignancy, with an average survival time of 12 to 14 months and a five-year survival rate of only 4% to 5% (3, 4). The mortality rate of glioma has been stable at 4-5/100,000, ranking among the top 10 in tumour mortality (5). At present, the

treatment of glioma is mainly by surgery, supplemented by radiotherapy and chemotherapy. However, because the tumour tissue is invasive and the boundary between the normal brain tissues (NBTs) is not clear, surgical resection is difficult (6). Glioma with a higher degree of malignancy is not sensitive to radiotherapy, and a high dose of radiation will cause normal brain tissue damage, so the clinical effective rate is only 50% (7). Most chemotherapy drugs cannot be used for treatment because they have difficulty crossing the blood-brain barrier. Overall, active research on the molecular mechanism of glioma is very important for the formulation of treatment strategies for glioma.

Current research has found that most sequences in the genome do not encode proteins and commonly known as non-coding RNAs (ncRNAs), which include circular RNAs (circRNAs), long non-coding RNAs (lncRNAs), and microRNAs (miRNAs) (8). Among them, lncRNAs are non-coding RNAs that do not have an open reading frame (ORF) and have a transcript length greater than 200 nucleotides (9). Initially, researchers found that the expression of many lncRNAs was dysregulated in a variety of tumours, including gliomas and that the expression levels of some lncRNAs could be used as prognostic indicators (10, 11). With further studies, researchers have found that lncRNAs can affect tumour progression by their involvement in a variety of cellular processes, such as proliferation, migration, invasion, autophagy, and epithelial-mesenchymal transition (EMT) (12–14). COX10 antisense RNA 1 (COX10-AS1) is a non-coding transcript located on chromosome 17 (14029292-14069458, complement). Till now, little is known about the role of COX10-AS1 in human diseases. Feng et al. reported that compared with that in healthy oral mucosa, COX10-AS1 was upregulated in oral squamous cell carcinoma tissues (15). Luan et al. found that COX10-AS1 was associated to autophagy and the prognosis of glioma patients (16). However, the regulatory network of COX10-AS1 in the progression of glioma has not been elucidated.

In our present study, we analysed the expression of COX10-AS1 in a public database and in clinical specimens. Consistent with the previous studies, COX10-AS1 was upregulated in glioma tissues and cell lines. Next, gain/loss-of-function assays indicated that COX10-AS1 participated in the proliferation, migration and invasion of glioma cells. Then, with the help of bioinformatics tools and related assays, we demonstrated that COX10-AS1 promoted glioma progression by sponging miR-641 to regulate E2F6. More interestingly, we found that E2F6, a well-known transcription factor (TF), could regulate COX10-AS1 expression by directly binding to its promoter region. By using rescue assays, we concluded that COX10-AS1/miR-641/E2F6 formed a positive feedback loop in glioma progression, which may provide a theoretical basis for the development of new treatment strategies for glioma.

MATERIALS AND METHODS

Clinical Specimens

Thirty glioma tissues and paired adjacent normal brain tissues were collected from patients who were diagnosed with glioma at Nanjing First Hospital. The tissues were frozen in liquid nitrogen and stored at -80°C immediately after surgical resection. All the participants signed written informed consent forms. This research was approved by the Ethics Committee of the Nanjing First Hospital.

Cell Lines

Glioma cell lines (U87, U118, T98G, A172 and LN229) were obtained from Procell (Wuhan, China). The normal human astrocytes (NHAs) obtained from JENNIO Biological Technology (Guangzhou, China). All six cell lines were cultured in Dulbecco's modified Eagle's medium (DMEM, Gibco, NY, USA, Cat. No. 11965092) containing 10% foetal bovine serum (FBS, ScienCell, LA, USA, Cat. No. 0500) and were incubated in an atmosphere containing 5% CO_2 at 37°C.

Interfering Nucleotide Transfection

The chemically synthesized oligonucleotides used in this study were designed and constructed by GenePharma (Shanghai, China). The transfections were performed using Lipofectamine 3000 (Invitrogen, Carlsbad, CA, USA, Cat. No. 2185325) according to the manufacturer's instructions. The interfering nucleotide used in this study were shown in **Table S1**.

RNA Isolation and Quantitative Real-Time Polymerase Chain Reaction (qRT-PCR)

RNA extraction and qRT-PCR were performed as described previously (17). Total RNA was extracted from clinical tissue and cells by TRIzol reagent (Invitrogen, Carlsbad, CA, USA, Cat. No. 15596018). qRT-PCR was conducted using an ABI Prism 7700 Sequence Detection System (Applied Biosystems, Thermo Fisher Scientific, MA, USA) according to the manufacturer's instructions. β-actin was used as an internal control. Relative expression levels of COX10-AS1, miR-641 and E2F6 were measured using the $2^{-\Delta\Delta Ct}$ method. The primers used in this study were shown in **Table S2**.

Nuclear and Cytoplasmic RNA Fraction Isolation

Nuclear and cytoplasmic RNA were isolated from each fraction using a Nuclear/Cytosol Fractionation Kit (BioVision, San Francisc, CA, USA, Cat. No. XY-K266-25) following the manufacturers' instructions. U6 and 18S were used as a nuclear control and cytoplasmic control, respectively.

Western Blot

Total protein was extracted from the cells by using RIPA buffer (KenGEN, Shanghai, China, Cat. No. KGB704), and the protein concentrations were quantified by using a BCA Protein Assay Kit (Beyotime, Shanghai, China, Cat. No. P0012S). The steps were the same as those described in our previous study (18).

The primary antibodies used in this assay were purchased from Abcam (Cambridge, UK, Cat. No. ab53061 & ab8227).

Fluorescence *In Situ* Hybridization (FISH)

FISH assays were performed with a FISH Kit (GenePharma, Shanghai, China, Cat. No. F11202) according to the manufacturer's instructions. The probe used in this study was synthesized and purchased from GenePharma (Shanghai, China). Cells were fixed in 4% paraformaldehyde for 20 min. Next, the cells were preincubated and incubated at 37°C for 30 min with PBS and hybridization solution, respectively. After that, cell nuclei were stained by using DAPI (4′,6-diamidino-2-phenylindole, Beyotime, Jiangsu, China, Cat. No. C1002). The images were captured using a fluorescence microscope (Zeiss, Germany).

RNA Pull-Down Assay

Biotinylated miR-641 and the corresponding mutant/negative control were synthesized and purchased from GenePharma (Shanghai, China). The oligonucleotides were transfected into U87 and LN229 cells using Lipofectamine 3000 (Invitrogen). Forty-eight hours later, the cell lysates were incubated with M-280 streptavidin magnetic beads (Invitrogen, Cat. No. 20164). qRT-PCR was used to detect the expression of COX10-AS1.

Chromatin Immunoprecipitation (ChIP)

ChIP assays were performed by using a ChIP Kit (Magna, Millipore, Bedford, MA, USA, Cat. No. 17-371). The collected cells were cross-linked by formaldehyde, and the reaction was terminated by glycine. After incubation with lysis buffer for 30 min, the cells were sheared by sonication and centrifuged. Then, the DNA–protein complexes were immunoprecipitated using antibodies (anti-E2F6, Abnova, China, Cat No. H00001876-PW1 and lgG, Proteintech, USA, Cat. No. 66360-3-Ig). qRT-PCR was used to detect the purified DNA.

Luciferase Reporter Assay

The fragments of COX10-AS1 or E2F6 containing the miR-641 binding sites (wild type, WT) and negative controls (mutant, MUT) were amplified and cloned into the pGL3 vector (Promega, Madison, WI, USA, Cat No. E1751). Then, U87 and LN229 cells were transfected with miR-641 mimics or controls by using Lipofectamine 3000 (Invitrogen) in accordance with the manufacturers' instructions. Forty-eight hours later, the luciferase activity of the cells was measured by the Dual-Luciferase Reporter Assay System (Promega, WI, USA).

Clone Formation Assay

300 cells were grown in culture plates (60 mm, Corning, NY, USA) and maintained in DMEM containing 10% FBS. 14 d later, cells were fixed with paraformaldehyde (4%) for 20 min. Then stained with 0.1% crystal violet for 15 min. Finally, visible colonies were counted.

5-Ethynyl-20-deoxyuridine (EdU) Assay

EdU assays were performed with an EdU Cell Proliferation Kit (RiboBio, Guangzhou, China, Cat No. 10310-3). The protocol was the same as that described in our previous study (19). A fluorescence microscope (Olympus, Japan) was used to acquire the images.

Transwell Assays

Transwell assays were performed as described previously (18). Matrigel (1:9 dilution, BD, NJ, USA, Cat No. 356234) was used to precoat the upper chamber for Transwell invasion assays. Forty-eight hours later, the cells were fixed, strained and counted in turn.

Immunohistochemistry (IHC)

Immunohistochemistry was performed as described previously (17). Paraffin-embedded tissues were incubated with a primary antibody against E2F6 (1:200, Abcam, Cambridge, UK, Cat. No. ab53061) or Ki-67 (1:200, CST, MA, USA, Cat. No. 9449) at 4°C for 12 h. Then, the tissues were incubated with a secondary antibody (1:1000, Boster, Wuhan, Hubei, China, Cat. No. BM3895 & BA1082) at room temperature for 1 h. After incubation with ABC-peroxidase at room temperature for 1 h, the tissues were stained with diaminobenzidine for 5 min. The images were captured using a fluorescence microscope (Olympus, Japan).

Terminal Deoxynucleotidyl Transfer-Mediated dUTP Nick end Labelling Staining (TUNEL)

The tissues were deparaffinized in xylene, followed by washing in alcohol. Apoptotic cells were detected by a TUNEL Kit (Roche, Mannheim, Germany, Cat. No.11767291910) according to the manufacturer's instructions.

Intracranial Tumour Mouse Model

Forty male nude mice purchased from the Chinese Academy of Sciences were randomly divided into four groups (10 mice per group). LN229 cells (2×10^6) stably expressing luciferase were transfected with sh-COX10-AS1, sh-E2F6 and the corresponding negative controls. Next, the cells were intracranially injected into the frontal lobe of nude mice. A bioluminescence imaging system was used to quantify the volumes of the tumours formed intracranially every ten days after implantation. The Living Images software package (Caliper Life Science, Waltham, MA, USA) was used to determine the integrated flux of photons (photons/s). Mouse survival data were recorded in detail until all the mice died. Brain tissue and the tumour tissue that formed in

the brain were removed intact for immunohistochemical analysis and other experiments. The animal experiments were approved by the Institutional Animal Care and Use Committee of Nanjing First Hospital.

Statistical Analysis

SPSS 20.0 (IBM, NY, USA) was used to analyse the data. The data are expressed as the means ± standard deviation (SD). Student's t-test or one-way ANOVA was used to evaluate the differences between groups. Overall survival was evaluated by the Kaplan–Meier method. P<0.05 indicates statistical significance. All experiments were carried out three times independently.

RESULTS

COX10-AS1 Was Upregulated in Glioma Tissues and Cell Lines

To detect the expression of COX10-AS1 in glioma, online databases (GEPIA, http://gepia.cancer-pku.cn/index.html) were utilized. The data from GEPIA showed that the expression of COX10-AS1 in glioma tissues was higher than that in normal brain tissues (**Figure 1A**). We also explored COX10-AS1 expression in clinical species collected during surgery, and the aresult was similarly to that of the online databases (**Figures 1B, C**). To evaluate whether COX10-AS1 can be used as an indicator to predict the recurrence of glioma, the expression level of COX10-AS1 in the tissues of primary and recurrent glioma was detected. Interestingly, the results showed that COX10-AS1 was upregulated in recurrent glioma, suggesting that COX10-AS1 is closely related to glioma recurrence (**Figure 1D**). Moreover, clinical data of 30 glioma patients was collected and Kaplan-Meier curves indicated that glioma patients with high COX10-AS1 expression had poorer survival than those with low COX10-AS1 expression (**Figure 1E**). The correlation of clinicopathological characteristics between COX10-AS1 and glioma patients was shown in **Table 1**. In addition, we measured COX10-AS1 expression in normal human astrocytes and glioma cell lines. The results showed that the COX10-AS1 levels in glioma cell lines were much higher than those in NHAs, especially in U87 and LN229 cells (**Figure 1F**). These findings suggest that COX10-AS1 is closely related to the malignant progression of glioma.

COX10-AS1 Promotes Glioma Proliferation, Migration and Invasion *In Vitro* and Glioma Growth *In Vivo*

To study the relationship between COX10-AS1 and the malignant progression of glioma, we transfected short hairpin RNAs targeting COX10-AS1 (sh-COX10-AS1-1 and sh-COX10-AS1-2), a COX10-AS1 expression plasmid (COX10-AS1) and

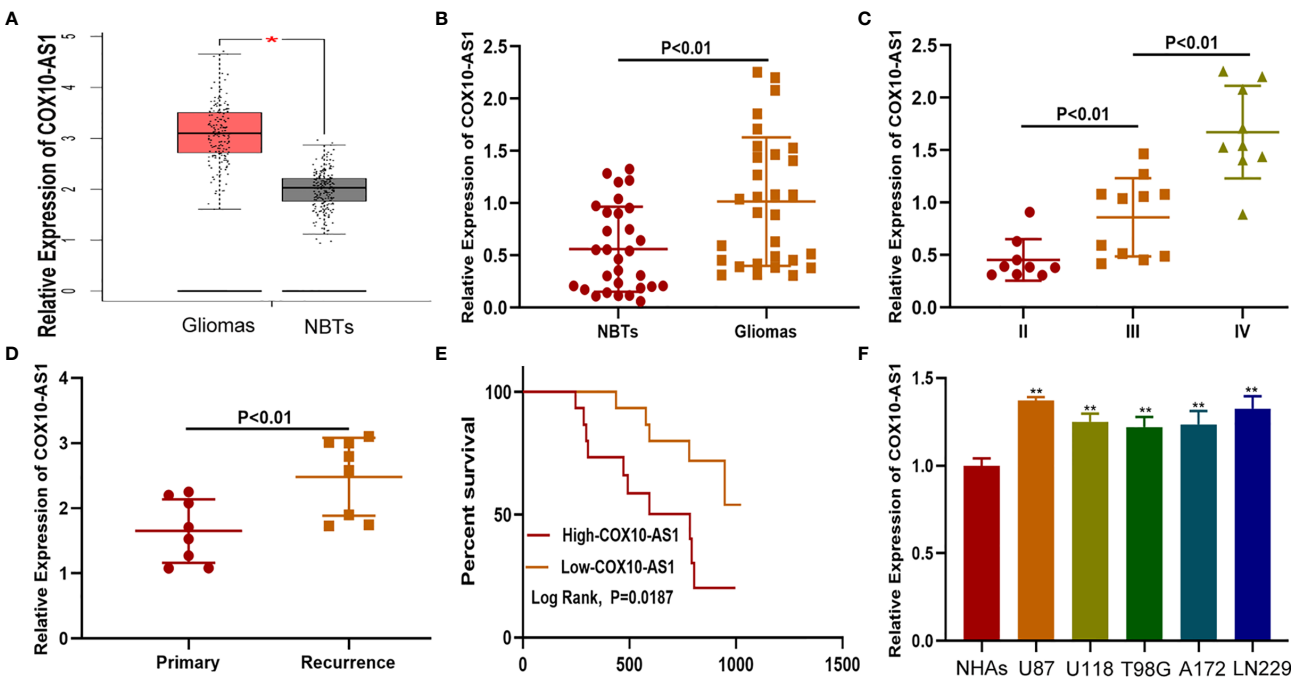

FIGURE 1 | COX10-AS1 is upregulated in glioma tissues and cell lines. **(A)** The relative expression of COX10-AS1 in GEPIA. **(B)** The relative expression of COX10-AS1 in clinical specimens. **(C)** The relative expression of COX10-AS1 in different grade of glioma. **(D)** The relative expression of COX10-AS1 in clinical specimens from patients with primary and recurrent glioma. **(E)** Kaplan–Meier curve analysis of the correlation between COX10-AS1 expression and overall survival from our clinical data. **(F)** The relative expression of COX10-AS1 in NHAs and glioma cell lines. *P < 0.05, **P < 0.01.

TABLE 1 | Correlation of clinicopathological characteristics between COX10-AS11 and glioma patients.

Clinicopathologic data	Case (n)	COX10-AS1 expression	P value
Gender			P = 0.8619
Male	17	1.0240 ± 0.5938	
Female	13	0.9859 ± 0.5361	
Age (years)			P = 0.6785
<60	11	0.9520 ± 0.6392	
≥60	19	1.0511 ± 0.5804	
Tumor diameter (cm)			P < 0.05
<3	13	0.7588 ± 0.4898	
≥3	17	1.2105 ± 0.6107	
WHO classification			P < 0.01
I+II	10	0.5304 ± 0.2749	
III+IV	20	1.2460 ± 0.5278	

corresponding controls into U87 and LN229 cells. The efficiency of these chemosynthetic sequences was verified by qRT-PCR (**Figures 2A, B**). Next, clone formation assays and EdU assays revealed that silencing COX10-AS1 decreased the proliferation ability of U87 and LN229 cells, while upregulation of COX10-AS1 had the opposite effect (**Figures 2C–H**). Transwell assays illustrated that downregulation of COX10-AS1 reduced cell migration and invasion, whereas upregulation of COX10-AS1 increased the migration and invasion of U87 and LN229 cells (**Figures 2I–L**). Furthermore, we injected LN229 cells transfected with a fluorescent lentivirus expressing sh-COX10-AS1 (including sh-COX10-AS1-1 and sh-COX10-AS1-2) or the corresponding controls into the brains of nude mice. In vivo imaging of the mice was performed on the indicated days (1 d, 10 d and 20 d) after implantation. The results showed that tumour growth was obviously inhibited after COX10-AS1 silencing (**Figures 3A, B**). Furthermore, we found that the mice in the sh-COX10-AS1 group had better survival than those in the negative group (**Figure 3C**). In addition, immunohistochemistry assays showed that Ki-67 was downregulated and TUNEL staining was upregulated in tumour tissues from mice in the sh-COX10-AS1 group (**Figures 3D, E**). These results suggest that COX10-AS1 exhibits important functions in glioma.

COX10-AS1 Acts as a Sponge for miR-641

There are several mechanisms by which lncRNAs affect tumour progression, of which their role as competing endogenous RNAs (ceRNAs) is an important one (20). By this mechanism lncRNAs can act as sponges for miRNAs to regulate targeted message RNAs (mRNAs), which can promote or suppress tumour progression. To reveal the underlying mechanism of COX10-AS1 in glioma, we measured the expression of COX10-AS1 at the subcellular level. The results of qRT-PCR and FISH showed that COX10-AS1 was localized in both the cytoplasm and the nucleus (**Figures 4A, B**), indicating that COX10-AS1 is likely to exert its function of regulation of tumour progression by acting as a ceRNA. To determine the targeted miRNA of COX10-AS1, bioinformatics prediction was performed with StarBase (http://starbase.sysu.edu.cn/), and miR-641 greatly aroused our interest (**Figure 4C**). Next, we detected the expression of miR-641 in clinical specimens and found that miR-641 was higher in normal brain tissues than in glioma tissues (**Figures 4D, E**). Compared with primary glioma tissues, miR-641 expression in recurrent glioma tissues was lower (**Figure 4F**). Similarly, miR-641 was higher in NHAs than that in glioma cell lines (**Figure 4G**). Moreover, RNA pull-down assays showed that COX10-AS1 was pulled down by miR-641 in both U87 and LN229 cells (**Figures 4H, I**). Moreover, luciferase reporter assays indicated that miR-641 could decrease the luciferase activity of COX10-AS1-WT but not COX10-AS1-MUT (**Figures 4J, K**). Overall, we concluded that COX10-AS1 acts as a sponge for miR-641 in glioma cells.

The Effect of COX10-AS1 on Glioma Is Partially Mediated by miR-641

To explore the function of miR-641 in COX10-AS1 promoting the malignant progression of glioma, four cell models were constructed with miR-641 inhibitor, sh-COX10-AS1 and the corresponding negative controls. qRT-PCR showed that sh-COX10-AS1 obviously upregulated miR-641 (**Figures 5A, B**). Clone formation assays and EdU assays indicated that the miR-641 inhibitor could promote the proliferation of glioma cells, and the promoting effect could be reversed by sh-COX10-AS1 (**Figures 5C–H**). Similarly, the Transwell assays showed that miR-641 inhibitor could facilitate the migration and invasion of glioma cells, and the facilitating effect was partially rescued by sh-COX10-AS1 (**Figures 5I–L**). These functional assays indicated that miR-641 plays an important role in the carcinogenic effect of COX10-AS1 on glioma progression.

E2F6 is the Functional Target of the COX10-AS1/miR-641 Axis

To verify the functional target of the COX10-AS1/miR-641 axis, we searched the StarBase database. Considering the database results and the expression data from our clinical specimens, we chose E2F6 for further study (**Figure 6A**). qRT-PCR showed that the expression of E2F6 in glioma tissues was higher than that in normal brain tissues and was correlated with the recurrence of glioma (**Figures 6B–D**). Pearson's correlation analysis indicated that there was a significant correlation between E2F6 and COX10-AS1/miR-641 (**Figures 6E, F**). We explored E2F6

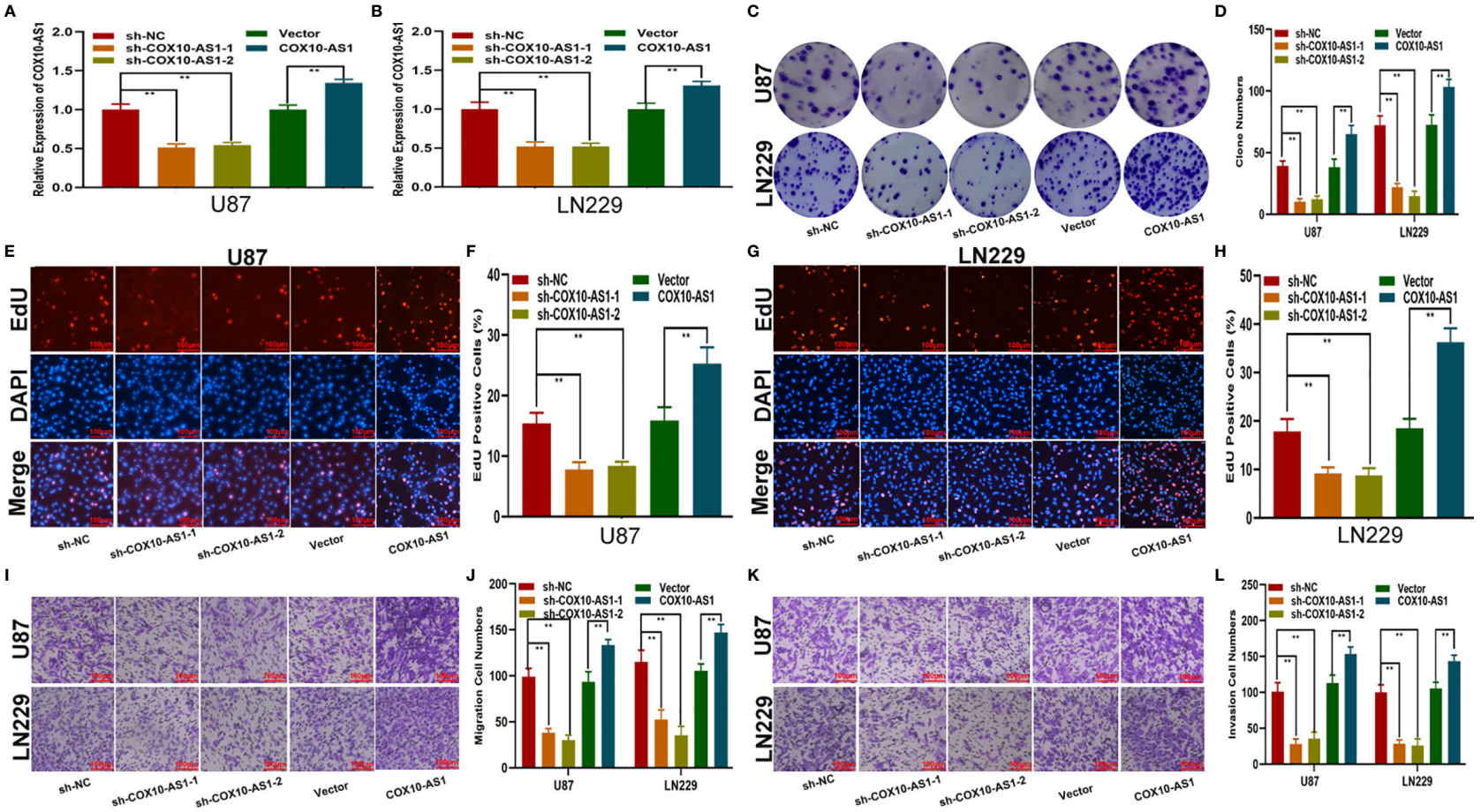

FIGURE 2 | COX10-AS1 promotes glioma proliferation, migration and invasion *in vitro.* **(A, B)** Relative expression of COX10-AS1 in U87 and LN229 cells transfected with sh-COX10-AS1 (including sh-COX10-AS1-1, sh-COX10-AS1-2), COX10-AS1 plasmid or the corresponding negative control, as measured by qRT-PCR. **(C, D)** The proliferation of U87 and LN229 cells transfected with sh-COX10-AS1, COX10-AS1 plasmid or the corresponding negative control, as measured by clone formation assays. **(E–H)** The proliferation of U87 and LN229 cells transfected with sh-COX10-AS1, COX10-AS1 plasmid or the corresponding negative control, as measured by EdU assays. **(I, J)** The migration of U87 and LN229 cells transfected with sh-COX10-AS1, COX10-AS1 plasmid or the corresponding negative control, as measured by Transwell assays. **(K, L)** The invasion of U87 and LN229 cells transfected with sh-COX10-AS1, COX10-AS1 plasmid or the corresponding negative control, as measured by Transwell assays. **P < 0.01.

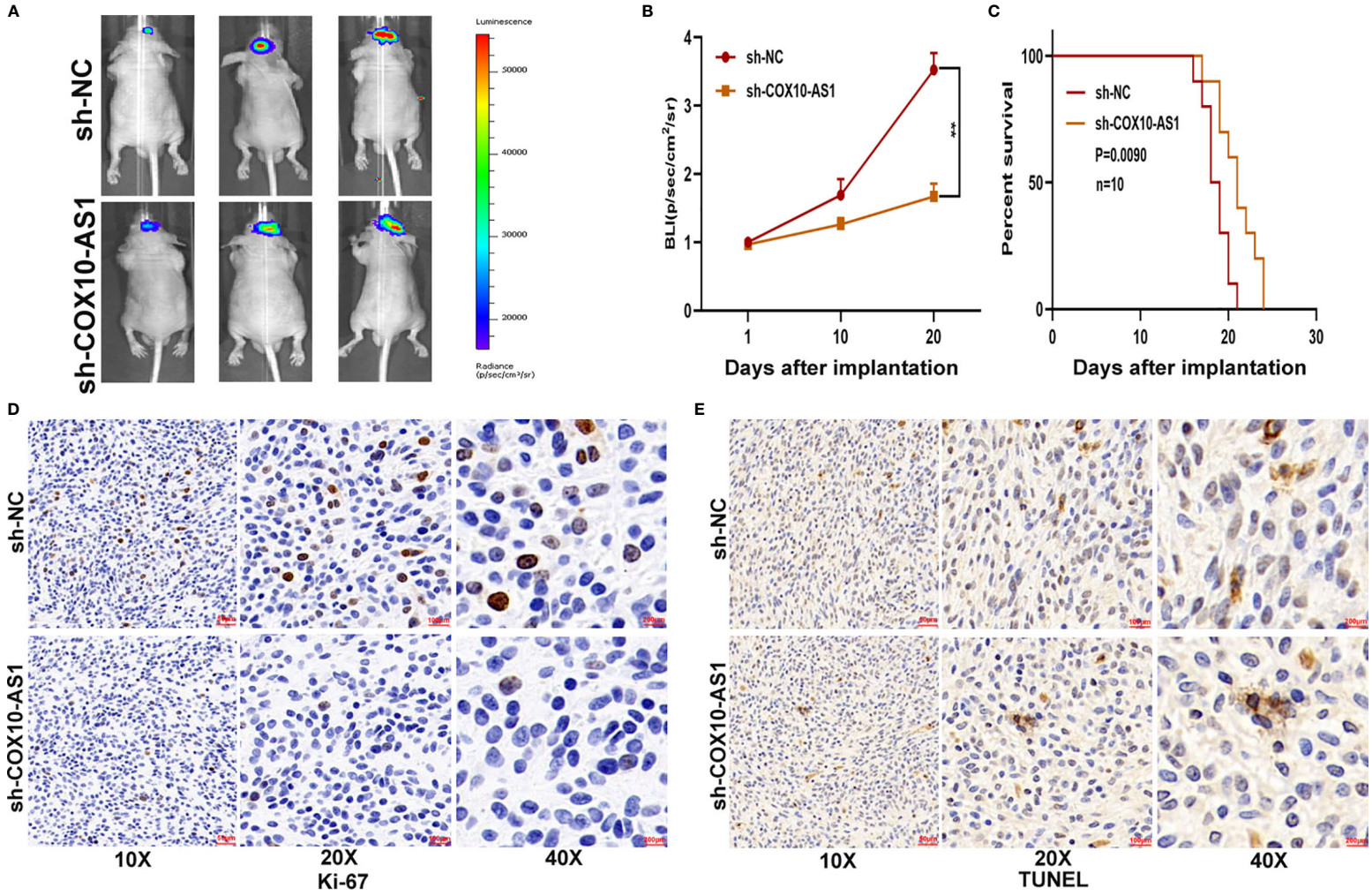

FIGURE 3 | COX10-AS1 promotes glioma growth *in vivo*. **(A, B)** The bioluminescent images of the tumours formed in the brains of nude mice were acquired at days 1, 10 and 20 after implantation. **(C)** Overall survival was compared between the sh-COX10-AS1 and sh-NC groups by Kaplan-Meier survival curves. **(D)** Immunohistochemistry for Ki-67 in the sh-COX10-AS1 and sh-NC groups. **(E)** TUNEL staining in the sh-COX10-AS1 and sh-NC groups. **P < 0.01.

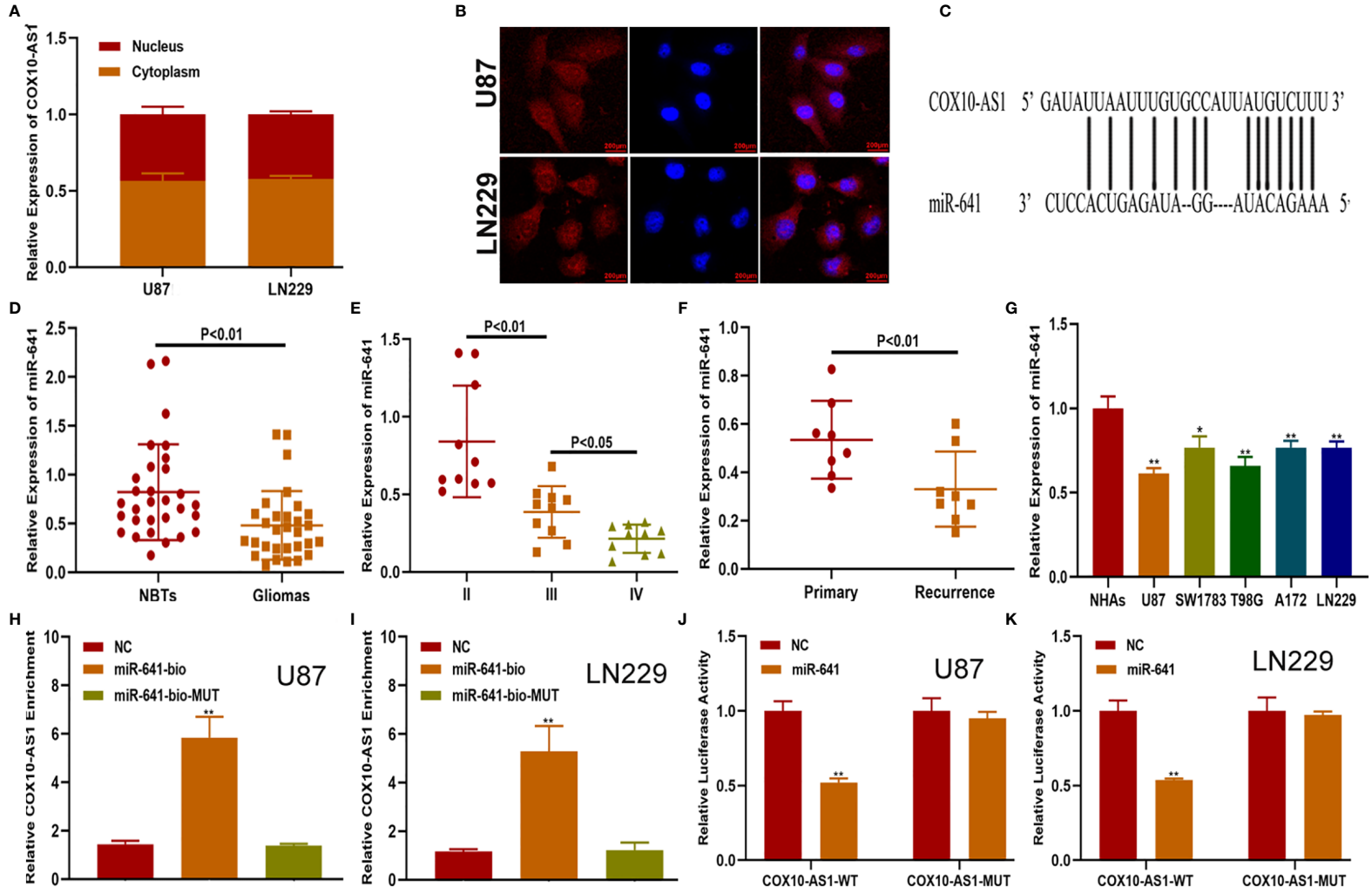

FIGURE 4 | COX10-AS1 acts as a sponge for miR-641. **(A)** RT-qPCR assays in nuclear and cytoplasmic RNA fractions detected the COX10-AS1 level in the cytoplasm and nucleus. **(B)** The distribution of COX10-AS1 in U87 and LN229 cells was evaluated by FISH assays. **(C)** The putative binding sites of miR-641 on COX10-AS1 were predicted by an online database. **(D)** The relative expression of miR-641 in clinical specimens. **(E)** The relative expression of miR-641 in different grade of glioma. **(F)** The relative expression of miR-641 in primary and recurrent glioma clinical specimens. **(G)** The relative expression of miR-641 in NHAs and glioma cell lines. **(H, I)** U87 and LN229 cells were assayed by biotin-based pull-down after transfection with biotin-labelled miR-641. **(J, K)** Luciferase reporter assay indicated that miR-641 reduced the luciferase activity of COX10-AS1-WT but not COX10-AS1-MUT. *P < 0.05, **P < 0.01.

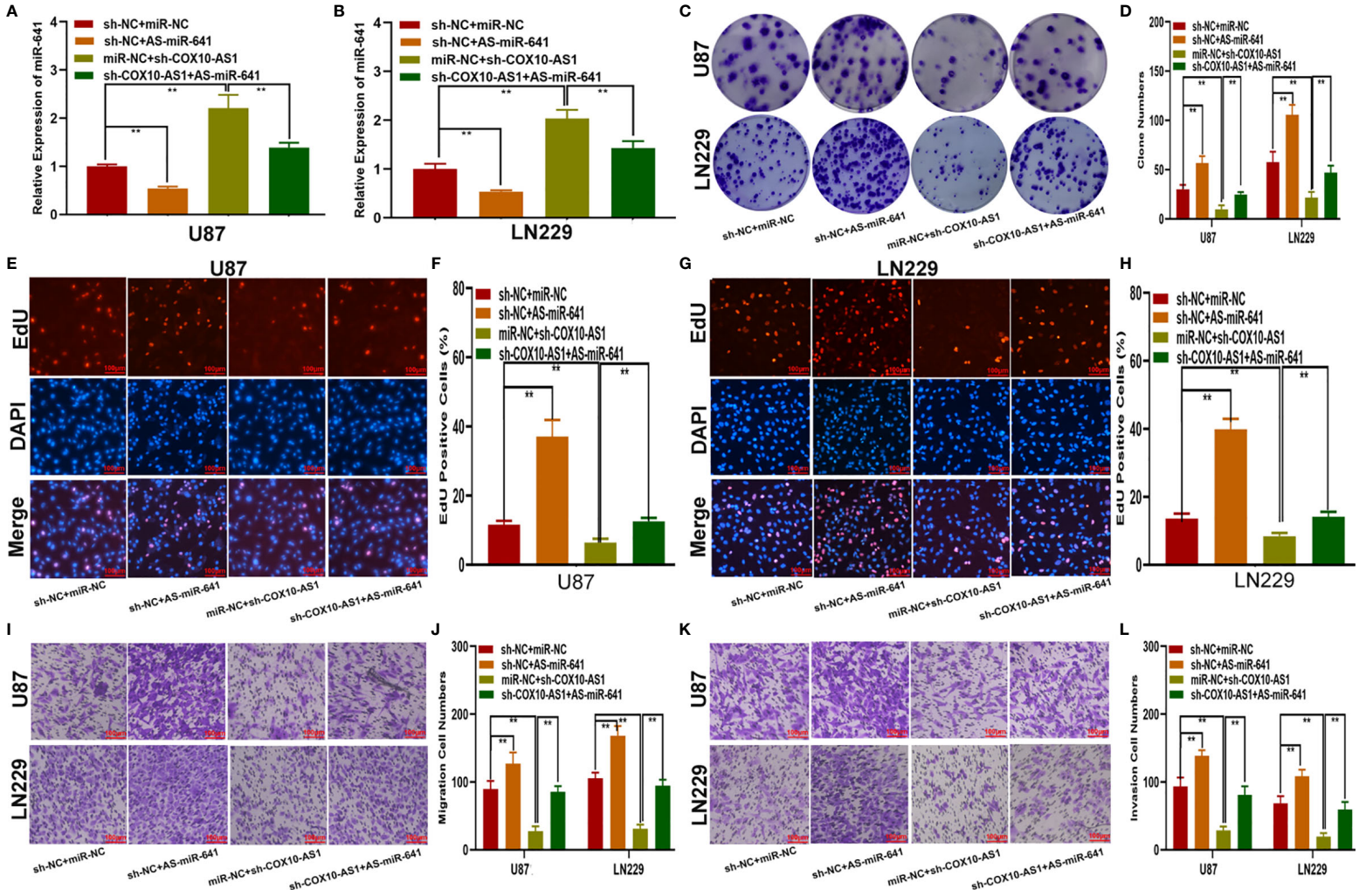

FIGURE 5 | The effect of COX10-AS1 on glioma is partially mediated by miR-641. **(A, B)** The relative expression of miR-641 in U87 and LN229 transfected with miR-641 inhibitor, sh-COX10-AS1 or the corresponding controls, as measured by qRT-PCR. **(C, D)** The proliferation of U87 and LN229 cells transfected with miR-641 inhibitor, sh-COX10-AS1 or the corresponding controls, as measured by clone formation assays. **(E–H)** The proliferation of U87 and LN229 cells transfected with miR-641 inhibitor, sh-COX10-AS1 or the corresponding controls, as measured by EdU assays. **(I, J)** The migration of U87 and LN229 cells transfected with miR-641 inhibitor, sh-COX10-AS1 or the corresponding controls, as measured by Transwell assays. **(K, L)** The invasion of U87 and LN229 cells transfected with miR-641 inhibitor, sh-COX10-AS1 or the corresponding controls, as measured by Transwell assays. **P < 0.01.

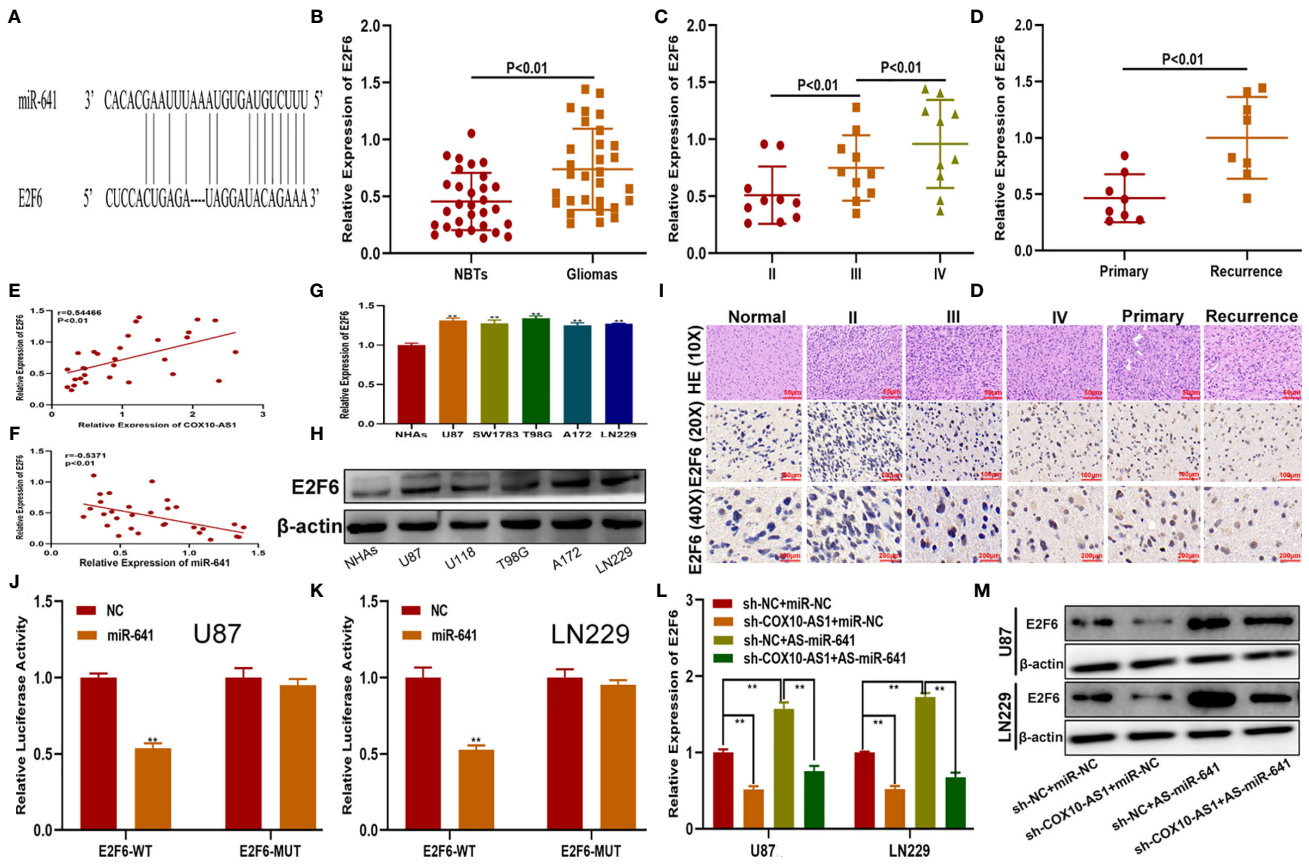

FIGURE 6 | E2F6 is the functional target of the COX10-AS1/miR-641 axis. **(A)** The putative binding sites of miR-641 on E2F6 were predicted by an online database. **(B)** The relative expression of E2F6 in clinical specimen. **(C)** The relative expression of E2F6 in different grade of glioma. **(D)** The relative expression of E2F6 in primary and recurrent glioma. **(E)** Pearson's correlation analysis of COX10-AS1 expression and E2F6 expression in clinical specimens. **(F)** Pearson's correlation analysis of miR-641 expression and E2F6 expression in clinical specimens. **(G, H)** The relative expression of E2F6 in NHAs and glioma cell lines measured by qRT-PCR and western blot. **(I)** The expression level of E2F6 in different grades of glioma detected by immunohistochemistry. **(J, K)** Luciferase reporter assay indicated that miR-641 reduced the luciferase activity of E2F6-WT but not E2F6-MUT. **(L, M)** The relative expression of E2F6 in U87 and LN229 cells transfected with sh-COX10-AS1, miR-641 inhibitor or sh-COX10-AS1 together with miR-641 inhibitor, as measured by qRT-PCR and western blot. **P < 0.01.

expression in NHAs and glioma cell lines by qRT-PCR and western blot as well. The results demonstrated that E2F6 was higher in glioma cells than in NHAs (**Figures 6G, H**). Immunohistochemistry assays showed the similar results (**Figure 6I**). Luciferase reporter assays indicated that, compared with that of E2F6-MUT, miR-641 obviously decreased the luciferase activity of E2F6-WT (**Figures 6J, K**). Otherwise, qRT-PCR and western blot assays showed that miR-641 inhibitor could upregulate the expression of E2F6 and that the promoting effect could be inhibited by sh-COX10-AS1 (**Figures 6L, M**). Thus, we concluded that E2F6 is the functional target of the COX10-AS1/miR-641 axis.

E2F6 Promotes Glioma Proliferation, Migration and Invasion *In Vitro* and Glioma Growth *In Vivo*

To explore whether E2F6 regulated the function of miR-641, three cell models were constructed with sh-E2F6, miR-641 inhibitor and the negative control. qRT-PCR and western blot assays confirmed that miR-641 inhibitor reversed the E2F6 downregulation caused by sh-E2F6 (**Figures 7A, B**). Clone formation assays and EdU assays demonstrated that sh-E2F6 could inhibit the proliferation of glioma cells and that the inhibitory effect could be rescued by miR-641 inhibitor (**Figures 7C–H**). Transwell assays showed a similar result whereby sh-E2F6 could inhibit the migration and invasion of glioma cells, and the inhibitory effect could be partly reversed by miR-641 inhibitor (**Figures 7I–L**). In addition, we explored the effect of E2F6 on glioma growth *in vivo*. The results demonstrated that downregulation of E2F6 inhibited tumour growth and extended the survival time (**Figures 8A–C**). Moreover, Ki-67 and TUNEL staining suggested that E2F6 was involved in the progression of glioma growth (**Figures 8D, E**).

E2F6 Regulates COX10-AS1 Expression by Binding to Its Promoter Region

To further explain the regulatory relationship among COX10-AS1, miR-641 and E2F6, we tested whether E2F6 could regulate

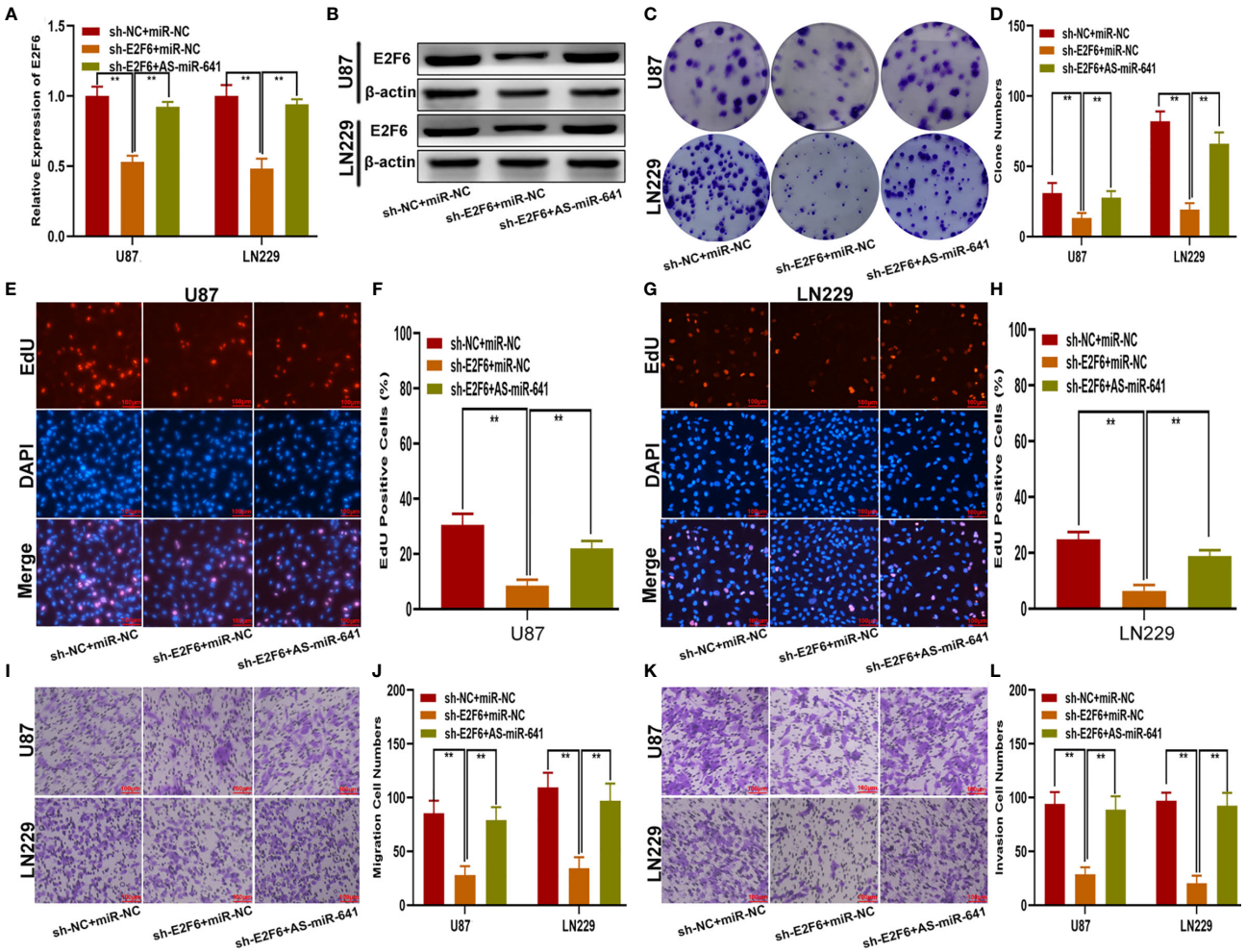

FIGURE 7 | E2F6 promotes glioma proliferation, migration and invasion *in vitro*. **(A, B)** The relative expression of E2F6 in U87 and LN229 cells transfected with sh-E2F6 or sh-E2F6 together with miR-641 inhibitor, as measured by qRT-PCR and western blot. **(C, D)** The proliferation of U87 and LN229 cells transfected with sh-E2F6 or sh-E2F6 together with miR-641 inhibitor, as measured by clone formation assays. **(E–H)** The proliferation of U87 and LN229 cells transfected with sh-E2F6 or sh-E2F6 together with miR-641 inhibitor, as measured by EdU assays. **(I, J)** The migration of U87 and LN229 cells transfected with sh-E2F6 or sh-E2F6 together with miR-641 inhibitor, as measured by Transwell assays. **(K, L)** The invasion of U87 and LN229 cells transfected with sh-E2F6 or sh-E2F6 together with miR-641 inhibitor, as measured by Transwell assays. **P < 0.01.

COX10-AS1. First, we searched the promoter sequence of COX10-AS1 *via* UCSC (https://genome.ucsc.edu/). With the help of the JASPAR website (http://jaspar.genereg.net/), we found that there are sites on E2F6 that could bind to the promoter sequence of COX10-AS1 (**Figures 9A–C**). By ChIP assays, we found that the affinity of the COX10-AS1 promoter (P2) to E2F6 was stronger than that to IgG (**Figures 9D, E**). To validate the effectiveness of the binding sites (including two sites), luciferase reporter assays was conducted, and the results indicated that the promoter activity of the predicted sites (-1804 ~ -1794) was enhanced significantly by E2F6 (**Figure 9F**). Finally, we found a positive correlation between E2F6 and COX10-AS1 by qRT-PCR and/or western blot (**Figures 9G–I**). Overall, we concluded that COX10-AS1/miR-641/E2F6 formed a positive feedback loop to regulate glioma progression.

DISCUSSION

In 1976, E Zuckerkandl reported that ncRNAs may exert their function by regulating the transcription process, which caused a paradigm shift because researchers generally believed that ncRNAs were useless and were therefore called "rubbish" (21). Over time, mounting advances in ncRNAs research have shown that dysregulation of ncRNAs is closely related to human diseases, including cancers. For instance, miR-452 regulates the progression of gastric cancer by targeting EPB41L3 (22); SNHG1 (small nucleolar RNA host gene 1) promotes the malignant development of glioma by acting as a sponge of miR-194 (19); and Circ_0079593 may function as a prognostic indicator in glioma (23). LncRNAs, an important class of ncRNAs longer than 200 nucleotides, have aroused great interest among

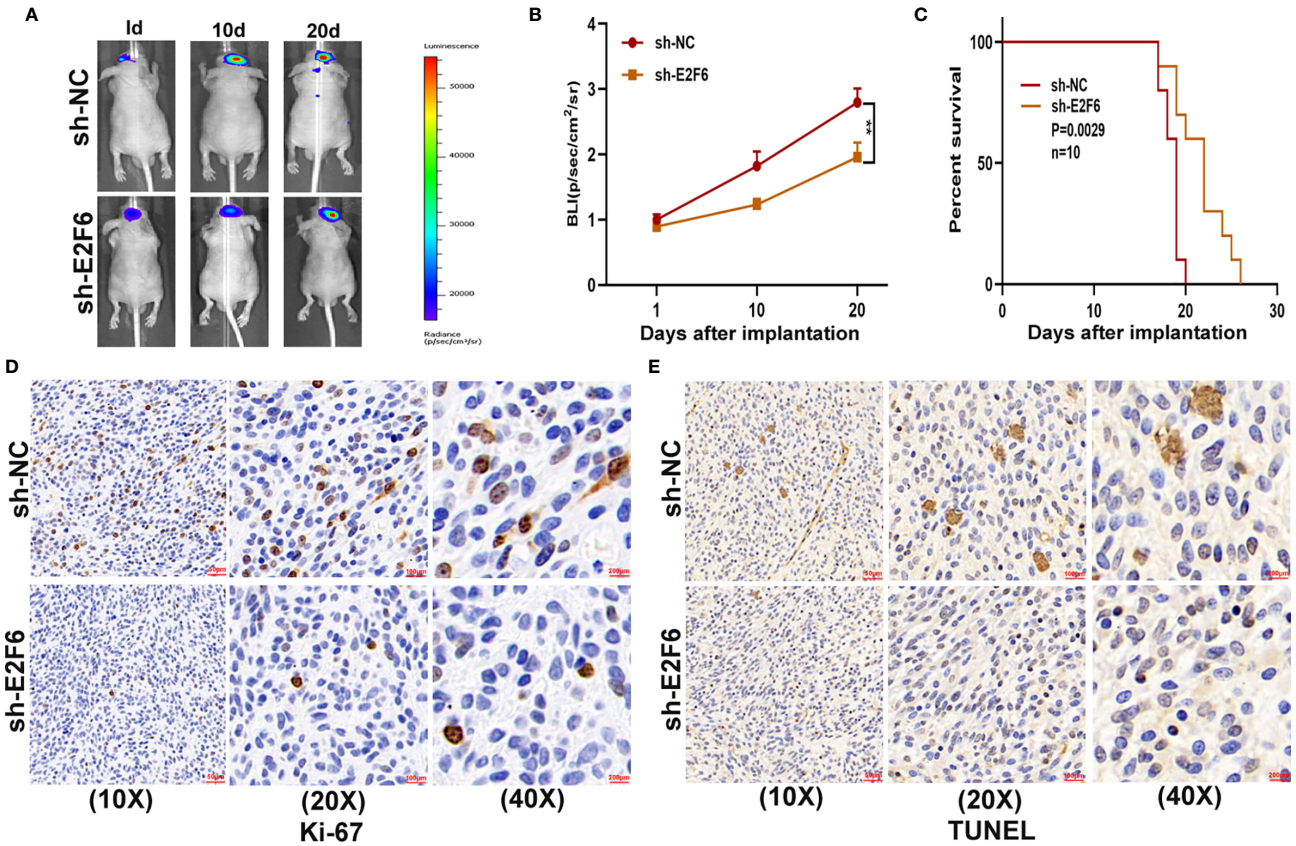

FIGURE 8 | E2F6 promotes glioma growth *in vivo*. **(A, B)** The bioluminescent images of the tumours formed in the brains of nude mice were acquired at days 1, 10 and 20 after implantation. **(C)** Overall survival was compared between the sh-E2F6 and sh-NC groups by Kaplan-Meier survival curves. **(D)** Immunohistochemistry for Ki-67 in the sh-E2F6 and sh-NC groups. **(E)** Immunohistochemistry for TUNEL staining in the sh-E2F6 and sh-NC groups.

researchers. Till now, multiple lines of research have suggested that lncRNAs have critical effects on tumour processes, such as proliferation, apoptosis, and invasion (24–26). COX10-AS1, a lncRNA transcript from chromosome 17, has been shown to be related to the development of human cancers. For example, Lu et al. demonstrated that COX10-AS1 is dysregulated in oral squamous cell carcinoma (15) and Luan et al. reported that COX10-AS1 is involved in the development of glioma via regulation of autophagy (16). Although existing research has indicated that COX10-AS1 is closely related to glioma, the underlying mechanism is elusive and has not been completely clarified. In the current study, through the public databases GEPIA, we determined that COX10-AS1 was upregulated in glioma. Consistent with the results from the public database, we detected the expression level of COX10-AS1 in clinical specimens collected during surgery and obtained a similar result. By analysis of the clinical data, we found that the expression level of COX10-AS1 was related to the prognosis and recurrence of patients with glioma. In addition, qRT-PCR demonstrated that the expression of COX10-AS1 in glioma cell lines was higher than that in NHAs, especially in U87 and LN229. To explore the function of COX10-AS1 in glioma, a series of gain- and loss-of-function assays were conducted. The results showed that downregulation of COX10-AS1 inhibited the proliferation, migration and invasion of glioma, whereas upregulation of COX10-AS1 caused the opposite effect. These findings indicated that COX10-AS1 plays a key role in glioma progression, which prompted us to investigate the potential mechanism.

By the ceRNA mechanism, a lncRNA can act as a sponge for miRNAs, leading to the latter being inactivated, thereby losing its regulatory effect on the targeted mRNAs (27). Recently, the ceRNA mechanism has been shown to be widely involved in human cancers. For example, Wang et al. indicated that NEAT1 aggravates endometrial cancer progression by sponging miR-144 (28); Yuan et al. reported that linc00994 is involved in the proliferation and invasion of gastric cancer by sponging miR-765-3p (29); and Liu et al. showed that HOTAIR acts as a sponge for miR-126 to regulate glutaminase in glioma (18). In the current study, the information from StarBase and the experiments we performed indicated that COX10-AS1 could sponge miR-641. qRT-PCR showed that miR-641 was downregulated in glioma and was correlated with glioma recurrence, which indicated that miR-641 may be involved in

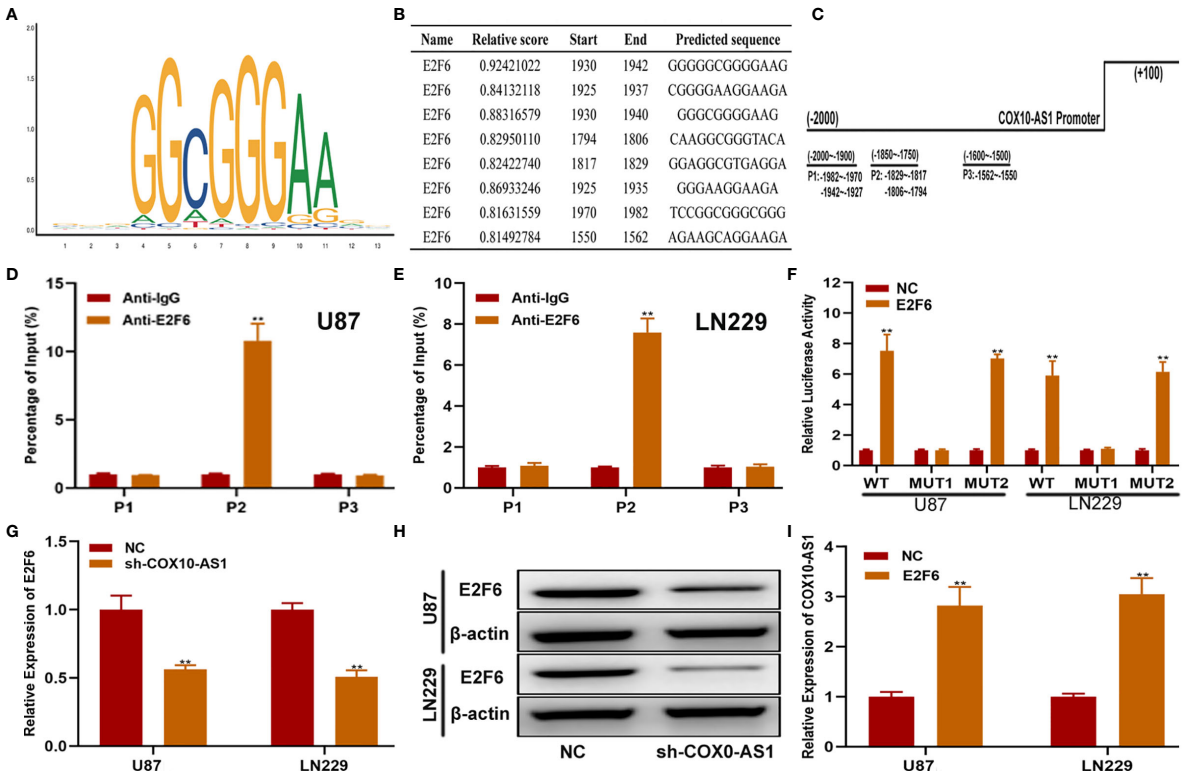

FIGURE 9 | E2F6 regulates COX10-AS1 expression by binding to its promoter region. **(A)** The binding motif of E2F6 determined from JASPAR. **(B, C)** The top five binding sites in the COX10-AS1promoter and their corresponding three counterparts in the promoter region are shown. **(D, E)** ChIP assays were performed to reveal the affinity of E2F6 to the COX10-AS1 promoter in U87 and LN229 cells. **(F)** Luciferase reporter assays were used to locate the binding sequences of E2F6 to the COX10-AS1 promoter. **(G, H)** The expression level of E2F6 in glioma cell lines transfected with sh-COX10-AS1 or sh-NC, as measured by qRT-PCR and western blot. **(I)** The expression level of COX10-AS1 in glioma cell lines transfected with E2F6 plasmid or NC, as measured by qRT-PCR. **P < 0.01.

the regulation of COX10-AS1 in glioma. Previous studies have demonstrated that miR-641 participates in the development of some tumours. For instance, Kong et al. reported that miR-641 inhibits the progression of lung cancer (30); Chen et al. showed that miR-641 is involved in the erlotinib resistance of non-small-cell lung cancer (31); and Yao et al. suggested that miR-641 acts as a tumour suppressor in cervical cancer (32). There is also a study that reported that miR-641 could target ATK2 to regulate glioma progression (33); however, the role and mechanism of miR-641 in glioma still need further study. In this research, we found that, consistent with a previous study, miR-641 was downregulated in glioma. Moreover, miR-641 could partly inhibit the promoting effect of COX10-AS1 on glioma progression.

To test our scientific hypothesis, we selected the target mRNAs of miR-641 from an online database. From these candidate genes, we found that E2F6 was upregulated in glioma tissues and cell lines, which was closely related to COX10-AS1 and miR-641. As a well-known member of the E2F family, E2F6 plays a critical role in human disease. Li et al. reported that E2F6 regulates gastric carcinoma development by targeting CASC2 (34); Shi et al. suggested that E2F6 acts as a target of TLX to regulate islet beta cell proliferation (35); and Cai et al. documented that E2F6 is involved in miR-425-mediated growth renal cell carcinoma (36). However, the role of E2F6 in glioma has never been reported. It is imperative to investigate the role and underlying mechanism of E2F6 in glioma. Through a series of assays, we confirmed that E2F6 is a functional target of the COX10-AS1/miR-641 axis to regulate proliferation, migration and invasion.

As COX10-AS1 is a ncRNA, there is no doubt that the transcription process of COX10-AS1 is regulated by transcription factors. E2F6 is a well-known transcription factor, and we were interested in whether E2F6 could regulate the transcription process of COX10-AS1, which is of great significance to further study the mechanism of COX10-AS1/miR-641/E2F6 in glioma. Through a literature search, we found that there is no research on the regulatory relationship between E2F6 and COX10-AS1. To address this issue, we used the JASPAR database. According to the prediction from JASPAR, there were existing sites in the promoter of COX10-AS1 to which E2F6 could bind. The effective binding sites of E2F6 on COX10-AS1 were verified by luciferase reporter assay and ChIP. In addition, the results of qRT-PCR and western blotting showed that downregulation of COX10-AS1 could repress E2F6 expression and that E2F6 could promote the transcription of COX10-AS1. These results suggested that COX10-AS1/miR-641/E2F6 formed a positive feedback loop to regulate glioma progression (**Figure 10**).

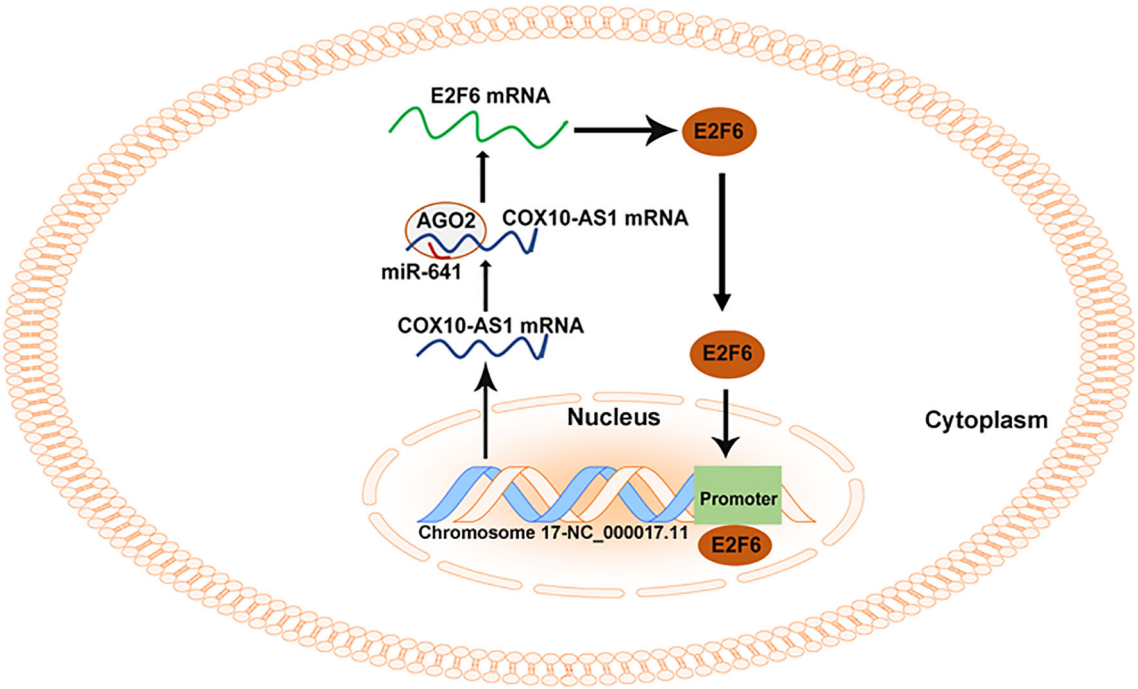

FIGURE 10 | Summary of the COX10-AS1/miR-641/E2F6 feedback loop in glioma progression.

Taken together, in present study, we showed that E2F6-induced COX10-AS1 promotes glioma progression by acting as a sponge for miR-641 to regulate E2F6. These findings indicated that the E2F6/COX10-AS1/miR-641 feedback loop plays an important role in glioma and may be considered a potential therapeutic target for glioma patients.

DATA AVAILABILITY STATEMENT

The raw data supporting the conclusions of this article will be made available by the authors, without undue reservation.

ETHICS STATEMENT

The studies involving human participants were reviewed and approved by Ethics Committee of the Nanjing First Hospital. The patients/participants provided their written informed consent to participate in this study. The animal study was reviewed and approved by Ethics Committee of the Nanjing First Hospital.

AUTHOR CONTRIBUTIONS

LL performed the cell functional experiments, analyzed the data, and prepared the figures. XiaoL performed the experiments and wrote the manuscript. HW designed the experiments and collected clinical specimen. YT performed the animal experiments. XianL discussed the manuscript. YS designed the experiments, supervised the research and revised the manuscript. All authors contributed to the article and approved the submitted version.

FUNDING

This study was supported by grants from National Natural Science Foundation of China (No. 81502168) and Nanjing Medical Science and technique Development Foundation.

SUPPLEMENTARY MATERIAL

The Supplementary Material for this article can be found online at: https://www.frontiersin.org/articles/10.3389/fonc.2021.648152/full#supplementary-material

REFERENCES

1. Shen J, Xiong J, Shao X, Cheng H, Fang X, Sun Y, et al. Knockdown of the Long Noncoding RNA XIST Suppresses Glioma Progression by Upregulating Mir-204-5p. *J Cancer* (2020) 11(15):4550–9. doi: 10.7150/jca.45676
2. Jovcevska I. Next Generation Sequencing and Machine Learning Technologies Are Painting the Epigenetic Portrait of Glioblastoma. *Front Oncol* (2020) 10:798. doi: 10.3389/fonc.2020.00798
3. Lin N, Li W, Wang X, Hou S, Yu D, Zhao X, et al. Upregulation of Mir-340 Inhibits Tumor Growth and Mesenchymal Transition via Targeting c-MET in

Glioblastoma. *Cancer Manag Res* (2020) 12:3343–52. doi: 10.2147/CMAR.S250772
4. Zhang S, Wang K. Mir-383 Down-Regulates the Oncogene CIP2A to Influence Glioma Proliferation and Invasion. *Onco Targets Ther* (2020) 13:4063–74. doi: 10.2147/OTT.S248116
5. Howell AE, Robinson JW, Wootton RE, McAleenan A, Tsavachidis S, Ostrom QT, et al. Testing for Causality Between Systematically Identified Risk Factors and Glioma: A Mendelian Randomization Study. *BMC Cancer* (2020) 20 (1):508. doi: 10.1186/s12885-020-06967-2
6. Zhu L, Nazeri A, Pacia CP, Yue Y, Chen H. Focused Ultrasound for Safe and Effective Release of Brain Tumor Biomarkers Into the Peripheral Circulation. *PloS One* (2020) 15(6):e0234182. doi: 10.1371/journal.pone.0234182
7. Khan L, Soliman H, Sahgal A, Perry J, Xu W, Tsao MN. External Beam Radiation Dose Escalation for High Grade Glioma. *Cochrane Database Syst Rev* (2020) 5:CD011475. doi: 10.1002/14651858.CD011475.pub3
8. Li Y, Shan G, Teng ZQ, Wingo TS. Editorial: Non-Coding RNAs and Human Diseases. *Front Genet* (2020) 11:523. doi: 10.3389/fgene.2020.00523
9. Shirahama S, Miki A, Kaburaki T, Akimitsu N. Long Non-Coding RNAs Involved in Pathogenic Infection. *Front Genet* (2020) 11:454. doi: 10.3389/fgene.2020.00454
10. Chen DY, Jiang RF, Li YJ, Liu MX, Wu L, Hu W. Screening and Functional Identification of lncRNAs in Antler Mesenchymal and Cartilage Tissues Using High-Throughput Sequencing. *Sci Rep* (2020) 10(1):9492. doi: 10.1038/s41598-020-66383-1
11. Zhang Z, Qiu M, Du H, Li Q, Yu C, Gan W, et al. Identification of Long Noncoding RNAs Involved in Adaptability to Chronic Hypoxic by Whole Transcriptome Sequencing. *3 Biotech* (2020) 10(6):269. doi: 10.1007/s13205-020-02272-8
12. Guo J, Li Y, Duan H, Yuan L. Metformin Suppresses the Proliferation and Promotes the Apoptosis of Colon Cancer Cells Through Inhibiting the Expression of Long Noncoding RNA-UCA1. *Onco Targets Ther* (2020) 13:4169–81. doi: 10.2147/OTT.S245091
13. Jin L, Li C, Liu T, Wang L. A Potential Prognostic Prediction Model of Colon Adenocarcinoma With Recurrence Based on Prognostic lncRNA Signatures. *Hum Genomics* (2020) 14(1):24. doi: 10.1186/s40246-020-00270-8
14. Mi LD, Sun CX, He SW, Du GY. Sp1-Induced Upregulation of Lncrna LINC00514 Promotes Tumor Proliferation and Metastasis in Osteosarcoma by Regulating miR-708. *Cancer Manag Res* (2020) 12:3311–22. doi: 10.2147/CMAR.S242464
15. Feng L, Houck JR, Lohavanichbutr P, Chen C. Transcriptome Analysis Reveals Differentially Expressed lncRNAs Between Oral Squamous Cell Carcinoma and Healthy Oral Mucosa. *Oncotarget* (2017) 8(19):31521–31. doi: 10.18632/oncotarget.16358
16. Luan F, Chen W, Chen M, Yan J, Chen H, Yu H, et al. An Autophagy-Related Long Non-Coding RNA Signature for Glioma. *FEBS Open Bio* (2019) 9 (4):653–67. doi: 10.1002/2211-5463.12601
17. Liu L, Cui S, Zhang R, Shi Y, Luo L. miR-421 Inhibits the Malignant Phenotype in Glioma by Directly Targeting MEF2D. *Am J Cancer Res* (2017) 7(4):857–68.
18. Liu L, Cui S, Wan T, Li X, Tian W, Zhang R, et al. Long Non-Coding RNA HOTAIR Acts as a Competing Endogenous RNA to Promote Glioma Progression by Sponging Mir-126-5p. *J Cell Physiol* (2018) 233(9):6822–31. doi: 10.1002/jcp.26432
19. Liu L, Shi Y, Shi J, Wang H, Sheng Y, Jiang Q, et al. The Long Non-Coding RNA SNHG1 Promotes Glioma Progression by Competitively Binding to miR-194 to Regulate PHLDA1 Expression. *Cell Death Dis* (2019) 10(6):463. doi: 10.1038/s41419-019-1698-7
20. Zhang XZ, Liu H, Chen SR. Mechanisms of Long Non-Coding RNAs in Cancers and Their Dynamic Regulations. *Cancers (Basel)* (2020) 12(5):1245. doi: 10.3390/cancers12051245
21. Zuckerkandl E. Gene Control in Eukaryotes and the C-Value Paradox "Excess" DNA as an Impediment to Transcription of Coding Sequences. *J Mol Evol* (1976) 9(1):73–104. doi: 10.1007/BF01796124
22. He X, Shu Y. miR-452 Promotes the Development of Gastric Cancer *Via* Targeting EPB41L3. *Pathol Res Pract* (2020) 216(1):152725. doi: 10.1016/j.prp.2019.152725
23. Qu Y, Zhu J, Liu J, Qi L. Circular RNA Circ_0079593 Indicates a Poor Prognosis and Facilitates Cell Growth and Invasion by Sponging miR-182 and miR-433 in Glioma. *J Cell Biochem* (2019) 120(10):18005–13. doi: 10.1002/jcb.29103
24. Da CM, Gong CY, Nan W, Zhou KS, Wu ZL, Zhang HH. The Role of Long Non-Coding RNA MIAT in Cancers. *BioMed Pharmacother* (2020) 129:110359. doi: 10.1016/j.biopha.2020.110359
25. Cao Q, Dong Z, Liu S, An G, Yan B, Lei L. Construction of a Metastasis-Associated ceRNA Network Reveals a Prognostic Signature in Lung Cancer. *Cancer Cell Int* (2020) 20:208. doi: 10.1186/s12935-020-01295-8
26. Xia P, Li Q, Wu G, Huang Y. An Immune-Related lncRNA Signature to Predict Survival In Glioma Patients. *Cell Mol Neurobiol* (2020) 41(2):365–75. doi: 10.1007/s10571-020-00857-8
27. Liu L, Li Y, Zhang R, Li C, Xiong J, Wei Y. MIR205HG Acts as a ceRNA to Expedite Cell Proliferation and Progression in Lung Squamous Cell Carcinoma Via Targeting miR-299-3p/MAP3K2 Axis. *BMC Pulm Med* (2020) 20(1):163. doi: 10.1186/s12890-020-1174-2
28. Wang W, Ge L, Xu XJ, Yang T, Yuan Y, Ma XL, et al. Lncrna NEAT1 Promotes Endometrial Cancer Cell Proliferation, Migration and Invasion by Regulating the miR-144-3p/EZH2 Axis. *Radiol Oncol* (2019) 53(4):434–42. doi: 10.2478/raon-2019-0051
29. Yuan L, Ma T, Liu W, Chen Y, Yuan Q, Ye M, et al. LINC00994 Promoted Invasion and Proliferation of Gastric Cancer Cell *Via* Regulating Mir-765-3p. *Am J Transl Res* (2019) 11(10):6641–9.
30. Kong Q, Shu N, Li J, Xu N. Mir-641 Functions as a Tumor Suppressor by Targeting MDM2 in Human Lung Cancer. *Oncol Res* (2018) 26(5):735–41. doi: 10.3727/096504017X15021536183490
31. Chen J, Cui JD, Guo XT, Cao X, Li Q. Increased Expression of miR-641 Contributes to Erlotinib Resistance in Non-Small-Cell Lung Cancer Cells by Targeting NF1. *Cancer Med* (2018) 7(4):1394–403. doi: 10.1002/cam4.1326
32. Yao R, Zheng H, Wu L, Cai P. miRNA-641 Inhibits the Proliferation, Migration, and Invasion and Induces Apoptosis of Cervical Cancer Cells by Directly Targeting ZEB1. *Onco Targets Ther* (2018) 11:8965–76. doi: 10.2147/OTT.S190303
33. Hinske LC, Heyn J, Hubner M, Rink J, Hirschberger S, Kreth S. Intronic miRNA-641 Controls Its Host Gene's Pathway PI3K/AKT and This Relationship is Dysfunctional in Glioblastoma Multiforme. *Biochem Biophys Res Commun* (2017) 489(4):477–83. doi: 10.1016/j.bbrc.2017.05.175
34. Li Y, Jiang L, Lv S, Xu H, Fan Z, He Y, et al. E2F6-Mediated lncRNA CASC2 Down-Regulation Predicts Poor Prognosis and Promotes Progression in Gastric Carcinoma. *Life Sci* (2019) 232:116649. doi: 10.1016/j.lfs.2019.116649
35. Shi X, Ma D, Li M, Zeng L, Chen J, Yang Y. Nuclear Receptor TLX Regulates Islet Beta Cell Proliferation Via E2F6. *Biochem Biophys Res Commun* (2019) 513(3):560–6. doi: 10.1016/j.bbrc.2019.04.033
36. Cai Q, Zhao A, Ren LG, Chen J, Liao KS, Wang ZS, et al. MiR-425 Involves in the Development and Progression of Renal Cell Carcinoma by Inhibiting E2F6. *Eur Rev Med Pharmacol Sci* (2018) 22(19):6300–7. doi: 10.26355/eurrev_201810_16040

Conflict of Interest: The authors declare that the research was conducted in the absence of any commercial or financial relationships that could be construed as a potential conflict of interest.

frontiers in Oncology

ORIGINAL RESEARCH
published: 27 July 2021
doi: 10.3389/fonc.2021.659353

Decorin Suppresses Invasion and EMT Phenotype of Glioma by Inducing Autophagy *via* c-Met/Akt/mTOR Axis

Yanfei Jia[1†], *Qian Feng*[2†], *Bo Tang*[1], *Xiaodong Luo*[1], *Qiang Yang*[1], *Hu Yang*[1] *and Qiang Li*[1*]

[1] Department of Neurosurgery, Second Hospital of Lanzhou University, Lanzhou, China, [2] Department of Respiratory Medicine, Second Hospital of Lanzhou University, Lanzhou, China

OPEN ACCESS

Edited by:
Marcos Vinicius Calfat Maldaun, Hospital Sirio Libanes, Brazil

Reviewed by:
Vadim Kumeiko, Far Eastern Federal University, Russia
Sumit Mukherjee, Cornell University, United States

***Correspondence:**
Qiang Li
xiehere2017@sina.com

[†]These authors have contributed equally to this work

Specialty section:
This article was submitted to Neuro-Oncology and Neurosurgical Oncology, a section of the journal Frontiers in Oncology

Received: 27 January 2021
Accepted: 23 April 2021
Published: 27 July 2021

Citation:
Jia Y, Feng Q, Tang B, Luo X, Yang Q, Yang H and Li Q (2021) Decorin Suppresses Invasion and EMT Phenotype of Glioma by Inducing Autophagy via c-Met/Akt/mTOR Axis. Front. Oncol. 11:659353. doi: 10.3389/fonc.2021.659353

Decorin exhibits inhibitory effects in tumorigenesis in various types of cancers. The clinical characteristics of 42 patients with GBM were reviewed and analyzed. Lentiviral constructs for decorin overexpression and shRNA-mediated silencing were established for U87MG cells and T98G cells, respectively. The expressions of EMT- and autophagy-associated markers were detected in GBM cell lines. The migration and invasion of the glioma cells were assayed to reflect the malignant behavior of GBM. A mouse xenograft model was used to verify the effect of decorin on autophagy *in vivo*. Reduced expression of decorin in glioma tissues was associated with a poor survival of the patients. Decorin overexpression suppressed cell migration, invasion and attenuated EMT phenotype in glioma cell lines. Further study indicated that decorin inhibited EMT phenotype through the induction of autophagy. The mechanisms include inhibiting the activation of c-Met/Akt/mTOR signaling and regulating the expressions of mesenchymal markers including Slug, vimentin and Twist, and epithelial marker E-cadherin. In addition, decorin overexpression in a mice model can also suppress the GBM invasion and EMT phenotype. In conclusion, decorin suppresses invasion and EMT phenotype of glioma by inducing autophagy *via* c-Met/Akt/mTOR axis.

Keywords: glioblastoma multiforme, decorin, extracellular matrix, epithelial to mesenchymal transition, autophagy

INTRODUCTION

Glioblastoma multiforme (GBM) is one of the deadliest malignant tumors that occurs in the central nervous system (1). Poor prognosis is commonly found in the GBM patients due to the high invasiveness and resistant to current treatments (2). The epithelial to mesenchymal transition (EMT), a crucial biological process associated with embryonic and post-natal development, has also been reported to regulate tumor aggressive invasion and metastasis in multiple tumors (3, 4),

including gliomas (5, 6). In GBM, multiple EMT activators including ZEB1 could induce glioma cells to acquire pseudopodia and higher invasive ability, which are special features of the mesenchymal cells (7). Furthermore, EMT may also initiate the dedifferentiation of the cells, allowing the cells to obtain malignant characteristics including tumor invasive ability and multidrug resistance (8, 9).

Autophagy is an evolutionary conserved homeostatic mechanism *via* degrading misfolded proteins and damaged organelles (10), and dysfunction of autophagy is related to several pathological conditions including cancer occurrence. Autophagy is shown to play double effects on cancer by either inhibiting tumorigenesis *via* protecting the genomic integrity or facilitating tumor growth under metabolic stress and promoting tumor aggressiveness (11). Therefore, the role of autophagy in tumor initiation and progression remains to be further elucidated. Current evidence has indicated that autophagy could maintain cells survival, but an unrestrained autophagy may lead to cell death (12, 13). However, the exact effects of autophagy on the EMT in GBM remain unknown.

Invasion and development of the GBM are promoted by remodeling and degradation of the extracellular matrix (ECM) surrounding the tumor (14). ECM of the central nervous system is composed of a higher content of proteoglycans including tenascin-C and decorin and glycosaminoglycans such as hyaluronic acid (2). These macromolecule components orchestrate the biological behavior of the GBM cells by modulating multiple cellular regulatory signals from the microenvironment of the tumors. Decorin, one of the most intensely studied small leucine-rich proteoglycans (SLRPs), exhibits diverse functions in a variety of pathophysiological processes, such as collagen fibrillogenesis (15, 16), wound healing (17), cell apoptosis, and angiogenesis (18, 19). Decorin is found to exhibit inhibitory effects in tumorigenesis in various types of cancers (20). Current evidence indicates that decorin plays role in tumor cell cycle arrest and cell apoptosis through epidermal growth factor receptor (EGFR) pathway, and decorin also inhibits tumor angiogenesis after formation of a heterodimeric complex with its key receptor Met (21).

In this study, we investigated the role of decorin in autophagy and EMT in GBM, and revealed a molecular mechanism of its inhibitory effects on the malignant behavior of GBM.

MATERIALS AND METHODS

Clinical Specimens and Characteristics

A total of 42 patients with GBM who had received both surgery and chemoradiotherapy were included. The patients were 23 male and 19 female, with a median age of 50.5 years, and ranged 27~69 years. The GBM tissue specimens were collected from the patients had not received other therapies during the surgery in the Second Hospital of Lanzhou University (China). All the fresh specimens were immediately frozen in liquid nitrogen and then stored at -80°C. Tissue sample used for immunohistochemical staining was fixed and embedded in paraffin. The clinical characteristics of the patients were reviewed and analyzed. This study was approved by the Ethics Committee of Second Hospital of Lanzhou University, and the patients signed written informed consent.

Cell Cultivation and Transfection

The human GBM cell lines including U87MG, T98G, U251, A172 and U118 were acquired from the American Type Culture Collection (ATCC; Rockville, MD). Human normal astrocyte cell line NHAs were acquired from Lonza (Rockland, ME). The cells were cultured in the Dulbecco's modified Eagle's medium (DMEM, Gibco, Thermo Fisher Scientific Inc., Waltham, MA) containing 4500 mg/L glucose and 4 mM L-glutamine, and supplemented with 10% fetal bovine serum (FBS, Gibco), 100 units/mL penicillin, and 100 μg/mL streptomycin (Sigma, St. Louis, MO). Cell culture was performed in a humidified atmosphere of 5% CO_2 and maintained at 37°C.

Lentiviral constructs for decorin overexpression and shRNA-mediated silencing were purchased from GeneChem (Shanghai, China). The vector sequence of decorin shRNA was: 5′-CCG GCCGCATTGCTGATACCAATATCTCGAGATAT TGGTATCAGCAATGCGGTTTTTG-3′. The U87MG, T98G and U251 cell lines were cultured in six-well plates at 20~30% cell density one day before transduction. U87MG and U251 cells were transfected with LV-decorin-puromycin at a multiplicity of infection (MOI) of 20, and LV-decorin-shRNA-puromycin was transduced into T98G and U251 cells at a MOI of 40. In addition, non-target virus (LV-puromycin) served as negative control (NC). The DMEM should be replaced by fresh medium 12 h after the incubation. Puromycin was added to the cultured cells to choose the cells transduced with the viruses 48 h after the incubation.

Reverse Transcription and Quantitative Real-Time Polymerase Chain Reaction (qRT-PCR)

Total RNA was extracted from GBM tissue samples using TRIzol reagent (Gibco, San Diego, CA). 1 μg of RNA was converted to cDNA using reverse transcriptase. qRT-PCR PCR was performed in an ABI PCR instrument (Applied Biosystems, Grand Island, NY) with a Fast SYBR-green Master Mix kit. GAPDH served as an internal control. The relative expression level of PCR product was calculated with the $2^{-\Delta\Delta Ct}$ method. The primers in this assay were decorin, forward: 5′-ATGAAG GCCACTATCATCCTCC-3′ and reverse: 5′-GTCGCGGT CATCAGGAACTT-3′; GAPDH, forward: 5′-GGAGCGAGA TCCCTCCAAAAT-3′ and reverse: 5′-GGCTGTTGTCA TACTTCTCATGG-3′.

Primary Glioma Cell Isolation and Cultivation

The primary glioma cells were isolated from three patients (No. 17, No.25 and No.35) and cultured as P017, P025 and P035. The tumor tissues were resected and debrided of the necrotic tissue under sterile conditions, and then digested with 0.25% Trypsin. The cells were harvested after the lysis of red blood cells, washed

with phosphate-buffered saline (PBS) and cultured in DMEM supplemented with 10% FBS. The cell medium should be exchanged every two days to remove the non-attached cells until the medium became clarified.

Western Blot Analysis

The total protein of the cells was extracted using RIPA protein extraction buffer (Beyotime, Shanghai, China) containing protease inhibitor. Proteins were separated using SDS-PAGE gels and transferred to a polyvinylidene fluoride (PVDF) membrane using a iBlot 2 Dry Blotting System (Life technologies, Thermo Fisher Scientific, Waltham, MA). The non-specific reactivity was blocked with nonfat milk at 4°C for one hour. The PVDF membranes were then incubated with primary antibodies including anti-decorin (1:1000), anti-E-cadherin (1:10000), anti-fibronectin (1:1000), anti-vimentin (1:1000), anti-Snail (1:1000), anti-Slug (1:1000), anti-Twist (1:1000), anti-LC3B (1:2000), anti-p62 (1:10000), anti-c-Met (1:1000), anti-p-c-Met (1:1000), anti-Akt (1:1000), anti-p-Akt (1:1000), anti-mTOR (1:10000), anti-p-mTOR, anti-ERK1/2 (1:10000), anti-p-ERK1/2, anti-β-actin (1:5000) and anti-GAPDH (1:5000) at 4°C overnight. These antibodies were from Abcam (Cambridge, MA). The membranes were then washed in TBST and incubated with Horseradish peroxidase-conjugated secondary antibodies (Beyotime, Shanghai, China) for 1 h. A Super ECL Plus Detection reagent (Applygen Technologies, Beijing, China) was used to develop the bands, which were captured by a Tanon-4200 Gel Imaging System (Tanon, Shanghai, China).

Wound-Healing Assay

The transduced U87MG or T98G cells were seeded in a 12-well plate until confluence. The cell monolayer was manually scratched with a 200 μL-pipette tip to from a straight line without corresponding cells. The wells were gently washed once with PBS to clean the visual field. To decrease the influence of FBS on the cell migration, the FBS concentration in the medium was changed to 0.5%. At least five continuous fields per well were recorded with a Zeiss Axio Observer Z1 inverted microscope (Carl Zeiss, Thornwood, NY) before and 24 h after migration. The ability of cell migration was expressed as the percentage of cell wound closure, which is calculated as (Scratching area - Wound area at 24 h)/Scratching area × 100%. The scratching area and wound area were quantified by the ImageJ software (NIH, Bethesda, MD).

Cell Invasion Assay

The invasion of transduced U87MG or T98G cells were determined by a BioCoat Matrigel Invasion Chamber (BD Biosciences, Franklin Lakes, NJ). Briefly, cells (1×10^5) in DMEM containing 0.5% FBS were seeded on the upper chamber with Matrigel-coated membrane in a 24-well plate. The bottom chamber was added with DMEM containing 10% FBS as a chemoattractant. After incubating for 24 h, cells on the upper chamber were removed by a cotton swab. The membrane with adhered cells were fixed using 2% paraformaldehyde, and then stained by 0.1% crystal violet PBS solution. Invasive cells were photographed in five random fields per treatment.

Immunofluorescence Analysis

The GBM cells were fixed with 4% paraformaldehyde in PBS for 15 min, and then permeabilized for 10 min with 0.1% Triton-X100. The cells were blocked with 3% BSA for 30 min. After washed with PBS, the cells were incubated with primary anti-LC3B (1:2000, Abcam) or anti-p62 (1:2000, Abcam) primary antibodies for 1 h at 37°C. The cells were washed and then incubated with corresponding IgG H&L (Alexa Fluor® 488) secondary antibodies (Abcam) for 1 h at room temperature. DAPI was used to stain the cell nucleuses. Images were acquired with an UltraVIEW VoX confocal imaging system (Perkin Elmer, Waltham, MA).

In Vivo Mouse Xenograft Model

Single cell suspension (1×10^6) of U251-decorin-shRNA (shRNA-mediated decorin silencing), U251-decorin (decorin overexpression) or U251-shNC cells were implanted into the subcutaneous tissues in the right abdominal flank of the BALB/c-nu/nu mice. Four weeks after implantation of the cells, the mice were sacrificed. The tumors were fixed in 4% paraformaldehyde, and were then paraffin-embedded for HE staining or immunohistochemical analysis.

Statistical Analysis

The data in this study were presented as mean ± S.D. Comparisons were performed using two-sided Student's t-test (two groups), or one-way ANOVA with *post hoc* Tukey's test (multiple groups). The Kaplan-Meier method was used to plot the survival curves. Survival analysis was performed with the GraphPad Prism 7 Software. $P<0.05$ is considered significant.

RESULTS

Reduced Expression of Decorin in Glioma Tissues Associated With a Poor Survival

To determine the relationship between decorin and the prognosis of GBM patients, the expression of decorin in GBM tissues was evaluated. qRT-PCR was used to analyze the expression level of decorin in 42 GBM samples and 3 paratumorous tissue samples, and the results were shown in **Figure 1A**. Western blot analysis in three paired tissue samples from some of these patients (No. 14, 31 and 37) indicated that decorin was highly expressed in paratumorous tissues, while it had a lower expressions in GBM tissues (**Figure 1B**). We defined 21 cases with a higher level of decorin expression than the median as the high-expression group or decorin (high). The other 21 cases were included in the low-expression group or decorin (low). According to the Kaplan-Meier survival curve, the 21 patients with higher decorin expression had significantly better overall survival than those with lower decorin expression ($P = 0.0159$, **Figure 1C**). We further assessed the decorin expression using Western blot on different GBM cells including normal human astrocyte cell line (NHAs), established (U87MG, T98G, U251, A172 and U118) and primary glioma cell lines (P017, P025 and P035). We found a

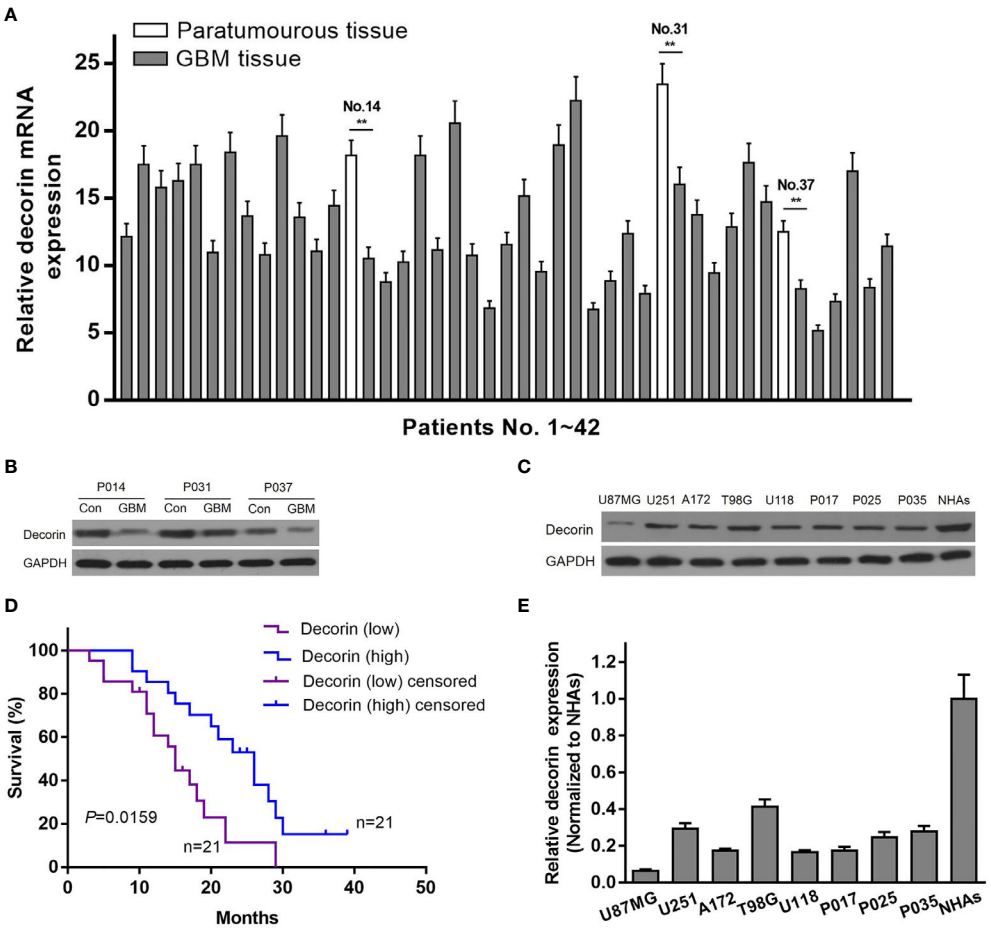

FIGURE 1 | Reduced expression of decorin in glioma tissues is associated with a poor survival. **(A)** The level of decorin expression was detected in 42 GBM samples and 3 paratumorous tissue samples using qRT-PCR. Values are means ± S.D. @ of 3 independent experiments.**P <0.01. **(B)** Western blot analysis in three paired tissue samples indicated that decorin was highly expressed in paratumorous tissues, while it had a lower expressions in GBM tissues. **(C)** Kaplan-Meier survival curve according to the levels of decorin expression. The 21 patients with higher decorin expression had significantly better overall survival than those with lower decorin expression (P = 0.0159). **(D)** Western blot analysis showed that decorin was highly expressed in human normal astrocyte cell line NHAs, while it had a lower expressions in established or primary glioma cell lines. **(E)** Measurement data of Western blot results (means ± S.D. @ of 3 independent experiments).

higher decorin expression level in normal astrocyte cell line while at low levels in all glioma cells studied (**Figures 1D, E**).

Decorin Suppresses Cell Migration, Invasion and Attenuates EMT Phenotype in Glioma Cell Lines

Because a low expression of decorin was correlated with a poor prognosis in patients with GBM, we then investigated whether decorin played a functional role in glioma cells. Lentiviruses-mediated overexpression of decorin in U87MG cells (U87MG-decorin), or expression of short hairpin RNAs (shRNA) to knock down decorin in T98G cell lines (T98G-decorin-shRNA) were performed. Wound-healing assay revealed that decorin overexpression dramatically decreased the cell migration in U87MG-decorin cells compared with that in U87MG-NC cells. In addition, T98G-decorin-shRNA cells showed a significantly increased cell migration compared to the T98G-shNC cells (**Figures 2A, B**). Consistently, overexpression of decorin significantly decreased the number of invasive U87MG cells. However, silencing of decorin significantly promoted cell invasion in T98G cells (**Figures 2C, D**).

To evaluate the potential effects of decorin on the regulation of EMT phenotype, the expression of EMT-associated markers was detected. The result of Western blot indicated that overexpression of decorin significantly increased the expression of E-cadherin, which was expressed in the neural tissue, but suppressed the mesenchymal markers vimentin and fibronectin, and the expressions of EMT-related proteins Snail, Slug and Twist were inhibited as well. In contrast, decorin-shRNA down-regulated the expression of E-cadherin, and up-regulated the mesenchymal markers and EMT-related proteins (**Figures 2E, F**). These results suggested that decorin significantly inhibited the occurrence of EMT, which could be promoted by decorin-shRNA.

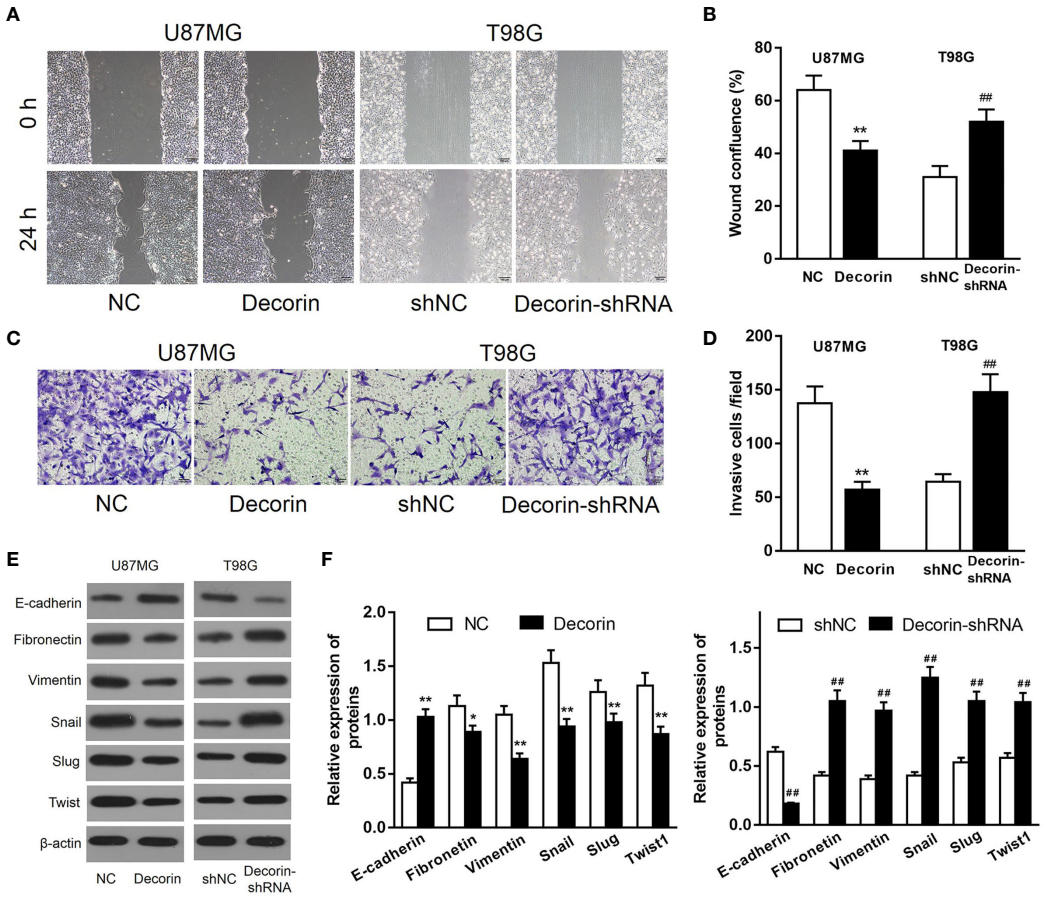

FIGURE 2 | Decorin inhibits cell migration, invasion and ameliorates EMT phenotype in glioma cell lines. **(A)** Wound-healing assay of U87MG and T98G cells with decorin overexpression and decorin silencing. Decorin overexpression dramatically decreased the cell migration in U87MG-decorin cells compared with that in U87MG-NC cells. T98G-decorin-shRNA cells showed a significantly increased cell migration compared to the T98G-shNC cells. **(B)** Measurement data of cell migration results (means ± S.D. @ of 3 independent experiments). **(C)** Overexpression of decorin significantly decreased the number of invasive U87MG cells. However, silencing of decorin significantly promoted cell invasion in T98G cells. **(D)** Measurement data of cell invasion results (means ± S.D. @ of 3 independent experiments). **(E)** Evaluation of the effects of decorin on the EMT phenotype. Western blot results showed that overexpression of decorin significantly increased the expression of E-cadherin, but suppressed the mesenchymal markers vimentin and fibronectin, and inhibited the expressions of EMT-related proteins Snail, Slug and Twist. In contrast, decorin-silencing down-regulated the expression of E-cadherin, and up-regulated the mesenchymal markers and EMT-related proteins. **(F)** Measurement data of Western blot results (means ± S.D. @ of 3 independent experiments). *P < 0.05, **P < 0.01 *vs.* NC; $^{\#\#}$P < 0.01 *vs.* shNC.

Decorin Induces Autophagy in Glioma Cell Lines

To determine the potential mechanism of the inhibitory effects of decorin overexpression on cell invasion and EMT, the levels of autophagy-related proteins were detected. Increased LC3B-I to LC3B-II conversion and reduced expression level of autophagy cargo protein p62 were both found in U87MG-decorin cells, indicating that autophagy was activated by decorin overexpression. In addition, decorin-silencing decreased the ratio of LC3B-II/LC3B-I and elevated the expression of p62 in T98G cells compared with those in shNC cells (**Figures 3A, B**). We then performed immunofluorescence assay to further detect the distribution of LC3B and p62 in U87MG cells. In consistent with western blot analysis, the results showed increased numbers of LC3B protein spots and decreased expression of p62 in the cytoplasm of decorin-overexpressed cells, suggesting that decorin overexpression could promote the cell autophagy (**Figure 3C**).

Decorin Inhibits EMT Phenotype Through the Induction of Autophagy in Glioma Cell Lines

To further discover the mechanisms underlying the inhibitory effects of decorin on the cell invasion and EMT phenotype, we examined whether autophagy–lysosome degradation system contributed to decorin-induced down-regulation of Slug and Twist expression, both of which play critical roles in the regulation of EMT. T98G-shNC or T98G-decorin-shRNA cells were treated with cycloheximide, a widely used protein synthesis inhibitor, or cycloheximide combined with proteasome inhibitor MG132, to block *de novo* synthesis and the ubiquitin-proteasome

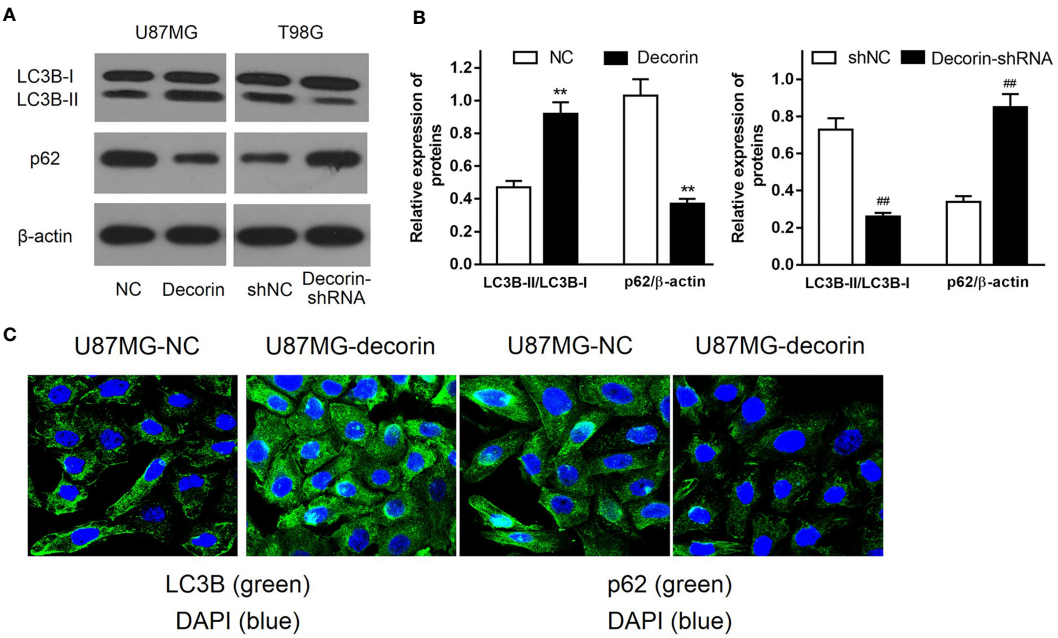

FIGURE 3 | Decorin stimulates autophagy in glioma cell lines. **(A)** Western blot analysis of autophagy related protein indicated that increased LC3B-I to LC3B-II conversion and reduced expression of p62 were both found in U87MG-decorin cells. Decorin-silencing decreased the ratio of LC3B-II/LC3B-I and elevated the expression of p62 in T98G cells. **(B)** Measurement data of Western blot results (means ± S.D. @ of 3 independent experiments). $^{**}P < 0.01$ *vs.* NC; $^{\#\#}P < 0.01$ *vs.* shNC. **(C)** Immunofluorescence analysis of LC3B and p62 in U87MG cells, in response to overexpression of decorin.

degradation of Slug and Twist. The result indicated that the degradation of Slug and Twist in T98G-shNC cells were much rapid than that in T98G-decorin-shRNA cells (**Figures 4A, B**). However, treatment of cells with both cycloheximide and MG132 could not change these effects between groups (**Figures 4C, D**). These data indicate that the decorin-mediated degradation of Slug/Twist does not depend on the ubiquitin-proteasome system.

The cells were then treated with cycloheximide and 3-MA, an inhibitor of autophagy. The result of Western blot indicated that the degradation rates of Slug and Twist were similar between T98G-shNC and T98G-decorin-shRNA cells, suggesting that 3-MA significantly attenuate the degradations of these proteins (**Figures 4E, F**). Therefore, a decorin-dependent mechanism is involved in degradation of Slug/Twist *via* activating the autophagy-lysosome system. Furthermore, 3-MA treatment could block the effects of decorin overexpression-induced inhibition of migration and invasion of U87MG cells (**Figures 4G, H**). Collectively, these findings suggest that decorin inhibits EMT phenotype through the induction of autophagy in glioma cell lines.

Decorin Suppresses EMT *via* c-Met/Akt Axis in Glioma Cells

As we had revealed decorin-mediated degradation of Slug/Twist, we then examined whether decorin directly inactivate EMT-prompting signal pathways. Mounting evidence has shown that decorin exert its oncosuppressive function as an endogenous pan-receptor tyrosine kinase inhibitor. Meanwhile, pathways mediated by tyrosine kinase receptors have been reported to participate in the activation of EMT-like related genes to promote GBM dissemination. Among these RTKs, the hepatocyte growth factor (HGF) binding receptor tyrosine kinase receptor c-Met is highly activated during GBM progression. The activated receptor is associated with a disassembly of adherent junction, resulting in increased cell migration and promoting EMT (22). Current evidence indicates that autophagy can be negatively regulated by PI3K/Akt protein pathway and positively regulated by ERK1/2 protein pathway (23). Thus, we sought to examine whether c-Met/PI3K/Akt axis is involved in decorin-induced EMT inhibition in glioma cells. First, we evaluated the phosphorylated levels of c-Met, Akt and mTOR in T98G-decorin-shRNA and U87MG-decorin cells, and the results indicated that phosphorylated levels of c-Met, Akt and mTOR were notably down-regulated by Western blot analysis. The level of p-ERK1/2 was increased in decorin-overexpressed U87MG cell lines compared with the U87MG-NC cells (**Figures 5A, B**). In contrast, the phosphorylated levels of c-Met, Akt and mTOR were significantly up-regulated, whereas the level of p-ERK1/2 was decreased in T98G-decorin-shRNA cells (**Figures 5A, B**). Although the carcinostatic function of decorin is specific, further investigation is urgently needed to illustrate the mechanism through which decorin affects the EMT and autophagy in tumors *via* the c-Met/Akt/mTOR and ERK1/2 signaling pathway. Thus, we used LY294002, a PI3K inhibitor, and the activator 740Y-P to treat the cells showing stable decorin

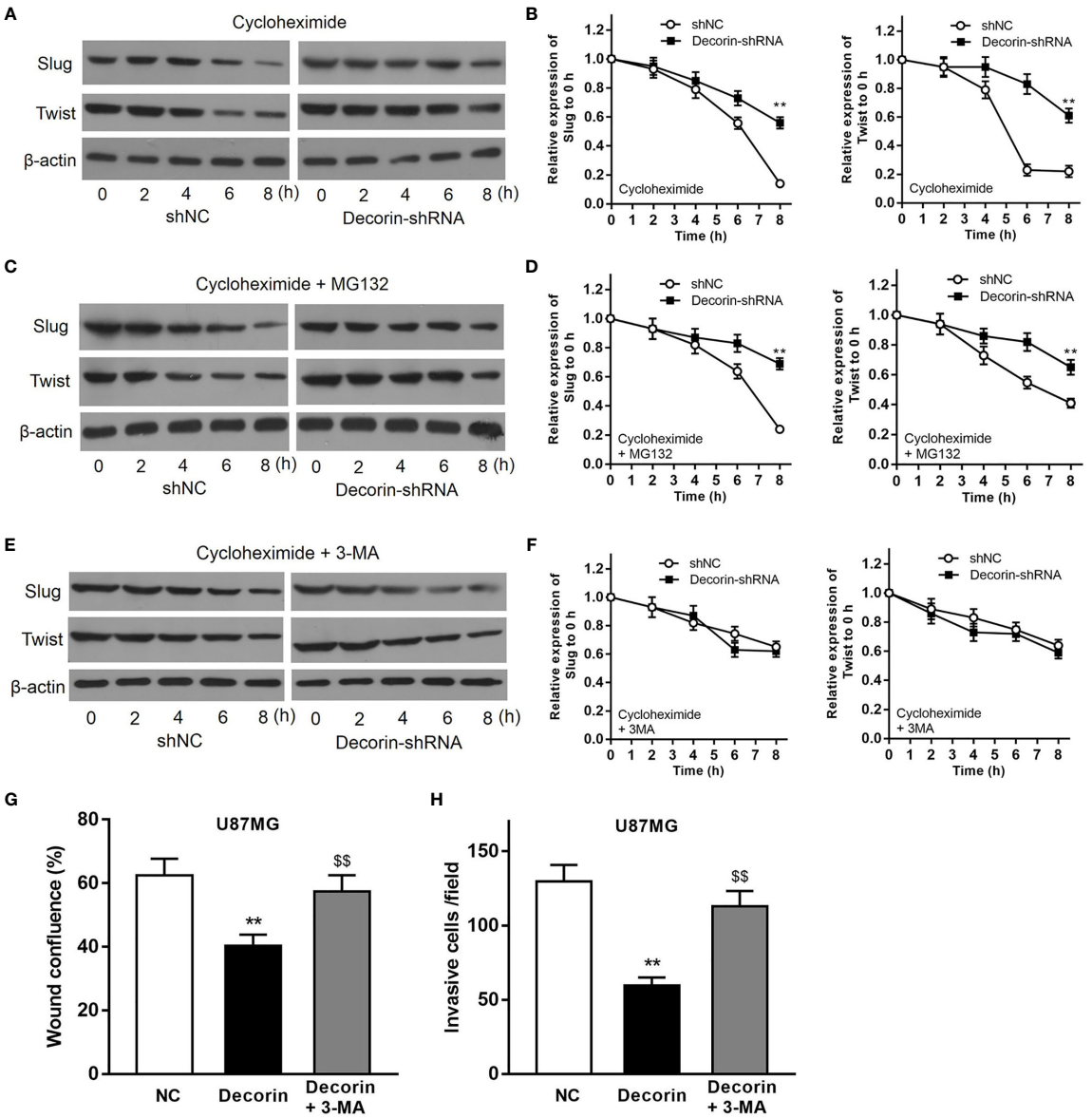

FIGURE 4 | Decorin inhibits EMT phenotype through the induction of autophagy in glioma cell lines. **(A)** T98G cells were infected with LV-decorin-shRNA vector. Cells were treated with 100 μg/mL of cycloheximide. Western blot results showed that the degradation of Slug and Twist in T98G-shNC cells were much rapid than that in T98G-decorin-shRNA cells. **(B)** Measurement data of **(A)** (means ± S.D. @ of 3 independent experiments). **P<0.01 *vs*. shNC. **(C)** Treatment of the cells with both cycloheximide and 10 μM of MG132 could not change these effects between groups. **(D)** Measurement data of **(C)** (means ± S.D. @ of 3 independent experiments). **P < 0.01 *vs*. shNC. **(E)** The degradation rates of Slug and Twist were similar between T98G-shNC and T98G-decorin-shRNA cells after the cells were treated with cycloheximide and 10 mmol/L 3-MA. **(F)** Measurement data of **(E)** (means ± S.D. @ of 3 independent experiments). **(G, H)** 3-MA treatment could block the effects of decorin overexpression-induced inhibition of migration and invasion of U87MG cells. (means ± S.D. @ of 3 independent experiments).). **P < 0.01 *vs*. NC; $^{\$\$}$P < 0.01 *vs*. Decorin.

knockdown or overexpression and evaluated the phosphorylated levels of c-Met, Akt, mTOR and ERK1/2, and the expressions of autophagy- and EMT-related markers by Western blot analysis. The results showed that in the U87MG-decorin cells, the expression levels of p-c-Met, p-Akt and p-mTOR were significantly increased, and p-ERK1/2 level was decreased after treatment with 740Y-P, but these expression changes were reversed in the T98G-decorin-shRNA cells after treatment with LY294002 (**Figures 5A, B**). In addition, the LC3B-II/LC3B-I expression ratio and E-cadherin was decreased in the decorin-overexpressed U87MG cells after 740Y-P treatment, but the levels of P62, Slug and Twist were augmented in these cells (**Figures 5C, D**). Contrarily, LY294002 treatment led to reduced expressions of p62, Slug and Twist, and up-regulated the expressions of p-ERK1/2, E-cadherin and LC3B-II/LC3B-I conversion, resulting in activation of ERK1/2 signaling and

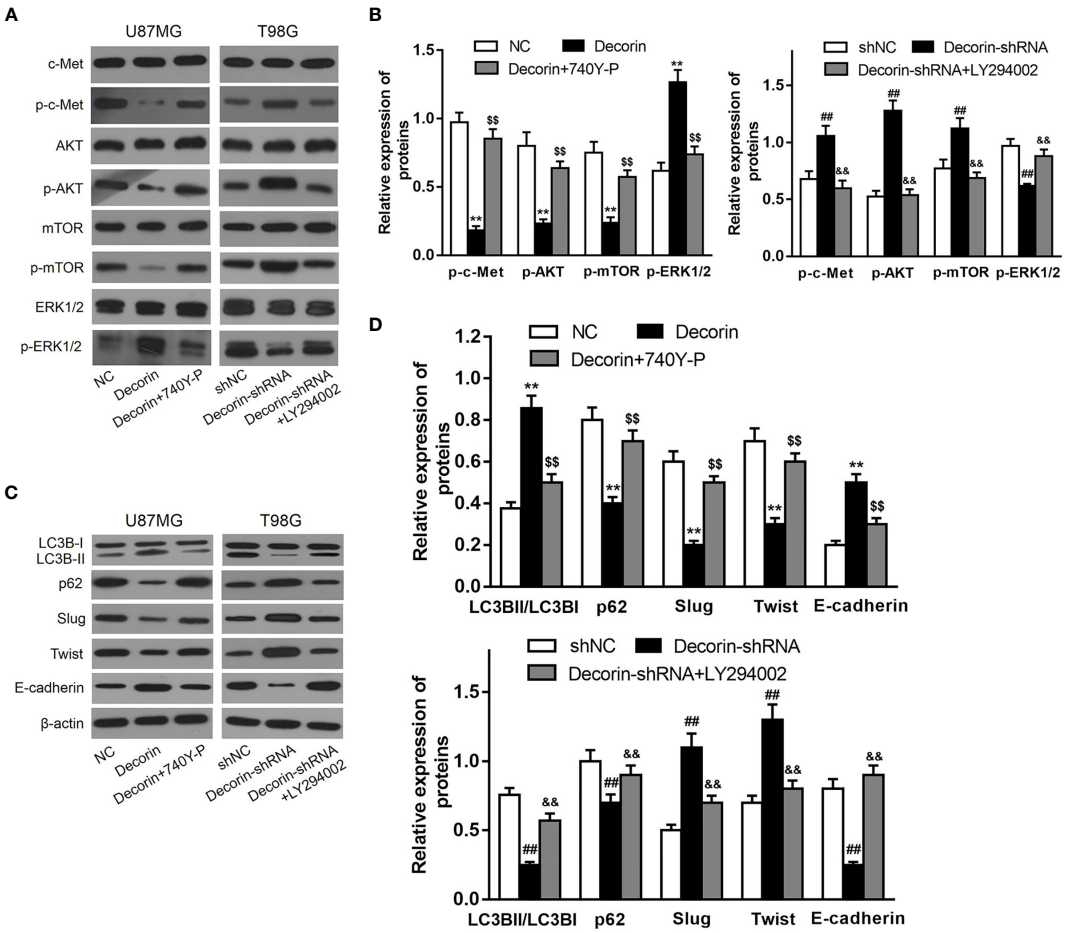

FIGURE 5 | Decorin suppresses EMT *via* c-MET/Akt/mTOR signaling pathway in glioma cells. **(A)** U87MG and T98G cells were infected with decorin-overexpressing lentivirus and decorin-shRNA lentivirus, respectively. U87MG were treated with 740Y-P, a PI3K activator, and T98G cells with the inhibitor LY294002. The cells were then harvested and lysed for the detection of p-c-Met, c-Met, p-Akt, Akt, p-mTOR, mTOR, p-ERK1/2 and ERK1/2 by western blot. The phosphorylated levels of c-Met, Akt and mTOR were notably down-regulated and the level of p-ERK1/2 was increased in decorin-overexpressed U87MG cell lines compared with the U87MG-NC cells. In contrast, the phosphorylated levels of c-Met, Akt and mTOR were significantly up-regulated, whereas the level of p-ERK1/2 was decreased in T98G-decorin-shRNA cells. The U87MG-decorin cells, the expression levels of p-c-Met, p-Akt and p-mTOR were significantly increased, and p-ERK1/2 level was decreased after treatment with 740Y-P, but these expression changes were reversed in the T98G-decorin-shRNA cells after treatment with LY294002. **(B)** Measurement data of **(A)** (means ± S.D. @ of 3 independent experiments). $^{**}P < 0.01$ *vs.* NC; $^{\$\$}P<0.01$ *vs*. Decorin; $^{\#\#}P < 0.01$ *vs.* shNC; $^{\&\&}P < 0.01$ *vs.* Decorin-shRNA. **(C)** LC3B-II/LC3B-I expression ratio and E-cadherin was decreased in the decorin-overexpressed U87MG cells after 740Y-P treatment, but the levels of P62, Slug and Twist were augmented in these cells. Contrarily, LY294002 treatment led to reduced expressions of p62, Slug and Twist, and up-regulated the expressions of p-ERK1/2, E-cadherin and LC3B-II/LC3B-I conversion. **(D)** Measurement data of **(C)** (means ± S.D. @ of 3 independent experiments). $^{**}P < 0.01$ *vs.* NC; $^{\$\$}P < 0.01$ *vs.* Decorin; $^{\#\#}P < 0.01$ *vs.* shNC; $^{\&\&}P < 0.01$ *vs.* Decorin-shRNA.

thereby the induction of autophagy and EMT inhibition (**Figures 5A, C, D**). Therefore, the regulatory effects of decorin on autophagy and the EMT can be partially attributed to the inhibition of PI3K-Akt-mTOR and activation of ERK1/2 signaling pathways.

Decorin Inhibits EMT Phenotype in Glioma Cells *via* Activation of Autophagy *In Vivo*

Along with the *in vitro* cellular data, we tested whether decorin could reduce tumor invasion and inhibit autophagy and the EMT phenotype *in vivo*. The role of decorin in a nude mouse model was analyzed. Lentiviral constructs for shRNA-mediated decorin silencing (U251-decorin-shRNA) and decorin overexpression (U251-decorin) were established in U251 cells. Compared to the U251-decorin tumor, U251-shNC and U251-decorin-shRNA tumors exhibited clear characteristics of invasion. The result of HE staining showed that U251-shNC tumor or U251-decorin-shRNA tumor tended to invade the neighboring normal tissue, however, the U251-decorin tumor kept a relative smooth edge (**Figure 6A**). The expression of mesenchymal markers including Slug and vimentin were up-regulated greatly in U251-decorin-shRNA tumors. The expressions of these proteins were decreased in U251-shNC tumors, and further significantly decreased in U251-decorin

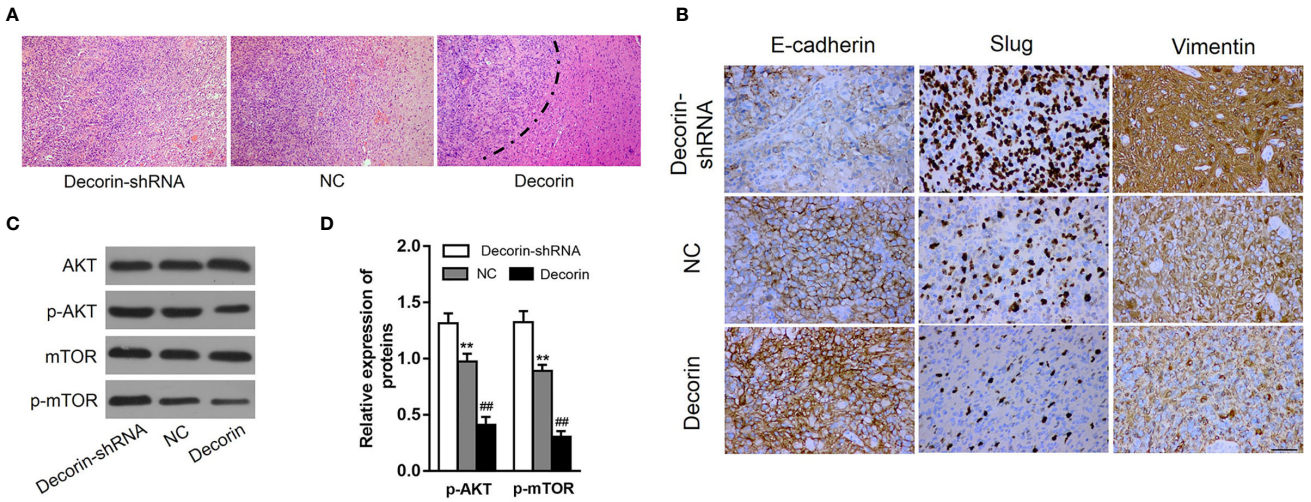

FIGURE 6 | Decorin overexpression suppresses GBM invasion and EMT phenotype. **(A)** The result of HE staining showed that U251-shNC tumor or U251-decorin-shRNA tumor tended to invade the neighboring normal tissue, however, the U251-decorin tumor kept a relative smooth edge. **(B)** The expression of mesenchymal markers including Slug and vimentin were up-regulated greatly in U251-decorin-shRNA tumors. The expressions of these proteins were decreased in U251-shNC tumors, and further significantly decreased in U251-decorin tumors. Conversely, the epithelial marker E-cadherin was down-regulated in U251-decorin-shRNA tumors, and the expression was increased in U251-shNC tumors, and further significantly increased in U251-decorin tumors. **(C)** The phosphorylated levels of Akt and mTOR were notably up-regulated in U251-decorin-shRNA tumors compared to those in U251-shNC tumors, and these phosphorylated levels were further decreased in U251-decorin tumors. **(D)** Measurement data of **(C)** (means ± S.D. @ of 3 independent experiments). $^{**}P < 0.01$ *vs.* Decorin-shRNA; $^{\#\#}P < 0.01$ *vs.* NC.

tumors. Conversely, the epithelial marker E-cadherin was down-regulated in U251-decorin-shRNA tumors, and the expression was increased in U251-shNC tumors, and further significantly increased in U251-decorin tumors. These data suggested that EMT was induced by decorin inhibition *in vivo* (**Figure 6B**). In addition, the phosphorylated levels of Akt and mTOR were notably up-regulated in U251-decorin-shRNA tumors compared to those in U251-shNC tumors, and these phosphorylated levels were further decreased in U251-decorin tumors (both P<0.01, **Figures 6C, D**). These data suggested that Akt/mTOR pathway was inhibited by decorin in the implantated tumors, which was consistent with the invasion data *in vivo*.

DISCUSSION

Proteoglycans are a macromolecule family with complex structures and high heterogeneity. Proteoglycans have a protein core and at least one covalently attached glycosaminoglycan chain. This unique structure provides the proteoglycans with the ability to regulate multiple pathophysiological processes including tumorigenesis (24). Decorin, which belongs to the small leucine-rich proteoglycan (SLRP) family, is a key component of ECM structure and function. Recent studies revealed that decorin exhibits potent oncosuppressive activities in multiple tumors (20, 21) through extracellular and intracellular mechanisms. In this study, we investigated the role of decorin in autophagy and EMT in GBM, and revealed that the high expression level of decorin correlates with the better overall survival of GBM patients. This differential expression was also observed in cultured cells that a higher decorin expression found in normal astrocyte cell line NHAs while it was at low levels in established glioma cells (U87MG, T98G, U251, A172 and U118) and the glioma cells isolated from three GBM patients. Notably, although GAPDH is a normally used reference gene for RT-qPCR assay, Rydbirk et al. reported that more stable reference gene such as UBE2D2 or RPL13 may be better for assessing gene expression in nerve tissues (25). In addition, we found that decorin regulates autophagy and the EMT phenotype through c-Met/Akt/mTOR and ERK1/2 pathway.

In addition to playing an essential role in embryonic development, EMT has also been implicated to modulate tumor invasion and metastasis in numerous tumors (26, 27) including GBM (28). Recent studies have shown that decorin not only exerts its actions within the tumor stroma, but also acts as a multifunctional signaling molecule in numerous pathological conditions such as hepatic fibrosis (29), immunomodulation (30, 31), obesity (32) and tumor initiation and progression (20, 33, 34). In this study, lentiviral constructs for decorin overexpression and shRNA-mediated silencing were established for U87MG cells and T98G cells, respectively. We observed that decorin overexpression in U87MG cells suppressed cell migration and invasion, accompanied by the reversion of EMT phenotype, which is characterized by down-regulation of mesenchymal marker fibronectin, vimentin, Snail, Slug and Twist, and up-regulation of epithelial marker E-cadherin. In contrast, silencing of decorin in T98G cells promoted cell migration, invasion and EMT process.

The current study further found that inhibition of the EMT by decorin was mediated by the activation of autophagy. Multiple autophagy-associated proteins are involved in this complicated process. In the present study, it was shown that overexpression of decorin in U87MG cells up-regulated the conversion of LC3B-II, and reduced the expression level of autophagy cargo protein p62. Immunofluorescence assay also confirmed the increased level of LC3B and decreased p62 level in U87MG cells transfected with decorin. These results suggest that decorin induces autophagy in human glioma cells. In addition, in U87MG cells normally lacking decorin expression, ectopic overexpression of decorin led to the autophagy-lysosome dependent degradation of Slug and Twist, two main promotors of EMT, to attenuate the EMT process in U87MG cells. In contrast, in T98G cells normally expressing decorin, silencing of decorin induced the accumulation of Slug and Twist, and activated the EMT process. Furthermore, autophagy inhibitor (3-MA) treatment could block the effects of decorin overexpression-induced inhibition of migration and invasion of U87MG cells. Thus, our study suggests that decorin shows its GBM-inhibitory effects through induction of autophagy activity to suppress the EMT process.

Recent reports have revealed that decorin can act as an anti-metastatic effector, suppressing migration and invasion of cancer cells (35–37). In a mice model of colon carcinoma, decorin inhibits the growth and migration of cancer cells through regulating the level of E-cadherin (38). The inhibitory effects of decorin on oncogenesis are associated with the activation of receptor complex (34). Using a discovery tool, such as a phosphotyrosine RTK array, a RTK, Met or HGF receptor was found to be specifically activated by soluble decorin proteoglycan or decorin protein core (39). Previous studies indicated that Met is a crucial receptor of decorin, and relays multiple oncosuppressive signals (39, 40). However, the relation between decorin, EMT and c-Met/Akt/mTOR axis remains unclear in glioma cells. Here, we characterized a specific signaling pathway in human glioma cells. Decorin overexpression in U87MG cells blocked the phosphorylation of c-Met, Akt and mTOR followed by downregulation of Slug, Twist and p62, and an increase of E-cadherin, LC3B-II to LC3B-I conversion. These effects were reversed when treated with PI3K activator 740Y-P. In contrast, the phosphorylation of c-Met, Akt and mTOR were inhibited, followed by downregulation of Slug, Twist and p62, and an increase of E-cadherin, LC3B-II to LC3B-I conversion in the decorin-knockdown T98G cells after treatment with the PI3K inhibitor LY294002.

Although implantation of the tumor cells into the brain is closer to the growth environment in the human, complicated operation and higher incidences of infection and death are major drawbacks of this model. Furthermore, it is also difficult to consecutively observe the growth of tumor. Thus, in this study, we used a mice model of subcutaneous implantation of tumor cells due to easy operation and observation. The *in vivo* result indicated that decorin overexpression can suppress the GBM invasion and EMT phenotype. In addition, the phosphorylated levels of Akt and mTOR were significantly decreased in U251-decorin tumors compared to those in both U251-decorin-shRNA tumors and U251-shNC tumors. Therefore, we demonstrated that decorin inhibits migration, invasion and EMT by the suppressing the c-Met/Akt/mTOR signaling pathway.

In conclusion, this study provides evidence that overexpressed decorin attenuated the EMT, migration and invasion of human glioma cells. The mechanisms include inhibiting the activation of c-Met/Akt/mTOR signaling and regulating the expression of the important mesenchymal markers including Slug, vimentin and Twist, and epithelial marker E-cadherin. These findings provide a basis for the action of decorin regulation in the GBM.

DATA AVAILABILITY STATEMENT

The raw data supporting the conclusions of this article will be made available by the authors, without undue reservation.

ETHICS STATEMENT

The animal study was reviewed and approved by Second Hospital of Lanzhou University.

AUTHOR CONTRIBUTIONS

QL conceived and designed the current study and contributed to writing the manuscript. YJ and QF performed the experiments. BT, XL, QY, and HY analyzed and interpreted the data. All authors read and approved the final manuscript.

REFERENCES

1. Tsidulko AY, Kazanskaya GM, Volkov AM, Suhovskih AV, Kiselev RS, Kobozev VV, et al. Chondroitin Sulfate Content and Decorin Expression in Glioblastoma Are Associated With Proliferative Activity of Glioma Cells and Disease Prognosis. *Cell Tissue Res* (2020) 379(1):147–55. doi: 10.1007/s00441-019-03127-2
2. Pogoda K, Bucki R, Byfield FJ, Cruz K, Lee T, Marcinkiewicz C, et al. Soft Substrates Containing Hyaluronan Mimic the Effects of Increased Stiffness on Morphology, Motility, and Proliferation of Glioma Cells. *Biomacromolecules* (2017) 18(10):3040–51. doi: 10.1021/acs.biomac.7b00324
3. Thompson EW, Williams ED. EMT and MET in Carcinoma–Clinical Observations, Regulatory Pathways and New Models. *Clin Exp Metastasis* (2008) 25(6):591–2. doi: 10.1007/s10585-008-9189-8
4. Gregory PA, Bert AG, Paterson EL, Barry SC, Tsykin A, Farshid G, et al. The miR-200 Family and miR-205 Regulate Epithelial to Mesenchymal Transition by Targeting ZEB1 and SIP1. *Nat Cell Biol* (2008) 10(5):593–601. doi: 10.1038/ncb1722
5. Elias MC, Tozer KR, Silber JR, Mikheeva S, Deng M, Morrison RS, et al. TWIST Is Expressed in Human Gliomas and Promotes Invasion. *Neoplasia* (2005) 7(9):824–37. doi: 10.1593/neo.04352
6. Freije WA, Castro-Vargas FE, Fang Z, Horvath S, Cloughesy T, Liau LM, et al. Gene Expression Profiling of Gliomas Strongly Predicts Survival. *Cancer Res* (2004) 64(18):6503–10. doi: 10.1158/0008-5472.CAN-04-0452
7. Kahlert UD, Maciaczyk D, Doostkam S, Orr BA, Simons B, Bogiel T, et al. Activation of Canonical WNT/beta-Catenin Signaling Enhances *In Vitro* Motility of Glioblastoma Cells by Activation of ZEB1 and Other Activators of

Epithelial-to-Mesenchymal Transition. *Cancer Lett* (2012) 325(1):42–53. doi: 10.1016/j.canlet.2012.05.024
8. Brabletz T. To Differentiate or Not–Routes Towards Metastasis. *Nat Rev Cancer* (2012) 12(6):425–36. doi: 10.1038/nrc3265
9. Chaffer CL, Brueckmann I, Scheel C, Kaestli AJ, Wiggins PA, Rodrigues LO, et al. Normal and Neoplastic Nonstem Cells Can Spontaneously Convert to a Stem-Like State. *Proc Natl Acad Sci USA* (2011) 108(19):7950–5. doi: 10.1073/pnas.1102454108
10. Catalano M, D'Alessandro G, Lepore F, Corazzari M, Caldarola S, Valacca C, et al. Autophagy Induction Impairs Migration and Invasion by Reversing EMT in Glioblastoma Cells. *Mol Oncol* (2015) 9(8):1612–25. doi: 10.1016/j.molonc.2015.04.016
11. Li H, Li J, Chen L, Qi S, Yu S, Weng Z, et al. HERC3-Mediated SMAD7 Ubiquitination Degradation Promotes Autophagy-Induced EMT and Chemoresistance in Glioblastoma. *Clin Cancer Res* (2019) 25(12):3602–16. doi: 10.1158/1078-0432.CCR-18-3791
12. Kocaturk NM, Akkoc Y, Kig C, Bayraktar O, Gozuacik D, Kutlu O. Autophagy as a Molecular Target for Cancer Treatment. *Eur J Pharm Sci: Off J Eur Fed Pharm Sci* (2019) 134:116–37. doi: 10.1016/j.ejps.2019.04.011
13. Debnath J, Baehrecke EH, Kroemer G. Does Autophagy Contribute to Cell Death? *Autophagy* (2005) 1(2):66–74. doi: 10.4161/auto.1.2.1738
14. Broekman ML, Maas SLN, Abels ER, Mempel TR, Krichevsky AM, Breakefield XO. Multidimensional Communication in the Microenvirons of Glioblastoma. *Nat Rev Neurol* (2018) 14(8):482–95. doi: 10.1038/s41582-018-0025-8
15. Reed CC, Iozzo RV. The Role of Decorin in Collagen Fibrillogenesis and Skin Homeostasis. *Glycoconjugate J* (2002) 19(4-5):249–55. doi: 10.1023/A:1025383913444
16. Ruhland C, Schonherr E, Robenek H, Hansen U, Iozzo RV, Bruckner P, et al. The Glycosaminoglycan Chain of Decorin Plays an Important Role in Collagen Fibril Formation at the Early Stages of Fibrillogenesis. *FEBS J* (2007) 274(16):4246–55. doi: 10.1111/j.1742-4658.2007.05951.x
17. Jarvelainen H, Puolakkainen P, Pakkanen S, Brown EL, Hook M, Iozzo RV, et al. A Role for Decorin in Cutaneous Wound Healing and Angiogenesis. *Wound Repair Regener* (2006) 14(4):443–52. doi: 10.1111/j.1743-6109.2006.00150.x
18. Grant DS, Yenisey C, Rose RW, Tootell M, Santra M, Iozzo RV. Decorin Suppresses Tumor Cell-Mediated Angiogenesis. *Oncogene* (2002) 21(31):4765–77. doi: 10.1038/sj.onc.1205595
19. Schonherr E, Sunderkotter C, Schaefer L, Thanos S, Grassel S, Oldberg A, et al. Decorin Deficiency Leads to Impaired Angiogenesis in Injured Mouse Cornea. *J Vasc Res* (2004) 41(6):499–508. doi: 10.1159/000081806
20. Sainio AO, Järveläinen HT. Decorin-Mediated Oncosuppression - a Potential Future Adjuvant Therapy for Human Epithelial Cancers. *Br J Pharmacol* (2019) 176(1):5–15. doi: 10.1111/bph.14180
21. Neill T, Schaefer L, Iozzo RV. Decorin as a Multivalent Therapeutic Agent Against Cancer. *Adv Drug Deliv Rev* (2016) 97:174–85. doi: 10.1016/j.addr.2015.10.016
22. Jiao D, Wang J, Lu W, Tang X, Chen J, Mou H, et al. Curcumin Inhibited HGF-Induced EMT and Angiogenesis Through Regulating C-Met Dependent PI3K/Akt/mTOR Signaling Pathways in Lung Cancer. *Mol Ther Oncolytics* (2016) 3:16018. doi: 10.1038/mto.2016.18
23. Zhu JF, Huang W, Yi HM, Xiao T, Li JY, Feng J, et al. Annexin A1-Suppressed Autophagy Promotes Nasopharyngeal Carcinoma Cell Invasion and Metastasis by PI3K/AKT Signaling Activation. *Cell Death Dis* (2018) 9(12):1154. doi: 10.1038/s41419-018-1204-7
24. Karamanos NK, Piperigkou Z, Theocharis AD, Watanabe H, Franchi M, Baud S, et al. Proteoglycan Chemical Diversity Drives Multifunctional Cell Regulation and Therapeutics. *Chem Rev* (2018) 118(18):9152–232. doi: 10.1021/acs.chemrev.8b00354
25. Rydbirk R, Folke J, Winge K, Aznar S, Pakkenberg B, Brudek T. Assessment of Brain Reference Genes for RT-qPCR Studies in Neurodegenerative Diseases. *Sci Rep* (2016) 6:37116. doi: 10.1038/srep37116
26. Wei R, Xiao Y, Song Y, Yuan H, Luo J, Xu W. FAT4 Regulates the EMT and Autophagy in Colorectal Cancer Cells in Part *via* the PI3K-AKT Signaling Axis. *J Exp Clin Cancer Res* (2019) 38(1):112. doi: 10.1186/s13046-019-1043-0
27. Chen C, Liang QY, Chen HK, Wu PF, Feng ZY, Ma XM, et al. DRAM1 Regulates the Migration and Invasion of Hepatoblastoma Cells *via* Autophagy-EMT Pathway. *Oncol Lett* (2018) 16(2):2427–33. doi: 10.3892/ol.2018.8937
28. Lu Y, Xiao L, Liu Y, Wang H, Li H, Zhou Q, et al. MIR517C Inhibits Autophagy and the Epithelial-to-Mesenchymal (-Like) Transition Phenotype in Human Glioblastoma Through KPNA2-Dependent Disruption of TP53 Nuclear Translocation. *Autophagy* (2015) 11(12):2213–32. doi: 10.1080/15548627.2015.1108507
29. Baghy K, Dezso K, Laszlo V, Fullar A, Peterfia B, Paku S, et al. Ablation of the Decorin Gene Enhances Experimental Hepatic Fibrosis and Impairs Hepatic Healing in Mice. *Lab Invest* (2011) 91(3):439–51. doi: 10.1038/labinvest.2010.172
30. Frey H, Schroeder N, Manon-Jensen T, Iozzo RV, Schaefer L. Biological Interplay Between Proteoglycans and Their Innate Immune Receptors in Inflammation. *FEBS J* (2013) 280(10):2165–79. doi: 10.1111/febs.12145
31. Merline R, Moreth K, Beckmann J, Nastase MV, Zeng-Brouwers J, Tralhao JG, et al. Signaling by the Matrix Proteoglycan Decorin Controls Inflammation and Cancer Through PDCD4 and MicroRNA-21. *Sci Signaling* (2011) 4(199):ra75. doi: 10.1126/scisignal.2001868
32. Bolton K, Segal D, McMillan J, Jowett J, Heilbronn L, Abberton K, et al. Decorin is a Secreted Protein Associated With Obesity and Type 2 Diabetes. *Int J Obes (Lond)* (2008) 32(7):1113–21. doi: 10.1038/ijo.2008.41
33. Theocharis AD, Skandalis SS, Neill T, Multhaupt HA, Hubo M, Frey H, et al. Insights Into the Key Roles of Proteoglycans in Breast Cancer Biology and Translational Medicine. *Biochim Biophys Acta* (2015) 1855(2):276–300. doi: 10.1016/j.bbcan.2015.03.006
34. Neill T, Schaefer L, Iozzo RV. Decorin: A Guardian From the Matrix. *Am J Pathol* (2012) 181(2):380–7. doi: 10.1016/j.ajpath.2012.04.029
35. Shintani K, Matsumine A, Kusuzaki K, Morikawa J, Matsubara T, Wakabayashi T, et al. Decorin Suppresses Lung Metastases of Murine Osteosarcoma. *Oncol Rep* (2008) 19(6):1533–9. doi: 10.3892/or.19.6.1533
36. Biaoxue R, Xiguang C, Hua L, Hui M, Shuanying Y, Wei Z, et al. Decreased Expression of Decorin and P57(KIP2) Correlates With Poor Survival and Lymphatic Metastasis in Lung Cancer Patients. *Int J Biol Markers* (2011) 26(1):9–21. doi: 10.5301/jbm.2011.6372
37. Stock C, Jungmann O, Seidler DG. Decorin and Chondroitin-6 Sulfate Inhibit B16V Melanoma Cell Migration and Invasion by Cellular Acidification. *J Cell Physiol* (2011) 226(10):2641–50. doi: 10.1002/jcp.22612
38. Bi X, Pohl NM, Qian Z, Yang GR, Gou Y, Guzman G, et al. Decorin-Mediated Inhibition of Colorectal Cancer Growth and Migration Is Associated With E-Cadherin *In Vitro* and in Mice. *Carcinogenesis* (2012) 33(2):326–30. doi: 10.1093/carcin/bgr293
39. Goldoni S, Humphries A, Nystrom A, Sattar S, Owens RT, McQuillan DJ, et al. Decorin Is a Novel Antagonistic Ligand of the Met Receptor. *J Cell Biol* (2009) 185(4):743–54. doi: 10.1083/jcb.200901129
40. Neill T, Schaefer L, Iozzo RV. Oncosuppressive Functions of Decorin. *Mol Cell Oncol* (2015) 2(3):e975645. doi: 10.4161/23723556.2014.975645

Conflict of Interest: The authors declare that the research was conducted in the absence of any commercial or financial relationships that could be construed as a potential conflict of interest.

frontiers in Neurology

ORIGINAL RESEARCH
published: 02 February 2022
doi: 10.3389/fneur.2022.819216

T2/FLAIR Abnormity Could be the Sign of Glioblastoma Dissemination

Mingxiao Li[1,2†], *Wei Huang*[1,2†], *Hongyan Chen*[3], *Haihui Jiang*[4], *Chuanwei Yang*[1,2], *Shaoping Shen*[1,2], *Yong Cui*[1,2], *Gehong Dong*[5], *Xiaohui Ren*[1,2,6*] *and Song Lin*[1,2,6*]

[1] Department of Neurosurgical Oncology, Beijing Tiantan Hospital, Capital Medical University, Beijing, China, [2] Department of Neurosurgery, Beijing Neurosurgical Institute, Capital Medical University, Beijing, China, [3] Department of Radiology, Beijing Tiantan Hospital, Capital Medical University, Beijing, China, [4] Department of Neurosurgery, Peking University Third Hospital, Peking University, Beijing, China, [5] Department of Pathology, Beijing Tiantan Hospital, Capital Medical University, Beijing, China, [6] Department of Neuroscience, Beijing Key Laboratory of Brain Tumor, Institute for Brain Disorders, Center of Brain Tumor, Beijing, China

OPEN ACCESS

Edited by:
Haotian Zhao,
New York Institute of Technology,
United States

Reviewed by:
Melanie Barz,
Technical University of Munich, Germany
Amaury De Barros,
INSERM U1214 Centre d'Imagerie Neuro Toulouse (ToNIC), France
Daniele Armocida,
Sapienza University of Rome, Italy

***Correspondence:**
Xiaohui Ren
xiaohuiren@aliyun.com
Song Lin
linsong2005@126.com

[†]These authors have contributed equally to this work

Specialty section:
This article was submitted to Neuro-Oncology and Neurosurgical Oncology, a section of the journal Frontiers in Neurology

Received: 21 November 2021
Accepted: 03 January 2022
Published: 02 February 2022

Citation:
Li M, Huang W, Chen H, Jiang H, Yang C, Shen S, Cui Y, Dong G, Ren X and Lin S (2022) T2/FLAIR Abnormity Could be the Sign of Glioblastoma Dissemination. Front. Neurol. 13:819216. doi: 10.3389/fneur.2022.819216

Purpose: Newly emerged or constantly enlarged contrast-enhancing (CE) lesions were the necessary signs for the diagnosis of glioblastoma (GBM) progression. This study aimed to investigate whether the T2-weighted-Fluid-Attenuated Inversion Recovery (T2/FLAIR) abnormal transformation could predict and assess progression for GBMs, especially for tumor dissemination.

Methods: A consecutive cohort of 246 GBM patients with regular follow-up and sufficient radiological data was included in this study. The series of T2/FLAIR and T1CE images were retrospectively reviewed. The patients were separated into T2/FLAIR and T1CE discordant and accordant subgroups based on the initial progression images.

Results: A total of 170 qualified patients were finally analyzed. The incidence of discordant T2/FLAIR and T1CE images was 25.9% (44/170). The median time-span of T2/FLAIR indicated tumor progression was 119.5 days (ranging from 57 days-unreached) prior to T1CE. Nearly half of patients (20/44, 45.5%) in the discordant subgroup suffered from tumor dissemination, substantially higher than accordant patients (23/126, 20.6%, $p < 0.001$). The median time to progression (TTP), post-progression survival (PPS), and overall survival (OS) were not statistically different (all $p > 0.05$) between discordant and accordant patients.

Conclusions: T2/FLAIR abnormity could be the sign of GBM progression, especially for newly emerged lesions disseminating from the primary cavity. Physicians should cast more attention on the dynamic change of T2/FLAIR images, which might be of great significance for progression assessment and subsequent clinical decision-making.

Keywords: glioblastoma (GBM), isocitrate dehydrogenase (IDH), gross total removal of tumor (GTR), supratotal maximal resection (SMR), T2/FLAIR, progression, dissemination, RANO

INTRODUCTION

The glioblastoma (GBM) is one of the most lethal malignancies and harbors profoundly intratumoral and intertumoral heterogeneity (1–3). This heterogeneity encompasses substantially molecular and spatial-temporal distinction and could be reflected on imaging (4). Though GBM typically presents as contrast-enhancing tumors (CET) on MRI, components beyond CE margins,

regarded as non-CE tumors (nCET), could also progress rapidly and evolve to CET that severely threaten survival (5). Recently, dozens of studies focusing on the nCET have proposed the innovative surgical strategy that nCET should be considered to be removed, which might be helpful to prolong prognosis (6–8). This informed us that more attention should be attached to the nCET.

Multicentric and multifocal GBM, consisting of 1–35% newly diagnosed GBM, tend to portend a worse prognosis than unifocal (9). In contrast to multicentric GBM, multifocal GBM presents obvious communication on T2-weighted-Fluid-Attenuated Inversion Recovery (T2/FLAIR) imaging. However, both the definition of multicentric and multifocal GBMs require CE rather than the non-CE (nCE) lesions as one of the centers or focuses (10). Till now, few researchers reported GBMs with nCE lesions as multi-focal or multicentric GBMs. Lasocki et al. firstly reported that nine (6%) of 151 patients with GBM had isolated nCE lesions and further proved GBM, which warned us to pay more attention to this phenomenon (11).

Multifocal or multicentric lesions could not only be diagnosed for primary GBM but for recurrent or progressed tumors. Though local recurrence dominates the patterns of progression, non-local progression, such as distant intracranial metastasis, subependymal spread, and leptomeningeal dissemination, and extracranial visceral metastasis, occurs in 2–34.5% patients with GBM (12, 13). The Response Assessment in Neuro-Oncology (RANO) and modified RANO criteria warrant new emerged or significantly enlarged CE lesions as the necessary and essential evidence to consider tumor progression for Bevacizumab-naïve patients (14–16), nevertheless, non-local recurrence could be similar to nCE multifocal or multicentric GBMs. They might not be visible on T1CE but T2/FLAIR images. Till now, no studies focused on this issue. Thus, we performed a retrospective study to explore whether T2/FLAIR could be more sensitive in distinguishing early progression than T1CE images, especially for non-local progressed GBM.

METHODS AND MATERIALS

Patients

A cohort of 246 consecutive adult patients from March 1, 2013 to August 31, 2020, surgically treated and pathologically defined as *de novo* supratentorial isocitrate dehydrogenase (IDH) wild-type GBM based on 2021 WHO classification of brain tumors was included in this retrospectively study (17). All tissue sections were meticulously reviewed by 3 senior neuropathologists to generate a consensus diagnosis. Patients with inadequate follow-up, lethal comorbidity, or other malignancies were excluded. Besides, patients without tumor progression were not included for subsequent analysis. Clinical, radiological, and pathological information was recorded.

Abbreviations: GBM, glioblastoma; IDH, isocitrate dehydrogenase; MGMT, O^6-methylguanine-DNA methyltransferase; KPS, Karnofsky Performance Status score; GTR, gross total removal of tumor; SMR, supratotal maximal resection; TTP, time to progression; OS, overall survival; PPS, post-progression survival.

Molecular Information

The 1p/19q codeletion, 7+/10–, epidermal growth factor receptor (EGFR) amplification status were determined by fluorescence *in situ* hybridization (FISH). For IDH1 R132 and IDH2 R172 mutations, telomerase reverse transcriptase (TERT) promoter C228T/C250T mutation was tested by Sanger sequencing (18, 19). The status of O^6-methylguanine-DNA methyltransferase (MGMT) promoter was determined by pyrosequencing, and patients were divided into methylated and unmethylated by the average methylation level of 12% (20). BRAF V600E, fibroblast growth factor receptor 1 (FGFR1), and H3K27M mutations were evaluated by Sanger sequencing for exclusion when required.

Collection of Radiological Data

All MRI studies were performed on 3.0-T clinical scanners (Siemens Trio Tim, or GE, Boston, MA USA) in the routine clinical workup. The protocol included axial T1-weighted (repetition time [TR] 1,750–2,250 ms, echo time [TE] 9.4–19.8 ms, matrix 256 × 198, slice thickness 5 mm), T2-weighted fast spin-echo (TR 4,900–6,711 ms, TE 97–116.6 ms, FA = 150°, matrix 256 × 320, slice thickness 5 mm, spacing 1 mm, field of view [FOV] = 220 × 220 mm, number of excitations [NEX] = 3), T2 FLAIR (TR = 7,000–8,000 msec, TE 91–152.0 msec, TI 2,340 ms, matrix 256 × 186; slice thickness 5 mm, spacing 1 mm, FOV = 220 × 220 mm, NEX = 3), and axial and coronal contrast-enhanced T1-weighted images (CE-T1WI; TR 1,779.2–2,110 ms, TE 9.4–19.8 ms, matrix: 320 × 288, FA = 15°, FOV = 240 × 188 mm, slice thickness 5 mm, spacing 1 mm, NEX = 1) with the administration of gadopentetate dimeglumine (0.2 mmol/kg).

MRI examinations were independently analyzed by 2 investigators (XHR, a neurosurgical oncologist with 15 years of experience and HYC, a radiologist with 25 years of experience). Both were blinded to clinical history, molecular status, and histopathologic diagnosis. Reassessment was performed when discordant results were acquired. If the disagreement persisted, a third reviewer (XZC, a radiologist in brain imaging with 25 years of experience), joined the discussion for final consensus.

Treatment and Follow-Up

All enrolled patients were surgically treated. After the operation and a waiting period of about 3–5 weeks, the Stupp's protocol, radiation with guideline-recommended dose concurrent daily temozolomide (TMZ; 75 mg/m^2/d), was finished, and following cycles of maintenance TMZ (150–200 mg/m^2 for 5 days every 28 days) adjuvant chemotherapy was administered.

Contrast-enhanced-MRI was meticulously followed within 4 weeks after concurrent chemoradiotherapy (CCRT) and regularly surveilled with an interval of 8–12 weeks or if necessary. The patterns of tumor progression were classified as local or *in situ* (obvious connection with the primary resection cavity), distant intracranial metastasis (newly emerged parenchyma lesions without a clear connection with the original tumor on T2/FLAIR images), subependymal spread (lesions disseminated along with the subependymal zone), and leptomeningeal dissemination (diffuse leptomeningeal enhancement around the contours of the gyri and sulci with/without multiple nodular deposited in

the subarachnoid space) based on the initial MR images with progression (12). We also employed the principles of RANO for low-grade glioma to evaluate the dynamic change of T2/FLAIR of this GBM cohort (21). MR spectrum (MRS), perfusion-weighted MRI (PWI) by dynamic susceptibility contrast (DSC), and ^{18}F-FDG-PET MRI were available to some but not all patients during the follow-up to provide valuable information to distinguish treatment response (pseudoprogression and radiation necrosis) from true progression.

To distinguish peritumor edema and true non-enhancing tumor, we introduced these definitions from the Visually Accessible Rembrandt Images (VASARI) feature set (https://wiki.nci.nih.gov/display/CIP/VASARI). Edema should be greater in signal than nCET and somewhat lower in signal than CSF. Pseudopods are the canonical characteristics of edema. The entire abnormality may be comprised of: (1) an enhancing component, (2) a non-enhancing component, (3) a necrotic component, and (4) an edema component for a typical GBM.

Time to progression (TTP) was defined as the duration from the initial surgery to the time of true tumor progression, and overall survival (OS) was termed as the duration between the initial surgery and the death, or date of the last follow-up (19, 22). Post-progression survival (the time span between tumor progression and death) was also calculated and documented for further analysis. All assessments were performed prior to Bevacizumab or other antiangiogenic therapy.

Statistical Analysis

The student's *t*-test was used for continuous variables, and the Mann-Whitney *U*-test was applied for non-parametric data. The Chi-square test or Fisher's exact test was used to compare the categorical variables. Graphpad Prism (Version 8.0.1, GraphPad Software, San Diego, CA, USA) was used for statistical analysis. The survival rate of patients was estimated with the Kaplan-Meier plot, and differences between curves were compared by the log-rank test. Probability values were obtained using 2-sided tests with statistical significance defined as $p < 0.05$.

RESULTS

Descriptive Characteristics and the Incidence of Different Patterns of Progression

A total of 246 patients were initially included in this study. Patients with no recurrence, ambiguous diagnosis of progression, or follow-up interval longer than 3 months were excluded for subsequent analysis (**Figure 1**). In 170 qualified GBM patients with assessable progression patterns, 25.3% (43/170) demonstrated non-local progression, such as distant intracranial metastasis (17/170, 10.0%), subependymal spread (20/170, 11.8%), and leptomeningeal dissemination (6/170, 3.5%), while local or diffuse recurrence was present in the other 127 (74.7%) patients (**Table 1**).

The Incidence of Discordant T2/FLAIR and T1CE Images for GBM

We observed the dynamic change discordance between T2/FLAIR and T1CE in a small subgroup of patients with GBM (44/170, 25.9%). The abnormal finding of T2/FLAIR was prior to T1CE in most cases (37/44, 84.1%), and the four of remaining patients received re-operation before the new or constantly enlarged T1CE lesions emerged, and the other three patients were only found T2/FLAIR abnormal space-occupying lesions without enhancement till the last follow-up.

The median time-span between T2/FLAIR and T1CE indicated progression was 119.5 days (ranging 57 days -unreached). In the discordant patients, two developed leptomeningeal dissemination (2/44, 4.5%), nine presented subependymal spread (9/44, 20.5%), nine showed distant intracranial metastases (9/44, 20.5%), and the remnant 24 patients suffered *in situ* recurrences (54.5%). Generally speaking, nearly half of discordant patients were observed with non-local tumor progression (20/44, 45.5%), while in an accordant subgroup, only 18.3% of patients suffered from non-local progression (23/126, $p < 0.001$; **Table 1**). Therefore, newly emerged non-CE lesions, especially for these distant from the primary tumor cavity, should be cast more attention because T2/FLAIR abnormal lesions could still be the sign of GBM progression.

A total of 96 patients achieved gross total removal of tumor (GTR), and in the discordant subgroups, the GTR rate was higher than accordant patients (32/44, 72.7% for discordant and 64/126, 50.8% for accordant, respectively, $p = 0.012$). In addition, the preoperative status was better in discordant than the accordant group (preoperative Karnofsky Performance Status [KPS] score >70: 36 of 44 (81.8%) patients for discordant and 81 of 126 (64.3%) patients for accordant, $p = 0.031$). The phenomenon informed us that the discordant subgroup achieved better local tumor control and resulted in a lower incidence of local progression (**Table 1**). While the mean age, gender distribution, preoperative KPS score, mean tumor volume, the incidence of ventricle infringement, MGMT promoter status, EFGR amplification, tumor location, and TERT promoter status was not different between discordant and accordant patients (**Table 1**).

Radiological and Pathological Finding

Distinguishing treatment-induced response, such as pseudoprogression and radionecrosis, from true progression is of utmost importance for subsequent clinical decision-making and prognosis assessment. In the whole discordant subgroup, eleven performed advanced imaging checks, such as MR spectrum (MRS), perfusion-weighted MRI (PWI), PET, or combined. Significantly increased choline (Cho)/N-acetyl-aspartate (NAA) ratio, relative cerebral blood volume (rCBV), and high glucose uptake were observed in these nine patients (9/11, 81.8%) while the other two showed mild-to-moderate perfusion and metabolic transformation.

Eleven patients in the discordant subgroup (three of them performed advanced imaging check, and seven of them

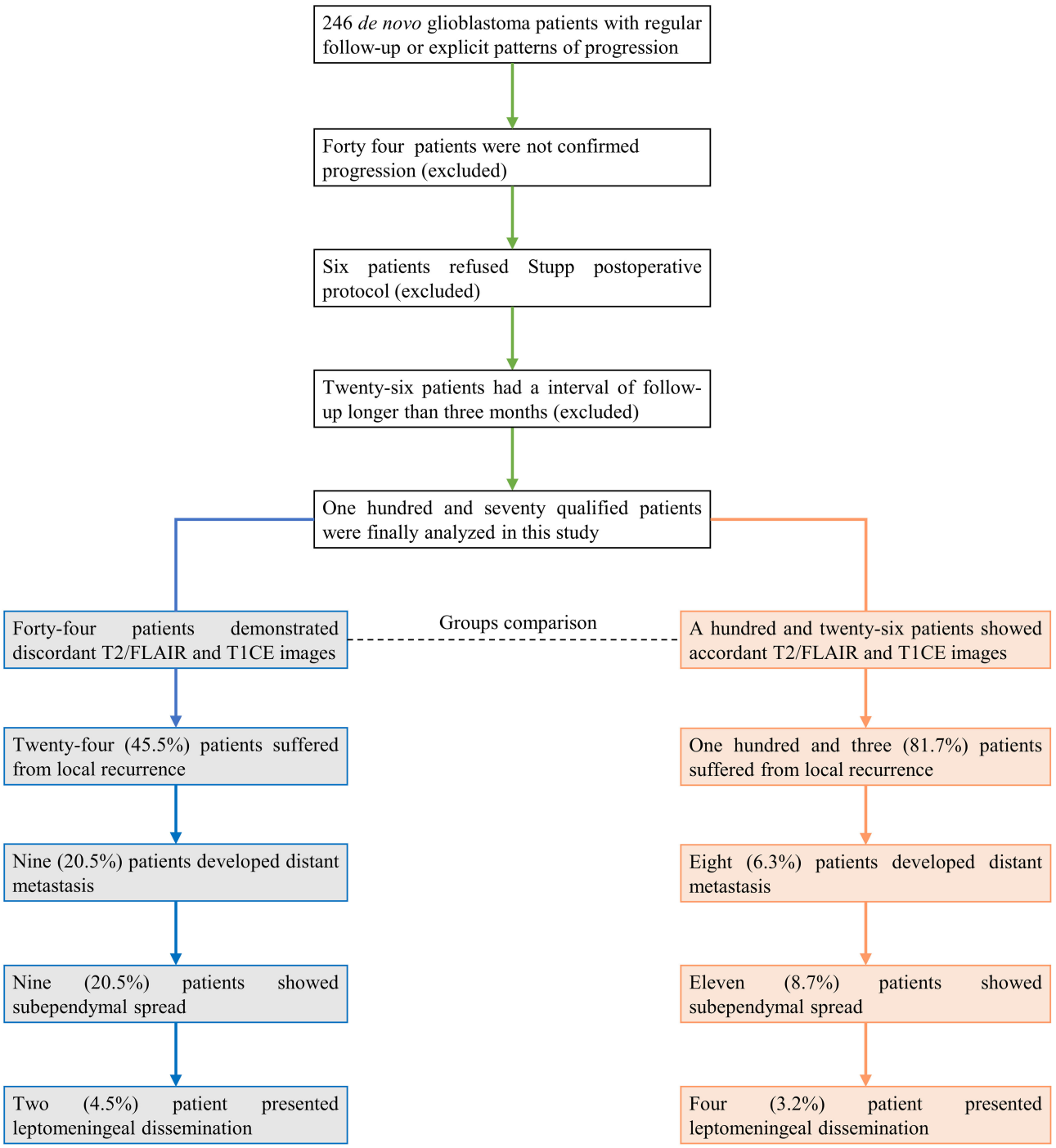

FIGURE 1 | Patients included in this study. The final analysis showed that 25.9% of patients (44/170) presented discordant results between T2/FLAIR and T1CE images.

were local recurrence) accepted reoperation, and eight of them were reported with GBM (all accepted re-operation till the tumor evolved into CE). The other three without enhancement were histologically confirmed astrocytoma with anaplastic characteristics (no obvious microvascular proliferation or necrosis were observed though this diagnosis should be refined as GBM based on the 2021 WHO brain tumor classification examples in **Figure 2**), and all of them were distant

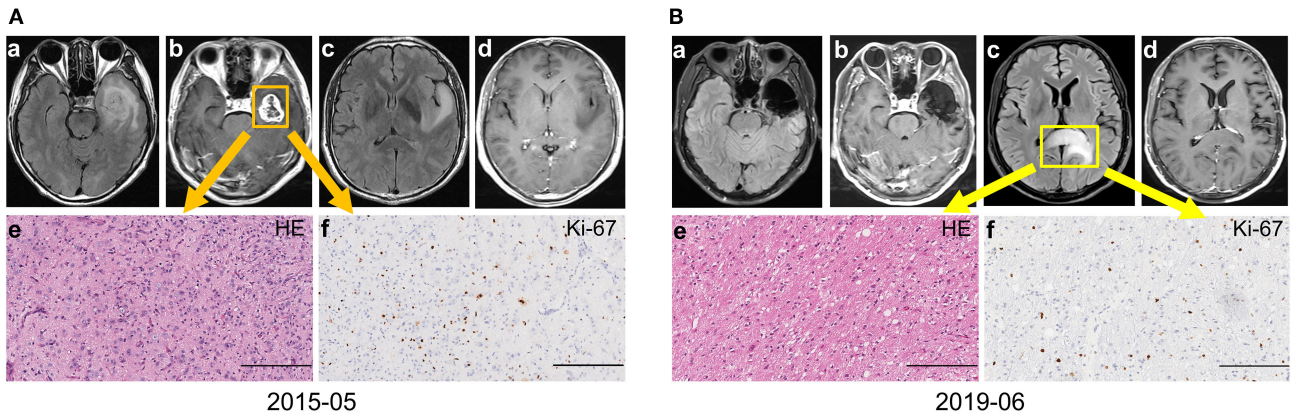

FIGURE 2 | A representative case for the discordant subgroup with distant intracranial metastasis. **(A)** The patient presented unbearable headache with contrast-enhancing (CE) lesion on left temporal (a–d). Craniotomy was performed and the tumor was totally removed. The final diagnose was primary GBM, IDH wild-type, WHO grade 4 (e–f). **(B)** Forty-nine months after the operation, a non-CE lesion on the splenium of the corpus callosum with space-occupying effect (a–d) was suspected tumor progression. The final pathology diagnosis was GBM, IDH wild-type, WHO grade 4 (e–f) based on the WHO 2021 brain tumor classification system (Bars, 200 μm). GBM, glioblastoma; IDH, isocitrate dehydrogenase.

metastasis. Therefore, highly aggressive GBM could transform into entities with histologically indicated gentle tumor behavior. This phenomenon was rare and has a close relationship with the distant non-CE lesion. Though most non-CE lesions evolved to CE lesions eventually, physicians should be aware that non-CE lesions might be the early sign of tumor progression for GBM, especially for distant lesions.

Similar Prognosis Between Discordant and Accordant Patients

For the whole cohort, the median TTP, OS, and PPS were 6.0, 19.0, and 11.0 months, respectively. The comparison of TTP, OS, and PPS between discordant and accordant patients was not significant (discordant vs. accordant, median TTP: 8.0 vs. 5.0 months, $p = 0.222$, **Figure 3A**; median OS: 21.0 vs. 19.0 months, $p = 0.164$, **Figure 3B**; median PPS: 11.5 vs. 10.5 months, $p = 0.171$, **Figure 3C**). The results demonstrated that though the discordant subgroup initially presented less aggressive tumor behavior with non-CE lesions, they progressed as fast as the CE lesions in accordant patients and harbored a lethal prognosis.

More discordant patients suffered from non-local tumor progression, thus simple comparison between discordant and accordant subgroups might overlook some critical information. Survival comparison demonstrated that the prognosis of non-local progression patients in the discordant subgroup was superior to accordant patients (median TTP: 7.1 vs. 5.0 months, $p = 0.083$, **Figure 3D**; median OS: 18.25 vs. 12.5 months, $p = 0.009$, **Figure 3E**; median PPS: 10.7 vs. 6.0 months, $p = 0.009$, **Figure 3F**). This result implied that the occurrence of tumor dissemination for discordant patients might be later due to better local tumor control, and disseminated nCE tumor cells might harbor a relatively gentle tumor behavior in discordant patients.

DISCUSSION

The IDH wild-type *de novo* GBM is one of the most lethal malignancies that embraces highly molecular, temporospatial, and radiological intratumoral and intertumoral heterogeneity (10). The RANO and modified RANO criteria for GBM request newly emerged or constantly enlarged CE lesions as the basic prerequisite to defining progression, regardless of T2/FLAIR (14–16). Our longitudinal observation demonstrated that extra attention should be paid to the dynamic change of T2/FLAIR, which might be the early sign of progression, especially for non-local progression GBMs.

Typically, GBM is highly aggressive, infiltrative, and invasive brain malignancy with prominent blood-brain barrier disruption (10). The canonical manifestation on radiology is pronounced CE lesions with surrounding T2/FLAIR abnormity areas (23). However, the inherently high heterogeneity renders neither all GBMs nor the whole body of GBMs is aggressive and destructive enough that could be reflected by CE MRI. Not only a minority of GBMs were non-CE but the ratio of nCE/CE in the GBMs varied significantly (24, 25). Both the CE and T2/FLAIR abnormal regions are enriched with malignant tumor cells that could reproduce and propagate rapidly (7, 26, 27). Contemporarily, no assessment criterion focusing on GBM was established according to radiological alteration of T2/FLAIR, neither treatment effect assessment for Bevacizumab-naïve patients nor progression surveillance. The extent of resection (EOR) of GBM is based on the percentage of CETs removed or the accurate resident volume of enhancement, regardless of T2/FLAIR. Complete response, partial response, stable disease, or progression after treatment for GBM of RANO was defined by dynamic alteration CE lesions for patients who did not receive antiangiogenic therapy (14, 28, 29). Studies reported the sensitivity of FLAIR signal increase prior to enhancement indicated *in situ* progression ranged from 34 to

TABLE 1 | Clinical, demographic and radiological characteristics of patients with/without discordant T2/FLAIR T1CE images.

Characteristics	Discordant	Accordant	*P*-value
Number of patients	44 (25.9%)	126 (74.1%)	-
Age at diagnosis (years)			
Mean	46.3 ± 12.8	49.6 ± 12.1	0.130
Median	50.0	51.0	0.847
Gender			
Male	30 (68.2%)	85 (67.5%)	0.930
Female	14 (31.8%)	41 (32.5%)	
Preoperative KPS			
>70	36 (81.8%)	81 (64.3%)	**0.031**
≤70	8 (18.2%)	45 (35.7%)	
Extent of resection			
GTR	32 (72.7%)	64 (50.8%)	**0.012**
Non-GTR	12 (27.3%)	62 (49.2%)	
Tumor volume (cm^3)			
Mean	36.8±33.1	44.5±51.7	0.352
Median	31.7	38.0	0.330
Ventricle infringement			
Yes	23 (52.3%)	79 (62.7%)	0.224
No	21 (47.7%)	47 (37.3%)	
MGMT promoter			
Methylated	19 (43.2%)	44 (35.8%)	0.384
Unmethylated	25 (56.8%)	79 (64.2%)	
Tumor location			
Frontal	13 (29.5%)	41 (32.5%)	0.926
Temporal	16 (36.4%)	40 (31.7%)	
Insular	9 (20.5%)	22 (17.5%)	
Parietal	4 (9.1%)	16 (12.7%)	
Occipital	2 (4.5%)	7 (5.6%)	
TERT promoter			
Mutant	11 (37.5%)	49 (42.3%)	0.080
Wild	17 (62.5%)	35 (57.7%)	
Patterns of progression			
Local recurrence	24 (54.5%)	103 (81.7%)	**0.003**
Distant metastasis	9 (20.5%)	8 (6.3%)	
Subependymal spread	9 (20.5%)	11 (8.7%)	
Leptomeningeal dissemination	2 (4.5%)	4 (3.2%)	

T1CE, T1 weighted contrast-enhancing images; KPS, Karnofsky Performance Status score; GTR, gross total removal of tumor; MGMT, O-6-methylguanine DNA methyltransferase. Bold: significant.

75% (27, 30–33), higher than ours, which might be accountable due to the difference in inclusion criteria, GTR, and ventricle infringement rate in our study. Our study firstly reported the incidence of T2-FLAIR discordance in dissemination monitoring and revealed its poor clinical outcome.

Traditionally, multifocal or multicentric GBM refers to the concept that synchronous multiple lesions at diagnosis, and the former was defined as multiple CE lesions embedded in a relatively large area with abnormal T2/FLAIR-weighted signal while the latter usually invading different hemisphere or lobe devoid of connection. Furthermore, multiple GBMs occurred at a distinct time without connection on MRI were also viewed as multicentric GBM (2, 34). However, these definitions were established based on the CE lesions with/without well-demarcated margins. Lasocki et al. firstly reported that the incidence of multicentric nCE lesions of GBM was 6% (9/151) at preoperative diagnosis, and the survival was much worse than patients without multicentric non-enhancement lesions. In four patients with follow-up MRIs, all developed enhancement and necrosis within 1 year (11). This phenomenon informed us that nCE lesions distant from the dominant lesion could be the reason for disease progression and treatment failure, and much more attention should be attached to the nCE lesions because they could not only be multicentric GBMs at diagnosis but at recurrence. Future response assessment criteria should incorporate the dynamic change of T2/FLAIR especially distant signal alteration to monitor GBM *in situ* recurrence or intracranial dissemination.

Local recurrence dominates the patterns of GBM progression (ranging from 60 to 85%) (12). The standard care of GBM demands radiotherapy to eliminate the residual tumor cells and postpone tumor recurrence. Demyelination caused by radiation in target volume could lead to evident T2/FLAIR abnormity (16). At the very early stage of progression, tumor-related edema or infiltration effect was quite obscure and totally covered by demyelination on T2/FLAIR images, but even tiny CE lesion on MRI could be extraordinarily conspicuous on T1CE images. Thus, for local recurrence and leptomeningeal dissemination monitoring, the newly emerged or constantly enlarged CE lesions could be more sensitive for recurrence predicting. Tumor cells could also migrate into areas out of beam target or the low dose of the target where demyelination was less pronounced. Tumor cells from nCE areas of initially dominant bulk could form new non-CE lesions out of the original target zone, or at the very early stage of new lesion forming, the transformation of T2/FLAIR was prior to T1CE images. Our results showed that 25.9% of patients could be found with an nCE lesion that eventually developed into CE lesions with necrosis, and three of them were pathologically confirmed as nCE GBM. Berzero et al. reported that histological grading was important for IDH wild-type glioma prognosis assessment (35), and our result confirmed this result in non-local progressed discordant patients. Thus, T2/FLAIR should be added to determine dissemination and predict prognosis for GBM, especially in the very early stage.

Currently, the concept of supratotal maximal resection (SMR), which is termed as total removal of both CE and T2/FLAIR abnormal regions for eligible patients, has raised great interest in neurosurgeons for GBM treatment. Some retrospective studies demonstrated that patients with GBM might derive a survival benefit from SMR while some were not (36–44). GBMs appropriate for SMR are commonly located on the prefrontal lobe, where a high percentage of GBMs was glioma-CpG island methylator phenotype (G-CIMP) subtype and MGMT promoter methylated (45, 46). The evidence level of SMR for GBM could never be equal to a multicenter, prospective trial due to the

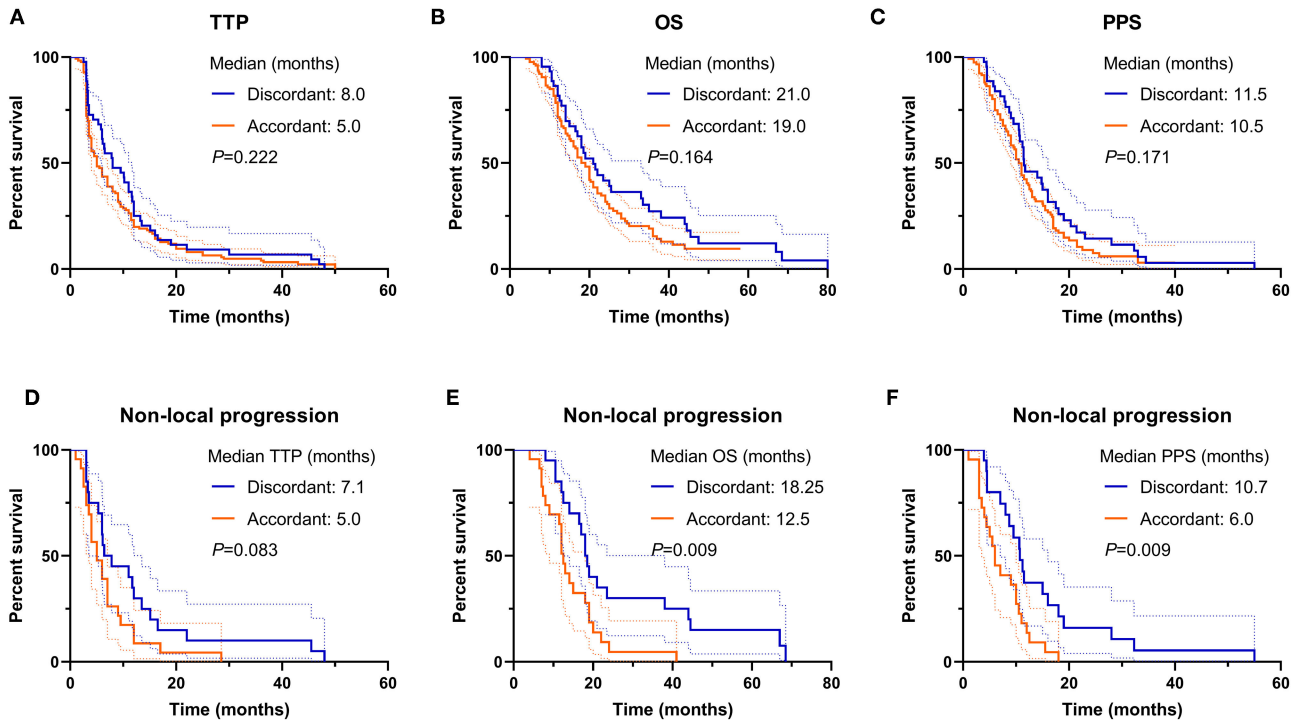

FIGURE 3 | Prognosis comparison between T2/FLAIR and T1CE discordant and accordant patients. **(A–C)** The TTP, OS, and PPS were not different between the two subgroups. **(D–F)** For non-local progression patients, the OS and PPS in discordant subgroup were favorable than accordant subgroup, but not for the TTP. TTP, time to progression; OS, overall survival; PPS, post-progression survival.

impractical nature of exploring the impact of EOR on survival. Though some results were contradictory, we still could not entirely deny the benefit yielded from SMR. This is the initial concern for T2/FLAIR abnormity for GBM, and we believe this would be inspirable and enlightened.

Multiple recurrences in GBM indicated a more aggressive and invasive tumor behavior and portended inferior prognosis without exception. There still lacks efficient and effective treatment modalities for GBM dissemination control. Some polite studies revealed that stereotactic radiosurgery (SRS) might be helpful for a single, small lesion with the satisfactory disease control (19, 47). For eligible patients, SRS might be an ideal choice to alleviate suffering and prolong survival.

Limitations do exist due to the nature of retrospective studies within a single institute. Acquisition of consecutive MRI data every 2–3 months in a large cohort of patients was quite difficult. Different medical centers for follow-up, poor compliance, and financial problems might be the major reasons that impede us from sufficient data. Till now, this is nevertheless one of the largest cohorts of studies with a series of MRI to dynamic monitor treatment response. Another limitation lies in that pathology confirmation was only achieved in a small part of patients. Furthermore, distinguishing peritumor edema from true non-enhancing tumors was difficult under certain circumstances. These limitations could not cover up the meaningful finding of this study, and neuro-oncologist should shed more light on the dynamic image change during follow-up, not only T1WI CE but T2/FLAIR images.

CONCLUSION

T2/FLAIR abnormity could be the early sign of GBM progression, especially for newly emerged lesions distant from the primary tumor cavity. The subsequent modified GBM assessment criterion should incorporate the T2/FLAIR information for disease monitoring, and physicians should cast more attention on the dynamic change of T2/FLAIR images for progression evaluation and subsequent clinical decision-making.

DATA AVAILABILITY STATEMENT

The original contributions presented in the study are included in the article/supplementary material, further inquiries can be directed to the corresponding authors.

ETHICS STATEMENT

The studies involving human participants were reviewed and approved by Capital Medical University, Beijing. The

patients/participants provided their written informed consent to participate in this study.

AUTHOR CONTRIBUTIONS

ML, XR, HJ, CY, YC, and SL contributed to literature search, study design, data collection, data interpretation, and writing. HC, SS, and XR contributed to MRI analysis. ML, SS, and CY contributed to data analysis. All authors contributed to the article and approved the submitted version.

FUNDING

This study was supported by the National Natural Science Foundation of China (81571632&81771309).

ACKNOWLEDGMENTS

The authors sincerely thank the patients and their families for their participation in the present study. We acknowledge Dr. Hongyan Chen, Dr. Qian Chen, and Dr. Xuzhu Chen (Beijing Tiantan Hospital) for collecting and interpreting the MRI data.

REFERENCES

1. Broekman ML, Maas SLN, Abels ER, Mempel TR, Krichevsky AM, Breakefield XO. Multidimensional communication in the microenvirons of glioblastoma. *Nat Rev Neurol.* (2018) 14:482–95. doi: 10.1038/s41582-018-0025-8
2. Georgescu M, Olar A. Genetic and histologic spatiotemporal evolution of recurrent, multifocal, multicentric and metastatic glioblastoma. *Acta Neuropathol Commun.* (2020) 8:10. doi: 10.1186/s40478-020-0889-x
3. Alexander BM, Cloughesy TF. Adult Glioblastoma. *J Clin Oncol.* (2017) 35:2402–9. doi: 10.1200/JCO.2017.73.0119
4. Park J, Kim H, Kim N, Park S, Kim Y, Kim J. Spatiotemporal heterogeneity in multiparametric physiologic MRI is associated with patient outcomes in IDH-wildtype glioblastoma. *Clin Cancer Res.* (2021) 27:237–45. doi: 10.1158/1078-0432.CCR-20-2156
5. Lasocki A, Gaillard F. Non-contrast-enhancing tumor: a new frontier in glioblastoma research. *AJNR Am J Neuroradiol.* (2019) 40:758–65. doi: 10.3174/ajnr.A6025
6. Jiang H, Cui Y, Liu X, Ren X, Li M, Lin S. Proliferation-dominant high-grade astrocytoma: survival benefit associated with extensive resection of FLAIR abnormality region. *J Neurosurg.* (2019) 132:998–1005. doi: 10.3171/2018.12.JNS182775
7. Choi Y, Ahn K, Nam Y, Jang J, Shin N, Choi H, et al. Analysis of heterogeneity of peritumoral T2 hyperintensity in patients with pretreatment glioblastoma: prognostic value of MRI-based radiomics. *Eur J Radiol.* (2019) 120:108642. doi: 10.1016/j.ejrad.2019.108642
8. Molinaro A, Hervey-Jumper S, Morshed R, Young J, Han S, Chunduru P, et al. Association of maximal extent of resection of contrast-enhanced and non-contrast-enhanced tumor with survival within molecular subgroups of patients with newly diagnosed glioblastoma. *JAMA oncology.* (2020) 6:495–503. doi: 10.1001/jamaoncol.2019.6143
9. Lasocki A, Gaillard F, Tacey M, Drummond K, Stuckey S. Multifocal and multicentric glioblastoma: Improved characterisation with FLAIR imaging and prognostic implications. *J Clin Neurosci.* (2016) 31:92–8. doi: 10.1016/j.jocn.2016.02.022
10. Barajas R, Hodgson J, Chang J, Vandenberg S, Yeh R, Parsa A, et al. Glioblastoma multiforme regional genetic and cellular expression patterns: influence on anatomic and physiologic MR imaging. *Radiology.* (2010) 254:564–76. doi: 10.1148/radiol.09090663
11. Lasocki A, Gaillard F, Tacey M, Drummond K, Stuckey S. The incidence and significance of multicentric noncontrast-enhancing lesions distant from a histologically-proven glioblastoma. *J Neurooncol.* (2016) 129:471–8. doi: 10.1007/s11060-016-2193-y
12. Jiang H, Yu K, Li M, Cui Y, Ren X, Yang C, et al. Classification of progression patterns in glioblastoma: analysis of predictive factors and clinical implications. *Front Oncol.* (2020) 10:590648. doi: 10.3389/fonc.2020.590648
13. Tu Z, Xiong H, Qiu Y, Li G, Wang L, Peng S. Limited recurrence distance of glioblastoma under modern radiotherapy era. *BMC Cancer.* (2021) 21:720. doi: 10.1186/s12885-021-08467-3
14. Wen PY, Chang SM, Van den Bent MJ, Vogelbaum MA, Macdonald DR, Lee EQ. Response assessment in neuro-oncology clinical trials. *J Clin Oncol.* (2017) 35:2439–49. doi: 10.1200/JCO.2017.72.7511
15. Ellingson BM, Wen PY, Cloughesy TF. Modified criteria for radiographic response assessment in glioblastoma clinical trials. *Neurotherapeutics.* (2017) 14:307–20. doi: 10.1007/s13311-016-0507-6
16. Wen PY, Macdonald DR, Reardon DA, Cloughesy TF, Sorensen AG, Galanis E, et al. Updated response assessment criteria for high-grade gliomas: response assessment in neuro-oncology working group. *J Clin Oncol.* (2010) 28:1963–72. doi: 10.1200/JCO.2009.26.3541
17. Louis DN, Perry A, Wesseling P, Brat DJ, Cree IA, Figarella-Branger D, et al. The 2021 WHO classification of tumors of the central nervous system: a summary. *Neuro Oncol.* (2021) 23:1231–51. doi: 10.1093/neuonc/noab106
18. Li M, Dong G, Zhang W, Ren X, Jiang H, Yang C, et al. Combining MGMT promoter pyrosequencing and protein expression to optimize prognosis stratification in glioblastoma. *Cancer Sci.* (2021) 112:3699–710. doi: 10.1111/cas.15024
19. Li M, Ren X, Jiang H, Yang K, Huang W, Yu K, et al. Supratentorial high-grade astrocytoma with leptomeningeal spread to the fourth ventricle: a lethal dissemination with dismal prognosis. *J Neurooncol.* (2019) 142:253–61. doi: 10.1007/s11060-018-03086-8
20. Li M, Ren X, Dong G, Wang J, Jiang H, Yang C, et al. Distinguishing pseudoprogression from true early progression in isocitrate dehydrogenase wild-type glioblastoma by interrogating clinical, radiological, and molecular features. *Front Oncol.* (2021) 11:627325. doi: 10.3389/fonc.2021.627325
21. van den Bent MJ, Wefel JS, Schiff D, Taphoorn MJ, Jaeckle K, Junck L, et al. Response assessment in neuro-oncology (a report of the RANO group): assessment of outcome in trials of diffuse low-grade gliomas. *Lancet Oncol.* (2011) 12:583–93. doi: 10.1016/S1470-2045(11)70057-2
22. Yang K, Ren X, Tao L, Wang P, Jiang H, Shen L, et al. Prognostic implications of epidermal growth factor receptor variant III expression and nuclear translocation in Chinese human gliomas. *Chin J Cancer Res.* (2019) 31:188–202. doi: 10.21147/j.issn.1000-9604.2019.01.14
23. Akbari H, Macyszyn L, Da X, Wolf R, Bilello M, Verma R, et al. Pattern analysis of dynamic susceptibility contrast-enhanced MR imaging demonstrates peritumoral tissue heterogeneity. *Radiology.* (2014) 273:502–10. doi: 10.1148/radiol.14132458
24. Lemée JM, Clavreul A, Menei P. Intratumoral heterogeneity in glioblastoma: don't forget the peritumoral brain zone. *Neuro Oncol.* (2015) 17:1322–32. doi: 10.1093/neuonc/nov119
25. Chow D, Chang P, Weinberg B, Bota D, Grinband J, Filippi C. Imaging genetic heterogeneity in glioblastoma and other glial tumors: review of current methods and future directions. *AJR Am J Roentgenol.* (2018) 210:30–8. doi: 10.2214/AJR.17.18754
26. Lundy P, Domino J, Ryken T, Fouke S, McCracken D, Ormond D, et al. The role of imaging for the management of newly diagnosed glioblastoma in adults: a systematic review and evidence-based clinical practice guideline update. *J Neurooncol.* (2020) 150:95–120. doi: 10.1007/s11060-020-03597-3
27. Gatson N, Bross S, Odia Y, Mongelluzzo G, Hu Y, Lockard L, et al. Early imaging marker of progressing glioblastoma: a window of opportunity. *J Neurooncol.* (2020) 148:629–40. doi: 10.1007/s11060-020-03565-x
28. Jiang T, Nam D, Ram Z, Poon W, Wang J, Boldbaatar D, et al. Clinical practice guidelines for the management of adult diffuse gliomas. *Cancer Lett.* (2020) 499:60–72. doi: 10.1016/j.canlet.2020.10.050

29. Lim M, Xia Y, Bettegowda C, Weller M. Current state of immunotherapy for glioblastoma. *Nat Rev Clin Oncol.* (2018) 15:422–42. doi: 10.1038/s41571-018-0003-5
30. Winterstein M, Münter M, Burkholder I, Essig M, Kauczor H, Weber M. Partially resected gliomas: diagnostic performance of fluid-attenuated inversion recovery MR imaging for detection of progression. *Radiology.* (2010) 254:907–16. doi: 10.1148/radiol09090893
31. Ito-Yamashita T, Nakasu Y, Mitsuya K, Mizokami Y, Namba H. Detection of tumor progression by signal intensity increase on fluid-attenuated inversion recovery magnetic resonance images in the resection cavity of high-grade gliomas. *Neurol Med Chir.* (2013) 53:496–500. doi: 10.2176/nmc.53.496
32. Sarbu N, Oleaga L, Valduvieco I, Pujol T, Berenguer J. Increased signal intensity in FLAIR sequences in the resection cavity can predict progression and progression-free survival in gliomas. *Neurocirugia (Asturias, Spain).* (2016) 27:269–76. doi: 10.1016/j.neucir.2016.04.002
33. Bette S, Gempt J, Huber T, Delbridge C, Meyer B, Zimmer C, et al. FLAIR signal increase of the fluid within the resection cavity after glioma surgery: generally valid as early recurrence marker? *J Neurosurg.* (2017) 127:417–25. doi: 10.3171/2016.8.JNS16752
34. Li Y, Zhang ZX, Huang GH, Xiang Y, Yang L, Pei YC, et al. A systematic review of multifocal and multicentric glioblastoma. *J Clin Neurosci.* (2021) 83:71–6.
35. Berzero G, Di Stefano A, Ronchi S, Bielle F, Villa C, Guillerm E, et al. IDH-wildtype lower grade diffuse gliomas: the importance of histological grade and molecular assessment for prognostic stratification. *Neuro Oncol.* (2020). doi: 10.1093/neuonc/noaa258
36. Tabor JK, Bonda D, LeMonda BC, D'Amico RS. Neuropsychological outcomes following supratotal resection for high-grade glioma: a review. *J Neurooncol.* (2021) 152:429–37. doi: 10.1007/s11060-021-03731-9
37. Moiraghi A, Roux A, Peeters S, Pelletier JB, Baroud M, Trancart B, et al. Feasibility, safety and impact on overall survival of awake resection for newly diagnosed supratentorial idh-wildtype glioblastomas in adults. *Cancers (Basel).* (2021) 13:2911. doi: 10.3390/cancers13122911
38. Bettag C, Schregel K, Langer P, Thomas C, Behme D, Stadelmann C, et al. Endoscope-assisted fluorescence-guided resection allowing supratotal removal in glioblastoma surgery. *Neurosurg Focus.* (2021) 50:E3. doi: 10.3171/2020.10.FOCUS20560
39. Jackson C, Choi J, Khalafallah AM, Price C, Bettegowda C, Lim M, et al. A systematic review and meta-analysis of supratotal versus gross total resection for glioblastoma. *J Neurooncol.* (2020) 148:419–31. doi: 10.1007/s11060-020-03556-y
40. Ene CI, Cimino PJ, Fine HA, Holland EC. Incorporating genomic signatures into surgical and medical decision-making for elderly glioblastoma patients. *Neurosurg Focus.* (2020) 49:E11. doi: 10.3171/2020.7.FOCUS20418
41. Dimou J, Beland B, Kelly J. Supramaximal resection: a systematic review of its safety, efficacy and feasibility in glioblastoma. *J Clin Neurosci.* (2020) 72:328–34. doi: 10.1016/j.jocn.2019.12.021
42. Roh TH, Kang SG, Moon JH, Sung KS, Park HH, Kim SH, et al. Survival benefit of lobectomy over gross-total resection without lobectomy in cases of glioblastoma in the noneloquent area: a retrospective study. *J Neurosurg.* (2019) 132:895–901. doi: 10.1093/neuonc/noz126.279
43. Ahmadipour Y, Kaur M, Pierscianek D, Gembruch O, Oppong MD, Mueller O, et al. Association of surgical resection, disability, and survival in patients with glioblastoma. *J Neurol Surg A Cent Eur Neurosurg.* (2019) 80:262–8. doi: 10.1055/s-0039-1685170
44. Esquenazi Y, Friedman E, Liu Z, Zhu JJ, Hsu S, Tandon N. The Survival Advantage of "Supratotal" Resection of Glioblastoma Using Selective Cortical Mapping and the Subpial Technique. *Neurosurgery.* (2017) 81:275–88. doi: 10.1093/neuros/nyw174
45. Brennan CW, Verhaak RG, McKenna A, Campos B, Noushmehr H, Salama SR, et al. The somatic genomic landscape of glioblastoma. *Cell.* (2013) 155:462–77. doi: 10.1016/j.cell.2013.09.034
46. Noushmehr H, Weisenberger DJ, Diefes K, Phillips HS, Pujara K, Berman BP, et al. Identification of a CpG island methylator phenotype that defines a distinct subgroup of glioma. *Cancer Cell.* (2010) 17510–22. doi: 10.1016/j.ccr.2010.03.017
47. Khan MN, Poulin A, Essig M. Fourth ventricular lesions in metastatic gliomas: a rare predilection? *Brain Tumor Res Treat.* (2017) 5:24–9. doi: 10.14791/btrt.2017.5.1.24

Conflict of Interest: The authors declare that the research was conducted in the absence of any commercial or financial relationships that could be construed as a potential conflict of interest.

frontiers in Oncology

ORIGINAL RESEARCH
published: 08 February 2022
doi: 10.3389/fonc.2021.788755

Transforming Growth Factor-Beta-Regulated LncRNA-MUF Promotes Invasion by Modulating the miR-34a Snail1 Axis in Glioblastoma Multiforme

Bakhya Shree, Shraddha Tripathi and Vivek Sharma *

Department of Biological Sciences, Birla Institute of Technology and Science, Hyderabad, India

OPEN ACCESS

Edited by:
Haotian Zhao,
New York Institute of Technology, United States

Reviewed by:
Quan Cheng,
Central South University, China
Runsheng Chen,
Chinese Academy of Sciences, China
Yikun Yao,
National Institutes of Health (NIH), United States

***Correspondence:**
Vivek Sharma
viveksharmabt@gmail.com; viveksharma@hyderabad.bits-pilani.ac.in

Specialty section:
This article was submitted to Neuro-Oncology and Neurosurgical Oncology, a section of the journal Frontiers in Oncology

Received: *03 October 2021*
Accepted: *13 December 2021*
Published: *08 February 2022*

Citation:
Shree B, Tripathi S and Sharma V (2022) Transforming Growth Factor-Beta-Regulated LncRNA-MUF Promotes Invasion by Modulating the miR-34a Snail1 Axis in Glioblastoma Multiforme. Front. Oncol. 11:788755. doi: 10.3389/fonc.2021.788755

Transforming growth factor beta (TGF-β)-regulated long-non-coding RNAs (lncRNAs) modulate several aspects of tumor development such as proliferation, invasion, metastasis, epithelial to mesenchymal transition (EMT), and drug resistance in various cancers, including Glioblastoma multiforme (GBM). We identified several novel differentially expressed lncRNAs upon TGF-β treatment in glioma cells using genome-wide microarray screening. We show that TGF-β induces lncRNA-MUF in glioma cells, and its expression is significantly upregulated in glioma tissues and is associated with poor overall survival of GBM patients. Knockdown of lncRNA-MUF reduces proliferation, migration, and invasion in glioma cells and sensitizes them to temozolomide (TMZ)-induced apoptosis. In addition, lncRNA-MUF downregulation impairs TGF-β-induced smad2/3 phosphorylation. In line with its role in regulating invasion, lncRNA-MUF functions as a competing endogenous RNA (ceRNA) for miR-34a and promotes Snail1 expression. Collectively, our findings suggest lncRNA-MUF as an attractive therapeutic target for GBM.

Keywords: glioblastoma, lncRNA, Snail1, miR-34a, TGF-β

1 INTRODUCTION

GBM is a heterogeneous malignancy of the central nervous system characterized by aggressive invasion into the surrounding tissue (1). Despite following an aggressive treatment approach involving surgical resection and radio- and chemotherapy with temozolomide (TMZ), it remains incurable with a dismal survival rate of about 15 months (2). One of the characteristic features of GBM is extensive infiltration and invasion of the tumor cells to the surrounding parenchyma, which leads to colonization and relapse of tumors (3). TGF-β is a cytokine with multiple functions regulating cell proliferation, differentiation, and tissue homeostasis (4, 5). TGF-β promotes cancer cell invasion, EMT, and chemoresistance (5). TGF-β is overexpressed in glioblastoma, and its elevated expression is associated with the increased histologic grade of GBM (6). TGF-β promotes proliferation, invasion, metastasis, angiogenesis, resistance to apoptosis, replicative immortality, evasion of growth suppression, evasion of immune checkpoint blockade, and chemoresistance in GBM (7–9).

Less than 3% of the human genome codes for proteins, while the rest of the genome pervasively transcribes several non-coding transcripts (10–12). Among these, lncRNA transcripts are the most abundant and are loosely defined as longer than 200 bp in length with no ability to code for proteins (10, 13). LncRNAs interact with proteins or other non-coding RNAs to regulate gene expression in *cis* and *trans* to modulate cancer phenotypes (10, 14). Several differentially expressed lncRNAs have been identified in GBM, which regulate various aspects of GBM pathology (15–20). TGF-β-regulated lncRNAs modulate invasion, metastasis, and EMT in various cancers (21). In glioma, TGF-β-regulated lncRNAs lncRNA-ATB, UCA1, LINC00645, and LINC00115 modulate proliferation, invasion, and glioma stem cell renewal (22–25). In addition, TGF-β-induced lncRNAs H19 and HOXD-AS2 confer TMZ resistance in glioma by regulating miR-198 biogenesis and competing with KSRP (9).

Using a microarray screen, we identified several previously uncharacterized TGF-β1-regulated lncRNAs in T98G cells and characterized the role of one of the TGF-β-induced lncRNA-mesenchymal upregulated factor (lncRNA-MUF/LINC00941) in glioma physiology. LncRNA-MUF was first identified by Yan et al., and they demonstrated that it regulates EMT in hepatocellular carcinoma (HCC) (26). However, the functions and mechanism of action of lncRNA-MUF in GBM were not known. We show that levels of lncRNA-MUF are upregulated in GBM tumor samples along with histological grade. Our results suggest that it functions as an oncogenic lncRNA to promote glioma cell growth and invasion by functioning as a miRNA sponge for miR-34a that targets and suppresses Snail1. In addition, we show that lncRNA-MUF depletion sensitizes glioma cells to TMZ-induced apoptosis. Collectively, our results suggest that the lncRNA-MUF/miR-34a/Snail1 signaling axis may serve as a novel therapeutic target for GBM treatment.

2 MATERIALS AND METHODS

2.1 Cell Culture and Treatments

T98G cells were purchased from the American Type Culture Collection (Manassas, VA). LN229, LN18, and U87-MG cells were purchased from NCCS, Pune. All cells were grown in complete medium, DMEM (Invitrogen) containing 10% fetal bovine serum (FBS) supplemented with 1 mM l-glutamine, and penicillin/streptomycin (Gibco). Cells were treated with TGF-β1 (10 ng/ml) PeproTech (#100-21) in serum-free medium (SFM) for dose and duration indicated in the figures and legends. SB505124 (Tocris # 3263), an inhibitor of TGFβRI/smad2/3, was used at a concentration of 6 μM for pretreatment of GBM cells to inhibit TGF-β signaling wherever indicated.

2.2 Microarray Analysis

Agilent SurePrint G3 Gene Expression Microarrays for Human (v3) for lncRNAs, containing 30,606 lncRNAs and 37,756 RefSeq-coding transcripts, were used to interrogate lncRNA and mRNA changes in vehicle versus TGF-β1 (10 ng/ml)-treated T98G cells after 24 h. RNA was isolated using MN NucleoSpin RNA Plus isolation kit (Cat. No. 740984.5). 10 μg of purified RNA samples was treated with recombinant DNAse I (Invitrogen Thermo Scientific—Cat. No. EN0521) as per manufacturer's instructions, and the RNA samples were column purified using the MN NucleoSpin column purification kit. Hybridization and analysis were performed at the Molecular Genomics Core at Genotypic Technology (Bangalore). Briefly, total RNA was end-labeled using Agilent Quick-Amp labeling Kit (p/n5190-0442) and hybridized to Agilent Human Gene Expression Microarray 8X60K. Fragmentation of labeled cRNA and hybridization were done using the Gene Expression Hybridization kit (Agilent Technologies, *In situ* Hybridization Kit, # 5190-0404). The hybridized slides were scanned using the Agilent Microarray Scanner (Agilent Technologies, Part Number G2600D). Data analysis was done by using GeneSpring GX software version 14.5. Gene expression in the test group (TGF-β) was compared with the control group (C) to identify differentially expressed genes (DEGs) upon TGF-β treatment. DEGs were selected based on log base 2 (fold ≥ 0.6) and log base 2 (fold ≤-0.6) with a statistical significance of p-value < 0.05.

2.3 Bioinformatic Analysis

LncRNA-MUF expression values and associated prognostic information from 693 glioma cases were obtained from the Chinese Glioma Genome Atlas (http://www.cgga.org.cn). These 693 samples comprised 505 WHO III and IV tumors and 188 WHO II tumors. The Kaplan–Meier estimation method was used for the overall survival analysis of patients based on lncRNA expression. miRNA targets of lncRNA-MUF were predicted by the RNAInter database (http://rnainter.org/). The interaction between lncRNA-MUF and miR-34a was confirmed by RNAhybrid (https://bibiserv.cebitec.uni-bielefeld.de/rnahybrid?id=rnahybrid_view_submission) and IntaRNA (https://www.rna-society.org/rnainter/IntaRNA.html). mRNA targets of miR-34a were identified using the miR-DB (http://mirdb.org/) and TargetScan (http://www.targetscan.org/vert_72/) databases. Kaplan–Meier survival analysis of miR-34a was performed by using data from the CGGA database.

2.4 siRNA Transfection

Transfections of siRNAs were performed using Lipofectamine® RNAiMAX Transfection Reagent (Life Technologies-Invitrogen, Cat. No.: 13778-075) and Opti-MEM (Invitrogen, 31985062) as per manufacturer's instructions. Glioma cells were transfected with 40 nM of siRNAs (Silencer Pre-Designed siRNA, Ambion, Thermo Fisher Scientific) targeting lncRNA-MUF. The siRNA duplexes used in this study are as follows: si-MUF-1 sense 5′ GCCUUCAACAUUCAGCACATT 3′, antisense 5′ UGUGCUG AAUGUUCAAGGCTG 3′; si-MUF-2 sense 5′ CCUCCAUAUU CAUGAACUATT 3′, antisense 5′ UAGUUCAUGAAUAU GGAGGCT 3′. Non-specific siRNA that does not target any known mammalian gene was purchased from Dharmacon ON-TARGETplus non-targeting control pool (Cat. No.: D-001810-10-20). To overexpress or inhibit miR-34a, we transfected glioma cells with mimics of human miR-34a (80 nM) (miRCURY LNA miRNA mimic, Qiagen, Cat. No.: 339173) and with inhibitors of miR-34a (80 nM) (miRCURY LNA miRNA inhibitor, Qiagen,

Cat. No.: 339121) using Lipofectamine according to the manufacturer's instructions.

2.5 RNA Isolation and Real-Time PCR

Total RNA was extracted from glioma cells using the MN NucleoSpin RNA plus isolation kit (Cat. No.: 740984.5). 1 μg of RNA was converted into cDNA using the PrimeScript first-strand cDNA kit from Takara (#6110A). Quantitative real-time PCR (qRT-PCR) was performed with the SYBR Green PCR Kit (#RR820A, Takara) in the Bio-Rad CFX96 real-time qPCR system. All reactions were performed in triplicates and normalized with TBP/HPRT as an internal control. The relative gene expression of each sample was calculated using the 2^{-ddct} formula. For miRNA expression analysis, RNA was isolated using Zymo Quick-RNA™ Miniprep Plus Kit (#R1057). miRNA cDNA was synthesized using the mir-X miRNA 1st-Strand Synthesis Kit (#638313, Takara). qRT-PCR of miRNA was carried out using the universal primer and the primer specific to miR-34a-5p (**Supplementary Table 1**). U6 was used as a normalizing control. The gene specific primer sequences are shown in **Supplementary Table 1**.

2.6 Nuclear and Cytoplasmic Extract Preparations

Cytoplasmic and nuclear fractions were separated, and RNA was purified as described previously (27). qRT-PCR was performed to identify relative RNA levels in each fraction by using GAPDH as a control for cytoplasmic fraction, and MALAT1 as a control for nuclear fraction.

2.7 Western Blot Analysis

Whole-cell lysates were isolated from T98G and U87-MG glioma cells with lysis buffer containing Triton X (1%), NaCl (150 mM), Tris base (10 mM), EDTA (1 mM), EGTA (0.2 mM), IGEPAL (0.5%), protease inhibitor (3 μl/ml), and phosphatase inhibitors $NaOVa_3$ (0.2 M) and NaF (0.5 M) 48 h after transfection. Cell lysates were incubated on ice for 20–30 min, with intermittent vortexing, and centrifuged at 14,000 rpm at 4°C for 20 min. The supernatant was collected in fresh prechilled tubes, and total protein was estimated using the BCA method, and extracts were frozen at −80°C until use. Western blotting was performed as described previously (28). Briefly, equal amounts of each sample protein were separated by sodium dodecyl sulfate polyacrylamide gel electrophoresis and transferred to a PVDF membrane, followed by blocking with 5% bovine serum albumin (A7906, Sigma) for 1.5 h. After that, the membrane was incubated with respective antibodies overnight at 4°C. The following primary antibodies (1: 2,500) were used: p-SMAD2/3 (CST #8828), total SMAD (CST #8685), Vimentin (CST #5741), N-cadherin (CST #13116), and Snail1 (CST #3895). Secondary antibodies (1:20,000)—HRP conjugated anti-rabbit (Vector Laboratories Cat. No.: P.I. 2000-1) or anti-mouse IgG (Invitrogen, Cat. No.: A16072)—were incubated for 2 h at room temperature. Immune blot bands were visualized with an ECL solution [Amersham ECL Prime Western Blotting Detection Reagent, GE Healthcare (Cat. No.: RPN2232)] and detected using VILBER Fusion Pulse ChemiDoc. Images were captured using Evolution Capture software. The blots were stripped and reprobed with β-actin antibody (1:100,000; Sigma #A1978) to determine equivalent loading as described previously (28). For stripping, blots were incubated at 50°C in stripping buffer containing 10% SDS, 0.5 M Tris–HCl, and 100 mM β-mercaptoethanol for 30 min, followed by PBST washes (5 times), blocking, and incubation with the primary antibody as described previously (29). The blot signals were quantified using ImageJ software for Microsoft Windows (National Institutes of Health, Bethesda, MD).

2.8 Chromatin Immunoprecipitation (ChIP)

Control or TGF-β-treated cells were fixed with 1% formaldehyde for 8 min at room temperature followed by quenching with a final concentration of 0.125 M glycine for 5 min. Cells were washed twice with ice-cold phosphate-buffered saline, harvested by scraping, pelleted, and resuspended in 250 μl of ChIP lysis buffer (50 mM Tris–HCl [pH 8.1], 0.9% SDS, 10 mM EDTA, protease inhibitor), and samples were incubated on ice for 1 h. Samples were sonicated using Bioruptor Plus (Diagenode) with sonication conditions: 30 s on, 30 s off for 20 cycles. After sonication, samples were centrifuged at 14,000 rpm at 4°C for 20 min. Supernatants were diluted 5-fold in ChIP dilution buffer (167 mM NaCl, 16.7 mM Tris–HCl pH 8.1, 1.2 mM EDTA, 1.1% Triton X-100, protease inhibitors), and 5% of the sample was taken as input. Samples were then incubated at 4°C overnight with Smad2/3 (1:200) (CST #8685S) or anti-rabbit IgG (CST #2729S) antibody. The following day, Dynabeads and protein G (Invitrogen #10004D) 50 μl per sample were added to the I.P. tubes and incubated for 2 h at 4°C. The beads were then washed once each with low-salt buffer (0.1% SDS, 1% Triton X-100, 2 mM EDTA, 20 mM Tris–HCl pH 8.1, 150 mM NaCl), high-salt buffer (0.1% SDS, 1% Triton X-100, 2 mM EDTA, 20 mM Tris HCl pH 8.1, 500 mM NaCl), LiCl buffer (0.25 M LiCl, 1% NP-40, 1% deoxycholate, 1 mM EDTA, 10 mM Tris–HCl pH 8.1), and TE buffer (pH 8.0). Following this, samples were reverse cross-linked by using decrosslinking buffer (222 mM NaCl, 50 mM Tris, 10 mM EDTA, 0.025% SDS), containing 5 μl proteinase K (NEB #P8107S, 800 U/ml) per sample with overnight incubation at 65°C. Genomic DNA was then extracted with a DNA purification kit (Zymo Kit Cat. No.: D3020), and lncRNA-MUF in immunoprecipitated samples was measured using qRT-PCR. The following primers specific to the lncRNA-MUF promoter were used for qRT-PCR analysis: forward primer, 5′ CTCAGTGCCTTCATGGTGGA 3′ reverse primer: 5′ GAGGG GCTTACAGATGTGGC 3′.

2.9 Cell Proliferation Assay

Colorimetric cell proliferation assay was performed by using the WST-1 reagent (Cat#. 05015944001, Roche) at the indicated time according to the manufacturer's instructions. Briefly, cells were seeded at a concentration of 2,500–5,000 cells/well in 96-well plates and transfected with siRNAs si-MUF-1, si-MUF-2, and si-NS at 40 nM, and cell proliferation was quantified at OD of 450 nm.

2.10 Colony Formation Assay

For clonogenic assays, cells were seeded into 96-well dishes and treated with si-NS or siRNAs against lncRNA-MUF. 24 h post-transfection, cells were trypsinized and seeded at a density of 200 cells per well in a 6-well dish and incubated at 37°C. Media were changed every 3 days. Colonies formed 14 days after plating were fixed with 4% paraformaldehyde and stained with crystal violet solution, and counted.

2.11 Caspase 3/7 Assay

Luminometric assay kit for caspase-3/7 (Promega, G8090) was used to determine the enzymatic activity of caspase-3/7 in glioma cells transfected with si-MUF-1 and 2. 48 h post-transfection, proluciferin DEVD substrate and caspase-Glo 3/7 buffer were added to the cells, and the assay was performed as per the manufacturer's instructions.

2.12 Invasion Assay

Glioma cells were transfected with control siRNA (si-NS) or si-MUF-1/si-MUF 2. After 24 h of transfection, cells were seeded into the upper chamber of transwell inserts (Corning, #3422) precoated with Matrigel (Corning, 356234) in serum-free media. Lower chambers had media containing 20% FBS. After 48 h, cells remaining on the upper surface of the membrane were gently removed with a cotton swab. Invaded cells were fixed with 4% PFA and stained with crystal violet solution (Sigma, V5265). Stained cells were visualized under Magnus INVI microscopy (×100), and invaded cells were counted at four different fields for each condition (23).

2.13 Migration Assays

For migration assay, si-MUF-1/si-MUF-2 or negative control siRNA-transfected glioma cells were seeded in a 12-well dish and cultured overnight. Scratch was made using a 20-µl pipette tip followed by PBS wash. Cells were maintained in 0.5% serum-containing media. Images of scratch were taken at 0, 24, and 48 h, and the migrating length was calculated using ImageJ (30).

2.14 Dual-Luciferase Reporter Assay

Dual-luciferase reporter assays were done to confirm the interaction between miR-34a-5p and lncRNA-MUF. The lncRNA-MUF region with miR-34a-5p sites was cloned into the pmirGLO vector (Promega) using NheI and SalI restriction sites. Cells were co-transfected with pmirGLO-lncRNA-MUF reporter plasmid and miR-34a-5p/N.C. mimics using Polyplus jetPRIME transfection reagent. 30 h post-transfection, the cells were lysed and subjected to luciferase assays using the Dual-Luciferase® Reporter Assay System (Promega, Cat. No.: E1910) according to the manufacturer's instructions on the SpectraMax iD3 Luminometer (Molecular Devices Corporation). Data were normalized to Renilla luciferase activity (23, 26).

For lncRNA-MUF promoter analysis, we cloned the -734-bp promoter region of lncRNA-MUF with predicted putative SBEs into the restriction sites of SacI and NheI of pGL3basic luciferase and renilla_polyA construct (a gift from Oskar Laur) (Addgene plasmid # 128046; http://n2t.net/addgene:128046; RRID: Addgene_128046). T98G and U87-MG cells were seeded at ~60%–70% confluency in 24-well plates. The next day, they were transiently transfected with 0.3 µg of lncRNA-MUF promoter containing pGL3basic luciferase and renilla_polyA reporter plasmid using jet prime transfection reagent. Eighteen hours post-transfection, cells were serum-starved for 6 h followed by treatment with 10 ng/ml TGF-β1 for the indicated time. Luciferase activity was measured using the Dual-Luciferase® Reporter Assay System according to the manufacturer's protocol (Promega) on the SpectraMax iD3 Luminometer (Molecular Devices Corporation). The results are expressed as a fold change in luciferase activity over control (28).

2.15 Statistical Analysis

Results are presented as mean ± SEM unless otherwise stated. We used paired Student's t-test for comparisons between two experimental groups. Additional statistical tests information is described in the figure legends. $p < 0.05$ was considered statistically significant.

3 RESULTS

3.1 Identification of TGF-β-Regulated LncRNAs in GBM Cells Using Microarray Screen

We sought to identify, in an unbiased fashion and at a genome-wide scale, differentially expressed lncRNAs upon TGF-β treatment in glioma cells. We performed gene expression analysis of control, and TGF-β1-treated T98G glioma cells using the Agilent SurePrint G3 Gene Expression Microarrays for Human (v3) for lncRNAs. Using a 1.5-fold change and p-value < 0.05 as a threshold, we identified 91 differentially expressed lncRNAs and 397 differentially expressed mRNAs in our screen (**Figures 1A, B** and **Supplementary Table 2**). LncRNAs constitute 18.3% of transcripts among the total number of DEGs identified upon TGF-β1 treatment in T98G cells (**Figure 1B**). We verified the TGF-β1-induced gene expression changes in levels of lncRNAs in T98G cells using qRT-PCR (**Figure 1C**). LncRNAs ENST00000409910 and LOC79160 get ~4-fold upregulated upon TGF-β treatment (**Figure 1C**). LncRNAs LINC00312, LOC101928710, lncRNA-MUF, and lnc-EGR2-1 get ~1.5–3-fold upregulated upon TGF-β treatment (**Figure 1C**). LncRNAs CTB-178M22.2 and KCNMA1-AS1 are significantly downregulated upon TGF-β treatment (**Figure 1C**). The expression of several TGF-β-regulated mRNAs identified from the microarray screen was also verified using qRT-PCR (**Figure S1A**). Among these upregulated lncRNAs, we further set out to characterize the role of lncRNA-MUF in glioma pathogenesis.

3.2 LncRNA-MUF Is Upregulated in GBM Tumor Samples and Is Associated With Poor Patient Prognosis

To investigate the role of lncRNA-MUF in GBM pathophysiology, we decided to evaluate its expression in GBM tumor samples using the CGGA database (http://www.cgga.org.cn/). Using the

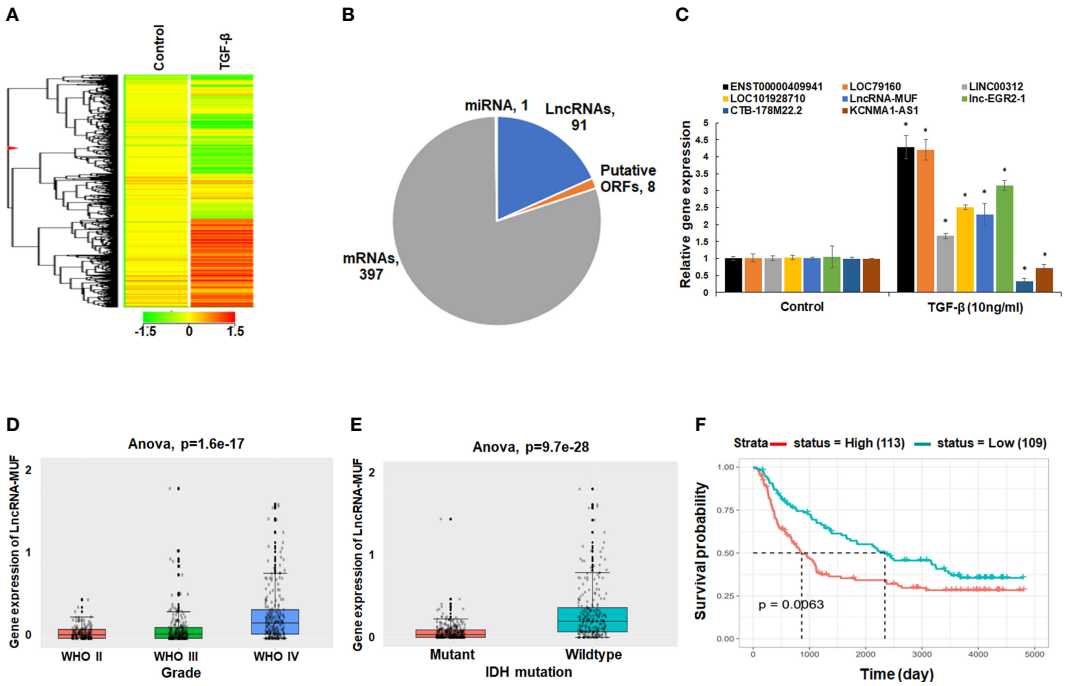

FIGURE 1 | LncRNA-MUF is overexpressed in GBM, and it is induced by TGF-β. **(A)** Heatmap representing the relative abundance of differentially expressed genes (DEGs, ≥1.5-fold, $p < 0.05$) in T98G cells upon TGF-β1 (10 ng/ml) treatment for 24 h. **(B)** Pie chart representing the class of DEGs ($p < 0.05$) identified from genome-wide microarray screening in T98G GBM cells upon TGF-β1 treatment for 24 h. **(C)** Validation of top TGF-β-regulated lncRNAs identified from microarray screening using qRT-PCR in T98G cells. RNA samples were analyzed by qRT-PCR, and error bars represent the mean ± SEM from three independent experiments. *Significant change in TGF-β-treated cells compared to control cells ($p < 0.05$). **(D)** LncRNA-MUF expression analysis in glioma tissues from the CGGA database. Elevated expression of MUF in GBM IV compared to lower-grade gliomas ($p=1.6e^{-17}$). **(E)** LncRNA-MUF levels are elevated in IDH wild-type GBM patients compared to IDH mutant cases as analyzed from the CGGA database (ANOVA, $p = 9.7e^{-28}$). **(F)** Kaplan–Meier survival analysis of lncRNA-MUF expression in glioma samples from CGGA databases shows that a high lncRNA-MUF expression is associated with poor overall survival in primary and recurrent GBM patients ($p = 0.0063$). Red line represents high lncRNA-MUF expression group, and green line represents the low lncRNA-MUF expression group.

mRNAseq_693 dataset of the CGGA database, we found that levels of lncRNA-MUF were significantly higher in GBM samples than normal brain tissues ($p = 6.3e^{-15}$) (**Figure S1B**). Moreover, lncRNA-MUF levels are significantly higher in grade IV GBM than in lower-grade gliomas ($p = 1.6e^{-17}$) (**Figure 1D**). GBM patients with IDH mutation show a better survival rate than the IDH wild-type group (1). Hence, we evaluated the expression of lncRNA-MUF in IDH mutant and wild-type glioma samples. We observed that the expression of lncRNA-MUF is significantly higher in gliomas with the IDH wild-type group than in the IDH mutant group ($p = 9.7e^{-28}$) (**Figure 1E**). In addition, high expression of lncRNA-MUF is correlated with poor overall survival in both primary and recurrent GBM patients ($p = 0.0063$) (**Figure 1F**). These results suggest that lncRNA-MUF expression is associated with aggressive phenotype and poor survival in glioma patients.

3.3 LncRNA-MUF Is Induced by TGF-β Through the Canonical SMAD2/3 Signaling Pathway in Glioma Cell Lines

LncRNA-MUF induction upon TGF-β1 treatment was dose-independent for TGF-β doses from 5 to 80 ng/ml for 24 h in T98G cells (**Figure S2A**). The time-course analysis-identified lncRNA-MUF gets induced upon TGF-β1 treatment as early as 1 h. However, a statistically significant increase of ~2-fold occurs only at 12 and 18 h of TGF-β treatment and then sustained at ~1.8-fold at 24, 36, and 48 h (**Figure 2A**). To assess the impact of TGF-β1 on the lncRNA-MUF expression on additional glioblastoma cell lines, we evaluated the lncRNA-MUF expression in LN18, LN229, U87-MG glioma cells. Upon TGF-β1 stimulation for 24 h, the expression of lncRNA-MUF was upregulated (≥2-fold) in glioma cell lines (T98G: 1.89-fold; U87-MG: 1.8-fold; LN229: 2.8-fold; LN18: 2.1-fold). These results indicate that lncRNA-MUF induction upon TGF-β1 treatment is not cell line-specific (**Figure 2B**). We then investigated the subcellular localization of lncRNA-MUF by measuring the lncRNA levels in nuclear and cytoplasmic fractions in T98G and U87-MG GBM cells. LncRNA-MUF showed 75% expression in the cytoplasm and 25% in the nucleus in T98G and U87-MG cell lines, respectively (**Figure S2B**).

TGF-β signal transduction occurs either through the canonical smad2/3 signaling pathway or through non-canonical pathways (4). To identify the transcription factors working downstream of the TGF-β pathway to regulate lncRNA-

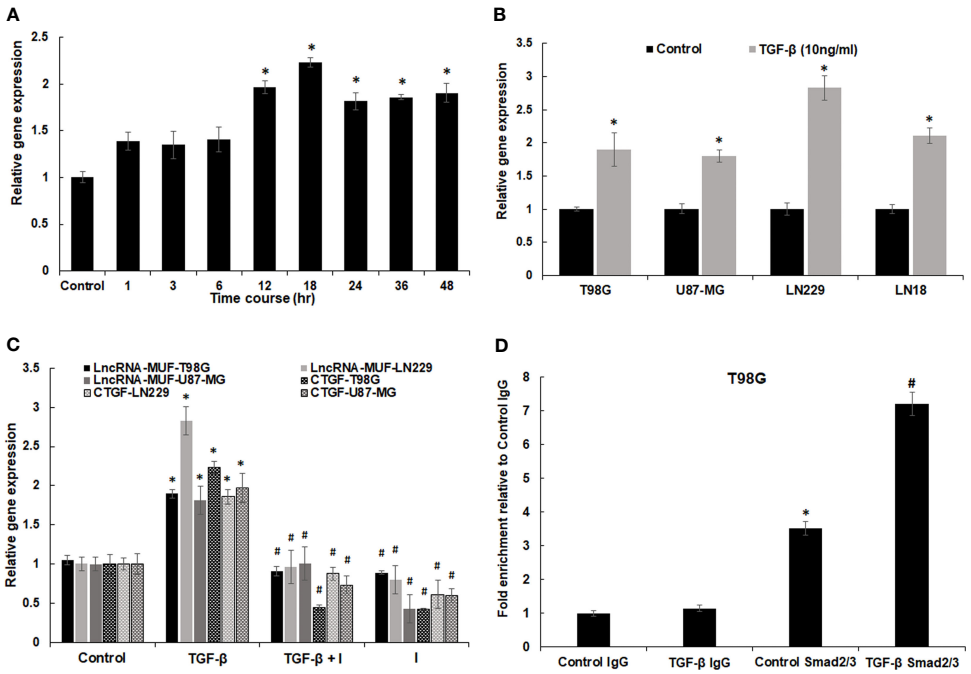

FIGURE 2 | Regulation of lncRNA-MUF expression through Smad2/3 signaling. **(A)** LncRNA-MUF is a delayed transcript with induction of ~2-fold at 12 and 18 h of TGF-β1 treatment (10 ng/ml), then reaching a plateau of ~1.8-fold at 24, 36, and 48 h. RNA levels were measured at the indicated time points using qRT-PCR. **(B)** LncRNA-MUF induction upon TGF-β treatment is not cell type-specific. The indicated GBM cell lines were treated with 10 ng/ml TGF-β for 24 h and lncRNA-MUF levels measured by qRT-PCR. **(C)** LncRNA-MUF induction upon TGF-β treatment is smad2/3 dependent. Human glioma cells (T98G, LN229, and U87-MG) were pretreated with 6 μM of SB505124 (TGFβR1/Smad2/3 inhibitor) for 2 h followed by co-treatment with TGF-β1 (10 ng/ml) for 24 h, and lncRNA-MUF transcript levels were determined by qRT-PCR. **(D)** ChIP-qPCR analysis of smad2/3 interaction with SBE in the lncRNA-MUF promoter in control and TGF-β-treated T98G cells. DNA was isolated from control and TGF-β-treated cells after immunoprecipitation with the anti-smad2/3 antibody and was amplified using specific primer sets. LncRNA-MUF promoter levels in immunoprecipitated samples were measured by qRT-PCR analysis, normalized to input, and represented as "fold enrichment relative to control IgG I.P." Values represent mean ± S.D. from two independent experiments. *Significant change compared to IgG ($p < 0.05$). #Significant change compared to control Smad2/3 ($p < 0.05$). Data information: RNA samples were analyzed by quantitative RT-PCR, normalized with TBP/HPRT. Error bars represent the mean ± SEM from 3 independent experiments. *Significant change compared to respective control samples ($p < 0.05$). #Significant decrease from TGF-β-treated cells ($p < 0.05$). Statistical comparisons were made using Student's t-test.

MUF expression, we looked at the lncRNA-MUF promoter using JASPAR (http://jaspar.genereg.net/) and found functional smad-binding elements (SBE) (5′ CAGAC 3′/5′ GTCTG 3′) at the -498, -1,321, -1,850, -2,413, and -2,942 positions. Hence, we evaluated lncRNA-MUF expression upon TGF-β treatment in the presence and absence of TGF-β inhibitor SB505124. To this end, GBM cells were treated with 6 μm SB505124 (TGFβR1/smad2/3 inhibitor) for 2 h before treatment with TGF-β1 (24 h). Blocking smad2/3 with SB505124 significantly abrogated TGF-β-induced lncRNA-MUF expression in glioma cells (~50% reduction in T98G, LN229, and U87-MG) (**Figure 2C**). As TGF-β-induced lncRNA-MUF expression and TGF-βRI inhibitor significantly abrogated lncRNA-MUF levels, we used luciferase reporter assay to confirm if lncRNA-MUF promoter can drive TGF-β-mediated luciferase activity. Transfection of T98G and U87-MG cells with the lncRNA-MUF-promoter-luciferase reporter construct followed by TGF-β treatment for 24 h resulted in a significant ~2.5- and 2-fold increase in luciferase activity over control, respectively (**Figure S2C**). Next, we performed ChIP-qPCR to determine whether TGF-β promotes increased binding of smad2/3 to SBE on the lncRNA-MUF promoter. ChIP-qPCR revealed increased binding of smad2/3 on SBE on the lncRNA-MUF promoter upon TGF-β stimulation (**Figure 2D**). These results suggest that TGF-β upregulates lncRNA-MUF expression through the canonical SMAD signaling pathway.

3.4 Knockdown of LncRNA-MUF Reduces Cell Proliferation, Induces Apoptosis, and Sensitizes Glioma Cells to TMZ-Mediated Apoptosis

To investigate the physiological function of lncRNA-MUF in glioma pathogenesis, we established lncRNA-MUF knockdown by siRNA using two different siRNAs (si-MUF-1 and si-MUF-2) in T98G and U87-MG cell lines. The knockdown of lncRNA-MUF with si-MUF-1 results in ~85% reduction, and si-MUF-2 results in ~67% reduction of lncRNA-MUF levels in T98G and U87-MG cells (**Figure S3**). LncRNA-MUF depletion using siRNAs results in a time-dependent reduction in cell

proliferation in glioma cells. Cell proliferation was reduced by ~40% and ~55% at 48 and 72 h post-lncRNA-MUF knockdown, respectively, in T98G cells (**Figure 3A**). A similar ~40%–50% reduction in cell proliferation was observed in LN229 and U87-MG glioma cells transfected with siRNA against lncRNA-MUF compared to cells transfected with non-specific siRNA (si-NS) (**Figure 3A**). Consistent with the reduction in cell proliferation upon lncRNA-MUF depletion, MUF knockdown resulted in a significant decrease in colony formation of ~62% and 70%, respectively, in T98G and U87-MG cells compared to respective control cells transfected with si-NS (**Figure 3B** and **Figure S4C**). Moreover, depletion of lncRNA-MUF by siRNA also results in apoptosis as demonstrated by an increase of ~1.75-fold, 3.6-fold, and 3.4-fold caspase 3/7 activity in T98G, U87-MG, and LN229, respectively, as compared to control cells (**Figure 3C**). Consistently, the levels of caspase 9 mRNA were ~2-fold increased following lncRNA-MUF knockdown in T98G and U87-MG cells (**Figure S4A**). TMZ is an oral alkylating drug that is used to treat GBM; however, 50% of GBM cases develop resistance to TMZ. Several GBM cell lines such as T98G and

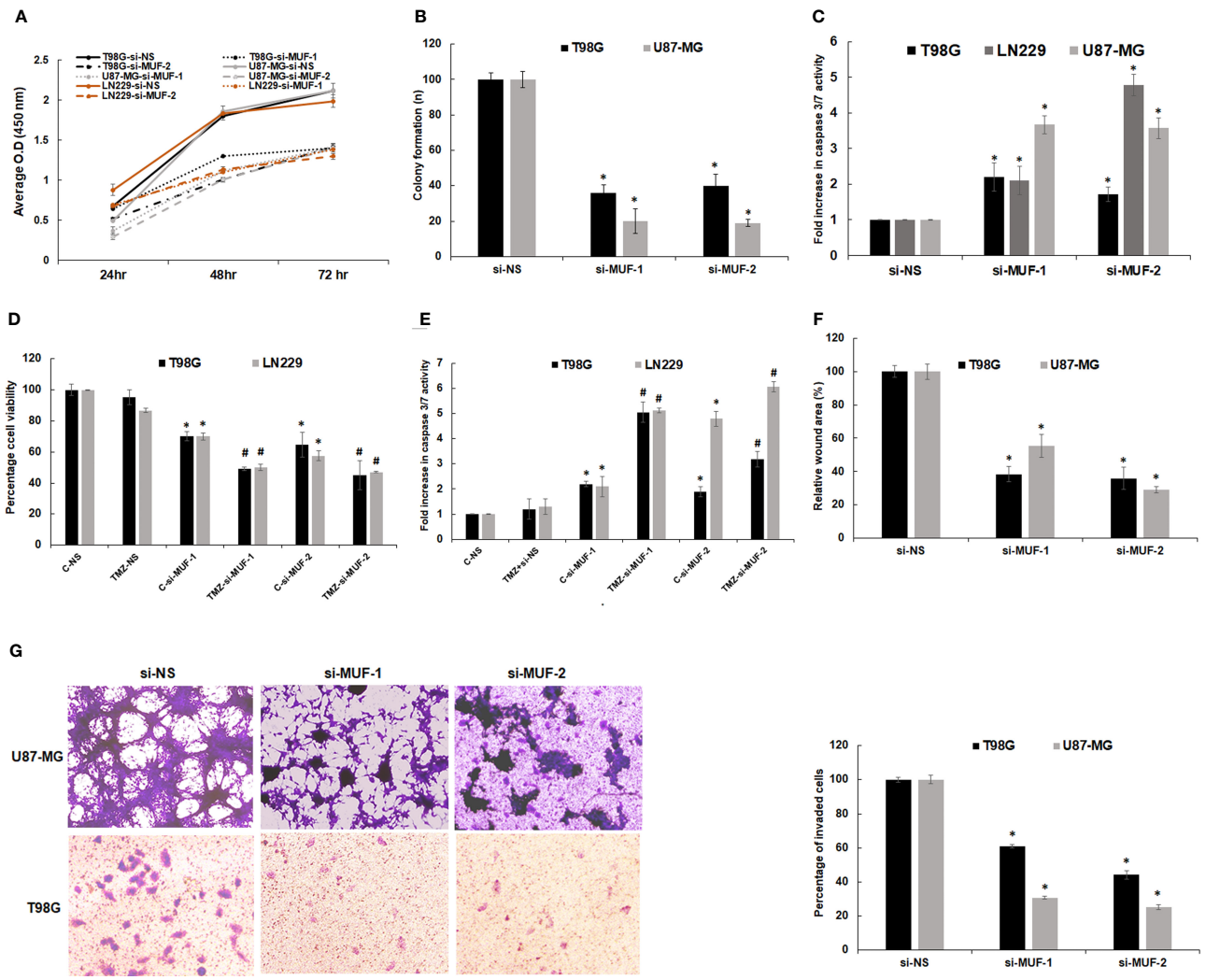

FIGURE 3 | Effect of lncRNA-MUF knockdown on glioma cell proliferation, migration, and invasion *in vitro*. **(A)** Human glioma cells were transfected with si-NS or si-MUF-1/si-MUF-2 (40 nM), and percentage cell viability was calculated at indicated times using WST1. Values represent mean ± S.D. from four independent experiments. *Significant change compared to si-NS cells at the corresponding time ($p < 0.05$). Statistical comparisons were made using Student's t-test. **(B)** Reduced colony formation ability of GBM cells with lncRNA-MUF knockdown. **(C)** Caspase 3/7 activity assay shows that lncRNA-MUF knockdown induces apoptosis in GBM cells. **(D)** LncRNA-MUF knockdown with a low dose of si-MUF1/si-MUF-2 (20 nM) in combination with TMZ treatment (600 μM) shows enhanced reduction of glioma cell (T98G and LN229) proliferation and increased sensitivity to TMZ, as analyzed using WST1 assay. **(E)** LncRNA-MUF knockdown (20 nM of si-MUF-1/si-MUF-2) combined with TMZ treatment (600 μM) show enhanced caspase 3/7 activity as compared to TMZ alone. **(F)** Wound healing assay demonstrates reduced GBM cell migration upon lncRNA-MUF knockdown. **(G)** Matrigel invasion assay shows that lncRNA MUF inhibition reduces glioma cell invasion. Values represent mean ± S.D. from four independent experiments. *Significant change compared to si-NS cells at the corresponding time ($p < 0.05$). Statistical comparisons were made using Student's t-test. # Significant decrease from C-si-MUF-1 and C-si-MUF-2 trabsfected cells ($p < 0.05$).

LN229 show resistance to TMZ, and TGF-β-induced lncRNAs are known to promote TMZ resistance (9, 31). Therefore, we evaluated the effect of lncRNA-MUF knockdown on TMZ sensitivity in T98G and LN229 cells. LncRNA-MUF depletion with low siRNA levels (20 nM) resulted in significantly reduced cell proliferation in TMZ-treated T98G and LN229 cells compared to si-NS-transfected cells treated with TMZ (**Figure 3D**). In addition, TMZ treatment in lncRNA-MUF knockdown resulted in a significantly higher increase in caspase 3/7 activity (~5-fold) compared to si-NS-transfected T98G and LN229 cells treated with TMZ (**Figure 3E**). These results suggest that lncRNA-MUF knockdown sensitizes glioma cells to TMZ-induced apoptosis. We then investigated the effect of lncRNA-MUF knockdown on glioma cell migration and invasion. Wound healing assay revealed that lncRNA-MUF-depleted T98G and U87-MG cells show ~63% and ~58% reduction in cell migration, respectively, compared to control cells (**Figures 3F** and **S4B**). Matrigel invasion assay during lncRNA-MUF depletion results in ~55% and ~70% inhibition of cell invasion in T98G and U87-MG cells, respectively, compared to control cells (**Figure 3G**). Thus, collectively these results suggest that lncRNA-MUF serves as an oncogene to promote proliferation, drug resistance, migration, and invasion in GBM cells, and targeting lncRNA-MUF is an attractive therapeutic strategy for GBM.

3.5 LncRNA-MUF Regulates Gene Expression of a Subset of TGF-β Target Genes in cis and trans

LncRNA transcripts often regulate gene expression in cis and trans (10). We first evaluated the effect of lncRNA-MUF knockdown on its cis genes (**Figure 4A**). We observed ~50% downregulation of the Caprin2 gene in T98G and U87-MG upon lncRNA-MUF knockdown with both the siRNAs (**Figure 4A**). This is consistent with Ai et al., who reported the cis-regulation of the Caprin2 gene by lncRNA-MUF through chromosome

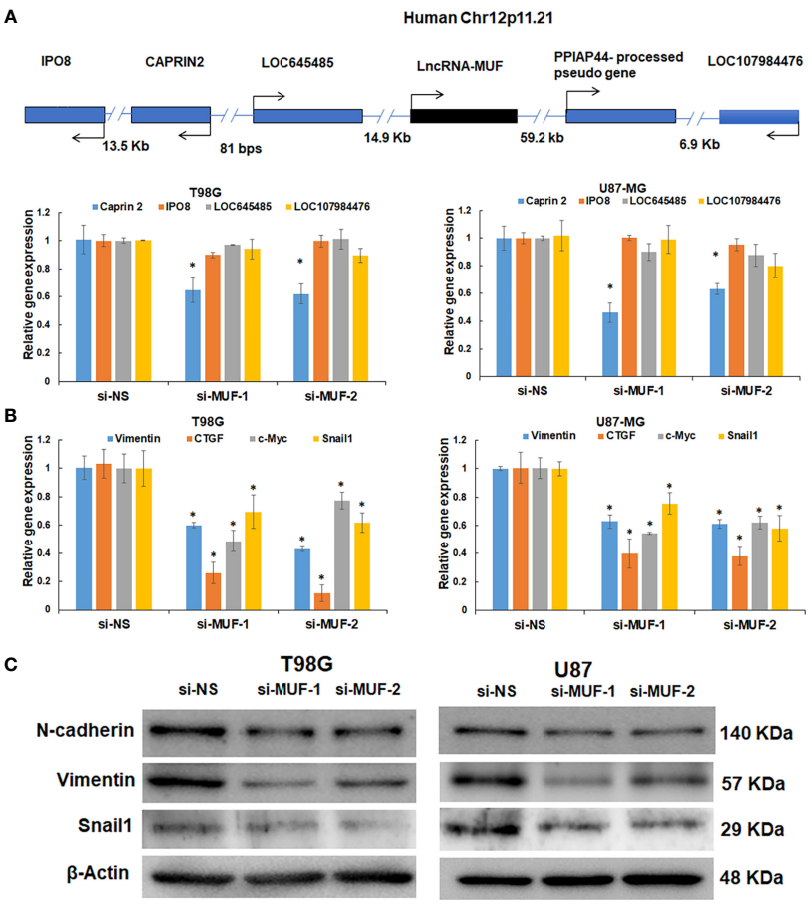

FIGURE 4 | LncRNA-MUF modulates gene expression in cis and trans and promotes EMT in glioma. **(A)** Validation of cis gene expression of lncRNA-MUF with lncRNA knockdown. LncRNA knockdown represses cis gene expression (Caprin2). **(B)** LncRNA-MUF modulates TGF-β target gene expression in trans in GBM. T98G and U87-MG glioma cells transfected with si-NS, si-MUF-1, or si-MUF-2 (25 nM), and transcript levels of indicated genes were measured 48 h post-transfection. RNA samples were analyzed by quantitative RT-PCR, and error bars represent the mean ± SEM from three independent experiments. **(C)** LncRNA-MUF promotes GBM EMT. Western blot analysis of EMT markers Vimentin, N-cadherin, and Snail1 followed by lncRNA-MUF knockdown in T98G and U87-MG cells. *Significant change compared to cells transfected with si-NS ($p < 0.05$). Values represent mean ± SD from three independent experiments.

looping in OSCC (32). However, the levels of other cis genes (IPO8, LOC645485, LOC107984476) remained unchanged upon lncRNA-MUF knockdown (**Figure 4A**). We also observed that the Caprin2 gene is upregulated by TGF-β in T98G GBM cells (1.7-fold) using qPCR assays (**Figure S5A**). These results suggest that lncRNA-MUF regulates TGF-β-induced expression of the Caprin2 gene in *cis* in glioma cells. Since lncRNA-MUF regulates genes involved in the WNT/β-catenin pathway (26, 32), we evaluated the impact of lncRNA-MUF knockdown on the WNT/β-catenin pathway genes in glioma cells. Surprisingly, we did not observe any significant change in their expression upon MUF depletion in glioma cells (**Figure S5B**). To further identify the genes regulated in *trans* by lncRNA-MUF in glioma cells, we evaluated the expression of the TGF-β gene ontology group upon its siRNA-mediated knockdown. Depleting MUF resulted in ~50% downregulation of Snail1, ~40% downregulation of vimentin, ~60% downregulation of CTGF, and ~30% downregulation of c-Myc in T98G cells and U87-MG cells (**Figure 4B**). Several other TGF-β-regulated genes did not show any change in expression with MUF knockdown (**Figure S5C**). Since lncRNA-MUF depletion inhibits invasion and Snail1 regulates EMT and invasion, we evaluated EMT marker expression upon lncRNA-MUF inhibition by Western blotting. In agreement with q-PCR data, knockdown of lncRNA-MUF resulted in ~40% decrease in N-cadherin, ~80% decrease in vimentin, and ~70% decrease in Snail1 protein levels in T98G and U87-MG cells (**Figures 4C** and **S5D**). These results indicate that lncRNA-MUF selectively regulates the expression of Snail1, vimentin, N-cadherin, CTGF, and c-Myc in GBM.

3.6 Knockdown of LncRNA-MUF Attenuates TGF-β Signaling

TGF-β-induced lncRNAs are known to regulate the TGF-β signaling pathway *via* an autocrine signaling loop (33). Hence, we asked if lncRNA-MUF is also involved in regulating TGF-β signaling. To test this, we evaluated the impact of lncRNA-MUF knockdown on TGF-β-induced phosphorylation of smad2/3. Silencing lncRNA-MUF in T98G results in a ~35% decrease in smad2/3 phosphorylation at 15 min and 30 min post-TGF-β treatment compared to si-NS cells treated with TGF-β. A similar reduction of ~30% is observed in p-smad2/3 levels upon TGF-β treatment in U87-MG cells compared to TGF-β1-treated si-NS cells (**Figures 5A** and **S6**). This is consistent with the fact that pathway analysis by the lncACTdb database suggests that the TGF-β signaling pathway is among the top 10 enriched signaling pathways regulated by lncRNA-MUF (**Figure 5B**). Our results indicate that lncRNA-MUF regulates smad2/3 phosphorylation downstream of the TGF-β pathway in glioma cells.

3.7 LncRNA-MUF Modulates TGF-β-Induced Invasion in Glioma *via* the miR-34a-5p/Snail1 Axis

LncRNAs function as endogenous miRNA sponges and participate in the ceRNA regulatory network (34, 35). Yan et al. have reported the direct binding of lncRNA-MUF and miR-34a using RNA immunoprecipitation (RIP) and RNA pull-down assays (26). In addition, they show that lncRNA-MUF regulates Snail1 expression by sponging miR-34a to modulate EMT in HCC cells (26). Using RNAhybrid and IntaRNA databases, we identified putative miR-34a-binding sites in lncRNA-MUF (**Figure S7A**). To identify the interaction between lncRNA-MUF and miR-34a-5p, we cloned the region of lncRNA-MUF with the miR-34a-binding sites into the pmirGLO vector downstream of the firefly luciferase gene. Co-transfection with the pmirGLO-lncRNA-MUF reporter plasmid and miR-34a mimics reduced the reporter activity significantly (~70%) compared to the control cells (**Figure 6D**).

Since miR-34a has a well-established tumor-suppressor role in several cancers, including GBM (36), we first evaluated its expression in glioblastoma tissue using the CGGA dataset. Expression of miR-34a is lowest in grade IV GBM ($p = 0.0038$) (**Figure 6A**). In addition, the Kaplan–Meier survival curve demonstrates that high expression of miR-34a positively correlates with better survival of glioma patients ($p = 0.016$) (**Figure 6B**). To understand the impact of miR-34a on lncRNA-MUF regulation, we first determined its levels upon miR-34a overexpression using miRNA mimics. We observed a significant ~40%–50% reduction in lncRNA-MUF expression in T98G and U87-MG cells upon treatment with miR-34a mimic (**Figure 6C**). Snail1 is a well-known target of miR-34a; consistent with this, we observed that transfection of miR-34a mimics in T98G and U87-MG glioma cells significantly reduced Snail1 protein levels and knockdown of miR-34a using miRNA inhibitors reversed this effect (**Figure 6E** and **Figure S7B**). Given that miR-34a targets lncRNA-MUF and Snail1 expression and because we observed downregulation of Snail1 upon lncRNA-MUF depletion, we explored if lncRNA-MUF could act as a ceRNA to sponge miR-34a for stabilizing Snail1 to regulate invasion in glioma cells. Invasion analysis revealed that reduction in invasion upon lncRNA-MUF knockdown is significantly reversed upon co-transfection with the miR-34a inhibitor (**Figures 6G, H**). Moreover, in accordance with the role of miR-34a in the regulation of invasion by Snail1, we observed that the miR-34a inhibitor significantly restores Snail1 downregulation caused by lncRNA-MUF depletion (**Figure 6F** and **Figure S7C**). These experiments indicate that TGF-β induced lncRNA-MUF sponges miR-34a to promote Snail1-induced invasion (**Figures 6G, H**).

4 DISCUSSION

Glioma is the most lethal and invasive malignant brain neoplasm with a poor prognosis and frequent recurrence after surgery. Prominent features of GBM that contribute to recurrence include the presence of glioma stem cells, resistance to TMZ, and invasion (25, 37). TGF-β secreted by glioma cells confers them with an aggressive pro-invasive phenotype and TMZ resistance (9). TGF-β induces the expression of several lncRNAs (LINC00645, LINC00115, UCA1, lnc-ATB) through the canonical or non-canonical signaling pathway to promote glioma progression (22–24, 30). Nie et al. identified eight differentially regulated lncRNAs (H19, HOXD-AS2, LINC00635, LINC00277, RP11-196G11.2,

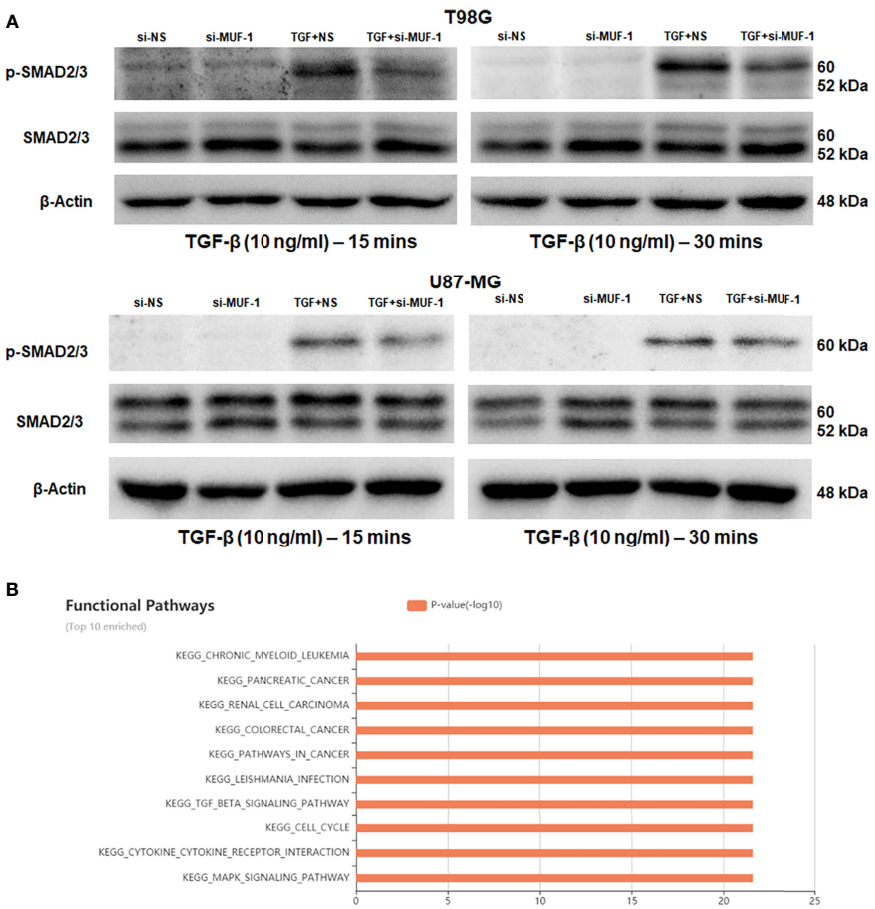

FIGURE 5 | LncRNA-MUF regulates TGF-β signaling. **(A)** LncRNA-MUF knockdown impairs phosphorylation of the smad2/3 complex. Western blot analysis of psmad2/3 and total smad2/3 levels in T98G and U87-MG cells treated with 10 ng/ml TGF-β1 (15 and 30 min), 48 h after lncRNA-MUF knockdown with si-MUF-1. A representative blot is shown from three independent experiments with similar results. Blots were reprobed for β-actin to establish equivalent loading. **(B)** Top 10 enriched signaling pathways regulated by lncRNA-MUF identified from the lncACTdb database.

LINC00152, MALAT1, and LOC100506207) in D54, P-GBM2 cells (9). They demonstrated that H19 and HOXD-AS2 confer TMZ resistance by regulating miR-198 biogenesis by competing with KSRP (9). LINC00115 regulates glioma stem cell tumorigenicity by enhancing ZNF596 by preventing the binding of miR-200 to the 5′ UTR of ZNF596 (25).

We identify several novel differentially expressed lncRNAs upon TGF-β treatment using a genome-wide microarray screen in T98G cells. Among the identified lncRNAs, we unveil the role of lncRNA-MUF in glioma pathobiology. LncRNA-MUF, also known as mesenchymal stem cell upregulated factor (lncRNA-MUF), promotes hepatocellular carcinoma by binding to ANXA2 to activate WNT/β-catenin signaling-mediated EMT (26). In addition, it sponges miR-34a in HCC cells leading to upregulation of Snail1 to promote EMT (26). We demonstrate that the levels of lncRNA-MUF are elevated in GBM tumor samples, and its expression is associated with poor survival and prognosis. This is consistent with the fact that the levels of lncRNA-MUF are also upregulated in gastric cancer, oral squamous cell carcinoma (OSCC), papillary thyroid carcinoma, colorectal cancer (CRC), lung cancer, colon cancer, and pancreatic cancer (32, 38–46).

ChIP-seq revealed that the lncRNA-MUF promoter upon TGF-β stimulation accumulates, activating H3K27ac marks (38). LncRNA-MUF induction by TGF-β in CRC cells is abrogated upon treatment with disitertide, an inhibitor of TGFβR1 (39). In line with these findings, we show that lncRNA-MUF induction by TGF-β is completely abrogated upon treatment with TGFβR1/smad 2/3 inhibitor SB505124 in glioma cells (**Figure 2C**). TGF-β-regulated lncRNA-MIR100HG regulates smad2/3 phosphorylation in prostate carcinoma (33). LncRNA-MUF also regulates the TGF-β signaling by preventing the SMAD4 degradation by competing with β-TrCP in CRC (39). We demonstrate for the first time that MUF downregulation attenuates TGF-β-induced phosphorylation of smad 2/3 in glioma cells. LncRNA-MUF promotes OSCC progression by mediating chromosome looping to the promoter of its cis gene, Caprin2, to activate the WNT/β-catenin signaling-mediated progression of OSCC (32). Although we observed a significant downregulation of the Caprin2 gene with lncRNA-MUF knockdown, we did not observe any change in the WNT/β-

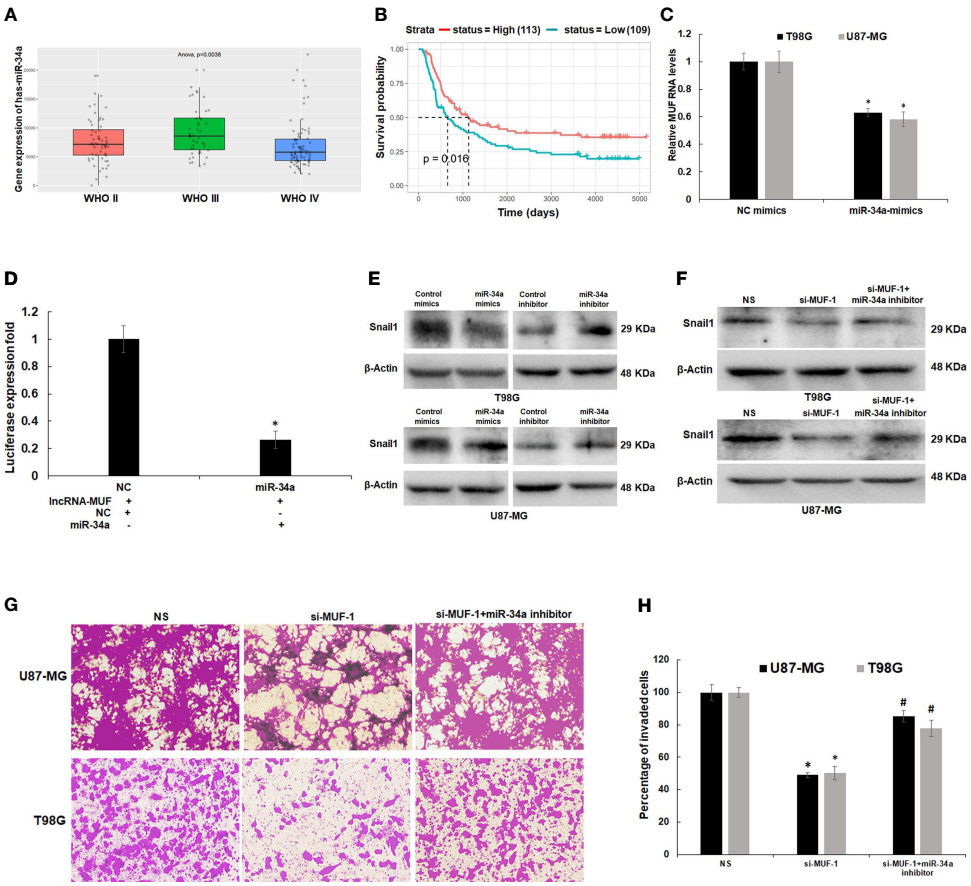

FIGURE 6 | LncRNA-MUF acts as a ceRNA by sponging miR-34a and regulates Snail1 expression. **(A)** Low expression of miR-34a in grade IV GBM as compared to lower-grade gliomas (p = 0.0038). Red bar represents miR-34a expression in the WHO grade II group, green bar represents miR-34a expression in WHO grade III, and blue bar represents miR-34a expression in the WHO grade IV glioma group. **(B)** Kaplan–Meier survival analysis showed that a high miR-34a expression was correlated with better survival in primary and recurrent GBM patients identified from the CGGA database (p = 0.016). Red line represents the high miR-34a expression group, and green line represents the low miR-34a expression group. **(C)** Downregulation of lncRNA-MUF transcript levels upon miR-34a overexpression measured by qRT-PCR in T98G and U87-MG cells. **(D)** Luciferase activity assay demonstrated that lncRNA-MUF could bind with miR-34a; relative luciferase activity was measured in HEK293T cells co-transfected with miR-34a-5p mimics and pmiRGLO-lncRNA-MUF constructs. Luminescence signals were measured 30 h post-transfection using dual luciferase assay. Data are shown as mean ± S.D. of three independent experiments; *p < 0.05. **(E)** Downregulation and upregulation of Snail1 protein levels upon treatment with miR-34a mimics and miR-34a inhibitor, respectively. T98G and U87-MG cells transfected with 80 nM of negative control mimics/inhibitor and miR-34a mimics/inhibitor. 48 h post-transfection protein lysates were collected, and Snail1 protein levels were analyzed by Western blotting. A representative blot is shown from three independent experiments with similar results. Blots were reprobed for β-actin to establish equivalent loading. **(F)** Rescue of Snail1 protein levels caused by lncRNA-MUF knockdown in T98G and U87-MG glioma cells upon miR-34a inhibition. A representative blot is shown from three independent experiments with similar results. Blots were reprobed for β-actin to establish equivalent loading. **(G)** Rescue of invasion caused by lncRNA-MUF knockdown in T98G and U87-MG glioma cells upon miR-34a inhibition. **(H)** Quantification of invaded cells upon lncRNA-MUF knockdown and miR-34a inhibition in T98G and U87-MG cells. # Significant decrease from C-si-MUF-1 transfected cells (p < 0.05).

catenin signaling genes. Our results suggest that apart from regulating Caprin2 expression, lncRNA-MUF modulates the expression of several genes involved in the TGF-β pathway in glioma cells (vimentin, CTGF, c-Myc, and Snail1) with Snail1 as one of the primary targets. However, the mechanism of regulation of vimentin, N-cadherin, CTGF, and c-Myc by lncRNA-MUF needs further investigation.

LncRNAs act as endogenous miRNA sponges for binding to miRNAs or participating in the ceRNA regulatory network (35). The cross talk between miRNAs and TGF-β-induced lncRNAs regulates the EMT and tumor invasion in glioma (23, 25). miR-34a suppresses the proliferation and invasion in glioma (47). It is downregulated in human glioma tumors as compared to normal brain tissue (47). miR-34a has a potential tumor-suppressor role in glioma by targeting several oncogenes and also induces differentiation of glioma stem cells (47). Dai et al. recently reported that LINC00665 sponges miR-34a, which targets the angiotensin II receptor type I (AGTR1) gene to impede glioma malignancy (48). Several studies have reported that Snail1 is a direct target of miR-34a (36, 49, 50). Snail1 is a crucial transcription factor that promotes tumor cell invasion and EMT (51). Snail1 is often upregulated in glioma, and high expression of Snail1 is associated

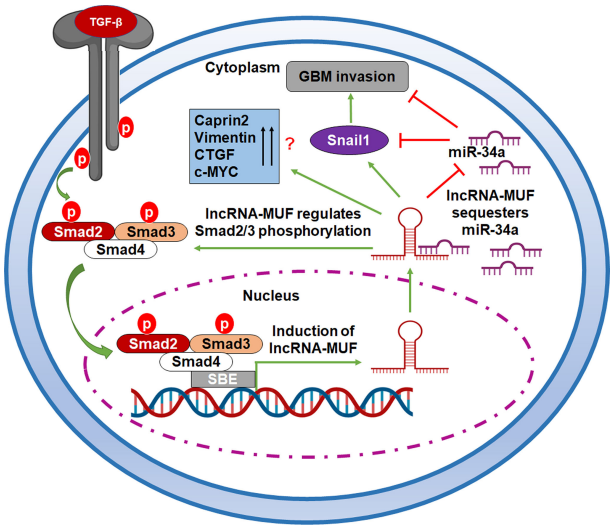

FIGURE 7 | A working model of TGF-β-activated lncRNA-MUF-driven glioma invasion. LncRNA-MUF is activated through the canonical TGF-β pathway, and it in turn regulates the phosphorylation of Smad2/3. It sequesters miR-34a from its binding target, Snail1, resulting in enhanced Snail1 expression and glioma invasion through the lncRNA-MUF/miR-34a/Snail1 signaling axis.

with poor survival of glioma patients (52). We observed a positive correlation between MUF and Snail1 expression in GBM tumor samples (**Figure S7D**). We also show that lncRNA-MUF depletion in glioma cells results in reduced migration and invasion, and lncRNA-MUF promotes GBM invasion by acting as an endogenous sponge for miR-34a and causing stabilization of its target Snail1 (**Figure 6G**). In addition, we show that loss of lncRNA-MUF expression reduces cell proliferation, induces apoptosis, and sensitizes glioma cells to TMZ-induced cell death. Our findings suggest that the TGF-β-regulated lncRNA-MUF/miR-34a/Snail1 signaling axis is a critical regulator of invasion in GBM (**Figure 7**). Our results warrant further preclinical studies on lncRNA-MUF using low-passage glioma patient-derived cell models, glioma stem cells, and *in vivo* models to firmly establish its role as a therapeutic target for GBM.

DATA AVAILABILITY STATEMENT

The datasets presented in this study can be found in online repositories. The names of the repository/repositories and accession number(s) can be found in the following: https://www.ncbi.nlm.nih.gov/, GSE183211.

AUTHOR CONTRIBUTIONS

BS: conceptualization, methodology, validation, formal analysis, investigation, visualization, writing—original draft. ST: methodology, validation, investigation, visualization. VS: conceptualization, methodology, investigation, visualization, formal analysis, resources, supervision, project administration, funding acquisition, writing—original draft, review, and editing. All authors contributed to the article and approved the submitted version.

FUNDING

This work was supported by extramural grants from the Government of India (DST-SERB ECR/2017/001953 and DBT-RLS 102/IFD/SAN/3499/2016-17) and intramural funds from an OPERA grant from BITS Pilani to VS. BS is supported by an SRF from ICMR No. 2020-7940/GEN-BMS.

ACKNOWLEDGMENTS

BS acknowledges a Ph.D. fellowship from BITS Pilani. We thank Sharma lab members for their help and support.

SUPPLEMENTARY MATERIAL

The Supplementary Material for this article can be found online at: https://www.frontiersin.org/articles/10.3389/fonc.2021.788755/full#supplementary-material

REFERENCES

1. Louis DN, Perry A, Reifenberger G, von Deimling A, Figarella-Branger D, Cavenee WK, et al. The 2016 World Health Organization Classification of Tumors of the Central Nervous System: A Summary. *Acta Neuropathol (Berl)* (2016) 131(6):803–20. doi: 10.1007/s00401-016-1545-1
2. Nørøxe DS, Poulsen HS, Lassen U. Hallmarks of Glioblastoma: A Systematic Review. *ESMO Open* (2016) 1(6):e000144. doi: 10.1136/esmoopen-2016-000144
3. Vollmann-Zwerenz A, Leidgens V, Feliciello G, Klein CA, Hau P. Tumor Cell Invasion in Glioblastoma. *Int J Mol Sci* (2020) 21(6):1932. doi: 10.3390/ijms21061932
4. Massagué J. TGFβ Signalling in Context. *Nat Rev Mol Cell Biol* (2012) 13 (10):616–30. doi: 10.1038/nrm3434
5. Colak S, ten Dijke P. Targeting TGF-β Signaling in Cancer. *Trends Cancer* (2017) 3(1):56–71. doi: 10.1016/j.trecan.2016.11.008
6. Roy L-O, Poirier M-B, Fortin D. Transforming Growth Factor-Beta and Its Implication in the Malignancy of Gliomas. *Target Oncol* (2015) 10(1):1–14. doi: 10.1007/s11523-014-0308-y
7. Han J, Alvarez-Breckenridge CA, Wang Q-E, Yu J. TGF-β Signaling and Its Targeting for Glioma Treatment. *Am J Cancer Res* (2015) 5(3):11.
8. Mao J, Sun Z, Cui Y, Du N, Guo H, Wei J, et al. *PCBP2* Promotes the Development of Glioma by Regulating *FHL3* /TGF-β/Smad Signaling Pathway. *J Cell Physiol* (2020) 235(4):3280–91. doi: 10.1002/jcp.29104
9. Nie E, Jin X, Miao F, Yu T, Zhi T, Shi Z, et al. TGF-β1 Modulates Temozolomide Resistance in Glioblastoma *via* Altered microRNA Processing and Elevated MGMT. *Neuro Oncol* (2021) 23(3):435–46. doi: 10.1093/neuonc/noaa198
10. Rinn JL, Chang HY. Long Noncoding RNAs: Molecular Modalities to Organismal Functions. *Annu Rev Biochem* (2020) 89(1):283–308. doi: 10.1146/annurev-biochem-062917-012708
11. Tripathi S, Shree B, Mohapatra S, Swati, Basu A, Sharma V. The Expanding Regulatory Mechanisms and Cellular Functions of Long Non-Coding RNAs

(lncRNAs) in Neuroinflammation. *Mol Neurobiol* (2021) 58(6):2916–39. doi: 10.1007/s12035-020-02268-8
12. Djebali S, Davis CA, Merkel A, Dobin A, Lassmann T, Mortazavi A, et al. Landscape of Transcription in Human Cells. *Nature* (2012) 489(7414):101–8. doi: 10.1038/nature11233
13. Statello L, Guo C-J, Chen L-L, Huarte M. Gene Regulation by Long Non-Coding RNAs and Its Biological Functions. *Nat Rev Mol Cell Biol* (2021) 22 (2):96–118. doi: 10.1038/s41580-020-00315-9
14. Huarte M. The Emerging Role of lncRNAs in Cancer. *Nat Med* (2015) 21 (11):1253–61. doi: 10.1038/nm.3981
15. Latowska J, Grabowska A, Zarębska Ż, Kuczyński K, Kuczyńska B, Rolle K. Non-Coding RNAs in Brain Tumors, the Contribution of lncRNAs, circRNAs, and snoRNAs to Cancer Development—Their Diagnostic and Therapeutic Potential. *Int J Mol Sci* (2020) 21(19):7001. doi: 10.3390/ijms21197001
16. Rezaei O, Tamizkar KH, Sharifi G, Taheri M, Ghafouri-Fard S. Emerging Role of Long Non-Coding RNAs in the Pathobiology of Glioblastoma. *Front Oncol* (2021) 10:625884. doi: 10.3389/fonc.2020.625884
17. Wang J, Zhang M, Lu W. Long Noncoding RNA GACAT3 Promotes Glioma Progression by Sponging miR-135a. *J Cell Physiol* (2019) 234(7):10877–87. doi: 10.1002/jcp.27946
18. Wei L, Yi Z, Guo K, Long X. Long Noncoding RNA BCAR4 Promotes Glioma Cell Proliferation *via* EGFR/PI3K/AKT Signaling Pathway. *J Cell Physiol* (2019) 234(12):23608–17. doi: 10.1002/jcp.28929
19. Xin S, Huang K, Zhu X-G. Non-Coding RNAs: Regulators of Glioma Cell Epithelial-Mesenchymal Transformation. *Pathol Res Pract* (2019) 215 (9):152539. doi: 10.1016/j.prp.2019.152539
20. Yadav B, Pal S, Rubstov Y, Goel A, Garg M, Pavlyukov M, et al. LncRNAs Associated With Glioblastoma: From Transcriptional Noise to Novel Regulators With a Promising Role in Therapeutics. *Mol Ther Nucleic Acids* (2021) 24:728–42. doi: 10.1016/j.omtn.2021.03.018
21. Papoutsoglou P, Moustakas A. Long Non-Coding RNAs and TGF-β Signaling in Cancer. *Cancer Sci* (2020) 111(8):2672–81. doi: 10.1111/cas.14509
22. Li Z, Liu H, Zhong Q, Wu J, Tang Z. LncRNA UCA 1 Is Necessary for TGF-β-Induced Epithelial–Mesenchymal Transition and Stemness *via* Acting as a Ce RNA for Slug in Glioma Cells. *FEBS Open Bio* (2018) 8(11):1855–65. doi: 10.1002/2211-5463.12533
23. Li C, Zheng H, Hou W, Bao H, Xiong J, Che W, et al. Long Non-Coding RNA Linc00645 Promotes TGF-β-Induced Epithelial–Mesenchymal Transition by Regulating miR-205-3p-ZEB1 Axis in Glioma. *Cell Death Dis* (2019) 10 (10):717. doi: 10.1038/s41419-019-1948-8
24. Tang F, Wang H, Chen E, Bian E, Xu Y, Ji X, et al. LncRNA-ATB Promotes TGF-β-Induced Glioma Cells Invasion Through NF-κb and P38/MAPK Pathway. *J Cell Physiol* (2019) 234(12):23302–14. doi: 10.1002/jcp.28898
25. Tang J, Yu B, Li Y, Zhang W, Alvarez AA, Hu B, et al. TGF-β-Activated lncRNA LINC00115 Is a Critical Regulator of Glioma Stem-Like Cell Tumorigenicity. *EMBO Rep* (2019) 20(12):e48170. doi: 10.15252/embr.201948170
26. Yan X, Zhang D, Wu W, Wu S, Qian J, Hao Y, et al. Mesenchymal Stem Cells Promote Hepatocarcinogenesis *via* lncRNA–MUF Interaction With ANXA2 and miR-34a. *Cancer Res* (2017) 77(23):6704–16. doi: 10.1158/0008-5472.CAN-17-1915
27. Chaudhary R, Gryder B, Woods WS, Subramanian M, Jones MF, Li XL, et al. Prosurvival Long Noncoding RNA PINCR Regulates a Subset of P53 Targets in Human Colorectal Cancer Cells by Binding to Matrin 3. *eLife* (2017) 6: e23244. doi: 10.7554/eLife.23244
28. Sharma V, Dixit D, Koul N, Mehta VS, Sen E. Ras Regulates Interleukin-1β-Induced HIF-1α Transcriptional Activity in Glioblastoma. *J Mol Med* (2011) 89(2):123–36. doi: 10.1007/s00109-010-0683-5
29. Sharma V, Shaheen SS, Dixit D, Sen E. Farnesyltransferase Inhibitor Manumycin Targets IL1β-Ras-HIF-1α Axis in Tumor Cells of Diverse Origin. *Inflammation* (2012) 35(2):516–9. doi: 10.1007/s10753-011-9340-6
30. Ma C-C, Xiong Z, Zhu G-N, Wang C, Zong G, Wang H-L, et al. Long Non-Coding RNA ATB Promotes Glioma Malignancy by Negatively Regulating miR-200a. *J Exp Clin Cancer Res* (2016) 35(1):90. doi: 10.1186/s13046-016-0367-2
31. Lee SY. Temozolomide Resistance in Glioblastoma Multiforme. *Genes Dis* (2016) 3(3):198–210. doi: 10.1016/j.gendis.2016.04.007
32. Ai Y, Wu S, Zou C, Wei H. LINC00941 Promotes Oral Squamous Cell Carcinoma Progression *via* Activating CAPRIN2 and Canonical WNT/β-Catenin Signaling Pathway. *J Cell Mol Med* (2020) 24(18):10512–24. doi: 10.1111/jcmm.15667
33. Papoutsoglou P, Rodrigues-Junior DM, Morén A, Bergman A, Pontén F, Coulouarn C, et al. The Noncoding MIR100HG RNA Enhances the Autocrine Function of Transforming Growth Factor β Signaling. *Oncogene* (2021) 40 (21):3748–65. doi: 10.1038/s41388-021-01803-8
34. Thomson DW, Dinger ME. Endogenous microRNA Sponges: Evidence and Controversy. *Nat Rev Genet* (2016) 17(5):272–83. doi: 10.1038/nrg.2016.20
35. Salmena L, Poliseno L, Tay Y, Kats L, Pandolfi PP. A ceRNA Hypothesis: The Rosetta Stone of a Hidden RNA Language? *Cell* (2011) 146(3):353–8. doi: 10.1016/j.cell.2011.07.014
36. Dong P, Xiong Y, Watari H, Hanley SJB, Konno Y, Ihira K, et al. MiR-137 and miR-34a Directly Target Snail and Inhibit EMT, Invasion and Sphere-Forming Ability of Ovarian Cancer Cells. *J Exp Clin Cancer Res* (2016) 35 (1):132. doi: 10.1186/s13046-016-0415-y
37. Bao S, Wu Q, McLendon RE, Hao Y, Shi Q, Hjelmeland AB, et al. Glioma Stem Cells Promote Radioresistance by Preferential Activation of the DNA Damage Response. *Nature* (2006) 444(7120):756–60. doi: 10.1038/nature05236
38. Gugnoni M, Manicardi V, Torricelli F, Sauta E, Bellazzi R, Manzotti G, et al. Linc00941 Is a Novel Transforming Growth Factor β Target That Primes Papillary Thyroid Cancer Metastatic Behavior by Regulating the Expression of Cadherin 6. *Thyroid* (2021) 31(2):247–63. doi: 10.1089/thy.2020.0001
39. Wu N, Jiang M, Liu H, Chu Y, Wang D, Cao J, et al. LINC00941 Promotes CRC Metastasis Through Preventing SMAD4 Protein Degradation and Activating the TGF-β/SMAD2/3 Signaling Pathway. *Cell Death Differ* (2021) 28(1):219–32. doi: 10.1038/s41418-020-0596-y
40. Luo C, Tao Y, Zhang Y, Zhu Y, Minyao DN, Haleem M, et al. Regulatory Network Analysis of High Expressed Long Non-Coding RNA LINC00941 in Gastric Cancer. *Gene* (2018) 662:103–9. doi: 10.1016/j.gene.2018.04.023
41. Liu H, Wu N, Zhang Z, Zhong X, Zhang H, Guo H, et al. Long Non-Coding RNA LINC00941 as a Potential Biomarker Promotes the Proliferation and Metastasis of Gastric Cancer. *Front Genet* (2019) 10:5. doi: 10.3389/fgene.2019.00005
42. Ren M-H, Chen S, Wang L-G, Rui W-X, Li P. LINC00941 Promotes Progression of Non-Small Cell Lung Cancer by Sponging miR-877-3p to Regulate VEGFA Expression. *Front Oncol* (2021) 11:650037. doi: 10.3389/fonc.2021.650037
43. Chang L, Zhou D, Luo S. Novel lncRNA LINC00941 Promotes Proliferation and Invasion of Colon Cancer Through Activation of MYC. *Onco Targets Ther* (2021) 14:1173–86. doi: 10.2147/OTT.S293519
44. Wang J, He Z, Xu J, Chen P, Jiang J. Long Noncoding RNA LINC00941 Promotes Pancreatic Cancer Progression by Competitively Binding miR-335-5p to Regulate ROCK1-Mediated LIMK1/Cofilin-1 Signaling. *Cell Death Dis* (2021) 12(1):36. doi: 10.1038/s41419-020-03316-w
45. Xu M, Cui R, Ye L, Wang Y, Wang X, Zhang Q, et al. LINC00941 Promotes Glycolysis in Pancreatic Cancer by Modulating the Hippo Pathway. *Mol Ther Nucleic Acids* (2021) 26:280–94. doi: 10.1016/j.omtn.2021.07.004
46. Fang L, Wang S-H, Cui Y-G, Huang L. LINC00941 Promotes Proliferation and Metastasis of Pancreatic Adenocarcinoma by Competitively Binding miR-873-3p and Thus Up-Regulates ATXN2. *Eur Rev Med Pharmacol Sci* (2021) 25(4):1861–8. doi: 10.26355/eurrev_202102_25081
47. Guessous F, Zhang Y, Kofman A, Catania A, Li Y, Schiff D, et al. microRNA-34a Is Tumor Suppressive in Brain Tumors and Glioma Stem Cells. *Cell Cycle* (2010) 9(6):1031–6. doi: 10.4161/cc.9.6.10987
48. Dai Y, Zhang Y, Hao M, Zhu R. LINC00665 Functions as a Competitive Endogenous RNA to Regulate AGTR1 Expression by Sponging Mir−34a−5p in Glioma. *Oncol Rep* (2021) 45(3):1202–12. doi: 10.3892/or.2021.7949
49. Siemens H, Jackstadt R, Hünten S, Kaller M, Menssen A, Götz U, et al. miR-34 and SNAIL Form a Double-Negative Feedback Loop to Regulate Epithelial-Mesenchymal Transitions. *Cell Cycle* (2011) 10(24):4256–71. doi: 10.4161/cc.10.24.18552
50. Kim NH, Kim HS, Li X-Y, Lee I, Choi H-S, Kang SE, et al. A P53/miRNA-34 Axis Regulates Snail1-Dependent Cancer Cell Epithelial–Mesenchymal Transition. *J Cell Biol* (2011) 195(3):417–33. doi: 10.1083/jcb.201103097
51. Alba-Castellón L, Olivera-Salguero R, Mestre-Farrera A, Peña R, Herrera M, Bonilla F, et al. Snail1-Dependent Activation of Cancer-Associated Fibroblast Controls Epithelial Tumor Cell Invasion and Metastasis. *Cancer Res* (2016) 76 (21):6205–17. doi: 10.1158/0008-5472.CAN-16-0176

52. Du L, Tang J-H, Huang G-H, Xiang Y, Lv S-Q. The Progression of Epithelial-Mesenchymal Transformation in Gliomas. *Chin Neurosurg J* (2017) 3(1):23. doi: 10.1186/s41016-017-0086-3

Conflict of Interest: The authors declare that the research was conducted in the absence of any commercial or financial relationships that could be construed as a potential conflict of interest.

Publisher's Note: All claims expressed in this article are solely those of the authors and do not necessarily represent those of their affiliated organizations, or those of the publisher, the editors and the reviewers. Any product that may be evaluated in this article, or claim that may be made by its manufacturer, is not guaranteed or endorsed by the publisher.

frontiers | Frontiers in Oncology

ORIGINAL RESEARCH
published: 14 April 2022
doi: 10.3389/fonc.2022.852940

Lucanthone Targets Lysosomes to Perturb Glioma Proliferation, Chemoresistance and Stemness, and Slows Tumor Growth *In Vivo*

Daniel P. Radin[1,2], *Gregory Smith*[1], *Victoria Moushiaveshi*[1], *Alexandra Wolf*[1], *Robert Bases*[3,4] *and Stella E. Tsirka*[1]*

[1] Department of Pharmacological Sciences, Renaissance School of Medicine at Stony Brook University, Stony Brook, NY, United States, [2] Stony Brook Medical Scientist Training Program, Renaissance School of Medicine at Stony Brook University, Stony Brook, NY, United States, [3] Department of Radiology, Montefiore Medical Center, New York City, NY, United States, [4] Department of Radiation Oncology, Montefiore Medical Center, New York City, NY, United States

OPEN ACCESS

Edited by:
Haotian Zhao,
New York Institute of Technology, United States

Reviewed by:
Vadim Le Joncour, University of Helsinki, Finland
Manabu Natsumeda, Niigata University, Japan
Tsung-I Hsu, Taipei Medical University, Taiwan

***Correspondence:**
Stella E. Tsirka
Styliani-anna.Tsirka@stonybrook.edu

Specialty section:
This article was submitted to Neuro-Oncology and Neurosurgical Oncology, a section of the journal Frontiers in Oncology

Received: 11 January 2022
Accepted: 22 March 2022
Published: 14 April 2022

Citation:
Radin DP, Smith G, Moushiaveshi V, Wolf A, Bases R and Tsirka SE (2022) Lucanthone Targets Lysosomes to Perturb Glioma Proliferation, Chemoresistance and Stemness, and Slows Tumor Growth In Vivo. Front. Oncol. 12:852940. doi: 10.3389/fonc.2022.852940

Glioblastoma is the most common and aggressive primary brain tumor in adults. Median survival time remains at 16-20 months despite multimodal treatment with surgical resection, radiation, temozolomide and tumor-treating fields therapy. After genotoxic stress glioma cells initiate cytoprotective autophagy, which contributes to treatment resistance, limiting the efficacy of these therapies and providing an avenue for glioma recurrence. Antagonism of autophagy steps has recently gained attention as it may enhance the efficacy of classical chemotherapies and newer immune-stimulating therapies. The modulation of autophagy in the clinic is limited by the low potency of common autophagy inhibitors and the inability of newer ones to cross the blood-brain barrier. Herein, we leverage lucanthone, an anti-schistosomal agent which crosses the blood-brain barrier and was recently reported to act as an autophagy inhibitor in breast cancer cells. Our studies show that lucanthone was toxic to glioma cells by inhibiting autophagy. It enhanced anti-glioma temozolomide (TMZ) efficacy at sub-cytotoxic concentrations, and suppressed the growth of stem-like glioma cells and temozolomide-resistant glioma stem cells. *In vivo* lucanthone slowed tumor growth: reduced numbers of Olig2$^+$ glioma cells, normalized tumor vasculature, and reduced tumor hypoxia. We propose that lucanthone may serve to perturb a mechanism of temozolomide resistance and allow for successful treatment of TMZ-resistant glioblastoma.

Keywords: autophagy, glioma, cancer stem cell, angiogenesis, hypoxia, lucanthone

INTRODUCTION

Gliomas are primary cancers of the central nervous system (CNS) (1). Among them, Glioblastoma (GBM), the highest grade and most aggressive glioma in adults, is the most commonly diagnosed and aggressive glioma in adults (1). The standard of care therapy for GBM consists of maximum safe surgical resection followed by fractional radiation, chemotherapy with the alkylating agent

temozolomide (TMZ) and adjuvant treatment with tumor-treating fields (2). Median survival time after diagnosis is approximately 16-20 months (2). As GBM is highly invasive, resection is typically incomplete, which accounts for rapid recurrence and contributes to the universal lethality of this malignancy.

During disease progression, patients often experience comorbidities including pharmacoresistant seizures, headaches, sleep disturbances and neurological deficits in addition to the side effects of radiation and chemotherapy (1), pointing to a great need for new treatment regimens. The search for treatment modalities is complicated by the fact that large molecules cannot pass efficiently through the blood brain barrier, so reagents demonstrating *in vitro* efficacy may not be useful *in vivo* because they never reach the brain. Gliomas are comprised of multiple cell populations including glioma cancer stem cells (GSC), pericytes, infiltrating bone-marrow derived macrophages (BMDM) and microglia (3–5). In glioma, BMDMs and microglia accumulate in tumor tissue attracted by chemokines, such as CSF1 and CCL2, secreted by tumor cells (6, 7) and constitute the glioma-associated macrophages/microglia (GAM). GAM promote glioma cell survival, neoangiogenesis and foster an immunosuppressive tumor microenvironment (TME) (3, 4, 6, 7). These processes constitute targets for novel methodologies to manage GBM.

Accumulating reports in the literature suggest that induction of autophagy in glioma cells promotes resistance to standard of care therapies and survival in hypoxia (8–11). Autophagic induction in tumor-associated pericytes and GAM fosters an immunosuppressive TME (5, 12). In addition induction of autophagy has been reported to limit the oncolytic capacity of cytotoxic T-lymphocytes (CTL) in other tumors (13, 14). Based on this evidence, we hypothesized that inhibiting autophagy may not only augment the efficacy of standard of care therapies, but may also reverse the immunosuppressive TME.

Lucanthone (marketed as Miracil D) is an anti-schistosome agent (15–20). It inhibits topoisomerase II and AP endonuclease 1 (APE1) (21–24). Lucanthone has shown efficacy against solid tumors when paired with ionizing radiation (25). It can cross the blood brain barrier and was shown to induce regression of breast cancer metastases (26) synergizing with TMZ against breast tumor cells *in vitro* (23). Inhibition of autophagy and lysosomal membrane permeabilization (27), may explain lucanthone's interaction with TMZ and radiation (23, 26). Of particular note, lysosomal membrane permeabilization by chloroquine resulted in repolarization of tumor-associated macrophages from an immune-suppressive/pro-tumor 'M2-like' to an immune-promoting/anti-tumor 'M1-like' phenotype (28). This phenotypic shift was denoted by a marked increase in pro-inflammatory markers (IFN-γ, TNF-α, CD86, iNOS), a decrease in the expression of anti-inflammatory proteins (IL-10, Arg1) and the induction of anti-tumor T-cell immunity (28). These data suggest that lucanthone's various mechanistic engagements may potentially serve to target multiple processes that support tumor growth, be it directly on the glioma cells, or indirectly on the GAM, thus augmenting the efficacy of TMZ and radiation, and modulating GAMs to exert anti-tumor effects and promote immune-mediated tumor rejection.

In this study we show that lucanthone targeted glioma cells at clinically relevant concentrations by blocking autophagy. Further, we show that this drug synergized with TMZ and preferentially targeted glioma stem-like cells *in vitro* and slowed tumor growth *in vivo*. Lucanthone normalized tumor vasculature, reduced hypoxia and increased cytotoxic T cell infiltration into the tumor core. All these events highlight the potential robust efficacy of this drug against TMZ-resistant gliomas, which are not normally conducive to chemotherapeutic treatment.

MATERIALS AND METHODS

Cell Culture

GL261 cells expressing luciferase (GLUC2) were obtained from the lab of Dr. Michael Lim. They are derived from a chemically induced astrocytoma in C57BL/6 mice (29). KR158 cells were obtained from the labs of Drs. Tyler Jacks and Behnam Badie, and are derived from genetically engineered Nf1/Tp53 mutants (30). Cells were maintained in DMEM, 10% serum, 1% antibiotic, 1% sodium pyruvate and incubated at 37°C with 5% CO_2. bEND.3 cells were cultured in DMEM with serum as above. Primary patient-derived human glioma cells (GBM43) which carries Nf1 and Tp53 mutations were obtained from Dr. Jann Sarkaria at the Mayo Clinic from the xenograft cell line panel. To enrich for glioma stem-like cells (GSC) in GLUC2, KR158 and GBM43 cells, serum was reduced step-wise over a week as described previously (31). GSC were cultured in serum-free DMEM medium containing F12 supplement along with pyruvate, antibiotics, N2 supplement, EGF, FGF and heparin (31).

Crystal Violet Studies

For single lucanthone treatment studies, GLUC2 and KR158 cells were plated at a density of 2,000 and 1,000 cells per well, respectively, in a 6-well plate and allowed to adhere overnight. They were then treated with 10 μM Lucanthone every 4 days for 12 days. On day 13, media were aspirated, and cells were fixed with 4% PFA for 10 minutes. Cells were then treated with 0.5% crystal violet solution for 20 minutes. Plates were washed and photographed.

For dual treatment studies (lucanthone and TMZ), GLUC2 and KR158 cells were plated at a density of 2,500 and 1,000 cells per well in a 12-well plate and allowed to adhere overnight. Cells were then treated with medium, TMZ, lucanthone, or a combination for 4 days. The media were aspirated, and the cells were washed with PBS once and incubated with standard medium for 3 days. The cells were fixed with PFA and treated with 0.5% crystal violet solution as above and photographed. Then lysis solution of 10% SDS in dH_2O was added to the plates overnight. To quantify relative crystal violet intensity, the absorbance of the crystal violet-containing supernatant was read under a spectrophotometer at 590 nm with a reference

wavelength of 670 nm. Data are graphed as percent of control (medium only-treated cells).

MTT Assay

Cells were plated in a 96-well plate and incubated overnight. Adherent tumor cells (2D cultures) were treated with lucanthone for 3 days and then subject to the MTT protocol as per manufacturer's instructions (Promega). GSC (3D cultures) were treated with lucanthone for 5 days, as this allowed sufficient time for spheroids to grow in culture. Prior to addition of the MTT reagent, plates were imaged under confocal microscopy with the addition of Calcein-AM and Ethidium homodimer to mark live cells and dead cells, respectively.

Acridine Orange Stain

GLUC2, KR158 and GBM43 cells were plated on glass-bottom 35mm plates overnight. They were then treated with medium or lucanthone for 48 hours. The cells were treated with 5μg/ml acridine orange for 15 minutes. Plates were washed with PBS 3x and then incubated in complete medium. Plates were then imaged for acidic vesicle accumulation (525/590nm) under confocal microscopy, according to manufacturer's instructions (Cayman chemical).

Immunocytochemistry

For immunocytochemical analysis, GLUC2, KR158 and GBM43 cells were plated on glass coverslips overnight. Cells were treated with medium or lucanthone for 48 hours. The medium was aspirated and cells were fixed with 4% PFA for 10 minutes. Plates were then washed 3x with 0.3% TX-100 in PBS and wells were blocked with 3% normal goat serum/0.3% TX-100 in PBS for 1 hour. Cells were stained with primary antibodies overnight (LC3, Ki67, Nestin, Olig2, SOX2, CD133, p62, Cathepsin D, γH2AX). The primary antibody was removed, and cells were again washed 3x with 0.3% TX-100 in PBS after which time cells were incubated with fluorescent secondary antibodies for an hour at room temperature. Cells were then washed 3x with PBS, counterstained with DAPI and imaged under confocal microscopy. GSC were induced to adhere to glass slides by precoating glass slides with Geltrex for an hour.

Western Blot

Immunoblotting was done as described previously (3). Briefly, cells were lysed in 50mM Tris-HCl (pH 7.4) with 1% Nonidet P-40, 0.25% sodium deoxycholate, 150mM NaCl, 1% SDS and 1mM sodium orthovanadate. Proteins were denatured by boiling with treatment with BME. Proteins were run on SDS-page gels, transferred to PVDF membranes (Immobilon; Millipore). Membranes were washed with Tris-buffered saline with 0.1% Tween 20 and blocked in a 5% non-fat dry milk powder for 1 hour. Membranes were then probed for LC3 (1:1000), p62 (1:1000), Olig2 (1:1000), SOX2 (1:1000) and B-Actin (1:2000; sigma Aldrich). Membranes were rinsed in TBS-T, probed with associated HRP-conjugated secondary antibodies and exposed to Pierce ECL substrate for 1 minute (Thermo Fisher Scientific) after which x-ray films were developed from membranes.

RNA Isolation and Quantitative RT-PCR

To prepare RNA, GLUC2 spheroids were spun down and lysed with Trizol and processed using the manufacturers protocol. To obtain cDNA, one microgram of RNA was reverse transcribed on a Veriti thermocycler using the High Capacity cDNA Reverse Transcription Kit. Amplification was performed on a StepOnePlus real-time PCR machine using a SYBR green kit (Applied biosystems). Primer sequences are as follows: GAPDH forward, 5′-GCACAGTCAAGGCCGAGAAT-3′; GAPDH reverse, 5′-GCCTTCTCCATGGTGGTGGA-3′; Olig2 forward, 5′- CAAATCTAATTCACATTCGGAAGGTTG -3′; Olig2 reverse, 5′- GACGATGGGCGACTAGACACC -3′. GAPDH was used as an internal control.

Animals

C57Bl6 mice were bred under maximum isolation on a 12:12 hour light:dark cycle with food *ad libitum*.

Murine Glioma Model

Gliomas were established in 3-4 month old male and female mice as described previously (3, 4, 32). GLUC2 GSC were dissociated with accutase and counted. Mice were anesthetized with 20mg/kg avertin, a midline incision was made in the scalp, the skin retracted and a small burr hole was drilled in the skull at the following stereotactic coordinates from bregma: -1mm anteroposterior and +2 mediolateral. $1x10^5$ GLUC2 GSC resuspended in PBS were injected over a period of 2 minutes at a depth of 3mm. At the end of the injection, the needle was kept in the injection site for a further 3 minutes. After needle removal, the incision was sutured and mice were placed on a heating pad until they fully recovered from anesthesia. During the disease course if mice were found to have lost more than 15% of their initial body weight, they were euthanized. All animal procedures were approved by the Stony Brook University Institutional Animal Care and Use Committee.

In Vivo Luciferase Imaging

GSC engraftment was visualized using the IVIS spectrum *in vivo* imaging system 7 days after inoculation and again on days 14 and 21. Briefly, mice were anesthetized using continuous isofluorane exposure. Their scalps were shaved. Mice were injected i.p. with 150mg/kg D-Luciferin, carefully placed in the IVIS spectrum machine and imaged every 3-4 minutes for 40 minutes. Relative signal was quantified by a researcher blinded to the treatment, and luminescence ratios of day 21 to day 7 were calculated to approximate disease progression throughout the course of treatment.

Lucanthone Treatment *In Vivo*

Lucanthone was supplied by Dr. Robert Bases. Lucanthone was solubilized in 10% DMSO, 40% HPCD in PBS. After confirming the presence of gliomas on day 7, mice were randomly divided to control and treatment groups, and treated with either saline or 50mg/kg Lucanthone i.p. every day from day 7 to day 20. On day 21, tumors were visualized by bioluminescent imaging, as above.

Immunohistochemistry

Mice were anesthetized with 20mg/kg avertin and transcardially perfused with 30ml PBS followed by 30ml 4% PFA in PBS. Brains were removed and post-fixed in 4% PFA in PBS overnight. They were dehydrated for 48 hours in 30% w/v sucrose in PBS. Brains were then embedded in optimal cutting temperature compound (OCT, Tissue-Tek) and 20µm coronal sections throughout the entire tumor were taken on a Leica cryostat (Nusslock, Germany) and collected on Superfrost plus microscope slides. To determine tumor volume, serial sections were taken from each animal and subjected to hematoxylin and eosin stain. Tumor volume was calculated as tumor area x 20 µm thickness, x number of slides (33).

For immunohistochemical analysis, slides were brought to room temperature, washed 3x with 0.3% TX-100 in PBS and then blocked with 1% BSA/0.3% TX-100 in PBS for 1 hour. Slides were incubated overnight with appropriate primary antibodies (**Supplementary Table 1**). The primary antibody was removed and slides were washed 3x 0.3% TX-100 in PBS and incubated with appropriate secondary antibodies for 1 hour. Slides were washed 3x with PBS, and counterstained with DAPI. Immunoreactivity was visualized by confocal imaging using the Leica SP8-x system, with white light and argon lasers.

Statistical Analysis

Data comparing two population means with a normal distribution were analyzed using Student's t-test. Data with non-normal distributions were analyzed using a Mann-Whitney test. Differences in cumulative distributions were assessed with the Kolomogorov-Smirnov test. To assess for synergistic interactions, King's synergy test was used (34–36). Blood vessel circularity was calculated using the equation $Circularity=4*\pi*(area/(perimeter^2))$. Alpha value was set at 0.05 prior to starting experiments. Power analysis was used to determine the appropriate number of animals used in each experiment. Experiments were replicated with the two tumor lines. Statistical analysis was performed using Graphpad Prism (Graphpad Software Inc, La Jolla, CA).

RESULTS

Lucanthone Targets Lysosomes and Inhibits Autophagy

To examine whether lucanthone affects the growth of the two murine glioma cell lines GLUC2 and KR158, lucanthone (**Figure 1A**) was added to glioma cultures at 10 µM every 4 days for 2 weeks (**Figure 1B**), which reflects concentrations observed in the serum of patients (26). The proliferation of both cell lines was hindered. To investigate whether the possible mechanism by which lucanthone acts on glioma cells engaged autophagy, we treated glioma cells with lucanthone for 48 hours, and then stained them with acridine orange, which accumulates in acidic vacuolar organelles and shifts from green to red fluorescence (37). In control conditions, only few lysosomes were present in the cell lines. After treatment with lucanthone,

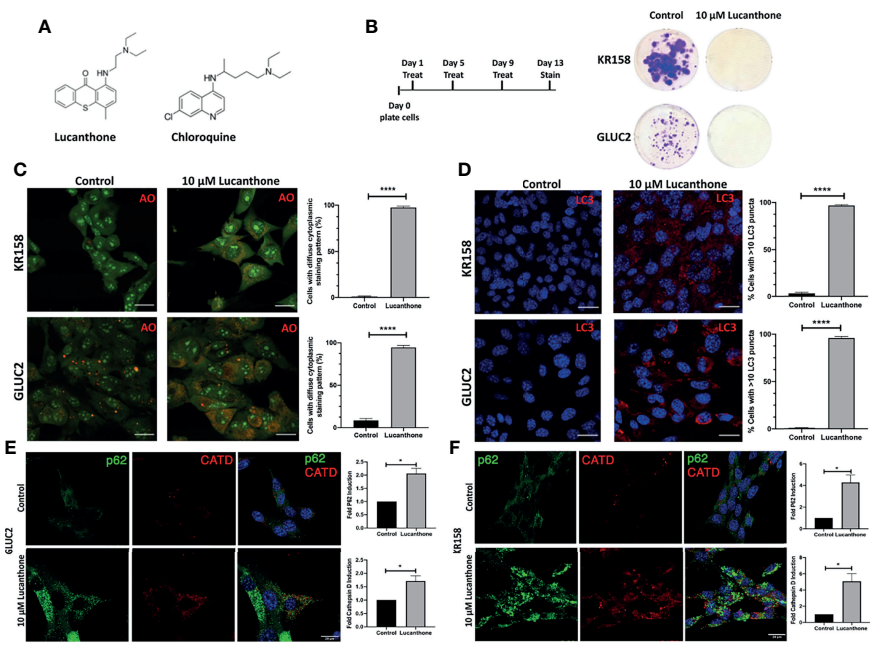

FIGURE 1 | Lucanthone compromises glioma cell growth. **(A)** Chemical structures of lucanthone and chloroquine. **(B)** Effects of long-term treatment of KR158 and GLUC2 cultures with 10 µM lucanthone on glioma cell proliferation. **(C)** Acridine orange (AO) marks lysosomes as punctae staining after 48 hour of lucanthone treatment. **(D)** LC3 marks autophagosome punctae levels after 48 hour treatment with lucanthone. **(E, F)** Effect of lucanthone on P62 and Cathepsin D levels in GLUC2 and KR158 cells, respectively. Scale bar = 30 µm. Bars are mean +/- SEM. N= 3-4 independent experiments. *p < 0.05, ****p < 0.0001, student's t-test.

cultures in both cell lines exhibited a remarkable diffuse cytoplasmic staining of dilated lysosomes (**Figure 1C**) with a corresponding increase in LC3 punctae (**Figure 1D**). These data parallel what has been observed after treatment with chloroquine in other tumor types (37) and suggest that lucanthone targets lysosomes and affects autophagic function at clinically relevant concentrations.

We also assessed the levels of the autophagy cargo receptor p62 and Cathepsin D. P62 accumulates in cells in which autophagy has been functionally inhibited and Cathepsin D is a lysosomal aspartyl protease (27). Our data demonstrate that after 48 hours of lucanthone treatment, P62 and Cathepsin D increase in both glioma cell lines, though we note a higher relative increase of both proteins in KR158 cells (**Figures 1E, F**). These findings illustrate lucanthone's ability to inhibit autophagy at clinically relevant concentrations.

To examine whether lucanthone exerts its functions by acting as an inhibitor of topoisomerase 2 or APE1, we assessed the extent to which lucanthone induced DNA damage in glioma cell lines. To that end, GLUC2 and KR158 cells were treated with lucanthone for 48 hours, after which levels of γH2AX, a DNA damage marker, were assessed (38). As a positive control, glioma cells were also treated with the FDA-approved topoisomerase 2 inhibitor etoposide. While etoposide produced a marked increase in γH2AX intensity, lucanthone only produced a minimal effect, indicating that it is exerting its effect most likely *via* autophagy inhibition. When the levels of cleaved caspase-3 were evaluated, only minimal induction of cleaved caspase-3 in GLUC2 and KR158 spheroids treated with 10 μM lucanthone for 48 hours were observed, indicating that lucanthone may not be inducing apoptosis in these glioma cell lines (**Figure S1**), as was shown for another autophagy inhibitor, thymoquinone, which induces cathepsin-mediated, but caspase-independent cell death (39).

Lucanthone Interacts With Temozolomide

The interaction between lucanthone and TMZ was investigated by performing combination studies *in vitro*. First, we performed an MTT assay to determine minimally effective concentrations of lucanthone in both cell lines. Lucanthone exerted a dose-dependent reduction in cell viability, with an IC50 of approximately 11-13 μM (**Figure 2B**). Two-way ANOVA illustrated that both cell lines were similarly sensitive to lucanthone, implying that this drug may be useful regardless of driver mutations. These data also pointed towards the use of 1 μM lucanthone for the combination studies, since this concentration exerted minimal effects alone on both cell lines.

It has been reported that GL261 and KR158 cells exhibit striking resistance to TMZ *in vitro* (40, 41). Therefore, we treated GL261 and KR158 cells with control medium, either drug alone, or both drugs for 4 days, and then allowed cultures to recover for 3 days before analysis. In this extended treatment format, 1 μM lucanthone alone, or 50 μM TMZ or 100 μM TMZ produced only a modest effect on GL261 and KR158 cells (**Figures 2B, C**). However, crystal violet intensity was markedly decreased when cells were treated with a combination of lucanthone and TMZ (**Figures 2B, C**, $p<0.05$, King's synergy test). Our data, in agreement with previous studies on breast tumor cells (23), suggest that even lower doses of lucanthone may be useful when paired with standard of care therapies to slow glioma progression.

To understand why lucanthone may augment the anti-tumor effects of TMZ, we tested for changes in the levels of γH2AX, a

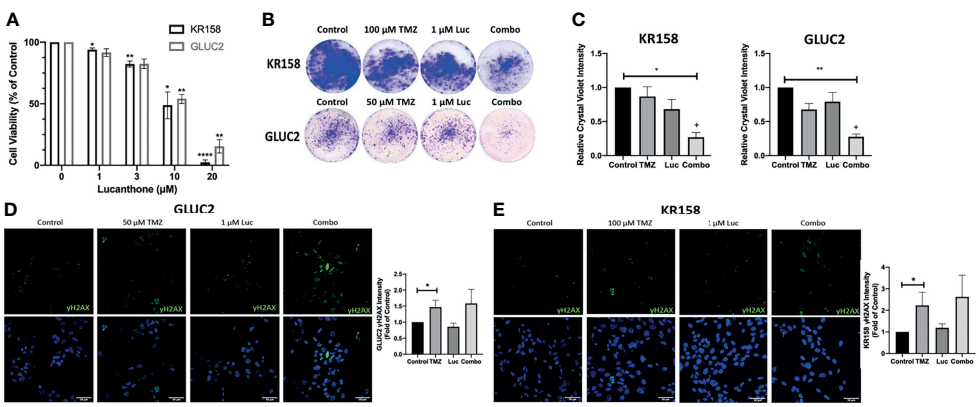

FIGURE 2 | Interaction between lucanthone and temozolomide. **(A)** KR158 and GLUC2 cells were treated with Lucanthone for 72 hours, after which an MTT assay was performed. Bars are mean +/- SEM, N=3-7 independent experiment. ANOVA $p<0.0001$. *$p < 0.05$, **$p < 0.01$, ****$p < 0.0001$, Dunnett's multiple comparison test to control-treated cells. **(B, C)** KR158 and GLUC2 cells were treated with lucanthone, TMZ, or the combination for 4 days and then allowed to recover in drug-free medium for 3 days. The cells were PFA-fixed and stained with crystal violet. Crystal violet-stained cells were then lysed and relative absorbance was measured to approximate culture viability. Representative wells are shown in **(B)**. **(C)** Quantification of crystal-violet stained cultures. Bars are mean +/- SEM, N=3-4 independent experiments. *$p < 0.05$, **$p < 0.01$, Dunnett's multiple comparison test to control-treated cells. +$p < 0.05$, King's synergy test, demonstrating significant interactions between lucanthone and TMZ in both cell lines. **(D)** Representative micrographs of γH2AX stained GLUC2 cells and quantification of γH2AX intensity per number of cells in the field of view in experiments where the GLUC2 cells were incubated with TMZ, or the combination of lucanthone and TMZ. **(E)** Representative micrographs of γH2AX stained KR158 cells. Quantification of γH2AX intensity per number of cells in the field of view in experiments where the KR158 cells were incubated with TMZ, or the combination of lucanthone and TMZ. Bars are mean +/- SEM, N=4 independent experiments. *$p < 0.05$, Mann-Whitney test.

marker of DNA damage, in both cell lines. After 48 hours, changes in γH2AX intensity were evident in cultures treated with TMZ, but not in those treated with lucanthone (**Figures 2D-F**). Cultures treated with both drugs exhibited slightly increased levels of γH2AX compared to cultures treated with TMZ alone, but this increase did not become statistically significant.

Lucanthone Targets Glioma Cancer Stem Cells and Overcomes Acquired Temozolomide Resistance

Cancer stem cells are defined as progenitor-like tumor cells that repopulate the tumor after what is considered "successful" treatment, driving tumor recurrence and fatality. It is now accepted that cancer stem cells (termed here GSC) are rapidly dividing (42) and resistant to both TMZ and radiation (43, 44). Recent data reveal that GSC preferentially rely on autophagy for their survival and resistance to TMZ (45, 46). To that end, we enriched for stemness characteristics in GLUC2 and KR158 cell lines (please see Materials and Methods). Both glioma cell lines grew as partially suspended spheroids. 1 week after culturing cells in stemness medium, GLUC2 spheroids stained positive for the stemness markers nestin, SOX2 and Olig2, while KR158 spheroids stained positive for nestin, CD133 and SOX2 (**Figure S2**). Cells staining positive for these markers also stained positive for the proliferation marker Ki67, demonstrating that these cells are indeed actively proliferating. Additionally, western blot analysis indicates that GLUC2 spheroids express higher levels of SOX2 and Olig2, while KR158 spheroids express higher levels of SOX2 than their adherent counterparts (**Figure S2**).

After determining that these cells expressed stemness markers, they were treated with increasing concentrations of lucanthone. Remarkably, doses as low as 3 μM produced a strong oncolytic effect in these GSC. Lucanthone reduced spheroid area in both cell lines (**Figures 3A, B**). Further, treatment with lucanthone in a dose-dependent manner resulted in reduced numbers of spheroids formed in culture and reduced viability of the cultures (**Figures 3C, D**). These data show that lucanthone may preferentially kill cells left behind after treatment with modalities such as TMZ and radiation. Additionally, the IC_{50} of lucanthone was approximately 2μM for KR158 and GLUC2 GSC. This is in contrast to an IC_{50} of 11-13 μM in cells cultured

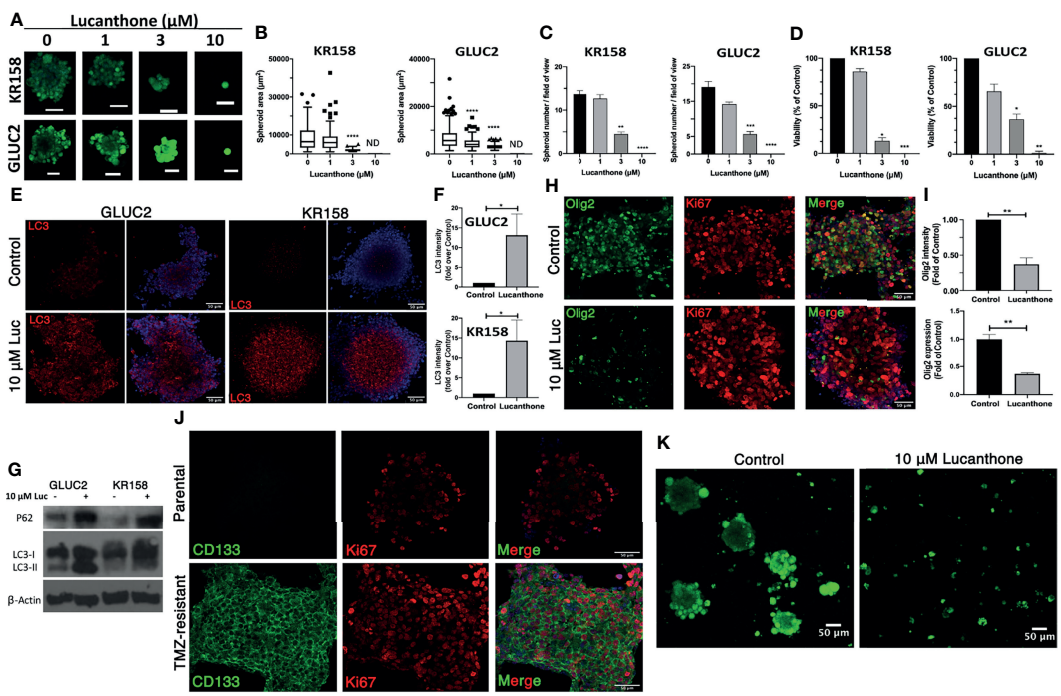

FIGURE 3 | Lucanthone targeted GSC and overcame acquired resistance to temozolomide. GLUC2 and KR158 spheroids were mechanically dissociated, plated overnight and treated with increasing concentrations of lucanthone for 5 days. After treatment, they were stained with Calcein-AM to visualize viable cells. **(A)** Representative images of KR158 and GLUC2 GSC treated with increasing concentrations of Lucanthone for 5 days; **(B)** Spheroid area distribution. ****$p < 0.0001$, Kolmogorov-Smirnov test comparing distributions to control-treated cultures; ND, Not Detected. **(C)** Spheroid number per field of view; **(D)** Viability of cultures as determined by MTT assay. Bars are mean +/- SEM, N=3-4 independent experiments. *$p < 0.05$, **$p < 0.01$, ***$p < 0.001$, Dunnett's multiple comparison test to control-treated cells. **(E)** LC3 staining in GLUC2 and KR158 spheroid cultures treated with media or 10 μM lucanthone for 48 hours; **(F)** LC3 intensity measured in the same cultures. *$p < 0.05$, Mann-Whitney test; **(G)** Olig2 staining in GLUC2 spheroid cultures treated with media (Control) and 10 μM lucanthone-treated for 48 hours; **(H)** Olig2 intensity and mRNA expression in the same cultures. **$p < 0.01$, t-test. N=3-4 independent experiments; **(I)** Immunoblot analysis of p62 and LC3 in protein extracts from GLUC2 and KR158 spheroids with media or 10 μM lucanthone for 48 hours; **(J)** GLUC2 cells treated with 5 cycles of TMZ stained for the stemness marker CD133 and for the proliferation marker Ki67; **(K)** TMZ-resistant GLUC2 cells treated with media or 10 μM lucanthone for 5 days.

with serum. These data indicate that stem-like glioma cells may be more susceptible to autophagy inhibiting drugs like lucanthone.

To gain mechanistic insight into how lucanthone reduces stemness, we allowed KR158 an GLUC2 GSC to form spheroids for 10 days, then treated spheroids with 10 μM lucanthone for 48 hours and assayed for alterations in levels of LC3and p62. By western blot analysis, we observed that lucanthone increased p62 levels in GLUC2 and KR158 GSC and increased levels of LC3-II as well (**Figures 3E, G**). We also observed increases in LC3 punctae in spheroids by immunocytochemistry and immunoblotting (**Figures 3E-G**). These data illustrate that the drug probably acted in a similar manner to that observed in adherent 2D cultures. It is worthy to note that in control conditions, LC3 punctae were also observed in spheroids, suggesting a higher level of baseline autophagy in GSC and a higher reliance on autophagy in general. In addition to assessing for changes in autophagic flux, we assessed for changes in the levels of stemness markers after treatment. We observed a strong reduction in Olig2 intensity in lucanthone-treated cultures (**Figures 3H, I**), while expression on nestin and SOX2 did not change. Using RT-qPCR we found that lucanthone reduced Olig2 mRNA expression in GLUC2 spheroids by >60% (**Figure 3I**). Minimal changes were also observed in Ki67 in these cultures.

Despite multimodal treatment, the recurrence rate for glioblastoma is ~100%. It has also been proposed that glioma cells change throughout the course of treatment such that the cells that survive treatment are functionally different than the parental tumor (47–49). We tested whether Lucanthone was able to exert oncolytic effects on glioma cells that have been selected for their ability to resist the standard chemotherapy temozolomide, TMZ. To that end, we treated GLUC2 cells with two cycles (48 hours of treatment and 7 days recovery per cycle) of 250 μM TMZ and 3 cycles of 500 μM TMZ. After the selection, we noticed that the surviving cells started forming spheres in serum-containing medium, similar to the ones we observe when culturing these cells in stemness-promoting medium. These spheroids expressed the prototypic stemness gene CD133 whereas parental GLUC2 spheroids did not (**Figure 3J**), suggesting that glioma cells dynamically respond to genotoxic therapy by acquiring stem-like morphology and characteristics (47). Cells selected for TMZ resistance were also less sensitive to TMZ treatment than parental GLUC2 cells (**Figure S3**). In spite of becoming more stem-like, these cultures were still markedly sensitive to 10 μM lucanthone (**Figure 3K**), suggesting that lucanthone could be used to slow the growth of TMZ-resistant malignant glioma cells.

To examine if lucanthone could target human glioma cells as well, we obtained patient-derived glioma cells from the Mayo Clinic (termed GBM43), which bear Tp53 and Nf1 mutations. After treatment with lucanthone, GBM43 cells exhibited a similar acridine orange cytoplasmic staining pattern as seen in GLUC2 and KR158 cells (**Figure 4A**). Additionally, there were

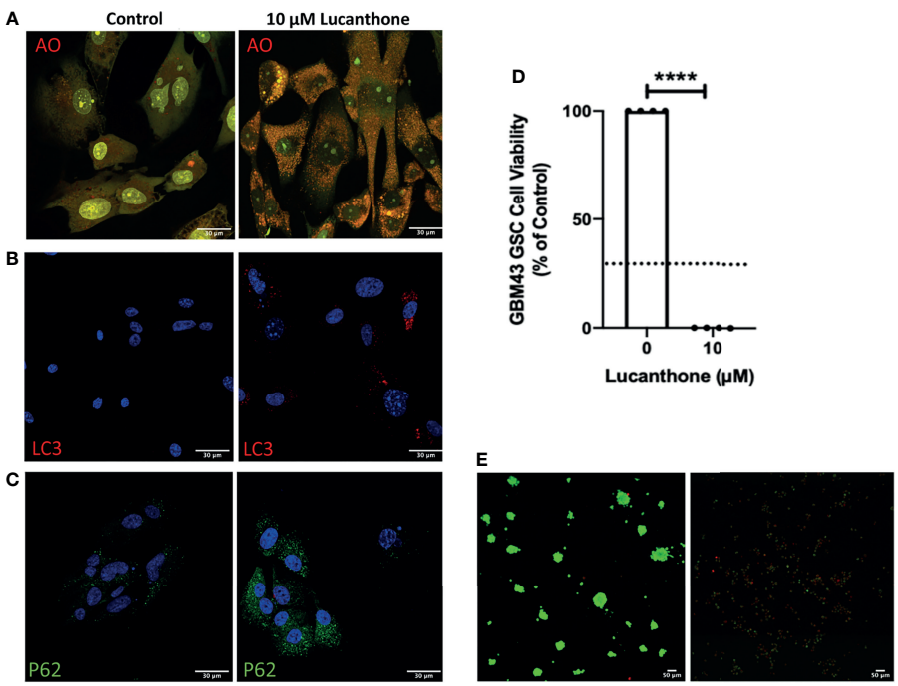

FIGURE 4 | Patient-derived glioma cells are susceptible to lucanthone. **(A)** GBM43 cells were treated with lucanthone and assessed for changes in acridine orange staining, **(B)** LC3 and **(C)** p62 levels. **(D)** GBM43 CSCs were treated with lucanthone for 5 days and then an MTT assay was performed. **(E)** GBM43 GSC were treated with media or lucanthone for 5 days, after which spheroids were visualized by Calcein-AM and Ethidium homodimer staining. Data are representative of 4 independent experiments. ****$p < 0.0001$, t-test. Dotted line represents culture viability prior to any treatment.

modest increases in LC3 and P62 (**Figures 4B, C**), suggesting that autophagy was inhibited in these cells. After enriching for stem-like qualities in these cells, treatment with 10 μM lucanthone drastically reduced cell viability (**Figure 4D**) and completely inhibited spheroid formation in these cultures (**Figure 4E**). Taken together, these data show that lucanthone can be used to inhibit autophagy in mouse and human glioma cells.

Lucanthone Slows Glioma Growth *In Vivo*

To assess translational potential, the efficacy of lucanthone was investigated in a mouse model of glioma. GLUC2 GSC were allowed to form spheroids for 10 days in culture. The spheroids were mechanically dissociated and 100,000 GLUC2 cells were implanted in the striatum of mice. Tumors were allowed to form for 7 days. Tumor cell presence was confirmed using IVIS imaging system on day 7, after which mice were segregated into two groups: one group received saline every day until day 21 while the other group received 50mg/kg lucanthone every day until day 21. The animals were imaged on days 14 and 21 (**Figure 5A**). On day 14, 5 of the 7 control mice exhibited a 2-fold increase in luminescence. In contrast, only 1 of 8 lucanthone-treated mice experienced a two-fold increase in luminescence, suggesting that lucanthone mitigated tumor growth between days 7 and 14 (chi-squared test, $p<0.05$). By day 21, control (saline)-treated glioma-bearing mice experienced a ~200-fold increase in tumor luminescence compared to day 7, whereas lucanthone-treated mice experienced only a 10-fold increase in tumor luminescence (**Figures 5B, C**). Upon histological analysis, the tumors of lucanthone-treated mice were approximately 60% smaller than those of saline-treated animals (**Figures 5D, E**). Moreover, saline-treated mice experienced cachexia (**Figure 5F**), whereas lucanthone-treated mice did not experience significant weight loss throughout the course of treatment (**Figure 5F**).

Lucanthone Reduces Olig2$^+$ Glioma Cells *In Vivo*

Standard of care therapies for glioma enrich for tumor stem-like cells, which is thought to play a role in glioma recurrence (43, 44). However, the *in vitro* data described so far suggest that lucanthone may reduce stem-like qualities of glioma cells, rather than solely target non-stem glioma cells. To that end, we interrogated how lucanthone affects glioma stem-like cells *in vivo*. The expression of stemness genes such as Olig2 and SOX2 was assessed in experimental tumors. Initial examination revealed that the density of Olig2$^+$ cells was highest near the periphery of the tumor (**Figures 6A, C, D**), though we did observe a significant number of Olig2$^+$ cells near the core as well. These data agree with previous findings that Olig2$^+$ glioma cells are present at increased numbers near the tumor periphery (50). According to the Ivy Glioblastoma Atlas, an anatomically annotated transcriptional dataset of human glioblastoma tumors (51), Olig2 expression is increased in areas of infiltrating tumor and cellular tumor, and reduced in areas of necrosis and around blood vessels (**Figure 6B**). These findings

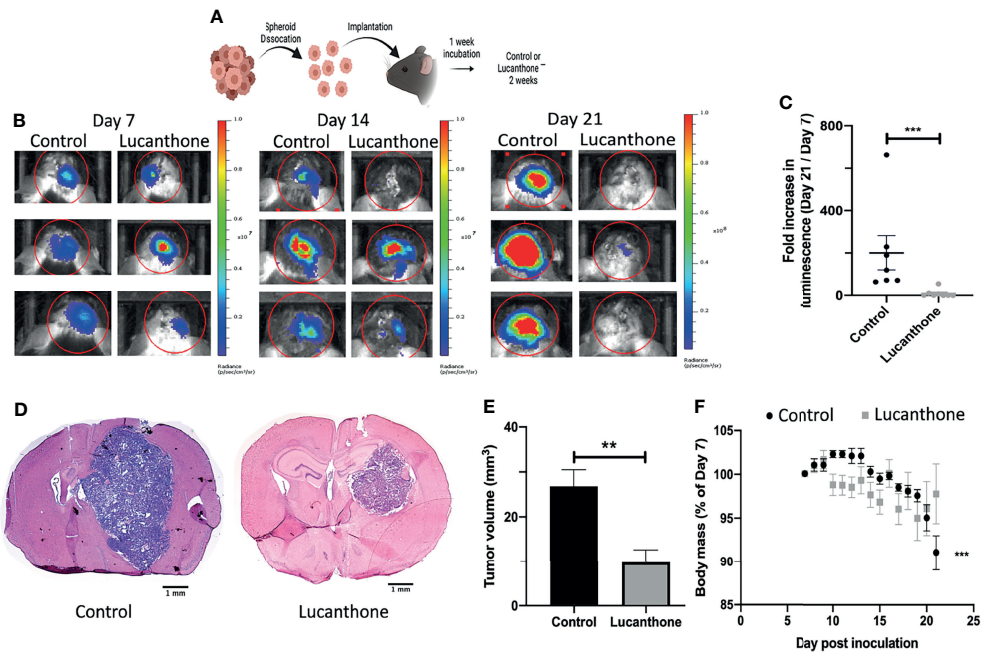

FIGURE 5 | Lucanthone mitigated the growth of dissociated GLUC2 spheroids *in vivo*. **(A)** Treatment scheme used for the study. **(B)** Representative images of *in vivo* luminescent imaging on Days 7, 14 and 21. **(C)** Fold increase in luminescence from day 7 to day 21. ***$p < 0.001$, Mann-Whitney test. **(D)** Tumor volume of control- and lucanthone-treated animals with representative images shown in **(E)** **$p < 0.01$, Mann-Whitney test. **(F)** Body mass depicted as a percentage of the start of treatment on day 7. ***$p < 0.001$, Mann-Whitney test, compared to relative body mass on day 7. Bars are mean +/- SEM, N=7-8 animals.

suggest that, with respect to spatial expression of Olig2, GLUC2 GSC may accurately reflect what is observed in the human disease.

In contrast to the abundant Olig2 expression observed in saline-treated mice, we noted a striking reduction in Olig2 positivity around the periphery of lucanthone-treated tumors and near the core of these tumors. Two-way ANOVA revealed that in both treatment conditions, Olig2 intensity is higher near the tumor border, and that lucanthone resulted in reduction of Olig2 intensity at the tumor periphery and in the tumor core (**Figure 6E**). Ki67 positivity was similar in both treatment conditions. Additionally, SOX2 expression was not significantly different between treatment conditions, which parallels the result when individual spheroids were treated with lucanthone *in vitro*. While lucanthone did not significantly modulate γH2AX *in vitro*, γH2AX positivity was modestly increased *in vivo* in lucanthone-treated tumors (**Figure S4**). Increases in γH2AX were most likely restricted to glioma cells, as most of the cells that exhibited increases in γH2AX were not staining for the GAM marker, F4/80 (**Figure S4**).

Tumor Microenvironmental Changes Induced by Lucanthone

In addition to assessing for tumor-cell specific effects of lucanthone *in vivo*, the extent to which other cell types in the tumor microenvironment may have been functionally affected by lucanthone treatment was examined. Previously, evidence has been provided that in addition to directly targeting tumor cells, chloroquine (another autophagy inhibitor) normalized the formation of blood vessels in the tumor microenvironment by directly acting on endothelial cells (52). Chloroquine augmented Notch1 signaling in endothelial cells, and as a consequence, reduced the blood vessel tortuosity and increased blood vessel patency. Because lucanthone and chloroquine exert their effects by a similar mechanism, we hypothesized that lucanthone may also modulate blood vessel formation in developing gliomas. To examine this possibility, tumor sections were stained for CD31, an endothelial cell marker. Blood vessel area, luminal area and overall blood vessel circularity were assessed. Interestingly, large blood vessels were observed in control tumors, though many of them exhibited a small luminal area. Accordingly, there were multiple tortuous blood vessels with minimal circularity. In lucanthone-treated tumors, the blood vessels were smaller, but those blood vessels typically showed an increased luminal area and the blood vessels themselves were more circular, suggesting that lucanthone may indeed be functionally affecting angiogenesis in the tumor microenvironment, potentially by acting directly on endothelial cells (**Figures 7A-D**). CD31 intensity was also diminished in lucanthone-treated tumors (**Figures 7A-D**). To examine if lucanthone acted directly on

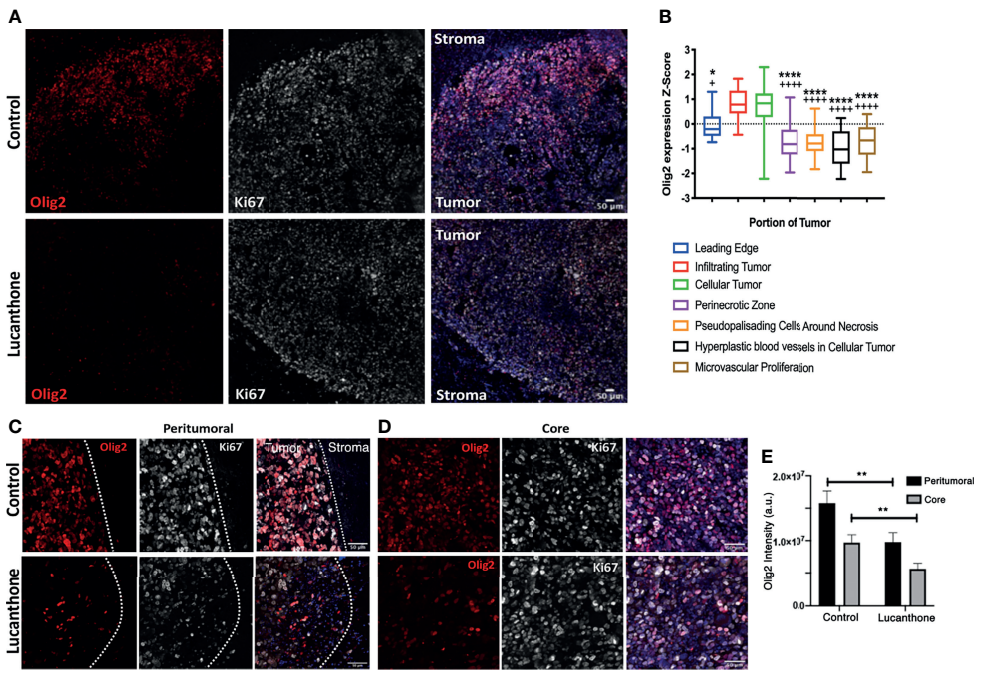

FIGURE 6 | Lucanthone reduced Olig2^{+} positivity in tumors *in vivo*. **(A)** Representative immunohistochemical images of Olig2 and Ki67 in tumors and surrounding stroma in saline- and lucanthone-treated mice. **(B)** Expression of Olig2 in different areas in human glioblastomas adapted from the Ivy Glioblastoma Atlas. ****p < 0.0001 Kruskal-Wallis test, demonstrating significant differences in Olig2 expression among various tumor areas. *p < 0.05, ****p < 0.0001 Dunn's test, compared to infiltrating tumor. $^{+}$p < 0.05, $^{++++}$p < 0.0001, Dunn's test, compared to cellular tumor. **(C, D)** Olig2 expression in tumor periphery and tumor core in both treatment conditions with intensity quantifications in **(E)** Two-way ANOVA p < 0.05. **p < 0.01, Bonferroni multiple comparison test. Bars are mean +/- SEM, N=4 animals per group.

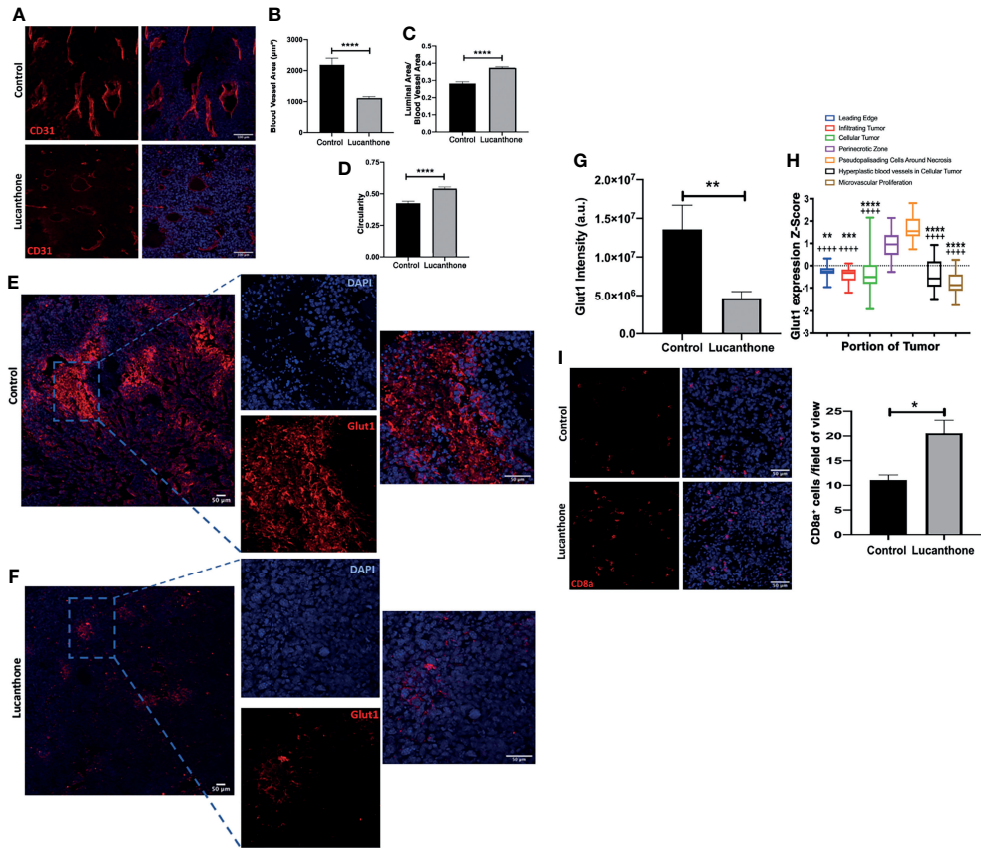

FIGURE 7 | Tumor microenvironmental changes induced by Lucanthone. **(A)** Representative images of blood vessels marked by CD31 of control- and lucanthone-treated tumors. **(B)** Blood vessel area. **(C)** Luminal area/blood vessel area. **(D)** Blood vessel circularity. ****p < 0.0001, Kolmogorov-Smirnov test. Bars are mean +/- SEM, N=4-5 animals per group. **(E, F)** Representative images of Glut1 levels in control- and lucanthone-treated tumors, respectively. **(G)** Quantification of Glut1 intensity in the tumor microenvironment. Bars are mean +/- SEM. N=5 mice **p < 0.01, t-test. **(H)** Glut1 expression in necrotic areas in clinical specimens. Data adapted from the Ivy Glioblastoma Atlas. ****p < 0.0001, Kruskal Wallis test. **p < 0.01, ***p < 0.001, ****p < 0.0001, Dunn's test, compared to perinecrotic zone, $^{++++}$p < 0.0001, Dunn's test, compared to pseudopalisading cells around necrotic areas. **(I)** $CD8a^+$ cells in the tumor microenvironment in control- and lucanthone-treated tumors. *p < 0.05, Mann-Whitney test Bars are mean +/- SEM, N=4 animals per group.

endothelial cells, we treated bEND.3 cells with lucanthone for 72 hours. Lucanthone exerted a dose-dependent effect on the cells, as at 20μM it significantly reduced bEND.3 cells viability after incubation for 72 hours (**Figure S5**).

To interrogate functional outcomes of normalized tumor vasculature, the extent to which tumors exhibited evidence of hypoxia was assessed. In addition to proteins such as Hif1a/Hif2a, there are multiple other proteins induced in areas of tumor hypoxia, including Carbonic Anhydrase IX (CAIX) and Glut1 (53). Tumors in both treatment conditions displayed little CAIX positivity. While control-treated tumors displayed remarkable Glut1 positivity, specifically in necrotic tumor areas (**Figure 7E**), lucanthone-treated tumors displayed minimal Glut1 positivity (**Figure 7F**). Quantification of Glut1 intensities is shown in **Figure 7G**. Glut1 expression in control tumors also mirrors expression patterns observed clinically (**Figure 7H**). These data illustrate that in addition to tumor-cell specific effects, lucanthone may modulate additional parameters of the tumor microenvironment. While Glut1 was reduced throughout the tumor, we observed that another glucose transporter, Glut4, was expressed throughout the tumor in saline- and lucanthone-treated conditions (**Figure S6**), suggesting that glucose transporter expression is not globally affected. As well, we observed an increase in the amount of cytotoxic T cells in the center of tumors in mice treated with lucanthone, which suggests that there may be a relief in the immunosuppressive nature fostered by gliomas after treatment (**Figure 7I**).

Targeting lysosomes is thought to exert effects on multiple cell types in the glioma microenvironment, potentially including GAM. Therefore, we assessed for differences in myeloid cell populations by staining for P2RY12 and TMEM119. In accordance with our previous work (32), P2RY12+ cells appeared mainly around the rim of gliomas in both treatment conditions (**Figure S7A**). However, we detected TMEM119+ cells throughout control-treated tumors and to a lesser extent in lucanthone-treated tumors (**Figures S7B, C**).

DISCUSSION

The pursuit of superior therapeutics for the treatment of high-grade glioma is limited in large part by the existence of the blood-brain barrier, which has evolved to exclude large and charged molecules from accumulating in the CNS at meaningful concentrations. Although substantial research has been conducted over the past several years to identify novel targets for targeting glioma without classical side effects associated with genotoxic stressors, failure of novel and repurposed drugs to reach the brain may limit their clinical use, even if they exert therapeutic effects in *in vivo* models of peripheral tumor (54). Additionally, the presence of GSC with their marked resistance to standard therapies, such as radiation and TMZ treatment, contribute to the inevitable recurrence and dismal prognosis of this disease (43, 44).

Our data show that lucanthone, a drug utilized for the treatment of schistosomal infections, targets autophagy in glioma cells, when administered systemically, and slows the growth of intracranial gliomas *in vivo*. These data, in addition to prior reports detailing its pharmacokinetic distribution in murine models (26), suggest that lucanthone may be able to enter the brain to act either as a monotherapy or work in concert with existing therapies.

Most interventions tailored to treating high-grade gliomas minimally prolong patient survival. Extensive research into the treatment resistance to TMZ, radiation, angiogenesis inhibitors, and tumor-treating fields therapy all point to the induction of cytoprotective autophagy as a means for treatment resistance and eventual disease progression (9–11, 45, 55–58). Oftentimes, chloroquine or hydroxychloroquine have been used as autophagy inhibitors in the pre-clinical setting and have been trialed in a myriad of different cancers. With specific respect to glioma, chloroquine exhibits poor penetration of the blood-brain barrier (59) and low potency (27), which may explain its lack of clinical efficacy. Lucanthone is a more potent autophagy inhibitor, and is well tolerated in the clinical setting. Additionally, our data show that at sub-cytotoxic concentrations, lucanthone may still be useful to augment the efficacy of TMZ (**Figure 2**). Future studies are warranted to detail its interaction with therapies such as radiation, angiogenesis inhibitors and tumor-treating fields *in vitro* and *in vivo*.

Lucanthone has been shown to act as a topoisomerase II poison as well as an APE1 inhibitor at high concentrations. Our results, however, advocate that its primary function would be the disruption of autophagy. After treatment, we observed extensive accumulation of autophagosomes in both KR158 and GL261 cells, also demonstrating that lucanthone exerts its effects independent of driver mutations. It is of particular interest that when glioma cells were cultured in stemness-promoting conditions, they exhibited increased sensitivity to lucanthone at doses as low as 3 μM. Since GSC are notoriously resistant to standard treatments, the development of adjuvant therapies that target a resistant sub-population may be useful in managing this disease and preventing recurrence. It is possible that lucanthone preferentially targets this sub-population by inducing lysosomal membrane permeabilization (LMP). Our data demonstrate that after lucanthone treatment, Cathepsin D is found throughout the cell, which may be due to lysosomal rupture and spilling of lysosomal contents into the cytoplasm. Prior reports have shown that GSC are susceptible to LMP (60–62), providing further evidence that interfering with lysosomal function may properly target cells spared from standard glioma treatments. We show here that lucanthone targeted glioma cells $CD133^+$ glioma cells that have acquired resistance to TMZ, recapitulating previous reports that temozolomide induces glioma cells to acquire more stem-like characteristics (47). As there are no therapies currently approved for the treatment of recurrent glioblastoma, it would be of interest to develop a robust pipeline in which drugs are tested against glioma cells with an acquired resistance to temozolomide ± ionizing radiation.

To mechanistically explain lucanthone's inhibitory effect on stemness, we probed for changes in LC3 and the stemness markers nestin, SOX2 and Olig2. We expected to observe increases in LC3 intensity in lucanthone-treated spheroid cultures. It should be noted that there were noticeable numbers of autophagosomes in control-treated spheroid cultures, strengthening the notion that GSC are more reliant on autophagy for survival at baseline conditions. However surprisingly there was a significant reduction in the number of cells in spheroids that stained positive for Olig2. In triple-negative breast tumor cells with constitutively active STAT3, the autophagy inhibitor chloroquine reduces active STAT3 (63). In glioma, inhibiting STAT3 activation by pharmacological or genetic means has been shown to reduce Olig2 levels (64), observations that may tie together lucanthone's mechanism with the observed reduction in Olig2. These *in vitro* results were recapitulated *in vivo*: Tumors derived from control-treated mice exhibited robust Olig2 intensity, especially at the tumor border. Lucanthone reduced Olig2 levels at the border and core of the tumors (**Figure 6**). $Olig2^+$ glioma cells exhibit increased resistance to standard therapies (65, 66), further encouraging the concomitant use of lucanthone with aforementioned interventions.

Gliomas exhibit dysregulated angiogenesis, which may contribute to the development of tumor hypoxia. Chloroquine was previously shown to act on endothelial cells in the melanoma tumor microenvironment. Chloroquine decreased the degradation of endothelial Notch 1, which functions to normalize tumor blood vessels and increases perfusion of the tumor. Herein, we find that the blood vessels of tumors treated with lucanthone exhibited increased circularity and reduced tortuosity. Decreasing tumor hypoxia may serve multiple functions, including increasing the delivery of systemic therapies to the whole tumor mass. In addition, eliminating pockets of hypoxia in gliomas through proper vessel perfusion could increase the efficacy of radiation therapy (67, 68) and restore the activity of cytotoxic T cells (69).

The advent of immunotherapies in the clinical setting has sparked an interest in understanding the role of both the innate and adaptive immune systems in the progression of aggressive tumor types, such as high-grade gliomas. Gliomas are comprised of multiple cell types specific to the CNS, and are heavily composed of CNS-resident microglia and blood-derived

macrophages (70). Offsetting the tumor-promoting functions of these cells may directly slow the growth of gliomas and interact favorably with TMZ (49, 71, 72) and radiation (73). Investigations in peripheral tumor types, such as melanoma and hepatocellular carcinoma, revealed that late-stage autophagy inhibition with chloroquine, which was shown to act as an inhibitor of palmitoyl-protein thioesterase 1 (Ppt1) (74–76), reverses the immunosuppressive nature of tumor-associated macrophages and thus increases the efficacy of T-cell targeted PD-1 therapies (28, 76). While we have not yet identified the direct protein target of lucanthone action that results in autophagy inhibition, we hypothesize that, due to the structural similarity between lucanthone and chloroquine, Ppt1 may be an additional interactor, along with TopII and Ape1. Given that lucanthone may augment T cell infiltration into the glioma microenvironment (**Figure 7I**), future research may examine the extent to which lucanthone modulates the pro-/anti-tumorigenic function of glioma-associated microglia and macrophages alone and in combination with targeted therapies such as PD-1 inhibitors or radiation.

Taken together, our data support the concept that lucanthone may represent a sorely needed therapy to treat (recurrent/TMZ-resistant) high-grade gliomas. It may favorably interact with existing therapies through its direct effects on glioma cells, and may enhance therapeutic efficacy by modulating the function of endothelial cells and glioma stem cells. Exploring combinations of lucanthone with DNA-damaging therapies and immune-stimulating therapies may yield synergistic effects and improve our ability to clinically manage this intractable disease.

DATA AVAILABILITY STATEMENT

The original contributions presented in the study are included in the article/**Supplementary Material**. Further inquiries can be directed to the corresponding author.

ETHICS STATEMENT

The animal study was reviewed and approved by IACUC Stony Brook University.

AUTHOR CONTRIBUTIONS

DR designed, performed and analyzed experiments and wrote drafts of the manuscript. GS, VM, and AW performed and analyzed experiments. RB provided lucanthone and assisted with experimental design and manuscript preparation. ST designed, supervised and analyzed experimental data, and edited manuscript drafts. All authors contributed to the article and approved the submitted version.

FUNDING

This work was partially supported by an NIH F30CA257677 (DR), NIH T32GM008444 (DR) and a Stony Brook University (SBU) OVPR Seed Grant and SBU Bridge funds (ST).

ACKNOWLEDGMENTS

The authors would like to thank members of the Tsirka lab for thoughtful discussions.

SUPPLEMENTARY MATERIAL

The Supplementary Material for this article can be found online at: https://www.frontiersin.org/articles/10.3389/fonc.2022.852940/full#supplementary-material

REFERENCES

1. Omuro A, DeAngelis LM. Glioblastoma and Other Malignant Gliomas: A Clinical Review. *JAMA* (2013) 310(17):1842–50. doi: 10.1001/jama.2013.280319
2. Stupp R, Taillibert S, Kanner A, Read W, Steinberg D, Lhermitte B, et al. Effect of Tumor-Treating Fields Plus Maintenance Temozolomide vs Maintenance Temozolomide Alone on Survival in Patients With Glioblastoma: A Randomized Clinical Trial. *JAMA* (2017) 318(23):2306–16. doi: 10.1001/jama.2017.18718
3. Miyauchi JT, Chen D, Choi M, Nissen JC, Shroyer KR, Djordevic S, et al. Ablation of Neuropilin 1 From Glioma-Associated Microglia and Macrophages Slows Tumor Progression. *Oncotarget* (2016) 7(9):9801–14. doi: 10.18632/oncotarget.6877
4. Miyauchi JT, Caponegro MD, Chen D, Choi MK, Li M, Tsirka SE. Deletion of Neuropilin 1 From Microglia or Bone Marrow-Derived Macrophages Slows Glioma Progression. *Cancer Res* (2018) 78(3):685–94. doi: 10.1158/0008-5472.CAN-17-1435
5. Valdor R, Garcia-Bernal D, Riquelme D, Martinez CM, Moraleda JM, Cuervo AM, et al. Glioblastoma Ablates Pericytes Antitumor Immune Function Through Aberrant Up-Regulation of Chaperone-Mediated Autophagy. *Proc Natl Acad Sci USA* (2019) 116(41):20655–65. doi: 10.1073/pnas.1903542116
6. Pyonteck SM, Akkari L, Schuhmacher AJ, Bowman RL, Sevenich L, Quail DF, et al. CSF-1R Inhibition Alters Macrophage Polarization and Blocks Glioma Progression. *Nat Med* (2013) 19(10):1264–72. doi: 10.1038/nm.3337
7. Chang AL, Miska J, Wainwright DA, Dey M, Rivetta CV, Yu D, et al. CCL2 Produced by the Glioma Microenvironment Is Essential for the Recruitment of Regulatory T Cells and Myeloid-Derived Suppressor Cells. *Cancer Res* (2016) 76(19):5671–82. doi: 10.1158/0008-5472.CAN-16-0144
8. Kanzawa T, Germano IM, Komata T, Ito H, Kondo Y, Kondo S. Role of Autophagy in Temozolomide-Induced Cytotoxicity for Malignant Glioma Cells. *Cell Death Differ* (2004) 11(4):448–57. doi: 10.1038/sj.cdd.4401359
9. Hori YS, Hosoda R, Akiyama Y, Sebori R, Wanibuchi M, Mikami T, et al. Chloroquine Potentiates Temozolomide Cytotoxicity by Inhibiting Mitochondrial Autophagy in Glioma Cells. *J Neurooncol* (2015) 122(1):11–20. doi: 10.1007/s11060-014-1686-9
10. Ye H, Chen M, Cao F, Huang H, Zhan R, Zheng X. Chloroquine, an Autophagy Inhibitor, Potentiates the Radiosensitivity of Glioma Initiating Cells by Inhibiting Autophagy and Activating Apoptosis. *BMC Neurol* (2016) 16(1):178. doi: 10.1186/s12883-016-0700-6
11. Abdul Rahim SA, Dirkse A, Oudin A, Schuster A, Bohler J, Barthelemy V, et al. Regulation of Hypoxia-Induced Autophagy in Glioblastoma Involves ATG9A. *Br J Cancer* (2017) 117(6):813–25. doi: 10.1038/bjc.2017.263
12. Xu J, Zhang J, Zhang Z, Gao Z, Qi Y, Qiu W, et al. Hypoxic Glioma-Derived Exosomes Promote M2-Like Macrophage Polarization by Enhancing

Autophagy Induction. *Cell Death Dis* (2021) 12(4):373. doi: 10.1038/s41419-021-03664-1
13. Liang X, De Vera ME, Buchser WJ, Romo de Vivar Chavez A, Loughran P, Beer Stolz D, et al. Inhibiting Systemic Autophagy During Interleukin 2 Immunotherapy Promotes Long-Term Tumor Regression. *Cancer Res* (2012) 72(11):2791–801. doi: 10.1158/0008-5472.CAN-12-0320
14. DeVorkin L, Pavey N, Carleton G, Comber A, Ho C, Lim J, et al. Autophagy Regulation of Metabolism Is Required for CD8(+) T Cell Anti-Tumor Immunity. *Cell Rep* (2019) 27(2):502–513 e505. doi: 10.1016/j.celrep.2019.03.037
15. Blair DM, Hawking F, Meeser CV, Ross WF. Miracil; Clinical Trial on Patients Infected With Schistosoma Haematobium and S. Mansoni. *Br J Pharmacol Chemother* (1949) 4(1):68–80. doi: 10.1111/j.1476-5381.1949.tb00517.x
16. Alves W. Further Studies on the Treatment of Urinary Bilharziasis With Lucanthone Hydrochloride. *Bull World Health Organ* (1958) 18(5-6):1109–11.
17. Berberian DA, Freele H, Rosi D, Dennis EW, Archer S. Schistosomicidal Activity of Lucanthone Hydrochloride, Hycanthone and Their Metabolites in Mice and Hamsters. *J Parasitol* (1967) 53(2):306–11.
18. Archer S. Recent Progress in the Chemotherapy of Schistosomiasis. *Prog Drug Res* (1974) 18:15–24. doi: 10.1007/978-3-0348-7087-0_3
19. Archer S, Miller KJ, Rej R, Periana C, Fricker L. Ring-Hydroxylated Analogues of Lucanthone as Antitumor Agents. *J Med Chem* (1982) 25(3):220–7. doi: 10.1021/jm00345a006
20. Archer S, Zayed AH, Rej R, Rugino TA. Analogues of Hycanthone and Lucanthone as Antitumor Agents. *J Med Chem* (1983) 26(9):1240–6. doi: 10.1021/jm00363a007
21. Bases RE, Mendez F. Topoisomerase Inhibition by Lucanthone, an Adjuvant in Radiation Therapy. *Int J Radiat Oncol Biol Phys* (1997) 37(5):1133–7. doi: 10.1016/s0360-3016(97)00113-2
22. Dassonneville L, Bailly C. Stimulation of Topoisomerase II-Mediated DNA Cleavage by an Indazole Analogue of Lucanthone. *Biochem Pharmacol* (1999) 58(8):1307–12. doi: 10.1016/s0006-2952(99)00221-x
23. Luo M, Kelley MR. Inhibition of the Human Apurinic/Apyrimidinic Endonuclease (APE1) Repair Activity and Sensitization of Breast Cancer Cells to DNA Alkylating Agents With Lucanthone. *Anticancer Res* (2004) 24 (4):2127–34.
24. Naidu MD, Agarwal R, Pena LA, Cunha L, Mezei M, Shen M, et al. Lucanthone and Its Derivative Hycanthone Inhibit Apurinic Endonuclease-1 (APE1) by Direct Protein Binding. *PloS One* (2011) 6(9):e23679. doi: 10.1371/journal.pone.0023679
25. Turner S, Bases R, Pearlman A, Nobler M, Kabakow B. The Adjuvant Effect of Lucanthone (Miracil D) in Clinical Radiation Therapy. *Radiology* (1975) 114 (3):729–31. doi: 10.1148/114.3.729
26. Del Rowe JD, Bello J, Mitnick R, Sood B, Filippi C, Moran J, et al. Accelerated Regression of Brain Metastases in Patients Receiving Whole Brain Radiation and the Topoisomerase II Inhibitor, Lucanthone. *Int J Radiat Oncol Biol Phys* (1999) 43(1):89–93. doi: 10.1016/s0360-3016(98)00374-5
27. Carew JS, Espitia CM, Esquivel JA2nd, Mahalingam D, Kelly KR, Reddy G, et al. Lucanthone Is a Novel Inhibitor of Autophagy That Induces Cathepsin D-Mediated Apoptosis. *J Biol Chem* (2011) 286(8):6602–13. doi: 10.1074/jbc.M110.151324
28. Chen D, Xie J, Fiskesund R, Dong W, Liang X, Lv J, et al. Chloroquine Modulates Antitumor Immune Response by Resetting Tumor-Associated Macrophages Toward M1 Phenotype. *Nat Commun* (2018) 9(1):873. doi: 10.1038/s41467-018-03225-9
29. Ausman JI, Shapiro WR, Rall DP. Studies on the Chemotherapy of Experimental Brain Tumors: Development of an Experimental Model. *Cancer Res* (1970) 30(9):2394–400.
30. Reilly KM, Loisel DA, Bronson RT, McLaughlin ME, Jacks T. Nf1;Trp53 Mutant Mice Develop Glioblastoma With Evidence of Strain-Specific Effects. *Nat Genet* (2000) 26(1):109–13. doi: 10.1038/79075
31. Yi L, Zhou C, Wang B, Chen T, Xu M, Xu L, et al. Implantation of GL261 Neurospheres Into C57/BL6 Mice: A More Reliable Syngeneic Graft Model for Research on Glioma-Initiating Cells. *Int J Oncol* (2013) 43(2):477–84. doi: 10.3892/ijo.2013.1962
32. Caponegro MD, Oh K, Madeira MM, Radin D, Sterge N, Tayyab M, et al. A Distinct Microglial Subset at the Tumor-Stroma Interface of Glioma. *Glia* (2021) 69(7):1767–81. doi: 10.1002/glia.23991
33. Zhai H, Acharya S, Gravanis I, Mehmood S, Seidman RJ, Shroyer KR, et al. Annexin A2 Promotes Glioma Cell Invasion and Tumor Progression. *J Neurosci* (2011) 31(40):14346–60. doi: 10.1523/JNEUROSCI.3299-11.2011
34. Kumar V, Radin D, Leonardi D. Probing the Oncolytic and Chemosensitizing Effects of Dihydrotanshinone in an *In Vitro* Glioblastoma Model. *Anticancer Res* (2017) 37(11):6025–30. doi: 10.21873/anticanres.12049
35. Radin DP, Purcell R, Lippa AS. Oncolytic Properties of Ampakines *In Vitro*. *Anticancer Res* (2018) 38(1):265–9. doi: 10.21873/anticanres.12217
36. Kumar V, Radin D, Leonardi D. Studies Examining the Synergy Between Dihydrotanshinone and Temozolomide Against MGMT+ Glioblastoma Cells *In Vitro*: Predicting Interactions With the Blood-Brain Barrier. *BioMed Pharmacother* (2019) 109:386–90. doi: 10.1016/j.biopha.2018.10.069
37. Xu J, Patel NH, Saleh T, Cudjoe EKJr., Alotaibi M, Wu Y, et al. Differential Radiation Sensitivity in P53 Wild-Type and P53-Deficient Tumor Cells Associated With Senescence But Not Apoptosis or (Nonprotective) Autophagy. *Radiat Res* (2018) 190(5):538–57. doi: 10.1667/RR15099.1
38. Tamamori-Adachi M, Koga A, Susa T, Fujii H, Tsuchiya M, Okinaga H, et al. DNA Damage Response Induced by Etoposide Promotes Steroidogenesis *via* GADD45A in Cultured Adrenal Cells. *Sci Rep* (2018) 8(1):9636. doi: 10.1038/s41598-018-27938-5
39. Racoma IO, Meisen WH, Wang QE, Kaur B, Wani AA. Thymoquinone Inhibits Autophagy and Induces Cathepsin-Mediated, Caspase-Independent Cell Death in Glioblastoma Cells. *PloS One* (2013) 8(9):e72882. doi: 10.1371/journal.pone.0072882
40. Ferrer-Font L, Villamanan L, Arias-Ramos N, Vilardell J, Plana M, Ruzzene M, et al. Targeting Protein Kinase CK2: Evaluating CX-4945 Potential for GL261 Glioblastoma Therapy in Immunocompetent Mice. *Pharmaceuticals (Basel)* (2017) 10(1):24. doi: 10.3390/ph10010024
41. Roberts NB, Alqazzaz A, Hwang JR, Qi X, Keegan AD, Kim AJ, et al. Oxaliplatin Disrupts Pathological Features of Glioma Cells and Associated Macrophages Independent of Apoptosis Induction. *J Neurooncol* (2018) 140 (3):497–507. doi: 10.1007/s11060-018-2979-1
42. Couturier CP, Ayyadhury S, Le PU, Nadaf J, Monlong J, Riva G, et al. Single-Cell RNA-Seq Reveals That Glioblastoma Recapitulates a Normal Neurodevelopmental Hierarchy. *Nat Commun* (20203406) 11(1):3406. doi: 10.1038/s41467-020-17186-5
43. Bao S, Wu Q, McLendon RE, Hao Y, Shi Q, Hjelmeland AB, et al. Glioma Stem Cells Promote Radioresistance by Preferential Activation of the DNA Damage Response. *Nature* (2006) 444(7120):756–60. doi: 10.1038/nature05236
44. Chen J, Li Y, Yu TS, McKay RM, Burns DK, Kernie SG, et al. A Restricted Cell Population Propagates Glioblastoma Growth After Chemotherapy. *Nature* (2012) 488(7412):522–6. doi: 10.1038/nature11287
45. Buccarelli M, Marconi M, Pacioni S, De Pascalis I, D'Alessandris QG, Martini M, et al. Inhibition of Autophagy Increases Susceptibility of Glioblastoma Stem Cells to Temozolomide by Igniting Ferroptosis. *Cell Death Dis* (2018) 9 (8):841. doi: 10.1038/s41419-018-0864-7
46. Abbas S, Singh SK, Saxena AK, Tiwari S, Sharma LK, Tiwari M. Role of Autophagy in Regulation of Glioma Stem Cells Population During Therapeutic Stress. *J Stem Cells Regener Med* (2020) 16(2):80–9. doi: 10.46582/jsrm.1602012
47. Lee G, Auffinger B, Guo D, Hasan T, Deheeger M, Tobias AL, et al. Dedifferentiation of Glioma Cells to Glioma Stem-Like Cells By Therapeutic Stress-Induced HIF Signaling in the Recurrent GBM Model. *Mol Cancer Ther* (2016) 15(12):3064–76. doi: 10.1158/1535-7163.MCT-15-0675
48. Azambuja JH, da Silveira EF, de Carvalho TR, Oliveira PS, Pacheco S, do Couto CT, et al. Glioma Sensitive or Chemoresistant to Temozolomide Differentially Modulate Macrophage Protumor Activities. *Biochim Biophys Acta Gen Subj* (2017) 1861(11 Pt A):2652–62. doi: 10.1016/j.bbagen.2017.07.007
49. Li J, Sun Y, Sun X, Zhao X, Ma Y, Wang Y, et al. AEG-1 Silencing Attenuates M2-Polarization of Glioma-Associated Microglia/Macrophages and Sensitizes Glioma Cells to Temozolomide. *Sci Rep* (2021) 11(1):17348. doi: 10.1038/s41598-021-96647-3

50. Bastola S, Pavlyukov MS, Yamashita D, Ghosh S, Cho H, Kagaya N, et al. Glioma-Initiating Cells at Tumor Edge Gain Signals From Tumor Core Cells to Promote Their Malignancy. *Nat Commun* (2020) 11(1):4660. doi: 10.1038/s41467-020-18189-y
51. Puchalski RB, Shah N, Miller J, Dalley R, Nomura SR, Yoon JG, et al. An Anatomic Transcriptional Atlas of Human Glioblastoma. *Science* (2018) 360 (6389):660–3. doi: 10.1126/science.aaf2666
52. Maes H, Kuchnio A, Peric A, Moens S, Nys K, De Bock K, et al. Tumor Vessel Normalization by Chloroquine Independent of Autophagy. *Cancer Cell* (2014) 26(2):190–206. doi: 10.1016/j.ccr.2014.06.025
53. Li Z, Bao S, Wu Q, Wang H, Eyler C, Sathornsumetee S, et al. Hypoxia-Inducible Factors Regulate Tumorigenic Capacity of Glioma Stem Cells. *Cancer Cell* (2009) 15(6):501–13. doi: 10.1016/j.ccr.2009.03.018
54. Mulkearns-Hubert EE, Torre-Healy LA, Silver DJ, Eurich JT, Bayik D, Serbinowski E, et al. Development of a Cx46 Targeting Strategy for Cancer Stem Cells. *Cell Rep* (2019) 27(4):1062–1072 e1065. doi: 10.1016/j.celrep.2019.03.079
55. Yan Y, Xu Z, Dai S, Qian L, Sun L, Gong Z. Targeting Autophagy to Sensitive Glioma to Temozolomide Treatment. *J Exp Clin Cancer Res* (2016) 35:23. doi: 10.1186/s13046-016-0303-5
56. Shteingauz A, Porat Y, Voloshin T, Schneiderman RS, Munster M, Zeevi E, et al. AMPK-Dependent Autophagy Upregulation Serves as a Survival Mechanism in Response to Tumor Treating Fields (TTFields). *Cell Death Dis* (2018) 9(11):1074. doi: 10.1038/s41419-018-1085-9
57. Kim EH, Jo Y, Sai S, Park MJ, Kim JY, Kim JS, et al. Tumor-Treating Fields Induce Autophagy by Blocking the Akt2/miR29b Axis in Glioblastoma Cells. *Oncogene* (2019) 38(39):6630–46. doi: 10.1038/s41388-019-0882-7
58. Shi J, Dong X, Li H, Wang H, Jiang Q, Liu L, et al. Nicardipine Sensitizes Temozolomide by Inhibiting Autophagy and Promoting Cell Apoptosis in Glioma Stem Cells. *Aging (Albany NY)* (2021) 13(5):6820–31. doi: 10.18632/aging.202539
59. Roy L, Poirier M, Fortin D. P11.39 Chloroquine as an Anti-Glioblastoma Therapeutic: Repurposing of an Old Drug. *Neuro-Oncology* (2019) 21 (Supplement_3):iii51–2. doi: 10.1093/neuonc/noz126.185
60. Le Joncour V, Filppu P, Hyvonen M, Holopainen M, Turunen SP, Sihto H, et al. Vulnerability of Invasive Glioblastoma Cells to Lysosomal Membrane Destabilization. *EMBO Mol Med* (2019) 11(6):e9034. doi: 10.15252/emmm.201809034
61. Jacobs KA, Andre-Gregoire G, Maghe C, Thys A, Li Y, Harford-Wright E, et al. Paracaspase MALT1 Regulates Glioma Cell Survival by Controlling Endo-Lysosome Homeostasis. *EMBO J* (2020) 39(1):e102030. doi: 10.15252/embj.2019102030
62. Zhou W, Guo Y, Zhang X, Jiang Z. Lys05 Induces Lysosomal Membrane Permeabilization and Increases Radiosensitivity in Glioblastoma. *J Cell Biochem* (2020) 121(2):2027–37. doi: 10.1002/jcb.29437
63. Maycotte P, Gearheart CM, Barnard R, Aryal S, Mulcahy Levy JM, Fosmire SP, et al. STAT3-Mediated Autophagy Dependence Identifies Subtypes of Breast Cancer Where Autophagy Inhibition Can Be Efficacious. *Cancer Res* (2014) 74(9):2579–90. doi: 10.1158/0008-5472.CAN-13-3470
64. Guryanova OA, Wu Q, Cheng L, Lathia JD, Huang Z, Yang J, et al. Nonreceptor Tyrosine Kinase BMX Maintains Self-Renewal and Tumorigenic Potential of Glioblastoma Stem Cells by Activating STAT3. *Cancer Cell* (2011) 19(4):498–511. doi: 10.1016/j.ccr.2011.03.004
65. Mehta S, Huillard E, Kesari S, Maire CL, Golebiowski D, Harrington EP, et al. The Central Nervous System-Restricted Transcription Factor Olig2 Opposes P53 Responses to Genotoxic Damage in Neural Progenitors and Malignant Glioma. *Cancer Cell* (2011) 19(3):359–71. doi: 10.1016/j.ccr.2011.01.035
66. Liu H, Weng W, Guo R, Zhou J, Xue J, Zhong S, et al. Olig2 SUMOylation Protects Against Genotoxic Damage Response by Antagonizing P53 Gene Targeting. *Cell Death Differ* (2020) 27(11):3146–61. doi: 10.1038/s41418-020-0569-1
67. Dings RP, Loren M, Heun H, McNiel E, Griffioen AW, Mayo KH, et al. Scheduling of Radiation With Angiogenesis Inhibitors Anginex and Avastin Improves Therapeutic Outcome *via* Vessel Normalization. *Clin Cancer Res* (2007) 13(11):3395–402. doi: 10.1158/1078-0432.CCR-06-2441
68. Sheehan J, Cifarelli CP, Dassoulas K, Olson C, Rainey J, Han S. Trans-Sodium Crocetinate Enhancing Survival and Glioma Response on Magnetic Resonance Imaging to Radiation and Temozolomide. *J Neurosurg* (2010) 113(2):234–9. doi: 10.3171/2009.11.JNS091314
69. Noman MZ, Janji B, Kaminska B, Van Moer K, Pierson S, Przanowski P, et al. Blocking Hypoxia-Induced Autophagy in Tumors Restores Cytotoxic T-Cell Activity and Promotes Regression. *Cancer Res* (2011) 71(18):5976–86. doi: 10.1158/0008-5472.CAN-11-1094
70. Radin DP, Tsirka SE. Interactions Between Tumor Cells, Neurons, and Microglia in the Glioma Microenvironment. *Int J Mol Sci* (2020) 21 (22):8476. doi: 10.3390/ijms21228476
71. Chuang HY, Su YK, Liu HW, Chen CH, Chiu SC, Cho DY, et al. Preclinical Evidence of STAT3 Inhibitor Pacritinib Overcoming Temozolomide Resistance *via* Downregulating miR-21-Enriched Exosomes From M2 Glioblastoma-Associated Macrophages. *J Clin Med* (2019) 8(7):959. doi: 10.3390/jcm8070959
72. Li J, Kaneda MM, Ma J, Li M, Shepard RM, Patel K, et al. PI3Kgamma Inhibition Suppresses Microglia/TAM Accumulation in Glioblastoma Microenvironment to Promote Exceptional Temozolomide Response. *Proc Natl Acad Sci USA* (2021) 118(16):e2009290118. doi: 10.1073/pnas.2009290118
73. Akkari L, Bowman RL, Tessier J, Klemm F, Handgraaf SM, de Groot M, et al. Dynamic Changes in Glioma Macrophage Populations After Radiotherapy Reveal CSF-1R Inhibition as a Strategy to Overcome Resistance. *Sci Transl Med* (2020) 12(552):eaaw7843 . doi: 10.1126/scitranslmed.aaw7843
74. Nicastri MC, Rebecca VW, Amaravadi RK, Winkler JD. Dimeric Quinacrines as Chemical Tools to Identify PPT1, a New Regulator of Autophagy in Cancer Cells. *Mol Cell Oncol* (2018) 5(1):e1395504. doi: 10.1080/23723556.2017.1395504
75. Rebecca VW, Nicastri MC, Fennelly C, Chude CI, Barber-Rotenberg JS, Ronghe A, et al. PPT1 Promotes Tumor Growth and Is the Molecular Target of Chloroquine Derivatives in Cancer. *Cancer Discov* (2019) 9 (2):220–9. doi: 10.1158/2159-8290.CD-18-0706
76. Sharma G, Ojha R, Noguera-Ortega E, Rebecca VW, Attanasio J, Liu S, et al. PPT1 Inhibition Enhances the Antitumor Activity of Anti-PD-1 Antibody in Melanoma. *JCI Insight* (2020) 5(17):e133225. doi: 10.1172/jci.insight.133225

Conflict of Interest: The authors declare that the research was conducted in the absence of any commercial or financial relationships that could be construed as a potential conflict of interest.

frontiers | Frontiers in Oncology

ORIGINAL RESEARCH
published: 09 June 2022
doi: 10.3389/fonc.2022.878849

High Expression Levels of SIGLEC9 Indicate Poor Outcomes of Glioma and Correlate With Immune Cell Infiltration

Heng Xu[1†], Yanyan Feng[2†], Weijia Kong[3†], Hesong Wang[1], Yuyin Feng[1], Jianhua Zhen[1], Lichun Tian[4*] and Kai Yuan[1*]*

[1] School of Life Sciences, Beijing University of Chinese Medicine, Beijing, China, [2] Shenzhen Bao'an Traditional Chinese Medicine Hospital, Guangzhou University of Chinese Medicine, Shenzhen, China, [3] Beijing Hospital of Traditional Chinese Medicine Clinical Medical College, Beijing University of Chinese Medicine, Beijing, China, [4] Beijing Research Institute of Chinese Medicine, Beijing University of Chinese Medicine, Beijing, China

OPEN ACCESS

Edited by:
Haotian Zhao,
New York Institute of Technology,
United States

Reviewed by:
Jin Wang,
Jinan University, China
Yu-Chan Chang,
National Yang Ming Chiao Tung University, Taiwan

***Correspondence:**
Jianhua Zhen
jianhuazhen@bucm.edu.cn
Lichun Tian
tianlch@bucm.edu.cn
Kai Yuan
yuankai@bucm.edu.cn

[†]These authors have contributed equally to this work

Specialty section:
This article was submitted to Neuro-Oncology and Neurosurgical Oncology, a section of the journal Frontiers in Oncology

Received: 18 February 2022
Accepted: 26 April 2022
Published: 09 June 2022

Citation:
Xu H, Feng Y, Kong W, Wang H, Feng Y, Zhen J, Tian L and Yuan K (2022) High Expression Levels of SIGLEC9 Indicate Poor Outcomes of Glioma and Correlate With Immune Cell Infiltration. Front. Oncol. 12:878849. doi: 10.3389/fonc.2022.878849

Objective: This study aimed to investigate the diagnostic value and underlying mechanisms of sialic acid-binding Ig-like lectin 9 (SIGLEC9) in gliomas.

Patients and Methods: The Cancer Genome Atlas (TCGA) and the Chinese Glioma Genome Atlas (CGGA) databases were used to analyze the association of *SIGLEC9* expression levels with tumor stages and survival probability. Immunohistochemical staining of SIGLEC9 and survival analysis were performed in 177 glioma patients. Furthermore, related mechanisms were discovered about SIGLEC9 in glioma tumorigenesis, and we reveal how SIGLEC9 functions in macrophages through single-cell analysis.

Results: TCGA and CGGA databases indicated that patients with high *SIGLEC9* expression manifested a significantly shorter survival probability than those with low *SIGLEC9* expression. *SIGLEC9* was upregulated significantly in malignant pathological types, such as grade III, grade IV, mesenchymal subtype, and isocitrate dehydrogenase wild-type gliomas. The immunohistochemical staining of tissue sections from 177 glioma patients showed that high-SIGLEC9-expression patients manifested a significantly shorter survival probability than low-SIGLEC9-expression patients with age ≧60 years, grade IV, glioblastoma multiforme, alpha thalassemia/intellectual disability syndrome X-linked loss, and without radiotherapy or chemotherapy. Furthermore, the *SIGLEC9* expression level was positively correlated with myeloid-derived suppressor cell infiltration and neutrophil activation. The *SIGLEC9* expression was also positively correlated with major immune checkpoints, such as *LAIR1*, *HAVCR2*, *CD86*, and *LGALS9*. Through single-cell analysis, we found that the *SIGLEC9* gene is related to the ability of macrophages to process antigens and the proliferation of macrophages.

Conclusion: These findings suggested that SIGLEC9 is a diagnostic marker of poor outcomes in glioma and might serve as a potential immunotherapy target for glioma patients in the future.

Keywords: glioma, SIGLEC9, diagnostic marker, mechanism, therapeutic target

INTRODUCTION

Gliomas are primary intra-axial brain tumors representing 80% of all malignant brain tumors (1). Patients with glioma often suffer from vomiting, headaches, seizure, and visual loss. The causes of gliomas include hereditary disorders, radiation, and inherited polymorphisms of DNA repair genes (2). Inherited polymorphisms of DNA repair genes might increase the risk of gliomas (3). DNA damage accumulation would occur when DNA repair gene expression is decreased, which might increase the frequencies of mutation. The classification of gliomas depends on tumor grade, cell type, and tumor location (4). Gliomas could be categorized from World Health Organization (WHO) grade I to WHO grade IV. WHO grade I represents the least advanced disease with the best prognosis, while WHO grade IV represents the most advanced disease with the worst prognosis. In addition, the classification of gliomas depends on histological features, including classical subtype (CL), proneural subtype (PN), mesenchymal subtype (ME), *etc.* (5). The treatment of gliomas is a combined method of radiation, surgery, and chemotherapy (6). The prognosis of gliomas varies from different grades and subtypes. Low-grade glioma patients have better 5- and 10-year survival rates. While high-grade glioma patients have poor survival rates, the median overall survival of glioblastoma multiforme is approximately 15 months (7). Patients with isocitrate dehydrogenase (IDH) 1 or 2 mutated gliomas have a higher survival rate than patients with IDH wild-type gliomas (8).

In recent years, immune checkpoint modulators (ICIs) have been found to be important means of treating cancer, and ICIs targeting CTLA-4 or PD-1/PD-L1 have been developed (9, 10). Sialic acid-binding Ig-like lectins (SIGLECs) act as inhibitory receptors on innate and adaptive immune cells to suppress immune responses, and SIGLEC9 on neutrophils and SIGLEC7 on NK cells can potentially suppress antitumor immune responses (11). SIGLEC9 can be targeted to enhance therapeutic antitumor immunity *in vivo* (12). SIGLEC9 is a putative adhesion molecule mediating sialic-acid-dependent binding to cells (11). It contains a cytoplasmic motif referring to the immunoreceptor tyrosine-based inhibitor motif regulating cellular response. The related pathways of SIGLEC9 are class I MHC-mediated antigen processing and presentation, which is an innate immune response. SIGLEC9 is mainly expressed in peripheral blood leukocytes, such as monocytes, neutrophils, and $CD56^+$ NK cells. In mice, the functionally equivalent paralog of SIGLEC9 is Siglec-E. In the inflammatory environment, SIGLEC9 in neutrophils and monocytes could induce apoptosis after generating reactive oxygen species. Previous studies have explored the correlation between SIGLEC9 and cancers. Haas *et al.* found that SIGLEC9 modulates memory $CD8^+$ T cells to congregate in the tumor microenvironment of melanoma (13). Stanczak *et al.* discovered that SIGLEC9 was upregulated in the tumor-infiltrating T cells in the tumor microenvironment of colorectal cancer, ovarian cancer, and non-small cell lung cancer (14). A high SIGLEC9 expression in T cells is correlated with a decreased survival prognosis of non-small cell lung cancer patients. Beatson *et al.* demonstrated that mucin MUC1 could regulate the tumor immunological microenvironment that follows the engagement of SIGLEC9 (15). Although the functions of SIGLEC9 were explored in some types of cancer, the diagnosis value and underlying mechanism of SIGLEC9 in glioblastoma multiforme (GBM) have not been investigated. Therefore, we will reveal the effect of SIGLEC9 as an immune checkpoint on the immune microenvironment of glioma and provide a theoretical basis for the further development of immunotherapeutic agents for glioma.

In this study, we assessed the correlation between the clinical characteristics and SIGLEC9 expression in glioma patients. The Cancer Genome Atlas (TCGA) and Chinese Glioma Genome Atlas (CGGA) databases were used to compare the expression of *SIGLEC9*. Then, we measured the expression of SIGLEC9 with immunohistochemical staining on 177 patients with gliomas to validate the results. Gene Set Enrichment Analysis (GSEA) was conducted to reveal the biological functions of SIGLEC9 in gliomas. Lastly, functional enrichment analysis was performed to discover the role of SIGLEC9 in gliomas.

METHODS

Patients and Samples

A total of 177 patients with gliomas undergoing surgery in Sanbo Brain Hospital Capital Medical University were included in this study. The diagnosis of gliomas for every patient was authenticated with laboratory examination, clinical features, and macroscopic and histological examinations. The characteristics of glioma samples, including grade, subtype, and IDH expression, were estimated by two pathologists specializing in brain tumor disorders. The follow-up information of 177 glioma patients was acquired. The endpoint of this study was defined as overall survival (OS), which is the period from the surgery date to death date without a specified cause of death. OS is a useful index to estimate the prognosis of tumor patients. The follow-up period of all patients ended in April 2019. The informed consent of biomedical research about tissue usage has been signed by every patient with glioma, with the project approved by the ethics committee of Sanbo Brain Hospital Capital Medical University (no. SBNK-2018-003-01). We ranked the 177 patients from low to high, and then we identified the first 25 patients as belonging to the low-SIGLEC9-expression group and the last 26 patients as belonging to the high-SIGLEC9-expression group based on the significant difference in survival between the high-SIGLEC9-expression group and the low-SIGLEC9-expression group. The remaining patients were categorized into the medium-SIGLEC9-expression group. The clinical data of 177 patients are shown in **Supplementary Table S1**.

Immunohistochemical Staining

The protein levels of SIGLEC9 were examined by immunohistochemical staining. Formalin-fixed paraffin-embedded slides of glioma were baked for 4 h. Then, the slides were deparaffinated with dimethylbenzene and dehydrated with

gradient ethanol. Furthermore, the slides were subjected to antigen retrieval with boiled citrate buffer, cyclooxygenase block with 3% hydrogen peroxide, and nonspecific antigen block with 10% goat serum. The primary antibody rabbit anti-human SIGLEC9 (Abcam, Cambridge, MA, USA) was diluted to 1:100 and incubated at 4°C overnight. On day 2, the second antibody, horseradish peroxidase-labeled goat anti-rabbit or mouse, was incubated for 1 h. Then, the slide was stained with 3′-diaminobenzidine reagent and counterstained by hematoxylin. Lastly, the total area of positive expression of SIGLEC9 was evaluated with ImageJ software by two researchers in the list of authors. The best cutoff value was determined by the survminer package of R.

Bioinformatic Analysis of *SIGLEC9* Expression

The normalized values of fragments per kilobase per million mapped reads of gliomas were obtained from TCGA dataset (https://portal.gdc.cancer.gov) before April 2019. The batch effect of low-grade glioma (LGG) and GBM was removed by "sva" package. The normalized datasets of RNA-Seq were conducted as input. TCGA is a useful dataset to catalog genetic mutations responsible for cancer with the method of bioinformatics and genome sequence. The comparison of SIGLEC9 expressions in normal tissue and glioma was conducted in GEPIA website (http://gepia.cancer-pku.cn/). GEPIA is a web server about cancer and normal gene expression. In addition, we downloaded the mRNA-seq data from the CGGA dataset before October 2019. CGGA is a powerful dataset that stores the data of about more than 2,000 samples from Chinese brain tumor patients. The data of CGGA included mRNA sequencing, mRNA microarray, microRNA microarray, whole-exome sequencing, and the matched patient clinical data. The expression of *SIGLEC9* was compared between different grades and subtypes of gliomas. SPSS20.0 was used to evaluate the statistical significance between different groups.

Gene Set Enrichment Analysis

In this study, we conducted GSEA to investigate the underlying mechanisms of SIGLEC9 in gliomas. GSEA is a method that provides insights into discovering the biological mechanisms of the genes. The correlation between leukocyte infiltration and *SIGLEC9* expression was conducted by single-sample GSEA (ssGSEA). The correlation between immune-related gene sets and *SIGLEC9* was also conducted by ssGSEA. The ssGSEA is the extension of GSEA to measure the separate enrichment scores of each gene set. The ssGSEA could transform to the profile of gene set enrichment, which allows featuring of the cell state of biological process activities and pathways. The correlation between immune-related gene sets and *SIGLEC9* was visualized in the bioinformatics website (https://www.immport.org/).

Functional Enrichment Analysis

In this study, we calculated the correlation of genes and *SIGLEC9* by Spearman method. We filtered genes with correlation >0.6. Gene Ontology (GO) analysis was used to conduct the functional enrichment analysis. The Database for Annotation, "clusterProfiler", and "enrichplot" packages were used to analyze and visualize the results. GO analysis is a useful tool to investigate the biological processes, cellular components, and molecular functions. We selected signaling pathways with false discovery rate (FDR) <0.01 and count >10 from the GO and Kyoto Encyclopedia of Genes and Genomes (KEGG) enrichment results.

Single-Cell Gene Analysis

The single-cell sequencing data of tumor tissues and adjacent tissues of glioma were downloaded from the GSE162631 dataset of the GEO database. We selected 4 tumor samples and 1 paracancerous tissue sample for single-cell transcriptome analysis. Raw gene expression matrices were imported and processed using the Seurat R package. The cells and genes with poor quality were filtered out. The genes expressed in at least 3 cells and high-quality cells with more than 200 genes and less than 5,000 genes were selected for the subsequent analysis. Low-quality cells containing more than 10% mitochondrial genes were excluded. Principal component analysis (PCA) with "FindNeighbors" and "FindClusters" functions was used to perform Uniform Manifold Approximation and Projection (UMAP) to screen the significant top 20 principal components. Then, we clustered the cells with a resolution of dim = 30 and visualized the clustering results using a UMAP scatterplot. Then, the different clusters were annotated to cell types based on the typical marker genes of the cells. Furthermore, we analyzed the expression of SIGLEC9 genes in tumor tissue and adjacent tissue. The ggplot2 package was used to identify the ratio of cells in tumors with adjacent tissue. We re-analyzed the macrophages separately to assess the subtypes of specific cell populations. We used Seurat standard procedures, including PCA dimensionality reduction and tSNE cell construction of clusters to extract cell subsets. Finally, we divided the macrophages into the high-SIGLEC9-expression group and the low-SIGLEC9-expression group according to the median of SIGLEC9 expression. The regulatory role of SIGLEC9 in macrophages was further analyzed.

Statistical Analysis

Statistical analysis was conducted by *t*-test and Spearman χ^2 test. Kaplan–Meier analysis was used to evaluate the survival rates. Cox proportional hazard model analysis was conducted to measure the hazard ratio and 95% confidence interval associated with *SIGLEC9* expression. Statistical significance was considered when P <0.05.

RESULTS

The Expression of *SIGLEC9* in Gliomas With TCGA and CGGA Databases

We investigated the *SIGLEC9* expression in different grades and subtypes of glioma patients with TCGA and CGGA databases. In TCGA database, SIGLEC9 expression was higher in tumor tissue than in adjacent normal tissue in LGG and GBM (**Figure 1A**). The expression of *SIGLEC9* in grade III and grade IV glioma patients was higher than in grade II glioma patients (**Figure 1B**). As for the four subtypes, including classic, mesenchymal, and proneural subtypes, *SIGLEC9* expression was higher in the

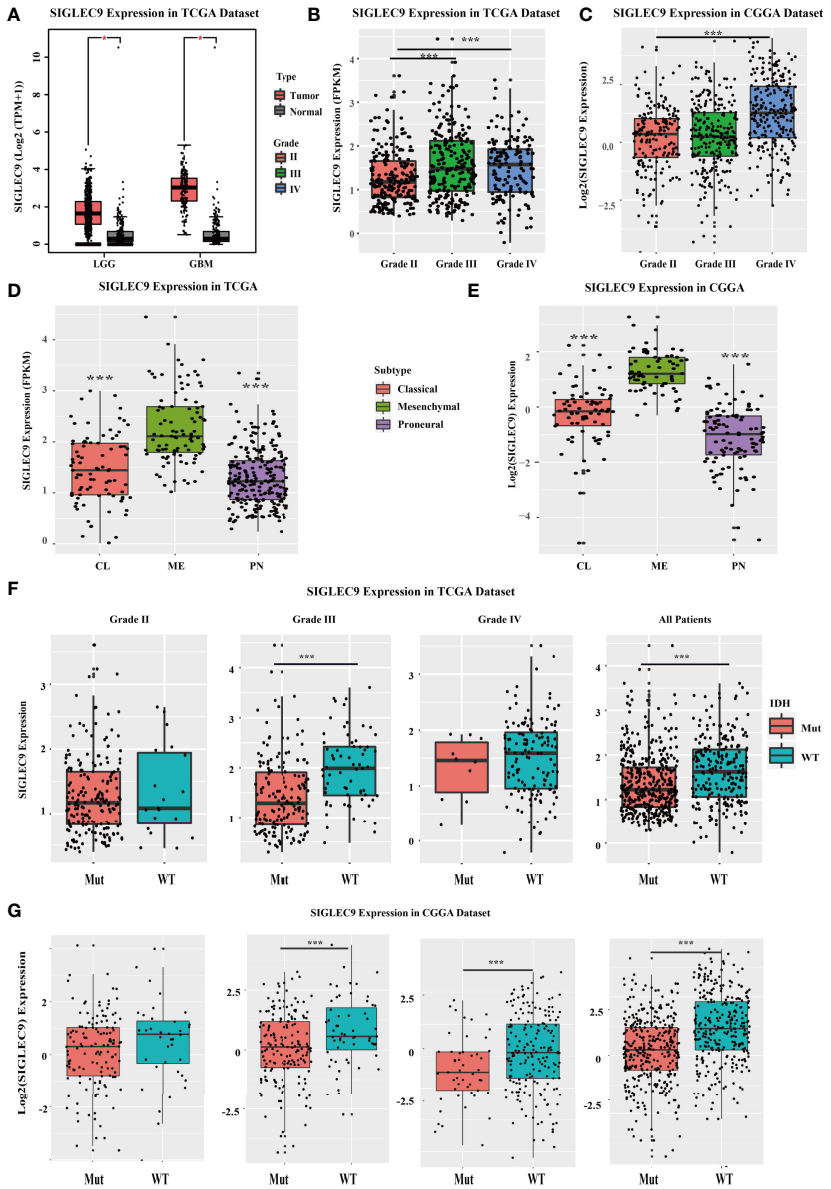

FIGURE 1 | The SIGLEC9 expression in different grades and subtypes with The Cancer Genome Atlas (TCGA) and the Chinese Glioma Genome Atlas (CGGA) databases. **(A)** The expression of SIGLEC9 in low-grade glioma (LGG) and glioblastoma multiforme (GBM) with TCGA database. In LGG patients, SIGLEC9 expression was higher in tumor tissue than in adjacent normal tissue (*<0.05). In GBM patients, SIGLEC9 expression was higher in tumor tissue than in adjacent normal tissue (*<0.05). **(B)** The SIGLEC9 expression in grade III patients was higher than in grade II patients with TCGA database (***<0.001). The SIGLEC9 expression in grade IV patients was higher than in grade II patients with TCGA database (***<0.001). **(C)** The SIGLEC9 expression in grade IV patients was higher than in grade II patients with CGGA database (***<0.001). **(D)** The SIGLEC9 expression in the mesenchymal subtype was higher than in the classic and proneural subtypes with TCGA database (***<0.001). **(E)** The SIGLEC9 expression in the mesenchymal subtype was higher than in the classic and proneural subtypes with CGGA database (***<0.001). **(F)** In grade II glioma patients with TCGA database, SIGLEC9 expression was higher in isocitrate dehydrogenase (IDH) wild-type patients than in IDH mutated patients (***<0.001). In all glioma patients with TCGA database, SIGLEC9 expression was higher in IDH wild-type patients than in IDH mutated patients (***<0.001). **(G)** In grade II and III glioma patients with CGGA database, SIGLEC9 expression was higher in IDH wild-type patients than in IDH mutated patients (***<0.001). In all glioma patients with CGGA database, SIGLEC9 expression was higher in IDH wild-type patients than in IDH mutated patients (***<0.001).

mesenchymal subtype than in the other two subtypes of gliomas in TCGA database (**Figure 1D**). IDH is regarded as an index for the survival prognosis of gliomas. The results of the TCGA database showed that *SIGLEC9* expression was higher in IDH wild-type glioma patients than in IDH mutated glioma patients (**Figure 1F**). The expression patterns of *SIGLEC9* in different grades and subtypes of glioma patients from the CGGA database were similar to that of TCGA database. In the CGGA database,

the expression of *SIGLEC9* in grade IV glioma patients was higher than in grade II patients (**Figure 1C**). The *SIGLEC9* level was higher in the mesenchymal subtype than in the other two subtypes of gliomas (**Figure 1E**). The *SIGLEC9* expression was higher in IDH wild-type gliomas than in IDH mutated gliomas (**Figure 1G**).

Furthermore, we used TCGA and CGGA databases to analyze the survival probability of glioma patients with different expression levels of *SIGLEC9*. In TCGA dataset, patients with a higher *SIGLEC9* expression had less survival probability than patients with a lower *SIGLEC9* expression ($P < 0.001$) (**Figure 2A**). In the CGGA dataset, patients with a higher *SIGLEC9* expression also had less survival probability than patients with a lower *SIGLEC9* expression ($P < 0.001$) (**Figure 2B**). Furthermore, Survival analysis in different subgroups with glioma between the high-SIGLEC9 and low-SIGLEC9 groups was performed, the result was shown in **Figure S1**.

The Expression of SIGLEC9 in Glioma Patients With Immunohistochemical Staining

We analyzed the expression of SIGLEC9 in 177 glioma patients with immunohistochemical staining. Based on the level of SIGLEC9 expression, the glioma patients were divided into three groups, and the clinical data of 177 patients are shown in **Supplementary Table S1**. As shown in **Figure 3A**, patients with a high SIGLEC9 expression manifested a significantly shorter survival probability than those patients with a low SIGLEC9 expression ($P = 0.019$). Then, we analyzed the relationship between clinical characteristics and SIGLEC9 expression in glioma patients. We found that, in glioma patients with age ≧60 years, high-SIGLEC9-expression patients presented a shorter survival probability than low-SIGLEC9-expression patients ($P = 0.007$). Similar phenomena were also observed in patients with grade IV or glioblastoma ($P = 0.032$), patients with ATRX loss glioma ($P = 0.002$), patients without radiotherapy ($P = 0.015$), or patients without chemotherapy ($P = 0.040$). The detailed information on the clinical forest is listed in **Figure 3B**. The immunohistochemical map of glioma patients is shown in **Figure 3C**, and it can be seen intuitively that there are apparent differences in the expression of SIGLEC9 between glioma patients.

The Correlation Between Immune Microenvironment and *SIGLEC9* Expression in Gliomas

In this study, we investigated the correlation between the immune microenvironment and the SIGLEC9 levels in gliomas. Firstly, we analyzed the correlation between immune cell infiltration and *SIGLEC9* expression in gliomas with TCGA database. As shown in **Figure 4A**, the *SIGLEC9* expression was mostly positively correlated with myeloid-derived suppressor cell (MDSC) infiltration (Cor = 0.84, $P < 2.2e{-}16$), effector memory $CD8^+$ T cell infiltration (Cor = 0.71, $P < 2.2e{-}16$), T follicular helper cell infiltration (Cor = 0.67, $P < 2.2e{-}16$), regulatory T cell infiltration (Cor = 0.63, $P < 2.2e{-}16$), mast cell infiltration (Cor = 0.58, $P < 2.2e{-}16$), and neutrophil infiltration (Cor = 0.27, $P < 9.6e{-}13$) in gliomas. The CGGA database was also used to explore the correlation between immune status and *SIGLEC9* expression, and similar results were observed. The *SIGLEC9* expression was positively correlated with MDSC infiltration (Cor = 0.88, $P < 2.2e{-}16$), effector memory $CD8^+$ T cell infiltration (Cor = 0.79, $P < 2.2e{-}16$), macrophage infiltration (Cor = 0.79, $P < 2.2e{-}16$), regulatory T cell infiltration (Cor = 0.77, $P < 2.2e{-}16$), natural killer T cell infiltration (Cor = 0.77, $P < 2.2e{-}16$), and neutrophil infiltration (Cor = 0.55, $P < 2.2e{-}16$) (**Figure 4B**).

As shown in **Figure 4C**, glioma patients with high SIGLEC9 expression have significantly enhanced infiltration of immune cells, such as T cells, NK cells, neutrophils, aDC, B cells, DC cells, iDC cells, macrophages, mast cells, Th1, Th2, Th17, and so on. The proportion of these immune cells infiltrated was significantly reduced (pDC and Treg). We also calculated the difference in

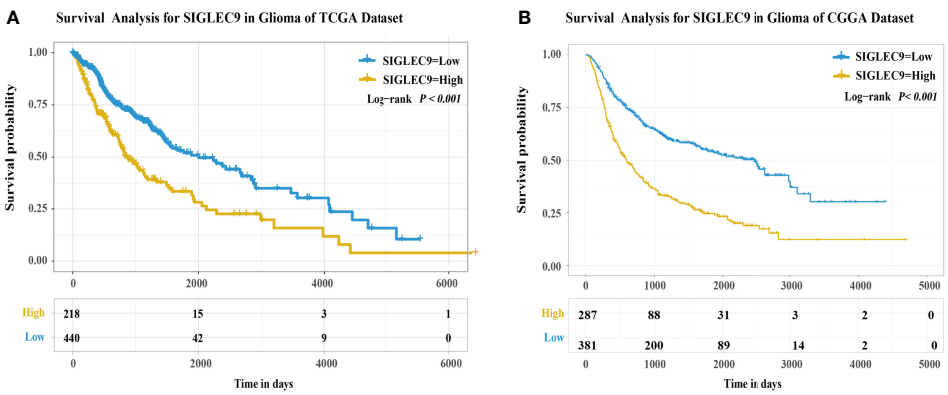

FIGURE 2 | The expression of SIGLEC9 in gliomas with The Cancer Genome Atlas (TCGA) and the Chinese Glioma Genome Atlas (CGGA) databases. **(A)** In TCGA database, the glioma patients with a high SIGLEC9 expression ($n = 218$) had a shorter survival probability than those patients with a low SIGLEC9 expression ($n = 440$) ($P < 0.001$). **(B)** In the CGGA database, the glioma patients with a high SIGLEC9 expression ($n = 287$) had a shorter survival probability than those patients with a low SIGLEC9 expression ($n = 381$) ($P < 0.001$).

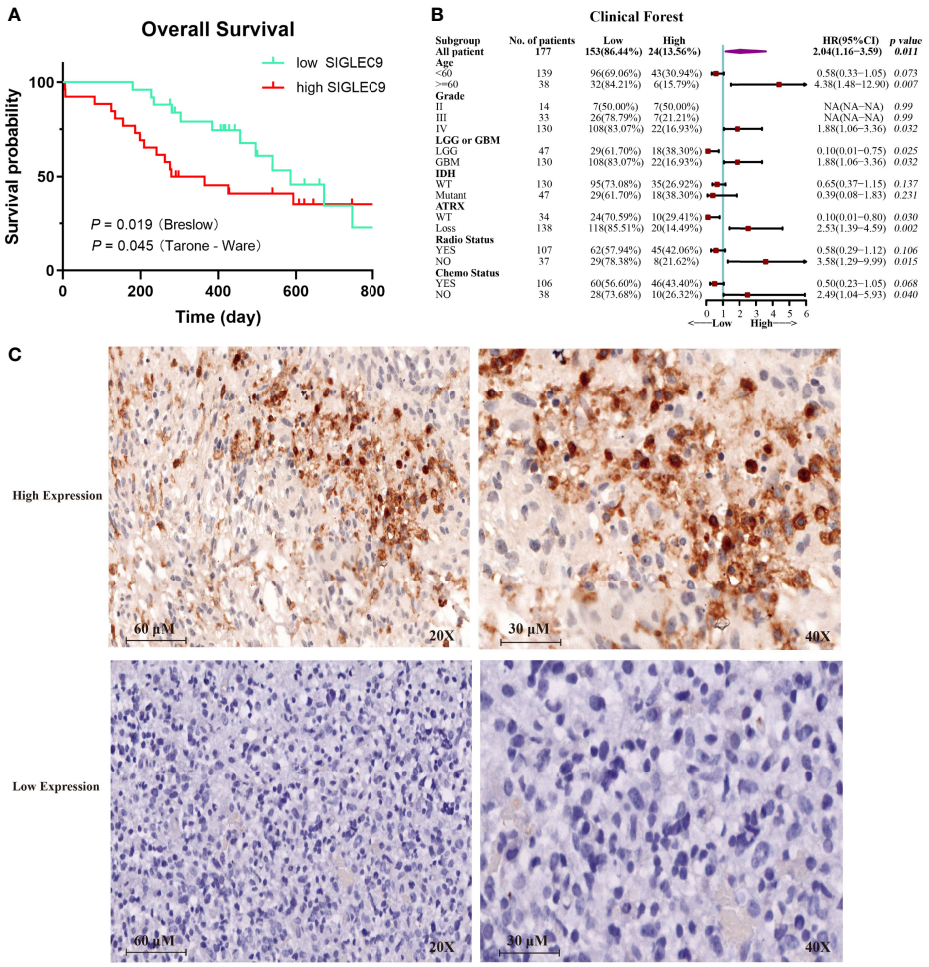

FIGURE 3 | The expression of SIGLEC9 in 177 glioma patients. **(A)** The glioma patients with a high SIGLEC9 expression (n = 26) had a shorter survival probability than those patients with a low SIGLEC9 expression (n = 25) (P = 0.019). **(B)** Clinical characteristics of SIGLEC9 expression in glioma patients. In glioma patients with the following characteristics—age ≧60 years (P = 0.007), grade IV (P = 0.032), glioblastoma (P = 0.032), alpha thalassemia/intellectual disability syndrome X-linked loss (P = 0.002), without radiotherapy (P = 0.015), or without chemotherapy (P = 0.040), respectively—those with a high SIGLEC9 expression had a shorter survival probability than those with a low SIGLEC9 expression. **(C)** Immunohistochemical staining of SIGLEC9 from glioma patients of Sanbo Brain Hospital Capital Medical University.

microenvironment scores between the high-SIGLEC9-expression group and the low-SIGLEC9-expression group by the ESTIMATE algorithm, and the results showed that the high-SIGLEC9-expression group had a higher immune score in StromalScore, ImmuneScore, and ESTIMATEScore (P < 0.001) (**Figure 4D**).

Then, we evaluated the expression correlation between SIGLEC9 and checkpoint members in tumor-induced immune response using Pearson correlation analysis with TCGA dataset. As shown in **Figure 4E** and **Supplementary Table S3**, SIGLEC9 had a high concordance with LAIR1 (Cor = 0.919, P < 0.001), HAVCR2 (Cor = 0.892, P < 0.001), CD86 (Cor = 0.870, P < 0.001), and LGALS9 (Cor = 0.810, P < 0.001).

Functional Enrichment Analysis of *SIGLEC9*-Correlated Genes

GO analysis was conducted to investigate the functions of *SIGLEC9*-correlated genes in data obtained from TCGA and CGGA databases. Based on the data of TCGA database, GO analysis showed that the *SIGLEC9*-correlated genes were mostly enriched in neutrophil activation, neutrophil degranulation, and neutrophil-mediated immunity (**Figure 5A**). The GO analysis based on the data of CGGA database also showed similar results (**Figure 5B**).

Moreover, GSEA was conducted to explore the biological functions of SIGLEC9 in gliomas. Based on the data of TCGA database, SIGLEC9 was positively correlated with the IL6-JAK-STAT3 signaling pathway (NES = 2.814, FDR = 0), KRAS signaling pathway (NES = 2.474, FDR = 0), reactive oxygen species pathway (NES = 1.896, FDR = 0), and TGF-β signaling pathway (NES = 1.928, FDR = 0) (**Figure 5C**). Similar results were obtained from the GSEA analysis based on the data of the CGGA database (**Figure 5D**), such as IL6-JAK-STAT3 signaling pathway (NES = 2.073, FDR = 0), KRAS signaling pathway (NES = 1.622, FDR = 0.001), reactive oxygen

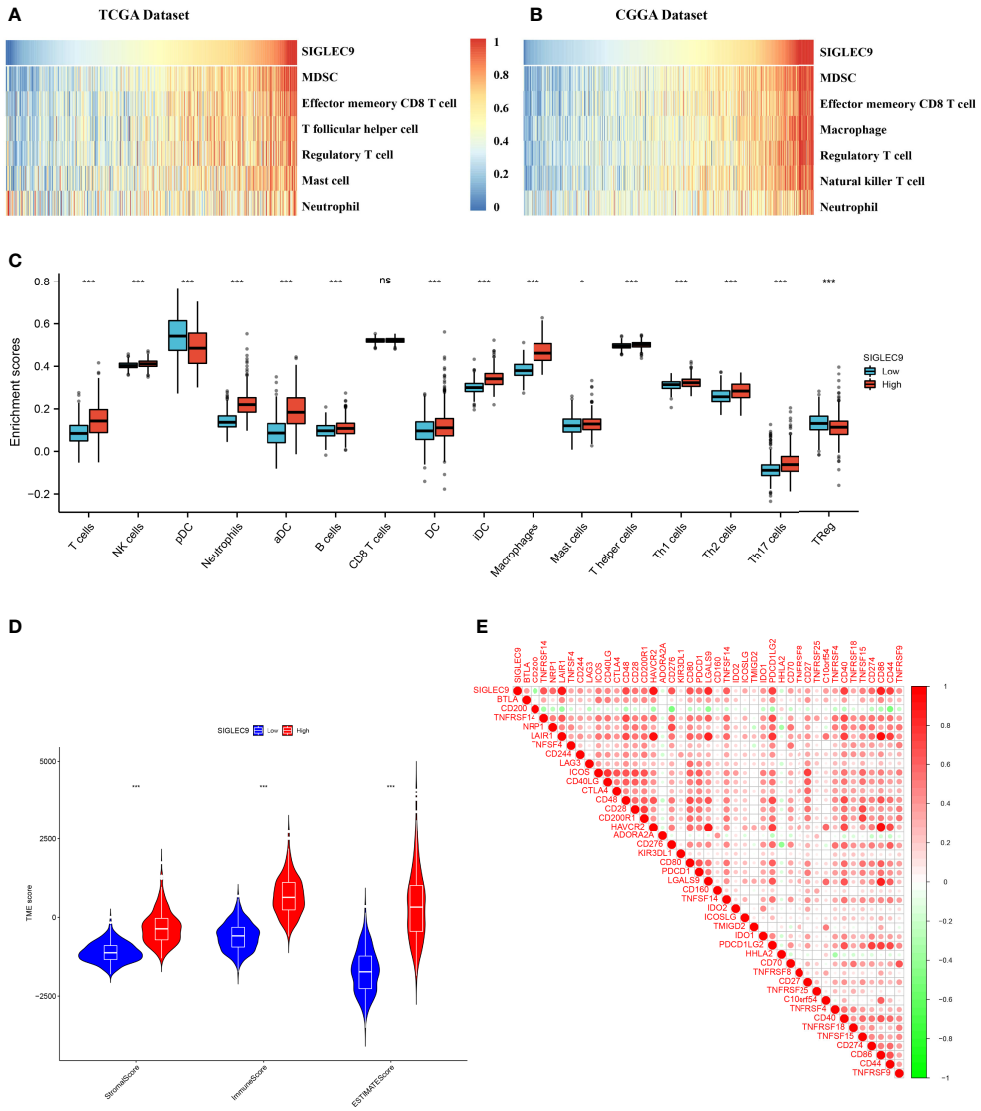

FIGURE 4 | Relationship between SIGLEC9 expression and immune microenvironment. **(A)** In glioma patients with The Cancer Genome Atlas (TCGA) database, SIGLEC9 expression was positively correlated with immune cell infiltration, including myeloid-derived suppressor cells (MDSCs), effector memory CD8 T cells, T follicular helper cells, regulatory T cells, macrophages, *etc.* **(B)** In glioma patients with TCGA database, SIGLEC9 expression was positively correlated with MDSCs, effector memory CD8 T cells, macrophages, regulatory T cells, natural killer T cells, neutrophils, *etc.* **(C)** Differences in immune cell infiltration between the high and the low expression of SIGLEC9, respectively. **(D)** Relationship between SIGLEC9 expression and immune microenvironment score. **(E)** Relationship between SIGLEC9 expression and immune checkpoints. ns, p≥0.05; *, p< 0.05; ***, p<0.001.

speciespathway (NES = 1.668, FDR = 4.40E-04), and TGF-β signaling pathway (NES = 1.700, FDR = 2.91E-04).

Single-Cell Analysis of Tumor Tissue and Adjacent Tissue

Firstly, we normalized and pooled single-cell data from all samples and filtered the low-quality cells (**Figures 6A, B**). Then, we merged the tumor and adjacent tissue sample to perform unsupervised clustering to identify distinguished cell populations. Seurat v3.0 with default parameters was conducted in this study. We classified different cell subsets according to the related typical marker genes in cells. We mainly identified 10 types of cells (**Figures 6C, D**), such as glial/neuronal cells (PTPRZ1 and FABP7), DCs (HLA-DQA1, HLA-DPB1, FCER1A, and CD1C), T cells (CD3E, CD3D, CD3G, GZMK, and GZMA), mural cell (RGS5, BGN, TAGLN, NOTCH3, and PDGFRB), neutrophil (IL1R2, CSF3R, FPR2, and CXCL1), endothelial (CLDN5, VWF, ABCG2, and CAVIN2), macrophage (proliferating) (MKI67 and TOP2A), macrophage (APOC1), microglia/microphage (CD163 and F13A1), microglia (P2RY13 and SLC1A3), and microglia (P2RY12 and CX3CR1). We calculated the proportion of various types of cells in each

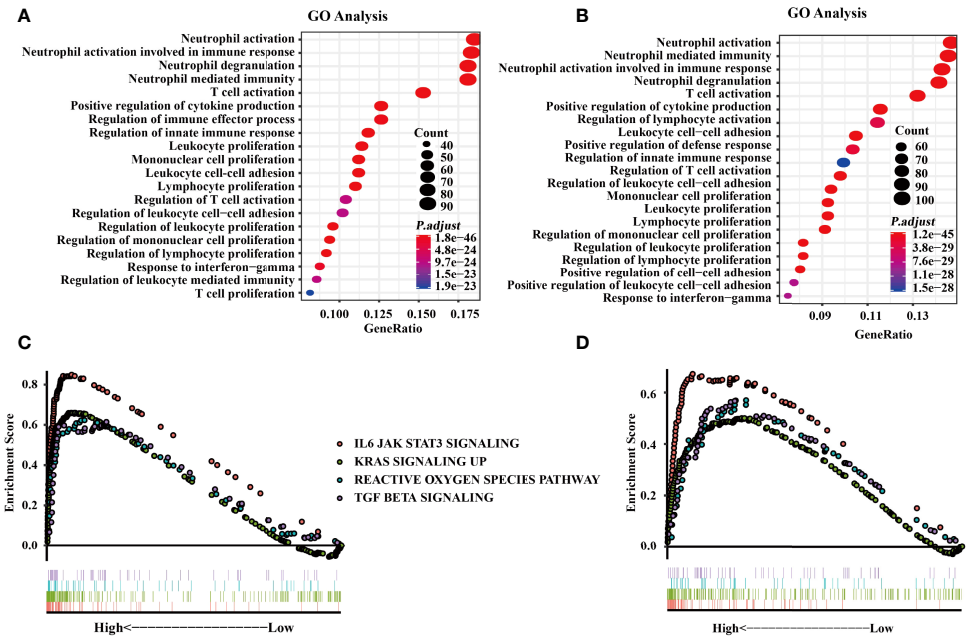

FIGURE 5 | Functional enrichment analysis with The Cancer Genome Atlas (TCGA) and the Chinese Glioma Genome Atlas (CGGA) databases. **(A)** Gene Ontology (GO) analysis from the TCGA database. **(B)** GO analysis from CGGA databases. **(C)** Gene Set Enrichment Analysis (GSEA) was conducted to investigate the biological functions of SIGLEC9 in gliomas from the TCGA database. **(D)** GSEA was conducted to investigate the biological functions of SIGLEC9 in gliomas from the CGGA database. The red lines represent SIGNALING as IL6 JAK STAT3. The green line represents KRAS signaling up. The turquoise line represents the reactive oxygen species pathway. The purple line represents TGF-β signaling.

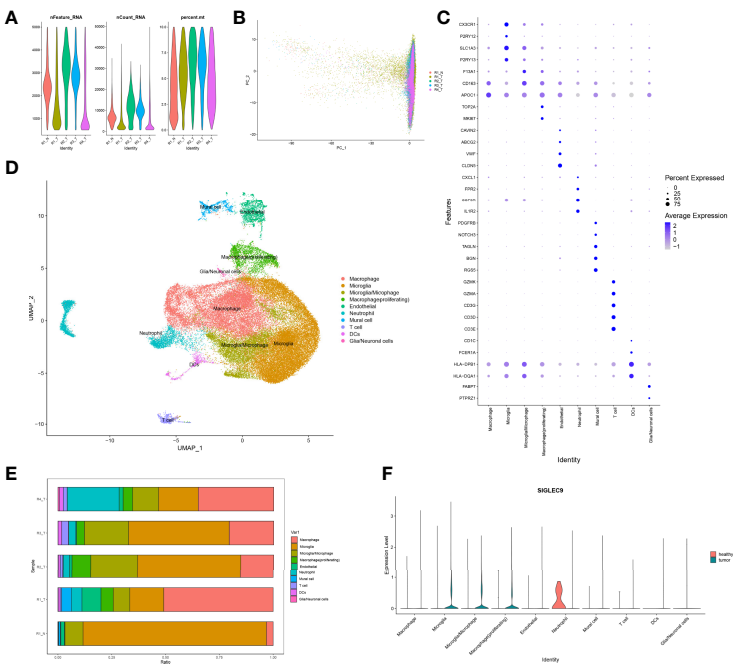

FIGURE 6 | Identification of differentially expressed genes and cell subsets in glioma with single-cell analysis. **(A)** High-quality cell filtration. The cells were filtrated with the number of genes in cells nFeature >200 and ≤5,000; the proportion of mitochondrial genes in cells (percent.mt <10). **(B)** Integration of all samples. **(C)** Bubble plot of marker gene expression in the identification of different cell types. **(D)** Exhibition of cell subsets. **(E)** Proportion of cells in each sample. **(F)** Expression of SIGLEC9 in tumor tissue and in adjacent tissue.

sample and found that the proportion of microglia in normal samples was significantly higher than that in tumor samples, but the proportion of macrophages was significantly lower than that in tumor samples (**Figure 6E**). Therefore, our further analysis also focused on macrophages in tumors. Finally, we calculated the expression of SIGLEC9 in these cell subsets between glioma tissue and adjacent tissue (**Figure 6F**). In macrophages (proliferating) and macrophages subsets, the expression of SIGLEC9 in cancer tissues was higher than that in adjacent tissues. Macrophages play an essential role in glioma, and SIGLEC9 may be an important regulator of macrophages.

Regulatory Role of SIGLEC9 in Macrophages and Macrophages (Proliferating) With Glioma

We extracted a subset of macrophages (macrophage) for analysis (**Figure 7A**), and we found that SIGLEC9 was positively correlated with genes (NCF2, PSMA7, VAMP3, and NCF4) ($P < 0.05$) that are involved in antigen processing and presentation of antigen (**Figure 7B**). Based on the median of SIGLEC9 expression, we divided the macrophages into two groups with high and low SIGLEC9 expression, and we further identified differential genes between these two groups. The GSEA analysis found that differential genes were associated with macrophage activation (16) (**Figure 7C**). The GO enrichment analysis found that upregulated differential genes were significantly enriched in pathways such as antigen processing and presentation of peptide antigen *via* MHC class II, antigen processing and presentation of peptide antigen, *etc.* (**Figure 7D**). In addition, the KEGG enrichment analysis found that upregulated differentially genes were enriched in Fc gamma R-mediated phagocytosis and antigen processing and presentation pathways (**Figure 7E**). Therefore, the differential genes of the two groups are involved in the pathway of antigen presentation, which also indicates that the expression of SIGLEC9 gene is related to the ability of macrophages to process antigens.

We also extracted macrophages (proliferating) for analysis and, as shown in **Supplementary Figure S2**, we found that SIGLEC9 was positively correlated with the proliferation genes (ANAPC11, CCNB1, and PLK1) ($P < 0.05$) of macrophages. According to the median of SIGLEC9 expression, we further divided the macrophages (proliferating) into two groups with a high expression and a low expression of SIGLEC9, respectively. We found the differential genes between the high-SIGLEC9-expression group and the low-SIGLEC9-expression group. The GSEA analysis found that upregulated genes were associated with macrophage maturation and M2 polarization (17). The GO enrichment found that upregulated genes were significantly

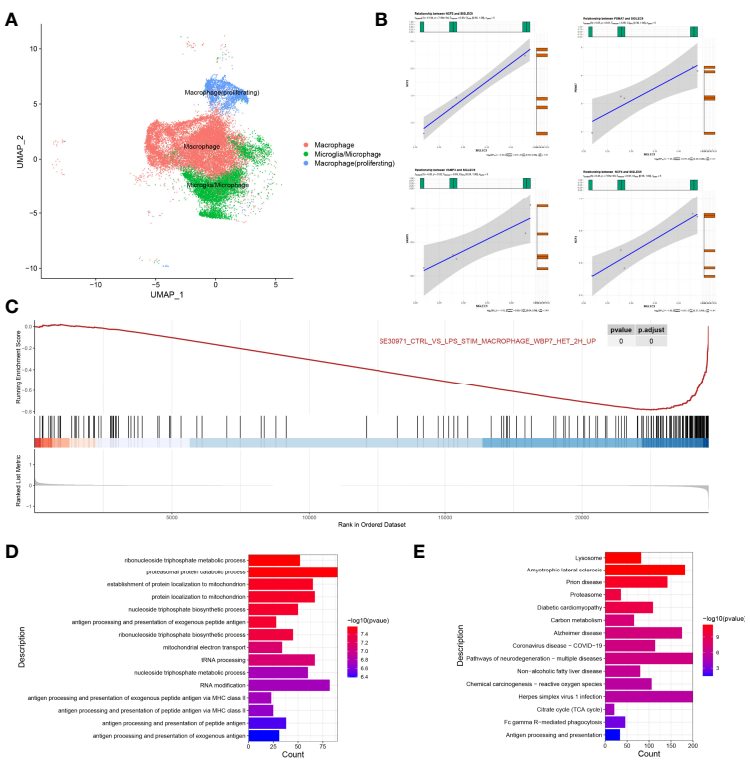

FIGURE 7 | Regulatory role of SIGLEC9 in macrophages with glioma. **(A)** Uniform Manifold Approximation and Projection plot of macrophage cluster. **(B)** Correlation between SIGLEC9 and macrophage activation genes (NCF2, PSMA7, VAMP3, and NCF4). **(C)** Gene Set Enrichment Analysis between high- and low-SIGLEC9 groups in macrophages. **(D)** Gene Ontology analysis between high- and low-SIGLEC9 groups in macrophages. **(E)** Kyoto Encyclopedia of Genes and Genomes analysis between high- and low-SIGLEC9 groups in macrophages.

enriched in the regulation of cell cycle phase transition, DNA replication, T cell activation, and other pathways, which are related to cell proliferation and replication. In addition, the KEGG enrichment found that upregulated genes were significantly enriched in pathways, such as DNA replication and cell cycle, which are also related to cell proliferation and replication. It indicates that the high expression of SIGLEC9 is related to the M2 macrophage polarization and proliferation of macrophages.

DISCUSSION

Glioma is a broad term of tumors occurring in the brain and spinal cord (18). There are more than 100 different pathological types of central nervous system and brain tumors, in which gliomas represent the largest proportion. The prognosis of gliomas after diagnosis varies significantly with the tumor grades, subtypes, and molecular biomarkers (19). The high-grade (III and IV) gliomas have a poor survival time. GBM also has poor overall survival, and the average length of survival after diagnosis is only 12 to 15 months. In the four molecular subtypes of GBM, the mesenchymal subtype tends to have the poorest overall survival than the other three subtypes (20). IDH is an enzyme that catalyzes the oxidative decarboxylation of isocitrate, and IDH wild-type glioma patients have a poor prognosis (21). The alpha thalassemia/intellectual disability syndrome X-linked (ATRX) gene is involved in telomere maintenance, and the loss of ATRX could reduce the median survival of glioma patients by promoting tumor growth (22).

In this study, we comprehensively analyzed the expression pattern of *SIGLEC9* in gliomas with TCGA and CGGA databases. High-*SIGLEC9*-expression patients had a shorter survival probability than low-*SIGLEC9*-expression patients. In addition, *SIGLEC9* expression was significantly upregulated in malignant pathological types such as grade III, grade IV, mesenchymal subtype, and IDH wild-type gliomas. Then, we investigated the protein levels of SIGLEC9 in 177 glioma patients from Sanbo Brain Hospital Capital Medical University. The results indicated that high-SIGLEC9-expression patients had a shorter survival probability than low-SIGLEC9-expression patients. In addition, high SIGLEC9 expression presented to have a shorter survival probability in patients with age ≧60 years, with grade IV glioma, with GBM, with ATRX loss glioma, without radiotherapy, or without chemotherapy. These parameters are all correlated with the poor overall survival of glioma patients as mentioned above. These results showed that SIGLEC9 expression was positively correlated with a malignant biologic process, indicating that SIGLEC9 might play important roles in the progression of gliomas.

Then, we investigated the underlying mechanisms of SIGLEC9 in gliomas, and our results showed that SIGLEC9 might regulate the tumor microenvironment (TME) in gliomas. TME is a dynamic condition in such a way that different immune cells interplay with cancer cells (23). TME has different inflammatory mediators, extracellular matrix, and signaling molecules to induce tumor progression and therapy resistance (24, 25). Tumor-infiltrated immune cells contain different types of cells, such as MDSCs, neutrophils, macrophages, dendritic cells, regulatory T cells (Treg), *etc.* (26, 27). Our results revealed that tumor-related immune cells, such as MDSCs, regulatory T cells, and neutrophils, were positively correlated with *SIGLEC9* expression in gliomas. *SIGLEC9* expression was mostly correlated with MDSC infiltration in glioma. MDSCs are a heterogenous group of immune cells with immature myeloid cells, including precursors of granulocytes, macrophages, and dendritic cells (28). MDSCs are strongly expanded in the site of cancer, such as gliomas, and have been demonstrated to be correlated with a poor prognosis and therapy resistance in cancer patients (29). MDSCs have strong abilities to exacerbate gliomas. Firstly, MDSCs induce the production of reactive oxygen species, nitric oxide, and arginase (30). Secondly, MDSCs could induce the maturity and development of tumor-induced regulatory T cells (31). Thirdly, MDSCs could increase the expression of prostaglandin E2 and cyclooxygenase 2 (32). These inflammatory mediators produced by MDSCs could increase the complexity of immune cell interactions in the TME of gliomas. Consistently, our data also showed that SIGLEC9 was positively correlated with the reactive oxygen species pathway in the GSEA analysis, and SIGLEC9 expression was positively correlated with regulatory T cell infiltration. Furthermore, SIGLEC9 expression was also positively correlated with immune checkpoints, including LAIR1, HAVCR2, CD86, and LGALS9. As an important member of the immune tumor microenvironment, macrophages play an important therapeutic role in glioma. Hara et al. have proven that macrophages can induce a transition of glioblastoma cells into mesenchymal-like (MES-like) states (33). They found that the state of MES-like glioblastoma is related to the increase in the expression of the medium germination program in the middle of macrophages, which has potential treatment for the widespread changes in the immune microenvironment. In the results of our single-cell sequencing analysis, compared with normal samples, we found that SIGLEC9 expresses highly in three types of macrophages [macrophage (proliferating), macrophage, and microglia/microphage] in tumor samples. Furthermore, we found that the SIGLEC9 gene is related to the ability of macrophages to process antigens and the proliferation of macrophages. In the future, we will demonstrate the regulatory role of SIGLEC9 in macrophages through further experiments. Thus, SIGLEC9 was considered to exacerbate the gliomas by suppressing the anti-tumor immune response.

Functional enrichment analysis showed that the *SIGLEC9*-correlated genes were enriched in neutrophil immune response. Neutrophils are the most abundant granulocytes to comprise approximately 70% of leukocytes in the peripheral blood of humans. Previous studies have revealed that the number of neutrophils is positively correlated with the severity and poor prognosis of glioma patients (34). In high-grade gliomas, neutrophilia was associated with poor survival to decreased overall survival (35). Cytokine granulocyte-colony stimulating

factor (G-CSF) is the growth factor of neutrophils, and G-CSF is over-produced in glioma patients (36). In addition, G-CSF is responsible for the high neutrophil–lymphocyte ratio (NLR) in glioma patients *via* switching bone marrow hematopoiesis from lymphocytes to granulocytes (37). A high neutrophil/lymphocyte ratio is correlated with a poor prognosis of glioma patients. Neutrophils are also related to the resistance of anti-angiogenic therapy, such as anti-vascular endothelial growth factor therapy of glioma patients (38). Tumor-infiltrated neutrophils can secrete elastase to promote the proliferation of glioma cells (39).

In summary, SIGLEC9 might regulate the TME in gliomas to exacerbate the disease, and MDSCs and neutrophils play an important role in the function of SIGLEC9. Moreover, SIGLEC9 might upregulate the expression of immune checkpoint genes to suppress the anti-tumor immune response in gliomas.

CONCLUSION

In this study, we analyzed the expression patterns and prognostic values of SIGLEC9 in glioma. *SIGLEC9* expression was significantly upregulated in malignant pathological types, such as grade III, grade IV, mesenchymal subtype, and IDH wild-type gliomas in TCGA and CGGA database. High *SIGLEC9* expression presented to have a shorter survival probability than low *SIGLEC9* expression in glioma patients. Our own clinical data also showed that high SIGLEC9 protein levels presented to have a shorter survival probability than low SIGLEC9 protein levels in patients with age ≧60 years, grade IV glioma, GBM, ATRX loss glioma, without radiotherapy, or without chemotherapy, which are all poor prognosis factors of gliomas. Furthermore, we investigated the underlying functions of SIGLEC9 in glioma pathogenesis, and we found that SIGLEC9 might regulate the TME to induce tumor growth, metastasis, and the therapy resistance of gliomas. We inferred that MDSCs and neutrophils might play an important role in the function of SIGLEC9. Moreover, SIGLEC9 might upregulate the expression of immune checkpoint genes to suppress the anti-tumor immune response in gliomas. These results indicated that high SIGLEC9 expression might serve as a poor prognosis marker for glioma patients and SIGLEC9 might be a therapeutic target for glioma in the future.

DATA AVAILABILITY STATEMENT

The original contributions presented in the study are included in the article/**Supplementary Material**. Further inquiries can be directed to the corresponding authors.

ETHICS STATEMENT

The studies involving human participants were reviewed and approved by the ethics committee of Sanbo Brain Hospital Capital Medical University (no. SBNK-2018-003-01). Written informed consent to participate in this study was provided by the participants' legal guardian/next of kin. Written informed consent was obtained from the individuals for the publication of any potentially identifiable images or data included in this article.

AUTHOR CONTRIBUTIONS

HX and YaF performed the statistical analysis and drafted the manuscript. WK, HW, and YuF contributed to database building. JZ, KY, and GH conceived the design of the study and revised the manuscript. All authors contributed to the article and approved the submitted version.

ACKNOWLEDGMENTS

This work was supported by the Projects of International Cooperation and Exchanges (grant number 2014DFA32950) and research program from Beijing University of Chinese Medicine (grant numbers BUCM-2019-JCRC006 and 2019-JYB-TD013).

SUPPLEMENTARY MATERIAL

The Supplementary Material for this article can be found online at: https://www.frontiersin.org/articles/10.3389/fonc.2022.878849/full#supplementary-material

REFERENCES

1. Davis ME. Epidemiology and Overview of Gliomas. *Semin Oncol Nurs* (2018) 34(5):420–9. doi: 10.1016/j.soncn.2018.10.001
2. Cahill D, Turcan S. Origin of Gliomas. *Semin Neurol* (2018) 38(1):5–10. doi: 10.1055/s-0038-1635106
3. Liu K, Jiang Y. Polymorphisms in DNA Repair Gene and Susceptibility to Glioma: A Systematic Review and Meta-Analysis Based on 33 Studies With 15 SNPs in 9 Genes. *Cell Mol Neurobiol* (2017) 37(2):263–74. doi: 10.1007/s10571-016-0367-y
4. Omuro A, DeAngelis LM. Glioblastoma and Other Malignant Gliomas: A Clinical Review. *JAMA* (2013) 310(17):1842–50. doi: 10.1001/jama.2013.280319
5. Wang Q, Hu B, Hu X, Kim H, Squatrito M, Scarpace L, et al. Tumor Evolution of Glioma-Intrinsic Gene Expression Subtypes Associates With Immunological Changes in the Microenvironment. *Cancer Cell* (2018) 33(1):152. doi: 10.1016/j.ccell.2017.12.012
6. Ghotme KA, Barreto GE, Echeverria V, Gonzalez J, Bustos RH, Sanchez M, et al. Gliomas: New Perspectives in Diagnosis, Treatment and Prognosis. *Curr Top Med Chem* (2017) 17(12):1438–47. doi: 10.2174/1568026617666170103162639
7. Chen R, Smith-Cohn M, Cohen AL, Colman H. Glioma Subclassifications and Their Clinical Significance. *Neurotherapeutics* (2017) 14(2):284–97. doi: 10.1007/s13311-017-0519-x
8. Picca A, Berzero G, Di Stefano AL, Sanson M. The Clinical Use of IDH1 and IDH2 Mutations in Gliomas. *Expert Rev Mol Diagn* (2018) 18(12):1041–51. doi: 10.1080/14737159.2018.1548935
9. Kim ST, Chu Y, Misoi M, Suarez-Almazor ME, Tayar JH, Lu H, et al. Distinct Molecular and Immune Hallmarks of Inflammatory Arthritis Induced by

Immune Checkpoint Inhibitors for Cancer Therapy. *Nat Commun* (2022) 13 (1):1970. doi: 10.1038/s41467-022-29539-3
10. Bailey CM, Liu Y, Liu M, Du X, Devenport M, Zheng P, et al. Targeting HIF-1α Abrogates PD-L1-Mediated Immune Evasion in Tumor Microenvironment But Promotes Tolerance in Normal Tissues. *J Clin Invest* (2022) 132(9):e150846. doi: 10.1172/JCI150846
11. Fraschilla I, Pillai S. Viewing Siglecs Through the Lens of Tumor Immunology. *Immunol Rev* (2017) 276(1):178–91. doi: 10.1111/imr.12526
12. Ibarlucea-Benitez I, Weitzenfeld P, Smith P, Ravetch JV. Siglecs-7/9 Function as Inhibitory Immune Checkpoints *In Vivo* and Can Be Targeted to Enhance Therapeutic Antitumor Immunity. *Proc Natl Acad Sci USA* (2021) 118(26): e2107424118. doi: 10.1073/pnas.2107424118
13. Haas Q, Boligan KF, Jandus C, Schneider C, Simillion C, Stanczak MA, et al. Siglec-9 Regulates an Effector Memory $CD8^+$ T-Cell Subset That Congregates in the Melanoma Tumor Microenvironment. *Cancer Immunol Res* (2019) 7 (5):707–18. doi: 10.1158/2326-6066.CIR-18-0505
14. Stanczak MA, Siddiqui SS, Trefny MP, Thommen DS, Boligan KF, von Gunten S, et al. Self-Associated Molecular Patterns Mediate Cancer Immune Evasion by Engaging Siglecs on T Cells. *J Clin Invest* (2018) 128 (11):4912–23. doi: 10.1172/JCI120612
15. Beatson R, Tajadura-Ortega V, Achkova D, Picco G, Tsourouktsoglou TD, Klausing S, et al. The Mucin MUC1 Modulates the Tumor Immunological Microenvironment Through Engagement of the Lectin Siglec-9. *Nat Immunol* (2016) 17(11):1273–81. doi: 10.1038/ni.3552
16. De Freitas A, Banerjee S, Xie N, Cui H, Davis KI, Friggeri A, et al. Identification of TLT2 as an Engulfment Receptor for Apoptotic Cells. *J Immunol* (2012) 188(12):6381–8. doi: 10.4049/jimmunol.1200020
17. Pello OM, De Pizzol M, Mirolo M, Soucek L, Zammataro L, Amabile A, et al. Role of C-MYC in Alternative Activation of Human Macrophages and Tumor-Associated Macrophage Biology. *Blood* (2012) 119(2):411–21. doi: 10.1182/blood-2011-02-339911
18. Ostrom QT, Gittleman H, Stetson L, Virk SM, Barnholtz-Sloan JS. Epidemiology of Gliomas. *Cancer Treat Res* (2015) 163:1–14. doi: 10.1007/978-3-319-12048-5_1
19. Reifenberger G, Wirsching HG, Knobbe-Thomsen CB, Weller M. Advances in the Molecular Genetics of Gliomas - Implications for Classification and Therapy. *Nat Rev Clin Oncol* (2017) 14(7):434–52. doi: 10.1038/nrclinonc.2016.204
20. Behnan J, Finocchiaro G, Hanna G. The Landscape of the Mesenchymal Signature in Brain Tumours. *Brain* (2019) 142(4):847–66. doi: 10.1093/brain/awz044
21. Masui K, Mischel PS, Reifenberger G. Molecular Classification of Gliomas. *Handb Clin Neurol* (2016) 134:97–120. doi: 10.1016/B978-0-12-802997-8.00006-2
22. Koschmann C, Calinescu AA, Nunez FJ, Mackay A, Fazal-Salom J, Thomas D, et al. ATRX Loss Promotes Tumor Growth and Impairs Nonhomologous End Joining DNA Repair in Glioma. *Sci Transl Med* (2016) 8(328):328ra28. doi: 10.1126/scitranslmed.aac8228
23. Wu T, Dai Y. Tumor Microenvironment and Therapeutic Response. *Cancer Lett* (2017) 387:61–8. doi: 10.1016/j.canlet.2016.01.043
24. Landskron G, de la Fuente M, Thuwajit P, Thuwajit C, Hermoso MA. Chronic Inflammation and Cytokines in the Tumor Microenvironment. *J Immunol Res* (2014) 2014:149185. doi: 10.1155/2014/149185
25. Gieryng A, Pszczolkowska D, Walentynowicz KA, Rajan WD, Kaminska B. Immune Microenvironment of Gliomas. *Lab Invest* (2017) 97(5):498–518. doi: 10.1038/labinvest.2017.19
26. Elliott LA, Doherty GA, Sheahan K, Ryan EJ. Human Tumor-Infiltrating Myeloid Cells: Phenotypic and Functional Diversity. *Front Immunol* (2017) 8:86. doi: 10.3389/fimmu.2017.00086
27. Boussiotis VA, Charest A. Immunotherapies for Malignant Glioma. *Oncogene* (2018) 37(9):1121–41. doi: 10.1038/s41388-017-0024-z
28. Kohanbash G, Okada H. Myeloid-Derived Suppressor Cells (MDSCs) in Gliomas and Glioma-Development. *Immunol Invest* (2012) 41(6-7):658–79. doi: 10.3109/08820139.2012.689591
29. Ding AS, Routkevitch D, Jackson C, et al. Targeting Myeloid Cells in Combination Treatments for Glioma and Other Tumors. *Front Immunol* (2019) 10:1715. doi: 10.3389/fimmu.2019.01715
30. Youn JI, Gabrilovich DI. The Biology of Myeloid-Derived Suppressor Cells: The Blessing and the Curse of Morphological and Functional Heterogeneity. *Eur J Immunol* (2010) 40(11):2969–75. doi: 10.1002/eji.201040895
31. Huang B, Pan PY, Li Q, Sato AI, Levy DE, Bromberg J. Gr-1+CD115+ Immature Myeloid Suppressor Cells Mediate the Development of Tumor-Induced T Regulatory Cells and T-Cell Anergy in Tumor-Bearing Host. *Cancer Res* (2006) 66(2):1123–31. doi: 10.1158/0008-5472.CAN-05-1299
32. Won WJ, Deshane JS, Leavenworth JW, Oliva CR, Griguer CE. Metabolic and Functional Reprogramming of Myeloid-Derived Suppressor Cells and Their Therapeutic Control in Glioblastoma. *Cell Stress* (2019) 3(2):47–65. doi: 10.15698/cst2019.02.176
33. Hara T, Chanoch-Myers R, Mathewson ND, Myskiw C, Atta L, Bussema L.. Interactions Between Cancer Cells and Immune Cells Drive Transitions to Mesenchymal-Like States in Glioblastoma. *Cancer Cell* (2021) 39(6):779–792.e11. doi: 10.1016/j.ccell.2021.05.002
34. Gabrusiewicz K, Rodriguez B, Wei J, Hashimoto Y, Healy LM, Maiti SN. Glioblastoma-Infiltrated Innate Immune Cells Resemble M0 Macrophage Phenotype. *JCI Insight* (2016) 1(2):85841. doi: 10.1172/jci.insight.85841
35. Schernberg A, Nivet A, Dhermain F, Ammari S, Escande A, Pallud J. Neutrophilia as a Biomarker for Overall Survival in Newly Diagnosed High-Grade Glioma Patients Undergoing Chemoradiation. *Clin Transl Radiat Oncol* (2018) 10:47–52. doi: 10.1016/j.ctro.2018.04.002
36. Nitta T, Sato K, Allegretta M, et al. Expression of Granulocyte Colony Stimulating Factor and G6ranulocyte-Macrophage Colony Stimulating Factor Genes in Human Astrocytoma Cell Lines and in Glioma Specimens. *Brain Res* (1992) 571(1):19–25. doi: 10.1016/0006-8993(92)90505-4
37. Albulescu R, Codrici E, Popescu ID, Mihai S, Necula LG, Petrescu D. Cytokine Patterns in Brain Tumour Progression. *Mediators Inflamm* (2013) 2013:979748. doi: 10.1155/2013/979748
38. Achyut BR, Shankar A, Iskander AS, Ara R, Angara K, Zeng P. Bone Marrow Derived Myeloid Cells Orchestrate Antiangiogenic Resistance in Glioblastoma Through Coordinated Molecular Networks. *Cancer Lett* (2015) 369(2):416–26. doi: 10.1016/j.canlet.2015.09.004
39. Iwatsuki K, Kumara E, Yoshimine T, Nakagawa H, Sato M, Hayakawa T. Elastase Expression by Infiltrating Neutrophils in Gliomas. *Neurol Res* (2000) 22(5):465–8. doi: 10.1080/01616412.2000.11740701

Conflict of Interest: The authors declare that the research was conducted in the absence of any commercial or financial relationships that could be construed as a potential conflict of interest.

frontiers | Frontiers in Oncology

TYPE Original Research
PUBLISHED 02 September 2022
DOI 10.3389/fonc.2022.818283

OPEN ACCESS

EDITED BY
Haotian Zhao,
New York Institute of Technology,
United States

REVIEWED BY
Congxin Dai,
Capital Medical University, China
Lin Qi,
Central South University, China
Fan Yang,
Jiangxi Agricultural University, China

*CORRESPONDENCE
Zongmao Zhao
zzm@hb2h.com

SPECIALTY SECTION
This article was submitted to Neuro-Oncology and Neurosurgical Oncology, a section of the journal Frontiers in Oncology

RECEIVED 19 November 2021
ACCEPTED 15 August 2022
PUBLISHED 02 September 2022

CITATION
Guo K, Zhao J, Jin Q, Yan H, Shi Y and Zhao Z (2022) CASP6 predicts poor prognosis in glioma and correlates with tumor immune microenvironment.
Front. Oncol. 12:818283.
doi: 10.3389/fonc.2022.818283

CASP6 predicts poor prognosis in glioma and correlates with tumor immune microenvironment

Kai Guo[1,2], Jiahui Zhao[3], Qianxu Jin[1], Hongshan Yan[1], Yunpeng Shi[1] and Zongmao Zhao[1]*

[1]Department of Neurosurgery, The Second Hospital of Hebei Medical University, Shijiazhuang, China, [2]Department of Neurosurgery, Affiliated Xing Tai People Hospital of Hebei Medical University, Xingtai, China, [3]Department of Neurology, Beijing Tiantan Hospital, Capital Medical University, Beijing, China

Background: Glioma is an aggressive tumor of the central nervous system. Caspase-6 (CASP6) plays a crucial role in cell pyroptosis and is a central protein involved in many cellular signaling pathways. However, the association between CASP6 and prognosis of glioma patients remains unclear.

Methods: Four bioinformatic databases were analyzed to identify differentially expressed genes (DEGs) between glioma and healthy tissues. Eighty-one protein-coding pyroptosis-related genes (PRGs) were obtained from the GeneCards database. The pyroptosis-related DEGs (PRDEGs) were extracted from each dataset, and *CASP6* was found to be aberrantly expressed in glioma. We then investigated the biological functions of CASP6 and the relationship between *CASP6* expression and the tumor microenvironment and immunocyte infiltration. The half maximal inhibitory concentration of temozolomide and the response to immune checkpoint blockade in the high- and low-*CASP6* expression groups were estimated using relevant bioinformatic algorithms. Quantitative real-time reverse transcription PCR and western blotting were carried out to confirm the different expression levels of CASP6 between human astrocytes and glioma cell lines (U251 and T98G). We determined the role of CASP6 in the tumorigenesis of glioma by knocking down *CASP6* in U251 and T98G cell lines.

Results: We found that *CASP6* was overexpressed in glioma samples and in glioma cell lines. *CASP6* expression in patients with glioma correlated negatively with overall survival. In addition, *CASP6* expression correlated positively with the degree of glioma progression. Functional analysis indicated that CASP6 was primarily involved in the immune response and antigen processing and presentation. Patients with high *CASP6* levels responded more favorably to temozolomide, while patients with low

expression of *CASP6* had a better response to immunotherapy. Finally, *in vitro* experiments showed that *CASP6* knockdown inhibited glioma proliferation.

Conclusions: The pyroptosis-related gene *CASP6* might represent a sensitive prognostic marker for patients with glioma and might predict their response of immunotherapy and temozolomide therapy. Our results might lead to more precise immunotherapeutic strategies for patients with glioma.

KEYWORDS

CASP6, glioma, pyroptosis, prognosis, immune microenvironment

Introduction

Glioma, which is derived from the neuroepithelial cell layer, is the most common cancer of the central nervous system (CNS). In 2016, the World Health Organization classified glioma into four histopathological grades on the basis of the degree of its progression. Grades I and II are defined as low-grade glioma (LGG), while grades III and IV are defined as high-grade glioma. Oligodendrogliomas and astrocytomas belong to the grade II class. Anaplastic oligodendrogliomas, anaplastic astrocytomas, anaplastic oligoastrocytomas, and anaplastic ependymomas are classified into grade III. Glioblastoma (GBM) is grade IV, which is the most malignant type of glioma (1). Surgical resection plus radiotherapy and chemotherapy are the mainstay therapeutic strategies to treat glioma patients. Due to the high aggressiveness, high recurrence rate, and resistance to radiotherapy and chemotherapy the overall survival (OS) of glioma patients is low (2), Despite the progress for glioma research in recent years no major breakthroughs have been made to improve glioma prognosis (3).

Pyroptosis is a form of programmed cell death characterized by cell swelling, lysis, and the release of pro-inflammatory factors (4). Recently, research has shown that pyroptosis plays a crucial role in inhibiting tumor cell proliferation and tumor growth in many kinds of cancer, such as colon cancer (5), non-small cell lung cancer (6), and hepatocellular carcinoma (7). In the field of glioma research, many potential treatments might exert an antitumor effect *via* pyroptosis. For example, the natural nutrient kaempferol was found to be an anti-glioma drug that possibly induces pyroptosis (8). MicroRNA miR-214 and circular RNA hsa_circ_0001836 were found to inhibit glioma growth *via* inducing pyroptosis (9, 10). Caspase 6 (CASP6) is activated in pyroptosis cascade and plays a critical role in this process. Caspase-6 can induce the activation of NLRP3 inflammasome, which is a core step of pyroptosis (11). Accumulating experimental evidence suggests that the apoptosis of hTERT-positive malignant glioma cells is markedly promoted by the induction of the hTERT/rev-caspase-6 complex (12). These findings indicated that CASP6 might play a critical role in the occurrence of glioma and could be a potential therapeutic target. However, the effects of CASP6 on glioma pyroptosis and its mechanism need further investigation.

In this study, we sought to identify pyroptosis-related differentially expressed genes (PRDEGs) through analyzing sequencing datasets obtained from glioma patient tissues. These analyses identified *CASP6* as one of the glioma-associated PRDEGs. Furthermore, we found that *CASP6* expression level was correlated with prognosis of glioma patients, and outcomes of chemotherapy and immunotherapy. In addition, we analyzed the biological functions of CASP6 in glioma and found that CASP6 was involved in the immune microenvironment and the infiltration of immune cells. Finally, the abnormal expression of *CASP6* in gliomas was verified using an external database and cell experiments. Our findings suggest that CASP6 is a marker to predict the prognosis of glioma patients and might be a potential target to treat glioma.

Abbreviations: AUC, Area under the curve; CCK-8, Cell Counting Kit-8; CNS, Central nervous system; CGGA, Chinese Glioma Genome Atlas; DEGs, Differentially expressed genes; ESTIMATE, Estimation of Stromal and Immune cells in Malignant Tumors using Expression data; GEO, Gene Expression Omnibus; GSE, Gene Expression Omnibus Series; GO, Gene Ontology; GSEA, Gene Set Enrichment Analysis; GDSC2, Genomics of Drug Sensitivity in Cancer 2; GTEx, Genotype-Tissue Expression; GBM, Glioblastoma; IC50, Half maximal inhibitory concentration; HR, Hazard ratio; HA, Human astrocytes; HPA, Human Protein Atlas; ICB, Immune checkpoint blockade; KEGG, Kyoto Encyclopedia of Genes and Genomes; OS, Overall survival; PRDEGs, Pyroptosis-related differential expressed genes; PRGs, Pyroptosis-related genes; qRT-PCR, Quantitative real-time reverse transcription PCR; ROC, Receiver operating characteristic; Tregs, Regulatory T cells; REMBRANDT, Repository for Molecular Brain Neoplasia Data; ssGSEA, Single sample gene set enrichment analysis; TMZ, Temozolomide; TCGA, The Cancer Genome Atlas; TIDE, Tumor Immune Dysfunction and Exclusion; TIME, Tumor immune microenvironment; TIMER, Tumor Immune Estimation Resource; TME, Tumor microenvironment; WHO, World Health Organization.

Materials and methods

Data collection and preparation

A total of 180 (23 non-tumor and 157 tumor) mRNA expression profiles from patients with glioma were collected from the Gene Expression Omnibus (GEO) database (GSE4290) (https://www.ncbi.nlm.nih.gov/). Data for 1018 patients with glioma were downloaded from the Chinese Glioma Genome Atlas (CGGA) database (http://www.cgga.org.cn/index.jsp). Non-tumor (n = 28) and tumor (n = 522) samples from patients with glioma in the GEO database (GSE108474), termed The Repository of Molecular Brain Neoplasia Data (REMBRANDT), were included. Biological information from patients with glioma (523 with LGG and 171 with GBM) and information from normal brain tissue were obtained from the UCSC Xena project (https://xena.ucsc.edu/). All raw data from The Cancer Genome Atlas (TCGA) (https://portal.gdc.cancer.gov/) and the Genotype-Tissue Expression (GTEx) database (https://www.gtexportal.org/home/) were recalculated using standard pipeline algorithm from the UCSC Xena project. This process minimized the discrepancy between expression data and made the digital data more compatible. Recurrent samples, secondary samples, non-glioma samples, and samples with incomplete clinical information were excluded. A total of 1920 primary glioma samples (TCGA: 662; GSE4290: 153; REMBRANDT: 454 CGGA: 651) and 257 normal tissues (TCGA-GTEx: 206; GSE4290:23; REMBRANDT:28) were included in this study.

Identification of differentially expressed genes related to pyroptosis in three databases

TCGA-GTEx, GSE4290, and REMBRANT datasets were separately analyzed to detect differentially expressed genes (DEGs) (Supplementary Figure 1). These analyses were performed using the R software version 4.1.0 (13). We set |log fold change (FC)|>1 and an adjusted P-values (p-adj) < 0.05 as the thresholds. The DEGs of TCGA-GTEx, GSE4290 and REMBRANT database were confirmed. We retrieved 81 protein-coding PRGs (Relevance Score>1) from the GeneCards database (https://www.genecards.org/) (Supplementary Table 1).

Validation of the identified biomarker

We estimated the prognostic value of *CASP6* in patients with glioma using the CGGA dataset as the validation dataset. Based on the median expression level, the cleaned data were divided into two groups: the high *CASP6* expression group and the low *CASP6* expression group. Survival analysis between the two groups was implemented in the R software using the "survival" and "survminer" packages. Finally, we built receiver operating characteristic (ROC) curves to evaluate the predictive efficacy of *CASP6*.

Functional enrichment analyses of *CASP6*

Hallmark, Gene Ontology (GO) enrichment analysis, and Kyoto Encyclopedia of Genes and Genomes (KEGG) pathway analysis were performed using the R package "clusterProfiler" (14). Gene set enrichment analysis (GSEA) was used to explore the potential regulatory mechanisms of *CASP6*. We selected the annotated gene sets "h.all.v7.4.symbols.gmt" obtained from the Molecular Signatures Database (MSigDB3) (15), as the reference gene sets. Visualization of the above results was carried out using the R package "enrichplot". We set 0.05 as the cutoff point for the adjusted *p*-value.

Prediction of the chemotherapy and immunotherapy response

The response to temozolomide chemotherapy of each patient with glioma in the CGGA was estimated using the "oncoPredict" R package (16). In this analysis, the Genomics of Drug Sensitivity in Cancer 2 (GDSC2) database (https://www.cancerrxgene.org/) was used as the training data. Meanwhile, this algorithm calculated the half maximal inhibitory concentration (IC50) of temozolomide. The Tumor Immune Dysfunction and Exclusion (TIDE) algorithm using a python (version 3.8.6) script (17) was used to evaluate the response to immune checkpoint blockade (ICB) agents.

Correlation analysis of immune infiltration and CASP6

The "Estimation of STromal and Immune cells in Malignant Tumors using Expression data" (ESTIMATE) (18) algorithm was adopted to predict the level of immune cell infiltration across different *CASP6* expression groups in glioma. The immune score in *CASP6* high- and low-expression groups was determined based on the ESTIMATE analysis. Furthermore, to explore the influence of *CASP6* on the TIME in glioma, we exploited the CIBERSORT (19), single sample gene set enrichment analysis (ssGSEA) (20) and Tumor Immune Estimation Resource (TIMER) (21) algorithms to calculate the infiltration fractions of 22 types of tumor-infiltrating immune cells.

Verification of CASP6 expression in the Human Protein Atlas

CASP6 immunohistochemical images of normal brains and glioma tissues were downloaded from the Human Protein Atlas (HPA) (http://www.proteinatlas.org). We provide the links to these images in Supplementary Table 2.

Cell culture

Human astrocytes (HAs) were cultured with HA culture medium (Astrocyte Medium) (both from ScienCell Research Laboratories, Inc. (San Diego, CA, USA)). And the glioma cell lines (U251 and T98G) were obtained from Procell Life Science & Technology Co., Ltd. (Wuhan, China). Roswell Park Memorial Institute (RPMI) -1640 medium (Gibco, Thermo Fisher Scientific, Shanghai, China) was used as the basal culture medium of U251 cells, while the basal culture medium of T98G was minimal essential medium (MEM) (Gibco, Thermo Fisher Scientific, Shanghai, China). U251 cells were cultured with RPMI-1640 medium supplemented with 10% fetal bovine serum (FBS) and 1% penicillin–streptomycin (P/S) (Biological Industries at Sartorius, Kibbutz Beit-Haemek, Israel). T98G cells were maintained in the presence of MEM, 10% FBS and 1% P/S. HAs, U251, and T98G cells were cultured in a sterile cell incubator at 37°C with 5% CO2.

Quantitative reverse transcription real-time PCR

Total RNA from HA, U251, and T98G cells were extracted using Superbrilliant™ 6 min High-quality RNA Extraction Kit (Zhongshi Gene Technology, Tianjin, China, Cat. No.: ZS-M11005). cDNA synthesis was carried out using the Supersmart ™ 6 min 1st Strand cDNA Synthesizer Kit (Zhongshi Gene Technology, Cat. No.: ZS-M14003). QPCR was performed with Supersmart 5xFast SYBR Green qPCR Mix Kit (Zhongshi Gene Technology, Cat. No.: ZS-M13001) on Bio-Rad Laboratories CFX Connect (TM) Real-time PCR Detection System (Bio-Rad, Hercules, CA, USA). The primers were obtained from Thermo Scientific (Shanghai, China), and included those amplifying *CASP6* (forward 5′-AGGTGGATGCAGCCTCCGTTTA-3′, reverse 5′-ATGAGCCGTTCACAGTTTCCCG-3′); *GAPDH* (encoding glyceraldehyde-3-phosphate dehydrogenase) (Forward: 5′-GCAGGGGGGAGCCAAAAGGG-3′, reverse: 5′-TGCCAGCCCCAGCGTCAAAG-3′). Relative mRNA levels were calculated using the $2^{-\triangle\triangle Ct}$ method (22). Each experiment was carried out independently three times.

Western blotting

Cells were transfected with the indicated plasmids for 4 h. 72h after the transfection, cells were collected, and lysed using Radioimmunoprecipitation assay (RIPA) buffer and protease and phosphatase inhibitors (Solarbio Science and Technology, Beijing, China). Proteins were separated using 10% sodium dodecyl sulfate polyacrylamide gel electrophoresis (SDS-PAGE; Solarbio Science and Technology), then transferred to polyvinylidene fluoride membranes (Millipore, Billerica, MA, USA). The membranes were blocked using 5% skim milk for 2 h and then incubated at 4°C for 12 h with the primary antibodies recognizing the following proteins: CASP6 (ABclonal Technology, Wuhan, China, Catalog NO: A19552) and α -Tubulin (Abways Biotechnology, Shanghai, China, Catalog NO: AB0049). Secondary goat anti-rabbit IgG antibodies (Abways Biotechnology, Catalog NO: AB0101) were then incubated with the membrane for 1 h at 25°C. The ECL Western Blotting Substrate (Solarbio Science and Technology, Catalog NO: PE0010) was used to visualize the immunoreactive proteins, which were detected and analyzed using the BioRad ChemiDoc imaging system (Bio-Rad, USA).

Cell Counting Kit-8 assay

U251 and T98G glioma cells were cultured in T25 cell culture flasks. When the cell density reached about 60%, the culture medium was replaced by serum-free medium. *CASP6* small interfering RNAs (siRNAs) were purchased from Zhongshi Gene Technology. The sequence of si-CASP6#1 (Lot:2146812) was 5'-GACUUCCUCAUGUGUUACUCUdTdT-3' and 5'-AGAGUAACACAUGAGGAAGUCdTdT-3'. The sequence of si-CASP6#2 (Lot:2146814) was 5′-CCUUUGGAUGUAGUAGAUAAUdTdT -3' and 5'-AUUAUCUACUACAUCCAAAGGdTdT -3'. The sequence of si-CASP6#3 (Lot:2146816) was 5'-GCUUUGUGUGUCUUCCUGAdTdT -3' and 5'-UCAGGAAGACACACACAAAGCdTdT -3'. The CASP6 siRNAs and prepared GP-transfect-Mate reagent (GenePharma, Shanghai, China, Cat. No.: G04009) were added to the T25 cell culture flasks. Six hours after transfection, the medium was replaced by complete medium. After 48 h of incubation, the cells were collected and seeded in 96-well plates (5000 cells/well). After the cells were incubated for 2 h, 10 μL CCK-8 reagent (Report bio&technology Co. Ltd, Shijiazhuang, China, Cat.No.:RP-RC3028) was added into each well and incubated in a cell culture incubator for 1 h. A microplate reader (Synergy H1, Biotek, USA) was then employed to measure the absorbance of the medium in the well. This result was recorded as the results of day 0. The assay was repeated at 1, 2, and 3 days after seeding in 96-well plates. Six replicates were set for each sample. And the experiments were repeated independently three times.

Colony formation assay

48 hours after transfection, the *CASP6* siRNAs transfected glioma cells (U251 and T98G) in good growth status were collected and seeded in 35-mm dishes at 500 cells/dish. The cells were cultured with complete medium in a sterile cell incubator at 37°C with 5% CO2 for 14 days. The medium was replaced every 2 days. After 14 days of incubation, the colonies were formed. The culture medium was aspirated off, and 800 μL of 4% paraformaldehyde was added in the dish for 40 minutes to fix the cells. Finally, colonies were stained using crystal violet for 20 minutes and counted under a microscope. The experiments were repeated independently three times.

Statistical analysis

Data analysis and statistical tests were performed using R (version 4.1.0). Comparisons between two groups were performed *via* a Wilcoxon rank-sum test. We conducted statistical analysis of categorical variables between groups using the chi-squared test. The OS analysis of patients with glioma was carried out using the Kaplan-Meier method. The independent prognostic value of *CASP6* and other clinical characteristics were calculated separately using univariate and multivariate Cox regression analyses. Correlation analysis was conducted using the Pearson correlation test. We used the R package "meta." to determine a pooled hazard ratio (HR) by invoking the random-effects meta-analysis model. A *P*-value < 0.05 was considered statistically significant.

Results

Analysis of pyroptosis-related differentially expressed genes in glioma patients

To identify PRDEGs in gliomas, a collection of 81 genes related to pyroptosis were collated from GeneCards database. Their expression was examined in datasets from GSE4290 REMBRANDT, and the TCGA-GTEx cohorts. In the GSE4290 dataset, 11 PRDEGs were identified, among which 10 were upregulated and one was downregulated. In the REMBRANDT dataset, 11 PRDEGs were uncovered, including three that were upregulated and eight that were downregulated. In TCGA-GTEx dataset, 57 PRDEGS were upregulated and one PRDEG was downregulated (Figures 1A–C). Overlap of PRDEGs from these cohorts demonstrated that CASP6 was the only one upregulated in all three datasets, while there was no common downregulated PRDEG (Figures 1D, E). Together, these results identified CASP6 as a candidate biomarker in glioma.

CASP6 expression could predict prognosis in the CGGA dataset

To explore the prognostic significance of *CASP6* in patients with glioma, we chose the CGGA database for further analyses (Table 1). Based on the median *CASP6* expression level, glioma samples were sub-classified into a group with high *CASP6* expression levels and a group exhibiting low levels of *CASP6* expression. Kaplan-Meier survival curve showed that patients with glioma with lower *CASP6* had a longer OS ($P < 0.0001$) (Figure 2A). The accuracy of *CASP6* expression to predict the 3-year-OS and 5-year-OS of patients with glioma was evaluated using a ROC curve. The AUC values for 3-, and 5-year OS were 0.733, and 0.759, respectively (Figure 2B). Consistently, analysis of TCGA and the REMBRANDT cohorts demonstrated that patients with glioma exhibiting lower *CASP6* expression levels had longer survival ($P < 0.0001$) (Supplementary Figures 2A, 3A). In ROC curves based on the 3-, and 5-year OS, groups of patients with glioma exhibiting higher *CASP6* expression were separated from those with glioma of lower *CAP6* expression, with AUC values ranging from 0.668 to 0.809 (Supplementary Figures 2B, 3B). Moreover, a 10-year time-dependent AUC was plotted to define the accuracy of different variables in predicting the OS of patients in the CGGA, TCGA, and REMBRANDT cohorts. Compared to AUC values based on gender, isocitrate dehydrogenase (IDH) activity, 1p19q codeletion, and *MGMT* (encoding O-6-methylguanine-DNA methyltransferase) gene promoter methylation, *CASP6* expression levels, age, and grade consistently showed higher AUC scores (Figure 2C; Supplementary Figures 2C, 3C). In agreement, univariate and multivariate Cox analysis showed that *CASP6* expression could be a predictor of prognosis in patients with glioma (Table 2). Furthermore, the CGGA dataset was categorized according to age, gender, chemotherapy, radiotherapy, WHO grade, IDH mutation, 1p19q co-deletion, and *MGMT* methylation status. Each category was classified in into high-expression or low-expression groups based the median *CASP6* expression levels. Stratified survival analyses verified that low *CASP6* expression in each subgroup of patients was associated with longer survival (Figure 3). Accordingly, similar results were obtained from analysis of the TCGA and REMBRANDT databases (Supplementary Figures 4, 5) Taken together, these data indicated that *CASP6* may represent a potential prognostic biomarker for patients with glioma.

CASP6 expression could predict differences in TIME

Infiltration and activation of immune cells is associated with the prognosis of glioma (23). To investigate the role of CASP6 in

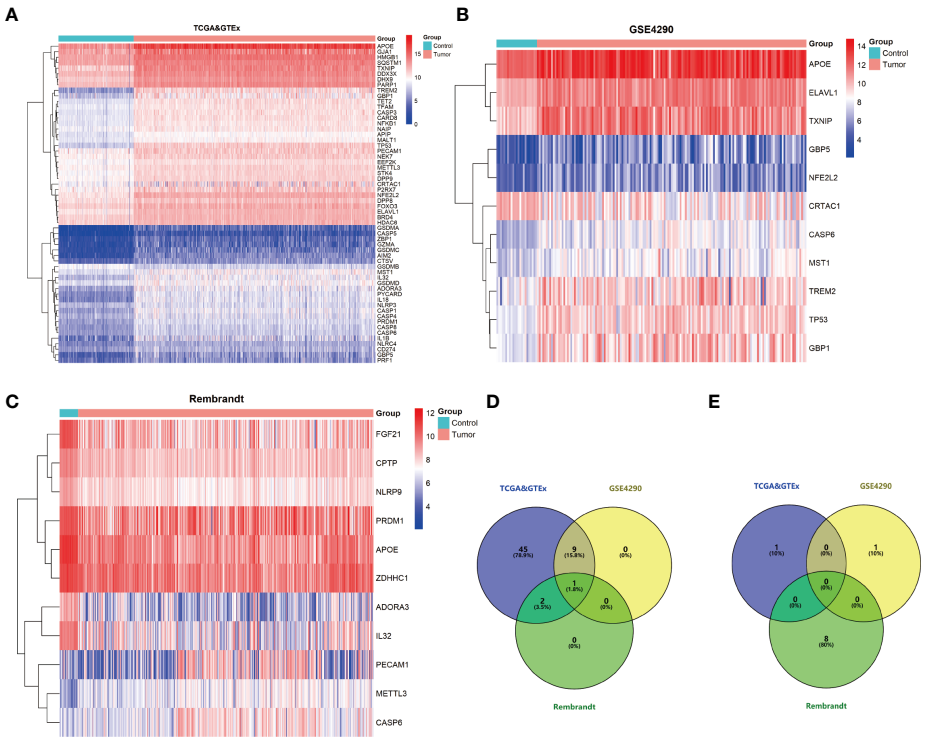

FIGURE 1
Pyroptosis-related differential expressed genes (PRDEGs) in glioma. **(A)** Heatmap of PRDEGs in the TCGA & GTEx datasets. **(B)** Heatmap of PRDEGs in the GSE4290 dataset. **(C)** Heatmap of PRDEGs in the REMBRANDT database. **(D)** Venn diagrams of up-regulated PRDEGs. **(E)** Venn diagrams of down-regulated PRDEGs.

the TIME of glioma, we evaluated the immune score and immune infiltration in glioma samples with low or high *CASP6* expression levels, respectively. In both CGGA and TCGA datasets, glioma sample group with increased levels of *CASP6* expression exhibited a higher immune score than the group with decreased *CASP6* expression (Figure 4A; Supplementary Figure 6A). The presence of immune cells and their identity in the CGGA and TAGA cohorts were analyzed using the CIBERSORT, ssGSEA, and TIMER algorithms. Compared to glioma sample group with lower *CASP6* expression levels, the proportions of naïve T cells, activated natural killer (NK) cells, and M0 macrophages were markedly decreased in glioma samples exhibiting higher levels of *CASP6* expression, whereas the proportions of gamma delta T cells, monocytes, M2 macrophages, activated dendritic cells, and neutrophils were significantly increased in this group (Figures 4B–D; Supplementary Figures 6B–D). To understand the effects of *CASP6* expression on TIME, we investigated the biological functions of CASP6. GO analysis showed that CASP6 was mainly involved in processes including "activation of immune response", "adaptive immune response", "aging", "ameboidal cell migration", and "antigen processing and presentation" (Figure 5A). Furthermore, the annotations of the KEGG pathway revealed an enrichment of CASP6 in pathways including "antigen processing and presentation", "cell cycle", "complement and coagulation cascades", "receptor interaction", and "focal adhesion" (Figure 5B). GSEA analysis showed that higher expression of *CASP6* was associated with hallmarks of tumorigenesis including "apoptosis", "allograft rejection", "coagulation", "complement", and "E2F targets" correlated markedly (Figure 5C; Supplementary Table 3). Taken together, these results indicated that CASP6 may play a role in regulating in immune cell infiltration in glioma.

CASP6 could serve as a biomarker to predict response to temozolomide and immunotherapy

As revealed by the GO and GSEA analyses, CASP6 was associated with "activation of the immune response", "cell cycle", and "apoptosis" processes. Thus, we investigated the predictive

TABLE 1 Clinical characteristics of 651 patients with primary glioma in the CGGA dataset according to *CASP6* expression.

CASP6 expression level		High	Low	P-value
Number		325	326	
CASP6_mRNA (median[IQR])		3.13 [2.79, 3.51]	1.81 [1.22, 2.12]	<0.001
Age (%)	≤42	133 (40.9)	181 (55.5)	<0.001
	>42	191 (58.8)	145 (44.5)	
Gender (%)	Female	130 (40.0)	136 (41.7)	0.714
	Male	195 (59.7)	190 (58.3)	
Grade (%)	II	70 (21.5)	162 (49.7)	<0.001
	III	87 (26.8)	107 (32.8)	
	IV	168 (51.7)	57 (17.5)	
Histology (%)	A (Astrocytoma)	57 (17.5)	74 (22.7)	<0.001
	AA (Anaplastic Astrocytoma)	73 (22.5)	47 (14.4)	
	AO (Anaplastic Oligodendroglioma)	14 (4.3)	44 (13.5)	
	AOA (Anaplastic Oligoastrocytoma)	0 (0.0)	16 (4.9)	
	GBM	168 (51.7)	57 (17.5)	
	O (Oligodendroglioma)	11 (3.4)	82 (25.2)	
	OA (Oligoastrocytoma)	2 (0.6)	6 (1.8)	
Survival (median[IQR])		22.7 [11.9, 51.8]	66.1 [30.2, 93.7]	<0.001
Status (%)	Alive	73 (22.5)	208 (63.8)	<0.001
	Dead	244 (75.1)	105 (32.2)	
IDH status (%)	Wildtype	215 (66.2)	72 (22.1)	<0.001
	Mutant	107 (32.9)	217 (66.6)	
1p19q (%)	Non-codel	302 (92.9)	144 (44.2)	<0.001
	Codel	22 (6.8)	120 (36.8)	
MGMTp methylation status (%)	un-methylated	148 (45.5)	114 (35.0)	0.037
	methylated	140 (43.1)	156 (47.9)	
Radio status (%)	No	43 (13.2)	71 (21.8)	0.006
	Yes	266 (81.8)	240 (73.6)	
Chemo status (%)	No	88 (27.1)	113 (34.7)	0.036
	Yes	217 (66.8)	191 (58.6)	

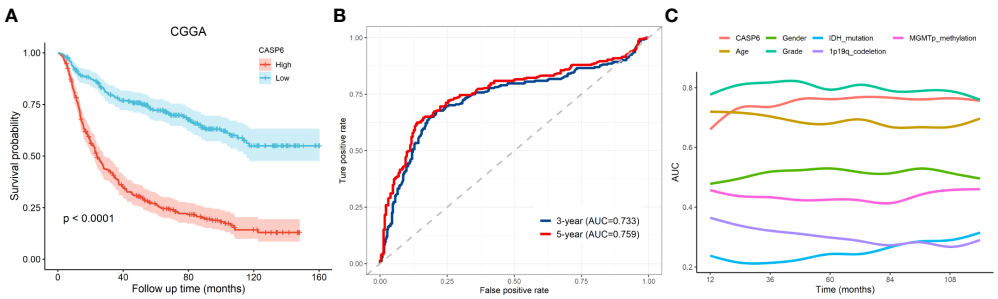

FIGURE 2
The prognostic value of *CASP6* in the CGGA database. **(A)** Kaplan-Meier survival analyses of overall survival and *CASP6* in patients with glioma in the CGGA database. **(B)** ROC curve analysis to evaluate the prognostic value of *CASP6* expression in glioma in terms of survival at 3 years and 5 years. **(C)** AUC analysis to evaluate the prognostic value of *CASP6* expression in glioma.

TABLE 2 Univariate and multivariate analysis of *CASP6* and clinical features in the CGGA datasets.

Univariate Cox analysis of CGGA (n=1018)			Multivariate Cox analysis CGGA (n=1018)		
Variables	***p* value**	**HR (95%CI)**	**Variables**	***p* value**	**HR (95%CI)**
CASP6	7.52E-30	2.1 (1.85-2.38)	CASP6	1.70E-06	1.64 (1.34-2.01)
Age	2.53E-21	1.04 (1.04-1.05)	Age	4.83E-05	1.02 (1.01-1.03)
Gender (Male vs. Female)	0.565	1.07 (0.86-1.32)	Gender (Male vs. Female)	0.861	0.98 (0.76-1.26)
Grade (WHOIV vs. WHOIII vs. WHOII)	2.65E-48	2.99 (2.58-3.46)	Grade (WHOIV vs. WHOIII vs. WHOII)	4.83E-09	1.89 (1.53-2.34)
Radio-status (Treated vs. Untreated)	0.0429	1.38 (1.01-1.88)	Radio-status (Treated vs. Untreated)	0.447	0.87 (0.6-1.26)
Chemo-status (Treated vs. Untreated)	0.0286	1.3 (1.03-1.65)	Chemo-status (Treated vs. Untreated)	0.00106	0.61 (0.46-0.82)
IDH (Mutant vs. Wildtype)	1.78E-37	0.22 (0.18-0.28)	IDH (Mutant vs. Wildtype)	0.127	0.77 (0.54-1.08)
1p19q (Codeletion vs. non-Codeletionl)	1.44E-19	0.14 (0.09-0.21)	1p19q (Codeletion vs. non-Codeletionl)	7.25E-05	0.35 (0.21-0.59)
MGMT (methyltransferase vs. non- methyltransferase	0.000936	0.68 (0.55-0.86)	MGMT (methyltransferase vs. non- methyltransferase	0.0353	0.76 (0.59-0.98)

HR, hazard ratio; IDH, isocitrate dehydrogenases; MGMT, O-6-methylguanine-DNA methyltransferase.

value of CASP6 expression in the response to temozolomide and immunotherapy. Temozolomide (TMZ) is one of the most common chemotherapeutic options for glioma treatment (24), and has been shown to improve the survival rate of patients newly diagnosed with glioma (25). Nonetheless, resistance to TMZ remains a conundrum in glioma chemotherapy. Simultaneously, immunotherapy has been increasingly applied to patients with glioma in recent years. Finding suitable molecular characteristics to predict the efficacy of immunotherapy is urgently required. We calculated the IC50 of TMZ associated with *CAPS6* expression to estimate its role in selecting the best treatment methods. Notably, TMZ presented a better therapeutic response in patients with glioma with high *CASP6* expression (Figure 6A). The outcome of TMZ response prediction in the TCGA cohort was consistent with that of the CGGA cohort (Supplementary Figure 8A). Meanwhile, the TIDE results further predicted that patients with high expression of *CASP6* would achieve a poorer response to immunotherapy than those with low *CASP6* expression (Figure 6B). Our findings revealed that the CASP6 could play a role in determining therapeutic strategies for patients with glioma.

Meta-analysis of *CASP6* and validation of *CASP6* expression in patients with glioma and cells

To improve the reliability of the results, a meta-analysis of the CGGA, TCGA, and REMBRANDT datasets was performed. The results confirmed that patients with high expression of *CASP6* had a shorter OS than patients with lower *CASP6* expression (HR = 2.18, 95% CI 1.24–3.82, Figure 7A). Further analysis of *CASP6* expression datasets obtained from the CGGA, REMBRANDT, TCGA, GSE4290 databases showed that higher *CASP6* expression was associated with the grade of glioma (Figure 7B). Immunohistochemical images of normal brain tissue, low-grade glioma, and high-grade glioma acquired from the HPA, confirmed that the protein level of CASP6 increased with increasing tumor grade (Figure 7C). Finally, qRT-PCR analysis revealed that the *CASP6* mRNA content in glioma cells (U251 and T98G) was almost two-fold higher than that in normal astrocyte cells (HA) (Figures 7D, E)

Knocking down of *CASP6* inhibits the proliferation of glioma cells

CCK-8 and colony formation assays were conducted to evaluate the effects of knocking down *CASP6* expression on glioma cell proliferation. The efficiency of *CASP6* knockdown was confirmed using qRT-PCR and western blotting. All three siRNAs significantly reduced the expression of CASP6 in U251 and T98G cell lines (Figures 8A–D). The CCK-8 assay showed that *CASP6* knockdown dramatically inhibited the proliferation of U251 and T98G cells (Figures 8E, F). Colony forming assays showed that the colony-forming capacity of U251 and T98G cells was reduced significantly after *CASP6* knockdown (Figure 8G). Collectively, these results demonstrated that the expression of *CASP6* correlated positively with glioma cell proliferation.

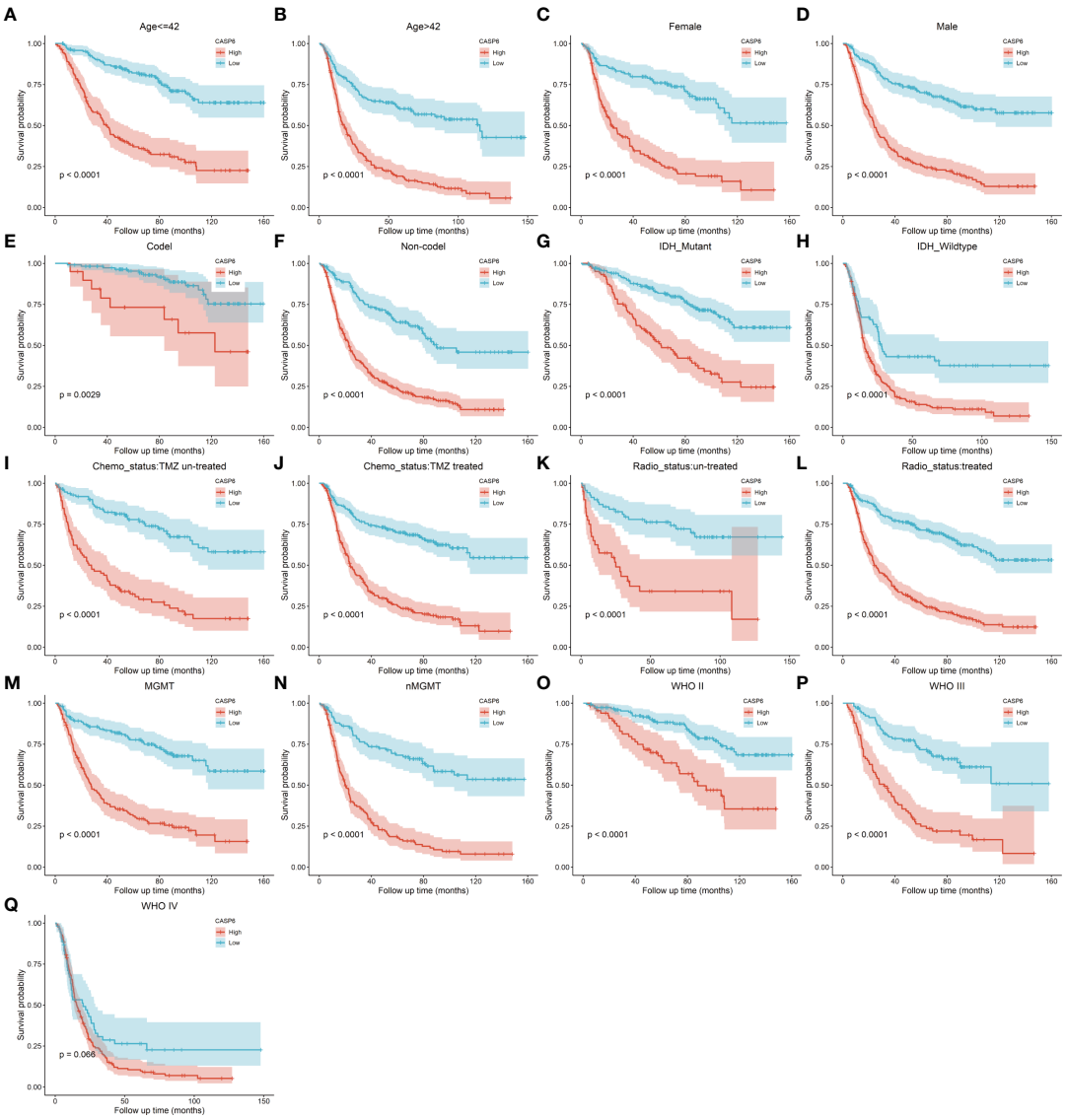

FIGURE 3
(A–Q) Stratified survival analysis of patients with low and high *CASP6* expression in the CGGA database, by age, sex, 1p19q codeletion, IDH mutation, chemotherapy status, radiotherapy status, MGMT status, and grade.

Discussion

Glioma is the most common primary brain neoplasm and is a leading cause of cancer-associated death worldwide (26). Recently, the therapeutic approaches to glioma have improved significantly, however, the clinical outcomes of patients with glioma remain poor (27). Immunotherapy can be effective in many tumors; however, the factors that influence the efficacy of immunotherapy remain complex and relatively unknown (28).

Pyroptosis plays a pivotal role in the onset and development of various diseases (29–31). Interestingly, pyroptosis plays conflicting roles in the promotion and inhibition of oncogenesis and the tumor microenvironment (32, 33). Furthermore, PRG-related prognostic models have been constructed for many neoplasms, including gastric cancer (34), skin cutaneous melanoma (35), breast cancer (36), and thyroid cancer (37). Previously, a prognostic model comprising three PRGs (*CASP4*, *CASP9*, and *NOD2* (encoding nucleotide binding oligomerization domain containing 2)) was constructed to predict the outcomes of patients with glioma (38). The results of the present study are more comprehensive because of the precise construction of the prognosis model,

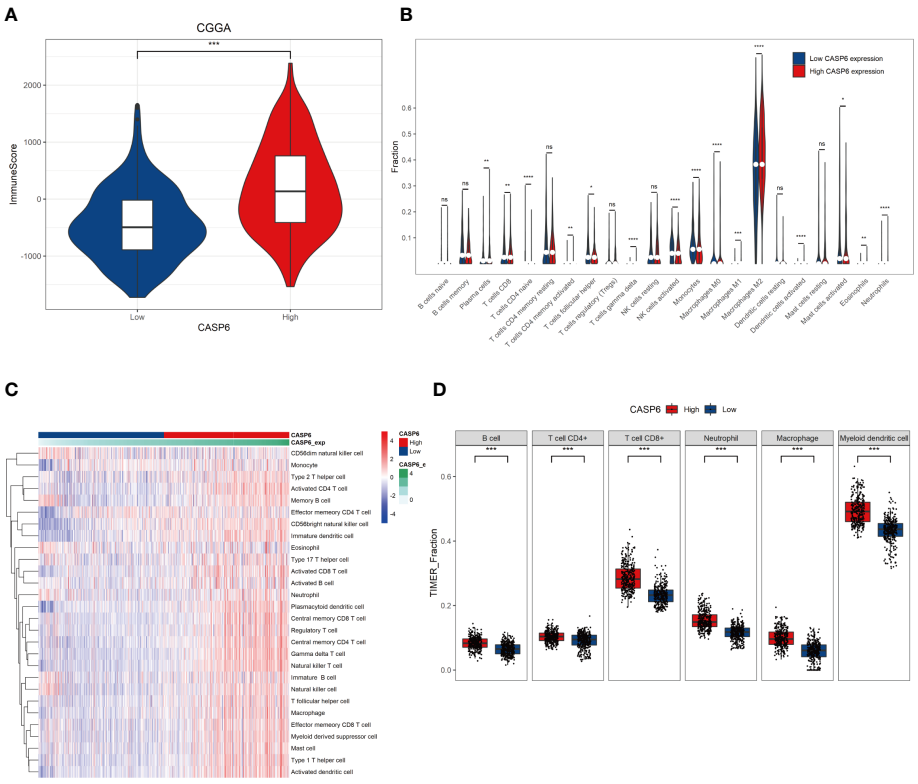

FIGURE 4
Relationships with *CASP6* in the tumor immune microenvironment from the CGGA database. **(A)** Correlation analysis of the ImmuneScore and *CASP6* levels. **(B)** The levels of infiltration of 22 types of immune cells in the low and high *CASP6* expression groups. **(C)** Results of ssGSEA analysis of CASP6 in the CGGA database. **(D)** Results of TIMER analysis of CASP6 in the CGGA database. **P* < 0.05, ***P* < 0.01, ****P* < 0.001, *****P* < 0.0001. ns, no significance

FIGURE 5
Related pathways analyzed by GSEA in the CGGA database. **(A)** GO analysis of *CASP6*. **(B)** KEGG analysis of *CASP6*. **(C)** Hallmark analysis of *CASP6*.

which was based on more databases, bioinformatic analysis and *in vitro* experiments.

CASP6 is an apoptotic caspase (39) that is involved in multiple cell death pathways. It can promote the activation of programmed cell death pathways including pyroptosis, apoptosis, and necroptosis (PANoptosis) (40). However, the status of *CASP6* as a PRG in glioma has been rarely reported (12, 41), therefore, the role of CASP6 in glioma was unclear. Our

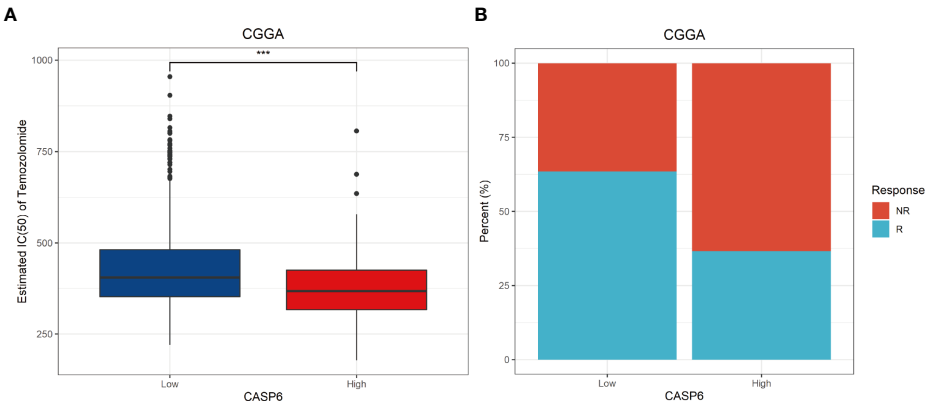

FIGURE 6
Potential predictive value of *CASP6* in chemotherapy and immunotherapy in the CGGA database. **(A)** IC50 of temozolomide in the low and high *CASP6* expression groups. Low *CASP6* expression group (n = 326), high *CASP6* expression group (n = 325) **(B)** Immunotherapy responses in the low and high *CASP6* expression groups. Low *CASP6* expression group [response: n = 207, (63.50%); non-response: n = 119, (36.50%)], high *CASP6* expression group (response: n = 119, (36.62%); non-response: n = 206, (63.38%)) ***$P < 0.001$.

results showed that *CASP6* was a significant biomarker to predict the prognosis of patients with glioma. In the OS analysis, patients with lower *CASP6* expression experienced longer survival. ROC analysis demonstrated that *CASP6* expression was a reliable marker to predict clinical outcomes in patients with glioma. Indeed, stratification survival analysis demonstrated the good predictive role of *CASP6* expression in glioma. Furthermore, univariate and multivariate Cox analyses identified *CASP6* expression as an independent prognostic risk factor for glioma patients.

PRGs regulate the TIME through various mechanisms (42, 43). According to the TME prognostic models, which are based on the characteristics of 33 cancers in the TCGA database, six "Immune Subtype" clusters (C1-C6) were identified (44). Glioma was grouped in cluster C4 (Lymphocyte Depleted), with features of a repressed Th1 response and a high M2 response. Conversely, LGG was classified into cluster C5 (Immunologically Quiet). Cluster C5 cluster has the lowest lymphocyte infiltration and the highest M2 macrophage responses. To explore the effects of CASP6 on the brain immune microenvironment of patients with glioma, we used several deconvolution algorithms. The ESTIMATE findings indicated that the high *CASP6* expression group had a higher ImmuneScore, which meant that immune cell infiltration was higher in the CASP6 high-expression group in the TIME. The proportion of M2 macrophages increased markedly in the high *CASP6* expression group. These results are consistent with the features of immune subtype clusters C4 and C5, and may support a malignant biological behavior of glioma cells (45). Conversely, patients with glioma with a higher proportion of regulatory T cell (Treg) infiltration were consistently associated with poor prognosis (46). Our findings support this conclusion. The high *CASP6* expression group, which was associated with poorer prognosis, exhibited higher infiltration of Tregs.

Considering the differences in the TIME between the two groups, we conducted GO and KEGG functional enrichment analyses to identify the underlying regulatory mechanism, which implied that CASP6 was primarily associated with the immune response and focal adhesion.

TMZ, the most common chemotherapeutic agent used to treat gliomas, can significantly prolong the survival of patients with glioma. However, the response to chemotherapy varies across individuals. To estimate the predictive value of *CASP6* expression in clinical therapy, sensitivity to TMZ was calculated based on gene expression profiles. The results indicated that patients with high *CASP6* expression were more sensitive to TMZ.

Studies have validated the importance of immune cell infiltration in patients with glioma (46). Immunotherapies can markedly improve patient survival and have shown significant antitumor outcomes in several clinical trials (47). The TME of glioma is shaped by the disease itself and not by the surrounding brain tissue. The innate immune system, instead of CD8+T cells, might have greater responsibility for the therapeutic effects of anti-programmed cell death-1 (PD-1) antibodies in glioblastoma. In glioblastoma, severe T cell exhaustion induced upregulation of multiple immune checkpoints, which inhibits immune modulation (48). Furthermore, not all patients with glioma can

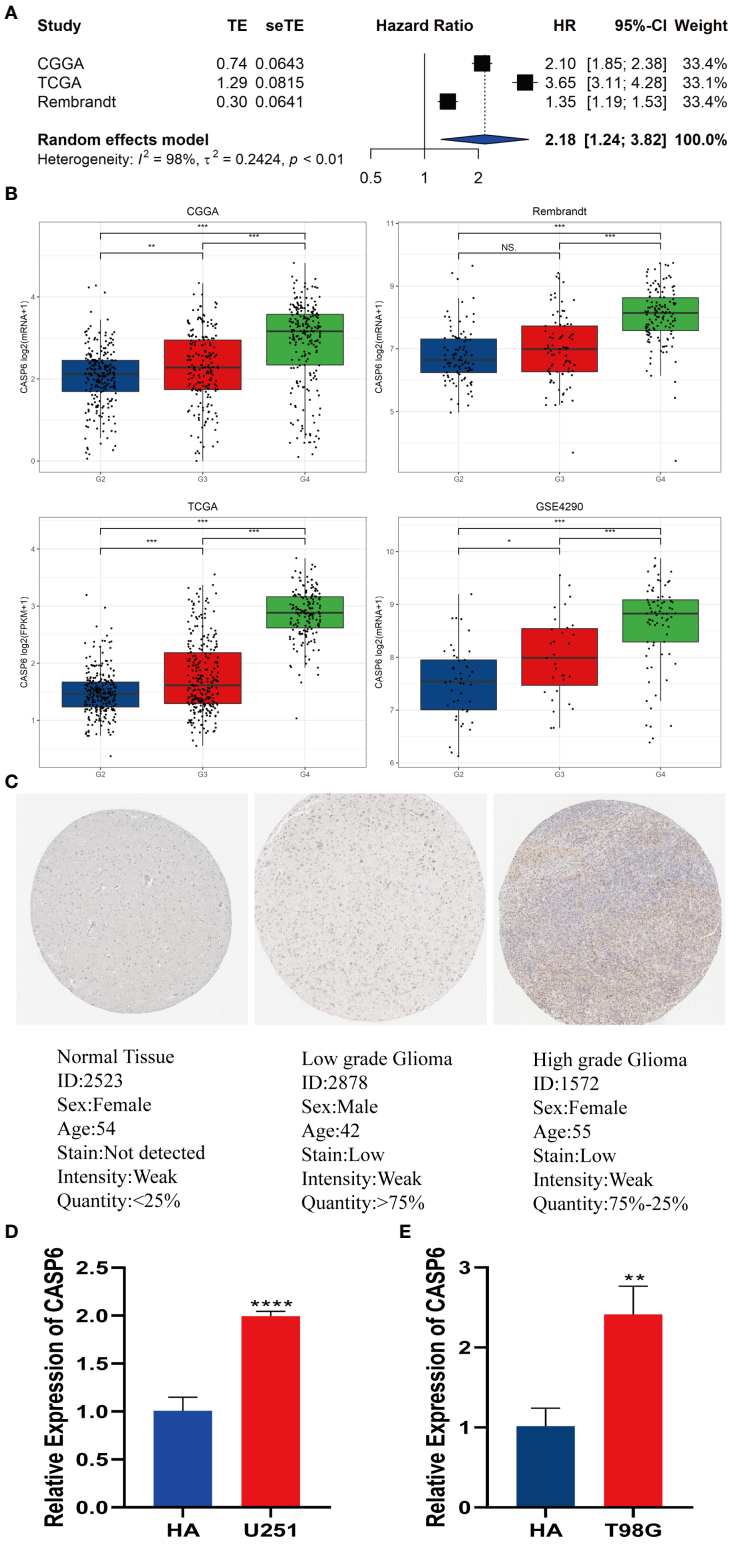

FIGURE 7
Meta-analysis of *CASP6* and its expression level in gliomas. **(A)** Meta-analysis of *CASP6* in the CGGA, TCGA and REMBRANDT databases. **(B)***CASP6* expression increased with disease progression of glioma (G2: Grade2, G3: Grade3, G4:Grade4). **(C)** Differentially expression of CASP6 in glioma and normal tissues in The Human Protein Atlas database. **(D)** qRT-PCR indicated that the expression of *CASP6* was upregulated in U251 cells compared with that in HAs. **(E)** qRT-PCR indicated that the expression of CASP6 was upregulated in T98G cells compared with that in HA. *P < 0.05, **P < 0.01, ***P < 0.001, ****P < 0.0001. NS: no significance.

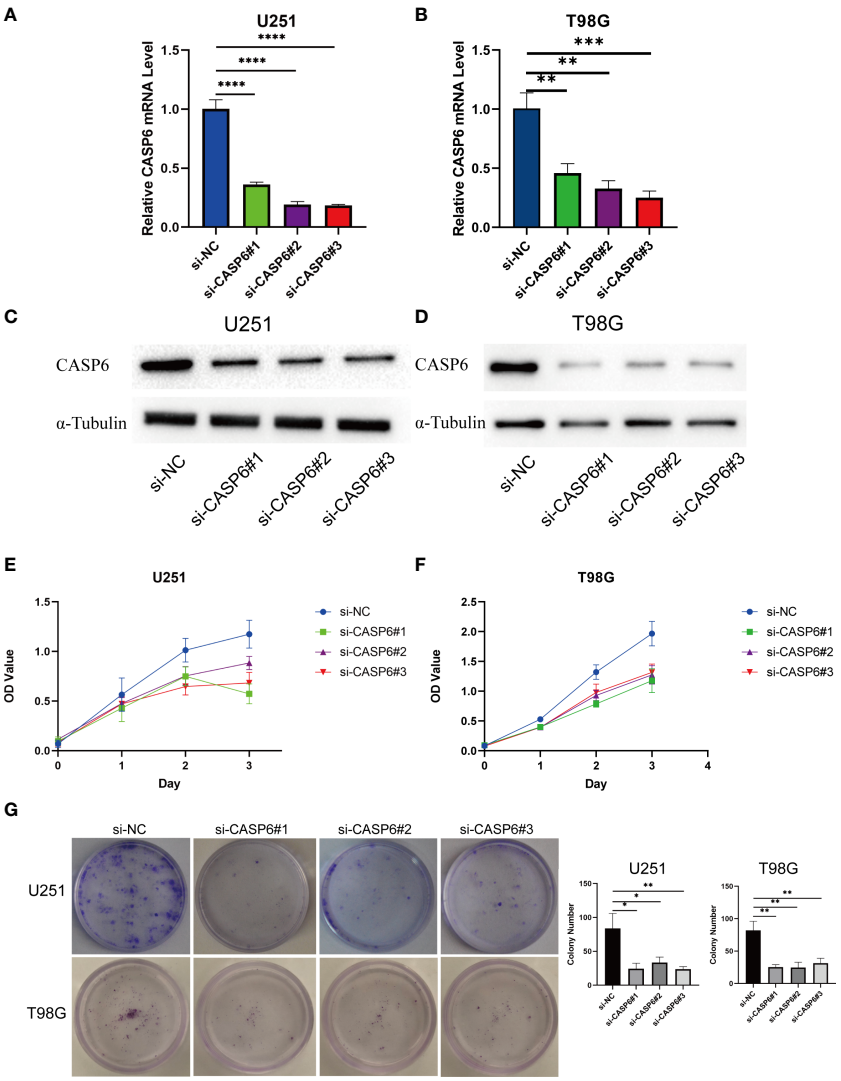

FIGURE 8
Results of loss of function experiments in U251 and T98G glioma cell lines. **(A, B)** The *CASP6* knockdown efficiency of different siRNAs in U251 and T98G cells. **(C, D)** Identification of *CASP6* knockdown efficiency by western blotting. **(E, F)** CCK-8 assays of U251 and T98G glioma cell lines knocked down for *CASP6*. **(G)** Colony formation assays of U251 and T98G glioma cell lines knocked down for *CASP6*. *P < 0.05, **P < 0.01, ***P < 0.001, ****P < 0.0001

benefit from monotherapy immune checkpoint inhibition (49). Therefore, new predictive biomarkers to improve precision immunotherapy for patients with glioma are required. In our study, patients with glioma with lower *CASP6* expression presented a better response to immunotherapy.

To further confirm the predictive value of *CASP6* expression as a new prognostic biomarker for glioma, we conducted a meta-analysis, which showed that based on its HR and 95% CI (2.18 and 1.24–3.82, respectively), *CASP6* expression is a robust prognostic indicator.

In addition, we performed experimental validation of aberrant *CASP6* expression in patients with different grades of glioma. The bioinformatics analysis showed that *CASP6* expression increased with the increasing degree of malignancy of glioma. The immunohistochemical images obtained from the HPA showed that CASP6 expression was lower in normal brain tissue than in glioma tissue. *CASP6* expression in normal human astrocytes was lower than that in human glioma cell lines (U251 and T98G), as confirmed by qRT-PCR. Furthermore, the HPA immunohistochemistry images showed that high-grade glioma tissues contained higher levels of CASP6 than low-grade glioma tissue. Thus, the above observations confirmed the findings of the bioinformatics analysis.

Finally, *in vitro* functional experiments showed that knockdown of *CASP6* inhibited the proliferation of glioma cells. CCK-8 and colony forming assays demonstrated that CASP6 is highly related to the proliferation of glioma. Thus, CASP6 might represent a potential target in the treatment of glioma.

In this study, we selected the CGGA as the validation cohort, because it is the largest Chinese sample database, containing clinical and follow-up information of patients with glioma. Furthermore, we excluded patients with secondary and recurrent glioma because of their complex biological characteristics. Nonetheless, the immunotherapy response of patients showed opposite trends when comparing the TCGA data with the CGGA data (Supplementary Figure 8B). We suspect that differences in ethnicities might be responsible for these contrasting results.

Conclusion

In the present study, we identified the PRDEG CASP6 as a biomarker for glioma. We propose that detecting *CASP6* expression combined with clinical features might improve the diagnostic accuracy in patients with glioma. *In vitro*, *CASP6* was verified as an oncogene in glioma, and CASP6 inhibition prevented glioma cell proliferation. The results of the present study might promote innovative strategies to assess immunotherapy outcomes and thus improve the prognosis of patients with glioma.

Data availability statement

The original contributions presented in the study are included in the article/Supplementary Material. Further inquiries can be directed to the corresponding author.

Author contributions

ZZ oversaw the overall design of this research. KG performed the experiments, analyzed the data, and wrote the manuscript. JZ contributed to the R software analysis and provided R language modification. QJ verified the data analysis. HY revised the figures and tables. YS revised the discussion of the article. All authors contributed to the article and approved the submitted version.

Funding

This work was supported by the National Key R & D Program Intergovernmental Cooperation on International Scientific and Technological Innovation of the Ministry of Science and Technology of China [grant number 2017YFE0110400]; the National Natural Science Foundation of China [grant number 81870984]; the Special Project for the Construction of Hebei Province International Science and Technology Cooperation Base [grant number 193977143D]; the Government Funded Project on Training of Outstanding Clinical Medical Personnel and Basic Research Projects of Hebei Province in the Year of 2019; and the Medical science research project of Hebei Province [grant number 20201567].

Acknowledgments

The authors would like to thank the CGGA, REMBRANDT, TCGA, GTEx and GEO databases for providing the data.

Conflict of interest

The authors declare that the research was conducted in the absence of any commercial or financial relationships that could be construed as a potential conflict of interest.

Publisher's note

Supplementary material

The Supplementary Material for this article can be found online at: https://www.frontiersin.org/articles/10.3389/fonc.2022.818283/full#supplementary-material

References

1. Louis DN, Perry A, Reifenberger G, von Deimling A, Figarella-Branger D, Cavenee WK, et al. The 2016 world health organization classification of tumors of the central nervous system: A summary. *Acta Neuropathol* (2016) 131:803–20. doi: 10.1007/s00401-016-1545-1

2. Ostrom QT, Bauchet L, Davis FG, Deltour I, Fisher JL, Langer CE, et al. The epidemiology of glioma in adults: a "state of the science" review. *Neuro Oncol* (2014) 16:896–913. doi: 10.1093/neuonc/nou087

3. Lim M, Xia Y, Bettegowda C, Weller M. Current state of immunotherapy for glioblastoma. *Nat Rev Clin Oncol* (2018) 15:422–42. doi: 10.1038/s41571-018-0003-5

4. Tang R, Xu J, Zhang B, Liu J, Liang C, Hua J, et al. Ferroptosis, necroptosis, and pyroptosis in anticancer immunity. *J Hematol Oncol* (2020) 13:110. doi: 10.1186/s13045-020-00946-7

5. Yu J, Li S, Qi J, Chen Z, Wu Y, Guo J, et al. Cleavage of GSDME by caspase-3 determines lobaplatin-induced pyroptosis in colon cancer cells. *Cell Death Dis* (2019) 10:193. doi: 10.1038/s41419-019-1441-4

6. Long K, Gu L, Li L, Zhang Z, Li E, Zhang Y, et al. Small-molecule inhibition of APE1 induces apoptosis, pyroptosis, and necroptosis in non-small cell lung cancer. *Cell Death Dis* (2021) 12:503. doi: 10.1038/s41419-021-03804-7

7. Shangguan F, Zhou H, Ma N, Wu S, Huang H, Jin G, et al. A novel mechanism of cannabidiol in suppressing hepatocellular carcinoma by inducing GSDME dependent pyroptosis. *Front Cell Dev Biol* (2021) 9:697832. doi: 10.3389/fcell.2021.697832

8. Chen S, Ma J, Yang L, Teng M, Lai ZQ, Chen X, et al. Anti-glioblastoma activity of kaempferol *via* programmed cell death induction: Involvement of autophagy and pyroptosis. *Front Bioeng Biotechnol* (2020) 8:614419. doi: 10.3389/fbioe.2020.614419

9. Jiang Z, Yao L, Ma H, Xu P, Li Z, Guo M, et al. miRNA-214 inhibits cellular proliferation and migration in glioma cells targeting caspase 1 involved in pyroptosis. *Oncol Res* (2017) 25:1009–19. doi: 10.3727/096504016X14813859905646

10. Liu Y, Wu H, Jing J, Li H, Dong S, Meng Q. Downregulation of I_circ_0001836 induces pyroptosis cell death in glioma cells *via* epigenetically upregulating NLRP1. *Front Oncol* (2021) 11:622727. doi: 10.3389/fonc.2021.622727

11. Lin W, Chen Y, Wu B, Chen Y, Li Z. Identification of the pyroptosis-related prognostic gene signature and the associated regulation axis in lung adenocarcinoma. *Cell Death Discov* (2021) 7:161. doi: 10.1038/s41420-021-00557-2

12. Komata T, Kondo Y, Kanzawa T, Hirohata S, Koga S, Sumiyoshi H, et al. Treatment of malignant glioma cells with the transfer of constitutively active caspase-6 using the human telomerase catalytic subunit (human telomerase reverse transcriptase) gene promoter. *Cancer Res* (2001) 61:5796–802.

13. R Core Team. R: A language and environment for statistical computing. In: *R foundation for statistical computing*. Vienna, Austria (2020). Available at: https://www.R-project.org/.

14. Yu G, Wang LG, Han Y, He QY. clusterProfiler: an r package for comparing biological themes among gene clusters. *OMICS* (2012) 16:284–7. doi: 10.1089/omi.2011.0118

15. Liberzon A, Birger C, Thorvaldsdóttir H, Ghandi M, Mesirov JP, Tamayo P. The molecular signatures database (MSigDB) hallmark gene set collection. *Cell Syst* (2015) 1:417–25. doi: 10.1016/j.cels.2015.12.004

16. Maeser D, Gruener RF, Huang RS. oncoPredict: an r package for predicting *in vivo* or cancer patient drug response and biomarkers from cell line screening data. *Brief Bioinform* (2021) 22:bbab260. doi: 10.1093/bib/bbab260

17. Jiang P, Gu S, Pan D, Fu J, Sahu A, Hu X, et al. Signatures of T cell dysfunction and exclusion predict cancer immunotherapy response. *Nat Med* (2018) 24:1550–8. doi: 10.1038/s41591-018-0136-1

18. Yoshihara K, Shahmoradgoli M, Martínez E, Vegesna R, Kim H, Torres-Garcia W, et al. Inferring tumour purity and stromal and immune cell admixture from expression data. *Nat Comm* (2013) 4:2612. doi: 10.1038/ncomms3612

19. Newman AM, Steen CB, Liu CL, Gentles AJ, Chaudhuri AA, Scherer F, et al. Determining cell type abundance and expression from bulk tissues with digital cytometry. *Nat Biotechnol* (2019) 37:773–82. doi: 10.1038/s41587-019-0114-2

20. Barbie DA, Tamayo P, Boehm JS, Kim SY, Moody SE, Dunn IF, et al. Systematic RNA interference reveals that oncogenic KRAS-driven cancers require Tbk1. *Nature* (2009) 462(7269):108–12. doi: 10.1038/nature08460

21. Li T, Fan J, Wang B, Traugh N, Chen Q, Liu JS, et al. Timer: A web server for comprehensive analysis of tumor-infiltrating immune cells. *Cancer Res* (2017) 77 (21):e108–e10. doi: 10.1158/0008-5472.CAN-17-0307

22. Livak KJ, Schmittgen TD. Analysis of relative gene expression data using real-time quantitative pcr and the 2(-delta delta C(T)) method. *Methods (San Diego Calif)* (2001) 25(4):402–8. doi: 10.1006/meth.2001.1262

23. Grabowski MM, Sankey EW, Ryan KJ, Chongsathidkiet P, Lorrey SJ, Wilkinson DS, et al. Immune suppression in gliomas. *J Neurooncol* (2021) 151:3–12. doi: 10.1007/s11060-020-03483-y

24. Yao T, Zhang CG, Gong MT, Zhang M, Wang L, Ding W. Decorin-mediated inhibition of the migration of U87MG glioma cells involves activation of autophagy and suppression of TGF-β signaling. *FEBS Open Bio* (2016) 6:707–19. doi: 10.1002/2211-5463.12076

25. Wang Y, Meng X, Zhou S, Zhu Y, Xu J, Tao R. Apatinib plus temozolomide for recurrent glioblastoma: An uncontrolled, open-label study. *Onco Targets Ther* (2019) 12:10579–85. doi: 10.2147/OTT.S226804

26. Bray F, Ferlay J, Soerjomataram I, Siegel RL, Torre LA, Jemal A. Global cancer statistics 2018: GLOBOCAN estimates of incidence and mortality worldwide for 36 cancers in 185 countries. *CA Cancer J Clin* (2018) 68:394–424. doi: 10.3322/caac.21492

27. Weller M, Wick W, Aldape K, Brada M, Berger M, Pfister SM, et al. Glioma. *Nat Rev Dis Primers* (2015) 1:15017. doi: 10.1038/nrdp.2015.17

28. Boussiotis VA, Charest A. Immunotherapies for malignant glioma. *Oncogene* (2018) 37(9):1121–41. doi: 10.1038/s41388-017-0024-z

29. Wu X, Ren G, Zhou R, Ge J, Chen FH. The role of Ca(2+) in acid-sensing ion channel 1a-mediated chondrocyte pyroptosis in rat adjuvant arthritis. *Lab Invest* (2019) 99(4):499–513. doi: 10.1038/s41374-018-0135-3

30. Zeng C, Wang R, Tan H. Role of pyroptosis in cardiovascular diseases and its therapeutic implications. *Int J Biol Sci* (2019) 15:1345–57. doi: 10.7150/ijbs.33568

31. Zu Y, Mu Y, Li Q, Zhang ST, Yan HJ. Icariin alleviates osteoarthritis by inhibiting NLRP3-mediated pyroptosis. *J Orthop Surg Res* (2019) 14:307. doi: 10.1186/s13018-019-1307-6

32. Yang X, Chen G, Yu KN, Yang M, Peng S, Ma J, et al. Cold atmospheric plasma induces GSDME-dependent pyroptotic signaling pathway *via* ROS generation in tumor cells. *Cell Death Dis* (2020) 11:295. doi: 10.1038/s41419-020-2459-3

33. Zhang Y, Yang J, Wen Z, Chen X, Yu J, Yuan D, et al. A nove' 3',5'-diprenylated chalcone induces concurrent apoptosis and GSDME-dependent pyroptosis through activating PKCδ/JNK signal in prostate cancer. *Aging* (2020) 12:9103–24. doi: 10.18632/aging.103178

34. Shao W, Yang Z, Fu Y, Zheng L, Liu F, Chai L, et al. The pyroptosis-related signature predicts prognosis and indicates immune microenvironment infiltration in gastric cancer. *Front Cell Dev Biol* (2021) 9:676485. doi: 10.3389/fcell.2021.676485

35. Ju A, Tang J, Chen S, Fu Y, Luo Y. Pyroptosis-related gene signatures can robustly diagnose skin cutaneous melanoma and predict the prognosis. *Front Oncol* (2021) 11:709077. doi: 10.3389/fonc.2021.709077

36. Ping L, Zhang K, Ou X, Qiu X, Xiao X. A novel pyroptosis-associated long non-coding RNA signature predicts prognosis and tumor immune microenvironment of patients with breast cancer. *Front Cell Dev Biol* (2021) 9:727183. doi: 10.3389/fcell.2021.727183

37. Wu P, Shi J, Sun W, Zhang H. Identification and validation of a pyroptosis-related prognostic signature for thyroid cancer. *Cancer Cell Int* (2021) 21:523. doi: 10.1186/s12935-021-02231-0

38. Li XY, Zhang LY, Li XY, Yang XT, Su LX. A pyroptosis-related gene signature for predicting survival in glioblastoma. *Front Oncol* (2021) 11:697198. doi: 10.3389/fonc.2021.697198

39. Man SM, Kanneganti TD. Converging roles of caspases in inflammasome activation, cell death and innate immunity. *Nat Rev Immunol* (2016) 16(1):7–21. doi: 10.1038/nri.2015.7

40. Zheng M, Karki R, Vogel P, Kanneganti TD. Caspase-6 is a key regulator of innate immunity, inflammasome activation, and host defense. *Cell* (2020) 181:674–87.e13. doi: 10.1016/j.cell.2020.03.040

41. Zhang L, Ren J, Zhang H, Cheng G, Xu Y, Yang S, et al. Her2-targeted recombinant protein immuno-Caspase-6 effectively induces apoptosis in Her2-overexpressing gbm cells in vitro and in vivo. *Oncol Rep* (2016) 36(5):2689–96. doi: 10.3892/or.2016.5088

42. Du T, Gao J, Li P, Wang Y, Qi Q, Liu X, et al. Pyroptosis, metabolism, and tumor immune microenvironment. *Clin Transl Med* (2021) 11:e492. doi: 10.1002/ctm2.492

43. Erkes DA, Cai W, Sanchez IM, Purwin TJ, Rogers C, Field CO, et al. Mutant BRAF and MEK inhibitors regulate the tumor immune microenvironment *via* pyroptosis. *Cancer Discov* (2020) 10:254–69. doi: 10.1158/2159-8290.CD-19-0672

44. Thorsson V, Gibbs DL, Brown SD, Wolf D, Bortone DS, Ou Yang TH, et al. The immune landscape of cancer. *Immunity* (2018) 48(4):812–30.e14. doi: 10.1016/j.immuni.2018.03.023

45. Qian M, Wang S, Guo X, Wang J, Zhang Z, Qiu W, et al. Hypoxic glioma-derived exosomes deliver microRNA-1246 to induce M2 macrophage polarization by targeting TERF2IP *via* the STAT3 and NF-κB pathways. *Oncogene* (2020) 39:428–42. doi: 10.1038/s41388-019-0996-y

46. Yang I, Han SJ, Sughrue ME, Tihan T, Parsa AT. Immune cell infiltrate differences in pilocytic astrocytoma and glioblastoma: Evidence of distinct immunological microenvironments that reflect tumor biology. *J Neurosurg* (2011) 115:505–11. doi: 10.3171/2011.4.JNS101172

47. Kamran N, Alghamri MS, Nunez FJ, Shah D, Asad AS, Candolfi M, et al. Current state and future prospects of immunotherapy for glioma. *Immunotherapy* (2018) 10:317–39. doi: 10.2217/imt-2017-0122

48. Ott M, Prins RM, Heimberger AB. The immune landscape of common CNS malignancies: implications for immunotherapy. *Nat Rev Clin Oncol* (2021) 18 (11):729–44. doi: 10.1038/s41571-021-00518-9

49. Hodges TR, Ott M, Xiu J, Gatalica Z, Swensen J, Zhou S, et al. Mutational burden, immune checkpoint expression, and mismatch repair in glioma: Implications for immune checkpoint immunotherapy. *Neuro Oncol* (2017) 19:1047–57. doi: 10.1093/neuonc/nox026

Frontiers in Oncology

Advances knowledge of carcinogenesis and tumor progression for better treatment and management

The third most-cited oncology journal, which highlights research in carcinogenesis and tumor progression, bridging the gap between basic research and applications to imrpove diagnosis, therapeutics and management strategies.

Discover the latest Research Topics

See more →

Frontiers

Avenue du Tribunal-Fédéral 34
1005 Lausanne, Switzerland
frontiersin.org

Contact us

+41 (0)21 510 17 00
frontiersin.org/about/contact